UAB
Universitat Autònoma de Barcelona

The role of the gut–brain axis in Parkinson's disease: insights from a novel neuromelanin–producing mouse model

Marina Lorente Picón

PhD Thesis

The role of the gut-brain axis in Parkinson's disease: insights from a novel neuromelanin-producing mouse model

Directors: Dra. Ariadna Laguna Tuset & Dr. Miquel Vila Bover

Tutor: Dr. Joan Xavier Comella Carnicé

PhD in Neurosciences

Insitut de Neurociències

Universitat Autònoma de Barcelona

Barcelona, 2025

CONTENTS

TABLE OF CONTENTS

LIST OF FIGURES

LIST OF TABLES

LIST OF ABBREVIATIONS

α-MSH and β-MSH	α- and β -melanocyte stimulating hormones
µl	Microliter
ºC	Degree Celsius
16S rRNA	16S ribosomal RNA gene
3-MT	3-Methoxytyramine
5-HIAA	5-hydroxyindole-3-acetic acid
5-HT	Serotonin
5-HT-d4	Serotonin-d4 Hydrochloride
5-SCD	5-S-cysteinyldopa
5-SCDA	5-*S*-cysteinyldopamine
6-OHDA	6-Hydroxydopamine
AAAs	Aromatic amino acids
AADC	L-amino acid decarboxylase
AAVs	Adeno-associated viruses
ABC	Avidin-Biotin-Peroxidase Complex
ABX	Antibiotic
AC	Aminochrome
ACh	Acetylcholine
ACh-d4	Acetylcholine-d4 Chloride
AChE	Acetylcholinesterase
ACR	Albumin/Creatinine ratio
ACTH	Adrenocorticotropic hormone
AD	Alzheimer's disease
AgPR	Agouti-related peptide
AI	Artificial Intelligence
AJ	Adherens junctions
ANS	Autonomic nervous systems
AP	Area postrema
ARA	Arachidonic acid
ARC	Arcuate
Arc*Pomc*$^{-/-}$	ARC POMC-deficient
ATP	Adenosine triphosphate
AUC	Area under the curve
BAT	Brown adipose tissue
BBB	Blood-brain barrier
BCAAs	Branched-chain amino acids
BDNF	Brain-derived neurotrophic factor
Bhmt	Betaine-Homocysteine S-Methyltransferase
Bpifb6	BPI Fold Containing Family B Member 6

BSA	Bovine serum albumin
C	Cholesterol
CA	Cervical afferents
CART	Amphetamine-regulated transcript
CBATEG	Center for Animal Biotechnology and Gene Therapy
CCH	Carbachol
cDNA	Complementary DNA
CEEA	Comitè Ètic d'Experimentació Animal
CIBEROBN	CIBER Fisiopatología de la Obesidad y Nutrición
CKD	Chronic kidney disease
CNS	Central nervous system
COMT	Catechol-O-methyltrtansferase
CRP	C-reactive protein
CSF	Cerebrospinal fluid
CTs	Thresholds cycles
CXCL8	CXC-chemokine ligand 8
DA	Dopamine
DAB	3,3'-diaminobenzidine
DA-d4	Dopamine-d4 hydrochloride
DAT	Dopamine transporter
DBH	Dopamine-beta-hydroxylase
DBS	Deep brain stimulation
DCT	DOPAchrome tautomerase
DDC	L-DOPA decarboxylase
DEA	Differential expression analysis
DEGs	Differentially expressed genes
DHI	5,6-dihydroxyundole
DHICA	5,6-dihydroxyindole-2-carboxylic acid
DI	Discrimination index
DLB	Dementia with Lewy bodies
DNV	Dorsal motor nucleus of the vagus nerve
DPP-IV	Dipeptidyl peptidase IV
DRs	Dopamine receptors
DVC	Dorsal vagal complex
e.g.	*exempli gratia* (example given)
EECs	Enteroendocrine cells
EFS	Electrical field stimulation
EGCs	Enteric glial cells
eNM	Extracellular NM
ENS	Enteric nervous system
EPA	Eicosapentaenoic acid
ESRD	End-stage renal disease
FA	Formic acid
FC	Fold change

FITC	Fluorescein isothiocyanate-conjugated
FMT	Fecal microbiota transplant
FSH	Follicle-stimulating hormone
GFR	Glomerular filtration rate
GH	Growth hormone
GI	Gastrointestinal
GLP-1	Glucagon-like peptide 1
Glyat	Glycine-N-Acyltransferase
Glycam1	Glycosylation-dependent cell adhesion molecule 1
GnRH	Gonadotropin-releasing hormone
GO	Gene Ontology
GSEA	Gene set enrichment analysis
GTT	Glucose tolerance test
GWAS	Genome-wide association studies
h	Hours
H2O	Water
HC	Healthy controls
HCl	Hydrochloric acid
HDL	High-density lipoprotein
HFD	High fat diet
HPA	Hypothalamic-pituitary-adrenal
HS	Horse serum
hTyr	Human tyrosinase
IBD	Inflammatory bowel disease
ICC	Interstitial cells of Cajal
IDL	Intermediate-density lipoproteins
IECs	Intestinal epithelial cells
IF	Immunofluorescence
IHC	Immunohistochemistry
ILBD	Incidental Lewy body disease
IS	Internal standard
Isc	Short-circuit current
JAMs	Junctional adhesion molecules
Klre1	Killer cell lectin-like receptor subfamily E member 1
KO	Knock out
Kyn	Kynurenine
LBDs	Lewy body disorders
LBP	Live biotherapeutic products
LBs	Lewy bodies
LC	Locus coeruleus
LDL	Low-density lipoprotein
L-DOPA	L-dihydroxyphenylalanine
LH	Luteinizing hormone
LHA	Lateral hypothalamic area

Lilrb4a	Leukocyte Immunoglobulin-Like Receptor, Subfamily B, Member 4A
LMWM	Low molecular weight multimers
L-NNA	Nω-nitro-L-arginine
LOD	Limit of detection
LOQ	Limit of quantitation
LP	Lewy pathology
LPC	Lysophosphatidylcholine
LPS	Lipopolysaccharides
LRRK2	Leucine-rich repeat kinase 2
m	Month
M cells	Microfold cells
MAO-B	Monoamine oxidase-B
MBs	Marinesco bodies
MC4Rs	Melanocortin 4 receptors
MCH	Melanin-concentrating hormone
min	Minute
mM	Milimolar
MPP+	1-methyl-4-phenylpyridinium ion
MPTP	1-methyl-4-phenyl-1,2,3,6-tetrahydropyridine
MRgFUS	Magnetic resonance-guided focused ultrasound
MRM	Multiple Reaction Monitoring
MRS2500	(1R,2S,4S,5S)-4-[2-Iodo-6-(methylamino)-9H-purin-9-yl]-2-(phosphonooxy)-bicyclo-[3.1.0]-hexane-1-methanol dihydrogen phosphate tetraammonium salt
MS	Multiple sclerosis
MSA	Multiple system atrophy
NANC	Non-adrenergic and non-cholinergic
NBM	Negative Binomial Model
NE	Noradrenaline
NGS	Normal goat serum
NM	Neuromelanin
NNNP	Non-nitrergic and non-purinergic
NO	Nitric oxide
NPY	Neuropeptide Y
NTS	Nucleus tractus solitarius
OB	Olfactory bulb
OD	Optical density
ORX-A	Orexin-A
OTUs	Operational taxonomic units
Paraquat	N, N’-dimethyl1-4-4-4’-bypiridinium
PB	Phosphate buffer
PB	Protein-bound
PBs	Pale bodies
PBS	Phosphate buffered saline

PCA	Principal Components Analysis
PCoA	Principal Coordinates Analysis
PD	Parkinson's Disease
PFA	Paraformaldehyde
PFC	Prefrontal cortex
PFFs	Pre-formed fibrils
PGI_2	Prostacyclin
PL	Glycerophospholipids
Pla2g2c	Phospholipase A_2, Group IIC
PLP-1	Proteolipid-protein-1
PNS	Peripheral nervous system
POMC	Proopiomelanocortin
PPN	Pedunculopontine nucleus
PRL	Prolactin
Ptgis	Prostaglandin I_2 Synthase
PUFAs	Polyunsaturated fatty acids
PVCA	Principal Variance Component Analysis
PYY	Peptide-YY
QC	Quality controls
RBD	REM sleep behavior disorder
REM	Rapid eye movement
RIPA	Radioimmunoprecipitation assay
r.p.m.	Revolutions per minute
ROS	Reactive oxygen species
RT	Room temperature
RT-qPCR	Real-time quantitative PCR
s	Seconds
SCFAs	Short-chain fatty acids
SCG	Sympathetic chain ganglia
SIBO	Small intestinal bacterial overgrowth
Slfn1	Schlafen 1
SM	Sphingomyelin
SNpc	Substantia Nigra pars compacta
SNPs	Single-nucleotide polymorphisms
SPCs	Spontaneous phasic contractions
STR	Striatum
T2D	Type 2 diabetes mellitus
Tarm1	T Cell-Interacting, Activating Receptor on Myeloid Cells 1
TBS	Tris buffered saline
TG	Triglycerides
TH	Tyrosine hydroxylase
TJs	Tight junctions
TLR-2	Toll-Like Receptor 2
TLR-4	Toll-Like Receptor 4

Tlr7	Toll-Like Receptor 7
TMS	Tetramethyl-silane
Trp	Tryptophan
TSH	Thyroid-stimulating hormone
TSP	Trimethylsilyl-propanoic acid
TYR	Tyrosinase
TYRP1	TYR-related protein-1
TYRP2	TYR-related protein-2
UAB	Universitat Autònoma de Barcelona
UC	Ulcerative colitis
UEB-VHIR	Statistics and Bioinformatics Unit at Vall d'Hebron Research Institute
UPLC-MS/MS	Ultra performance liquid chromatography-tandem mass spectrometer
VHIR	Vall d'Hebron Research Institute
VLDL	Very low-density lipoprotein
VMAT2	Vesicular monoamine transporter 2
VNS	Vagus nerve stimulation
VTA	Ventral tegmental area
WAT	White adipose tissue
WB	Western blot
ZO	Zonula occludens
ZO-1	Zonula occludens-1
ZO-2	Zonula occludens-2

ABSTRACT

ABSTRACT

Accumulating evidence indicates that gastrointestinal (GI) dysfunction and gut microbiota alterations represent a risk factor for Parkinson's disease (PD). Disruptions of the gut-brain axis can affect both the enteric and central nervous systems, contributing to disease pathophysiology and opening new avenues for the development of disease-modifying therapeutic strategies.

To assess the involvement of the gut-brain axis in PD pathogenesis and/or in modulating the manifestation of PD symptoms, we used a new transgenic neuromelanin (NM)-producing mouse model (tgNM) that mimics the human-like, age-dependent accumulation and brain-wide distribution of NM. We demonstrated that tgNM mice, particularly females, develop early sensorimotor impairments, GI dysfunction, gut barrier disruption, gut dysbiosis, low-grade systemic inflammation, and metabolic and neuroendocrine dysregulations. All these occurred during the prodromal phase, prior to dopaminergic neuronal loss in the substantia nigra pars compacta (SNpc). Next, we explored whether gut microbiota modulation could influence PD-like phenotypes. Chronic high fat diet (HFD) feeding induced a metabolic dysregulation phenotype, further exacerbating gut permeability and systemic inflammation, worsening neuroendocrine imbalances, and accelerating NM accumulation and neuroinflammation in key catecholaminergic nuclei, particularly in tgNM females. Finally, we assessed the therapeutic potential of rejuvenating the gut microbiota through fecal microbiota transplantation (FMT) from young healthy wt donors. While FMT successfully modified the microbiota composition in wt mice, it failed to induce persistent microbial changes, intestinal barrier function or behavioral improvements in tgNM females, suggesting that ongoing central nervous system pathology creates a hostile gut environment resistant to microbial interventions.

Collectively, our findings indicate that modelling human brain pigmentation in mice is sufficient to induce prodromal GI dysfunction, systemic metabolic dysregulation, increased neuronal vulnerability and glial reactivity. These results highlight the impact of metabolic stressors, such as diet, on neurodegenerative processes like PD. Moreover, they emphasize the need to consider sex differences, systemic inflammation and microbiota-host interactions in PD pathophysiology and for successful disease modifying therapeutic development. Overall, this thesis highlights that the tgNM mouse model represents a valuable tool to investigate gut-brain axis mechanisms and disease-modifying strategies in the context of PD and brain aging.

INTRODUCTION

1 Parkinson's disease

1.1 Brief history

Parkinson's disease (PD) was first described over two centuries ago by British physician James Parkinson in his seminal work, An Essay on the Shaking Palsy (1817). In this essay, Parkinson detailed a neurological condition characterized by primary motor symptoms such as resting tremor, flexed posture, and bradykinesia, emphasizing its progressive nature and late onset (Parkinson, 1817).

Approximately fifty years later, in 1872, French neurologist Jean-Martin Charcot expanded upon Parkinson's observations, providing a more comprehensive clinical characterization of the disease. Charcot identified bradykinesia and rigidity as hallmark features and introduced the term "Parkinson's disease," replacing earlier labels like "paralysis agitans" or "shaking palsy." Charcot's decision stemmed from his recognition that PD patients did not exhibit significant muscle weakness and did not always present with tremors, refining the understanding of this disorder's clinical spectrum (Charcot, 1872; Goetz, 2011; Obeso et al., 2017).

Later in the 1890s, Blocq, Marinesco, and Brissaud were the first to identify the Substantia Nigra pars compacta (SNpc) as the primary region affected in PD, despite its first description in 1786 by Félix Vic D'Azyr (d'Azyr, 1786; Fénelon & Walusinski, 2021). This conclusion was based on their observation of unilateral resting tremors in a patient with a tuberculoma in the cerebral peduncle contralateral to the body's affected side (Blocq et al., 1893). Two decades later, in the 1920s, Trétiakoff provided the first detailed description of neuropathological alterations in the SNpc of PD patients. He identified two key morphological lesions in PD, the loss of pigmented nerve cells, also known as neuromelanin (NM)-containing neurons, and the presence of intracellular inclusion bodies in idiopathic paralysis agitans. These inclusions, which he termed "Corps de Lewy" had been previously described by F. H. Lewy in 1912 (Holdorff, 2019; Lewy FH, 1912; Tretiakoff C, 1919). These observations established the loss of NM-containing dopaminergic neurons and the presence of Lewy Bodies (LBs) as key neuropathological hallmarks and diagnostic criteria for PD (N. L. G. Del Rey et al., 2018).

1.2 Epidemiology

PD is the most common neurodegenerative movement disorder and the second most prevalent neurodegenerative disease after Alzheimer's disease (AD), affecting over 10 million people worldwide (Marras et al., 2018). With increasing global life expectancy, the number of individuals diagnosed with PD has risen significantly. According to the 2016 Global Burden of Disease study, the crude prevalence of PD increased by 74% from 1990 to 2016, though this growth was more modest (22%) when adjusted for population aging (Ray Dorsey et al., 2018). However, estimating global prevalence and mortality remains challenging due to limited high-quality data, and extrapolations based on high-income countries may not

accurately represent trends in other regions. PD prevalence varies significantly by geography, ethnicity, age and sex (Ben-Shlomo et al., 2024). PD predominantly affects individuals aged over 65 years and is more common in men than in women (Ou et al., 2021). These differences are interconnected and influenced by disparities in education, healthcare access, and socioeconomic status, complicating efforts to isolate biological and environmental PD risk factors (Ben-Shlomo et al., 2024).

1.3 Neuropathology

The primary neuropathological hallmarks of PD are the loss of dopaminergic neurons in SNpc, leading to reduced dopamine (DA) levels in the striatum (STR), and the widespread accumulation of intracellular α-synuclein aggregates, known as LBs. These two features are specific for a definitive postmortem diagnosis of idiopathic PD (Poewe et al., 2017). Beyond the SNpc, other neuronal populations are also affected in PD (Giguère et al., 2018). Additionally, neuroinflammatory responses associated with neuronal degeneration have been consistently observed in postmortem PD brains (Galiano-Landeira et al., 2020; McGeer et al., 1988; Tansey et al., 2022) .

1.3.1 Selective neurodegeneration

In idiopathic PD, the brain often exhibits mild atrophy of the frontal cortex. However, the most defining morphological alterations are observed in the brainstem, where the SNpc shows a marked loss of pigmentation. This loss results from the degeneration and death of NM-containing dopaminergic neurons in the SNpc, which project to the basal ganglia, thus affecting the nigrostriatal pathway leading to the classical motor symptoms of PD (Dickson, 2012). Additionally, significant cell loss occurs in several subcortical nuclei, including the ventral tegmental area (VTA), the locus coeruleus (LC), the nucleus basalis of Meynert, the dorsal motor nucleus of the vagus nerve (DNV), the pedunculopontine nucleus, the raphe nuclei, the hypothalamus and the thalamus (Figure 1) (Giguère et al., 2018). Neurodegeneration in these regions leads to widespread disruptions in multiple neurotransmitter systems, including the cholinergic, adenosinergic, glutamatergic, GABAergic, noradrenergic, serotonergic, and histaminergic pathways also contributing to the spectrum of non-motor symptoms of the disease (Kalia et al., 2013). Overall, the detection of neurodegeneration in different anatomical structures involving various neurotransmitter systems defines PD as a multisystem disorder (Khan et al., 2023).

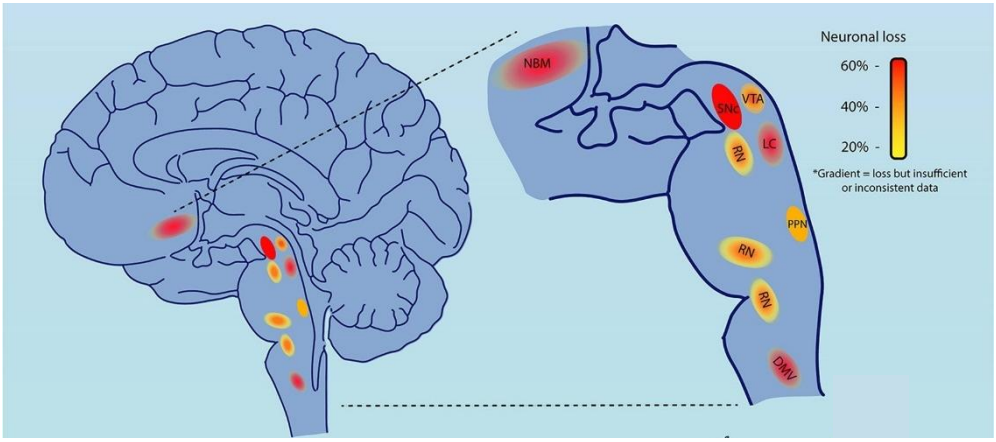

Figure 1. Cellular vulnerability in PD. Cellular vulnerability in PD. Schematic representation of brain regions demonstrating cell loss in PD. Color represents evidence of cell loss. Red = 60%, orange = 40%, and yellow = 20%. Color gradients indicate uncertainty in the extent of this cell loss. Adapted from (Giguère et al., 2018)

1.3.2 LB pathology and Marinesco bodies (MBs)

Another key neuropathological PD hallmark is the presence of abnormal cytoplasmic inclusions within neuronal cell bodies known as LBs. These spherical inclusions, along with thread-like Lewy neurites, are primarily composed of aggregated α-synuclein. However, they also include a diverse number of different molecules, proteins and organelles, including ubiquitin, tubulin, p62, neurofilaments, lipids and mitochondria (Shults, 2006). Another type of inclusion, considered precursors of LBs, are Pale bodies (PBs). These are characterized by rounded granular, pale-staining eosinophilic material that displaces NM in brainstem neurons (Choong & Mochizuki, 2022). Additionally, MBs, commonly found in pigmented neurons of the SNpc and LC, represent another type of inclusion in PD. Unlike LBs, MBs are localized within the cell nucleus and are more frequent with advancing age. They are also prevalent in AD, dementia with LBs, and other neurodegenerative disorders. Interestingly, in aging brains, MBs frequency correlates with striatal dopaminergic depletion (Beach et al., 2004).

1.3.2.1 Braak's staging

In 1942, Lewy observed that pathological changes in PD were not confined to the SNpc but were widespread throughout the central nervous system (CNS) (Lewy, 1942). Decades later, Braak *et al*. proposed a staging system for PD pathology based on the distribution of α-synuclein in a large series of autopsy cases. This staging system correlated the progressive spread of LB pathology with the clinical progression of the disease (Braak, Del Tredici, et al., 2003). Braak's scheme consists of six stages. In the earliest stage 1, neuronal pathology is observed in the DNV in the medulla and the anterior olfactory nucleus in the olfactory bulb (OB). By stage 2, the LC becomes affected, often coinciding with early non-

motor symptoms, though patients may still be asymptomatic. In stage 3, pathology advances to SNpc. At stage 4, significant neurodegeneration of the pigmented neurons in the SNpc becomes evident and the pathology progresses to involve the basal forebrain, amygdala and the medial temporal lobe structures. In the later stages 5 and 6, the pathology extends further into neocortical regions, eventually affecting primary sensory and motor areas (Figure 2) (Braak, Del Tredici, et al., 2003). While the Braak staging scheme offers a useful model for understanding the progression of PD pathology, it is important to note that it is based on the distribution of abnormal α-synuclein deposits rather than the pattern of neuronal loss. The relationship between α-synuclein deposition and the progression of neuronal degeneration has not been rigorously validated, and as such, the staging system should be interpreted with caution (Dickson, 2012; Halliday et al., 2012). Subsequent studies have reported that Braak's stereotypic staging is applicable to most PD cases but not all. Notably, a study found that 7% of the studied cases showed no affectations in the DNV, despite the presence of α-synuclein inclusions in the SNpc and cortical regions (Kalaitzakis et al., 2008). Additionally, in PD cases linked to genetic mutations, the pattern of LBs pathology often differs significantly from that seen in idiopathic PD (Doherty et al., 2013).

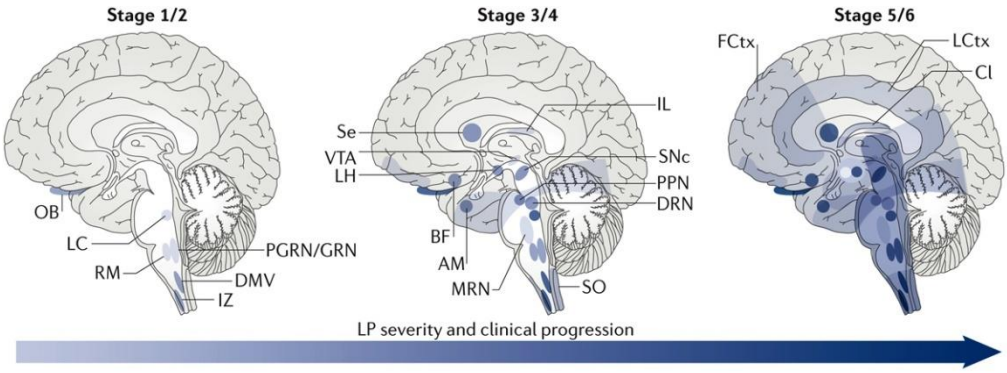

Figure 2. Staging of Lewy pathology (LP) in clinical PD. Schematic representation of the spread of LP within different brain structures, based on the stages proposed by Braak (Braak, Del Tredici, et al., 2003). The anatomical progression of disease through the brain increases over time (from left to right), and the darker the color the more LP is present in each region at a given stage. Retrieved from (Surmeier et al., 2017).

1.3.2.2 α-synuclein

The role of α-synuclein in the pathogenesis of PD was first recognized over two decades ago when genetic forms of PD were identified (Polymeropoulos et al., 1997; Spillantini et al., 1997). Abnormal aggregates of α-synuclein have since been implicated in several sporadic neurodegenerative disorders collectively referred to α-synucleinopathies. These include idiopathic PD, dementia with Lewy Bodies (DLB), multiple system atrophy (MSA), pure autonomic failure and REM sleep behavior disorder (RBD) (Arai et al., 2000;

Galvin et al., 2001; Krohn et al., 2020). Despite these advances, significant questions remain regarding the physiological function of α-synuclein and how to effectively target this protein to prevent neurodegenerative diseases (Calabresi et al., 2023).

1.3.3 Neuroinflammation

Neuroinflammation is another recognized hallmark of PD, as demonstrated by extensive evidence from postmortems, brain imaging, epidemiological and animal studies, that highlight the involvement of both innate and adaptive immunity in PD pathogenesis (Block et al., 2007; Brochard et al., 2009; H. Chen et al., 2005; Galiano-Landeira et al., 2020; McGeer et al., 1988). While innate immunity does not require the presence of a specific antigen to develop, adaptive immunity occurs when specific antigens are presented and recognized by lymphocytes (E. C. Hirsch et al., 2012). Traditionally considered a secondary response to neuronal cell death, recent research suggests that neuroinflammation may play an active and potentially pivotal role in the disease progression.

1.3.3.1 Innate immunity

The connection between neuroinflammation and PD pathogenesis was first reported in 1988, when McGeer et al. identified HLA-DR+ reactive microglia in postmortem PD brain tissue (McGeer et al., 1988). Historically, microglia in regions of neurodegeneration were described as ‘activated’, implying a harmful inflammatory state characterized by ameboid morphology. However, evidence now suggests that microglia exist along a spectrum of phenotypes and play diverse roles in PD pathogenesis (Joers et al., 2017). Microglia can contribute to neuronal death by releasing pro-inflammatory mediators such as TNF, IL-1β, TGFβ, IL-6, reactive oxygen species (ROS), nitric oxide (NO) species and pro-apoptotic proteins, which are elevated in the SNpc, STR, and cerebrospinal fluid (CSF) of PD patients (Nagatsu et al., 2000; Nagatsu & Sawada, 2005). Microglia may also interact with α-synuclein (Bido et al., 2021; Thi Lai et al., 2024) and NM contributing to PD pathology (W. Zhang et al., 2009). Conversely, microglia can exhibit protective functions by producing neurotrophic factors (Chung et al., 2016) and maintaining high phagocytic capacity for the clearance of misfolded proteins (Gao et al., 2023; Le et al., 2016). Thus, neuronal death in PD likely results, at least in part, from pro-inflammatory immune activation. Whether this reflects a loss of anti-inflammatory function, or a gain of pro-inflammatory activity remains unclear, as does the timing of these immune responses during disease progression. Microglial activation has been observed in PD postmortem brains, even in areas where significant neuronal loss is absent (Imamura et al., 2003), and confirmed in vivo by using PET imaging (Gerhard et al., 2006; Ouchi et al., 2005).

1.3.3.2 Adaptive immunity

The role of adaptive immunity in PD pathogenesis is supported by substantial evidence. Studies have investigated T cell subsets in both the brain and periphery to elucidate their contribution to PD-associated inflammation. In the brain, increased levels of CD4+ and CD8+ T cells have been identified in the SNpc of PD patients compared to controls (Brochard et al., 2009). Notably, a nigral infiltration by cytotoxic CD8+ T cells has been observed in early stages of α-synucleinopathy before dopaminergic neuronal death, with later stages showing a correlation between T cell activity and neuronal loss (Galiano-Landeira et al., 2020). Further evidence implicates adaptive immunity in PD pathogenesis, as CD4+ T cells have been shown to recognize specific α-synuclein peptides (Sulzer et al., 2017). Despite discrepancies in findings regarding T cell populations and their roles, variability may be explained from the heterogeneity of patient cohorts studied. Nonetheless, it is evident that dysregulated immune cell trafficking promotes a pro-inflammatory environment that exacerbates neuronal cell death in PD (Tansey et al., 2022).

Collectively, findings from studies on both the innate and adaptive immune systems suggest that immune dysregulation, occurring in both the brain and the periphery, drives upregulation of inflammatory cytokines. This triggers a cascade of pro-inflammatory signaling pathways that ultimately contribute to the neurotoxicity characteristic of PD. Similar to the inflammatory changes observed in the brain, increased levels of pro-inflammatory cytokines, including TNF, IFN-γ, IL-1β, IL-6, IL-2, CXC-chemokine ligand 8 (CXCL8 – IL-8) and CCL2, have been detected in the serum of PD patients, with these elevations correlating with disease progression and the degree of disability (Brodacki et al., 2008; Reale et al., 2009).

1.4 Neuromelanin

The equivalent of peripheral melanin in the brain is called NM because of its similar appearance, although it is exclusively found in catecholamine-producing regions and forms only in neurons (Vila, 2019). Its accumulation begins around 3 years of age in the human SNpc and continues through life, as neurons lack the ability to degrade or eliminate this pigment. Consequently, intracellular NM progressively accumulates, eventually occupying most of the neuronal cytoplasm with age (Fedorow et al., 2006).

1.4.1 Synthesis of melanin and NM

The synthesis, structure and functionality of NM remain subjects of ongoing debate, as decades of research have yet to provide definitive answers. However, the synthesis of peripheral melanin's, such as eumelanin and pheomelanin in melanocytes, is well-characterized (Ito & Wakamatsu, 2008). Melanogenesis begins with the oxidation of L-tyrosine or L-dihydroxyphenylalanine (L-DOPA) to L-DOPAquinone, a highly reactive intermediate, catalyzed by the enzyme tyrosinase (TYR) (Körner & Pawelek, 1982). In the absence of cysteine, L-DOPAquinone undergoes autooxidation to form

DOPAchrome, which is subsequently converted into 5,6-dihydroxyundole (DHI) or 5,6-dihydroxyindole-2-carboxylic acid (DHICA) by DOPAchrome tautomerase (DCT), also known as TYR-related protein-2 (TYRP2). DHI and DHICA are then oxidized and polymerized by TYR-related protein-1 (TYRP1) into complex polymeric structures forming eumelanin, a black-brown pigment (Prota, 2000). In contrast, pheomelanin synthesis involves the interaction of cysteine with L-DOPAquinone, forming cysteinyldopa, which is further oxidized into benzothiazine intermediates that polymerize into pheomelanin, a yellow-red pigment (Ito & Wakamatsu, 2008; Prota, 2000). The balance between eumelanin and pheomelanin production is determined by TYR activity and the availability of cysteine (Figure 3) (Krainc et al., 2023).

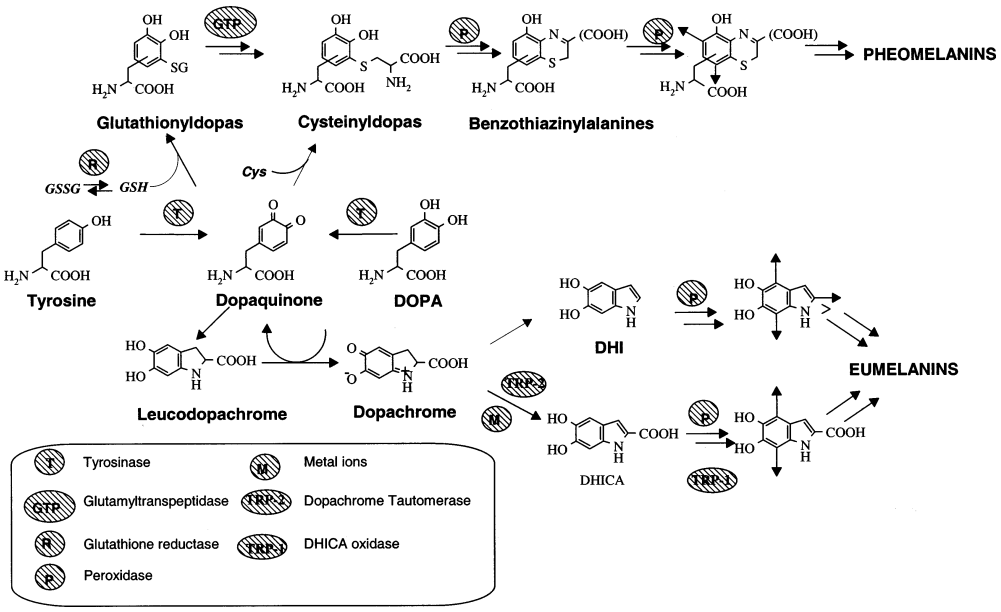

Figure 3. Overall view of melanogenesis. Biosynthetic pathways lead to eumelanin and pheomelanin production. Retrieved from (Prota, 2000).

Studies have demonstrated that NM consists of aggregated structures characterized by a pheomelanin-rich core surrounded by eumelanin surface, with a pheomelanin-to-eumelanin ratio of approximately 3:1 (Bush et al., 2006; Wakamatsu et al., 2003). These NM granules are heterogeneous organelles that also incorporate various cellular components, including lipids (18%) and peptides (12–15%), and their accumulation increases with aging (Figure 4) (Engelen et al., 2012; Zecca et al., 2000, 2008; Zucca et al., 2014).

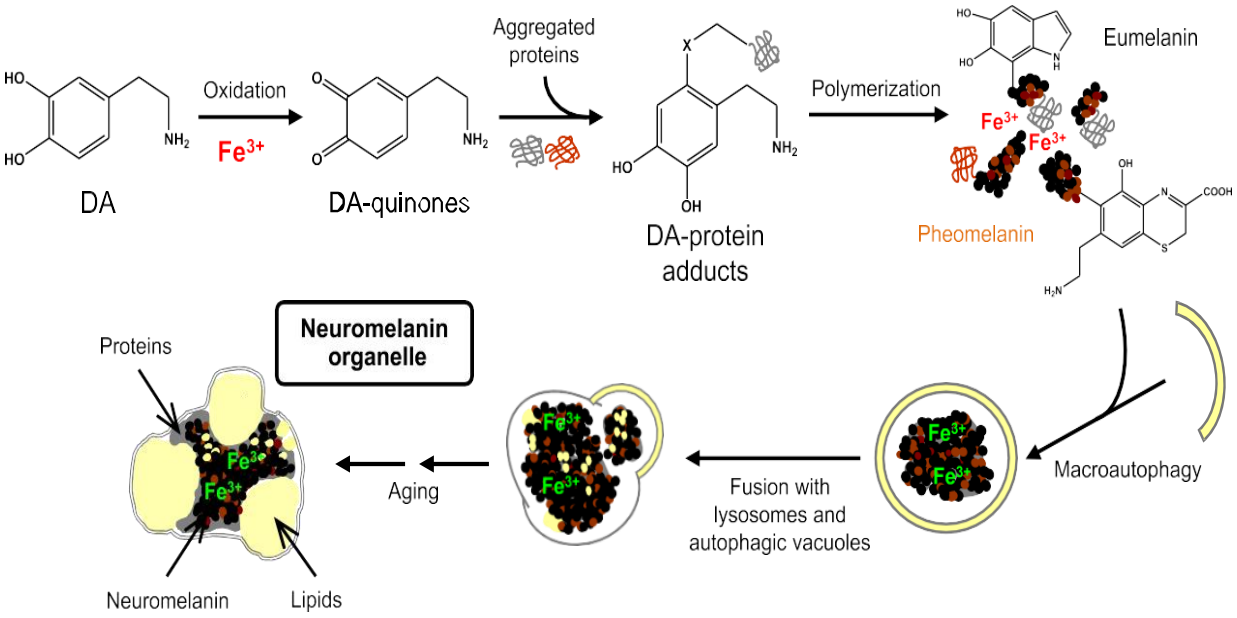

Figure 4. Proposed mechanism for NM pigment biosynthesis and for the formation of NM-containing organelles. Proposed process by which NM pigment is synthesized, and NM-containing organelles are formed in human SN neurons. Excess DA in the cytosol can undergo oxidation to quinones via iron catalysis. These reactive quinones can bind to aggregated proteins which accumulate in the cytosol, initiating oxidative polymerization and leading to the formation of the melanin-protein complex. This complex includes eumelanin and pheomelanin moieties, which have a high binding affinity for metals, particularly iron. Through the process of macroautophagy, this undegradable material is taken into autophagic vacuoles. These vacuoles subsequently fuse with lysosomes and other autophagic structures containing lipids and proteins, resulting in the formation of mature NM-containing organelles. These organelles consist of NM pigments along with metals, lipid bodies and protein matrix. Retrieved from (Sulzer et al., 2018).

The enzymatic control of NM synthesis remains controversial. Unlike peripheral melanin, NM may be formed through nonenzymatic processes driven by the autooxidation of DA (Vila, 2019). *In vitro* studies have shown that NM synthesis occurs when excess cytosolic catecholamines, such as DA, are not sequestered into synaptic vesicles. The addition of L-DOPA to cell cultures resulted in NM granule formation and accumulation, which was significantly reduced by overexpression of the vesicular monoamine transporter 2 (VMAT2). VMAT2 enhances DA uptake into synaptic vesicles, thereby lowering free cytosolic DA levels and reducing NM synthesis. NM formation was also diminished by the addition of iron chelators, suggesting that both free cytosolic DA and iron levels are critical for NM synthesis (Sulzer et al., 2000). However, several observations challenge the idea that NM synthesis is solely a result of DA autooxidation. For instance, the distribution of NM does not fully align with that of tyrosine hydroxylase (TH), the key enzyme in DA synthesis, as certain some DA and noradrenaline (NE)-producing neurons lack NM entirely (Gaspar et al., 1983). Additionally, NM is absent in most animal species, even in those with

significant DA levels, suggesting that its formation may not arise simply as a byproduct of DA oxidation (Marsden, 1961). Furthermore, PD patients treated with high doses of L-DOPA do not show increased NM levels in their surviving SNpc neurons, as might be expected if NM was purely the result of DA autooxidation (Fahn, 2015).

A potential enzymatic contributor to NM synthesis is TYR, the rate-limiting enzyme in peripheral melanogenesis. However, the expression of TYR in the adult human brain is debatable. Some studies have reported low levels of TYR-like activity and expression in the SNpc of human and murine brains (Carballo-Carbajal et al., 2019; Greggio et al., 2005; Miranda et al., 1984; Tief et al., 1998; Y. Xu et al., 1997). In contrast, other studies have failed to detect TYR in the human SNpc using other techniques such as western blot (WB), immunohistochemistry (IHC) or mass spectrometry analyses of the proteomic profile of NM granules (Tribl et al., 2007; Wulf et al., 2022). If TYR was present in sufficient amounts in human catecholaminergic neurons, it could provide an alternative enzymatic pathway for NM synthesis alongside DA autooxidation (Nagatsu et al., 2023). Consequently, the question of whether TYR or other related enzymes contribute to NM synthesis remains unresolved.

1.4.2 NM relation to PD pathogenesis

The functional significance of NM remains a subject of ongoing debate. Recent studies suggest that NM plays a dual role, acting either as a protective or a toxic factor depending on the cellular context (Zucca et al., 2014a). Its synthesis is believed to prevent the accumulation of toxic catecholamine derivates by incorporating them into its polymer structure (Zecca et al., 2003). Similar to peripheral melanins, NM exhibits antioxidant and radical-scavenging properties, mitigating oxidative stress. NM synthesis may also serve as a protective mechanism by trapping cytosolic quinones and semiquinones, thereby neutralizing their toxicity (Sulzer et al., 2000). Furthermore, NM protects neurons by binding and isolating toxins, including 1-methyl-4-phenylpyridinium ion (MPP+) (D'Amato et al., 1986) and the herbicide paraquat (Lindquist et al., 1988), reducing their deleterious effects on cellular organelles. However, NM's protective role may shift under certain conditions, implicating it as a potential vulnerability factor in PD. NM-containing neurons are particularly susceptible to neurodegeneration (E. Hirsch et al., 1988). Studies have shown that surviving neurons in the SNpc of PD patients exhibit decreased NM content compared to controls (Mann & Yates, 1983). In contrast, neuronal loss in non-melanized brain regions is inconsistent, nonspecific to PD, or occurs secondarily due to the loss of NM-containing interconnected neurons (Sulzer & Surmeier, 2013).

The mechanisms underlying NM's contribution to neuronal vulnerability remain speculative but are supported by experimental evidence. When intracellular iron levels exceed NM's binding capacity, redox-active iron is released, triggering oxidative stress (Zucca et al., 2014). Additionally, the accumulation of NM-containing autophagic vacuoles, formed through macroautophagy, may initially protect neurons by

sequestering oxidative stressors. However, excessive accumulation of these vacuoles can disrupt normal degradative pathways and interfere with vital cellular processes, such as growth factor signaling, ultimately compromising neuronal survival (Sulzer et al., 2000, 2008). Another toxic mechanism involves NM released into the extracellular space following neuronal death, which activates microglia. This activation sustains chronic neuroinflammation, exacerbating neuronal damage (W. Zhang et al., 2013). Activated microglia release neurotoxic mediators, including cytokines, NO and ROS, amplifying oxidative stress and neuronal vulnerability (W. Zhang et al., 2009). Additionally, extracellular NM (eNM) debris release sequestered redox-active metals, such as iron, and other toxic compounds, further promoting inflammation and neurodegeneration (Zucca et al., 2014a). This process creates a self-perpetuating cycle of neuronal death, NM release, and chronic inflammation, driving the progression of PD (Wilms et al., 2003).

Despite NM presence in the brain of all humans, only a small subset of individuals, (1% to 5% of the population over 60 years, with prevalence increasing with age) develop PD (Ben-Shlomo et al., 2024). Evidence suggests that PD may manifest in individuals who reach a pathogenic threshold of intracellular NM accumulation earlier in life. Supporting this hypothesis, one study from our group has shown that NM levels in the brains of PD patients and pre-symptomatic individuals, such as those with incidental LB disease (ILBD), exceed this pathogenic threshold (Carballo-Carbajal et al., 2019). In contrast, age-matched healthy individuals maintain intracellular NM levels below this threshold. The accelerated intracellular buildup of NM in PD could result from several factors. One possibility is the abnormal upregulation or increased activity of enzymes involved in NM production, such as TYR or TYRP2 (Fernández-Santiago et al., 2015). Another contributing factor is elevated cytosolic DA levels, resulting from impairments in VMAT2-mediated DA sequestration into synaptic vesicles, a defect observed in early PD cases (Gonzalez-Sepulveda et al., 2023). These mechanisms may accelerate NM accumulation, pushing neurons beyond the pathogenic threshold and contributing to neurodegeneration in PD.

1.5 Symptomatology

The clinical features historically associated with PD are motor symptoms which include resting tremors, muscular rigidity, bradykinesia and postural instability. These symptoms typically emerge as the disease progresses and are linked to the loss of dopaminergic neurons in the SNpc leading to DA depletion in the STR. The hallmark motor symptoms and their characteristic improvement with levodopa (L-DOPA) therapy remain central to the clinical diagnosis of PD (Hughes et al., 1992). The average age of onset is in the late fifties, with a broad range from <50 to >80 years of age. Early-onset PD is defined by an age of onset after 21 years but before 50 years (Mehanna et al., 2022; Poewe et al., 2017).

However, PD is now recognized as a multi-system neurodegenerative disorder combining both motor and non-motor symptoms (Figure 5). Non-motor symptoms, which often precede the onset of motor features

by decades, have a profound impact on patient's quality of life. These include sleep disturbances, neuropsychiatric symptoms, sensory symptoms, autonomic dysfunction, cognitive impairment, gastrointestinal (GI) disturbances and others (Chaudhuri et al., 2006). Recent years have seen growing efforts in epidemiological studies to identify risk factors and biomarkers that correlate with a later diagnosis of PD, providing valuable insights into early disease detection and intervention. Identifying markers associated with the prodromal symptoms of PD has become increasingly important for early detection. Additionally, identifying subjects with prodromal PD or individuals at risk of developing PD is essential for their inclusion in neuroprotective trials aimed at testing new potential therapies. Finally, the identification of these biomarkers is critical for understanding the etiopathogenic mechanisms underlying the onset of PD, enabling the design of targeted interventions to modify disease progression.

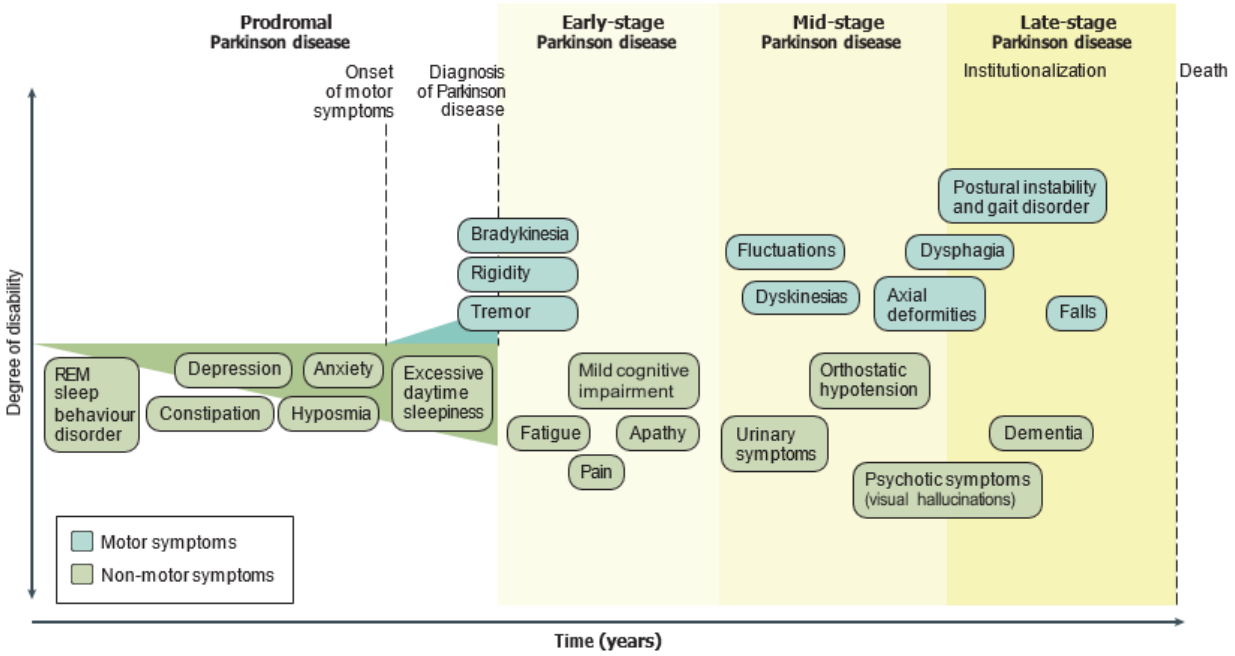

Figure 5. Clinical symptoms associated with PD progression. Schematic representation of the different clinical stages of PD associated with the appearance of non-motor and motor symptoms. Retrieved from (Poewe et al., 2017).

1.6 Treatment

Currently, no therapeutic interventions are available to halt or reverse the progression of PD. Symptom management remains focused around DA replacement therapies, with levodopa continuing to be the gold-standard treatment for symptom control (Antonini et al., 2018). As the disease advances, therapeutic approaches must adapt to manage motor complications, often incorporating neuromodulatory device-aided therapies. However, even the most advanced pharmacological and neuromodulatory techniques

fail to fully control motor complications, underscoring the ongoing challenge of maintaining continuous dopaminergic stimulation (Antonini et al., 2022; Demailly et al., 2024). This limitation is partly due to peripheral factors affecting levodopa pharmacokinetics, such as absorption and transport, as well as central changes involving synaptic alterations and interactions among dopaminergic and other catecholaminergic systems (Stocchi et al., 2024).

1.6.1 Treatment of motor symptoms

In early stages, levodopa is commonly administered as monotherapy or in combination with DA agonists (e.g., ropinirole, pramipexole, rotigotine) or monoamine oxidase-B (MAO-B) inhibitors (e.g., selegiline, rasagiline) (Pringsheim et al., 2021). DA agonists are often used to delay the initiation of levodopa therapy or, when combined with levodopa, to reduce “off” periods, characterized by the recurrence or worsening of the motor symptoms. Similarly, MAO-B inhibitors extend DA availability and are used for mild symptom relief or to enhance the efficacy of levodopa during “off” episodes (Stocchi et al., 2024). For patients with motor fluctuations, therapeutic approaches include dose adjustments, shortening levodopa intervals, and introducing adjunct therapies such as catechol-O-methyltransferase (COMT) inhibitors (e.g., entacapone, opicapone), additional MAO-B inhibitors, or amantadine to manage dyskinesia (Ferreira et al., 2022; Rascol et al., 2021; Rivest et al., 1999). Newer agents like safinamide, which have dual dopaminergic and glutamatergic effects, have shown promise in reducing motor fluctuations and improving non-motor symptoms such as mood and sleep (Abbruzzese et al., 2021).

1.6.2 Device-aided and surgical interventions

In some cases, device-aided therapies become essential. Continuous dopaminergic stimulation can be achieved through subcutaneous apomorphine infusions or levodopa–carbidopa intestinal gel systems, both of which reduce "off" periods and mitigate motor complications. Deep brain stimulation (DBS), targeting the subthalamic nucleus or globus palidus internus, is a well-established surgical approach that significantly improves motor symptoms and enhances quality of life (Groiss et al., 2009). Emerging non-invasive techniques, such as magnetic resonance-guided focused ultrasound (MRgFUS), have demonstrated significant improvements in medication-resistant symptoms like tremors. However, the long-term efficacy of MRgFUS requires further investigation, as its therapeutic benefits may decline over time (Ko et al., 2023). Vagus nerve stimulation (VNS), another non-invasive technique, has also emerged as a potential therapeutic to treat gait impairment in PD, however the evidence is also limited, and further studies are needed (Evancho et al., 2024; Marano et al., 2024; Morris et al., 2019; Torrecillos et al., 2022; H. Zhang et al., 2023).

1.6.3 Treatment of non-motor symptoms

As a multisystemic and multisymptomatic disorder, PD involves dysfunction in various neurotransmitter pathways, including serotonergic, noradrenergic, glutamatergic, GABAergic and cholinergic systems, which are not targeted by levodopa therapy. Non-motor symptoms encompass a wide range of neuropsychiatric, GI, cardiovascular, and autonomic disturbances that significantly affect quality of life. These symptoms can arise from the disease itself, or as side effects of dopaminergic therapies, leading to behaviors such as addiction, hypomania and nocturnal hyperactivity (Béreau et al., 2018).

A comprehensive evaluation of current treatments for non-motor symptoms has identified effective options: pramipexole (DA agonist), tricyclic antidepressants and venlafaxine (serotonin (5-HT) and NE reuptake inhibitor) for depressive symptoms; cognitive-behavioral therapy for depression and impulse control disorders; rivastigmine (acetylcholinesterase inhibitor) for apathy, dementia and mild cognitive impairment; clozapine and pimavanserin (modulating DA and 5-HT) for psychosis; droxidopa (NE precursor) for orthostatic hypotension; botulinum toxin A and B for sialorrhea; domperidone (DA antagonist) for nausea and gastroparesis; and macrogol, lubiprostone, probiotics and prebiotic fibers for constipation (Seppi et al., 2019).

Despite these therapeutic advances, limitations remain in effectively managing non-motor symptoms, particularly in the late stages of PD, highlighting the need for further research. The efficacy of neurotransmitter-targeting drugs reinforces the involvement of multiple systems in PD pathology. Therefore, continued investigation into pathophysiology-based interventions is essential to develop disease-modifying or restorative treatments (Lorente-picón & Laguna, 2021).

1.7 Etiology and risk factors

1.7.1 Genetic factors

Advances in genetic research have significantly improved our understanding of the genetic contributions to PD. The first causative gene linked to PD, SNCA (α-synuclein), was identified in families with inherited forms of the disease, marking a significant breakthrough (Polymeropoulos et al., 1997). Since then, a range of genes responsible for monogenic forms of PD has been well established. These monogenic cases are attributed to rare pathogenic variants in a single gene and are typically classified based on their inheritance patterns. Autosomal dominant forms of PD have been linked to mutations in genes such as SNCA, LRKK2 and VPS35, while autosomal recessive forms, usually associated with early-onset PD, involve mutations in PRKN, PINK and PARK7 (DJ-1). Other autosomal recessive genes, including PLA2G6, ATP13A2, FBXO7, SYNJ1, DNAJC6, VPS13C, PTPA, and DAGLB, are also associated with PD, but these cases are often accompanied by atypical clinical features (Table 1) (Lim et al., 2024). Although monogenic forms of PD account for approximately 5–15% of all cases, they offer critical insights into the molecular mechanisms

underlying the disease (Poewe et al., 2017). For instance, genetic variants in these forms frequently highlight disruptions in key pathways, such as mitochondrial function and the autophagy-lysosomal pathway, which are central to PD pathogenesis (Lim et al., 2024).

In idiopathic PD, genetic risk factors have been extensively studied through large genome-wide association studies (GWAS). These studies have identified more than 90 single-nucleotide polymorphisms (SNPs) affecting other pathways, including cytoskeleton organization, vesicular trafficking, neurotransmission, lipid metabolism, among others; associated with an increased risk of developing PD (Table 2) (Vázquez-Vélez & Zoghbi, 2021). Among these, LRRK2 represents the most common genetic cause of autosomal dominant PD, while variants in GBA1, a gene involved in lysosomal function, are recognized as the most frequent risk factor across various populations. For autosomal recessive PD, PRKN and PINK1 remain the most implicated genes. These genetic findings underscore the complex interplay between inherited factors and cellular processes in the development of both familial and idiopathic PD (Lim et al., 2024).

Table 1. PD-related genes registered in Online Mendelian Inheritance in Man (OMIM) database. Adapted from (Funayama et al., 2022; Lim et al., 2024).

Loci	Chromosomal position	Gene
PARK1/4	4q21.3-q22	SNCA
PARK2	6q25.2-27	PRKN
PARK3	2p13	unknown
PARK5	4p13	UCH-L1
PARK6	1p36.12	PINK1
PARK7	1p36.23	DJ-1
PARK8	12q12	LRRK2
PARK9	1p36	ATP13A2
PARK10	1p32	RAB7L1
PARK11	2q36-q37	GIGYF2
PARK12	Xq21-q25	unknown
PARK13	2p13.1	HTRA2
PARK14	22q13.1	PLA2G6
PARK15	22q11.2-qter	FBXO7
PARK16	1q32	unknown
PARK17	16q12	VPS35
PARK18	3q27-qter	EIF4G1
PARK19	1p31.3	DNAJC6
PARK20	21q22.11	SYNJ1
PARK21	3q22.1	DNAJC13
PARK22	7p11.2	CHCHD2
PARK23	15q22.2	VPS13C
PARK24	10q22.1	PSAP
	6q24.3	RAB32
	9q94.3	PTPA
	7p22.1	DAGLB

Table 2. Genes associated with SNPs that modulate PD risk. Adapted from (Vázquez-Vélez & Zoghbi, 2021)

Category	Candidate genes
Cytoskeleton	CAB39L, TUBG2, MAPT, DNAH17, ANK2, PDLIM2, SORBS3
Endosomal and vesicular trafficking	VAMP4, SIPA1L2, SNCA, CHMP2B, LRRK2, BIN3, RIMS1, DDR GK1, SYT4, ATP6V0A1, GBF1, ARHGAP27, SH3GL2
Immune system	FCGR2A, IL1R2, HLA-DRB6, HLA-DQA1, FYN, CD19, CD38, NOD2, TRIM40, FAM49B, ITIH3, ITI H4, TLR9, STAB1
Ion channels, transporters, and neurotransmitter signaling	KCNS3, KCNIP3, TMEM163, SCN3A, CHRNB1, CLCN3, GCH1, NCKIPSD, CAMK2D
Lipid metabolism and signaling	SPTSSB, ELOVL7, DGKQ
Lysosome and autophagosome	GBA, CTSB, GALC, KAT8, TMEM175
Mitochondria	SLC41A1, COQ7, VPS13C, BAG3, MCCC1, CRLS1, MICU3
Nucleus and gene regulation	NUCKS1, CCNT2, SATB1, KPNA1, MED12L, LCORL, MBNL2, MEX3C, MIR4697, TOX3, UBTF, LSM7, BRIP1, ASXL3, RPS6KL 1, PSMC3IP, SREBF1, RAI1, KANSL1, RNF141, RPS12, CDC71, PHF7, NUPL2, ZNF184
Ubiquitin pathway	UBAP2, BAP1, KLHL7
Miscellaneous	ITPKB, LINC00693, DYRK1A, OGFOD2, FAM171A2, ZNF646, F AM47E, FBRSL1, MIPOL1, SCAF11, PAM, TMEM229B, CRHR1 , STH, SPPL2C, DLG2, C5orf24, C8orf58, GS1–124K511, ALAS1, NISCH, GPNMB, FAM200B, STK39

1.7.2 Non-genetic factors

A wide range of non-genetic factors has been implicated in increasing the risk of developing PD. These include aging, sex, lifestyle habits, demographic variables, environmental exposures, dietary influences, medical history, comorbid conditions and certain medications (Ascherio & Schwarzschild, 2016; Chade et al., 2006; Y. Chen et al., 2021; Hubble et al., 1993). Among these, aging is the most prominent risk factor, as the incidence of PD increases sharply with advancing age (Reeve et al., 2014). Another significant factor is sex; PD is approximately twice as prevalent in men compared to women, although women tend to experience faster disease progression and higher mortality rates (Cerri et al., 2019a). Lifestyle and health-related habits also influence PD risk. Smoking and coffee consumption are consistently associated with reduced risk of developing PD (Rose et al., 2024; Y. Zhao et al., 2024). On the other hand, environmental exposures such as pesticides and herbicides, often encountered in agricultural work or through contaminated water well, have been strongly linked to an increased PD risk (Bloem & Boonstra, 2023; Brouwer et al., 2017). Similarly, exposure to heavy metals and air pollution has been identified as a contributing factor (D. Kwon, Paul, et al., 2024; Pyatha et al., 2022). Other factors associated with an elevated risk include viral infections, inflammatory bowel disease (IBD), and disruptions in the gut microbiota, highlighting the potential role of immune and GI factors to PD pathogenesis. Additionally, specific dietary habits have also been implicated in altering disease risk (H. S. Lee et al., 2021; Lorente-picón & Laguna, 2021; Smeyne et al., 2021).

2 The gut-brain axis in PD

2.1 Brief introduction

The gut-brain axis is a complex bidirectional communication network connecting the CNS and the enteric nervous system (ENS). This intricate system involves the neuroendocrine, neuroimmune, and autonomic nervous systems (ANS), along with the hypothalamic-pituitary-adrenal (HPA) axis and the gut microbiota (Carabotti et al., 2015; L. Liu & Zhu, 2018). Through pathways such as the vagus nerve and signaling molecules, the gut-brain axis regulates numerous physiological processes and behaviors, illustrating how the gut and the brain influence each other in both health and disease (Bonaz et al., 2018). The gut microbiota, which comprises bacteria, archaea, fungi, and viruses, plays a pivotal role in modulating CNS activity and neuronal communication, further underscoring its importance in this axis (Haikal et al., 2019; Parashar & Udayabanu, 2017; Scheperjans et al., 2018).

2.2 Structural anatomy of the GI tract

The intestinal tissue is organized into distinct layers, each with specialized functions (Figure 6). The mesentery anchors the intestines and acts as a pathway for major blood vessels, lymphatics, and nerve fibers, while also housing mesenteric lymph nodes, which are essential for lymphocyte transport and immune system development. Adjacent to the mesentery, the serosa forms the outer protective layer, providing lubrication that supports smooth peristaltic contractions. Underlying the serosa, the muscularis externa is comprised of an outer longitudinal layer and an inner circular layer, which together provide flexibility and coordinated contractility essential for intestinal motility. The myenteric plexus is located between these muscle layers, while the submucosal plexus lies closer to the lumen; both networks form extensive neuronal and glial circuits that regulate communication between different intestinal compartments, including the mucosal layer. Within the submucosa, immune structures such as Peyer’s patches and lymphoid follicles extend into the mucosa, which is composed of the lamina propria and the epithelial layer. Peyer's patches are integral components of the gut-associated lymphoid tissue and play a crucial role in immune surveillance and response. These lymphoid structures are strategically positioned in the small intestine facilitating the induction of immune responses (Heel et al., 1997).

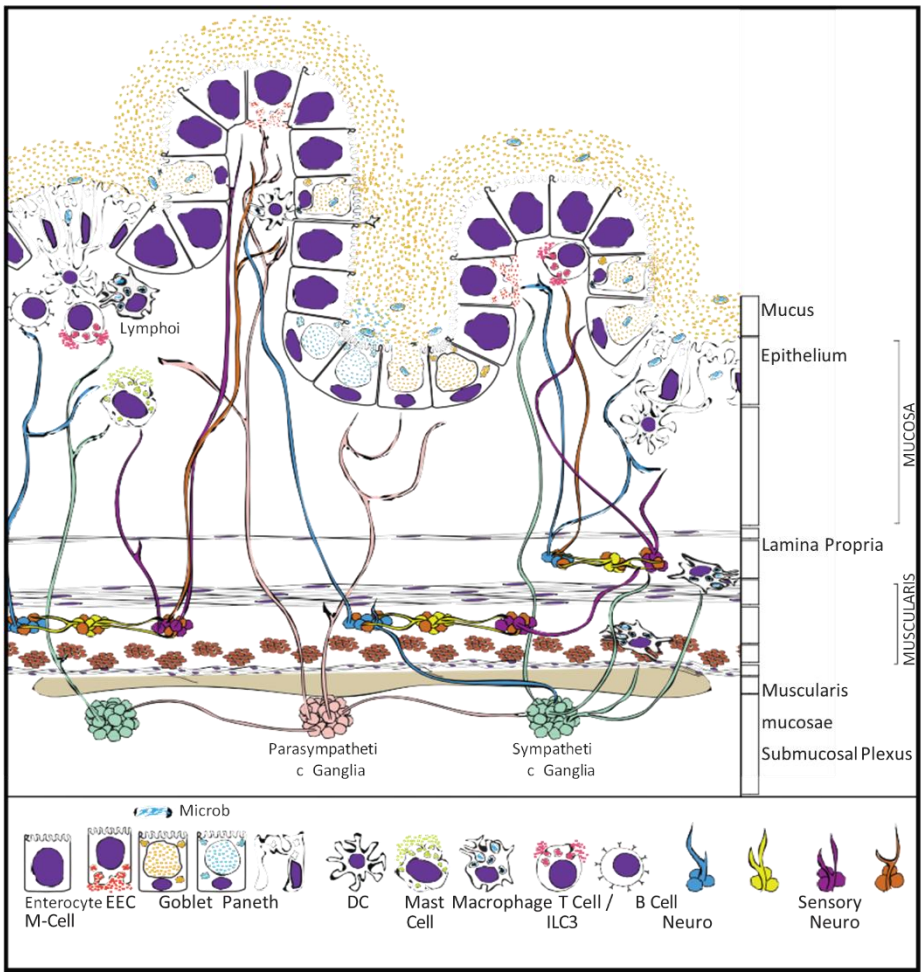

Figure 6.Anatomy of the GI tract. Representation of the different layers of the GI tract and the different cell types that compose it. Retrieved from (B. B. Yoo & Mazmanian, 2017).

The lamina propria is rich in connective tissue and harbors diverse populations of innate and adaptive immune cells, whereas the epithelial layer acts as a barrier separating the lumen contents from the underlying tissue. The epithelial layer comprises several specialized cell types, most notably enterocytes, goblet cells, Paneth cells and enteroendocrine cells (EECs). Enterocytes are the primary absorptive cells, and they present apical microvilli structures to maximize surface area, while goblet cells secrete mucins that contribute to the mucus layer. Paneth cells are predominantly located in the crypts and release antimicrobial peptides to maintain microbial homeostasis. Finally, EECs synthesize neuroendocrine factors that modulate different gut functions. In addition, intestinal epithelial cells (IECs) are important for directing innate and adaptive immunological responses to luminal antigens. Microfold cells (M cells) aid in the immunological sampling of antigens across the epithelium. In addition, M cells are typically found in close association with dendritic cells on the luminal side of Peyer's patches and facilitate antigen sampling, thereby preparing adaptive immune responses. Finally, the intestinal lumen, which hosts a

complex microbiome and various host-derived molecules, forms a dynamic interface between the external environment and the organism, playing a pivotal role in nutrient processing and immune modulation (Goto, 2019; B. B. Yoo & Mazmanian, 2017).

2.2.1 The enteric nervous system (ENS)

The GI tract is autonomously regulated by the ENS, the largest and most complex unit of the peripheral nervous system (PNS), which extends from the esophagus to the anal canal (Fleming et al., 2020). The ENS operates largely independently of the CNS, forming an integrated neural network responsible for controlling gut motility, fluid-electrolyte balance, mucosal immunity, blood flow, and the secretion of gut hormones (Constantinescu, 2016; Sasselli et al., 2012).

Structurally, the ENS comprises two interconnected ganglionated plexuses: the Auerbach plexus (myenteric plexus) and the Meissner plexus (submucosal plexus). These plexuses innervate the circular and longitudinal muscular layers, the lamina propria and the basolateral region of the epithelial mucosa (Sasselli et al., 2012). The myenteric plexus primarily regulates muscle contractions for the propulsion of GI contents, while the submucosal plexus oversees secretion and absorption processes (N. J. Spencer & Hu, 2020). Unlike skeletal muscle, which is only innervated by excitatory neurons, the smooth muscle cells of the GI tract are densely innervated by both excitatory and inhibitory motor neurons. The ENS contains millions of neurons and an even larger population of supporting cells, including enteric glial cells (EGCs) and interstitial cells of Cajal (ICC), which act as pacemakers for gut motility (Fleming et al., 2020; Furness et al., 2014; Pasternak et al., 2016). Neuronal populations within the ENS include sensory neurons, motor neurons, secretomotor neurons, and interneurons, producing a diverse array of neurotransmitters such as acetylcholine (ACh), NO, catecholamines, 5-HT, GABA and various neuropeptides (Furness, 2000; Hens et al., 2001; Z. D. Qu et al., 2008). EGCs, which exhibit diverse morphologies and chemical profiles, express markers such as S100B, GFAP, PDGFRα, and proteolipid-protein-1 (PLP-1), highlighting their complexity comparable to CNS glial cells (Grundmann et al., 2019).

Although the ENS can operate autonomously, it is influenced by extrinsic sympathetic and parasympathetic inputs from the CNS, primarily through the vagus nerve. Approximately 80% of the vagus nerve consists of afferent fibers that transmit visceral and somatic information from the gut to the CNS, while the remaining 20% comprises efferent fibers that regulate gut motility, secretion, and the cholinergic anti-inflammatory pathway (Bonaz et al., 2017). Vagal efferents originate from preganglionic neurons in the DNV and interact with the ENS via postganglionic neurons, with ACh as the primary neurotransmitter at these connections. Vagal afferents, originating from intestinal layers, terminate in the nucleus tractus solitarius (NTS), a key component of the dorsal vagal complex (DVC), which also includes the DNV and the area postrema (AP) (Bonaz et al., 2017; Sawchenko, 1983). The NTS acts as a central reflex hub for the ANS, relaying visceral information to higher brain regions such as the

hypothalamus, amygdala, thalamus, and LC, thus integrating gut-derived signals into autonomic, endocrine, and behavioral responses (Forstenpointner et al., 2022). Beyond vagal input, the gut is also influenced by sympathetic fibers, which connect the ENS to thoracic segments of the spinal cord via prevertebral ganglia (Browning & Travagli, 2014). Moreover, a recent study has highlighted the roles of both sympathetic and parasympathetic systems in Lewy body disorders (LBDs) onset and progression (Andersen et al., 2025). This complex interplay between the ENS, CNS, and autonomic inputs highlights the multifaceted regulation of GI function and its integration with the broader physiological systems of the body.

2.2.2 Intestinal epithelial barrier

The intestinal epithelial barrier serves as a critical defense mechanism, protecting the host from the potentially hostile environment within the gut lumen while ensuring the efficient absorption of nutrients, water and ions. Under homeostatic conditions, this barrier is composed of tightly packed epithelial cells joined by various junctional complexes, including tight junctions (TJs), adherens junctions (AJ), desmosomes and GAP junctions. TJs, consisting of proteins such as claudins, occludins, and junctional adhesion molecules (JAMs), are anchored to the cytoskeleton through zonula occludens (ZO) and cingulin. AJs, formed by cadherins linked to catenins, also interact with the cytoskeleton, while desmosomes connect to intermediate filaments via desmoplakin. Together, these junctions maintain the barrier's structural integrity and prevent paracellular leakage (Fortea et al., 2021; T. Suzuki, 2013; Van Ijzendoorn & Derkinderen, 2019). The integrity and structure of epithelial cells are mostly modulated by the cytoskeleton, primarily composed of actin, myosin, and intermediate filaments (Figure 7) (Fortea et al., 2021).

The gut microbiota is essential for maintaining epithelial barrier integrity under healthy conditions. It fosters a balanced coexistence of symbiotic microbes, mitigates inflammation, and shields the host from pathogens, thereby preserving intestinal and systemic homeostasis (Al-Asmakh & Hedin, 2015). However, external factors such as pathogens, toxins, dietary imbalances, and environmental stressors can disrupt this equilibrium, leading to gut microbiota dysbiosis and epithelial barrier disruption (Erny et al., 2015; Houser & Tansey, 2017). Impaired intestinal barrier permits trans- and paracellular passage of lumen contents into de lamina propria, enabling antigen penetration and triggering immune activation and cell recruitment. Cytokines such as TNF-α and IFN-γ can modulate TJs, impairing their function and further compromising barrier integrity (Turner, 2009). These inflammatory and immune responses also interact with the ENS, affecting neurons and EGCs in the submucosal and myenteric plexuses possibly modulating the CNS (Fortea et al., 2021).

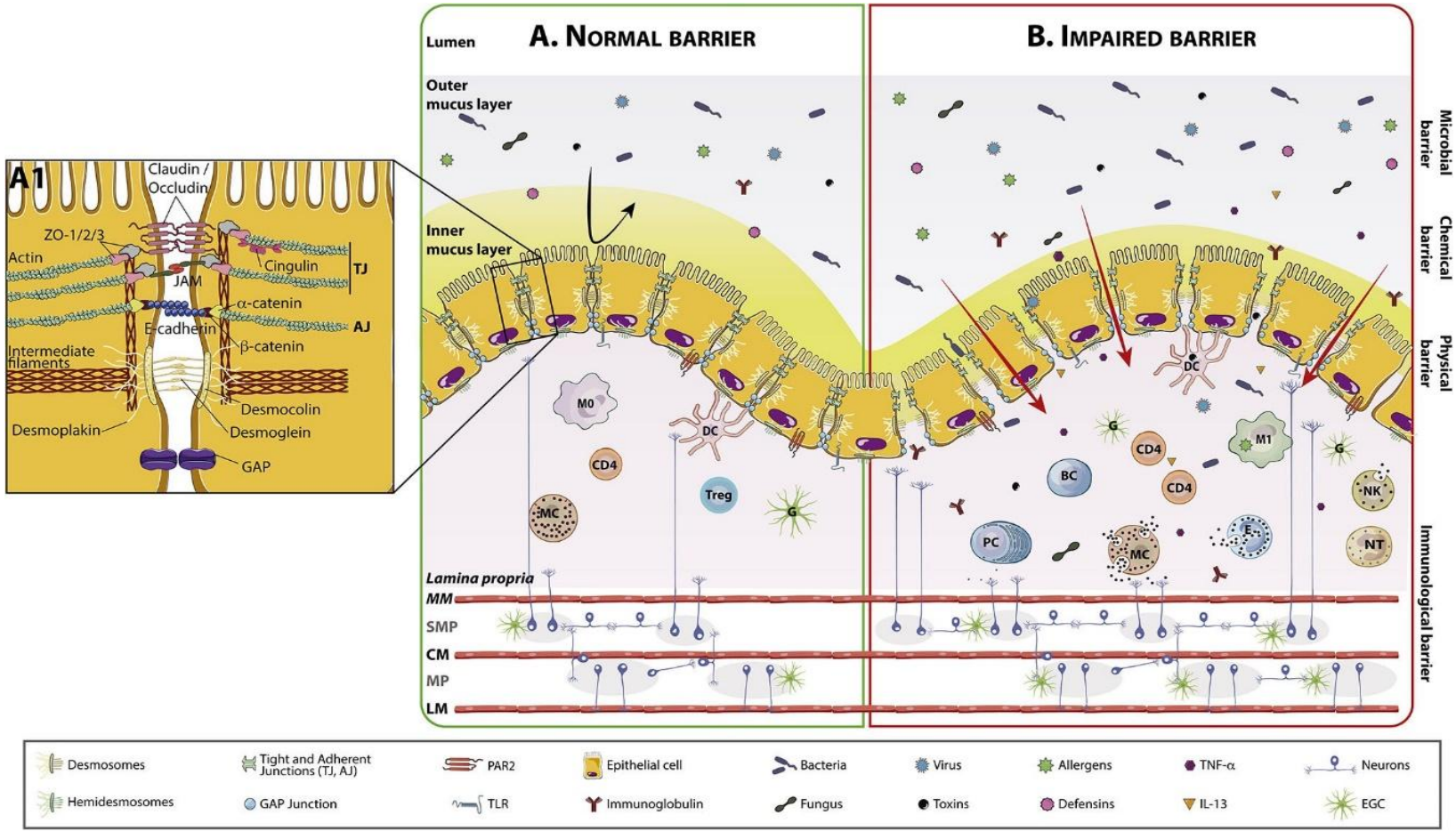

Figure 7. Representation of the intestinal epithelial barrier anatomy and its constituents under normal and impaired conditions. AJ: Adherens junctions; BC: B Cell; CD4: Lymphocyte T helper CD4+; CLDN: Claudin; CM: Circular muscle; D: Desmosomes; D: Dendritic cell; EGC: Enteric glial cell; ENS: Enteric nervous system; IL-13: Interleukin 13; JAM: Junctional adhesion molecule; LM: Longitudinal muscle; M0: Macrophages type 0; M1: Macrophages type 1; MC: Mast cell; MM: Muscularis mucosae; MP: Myenteric plexus; NK: Natural killer; NT: Neutrophil; OCLN: occludin; PC: Plasma cell; SMP: Submucous plexus; TJ: Tight junctions; TNF-α: Tumor necrosis factor alpha; Treg, T regulatory lymphocyte. Retrieved from (Fortea et al., 2021).

2.3 Clinical evidence of GI system involvement in PD

Historically, GI symptoms in PD were often overlooked by neurologists and movement disorders specialists, despite early clinical and neuropathological evidence highlighting significant GI involvement (Den hartog jager & Bethlem, 1960; Eadie & Tyrer, 1965b, 1965a). Today, non-motor symptoms related to the GI tract are recognized as critical prodromal markers of early-stage PD, according to the International Movement Disorders Society (Heinzel et al., 2019). These symptoms, which can precede the onset of classical motor symptoms by several years (Jost, 2010), include dysphagia, sialorrhea, bloating, nausea, gastroparesis, small bacteria overgrowth (SIBO), *Helicobacter pylori* infection, malnutrition, swallowing disorders and constipation (Fasano et al., 2015).

Increasing evidence supports the hypothesis that GI dysfunction is not merely a consequence of PD but may actively contribute to its onset and progression, in particular through gut microbiota dysbiosis and intestinal inflammation. Dysregulated expression of TJs such as occludin and ZO has been observed in fecal samples, serum and GI biopsies from PD patients, linking TJs disruption to increased gut permeability and inflammation (Aho et al., 2021; Boncuk Ulaş et al., 2023; Clairembault et al., 2015; Dumitrescu et al., 2021; Perez-Pardo et al., 2018; Rajkovaca Latic et al., 2024; Schwiertz et al., 2018). Additionally, elevated levels of calprotectin, a biomarker of intestinal inflammation released by infiltrating immune cells, have been reported in PD patients (Aho et al., 2021; Dumitrescu et al., 2021; Mulak et al., 2019; Schwiertz et al., 2018). Colonic biopsies and fecal studies have also revealed increased levels of cytokines such as TNF-α, IFN-γ, IL-6, IL-1β, as well as heightened expression of cyclooxygenase-2 (COX-2), providing further evidence of intestinal inflammation in PD (Devos et al., 2013; Dumitrescu et al., 2021; Mulak et al., 2019; Pochard et al., 2018) Notably, epidemiological studies demonstrate a higher risk of PD in individuals with IBD (H. S. Lee et al., 2021; Villumsen et al., 2019; Weimers et al., 2019; F. Zhu et al., 2019a; Y. Zhu et al., 2022) and a reduced risk in those receiving anti-inflammatory treatments, emphasizing the potential contribution of gut inflammation to PD pathophysiology (S. Park et al., 2019). Supporting this epidemiological link, shared genetic factors, particularly common alleles in the leucine-rich repeat kinase 2 (LRRK2) gene, have been identified in both PD and Crohn's disease patients (Hui et al., 2018). Moreover, clinical and animal studies have reported that truncal vagotomy could reduce the risk of developing PD, suggesting that the vagus nerve may be involved in the pathogenesis of PD (S. Kim et al., 2019; B. Liu et al., 2017; Svensson et al., 2015). Moreover, studies in *Pink1*$^{-/-}$ mice model reported that the absence of PINK1 during intestinal infection activates immune responses that contribute to PD pathology (Kazanova et al., 2024; Matheoud et al., 2019).

Thus, to better understand PD etiology, it's important to know how the extrinsic environmental and intrinsic vulnerability factors interact with the GI tract, as it has a role as a gateway to the brain (Adams-Carr et al., 2016; Frazzitta et al., 2019; S.-M. Hou et al., 2022).

2.4 Brain-first vs. Body-first hypothesis in PD pathogenesis

Accumulating evidence suggests that PD is a heterogeneous disorder with distinct subtypes characterized by different clinical and neuropathological progression patterns (Berg et al., 2021; Mestre et al., 2021; E. Qian & Huang, 2019; Van Rooden et al., 2011). There is a need to better describe this heterogeneity at the individual patient level to better predict disease progression and treatment response, and to identify new therapeutic targets (Marras et al., 2024). Post-mortem studies have identified two predominant α-synuclein pathology patterns: (i) a brainstem-predominant pattern, where pathology originates in the lower brainstem and spreads rostrally, and (ii) a limbic/amygdala-predominant pattern, where pathology is concentrated in midbrain and limbic structures (Borghammer, 2021; Borghammer et al., 2022; Borghammer & Van Den Berge, 2019; Braak, Del Tredici, et al., 2003; Raunio et al., 2019; Tanei et al., 2020). Recent evidence from neuroimaging studies further supports these differing pathological profiles corresponding to different clinical phenotypes(Horsager et al., 2020; Horsager & Borghammer, 2024). These studies have led to a new hypothesis proposing a brain-first vs body-first classification for the onset and progression of PD (Figure 8).

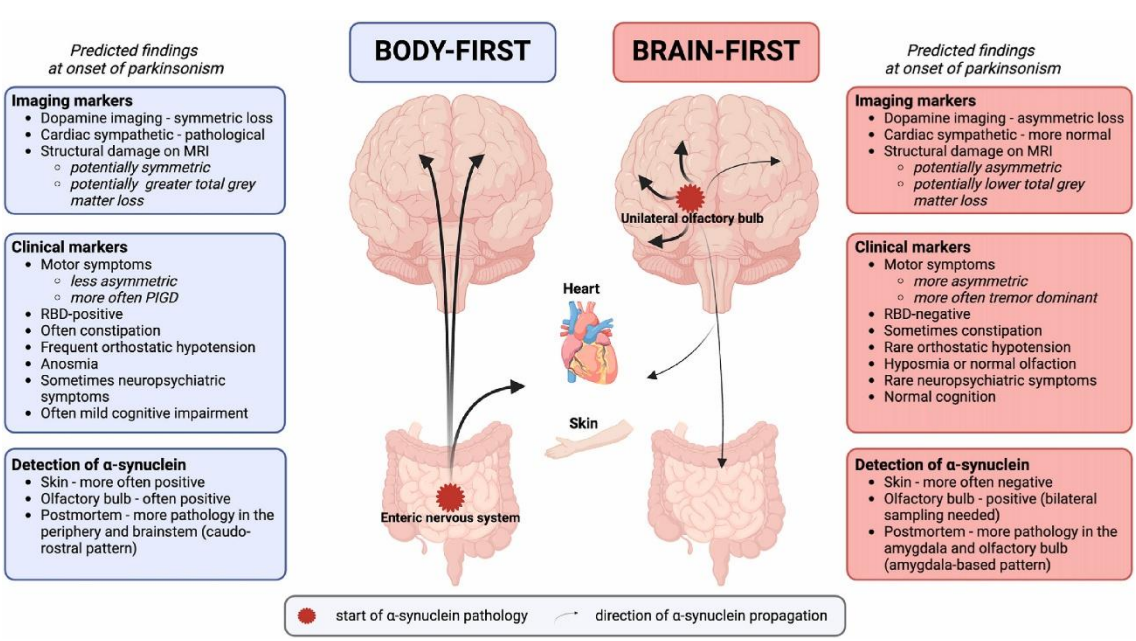

Figure 8. Simplified illustration of the spreading routes in the body-first and brain-first PD model. Key imaging, clinical and α-synuclein detection markers are specified. The proposed bi-directional spread of pathology suggests that body-first subjects should display early peripheral pathology in organs like the heart and skin, many years before PD diagnosis. In contrast, brain-first subjects are expected to show peripheral pathology only during the late prodromal stage or sometimes even after the PD diagnosis. Retrieved from (Horsager & Borghammer, 2024).

2.4.1 Body-first PD and the gut-brain axis

The body-first subtype is strongly associated with RBD in the prodromal phase. RBD, characterized by abnormal motor activity during rapid eye movement (REM) sleep, is a strong predictor of synucleinopathies, with over 90% of RBD patients eventually developing PD or a related disorder (Postuma et al., 2019; Schenck et al., 2013). Histopathological analyses confirm that RBD-positive PD patients exhibit greater LP in peripheral tissues, supporting the notion that RBD represents an early marker of body-first α-synuclein pathology (Leclair-Visonneau et al., 2017). The hypothesis that PD pathogenesis may originate in the GI tract has received considerable attention, with increasing evidence suggesting that α-synuclein aggregation may begin in the ENS before spreading to the CNS via DNV (Borghammer et al., 2021; Borghammer & Van Den Berge, 2019; Braak, Del Tredici, et al., 2003; Braak, Rüb, et al., 2003; Hawkes et al., 2007; Visanji et al., 2014). Histological studies support this gut-to-brain hypothesis, showing LB pathology in the GI tract of prodromal and sporadic PD patients (Beach et al., 2010; Kupsky et al., 1987; Wakabayashi et al., 1988, 1990). Experimental models have further demonstrated that α-synuclein aggregates can propagate trans-synaptically from the gut along the vagus nerve, reinforcing the concept of prion-like α-synuclein transmission (Challis et al., 2020; Holmqvist et al., 2014; S. Kim et al., 2019; Manfredsson et al., 2018; Van Den Berge et al., 2019; Xiang et al., 2024).

Beyond direct α-synuclein transmission, gut microbiota dysbiosis and inflammation have been implicated in triggering or accelerating α-synuclein misfolding. Bacterial amyloid proteins, such as curli secreted by *Escherichia coli*, and Tau proteins, have been shown to exacerbate α-synuclein aggregation and neuroinflammation (S. G. Chen et al., 2016; Pan et al., 2022; Schmit et al., 2023; Xiang et al., 2024). Additionally, increased intestinal permeability has been linked to pathogenic α-synuclein accumulation, supporting a body-first disease mechanism (Forsyth et al., 2011; O'Donovan et al., 2020; Rolli-Derkinderen et al., 2020; Scheperjans et al., 2015).

2.4.2 Brain-first PD and alternative entry routes

In contrast, the brain-first subtype is characterized by early dopaminergic deficits without significant peripheral autonomic dysfunction. RBD-negative PD patients exhibit relatively preserved peripheral innervation but show pronounced pathology in the upper brainstem and telencephalon, with nigrostriatal degeneration preceding autonomic involvement (Knudsen et al., 2021). These patients often present with asymmetric dopaminergic dysfunction, suggesting a distinct disease trajectory compared to body-first PD. Despite these early differences, both subtypes converge at advanced disease stages, leading to widespread neurodegeneration in both central and peripheral structures (Horsager et al., 2020).

An alternative but complementary hypothesis proposes two distinct entry routes for α-synuclein pathology: (i) a nasal pathway, where α-synuclein pathology originates in the OB and spreads to limbic

and cortical regions; (ii) a gastric pathway, where α-synuclein aggregates propagate from the ENS to the brainstem via the vagus nerve (Hawkes et al., 2007, 2009).

While gut-mediated transmission has been widely explored, the OB as a potential initiation site remains less studied. Early investigations failed to detect its spread beyond the olfactory cortex (Braak, Del Tredici, et al., 2003; Braak, Rüb, et al., 2003), yet olfactory dysfunction is considered one of the earliest PD symptoms. Emerging data indicates that OB pathology may contribute to PD initiation, with isolated OB pathology found in incidental LB disease and limbic-predominant LP in DLB (Adler & Beach, 2016; Beach et al., 2010; N. L. Rey et al., 2019). However, isolated OB pathology is rare, making its role in PD initiation uncertain. Interestingly, some studies suggest that α-synuclein aggregates detected in the ENS may originate in the brain and secondarily spread to the gut, rather than the gut being the primary site of pathology (Lawson et al., 2010; McFleder et al., 2023; Ulusoy et al., 2017).

Although the brain-first and body-first PD subtypes propose distinct initiation sites and propagation mechanisms, these hypotheses are not mutually exclusive, and ongoing debate continues regarding their relative contributions to disease progression (Borghammer, 2018; Leclair-Visonneau et al., 2020; Liddle, 2018; Lionnet et al., 2018; Scheperjans et al., 2018).

2.5 Gut dysbiosis in PD

In recent years, the gut microbiome has been extensively studied in the context of PD. While no universal definition of a “healthy” gut microbiome exists, it is widely recognized that high taxonomic diversity, microbial gene richness and a stable functional core enhance resilience to disturbances and facilitate recovery to a balanced state (Lloyd-Price et al., 2016). Aging, one of the main risk factors for PD, significantly affects gut microbiota composition and diversity. From infancy to adulthood, microbial diversity increases, but it declines sharply in later life (Heintz & Mair, 2014; Odamaki et al., 2016; Yatsunenko et al., 2012). Elderly individuals exhibit distinct gut microbiota profiles influenced by factors such as lifestyle, medications, infections, organ dysfunction, and age-related diseases (Claesson et al., 2011; Nagpal et al., 2018). This age-related decline in gut microbiota diversity contributes to inflammaging, oxidative stress and neural dysfunction (Calabrese et al., 2018; Franceschi et al., 2006) highlighting the gut microbiome as a promising therapeutic target in PD.

Advances in metagenomics approaches, including shotgun sequencing and 16S ribosomal RNA (16S rRNA) gene analysis, have enabled detailed exploration of gut microbial communities in human cohorts. These tools have been instrumental in identifying associations between gut microbiota dysbiosis, GI dysfunction and PD. Numerous studies, summarized in Table 3, have reported consistent alterations in gut microbiota composition in PD patients (Barichella et al., 2019; Bedarf et al., 2017; Cilia et al., 2020; Hasegawa et al., 2015; Heintz-Buschart et al., 2018; Heinzel et al., 2020; Hill-Burns et al., 2017; Keshavarzian et al., 2015; C. Li et al., 2019; W. Li et al., 2017; A. Lin et al., 2018; C. H. Lin et al., 2019; S. Nie et al., 2023; Petrov et al.,

2017; Y. Qian et al., 2020; Romano et al., 2021; Toh et al., 2022; Unger et al., 2016; Vascellari et al., 2020; Wallen et al., 2020, 2022; Weis et al., 2019; F. Zhang et al., 2020). At the phylum level, the decrease of Bacteroidetes and the increase of Actinobacteria, Proteobacteria and Verrucomicrobia were reported in different studies. At the family level, decreased relative abundances of Prevotellaceae and Lachnospiraceae were noted, while Bifidobacteriaceae, Christensenellaceae, Lactobacillaceae, Enterobacteriaceae and Verrucomicrobiaceae were consistently elevated. At the genus level, reductions in *Prevotella*, *Blautia*, *Roseburia* and *Faecalibacterium* were frequently reported, alongside increases in *Bifidobacterium*, *Alistipes, Christensenella, Lactobacillus* and *Akkermansia* (Table 3). These findings collectively confirm that gut microbiota composition is altered in PD, underscoring its potential role in the disease's pathophysiology and its relevance as a therapeutic target.

Several bacterial taxa reduced in PD such as members of Prevotellaceae, Lachnospiraceae, and genera like *Blautia*, *Roseburia*, and *Faecalibacterium* are involved in maintaining the gut mucosal barrier and generating short-chain fatty acids (SCFAs), including butyrate, propionate, and acetate (Machiels et al., 2014; Shen et al., 2018; Sokol et al., 2008; Venegas et al., 2019; Ye et al., 2023). SCFAs have a direct impact in GI physiology and gut barrier function. They play different roles in supporting gut barrier integrity, modulating immune responses by promoting anti-inflammatory cytokines, and regulating intestinal motility (Den Besten et al., 2013; Duan et al., 2023; M. H. Kim et al., 2013; Koh et al., 2016; M. Li et al., 2018; Seethaler et al., 2022; Y. P. Silva et al., 2020; Soret et al., 2010). Their reduction in PD is associated with increased gut permeability and heightened susceptibility to bacterial antigens and endotoxins, potentially triggering inflammation and neurodegeneration (Aho et al., 2021; Bedarf et al., 2024; S. J. Chen et al., 2022; Duan et al., 2023; Mulak, 2018; Nishiwaki et al., 2020, 2022; Unger et al., 2016; Wu et al., 2022).

Table 3. Different abundant taxa between PD patients and healthy controls (HC). Summary of the findings observed in different metagenomics studies.

Phylum	Family	Genus	Increased abundance	Decreased abundance	References
Actinobacteria			3	0	(Cirstea et al., 2020; W. Li et al., 2017; Zhang et al., 2020)
Actinobacteria	Bifidobacteriaceae		4	0	(Aho et al., 2019; Barichella et al., 2019; Hill-Burns et al., 2017; A. Lin et al., 2018)
Actinobacteria	Bifidobacteriaceae	Bifidobacterium	10	0	(Aho et al., 2019; Cirstea et al., 2020; Hill-Burns et al., 2017; Nie et al., 2023; Petrov et al., 2017; Romano et al., 2021; Tan et al., 2021; Unger et al., 2016; Wallen et al., 2020, 2022)
Bacteroidetes			1	3	(Keshavarzian et al., 2015; W. Li et al., 2017; Unger et al., 2016; Zhang et al., 2020)
Bacteroidetes	Bacteroidaceae		1	0	(Keshavarzian et al., 2015)
Bacteroidetes	Bacteroidaceae	Bacteroides	1	3	(Keshavarzian et al., 2015; F. Li et al., 2019; Petrov et al., 2017; Qian et al., 2020)
Bacteroidetes	Prevotellaceae		0	5	(Aho et al., 2019; F. Li et al., 2019; Scheperjans et al., 2015; Toh et al., 2022; Unger et al., 2016)
Bacteroidetes	Prevotellaceae	Prevotella	1	5	(Aho et al., 2019; Bedarf et al., 2017; C. H. Lin et al., 2019; Petrov et al., 2017; Wallen et al., 2020, 2022)
Bacteroidetes	Rikenellaceae	Alistipes	6	0	(Aho et al., 2019; C. Li et al., 2019; Y. Qian et al., 2020; Romano et al., 2021; Toh et al., 2022; Wallen et al., 2022)
Firmicutes			2	2	(Bedarf et al., 2017; Keshavarzian et al., 2015; A. Lin et al., 2018; Zhang et al., 2020)
Firmicutes	Enterococcaceae		2	1	(Hopfner et al., 2017; Pietrucci et al., 2019; Unger et al., 2016)
Firmicutes	Lachnospiraceae		0	11	(Barichella et al., 2019; Cirstea et al., 2020; Hill-Burns et al., 2017; Keshavarzian et al., 2015; A. Lin et al., 2018; Pietrucci et al., 2019; Romano et al., 2021; Toh et al., 2022; Vascellari et al., 2020; Wallen et al., 2020, 2022)
Firmicutes	Lachnospiraceae	Blautia	0	9	(Aho et al., 2019; Hill-Burns et al., 2017; Keshavarzian et al., 2015; W. Li et al., 2017; Romano et al., 2021; Vascellari et al., 2020; Wallen et al., 2020, 2022; Zhang et al., 2020)
Firmicutes	Lachnospiraceae	Roseburia	1	8	(Cirstea et al., 2020; Hill-Burns et al., 2017; Keshavarzian et al., 2015; C. Li et al., 2019; S. Nie et al., 2023; Romano et al., 2021; Toh et al., 2022; Vascellari et al., 2020; Wallen et al., 2020, 2022)

Firmicutes	Lachnospiraceae	Coprococcus	0	1	(Keshavarzian et al., 2015)
Firmicutes	Ruminococcaceae		3	2	(C. Li et al., 2019; F. Li et al., 2019; Romano et al., 2021; Scheperjans et al., 2015; Wallen et al., 2020)
Firmicutes	Ruminococcaceae	Ruminococcus	1	2	(C. Li et al., 2019; W. Li et al., 2017; Wallen et al., 2022)
Firmicutes	Christensenellaceae		5	0	(Barichella et al., 2019; Hill-Burns et al., 2017; Romano et al., 2021; Tan et al., 2021; Wallen et al., 2020)
Firmicutes	Christensenellaceae	Christensenella	4	0	(Petrov et al., 2017; Tan et al., 2021; Toh et al., 2022; Wallen et al., 2022)
Firmicutes	Clostridiaceae		1	0	(Keshavarzian et al., 2015)
Firmicutes	Clostridiaceae	Faecalibacterium	0	6	(W. Li et al., 2017; Petrov et al., 2017; Romano et al., 2021; Wallen et al., 2020, 2022; Weis et al., 2019)
Firmicutes	Clostridiaceae	Faecalibacterium prausnitzii	0	3	(Cirstea et al., 2020; Hill-Burns et al., 2017; Unger et al., 2016)
Firmicutes	Lactobacillaceae		7	1	(Barichella et al., 2019; Hill-Burns et al., 2017; Hopfner et al., 2017; C. Li et al., 2019; Pietrucci et al., 2019; Scheperjans et al., 2015; Tan et al., 2021; Unger et al., 2016)
Firmicutes	Lactobacillaceae	Lactobacillus	10	1	(Hasegawa et al., 2015; Hill-Burns et al., 2017; C. Li et al., 2019; C. H. Lin et al., 2019; Nie et al., 2023; Petrov et al., 2017; Qian et al., 2020; Romano et al., 2021; Tan et al., 2021; Wallen et al., 2020)
Proteobacteria			3	0	(Barichella et al., 2019; Keshavarzian et al., 2015; W. Li et al., 2017)
Proteobacteria	Enterobacteriaceae		3	0	(Barichella et al., 2019; Pietrucci et al., 2019; Unger et al., 2016)
Proteobacteria	Desulfovibrionaceae		2	0	(Cirstea et al., 2020; A. Lin et al., 2018)
Proteobacteria	Desulfovibrionaceae	Desulfovibrio	2	0	(S. Nie et al., 2023; Toh et al., 2022)
Verrucomicrobia			6	0	(Barichella et al., 2019; Keshavarzian et al., 2015; C. Li et al., 2019; C. H. Lin et al., 2019; Qian et al., 2020; Zhang et al., 2020)
Verrucomicrobia	Verrucomicrobiaceae		9	0	(Barichella et al., 2019; Bedarf et al., 2017; Heintz-Buschart et al., 2018; Hill-Burns et al., 2017; Keshavarzian et al., 2015; C. Li et al., 2019; F. Li et al., 2019; Scheperjans et al., 2015; Tan et al., 2021)
Verrucomicrobia	Verrucomicrobiaceae	Akkermansia	12	0	(Bedarf et al., 2017; Heintz-Buschart et al., 2018; Hill-Burns et al., 2017; Keshavarzian et al., 2015; C. Li et al., 2019; C. H. Lin et al., 2019; Qian et al., 2020; Romano et al., 2021; Tan et al., 2021; Toh et al., 2022; Wallen et al., 2020; Zhang et al., 2020)

2.6 Microbiota-based therapies

Therapeutic strategies targeting the gut microbiota have garnered attention as promising approaches for managing PD, given the relative accessibility of the gut compared to the brain. With growing evidence linking the gut microbiota to both PD risk and progression, microbiota-based interventions, including dietary approaches, probiotics, prebiotics and fecal microbiota transplants (FMT), have the potential to complement traditional PD treatments (Lorente-picón & Laguna, 2021). These approaches aim to modulate both motor and non-motor symptoms, thereby advancing PD management and improving patient outcomes.

2.6.1 Dietary approaches, probiotics and prebiotics

Dietary interventions are increasingly recognized for their potential to influence gut microbial populations and restore gut homeostasis. Specific dietary patterns have been linked to PD risk and progression (Kwon, Zhang, et al., 2024b). Among these, the Mediterranean diet, rich in vegetables, legumes, fruits, nuts, whole grains and healthy fats, has demonstrated multiple brain health benefits and improved gut microbiota composition (Alcalay et al., 2012; Bisaglia, 2022; Gardener & Caunca, 2018). This diet promotes the growth of fiber-utilizing bacteria that produce SCFAs, which are essential for maintaining intestinal barrier integrity, regulating gene expression, and supporting mitochondrial function (Duan et al., 2023; González-Bosch et al., 2021; Makki et al., 2018; Seethaler et al., 2022). Notably, SCFAs levels are often reduced in the fecal samples of PD patients, highlighting their potential role in PD pathology (S. J. Chen et al., 2022; Unger et al., 2016). Prebiotic fibers play a significant role in shaping the microbiota composition and influencing SCFAs levels (Cantu-Jungles et al., 2019). These fibers are not hydrolyzed by mammalian enzymes but instead fermented by bacteria in the GI tract. Since different bacterial groups have specific preferences for physical and chemical characteristics of fibers, this information can be leveraged to select a mixture of prebiotic fibers that promotes the growth of distinct SCFAs-producing bacterial groups (Cantu-Jungles et al., 2019; Gibson & Roberfroid, 1995; Hamaker & Tuncil, 2014; Hutkins et al., 2016). Studies have demonstrated that prebiotic interventions are well tolerated by PD patients and are safe, and it's associated with beneficial biological changes in the microbiota, SCFAs, inflammation, and neurofilament light chain (Bedarf et al., 2024; Hall et al., 2023) .

In contrast, the Western diet, characterized by high fat and sugar content and low dietary fiber intake, has been associated with gut dysbiosis and increased levels of lipopolysaccharides (LPS), exacerbating intestinal inflammation (Jackson et al., 2019; Palavra et al., 2021; Statovci et al., 2017; Zapała et al., 2022). Metabolic syndrome, often linked to poor dietary habits, is another significant risk factor for PD. It is characterized by central obesity, insulin resistance, dyslipidemia, and hypertension, all of which contribute to oxidative stress, neuroinflammation and mitochondrial dysfunction, further increasing PD

risk (De Lau et al., 2005; Hantikainen et al., 2022; Miyake et al., 2010; A. P. da S. Souza et al., 2021a; Swarup et al., 2024).

Probiotics have also emerged as a potential tool for managing PD-associated dysbiosis and GI dysfunction. While current evidence on their efficacy remains limited, several studies suggest that probiotics may help alleviate constipation, bloating, and other GI symptoms, thereby improving overall gut health in PD patients (Barichella et al., 2016; J. M. Park et al., 2023; Tan, Lim, et al., 2021; Xie et al., 2023; C. Zhang et al., 2020). The effectiveness of probiotics depends on the specific genera and species used, and the mechanisms underlying their benefits remain poorly understood (Dutta et al., 2019; Kechagia et al., 2013; Suez et al., 2019). Advanced tools like metagenomics and metabolomics are essential for unraveling the complex interactions between probiotics, gut microbes, and the host GI tract, and for designing long-term clinical trials to validate their therapeutic potential in PD.

Levodopa, the main pharmacological PD treatment, is often co-administered with carbidopa or benserazide to enhance its absorption and prevent premature peripheral conversion to DA. However, several factors, including drug kinetics, disease progression, GI dysfunction, and dietary protein intake, influence its chronic absorption (Demailly et al., 2024). Dietary proteins, broken into free amino acids, compete with levodopa for transport across intestinal and blood-brain barrier (BBB), reducing its bioavailability (Camargo & Verrey, 2014). To address this, low-protein and protein redistribution diets have been proposed as effective dietary strategies (C. Rusch et al., 2023). Host-microbiome interactions also play a crucial role in levodopa metabolism. Gut microbial activity, including infections like *Helicobacter pylori* and SIBO, can impair levodopa absorption (van Kessel & El Aidy, 2019). Certain gut bacteria, such as *Enterococcus faecalis* and *Lactobacillus brevis*, express L-tyrosine decarboxylase, converting levodopa into DA in the gut, potentially leading to heterogenous responses and side effects (Rekdal et al., 2019; van Kessel et al., 2019). Nutritional interventions targeting constipation, gastroparesis and dehydration may help optimize levodopa bioavailability. However, symptoms like anosmia, ageusia, and dysphagia can complicate dietary adherence in PD patients (Ma et al., 2018).

Although dietary approaches and probiotics are promising for improving gut health, reducing GI symptoms, and potentially modulating PD progression, further research is needed. Identifying specific dietary components, optimal dosages, and their mechanisms of action will be critical for designing effective interventions.

2.6.2 Fecal microbiota transplantation (FMT)

FMT is a promising approach for inducing comprehensive and sustained modifications in gut microbiota composition. This procedure involves the transfer of fecal microbiota from healthy donors into the GI tracts of patients to restore microbial environment and potentially mitigate disease progression by modulating gut microbiota-associated pathways (Z. Zhao et al., 2021). FMT has been successfully

implemented as a standard treatment for recurrent *Clostridioides difficile* infections, where it remains an approved therapeutic intervention (Bakken et al., 2011). Beyond infectious diseases, FMT has demonstrated beneficial effects in various neurological disorders, including autism spectrum disorder and multiple sclerosis (MS) (Vendrik et al., 2020), further supporting the role of gut microbiota in neuroimmune regulation. Despite growing interest, evidence for the efficacy of FMT in PD remains limited, primarily derived from case reports and small-scale open-label studies. Some studies have suggested potential benefits, reporting improvements in both motor and non-motor symptoms, particularly in alleviating constipation. However, other studies have found FMT to be well-tolerated but without significant clinical benefits (Bruggeman et al., 2024; Chernova et al., 2023; H. Huang et al., 2019; Kuai et al., 2021; Scheperjans et al., 2024; Segal et al., 2021; Xue et al., 2020). The inconsistences in reported outcomes are likely attributable to variations in study design, including differences in patient selection criteria, donor microbiota composition, FMT preparation and administration methods, clinical assessment tools, and follow-up durations. Furthermore, the absence of well-powered, placebo-controlled clinical trials raises concerns about potential placebo effects and limits the generalizability of current findings (Gheorghe et al., 2021).

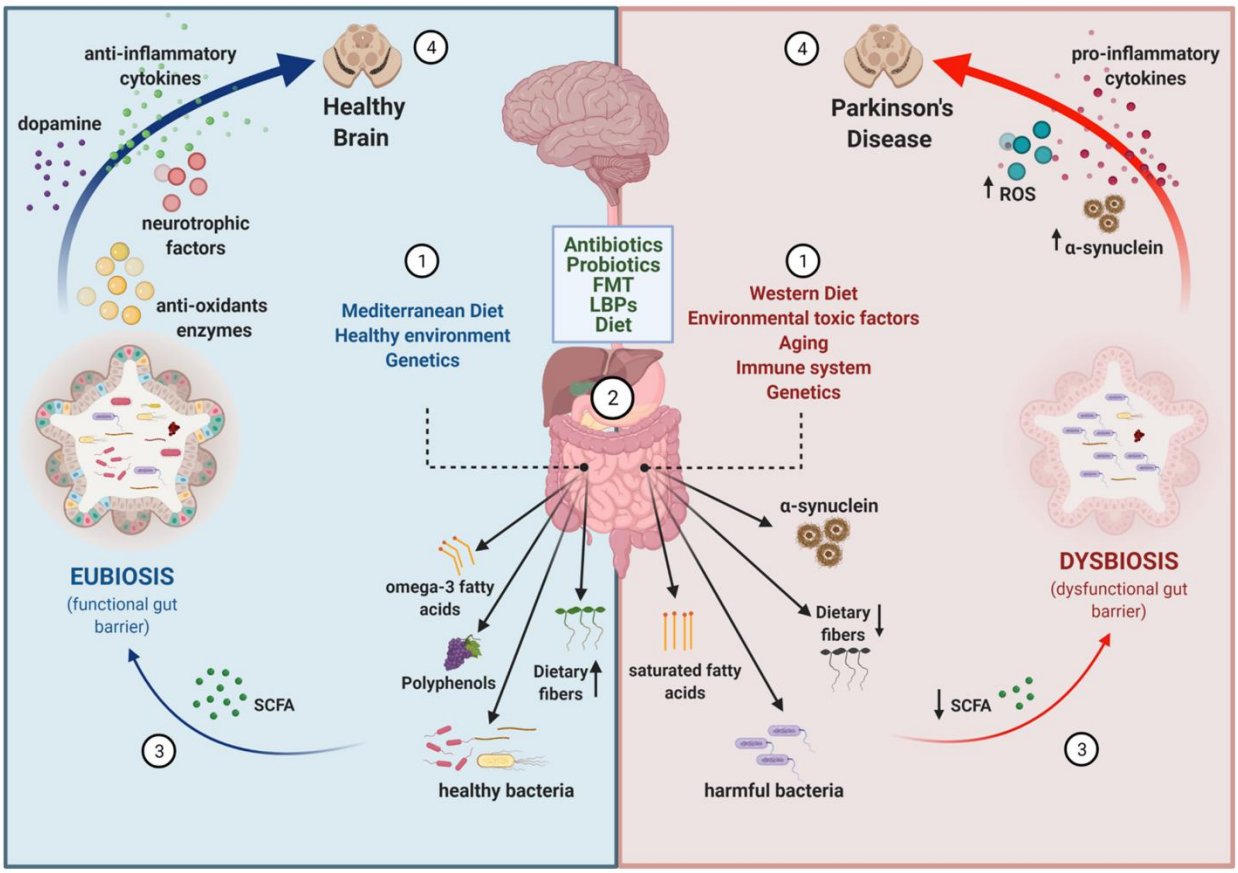

Figure 9. Schematic summary of PD-modifying strategies based on the gut microbiota. (1) Determinants of gut microbiota composition. The composition of the gut microbiota is influenced by intrinsic factors such as genetics, aging and immune system function, as well as extrinsic factors including dietary habits and environmental influences.

(2) Interventions to modify gut microbiota. A variety of strategies can be used to shift dysbiotic microbiota towards a healthier state. These include the use of ABX, probiotics, FMT, live biotherapeutic products (LBP), and dietary modifications. **(3) Microbial and metabolic consequences.** These interventions alter the balance between beneficial and harmful bacteria, affect the availability of dietary fibers, and modulate the production of metabolites with antioxidant/oxidant and anti-/pro-inflammatory properties. They also influence the aggregation of proteins, such as α-synuclein, within the gut. **(4) Impact on the gut-brain axis.** Due to the bidirectional communication between the gut and the brain, changes in the gut microbiota can directly impact brain function. This occurs through alterations in the levels of neurotransmitters, cytokines, ROS, neurotrophic factors, and α-synuclein aggregation. Overall, changes in gut microbiota composition have the potential to either alleviate or exacerbate the neurodegenerative processes associated with PD. Retrieved from (Lorente-picón & Laguna, 2021).

3 PD experimental mouse models

Modeling PD remains a complex challenge due to its etiological heterogeneity and the involvement of multiple pathological pathways. No single model completely replicates the clinical and pathological spectrum of PD; therefore, different approaches are used to address specific research objectives (Impellizzeri et al., 2023). Neurotoxin-induced models are cost-effective and rapidly induce PD-like phenotypes, making them well-suited for drug validation and symptomatic treatment studies. Conversely, genetic models, based on human PD-associated mutations, offer valuable insights into molecular mechanisms underlying disease development. Additionally, models utilizing pre-formed fibrils (PFFs) or viral vectors encoding the SNCA gene help to elucidate the mechanisms of α-synuclein pathology and its propagation. Given the limitations of individual models, combining multiple approaches enhances the ability to capture key aspects of PD pathogenesis (Bezard & Przedborski, 2011; Dawson et al., 2018; Dovonou et al., 2023).

Historically, PD research has focused on nigrostriatal dysfunction, leading to the development of models that replicate dopaminergic neurodegeneration and facilitate the evaluation of DA replacement therapies. However, as our understanding of PD has expanded to include extra-nigral pathologies, non-motor symptoms, and peripheral α-synuclein accumulation, newer models have been developed to reflect these complexities (Butkovich et al., 2020; Challis et al., 2020; Dautan et al., 2024; S. Kim et al., 2019; La Vitola et al., 2024).

Still, a key unresolved question is how PD initiation and progression differ between brain-first and body first subtypes, particularly in the prodromal phase. Experimental models capable of recapitulating distinct pathological trajectories are needed to investigate these mechanisms. While current neurotoxin-based genetic models have significantly advanced our understanding, they lack the complexity required to fully capture human PD heterogeneity. Future research should focus on refining preclinical models that accurately mimic multiple disease initiation sites, thereby improving the translation of basic research into clinical applications (Dovonou et al., 2023; Van Den Berge & Ulusoy, 2022).

3.1 Neurotoxin models

Neurotoxin-based models are among the most well-established and widely used in PD research. These models, which employ specific neurotoxins to induce selective nigrostriatal degeneration, have played a key role in the development of levodopa, DA agonists, MAO-B inhibitors, DBS, and cell transplantation therapies.

3.1.1 6-Hydroxydopamine (6-OHDA) model

The 6-OHDA model was the first developed for PD research (Ungerstedt, 1968). Since 6-OHDA does not cross the BBB, it must be injected directly into the STR, SNpc or medial forebrain bundle (Masini et al., 2021). Unilateral lesions facilitate internal comparisons between hemispheres, making it useful for studying motor asymmetry and basal ganglia dysfunction. The model successfully replicates bradykinesia and motor deficits, making it ideal for DA replacement and levodopa-induced dyskinesia studies (Lundblad et al., 2004). However, a key limitation is the lack of α-synuclein pathology.

3.1.2 MPTP model

The neurotoxin 1-methyl-4-phenyl-1,2,3,6-tetrahydropyridine (MPTP) unlike 6-OHDA, crosses the BBB and is metabolized into MPP+, which is taken up by dopaminergic neurons via the DA transporter (DAT). Once inside, MPP+ inhibits mitochondrial Complex I, leading to oxidative stress and neuronal death (Przedborski et al., 2004). This model selectively destroys nigral dopaminergic neurons, resulting in nigrostriatal degeneration and motor impairments (Blesa & Przedborski, 2014). Additionally, MPTP induces non-motor symptoms such as olfactory deficits, cognitive decline, and GI dysfunction (N. R. Han et al., 2021). Although MPTP increases α-synuclein expression, the formation of LB-like inclusions remains rare (Vila et al., 2000).

3.1.3 Paraquat and Rotenone model

Paraquat (N, N'-dimethyl1-4-4-4'-bypiridinium) is a widely used herbicide identified as a neurotoxin. It crosses the BBB and exerts toxicity through redox cycling, leading to oxidative stress (Berry et al., 2010; Richardson et al., 2005). Systemic paraquat treatment in mice results in a dose- and age-dependent loss of TH-positive neurons (McCormack et al., 2002). Rotenone, another pesticide and mitochondrial Complex I inhibitor, has been linked epidemiologically to PD risk. Systemic rotenone injections induce dopaminergic and noradrenergic neurodegeneration in SNpc and LC, respectively, together with motor impairments (Betarbet et al., 2000; L. Jing et al., 2021; Tanner et al., 2011). Importantly, rotenone also induces α-synuclein aggregation in both the CNS and PNS, supporting its relevance in PD research (Dodiya et al., 2020; Francisco Pan-Montojo et al., 2010).

3.2 Brain and gut injections of fibrillar α-synuclein forms

PFFs and human PD brain homogenates are used to induce pathological aggregation of endogenous α-synuclein. These models have been instrumental in studying α-synuclein propagation mechanisms. PFFs are generated *in vitro* from recombinant monomeric α-synuclein and injected into the brain (Volpicelli-Daley et al., 2011). Intracerebral PFF injections are most performed in the STR, with pathological α-synuclein accumulation subsequently detected in interconnected regions such as the SNpc, cortex, amygdala, hypothalamus, LC, and OB (Paumier et al., 2015; N. L. Rey et al., 2018). These exogenous fibrils act as seeds, triggering aggregation, hyperphosphorylation, and ubiquitination of endogenous α-synuclein, replicating key PD pathological features (Abdelmotilib et al., 2017; Karampetsou et al., 2017; Luk et al., 2012). Additionally, PFFs have been used to investigate gut-to-brain propagation of pathology along vagal and sympathetic nerves, supporting the body-first hypothesis of PD initiation (Arotcarena et al., 2020; Challis et al., 2020; Dautan et al., 2024; Holmqvist et al., 2014; S. Kim et al., 2019; Manfredsson et al., 2018; Uemura et al., 2018).

3.3 Viral vector-mediated α-synuclein overexpression

Viral vector-mediated gene delivery is a valuable tool for studying α-synuclein pathology. Among the various vectors, adeno-associated viruses (AAVs) are preferred due to their high neuronal transduction efficiency and long-term gene expression (Fischer et al., 2016). These models have demonstrated α-synuclein propagation from the midbrain to peripheral regions, supporting prion-like spreading (Ulusoy et al., 2017). Further studies have revealed that α-synuclein overexpression in the SNpc leads to submucosal neuronal loss and gut microbiota alterations, reinforcing the gut-brain axis hypothesis in PD (O'Donovan et al., 2020).

3.4 Viral NM-like production model

Investigating the role of NM in PD has been challenging due to its absence in common rodent models. Our group developed a viral-mediated approach expressing human tyrosinase (hTyr) in the SNpc of rodents leading to age-dependent NM-like accumulation in dopaminergic neurons. This model recapitulates key PD hallmarks, including mitochondrial dysfunction, autophagic impairment, neuroinflammation, impaired DA release, striatal denervation, dopaminergic neurodegeneration, and motor deficits. Additionally, LB-like inclusions are observed, making this model a valuable tool for studying NM accumulation and its role in PD pathophysiology (Carballo-Carbajal et al., 2019).

3.5 Genetic models

3.5.1 Transgenic and knock-out (KO) models for PARK genes

Genetic models have been developed to investigate the etiopathogenic mechanisms underlying familial PD. Several genes linked to PD risk have been identified, including Parkin (PRKN), PINK1, LRRK2, DJ-1, UCH-L1 and GBA1. Animal models with genetic modifications of these genes have successfully replicated key pathological features of idiopathic PD, such as LB-like inclusions, mitochondrial dysfunction, and lysosomal impairment. Notably, mutations in the SNCA gene, encoding α-synuclein, are implicated in both familial and sporadic PD cases. SNCA transgenic models, including those expressing WT, A53T, A30P, and E46K mutations, have been widely used to recapitulate α-synuclein pathology *in vivo* (Dovonou et al., 2023).

3.5.2 Transgenic mice expressing and accumulating brain-wide and age-dependent human-like NM

As mentioned before, one of the major limitations in modeling PD and other neurodegenerative disorders has been the inability to replicate NM accumulation in laboratory rodent models. To overcome this limitation, our group has recently developed a novel transgenic mouse model, termed tgNM to mimic progressive, brain-wide NM accumulation in catecholaminergic neurons, closely resembling the human condition. This model is based on the constitutive catecholaminergic-specific overexpression of hTyr under the TH promoter, enabling NM synthesis in catecholaminergic neurons. Unlike the previous viral vector-mediated NM production model, which was restricted to focal NM expression at the injection site, tgNM mice exhibit widespread and progressive NM accumulation across all catecholaminergic regions, following a caudorostral gradient, a pattern closely resembling human NM distribution (Figure 10) (Laguna et al., 2024).

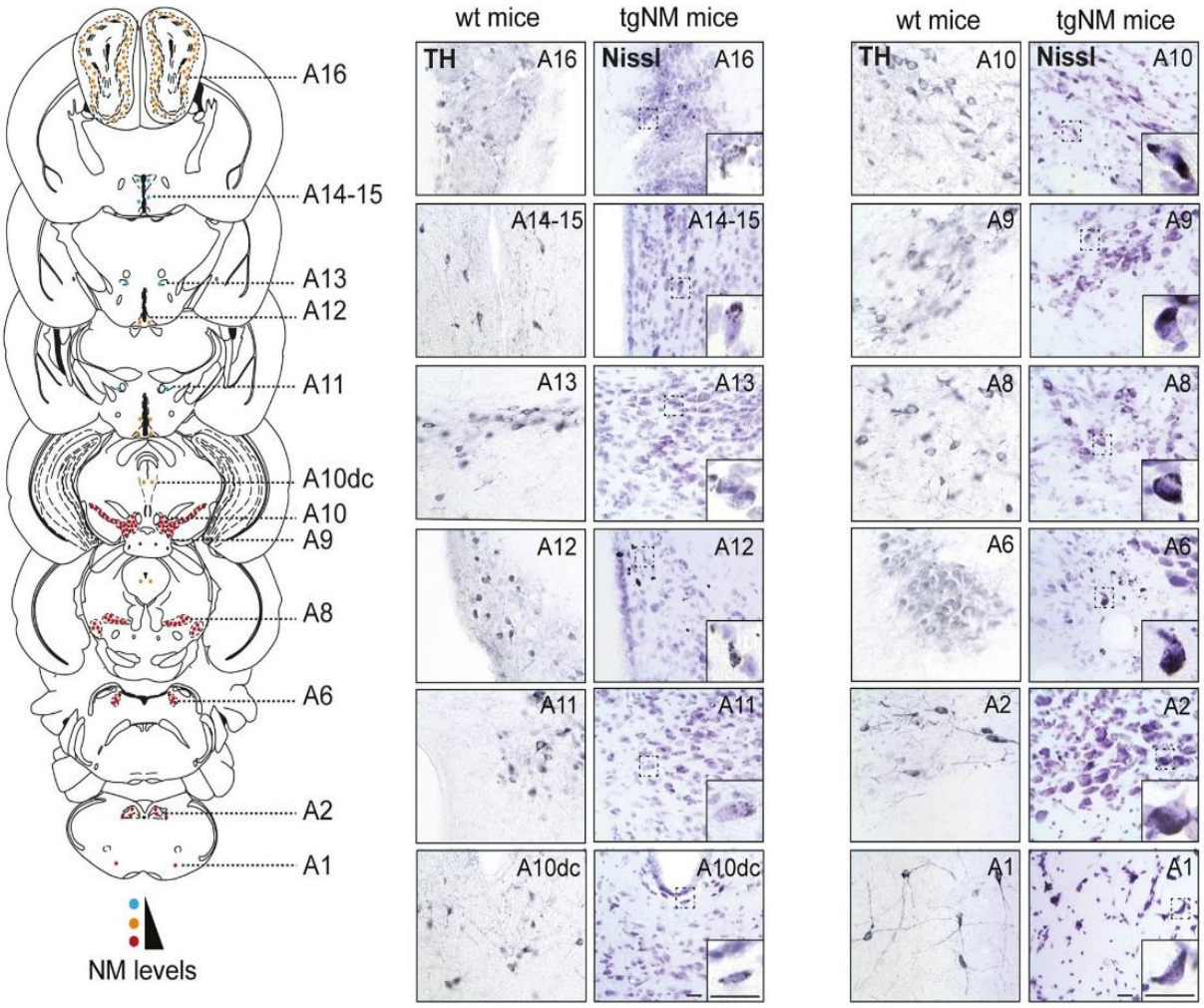

Figure 10. Brain-wide NM distribution in catecholaminergic brain nuclei from tgNM mice. Qualitative mouse brain atlas illustrating NM accumulation across catecholaminergic nuclei (A1-A16) in tgNM mice. Left, Schematic mouse brain atlas. The number of dots represents the quantity of NM-accumulating cells and dot color represents the levels of intracellular NM from very low levels (blue) to higher levels of NM accumulation (red). Right, Representative images of catecholaminergic regions. TH immunostaining in wt mice and Nissl-stained sections in tgNM mice for comparison. Adapted from (Laguna et al., 2024).

In tgNM mice, progressive NM accumulation in the SNpc and VTA leads to age-dependent dopaminergic dysfunction, the emergence of PD-like neuropathological hallmarks (including LB-like and MB inclusions), early neuroinflammatory changes, and incipient neurodegeneration. Although no significant neuronal loss is observed, striatal DA release deficits and motor impairments emerge with age, resembling the prodromal and early stages of PD. Notably, tgNM mice also exhibit early LC neurodegeneration, preceding nigral dopaminergic dysfunction. Stereological analyses reveal a significant reduction in TH-positive neurons in the LC detectable as early as one month (m) of age, which, in contrast to the SNpc and VTA, corresponds to actual neuronal degeneration rather than phenotypic downregulation. This LC neurodegeneration is accompanied by a marked reduction in NE levels in both the LC and projection areas,

such as the prefrontal cortex (PFC), leading to anxiety-related behaviors, emotional memory deficits and sleep disturbances, all of which are hallmark non-motor symptoms of PD. Furthermore, cholinergic dysfunction is evident in old tgNM mice, where a significant reduction in ChAT-positive neurons was detected in the nucleus basalis of Meynert and pedunculopontine nucleus (PPN), two key cholinergic structures interconnected with catecholaminergic brainstem nuclei. Despite the absence of significant serotonergic cell loss in the dorsal raphe nucleus, tgNM mice exhibited increased depressive-like behavior in the tail suspension test, indicating functional serotonergic dysregulation like what is observed in PD patients. In addition to central neurodegeneration, tgNM mice develop autonomic dysfunction with age. Although no significant overall loss of TH-positive neurons was observed in the DVC, a selective reduction in pigmented TH-positive neurons was detected. In adult tgNM mice, this loss primarily reflects TH downregulation, whereas in older animals, it progresses to actual neuronal loss, accompanied by extensive eNM debris and microglial activation, indicative of incipient neurodegeneration. Functionally, old tgNM mice develop bradycardia despite normal blood pressure, along with an increased respiratory rate, reflecting autonomic dysfunction, a common feature of PD. This dysautonomia contributes to a shortened lifespan, further reinforcing tgNM mice as a relevant model for prodromal and early PD. Additionally, NE and ACh imbalances were detected in vagal-innervated peripheral organs, including the heart and the GI tract, further emphasizing the systemic nature of PD pathophysiology in this model (Figure 11) (Laguna et al., 2024).

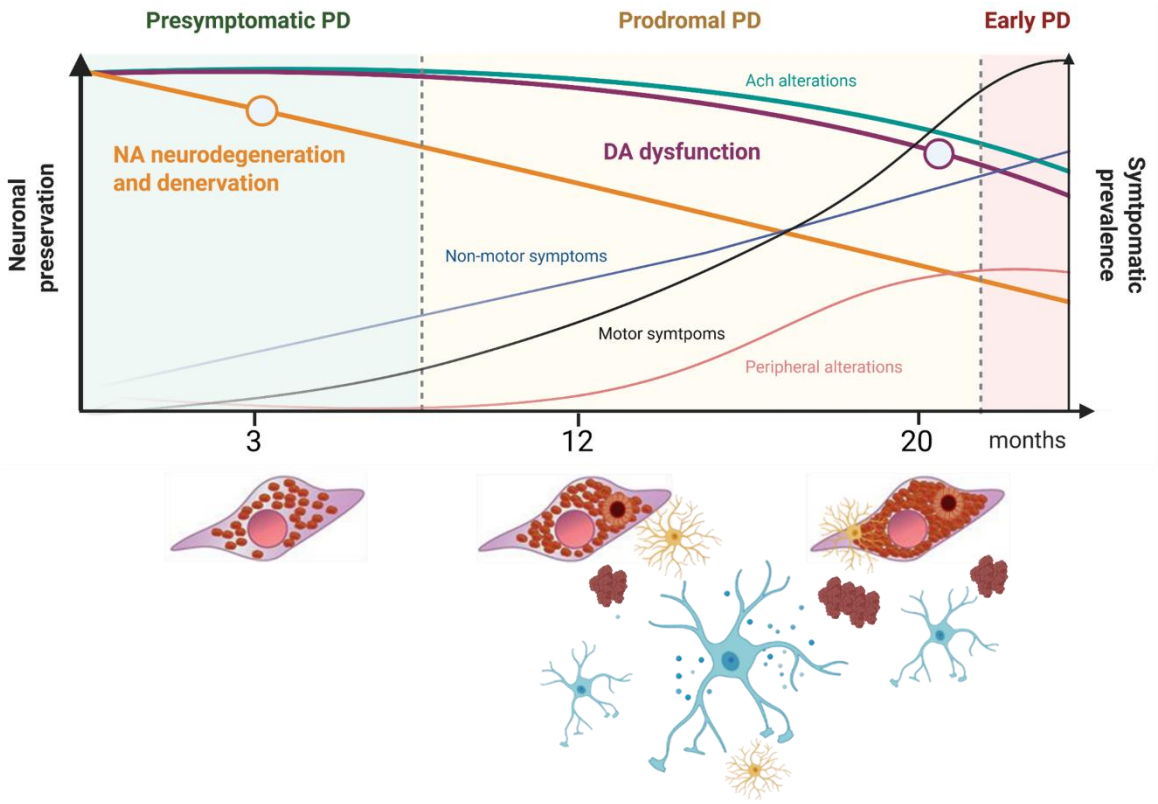

Figure 11. Schematic summary of tgNM mice PD-like features. TgNM mice model a prodromal phase of PD in which nigral dopaminergic cell loss has not been yet manifested, although dopaminergic dysfunction and neuroinflammation is present. It recapitulates PD-like motor and non-motor alterations, as well as autonomic dysfunction. TgNM mice offer a valuable tool to study and evaluate neuroprotective and disease-modifying therapies. Adapted from (Laguna et al., 2024).

HYPOTHESIS AND OBJECTIVES

Overall aim of the thesis

The primary objective of this PhD thesis is to investigate whether alterations in the gut-brain axis contribute to the manifestation of PD-like symptomatology and impact disease pathophysiology in NM-producing mice, a new preclinical rodent model of PD. By elucidating the mechanisms of neurodegeneration and gut dysfunction, we aim to contribute to the understanding of potential microbiota-based therapeutic strategies for treating GI disturbances and, potentially, other non-motor and motor symptoms in PD.

OBJECTIVE 1. Characterize the neuronal and GI alterations linked to age-dependent intracellular NM accumulation in tgNM mice.

Hypothesis: NM accumulation in tgNM mice induces motor and non-motor symptoms, including GI dysfunction.

Specific objectives:

i) Assess the behavioral phenotype of tgNM mice across lifespan.
ii) Assess the GI phenotype of tgNM mice across lifespan.
iii) Characterize the gut-brain axis of tgNM mice in terms of:
   a. Morphology
   b. Neurotransmission
   c. Gut microbiota composition
   d. Molecular profiles
   e. Inflammation
   f. Neuroendocrine function

OBJECTIVE 2. Determine if a high fat diet (HFD) can exacerbate the manifestation of PD-like symptoms in tgNM mice.

Hypothesis: Mice fed with a HFD have an altered gut microbiota composition that disturbs gut homeostasis, promotes a pro-inflammatory state, and exacerbates brain neuropathology, affecting both behavior and GI function in tgNM mice.

Specific objectives:

i) Characterize gut microbiota composition after HFD.
ii) Assess the behavioral phenotype of tgNM mice after HFD.
iii) Assess the GI phenotype of tgNM mice after HFD.
iv) Characterize the gut-brain axis of tgNM mice after HFD in terms of:
   a. Morphology
   b. Neurotransmission
   c. Molecular profiles
   d. Inflammation
   e. Neuroendocrine function

v) Assess the metabolic phenotype of tgNM mice after HFD.
vi) Assess brain neuropathology in tgNM mice after HFD.

OBJECTIVE 3. Determine if rejuvenation of the gut microbiota by FMT can slow down the manifestation of PD-like symptoms in tgNM mice.

Hypothesis: FMT from young wild-type mice will modify gut microbiota composition of adult tgNM mice, restore gut homeostasis, reduce GI inflammation, and consequently slow down brain neurodegeneration, thereby preventing the worsening of behavioral and GI alterations in aged tgNM mice.

Specific objectives:

i) Establish a stable donor microbiota graft.
ii) Characterize gut microbiota composition after FMT.
iii) Assess the behavioral phenotype of tgNM animals after FMT.
iv) Assess the GI phenotype of tgNM animals after FMT.

MATERIALS AND METHODS

1 Animals

1.1 TgNM mouse colony

Transgenic mice were generated through pronuclear microinjection of the full-length hTyr complementary DNA (cDNA) linked to the rat TH promoter (tg-TH-TYR – tgNM) into C57BL6-SJL mouse zygotes at the Center for Animal Biotechnology and Gene Therapy (CBATEG). The mice underwent backcrossing for 8-10 generations with C57BL/6J mice from Charles River and were maintained in heterozygosity. Animals were housed in groups of two to five per cage, separated by sex and genotype to avoid coprophagy in the CELLEX animal facility at the Vall d'Hebron Research Institute (VHIR) with *ad libitum* access to food and water within a 12-hour light/dark cycle under controlled humidity and temperature conditions (20-22ºC). All experimental and surgical procedures adhered to European (Directive 2010/63/UE) and Spanish regulations (Real Decreto 23/2013; Generalitat de Catalunya Decret 214/97) concerning the protection of animals used for experimental and scientific purposes. Approval for these procedures was obtained from VHIR Comitè Ètic d'Experimentació Animal (CEEA).

1.2 Genotyping

Animals were genotyped two weeks after birth before being weaned later on at three weeks. The total DNA was obtained from mouse ear samples following the kit AccuStart™ II Mouse Genotyping Kit (QuantaBio, #95135) instructions. To detect the presence of TYR gene, a PCR using a 9800 Fast Thermal Cycler (Applied Biosystems) was performed by mixing 1 µl of the extracted DNA and the following primers concentrated at 500nM:

$$TYR - Forward\ (TTCAGACCCAGACTCTTTTCAA)$$
$$TYR - Reverse\ (GCTGCTTTCTCTTGTGACGA)$$

The amplificated product is observed through electrophoresis separation in a 1.8% agarose gel and visualized using the GelDoc XR (BioRad).

1.3 HFD treatment

1.3.1 Diets

The treatment animals received a HFD composed of: 20Kcal% protein, 60Kcal% fat and 20Kcal% carbohydrate (Research Diets INC, #D12492); while control animals received a standard CHOW diet composed of 21Kcal% protein, 12.6Kcal% fat and 66.4Kcal% carbohydrate (SAFE® diets, #SAFE150).

1.3.2 Animals

Two-month-old littermates were fed during 4 m with two different diets, CHOW or HFD, till they were 6 m old. Mice were divided by sex and genotype into 8 groups: Females: (i) wt mice fed with CHOW diet; (ii) tgNM mice fed with CHOW diet; (iii) wt mice fed with HFD; (iv) tgNM mice fed with HFD; Males: (v) wt mice fed with CHOW diet; (vi) tgNM mice fed with CHOW diet; (vii) wt mice fed with HFD; (viii) tgNM mice fed with HFD.

1.4 FMT

1.4.1 Animals

Twelve-month-old littermates' wt and tgNM female mice were divided by genotype into 4 groups: (i) wt females receiving antibiotic (ABX)+FMT treatment; (ii) wt females receiving phosphate buffered saline (PBS) 1x treatment; (iii) tgNM females receiving ABX+FMT treatment; (iv) tgNM females receiving PBS 1x treatment.

1.4.2 Donor stool collection and storage

Three months-old wt female mice were placed individually in a clean cage without bedding and allowed to defecate normally for a maximum of 30 minutes (min). The fecal pellets were collected, a total of 5 fecal pellets were introduced in a microcentrifuge tube containing sterile autoclaved 1 ml PBS 1x and placed on ice till the end of the collection and during transportation. Within a period of 1 h after collection, pellets were resuspended with a vortex and by mechanical disruption using a pipette tip. After resuspension, samples were centrifuged at 2,500 r.p.m. (500G) for 1 min to remove insolubilized material. Supernatants were collected and merged into 5 ml aliquots containing 10% glycerol and stored at −80°C until use.

1.4.3 ABX treatment

The ABX treatment was given just to the group receiving FMT treatment. During 3 consecutive days and after 6 h fasting, mice received by oral gavage 200 µl of ABX cocktail containing: 1 g/l ampicillin (Sigma-Aldrich, #a9393); 0.5 g/l neomycin (Sigma-Aldrich, #n6386); 0.5 g/l vancomycin (Sigma-Aldrich, #v2002) and 1 g/l metronidazole (Sigma-Aldrich, #m1547). The cocktail was prepared fresh every day.

1.4.4 FMT treatment

The next day after ABX treatment, mice received 200 µl of FMT treatment via oral gavage 1 time every 3 days for 2 weeks. Then, we treated the animals once a week for the remainder of the study that lasted 6 m (24 total doses of FMTs). The control group received 200 µl of sterile PBS 1x instead.

2 Behavioral assessment

2.1 Beam test

Mice were placed at the beginning of an elevated horizontal plexiglass beam bar covered on white tape to avoid limb slip (1 m length – 2.5 cm width- 0.5 m elevation). At the beginning of the beam there was placed a little lamp and at the end of the beam, the animal cage to motivate the animal to cross the bar. Mice were allowed to explore the beam bar and receive two assisted trials to cross it before the test. After the two assisted trials, the test started, and animals were able to traverse the entire length of the beam unassisted for two consecutive times. The time it takes to the mouse to cross the beam was measured for a maximum of 120 s. If one mouse did not want to cross or went backwards, it was removed from the test. However, if the mouse fell off the beam, a maximum of 120 s was recorded for that trial. The average time after the two trials was calculated to obtain the result.

2.2 Habituation and dishabituation test (olfaction)

Each mouse was individualized in a new cage with new bedding. A cotton swab suspended in the middle of the cage was presented to the animal for object habituation during 10 min. A second swab impregnated with water was presented to the animal for 3 min after removing the first one. During this time, it was measured the number of times the animal went towards the new cotton swab and the total time the animal spent sniffing it. Finally, a third swab impregnated with lemon essence (Essenciales) was presented to the animal for 3 min after removing the second one. As before, the number of times the animal went towards the third cotton swab and the total time it spent sniffing it was measured. To calculate the discrimination index (DI) the following formula was used:

$$\frac{\text{Time exploring lemon essence} - \text{Time exploring water}}{\text{Time exploring lemon essence} + \text{Time exploring water}}$$

2.3 Tail suspension test

Animals were suspended by the tip of their tails with tape in a suspension bar elevated 50 cm. To avoid the tail climbing behavior, a 2 cm methacrylate tube was placed through the tail before suspending the animal. Right after suspending the animal, it was calculated the latency to surrender (s) as the time it took for the animal not to have any escape-oriented behaviors (i.e. fore and hind limbs movement). Moreover, during the following 6 min it was measured the total immobilization time (s) as the total time the mice spent without having any escape-oriented behaviors.

2.4 Vocalizations test

Mice were suspended by the tip of their tails with tape in a suspension bar elevated 50 cm. For a maximum of 3 min period, animals that vocalized once were registered with a yes/no score and were taken down from the bar.

2.5 Grip strength test

Animals were held by the middle/base of the tail and allowed to grasp a tangled fine gauge stainless steel wire attached to a steel chain with their forepaws. The test consisted of a maximum of 6 levels, in one of each the steel chain weight is incremented (13,2 g; 19,7 g; 25,9 g; 32,1 g; 38,1 g; 44,6 g). The criterion followed to pass each level is that the animal holds the suspended weight in the air for 5 s. The grip latency is the sum of the seconds (s) the animal is capable to maintain the different weights (e.g., if an animal passes 4 levels and on the fifth, holds the weight for 3 s, it scores 23).

2.6 Step down test – Passive avoidance

The set up of the Passive Avoidance - Step Down for Mice (vibrating platform) (Ugo Basile, #40570) cage consists in a dark box with a circled plexiglass platform placed in the middle of a controllable electrified net. The animals were trained 24 h prior to the test. First, the net was electrified with 0.6 mA; next, the mouse was introduced in in the cage and placed in the middle of the platform. The time it took to the animal to step down the platform and receive an electric shock was measured. The electrified net was immediately stopped, and the animal was removed from the cage. After 24 h, the mouse was placed again in the platform and the time to step down the platform was measured again, however this time the net was not electrified. The latency to step down the platform (s) was calculated by subtracting the latency time from the first day to that of the second day to normalize for the inter-individual variability.

2.7 Marble burying test

Cages were filled approximately 8 cm deep with wood chip bedding, lightly tamped down to make a flat, even surface. A total of 12 green glass marbles were placed on the surface, evenly spaced, each about 4 cm apart. Individualized animals were placed in each cage and left for 10 min. Afterwards, the number of marbles buried (to 2/3 their depth) with bedding was counted.

2.8 Pole test

Mice are placed at the top of a 50 cm long pole with their head oriented upward. To complete the task, animals must reorient themselves downward and descend the length of the pole to return to their home cage placed at the base. The time required for the mice to downward (time to turn) and the total time

taken to reach the base (total time) are recorded over two trials. Two further qualify the performance, we implemented a scoring system evaluating both the time taken to turn (scored from 1 to 5) and the way the mice descended the pole (scored from 1 to 3), with 1 representing the best performance and 5 the poorest. Results are presented as the average score obtained from the two trials.

Table 4. Scores used during the Pole test.

POLE SCORE
Turns <15 s = 1
Turns 15-30 s = 2
Turns 30-45 s = 3
Turns 45-60 s = 4
Walks down - 1
Slips down the pole - 2
Falls - 3

3 GI functional assessment

3.1 Body weight, food and water intake follow-up

Animals were weighed at the beginning of the week from 1 m old to 18 m for body weight control. The food and water content from each cage were also measured for food and water intake follow-up throughout the lifespan. Food and water bottles were refiled every week to maintain a constant supply for the mice. Data was normalized to the number of animals co-living in the same cage and results are shown as individual consumption values.

3.2 Stool collection, fecal water content measurement and Bristol scale

Animals were individualized in transparent plastic cages without any environmental enrichment factors or bedding. Fecal pellets were counted every 5 min for a total time of 60 min. The changes in stool form and pellet size were observed and recorded before collection, the Bristol scale was used to score the fecal pellets. Bristol scale rates stools depending on their shape and consistency from 1 (hard, solid stool) to 7 (loose/liquid stools). Type 3, 4 and 5 are considered as normal feces, 1 and 2 as a signal for constipation and 6 and 7 as an indication for diarrhea (Figure 19 g) (Blake et al., 2016). Afterwards, feces were collected every 10 min in microcentrifuge tubes previously weighed (*weight 1*) and weighed again (*weight 2*). To calculate the raw fecal weight, *weight 1* was subtracted from *weight 2*. Afterwards, tubes were placed O/N at 65ºC inside a stove. Next day, the tubes were weighed again (*weight 3).* To calculate the dry fecal weight, *weight 1* was subtracted from *weight 3*. To calculate the % of humidity the following equation was used:

$$\%humidity = \left(\frac{raw\ fecal\ weight - dry\ fecal\ weight}{raw\ fecal\ weight}\right) x100$$

3.3 Total intestinal transit time

Mice were oral gavage with 300 ml dose (approx. 10ml/kg body weight) of a red dye (Carmine red dye (Sigma-Aldrich, #C1022) in 0,5% methylcellulose (Sigma-Aldrich, #M7027) and placed in individual transparent plastic cages without any environmental enrichment factors nor bedding. The time until the red dye was observed in the feces was calculated as total intestinal transit time (min). To prepare the solution shake 0.1 g of methyl cellulose powder into 20 ml hot water (miliQ) (86-90 ºC) and stir rapidly while cooling the solution to 5 °C in an ice water bath while adding 1.2g red carmine. The solution is stable at room temperature but stored in tightly closed containers (i.e. 50ml falcon).

3.4 Small intestine propulsion rate

Mice were fasted for 12 h and oral gavage with 200 ml dose of a red dye (Carmine red dye (Sigma-Aldrich, #C1022) in 0,5% methylcellulose (Sigma-Aldrich, #M7027) and placed in individual transparent plastic cages without any environmental enrichment factors nor bedding. After 1 h, animals were euthanized and the whole intestine was collected to measure the travelled distance of the red dye. The distance covered by the red dye and the total length of the small intestine (from pylorus to cecum) were measured to calculate the small intestine propulsion rate. The following formula was used:

$$Propulsion\ rate\ (\%) = \frac{Distance\ traveled\ by\ the\ red\ dye}{Total\ length\ of\ the\ small\ intestine}\ x\ 100$$

3.5 Gut permeability test – FITC-dextran

Mice were fasted for 5 to 6 h before gavage with 44 mg/100g body weight of FITC-dextran (molecular weight 4.4 kDa; Sigma-Aldrich, #FD4) at a concentration of 80 mg/mL in sterile PBS 1X. For example, if a mouse weight was 50 mg, the dose would be 275 µl of FITC-Dextran. Blood was collected through submandibular vein after 1 h FITC-dextran administration, serum was isolated by centrifuging at 1000 G for 10 min at room temperature (RT). Serum was collected and fluorescence was quantified by fluorospectrometry (Varioskan LUX, Thermo Scientific) with the excitation and emission wavelength at 485 nm and 528 nm, respectively. Concentrations were obtained using a standard curve of serially diluted FITC-dextran.

3.6 Intestinal motility study

These procedures were performed in collaboration with the Neuroimmune-Gastroenterology (NeuroGast) group from Universitat Autònoma de Barcelona (UAB).

3.6.1 Tissue preparation

Animals were euthanized by cervical dislocation and intestines were quickly removed from the abdominal cavity. Proximal and distal colon samples were dissected, rinsed and placed in Krebs solution on a dissection dish and the mucosal layer was gently removed. Circular muscle strips 10 x 4 mm were cut in circular and longitudinal directions.

3.6.2 Solutions and drugs

The composition of the Krebs solution used was (in mmol/L): glucose 10.10, NaCl 115.48, $NaHCO_3$ 21.90, KCl 4.61, NaH_2PO_4 1.14, $CaCl_2$ 2.50, and $MgSO_4$ 1.16, bubbled with a mixture of 5% CO_2-95% O_2 (pH 7.4).
The following drugs were used: Nω-nitro-L-arginine (L-NNA) (Sigma Chemicals, USA), (2-hydroxyethyl) trimethylammonium chloride carbamate (carbachol-CCH), (1R,2S,4S,5S)-4-[2-Iodo-6-(methylamino)-9H-purin-9-yl]-2-(phosphonooxy)-bicyclo-[3.1.0]-hexane-1-methanol dihydrogen phosphate tetraammonium salt (MRS2500) (Tocris, UK), propranolol (Tocris, Bristol, UK), atropine and phentolamine (Sigma-Aldrich, St.Louis, MO, USA). Stock solutions were prepared by dissolving drugs in distilled water except for L-NNA, which was dissolved in Krebs solution by sonication.

3.6.3 Mechanical studies

Circular and longitudinal oriented muscle strips were set up in a 10-mL organ bath filled with Krebs solution and maintained at a temperature of 37 ± 1 °C and carbogenated (95% 0_2 and 5% $C0_2$). A tension of 1 g was applied, and tissues were equilibrated for 1 hour. After this period, strips displayed spontaneous phasic contractions (SPCs). Mechanical activity was measured using an isometric force transducer (UF-1 Harvard Apparatus) connected to a computer through an amplifier. Data were digitally recorded at a rate of 25 Hz using DATAWIN1 2001 software (Panlab, Barcelona, Spain) coupled with an analog-to-digital card installed in a computer. Grass S88 Stimulator (Grass Instruments Co., MA, USA) and Stim-Spiller II (MedLab Instruments, CO, USA) were used to deliver the pulses to the electrodes. Electrical field stimulation (EFS) was applied through two platinum electrodes placed on the support holding the tissue, to study the release of inhibitory and excitatory neurotransmitters.
We evaluated the (i) spontaneous myogenic contractility, (ii) CCH induced contractility and EFS-induced neural-mediated (iii) excitatory and (iv) inhibitory responses.

3.6.3.1 CCH induced contractility

In this experiment, tissues were incubated with the muscarinic agonist CCH at increasing concentrations from 10^{-8} to 10^{-5} M in intervals of 5 min which cause an increase of contractile activity.

3.6.3.2 Neural-mediated excitatory responses

To evaluate the effect of excitatory neurotransmitters released by neurons, the release of inhibitory neurotransmitters was inhibited incubating the muscle strips under non-nitrergic and non-purinergic (NNNP) conditions with L-NNA 1 mM and MRS2500 1 µM. We next used an EFS involving the application of trains of increasing frequency (Hz). EFS (voltage: 30 V; pulse duration: 0.4 ms; frequency: 1, 10, 20, 30, 40, 50 Hz; and train duration: 300 ms) was applied once every 140 s.

3.6.3.3 Neural-mediated inhibitory responses

To selectively isolate the response associated with inhibitory motoneurons, the effect of excitatory neurotransmitters was inhibited by incubating tissues in non-adrenergic and non-cholinergic (NANC) conditions with atropine, propranolol and phentolamine 1 µM. We next used an EFS involving the application of trains of increasing voltage (V). EFS (voltage: 5, 6, 7, 8, 10, 20, 30 V; pulse duration: 0.4 ms; frequency: 5 Hz; and train duration: 2 min) was applied.

3.6.4 Data analysis

The amplitude (mg), frequency (contractions/min) and tone (mg) were measured to estimate the SPCs between groups. The area under the curve (AUC; mg x min) of contractions calculated from the baseline was measured to estimate the response to inhibitory EFS and CCH. For the inhibitory EFS, to normalize data, responses were expressed as a percentage of the basal AUC obtained before the EFS. The following formula was used:

$$100\ x\ (AUC\ during\ EFS/AUC\ before\ EFS)$$

In this formula, 0% response represents the complete cessation of any activity, whereas 100% denotes no changes compared with basal activity. The amplitude (mg) of the subsequent off-response was also measured. To assess the effect of CCH-induced contractions, a nonlinear regression analysis was performed using the following formula:

$$Y\ =\ 100/(1\ +\ 10\hat{}((LogIC50\ -\ X)\ *\ Hill\ slope))$$

4 Glucose tolerance test (GTT)

This test was performed in collaboration with the Metabolism and Obesity group from VHIR.

GTT was performed on 5-6 h fasted mice. First, blood glucose was measured at time 0. Afterwards, an intraperitoneal injection of glucose (2 g/Kg body weight or 1g/kg depending on the experiment) was given to the mice and blood glucose was measured at 15, 30, 60, and 90 min. Glucose levels were measured in blood using a glucometer and test strips (ACCU-CHEK, AVIVA, Roche).

5 Histological analysis

5.1 Tissue processing

5.1.1 Brain samples

Animals were deeply anesthetized with isoflurane 4% and perfused through intracardial perfusion with saline [0.9% (weight/volume)] followed by paraformaldehyde (PFA) 4% solution in PBS 1X (PanReac, #252931). Brains were removed and post-fixed for 24h in PFA 4%, subsequently cryoprotected for 24h-48h in 30% sucrose solution at 4ºC and finally snap frozen with isopentane (PanReac, #123501). Frozen brains were sectioned using a cryostat at 30 µm (Leica, Germany) and sections were kept at 4ºC in PB (phosphate buffer) 0.1M + sodium azide 0.01% (Sigma-Aldrich, #S8032) solution.

5.1.2 Intestinal samples

Animals were deeply anesthetized with isoflurane 4% and intestines were quickly removed from the abdominal cavity. Mice were then perfused through intracardial perfusion with saline [0.9% (weight/volume)] followed by PFA 4% solution in PBS 1X (PanReac, #252931).

Wholemounts. Duodenal, proximal and distal colon samples were rinsed using a syringe with saline and post-fixed for 24 h in PFA 4% and kept at 4ºC in PBS 1X + sodium azide 0.01%. Whole mounts of longitudinal muscle and myenteric plexus were obtained by microdissection. Briefly, intestines sections were pinned in a Sylgard-coated plate and cut open by the mesenteric attachment over the length of the tissue. Afterwards, sections were stretched, flatten and pinned down with minutien pins with the mucosa facing up prior to microdissection of the different layers. Wholemounts were fixed again for 3 h in PFA 4% at RT and kept at 4ºC in PBS 1X + sodium azide 0.01%.

Paraffin samples. Duodenal, jejunum, ilium, proximal and distal colon samples were dissected and rinsed using a syringe with saline and post-fixed for 24 h in PFA 4% and kept at 4ºC in PBS 1X + sodium azide 0.01% prior to being paraffin embedded. Sectioning was performed with a sliding microtome (Leica, Germany) at 5 µm-thickness.

5.1.3 Renal samples

Paraffin samples. Kidneys were dissected and fixed for 24h in PFA 4% and kept at 4ºC in PBS 1X + sodium azide 0.01% prior to being paraffin embedded. Sectioning was performed with a sliding microtome (Leica, Germany) at 5 µm-thickness.

5.2 Immunohistochemistry (IHC)

5.2.1 Brain samples

Brain sections were quenched for 15 min in 3% H_2O_2 + 10% methanol (volume/volume) in Tris buffered saline 0.1M (TBS). Sections were rinsed 3 times for 5 min in TBS 1X between each incubation period. For a period of 1 h, sections were blocked with 5% normal goat serum (NGS) (Vector Laboratories, #S-1000) in TBS 1X. Later, tissues were incubated 48 h at 4ºC with primary antibody (Table 5) in 2% NGS + TBS 1X solution. Subsequently after washing 3 times with TBS 1X, the corresponding secondary biotinylated antibody (Table 6) diluted in 2% NGS + TBS 1X solution, was added and incubated at RT for 1 h. Afterwards, sections were rinsed again 3 times with TBS 1X, and avidin-biotin-peroxidase complex (ABC) solution (Thermo Fisher Scientific, ABC Peroxidase Standard Staining kit #32020 or Ultra-Sensitive ABC Peroxidase Standard Staining kit #32050) was applied and left to incubate for 1 h at RT. Peroxidase activity was developed by means of either 3,3'-diaminobenzidine (DAB) substrate or Vector® SG substrate (Vector®, #SK-4100 and SK-4700) and then sections were mounted and cover-slipped with DPX mounting medium (Sigma-Aldrich, #06522). Bright-field section images were obtained using Olympus Slideview VS200 slide scanner and the Olyvia 3.3 software.

5.2.2 Renal samples

Kidney sections were deparaffinized using xylene and rehydrated through graded alcohols. Endogenous peroxidases were blocked after deparaffination in an aqueous solution of 3% H_2O_2 - 10% (volume/volume, vol/vol) methanol. Antigen retrieval was performed with a citrate buffer (10mM citric acid, pH 6.0) at 95ºC for 20 min. Next, sections were blocked in 5% of bovine serum albumin (BSA) + TBS 1X. The sections were incubated for 16 h at 4ºC with primary antibody (Table 5) in 2% BSA + TBS 1X. After rinsing 3 times with TBS 1X, the corresponding secondary biotinylated antibody (Table 6) diluted in 2% BSA + TBS 1X solution, was added and incubated at RT for 1 h. Afterwards, sections were rinsed again 3 times with TBS 1X, and ABC solution (Thermo Fisher Scientific, ABC Peroxidase Standard Staining kit #32020) was applied and left to incubate for 1 h at RT. Peroxidase activity was developed by using DAB (D3939, Millipore-Sigma). Counterstaining of the slides was done with Hematoxylin Gill Nº 3 solution.

5.3 Immunofluorescence (IF)

5.3.1 Brain samples

Brain sections were selected and blocked at RT for 1 h with 5% NGS (Vector Laboratories, #S-1000) + 0.1% Triton-1X (Sigma-Aldrich, #T9284) + PBS 1X under agitation. Later, sections were incubated with the corresponding primary antibody (Table 5) in 2% NGS+ 0.1% Triton-1X + PBS 1X solution O/N at 4ºC. Subsequently after washing 3 times for 5 min in PBS 1X, the corresponding secondary antibody (Table 6) diluted in 2% NGS+ 0.1% Triton-1X + PBS 1X was added and incubated at RT for 1 h. After washing, sections were mounted and cover-slipped with DakoCytomation Fluorescent mounting medium (Dako, #S302380-2). IF high resolution micrographs were acquired with an Olympus Slideview VS200 slide scanner and the Olyvia 3.3 software.

5.3.2 Intestinal samples

These experimental procedures were performed in collaboration with the research group of The Enteric Nervous System in Gut and Brain Diseases from Inserm-University of Nantes.

Intestinal segments were permeabilized with PBS 1X containing 10% horse serum (HS) + 3% Triton X-100 + 0.05% saponin for 24 h at RT under agitation. Tissues were then incubated with the corresponding primary antibodies (Table 5) for 24 h in permeabilized buffer without saponin at RT under agitation. After washing 3 times, samples were incubated for 3 h in permeabilized buffer without saponin with corresponding secondary antibodies (Table 6) at RT in the dark under agitation. Washed tissues were mounted and cover-slipped with antifading ProLong™ Gold mounting medium (Thermofisher, #P36930). Images from inmmunostained tissues were acquired with AxioZoom.V16 (Zeiss, Marly le Roi, France) associated with Apotome2. Confocal images were also obtained using the confocal microscope Nikon A1 RSi (Nikon SAS, Champigny sur Marne, France) with two objectives 63x and 20x.

Table 5. Primary antibodies used in IHC, IF and WB.

Primary Antibody	Manufacturer and Reference	Dilution and application
CD68	Bio Rad #MCA1957	1:100 (IF)
ChAT	Milipore #AB144P	1: 500 (IHC for DVC) 1:500 (IF for intestinal tissue)
Iba1	Abcam #Ab178846	1:1000 (IHC)
nNOS	ENZO #ALX-210529-C100	1:1000 (IF)
p62	Progen #GP62-C	1:500 (IF)
TH	Sigma Aldrich #657012	1:40000 (IHC for SN and VTA) 1:10000 (IHC for STR) 1:10000 (IHC for DVC) 1:1000 (IF/WB)
WT-1	Abcam #ab89901	1:100 (IHC)
α-synuclein	BD Biosciences #610787	1:1000 (WB)
FAK	Invitrogen #39-6500	1:1000 (WB)

GFAP (G-A-5)	Sigma Aldrich #IF03L	1:1000 (WB)
Occludin	Invitrogen #33-1500	1:1000 (WB)
PGP 9.5	Invitrogen #MA1-83428	1:1000 (WB)
Phospho-α-synuclein (Ser129 – D1R1R)	Cell Signaling #23706	1:1000 (WB)
TAU-5	Invitrogen #MA5-12808	1:1000 (WB)
ZO-1	Invitrogen #40-2200	1:500 (WB)

Table 6. Secondary antibodies used in IHC, IF and WB.

Primary Antibody	Manufacturer and Reference	Dilution and application
Anti-mouse Alexa 488	Invitrogen #A21202	1:200 (IF for intestinal tissue)
Anti-rabbit Cy3	Jackson ImmunoResearch Lab #711-165-152	1:500 (IF for intestinal tissue)
Anti-human Alexa 647	Jackson ImmunoResearch Lab #709-605-149	1:500 (IF for intestinal tissue)
Anti-guinea pig Alexa 488	Gibco, #A11073	1:1000 (IF for brain tissue)
Anti-rabbit Alexa fluor 647	Life technologies, #A31573	1:1000 (IF for brain tissue)
Anti-mouse HRP	Sigma Aldrich #A9044	1:1000 (WB)
Anti-rabbit HRP	Invitrogen #31460	1:1000 (WB)
Anti-rabbit biotinylated	Vector laboratories, #BA1000	1:1000 (IHC)
Anti-rat biotinylated	Vector laboratories, #BA9400	1:1000 (IHC)
Anti-goat biotinylated	Vector Laboratories # BA-9500	1:250 (IHC)

5.4 Myenteric plexus cell counting

Quantification of Hu-positive, ChAT-positive and nNOS-positive neurons in the myenteric plexus of duodenal and proximal colon samples was performed manually using Image J software (NIH, USA). Briefly, the investigator randomly selected 10 ganglions per animal and quantified the number of neurons expressing the indicated markers. The proportion of ChAT-positive and nNOS-positive neurons was calculated relative to the total number of Hu-positive neurons within each ganglion and expressed as a percentage. All quantifications were performed by an investigator blinded to the experimental groups.

5.5 Dopaminergic cell counting

Quantification of (i) the total number of TH-positive (TH+NM+; TH+NM-) neurons, (ii) the number of NM-positive neurons (TH-NM+), (iii) the number of eNM aggregates in the SNpc, VTA and DVC; and (iv) the total number of ChAT-positive (ChAT+) neurons in DVC, was performed using a specific artificial intelligence (AI)-assisted algorithm and the Olympus V200 Desktop 3.3 software. Serial 30 µm-thick cryosections (every fourth section for SNpc and VTA; every sixth sections for DVC) covering the entire nuclei were included in the counting procedure. High resolution micrographs were acquired with an

Olympus Slideview VS200 slide scanner and the Olyvia 3.3 software. Data for the total numbers of TH+ neurons and ChAT+ neurons are expressed as absolute numbers. The total number of catecholaminergic SNpc, VTA and DVC neurons was calculated by considering all TH+NM+, TH-NM+ and TH+NM- neurons. The percentage (%) of TH downregulation was calculated by considering the total number of TH-NM+ with respect to the total number of neurons containing NM in the different experimental groups. All quantifications were performed by an investigator blinded to the experimental groups.

5.6 Neuropathological markers assessment

Quantification of the number of p62-positive MB and LB-like inclusions was performed manually using Image J software (NIH, USA). This quantification was based on fluorescent immunostaining (Table 5), and the total count of inclusions in each category was conducted from a representative coronal section of SNpc, VTA and DVC nuclei for each animal. All quantifications were performed by an investigator blinded to the experimental groups.

5.7 Neuroinflammation markers assessment

Quantification of the number of Iba1-positive (Iba1+) and CD68-positive (CD68+) in the SNpc, VTA and DVC representative coronal section was performed using a specific artificial intelligence (AI)-assisted algorithm and the Olympus V200 Desktop 3.3 software. The quantification of Iba1+ cells was divided into three categories depending on their activation state, i) ameboid - activated state microglia, ii) intermediate activated state microglia, and iii) ramified – non-activated state microglia. All quantifications were performed by an investigator blinded to the experimental groups.

5.8 Striatal optical densitometry (OD) analysis

Quantification of TH-positive fibers density in the dorsal STR was measured by OD using ImageJ. Four serial coronal 30 µm-thick cryosections, covering the entire nuclei, were TH-inmmunostained and scanned with an Epson Perfection v750 Pro scanner. Striatal densitometry values were corrected for non-specific background staining by subtracting densitometric values obtained from the corpus callosum and anterior commissure in the same images. Data are expressed as OD defined by the logarithmic intensity of the light transmitted through the material using the formula:

$$-log10(Striatum\ Intensity/Cortex\ Intensity)$$

All quantifications were performed by an investigator blinded to the experimental groups.

5.9 Intracellular NM quantification

Quantification of intracellular NM in representative sections of the SN, VTA, and DVC were measured by OD using ImageJ software (NIH, USA). Unstained 30µm-thick cryopreserved sections were selected and scanned with an Olympus Slideview VS200 slide scanner and the Olyvia 3.3 software. Catecholaminergic neurons were identified by the visualization of unstained NM brown pigment. NM DO values were corrected for non-specific background by subtracting densitometric values obtained from the extracellular space in the same images. Data are expressed as OD defined by the logarithmic intensity of the light transmitted through the material using the formula:

$$-log10(\frac{intracellular\ NM\ intensity}{extracellular\ space\ intensity})$$

All quantifications were performed by an investigator blinded to the experimental groups.

5.10 Podocyte density assessment

Quantification of the podocyte density in renal sections was performed by the Nephrology and kidney transplantation research group from VHIR.

Briefly, stained 5µm-thick sections with WT1 by IHC (a protein highly expressed in mature podocytes) were evaluated using QuPath software. Podocyte density (expressed as number of podocytes per mm^2 of glomerular area) was evaluated in 20 representative cortical glomeruli.

5.11 Glomerular hypertrophy assessment

Glomerular hypertrophy was quantified by the Nephrology and kidney transplantation research group from VHIR.

Briefly, the glomerular tuft cross-sectional area was measured using Image J (NIH) analysis software. Glomerular hypertrophy was assessed by measuring the tuft area from glomeruli in which the vascular pole was evident (using at least 20 glomeruli per section). This was performed to reduce the possibility of including tangentially cut glomeruli.

6 Real-time quantitative PCR (RT-qPCR)

6.1 Inflammatory markers

Total RNA was isolated from dissected duodenal and colon tissue using the RNeasy Mini Kit (Qiagen, #74104). The procedure was performed according to the manufacturer's specification. The yield and purity of the RNA was measured using a NanoDrop ND-1000 Spectrophotometer. 500 ng of total RNA

were retrotranscribed using High-Capacity cDNA Reverse Transcription kit (Thermo Fisher Scientific, #4368814). The RT-qPCR was performed with 10 ng of cDNA per well in technical triplicates using PowerUp™ SYBR™ Green Master Mix (Thermo Fisher Scientific, #A25776) mixed with the specific primers (Table 7) diluted at 500 nM. Water was added in the reaction as a negative control, serving as a non-template. The recommended standard cycling condition was used in a LightCycler® 480 System (Roche). To analyze the data, the software LightCycler® 480 SW 1.5.1 was used to obtain the thresholds cycles (CTs) for each sample. Fold changes (FC) for each transcript and sample were calculated normalizing the arithmetic mean of technical triplicates CTs to the mean of the endogenous control gene (RPS6) and then normalized to experimental control expression (wt mice) using the comparative method (ΔΔCt-method).

Table 7. Sequences of primers used for SYBR Green Assays

Primer Set	Forward Primer (5'-3')	Reverse Primer (5'-3')
α-synuclein	CACTGGCTTTGTCAAGAAGGACC	CATAAGCCTCACTGCCAGGATC
AADC	TCCCCACGGCTAGCTCATACCC	TTCCCCAGCCAGTCCATCATCA
b-actin	CATCCGTAAAGACCTCTATGCCAAC	ATGGAGCCACCGATCCACA
CART	CCCCTTCACAAGCACTTCAA	AAGTCCAGCACCATGGAGAG
Cldn-2	GAAAGGACGGCTCCGTTTTC	TCTTCGGAGCCTGTTTGCTT
CRH	GGCATCCTGAGAGAAGTCCCTC	ACAGAGCCACCAGCAGCATG
GADPH	CTCGCTCCTGGAAGATGGTG	GGTGAAGGTCGGTGTGAACG
GFAP	CACCTACAGGAAATTGCTGGAGG	CCACGATGTTCCTCTTGAGGTG
IL-1b	GCCTCGTGCTGTCGGACCCATA	TTGAGGCCCAAGGCCACAGGT
IL-10	GACTTTAAGGGTTACTTGGGTTGC	AGAAATCGATGACAGCGCCTC
IL-6	TCCAGTTGCCTTCTTGGGAC	AGTCTCCTCTCCGGACTTGT
INF-γ	CTGGAGGAACTGGCAAAAGGAT	GGTTGTTGACCTCAAACTTGGC
MCH	TCTTCCTACATGTTAATGCTGGCT	TCCTTATGGACTTGGAAGCTGA
NPY	TGGTTTCAGGGGATGAGATG	GCTCTGCGACACTACATCAA
occludin	GGTTAAAAATGTGTCTGCAGGCAC	GAGGCTGCCTGAAGTCATCCAC
Orexin-A	CTTCAGGCCAACGGTAACCAC	CCGGGGTGCTAAAGCGGTG
Oxytocin	CGGTGGATCTCGGACTGAAC	TAGCAGGCGGAGGTCAGAG
POMC	TTTTCAGTCAGGGGCTGTTC	CTCCTGCTTCAGACCTCCA
RPS6	GAAGCGCAAGTCTGTTCGTG	GTCCTGGGCTTCTTACCTTCT
s100b	AGAGGGTGACAAGCACAAGCTG	GAACTCCTGGAAGTCACACTCC
Sox-10	TGGACCACCGGCACCCAGAA	CGTGGGCAGAGCCACACCTG
TH	ATGCCTCCTCACCTATGCAC	CAGCCAACATGGGTACGTGT
TLR-2	GCCACCATTTCCACGGACT	GGCTTCCTCTTGGCCTGG
TLR-4	AGAAATTCCTGCAGTGGGTCA	TCTCTACAGGTGTTGCACATGTCA
TNF-α	GAACTTCGGGGTGATCGGTC	GCCACTCCAGCTGCTCCTCC
TRH	GGCTGATGATGGCTCTGGCTTT	ACGTCTTCCTCCTTCTCCTCCCTTT
Vasopressin	TCGCCAGGATGCTCAACAC	TTGGTCCGAAGCAGCGTC
ZO-2	CTAGACCCCCAGAGCCCCAGAAA	TCGCAGGAGTCCACGCATACAAG

7 Western blot (WB)

These experimental procedures were performed in collaboration with the research group of The Enteric Nervous System in Gut and Brain Diseases from Inserm-University of Nantes.

Samples of duodenum and proximal colon samples of approximately 50 mg were dissected and homogenized in ice-cold radioimmunoprecipitation assay (RIPA) Lysis buffer (Sigma-Aldrich, #20-188) complete with protease inhibitor (Sigma-Aldrich, #66373700), a phosphatase inhibitor cocktail (Sigma-Aldrich, #P0044), and sodium orthovanadate (Sigma-Aldrich, #S6508). Samples were lysed with the Precellys® 24 tissue homogenizer (Bertin Instruments, France). Protein concentrations were quantified using the Pierce™ BCA Protein Assay Kit (Thermo Scientific, #23227). Samples were further prepared for electrophoresis by diluting them with NuPAGE™ sample reducing agent 10X (Invitrogen, #NP0009), sonicated and denatured for 5 min at 98°C. Twenty micrograms of proteins were separated using the NuPAGE™ 4–12% Bis-Tris Midi Gel (Invitrogen, #WG1402BX10) or NuPAGE™ 3–8% Tris-Acetate Midi Gel (Invitrogen, #WG1603BX10) together with the NuPAGE™ MES SDS (20X) (Invitrogen, # NP0002) running buffer before electrophoretic transfer to nitrocellulose membranes (Life Technologies, #IB23001) with the iBlot™ 2 Dry Blotting System (Life Technologies, #IB21001). Nitrocellulose membranes were treated with PFA 4% and 0.01% (v/v) glutaraldehyde (Sigma-Aldrich, #G6257) to enhance membrane retention of α-synuclein. Membranes were then rinsed 3 times with TBS 1X and blocked for 1 h at RT in TBS 1X + 0.1% (v/v) Tween-20 (Sigma, #P1379) and 5% (w/v) non-fat dry milk. Later, membranes were incubated O/N at 4°C with the primary antibodies (Table 5). Membranes were 3 times rinsed with TBS 1X and incubated for 1 h at RT with the secondary antibodies (Table 6) and visualized later by enhanced chemiluminescent detection using SuperSignal™ West Pico PLUS Chemiluminescent Substrate (Thermo Scientific, #34580). Band densitometry was measured using Image Lab software (Bio Rad).

8 Chromatographic determination of dopaminergic metabolites in intestinal samples

Ultra performance liquid chromatography-tandem mass spectrometer (UPLC-MS/MS) analysis of GI tract and brain samples was performed using a previously validated method with some modifications (Gonzalez-Sepulveda et al., 2020).

8.1 Sample preparation

8.1.1 GI tract samples

Duodenal and proximal colon samples from wt and tgNM animals fed with CHOW or HFD were dissected and flushed clean with PBS 1X prior to being snap frozen in liquid nitrogen and kept at -80ºC until analysis.

The day of analysis, samples were homogenized with 300 µl of 250 mM formic acid (FA) and split in three: 55 µl for ACh, 240 µl for catecholaminergic and serotonergic determination and 20 µl for protein determination by Pierce™ BCA Protein Assay Kit (Thermo Scientific, #23227). For ACh quantification, samples were diluted 1:4 with 0.1% FA in acetonitrile containing 100 nM of ACh-d4 Chloride (ACh-d4) as internal standard (IS) and centrifuged at 20.000 G during 10 min at 4ºC. After centrifugation, supernatants were filtered using an Ostro™ protein precipitation and phospholipid removal plate (Waters, USA) prior the injection in the UPLC-MS/MS system. For catecholaminergic and serotonergic determination, after addition of a mixture (500 nM each) of dopamine-d4 hydrochloride (DA-d4) and serotonin-d4 Hydrochloride (5-HT-d4) as IS, samples were centrifuged at 20.000 G during 10 min at 4ºC. Then, reductive hydrolysis and alumina extraction of catecholic compounds in supernatant was performed using the method of Murakami et al. 2008 (K. Murakami et al., 2008) with some modifications. 100 µl of the supernatant were added to a tube containing 50 mg of previously weighed acid-washed alumina. Next, we added 200 µl of 1% $Na_2S_2O_5$ – 1% EDTA.2Na and 500 µl 2.7 M Tris. HCl – 2% EDTA.2Na (pH 9.0). Tubes were vigorously mixed on a microtube mixer for 5 min and then centrifuged at 20.000 G for 10 min at 4 ºC. After removal of the supernatant, the alumina was washed with 1 ml of MilliQ water and centrifuged at 20.000 G for 10 min at 4ºC three times. Metabolites of interest were finally eluted from alumina with 100 µl of 0.4 M $HClO_4$ by shaking for 2 min on a microtube mixer. Afterwards, 7 µl were injected into the UPLC-MS/MS system.

8.1.2 Brain samples

Midbrain sections including SNpc and VTA were dissected from fresh brains using a brain matrix, next they were snap frozen in liquid nitrogen and kept at -80ºC until analysis.

Samples were homogenized with 300 µl of 250 mM formic acid (FA) and split in two: 20 µl were taken for protein determination by BCA and 224 µl for catecholaminergic UPLC-MS/MS quantification, to which 32 µl DA-4d were added as IS. Samples were then centrifuged at 20.000 G during 10 min at 4ºC. After centrifugation, supernatants were filtered using an Ostro™ protein precipitation and phospholipid removal plate (Waters, USA) prior the injection in the UPLC-MS/MS system. On the other hand, the pellet was further processed to determine the “protein-bound” (PB) fraction of 5-*S*-cysteinyldopa (5-SCD) and 5-*S*-cysteinyldopamine (5-SCDA). Preparation of the PB fraction samples was performed using the reductive hydrolysis and alumina extraction method of Murakami et al. 2008 (K. Murakami et al., 2008) with some modifications. The pellet was washed with 1 ml of a 1:1 mixture of methanol and chloroform, vortex-mixed and centrifuged at 20,000 G for 10 min at 4 °C. After centrifugation and aspiration, 300 µl of a mixture containing 6 M HCl, 5% thioglycolic acid and 1% phenol were added to the resulting pellet into a sealed-capped tube. Tubes were then purged with a stream of nitrogen, sealed and incubated for 16 h at 110 °C. After cooling, samples were centrifuged at 20,000 G for 10 min at 4ºC. Next, 100 µl of the

hydrolysate were added to a tube containing 50 mg of acid-washed alumina prior the addition of 200 µl of 1% $Na_2S_2O_5$ – 1% EDTA.2Na and 500 µl 2.7 M Tris. HCl – 2% EDTA.2Na (pH 9.0). Tubes were vigorously mixed in a microtube mixer for 5 min and then centrifuged at 20,000 G for 10 min at 4ºC. After removal of the supernatant, the alumina was washed with 1 ml of MilliQ water and centrifuged at 20,000 G for 10 min at 4 °C three times. 5-SCD and 5-SCDA were finally eluted from alumina with 100 µl of 0.4 M $HClO_4$ by shaking for 2 min on a microtube mixer. 7 µl of the supernatant were injected into the UPLC-MS/MS system.

8.2 UPLC-MS/MS analysis.

8.2.1 Chromatographic separation of ACh

The chromatographic separation of samples for ACh determination was performed on a Cortecs UPLC HILIC (1.6 µm; 2,1x75 mm) column coupled to a Cortecs UPLC HILIC VanGuard pre-column (Waters). Column temperature was set at 50 ºC and samples were maintained at 6 ºC in the thermostatic autosampler. The mobile phase consisted of solvent A (Acetonitrile + 0.1% FA) and solvent B (10 mM ammonium acetate in MilliQ water) at a flow of 0.5 mL/min with isocratic 70% A- 30% B conditions during 2.2 min.

8.2.2 Chromatographic separation of serotonergic and dopaminergic metabolites

An Acquity HSS T3 (1.8 µm, 2.1 mm × 100 mm) column coupled to an Acquity HSS T3 VanGuard (100 Å, 1.8 µm, 2.1 mm × 5 mm) pre-column was used. Column temperature was set at 50ºC for serotonergic and at 45 ºC for dopaminergic metabolites. Samples were maintained at 6 ºC in the thermostatic autosampler and injected several times into the UPLC-MS/MS system to analyze different sets of compounds, organized in working mixes i.e. MIX1, MIX2 and MIX3. MIX1 includes 5-HT, tryptophan (Trp), 5-hydroxyindole-3-acetic acid (5-HIAA) and kynurenine (Kyn); MIX2 includes DA, NE, L-DOPA, 3-methoxytyramine (3-MT) and aminochrome (AC) and MIX3 includes 5-SCD and 5-SCDA. The mobile phase consisted of solvent A (methanol 100%) and solvent B (25 mM FA in MilliQ water) at a flow of 0.5 ml/min for MIX1 or 0.4 ml/min for MIX2 and MIX3 with the following gradient profile: 0.5% B maintained for 0.5 min, 5% B at 0.9 min maintained for 2.1 min, 50% B at 2.8 min maintained for 1.2 min, 0.5% B at 4.1 min maintained 0.2 min for equilibration.

8.2.3 Mass spectrometry quantification

The mass spectrometer detector operated under the following parameters: source temperature 150 ºC, desolvation temperature 450 ºC, cone gas flow 50 L/hr, desolvation gas flow 1100 L/hr and collision gas flow 0.15 ml/min. Argon was used as the collision gas. The capillary voltage was set at: 3 kV (MIX1) or 0.5

kV (MIX2, MIX3). The electrospray ionization source was operated in positive mode. Multiple Reaction Monitoring (MRM) acquisition settings for the targeted metabolites are summarized in (Table 8). Samples with a concentration between limit of detection (LOD) and limit of quantitation (LOQ) or bigger than LOQ were considered acceptable; samples with a concentration lower than LOD were considered as the LOD value. Catechol oxidation was measured using the formula AC + 5-SCDA + 5-SCDA-PB/DA and 5-SCD + 5-SCD-PB/L-DOPA. Data was normalized by protein concentration and presented as the percentage of the CHOW-fed wt concentration or ratio.

Table 8. MRM acquisition settings. RT: retention time; CV: cone voltage; CE: collision energy; CpV: capillary voltage. b: Parent mass after loss of water.

Analyte	MRM transition (m/z)	MIX	RT (min)	CV (V)	CE (eV)	CpV (kV)
ACh-d4 (IS)	150 > 91	1	1,5	28	12	3
ACh	145,98 > 86,80	1	1.5	10	15	3
NEb	151,75 > 106,94	2	0,69	15	20	0,5
DA-d4 (IS)	157,83 > 94,8	2	1,44	10	20	0,5
DA	153,93 > 90,57	2	1,46	10	20	0,5
L-DOPA	198,1 > 152,1	2	1,48	15	15	0,5
3-MTb	150,7 > 90,96	2	3,09	35	20	0,5
AC	149,61 > 121,91	2	3,36	25	25	0,5
5-SCDA	273,1 > 166,9	2	1,73	20	20	0,5
5-SCD	317 > 154,86	2	2,01	24	30	0,5
5-HT-d4 (IS)	181 >164	3	0,97	10	5	0,5
5-HT	177 > 160	3	0,97	10	5	0,5
5-HIAA	192 > 146	3	1,5	25	20	0,5
Trp	205 > 188	3	2,1	15	10	0,5
Kyn	209>146	3	1,6	15	20	0,5

8.3 Protein extraction from fecal samples

Fecal pellets were collected fresh in microcentrifuge tubes, snap frozen on dry ice and kept at -80 ºC until analysis. Protein was extracted from fecal samples using the extraction buffer from S100A8/S100A9 ELISA kit (Immundiagnostik AG, Germany, #K6936) in combination with protease/phosphatase inhibitor cocktail (Cell Signaling, #5872S). Pellets of approximately 20 mg were dissolved and homogenized in 1 ml (1:50) extraction buffer + protease/phosphatase inhibitors, vortex and centrifuged 3000 G for 10 min at 4ºC. The supernatant was collected and stored at -80 ºC for further analysis. Protein samples were quantified using the Pierce™ BCA Protein Assay Kit (Thermo Scientific, #23227).

8.4 Serum extraction

Animals were fasted previously for 6 h and anesthetized with 4% isoflurane, then a direct intracardiac puncture was performed for blood collection. Approximately 500 to 900 µl of blood were collected into

clotting activator tubes (Sarstedt, #41.1500.005) and kept at RT for 30 min. After coagulation, tubes were centrifuged at 1500G for 10 min at RT and rapidly stored at -80 ºC for further analysis.

8.5 Urine extraction

Animals were individualized in cages having a small grid preventing them from touching the cage floor. Urine samples were collected with a micropipette from the bottom of the cage and stored at -80ºC in microcentrifuge tubes.

8.6 Cytokine profile assessment

For cytokine profile characterization in mouse fecal and serum samples, the LEGENDplex™ Mouse Inflammation Panel (13-plex) immunoassay (BioLegend, #740150) was used according to the manufacture's guidelines. It allowed to quantify simultaneously 13 mouse cytokines, including IL-23, IL-1α, INF-γ, TNF-α, CCL2 (MCP-1), IL-12p70, IL-1b, IL-10, IL-6, IL-27, IL-17A, INF-β and GM-CSF. Serum samples were diluted 1:2 with assay buffer. Flow cytometer BD® LSRFortessa™ (Biosciences) was used for data acquisition and assay files were analyzed using LEGENDplex™ data analysis software (BioLegend).

8.7 Calprotectin assessment

For calprotectin assessment in mouse fecal samples, the S100A8/S100A9 ELISA kit mice (Immundiagnostik AG, Germany, #K6936) was used according to the manufacture's guidelines. For absorption measurement the Varioskan LUX (Thermo Scientific) was used at 450 nm. The data was analyzed using 4 parameter logistic curve fitting. Levels of calprotectin were normalized to the total protein concentration measured in each sample.

8.8 Corticosterone assessment

Corticosterone was assessed in mouse serum samples using Corticosterone ELISA kit (Enzo, #ADI-900-097) in accordance with the manufacturer's protocol. Serum samples did not need dilution and 10 µl of each sample was used. For absorption measurement the Varioskan LUX (Thermo Scientific) was used at 405 nm. The data was analyzed using 4 parameter logistic curve fitting.

8.9 Metabolic hormones assessment

For metabolic hormones profile characterization in mouse serum samples, the MILLIPLEX® Mouse Metabolic Hormone Expanded Panel - Metabolism Multiplex Assay (Milipore, #MMHE-44K) was used following the manufacturer's instructions. This multiplex kit allowed to quantify simultaneously 7 analytes, including ghrelin, active glucagon-like peptide 1 (GLP-1), glucagon, insulin, leptin, peptide-YY (PYY) and amylin. Serum samples were not diluted previously to the assay. However, we added to the

blood samples 3 µl of Dipeptidyl peptidase IV (DPP-IV) inhibitor (Milipore, #DPP4-010) and Protease inhibitor cocktail (Sigma-Aldrich, #P2714). The Luminex® analyzer (MAGPIX®) (ThermoFisher Scientific) was used to acquire the data and the ProcartaPlex Analysis software to analyze it.

8.10 Pituitary hormones assessment

For pituitary hormones profile characterization in mouse serum samples, the MILLIPLEX® Mouse Pituitary Panel (7-plex) (Milipore, #MPTMAG-49K) was used following the manufacturer's instructions. This multiplex kit allowed to quantify simultaneously 7 analytes, including adrenocorticotropic hormone (ACTH), brain-derived neurotrophic factor (BDNF), follicle-stimulating hormone (FSH), growth hormone (GH), prolactin, thyroid-stimulating hormone (TSH) and luteinizing hormone (LH). Serum samples were not diluted previously to the assay. The Luminex® analyzer (MAGPIX®) (ThermoFisher Scientific) was used to acquire the data and the ProcartaPlex Analysis software to analyze it.

8.11 Testosterone and estradiol assessment

For testosterone and estradiol assessment in mouse serum samples, the Estradiol and Testosterone ELISA kit (Demeditec, #DE2693 and #DE1559) were used in accordance with the manufacturer's instructions. Serum samples did not need dilution and 25 µl of each sample was used. For absorption measurement the Varioskan LUX (Thermo Scientific) was used at 450 nm. The data was analyzed using 4 parameter logistic curve fitting.

8.12 Urinary albumin assessment

Urinary albumin was assessed in mouse urinary samples using Albuwell™ M (Ethos Biosciences, #1011) in accordance with the manufacturer's instructions. Urine samples were diluted 1:4 following the protocol instructions. For absorption measurement the Varioskan LUX (Thermo Scientific) was used at 450 nm. The data was analyzed using 4 parameter logistic curve fitting.

9 Colorimetric and fluorometric assays

9.1 Urinary glucose assessment

Urinary glucose was assessed in mouse urinary samples using Mouse Glucose Assay Kit (Crystal Chem, #81692) in accordance with the manufacturer's instructions. Urine samples did not need dilution and 2 µl of each sample was used. For absorption measurement the Varioskan LUX (Thermo Scientific) was used at 450 nm. The data was analyzed using 4 parameter logistic curve fitting.

9.2 Urinary creatinine assessment

Urinary creatinine was assessed in mouse urinary samples using The Creatinine Companion (Creatinine Assay) (Ethos Biosciences, #1012) in accordance with the manufacturer's instructions. Urine samples did not need dilution and 2 µl of each sample was used. For absorption measurement the Varioskan LUX (Thermo Scientific) was used at 500 nm. The data was analyzed using the least squares regression line to obtain the concentration.

10 Glomerular filtration rate (GFR) assessment

GFR was performed by the Nephrology and kidney transplantation research group from VHIR.

GFR was measured in mice before and after treatment by transcutaneous measurement of FITC-sinistrin (MediBeacon, #29389090). Briefly, mice were anesthetized with isoflurane while a part of their back skin was shaved. A fluorescent signal measuring device (Transdermal GFR monitor, MediBeacon) was attached to the animal with an adhesive patch. The background signal of the skin was recorded for 5 min. Afterwards, an intravenous bolus of a FITC-sinistrin was administrated at a dose of 15mg/100g of body weight. Then the anesthesia was stopped, and the signal decay of the fluorescent agent was recorded during 1 h. The data obtained was analyzed with the specific software (MPD Studio Version RC15, MediBeacon) using a 3-compartment model to obtain FITC-sinistrin half-life, which was converted to µl/100g/min using a previously validated formula (Schreiber et al., 2012).

11 ^{1}H-NMR metabolomic characterization

11.1 Samples

Fecal pellets from wt and tgNM 6 and 18 m old animals were collected fresh in microcentrifuge tubes and snap frozen. Serum samples from wt and tgNM fasted animals at 18 m were collected. Both serum and fecal pellets were processed and analyzed by Biosfer Teslab (Reus, Spain).

11.2 Technical approach

Prior to analysis, aqueous and lipid extracts were obtained using the Folch method with slight modifications (Folch et al., 1957). Briefly, 1440 µL of dichloromethane: methanol (2:1, v/v) were added to 25 mg of previously lyophilized sample followed by three 5 min sonication steps with one shaking step in between. Next, 400 µL of ultrapure water was added, mixed, and centrifuged at 25100 G during 5 min at 4 °C. Aqueous and lipid extracts were transferred to a new microcentrifuge tube and completely dried in SpeedVac to achieve solvent evaporation and frozen at -80 °C until ^{1}H-NMR analysis. Aqueous extracts were reconstituted in a solution of 45 mM PBS containing 2.32 mM of Trimethylsilyl-propanoic acid (TSP) as a chemical shift reference and transferred into 5-mm NMR glass tubes. ^{1}H-NMR spectra were recorded

at 300 K operating at a proton frequency of 600.20 MHz using an Avance III-600 Bruker spectrometer. One-dimensional ^{1}H pulse experiments were carried out using the nuclear Overhauser effect spectroscopy (NOESY)-presaturation sequence to suppress the residual water peak at around 4.7 ppm and a total of 64 k data points were collected. The acquired spectra were phased, baseline-corrected and referenced before performing the automatic metabolite profiling of the spectra dataset through and adaptation of Dolphin (Gómez et al., 2014). Several database engines (BBioref AMIX database (Bruker), Chenomx and HMDB (Gómez et al., 2014), and literature (Vinaixa et al., 2010) were used for 1D-resonances assignment and metabolite identification. Lipid extracts were reconstituted in a solution of $CDCl_3$:CD_3OD:D_2O (16:7:1, v/v/v) containing Tetramethyl-silane (TMS) and transferred into 5-mm NMR glass tubes. ^{1}H-NMR spectra were recorded at 286 K operating at a proton frequency of 600.20 MHz using an Avance III-600 Bruker spectrometer. A 90° pulse with water pre-saturation sequence (ZGPR) was used. Quantification of lipid signals in ^{1}H-NMR spectra was carried out with LipSpin (Barrilero et al., 2018), an in-house software based on Matlab. Resonance assignments were done based on literature values (Vinaixa et al., 2010). The lipoprotein profile and the presence of glycosylated proteins were measured using the Liposcale® and the Glycoscale tests, respectively. The Liposcale® test is a CE marked and previously reported method based on 2D diffusion-ordered ^{1}H NMR spectroscopy to estimate the size (-Z) of the three main types of lipoproteins (very low-density lipoprotein (VLDL), low-density lipoprotein (LDL), and high-density lipoprotein (HDL)), and the concentration (-P) of particles of three subtypes (large, medium, and small sized particles) of the main types of lipoproteins, as well as the lipid content [cholesterol (-C) and triglycerides (-TG)] of the three main classes, together with intermediate-density lipoproteins (IDL). The glycoscale uses the same technique to determine the presence of glycosylated proteins in the serum. More specifically, it determines *N*-acetlyglucosamine and *N*-acetylgalactosamine bound to protein (GlycA), *N*-acetylneuraminic acid bound to protein (GlycB), and any of the three acetyl groups not bound to protein (GlycF). From these three peaks, it distinguishes their area (associated with concentration) and the ratio hight/width (describing the peak shape) (Amigó et al., 2021) .

12 Metagenomics

12.1 Samples

Frozen fecal samples from wt and tgNM females aged 1, 3, 6 and 18 m and from wt and tgNM males only at 6 m, were processed and analyzed by Microomics Systems S.L.

12.2 Technical approach

The composition and structure of the sampled microbial communities was assessed through the amplification and sequencing of the V3-V4 variable regions of the prokaryotic 16S rRNA gene. Briefly,

amplification was performed after 25 PCR cycles. In this procedure, positive and negative controls were used to ensure quality control. The positive control was a Mock Community control, which is a well-defined, accurately characterized community consisting of Gram-negative and Gram-positive bacteria and yeast with varying sizes and cell wall composition. The obtained libraries were sequenced using Illumina MiSeq™ System (300×2).

12.3 Bioinformatics processing and analysis

Raw demultiplexed forward and reverse reads were processed as shown in the following table (Table 9) using QIIME2 (Bolyen et al., 2019) and Dada2 software (Callahan et al., 2016):

Table 9. Dada2 software steps followed to demultiplex the samples.

Step	Software
Read trimming	Dada2
Quality filtering	Dada2
Denoising	Dada2
Pair- end merging	Dada2
Phylotype calling	Dada2

12.4 Statistical analysis

Alpha diversity comparisons were performed depending on the study, or using Kruskal-Wallis non-parametric test, or using a Generalized Linear Model. When using a Generalized Linear Model, the R package MASS v.7.3-54 (Venables, 2002) was used for richness and the R package glmmTMB v.1.1.8 (Brooks et al., 2017) was used for evenness. If a Generalized Linear Mixed Model was calculated, the R package NBZIMM v.1.0 (X. Zhang & Yi, 2020) was used for richness and the R package betareg v.3.1-4 (Cribari-Neto & Zeileis, 2010) for evenness. A significant threshold was set at 0.05.

Phylogenetic distances between operational taxonomic units (OTUs) were assessed using MAFFT (Katoh & Standley, 2013) and FastTree (Price et al., 2009) software's. OTUs and phylogenetic data were used to calculate the beta diversity metrics including Unweighted Unifrac, Weighted Unifrac, Jaccard and Bray-Curtis.

Beta diversity distance matrices were used to calculate principal coordinates analysis (PCoA) and to make ordination plots using R software package version 4.2.0. The significance of groups was tested using permutational multivariate analysis of variance (PERMANOVA) and ANOSIM tests. Permdisp test was used to identify location vs. dispersion effects (Anderson & Walsh, 2013). A significant threshold was set at 0.05. Taxonomic assignment of phylotypes was performed using a Bayesian Classifier (Q. Wang et al., 2007) trained with Silva database version 138 (99% OTUs full-length sequences) (Pruesse et al., 2007). Differential relative abundance of taxa was tested using different methods depending on the study: (i)

Kruskal Wallis non-parametric test with Conover's test with FDR Benjamini-Hochberg correction added for pairwaise comparison; (ii) Negative Binomial Generalized Linear Models. Either a Generalized Linear Model using the R package MASS v.7.3-54 (Venables and Ripley, 2002)or a Generalized Linear Mixed Model using the R package NBZIMM v.1.0 (X. Zhang & Yi, 2020) were calculated. A significant threshold was set at 0.05.

BiodiversityR v2.14-1, PMCMRplus v1.9.4, RVAideMemoire v0.9-8 and vegan v2.5-6 packages were used for the different statistical analysis carried out. The following figure (Figure 12) represents the steps of the analysis.

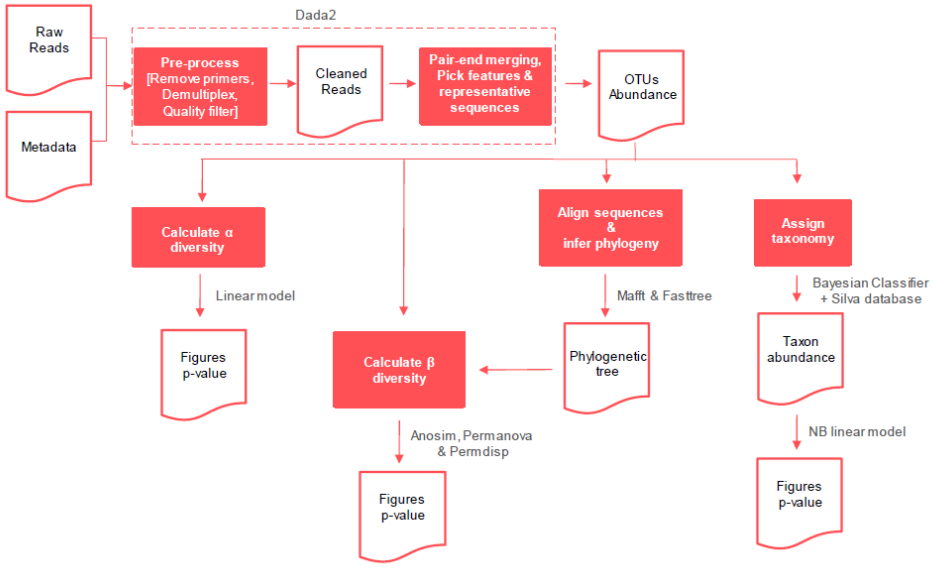

Figure 12. Sequence processing and analysis pipeline. The previously flowchart shows the steps of the analysis. Adapted from Microomics® (2024).

13 Transcriptomic microarrays

13.1 Transcriptomic microarrays

Duodenum RNA samples extracted from wt and tgNM female and male animals aged 6m that passed the RNA quality control, were analyzed in the High Technology Unit from Vall d'Hebron Research Institute (VHIR-UAT). Affymetrix GeneTitan microarray platform and the Genechip Mouse Clariom S array plate were used for this experiment. This array analyzed gene expression patterns on a whole-genome scale on a single array with probes covering many exons on the target genomes and thus permitting an accurate expression summarization at gene level. The starting material was 200ng of the total RNA of each sample. Quality of isolated RNA was first measured by Bioanalyzer Assay (Agilent). Briefly, sense ssDNA suitable for labelling was generated from total RNA with the GeneChip WT Plus Reagent Kit from Affymetrix

(Thermofisher - Affymetrix, UK) according to the manufacturer's instructions. Sense ssDNA was fragmented, labelled and hybridized to the arrays with the GeneChip WT Terminal Labeling and Hybridization Kit from the same manufacturer. Arrays plates were scanned to obtain .cel files. A first control of the technical quality was made with the software Expression Control.

13.2 Experimental design

The experimental conditions considered in this study were:

1. Genotype:
    i. tgNM mice samples
    ii. wt mice samples
2. Sex
    i. Female mice samples
    ii. Male mice samples

We used n=6 wt and n=6 tgNM females; n=5 wt and n=7 tgNM males.

13.3 Quality control

Bioinformatics analysis was performed by the Statistics and Bioinformatics Unit at Vall d'Hebron Research Institute (UEB-VHIR) using the statistical language R (R version 4.1.0 (2021-05-18), Copyright (C) 2021 The R Foundation for Statistical Computing), and the libraries developed for microarray analysis in the Bioconductor Project (Bioconductor).

Different types of quality controls (QC) were performed in the analysis, such as Intensity plots of the raw data, Principal Components Analysis (PCA), Heatmaps and Hierarchical clustering (Figure 13). However, in this study, all the samples were accepted for normalization process. First, arrays were normalized using the RMA method (Gentleman et al., 2005; Irizarry et al., 2003). The exon-level values were averaged to yield one expression value per gene. We found n=4 samples that clustered separately from the rest of the samples both in the PCA and hierarchical clustering analysis, suggesting higher differences in these samples. The Principal Variance Component Analysis (PVCA) was used to estimate the main sources of variability and identified the RIN and date of RNA extraction as main sources of "unwanted" variability. Therefore, these covariates were included in the linear model used for differential expression analysis (DEA).

13.4 Selection of differentially expressed genes (DEGs)

The analysis to select differentially expressed genes was based on adjusting a linear model with empirical Bayes moderation of the variance. This is a technique similar to ANOVA specifically developed for microarray data analysis by Gordon K Smyth (Smyth, 2004). A threshold of raw p-value <0.01 and absolute

logarithmic (FC)>|1.5| was applied to identify statistically DEGs. To obtain the Venn diagram and the Heatmaps, we also used genes with a raw p-value <0.01 and absolute logarithmic (FC)>|1.5|.

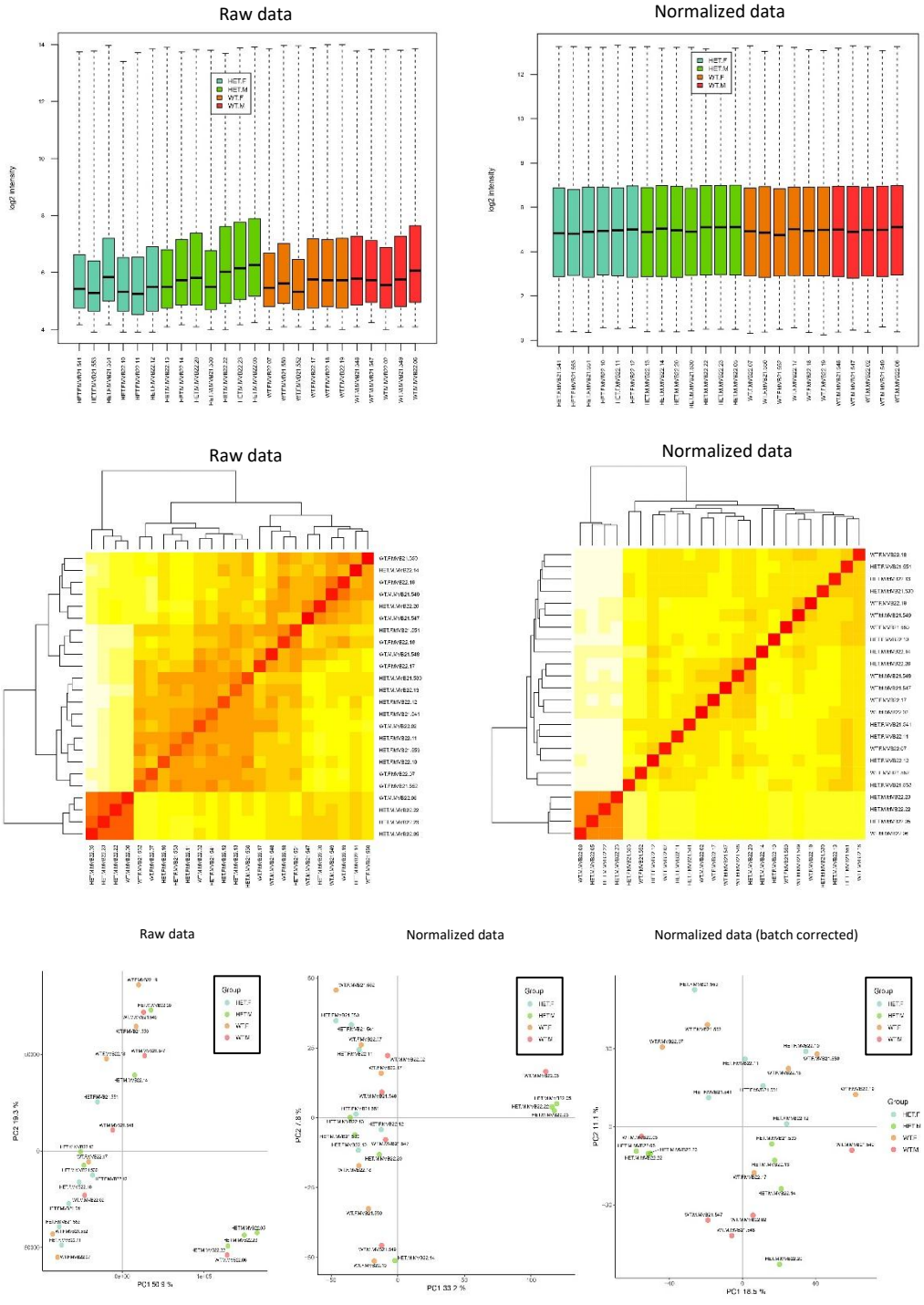

Figure 13. Transcriptomic microarray quality control analysis: Normalization and batch effect correction. a) Box plot summarizing signal intensity distributions of the arrays before (left) and after (right) normalization. Ideally, the boxes should exhibit similar positions and widths. b) Heatmap illustrating the distances between arrays and the hierarchical clustering of raw samples (left) and normalized samples (right). The color scale is selected to encompass

the range of distances present in the dataset. Patterns in this plot may indicate clustering of arrays due to biological, experimental or technical factors. Typically, distances between arrays should be uniform; significant deviations suggest outliers. Hierarchical clustering, represented by the lines grouping samples in the heatmap, calculates the distances between arrays to evaluate how the samples are grouped. c) PCA plots for raw data (left), normalized data (middle) and normalized data after batch effect correction (right).

14 Statistical analysis

Statistical analyses were performed using GraphPad Prism software (v10.2.2, GraphPad Software Inc, USA). The specific statistical test applied is detailed in the corresponding figure legends. Outlier values were identified by ROUT method and excluded from analyses when applicable. Data is represented as box-and-whisker plots showing the median, minimum, maximum and interquartile range. Given the relatively small samples sizes in our study, non-parametric tests were preferentially used. For comparisons between two groups, the Mann-Whitney test was employed. For comparisons involving two variables, a two-way ANOVA followed by a Fisher's least significant difference (LSD) post-hoc test for multiple comparisons was used. In all analyses, the null hypothesis was rejected at the 0.05 level ($p\text{-value} \leq 0.05$).

RESULTS

1 CHAPTER 1. Characterization of behavioral and GI alterations linked to age-dependent intracellular NM accumulation in mice.

1.1 TgNM basal colony characterization

As mentioned in the introduction, our group has generated and characterized a new tgNM mouse model that mimics the human age-dependent brain-wide distribution of NM within catecholaminergic regions in parallel to progressive human-like NM pigmentation. In this study, we aimed to assess the role of NM-mediated neurodegeneration in relation to gut dysbiosis and GI dysfunction in this novel mouse model. Accordingly, a new colony was established where mice were separated by genotype after weaning to prevent coprophagy between animals, which has been shown to normalize the microbiome of co-housed mice (Caruso et al., 2019). The life expectancy of tgNM mice was evaluated in both sexes, revealing a significant decrease in lifespan compared to their wt littermates (Figure 14 a, b) consistent with observations from the previous colony (Laguna et al., 2024).

Body weight, along with food and water intake, were monitored weekly from 3 m of age until euthanasia or natural death (Figure 14 e, h, k). TgNM animals exhibited an increased body weight over their lifespan. Notably, tgNM females began gaining weight significantly at 3 m of age (Figure 14 c), whereas tgNM males started to show body weight differences at 6 m of age (Figure 14 d). Moreover, analysis of feeding and water intake behavior indicated significantly elevated food and water consumption in tgNM females starting at 3 m (Figure 14 f, i). Although tgNM males seem to consume more food and water at 12 m of age, these differences were not statistically significant (Figure 14 g, j).

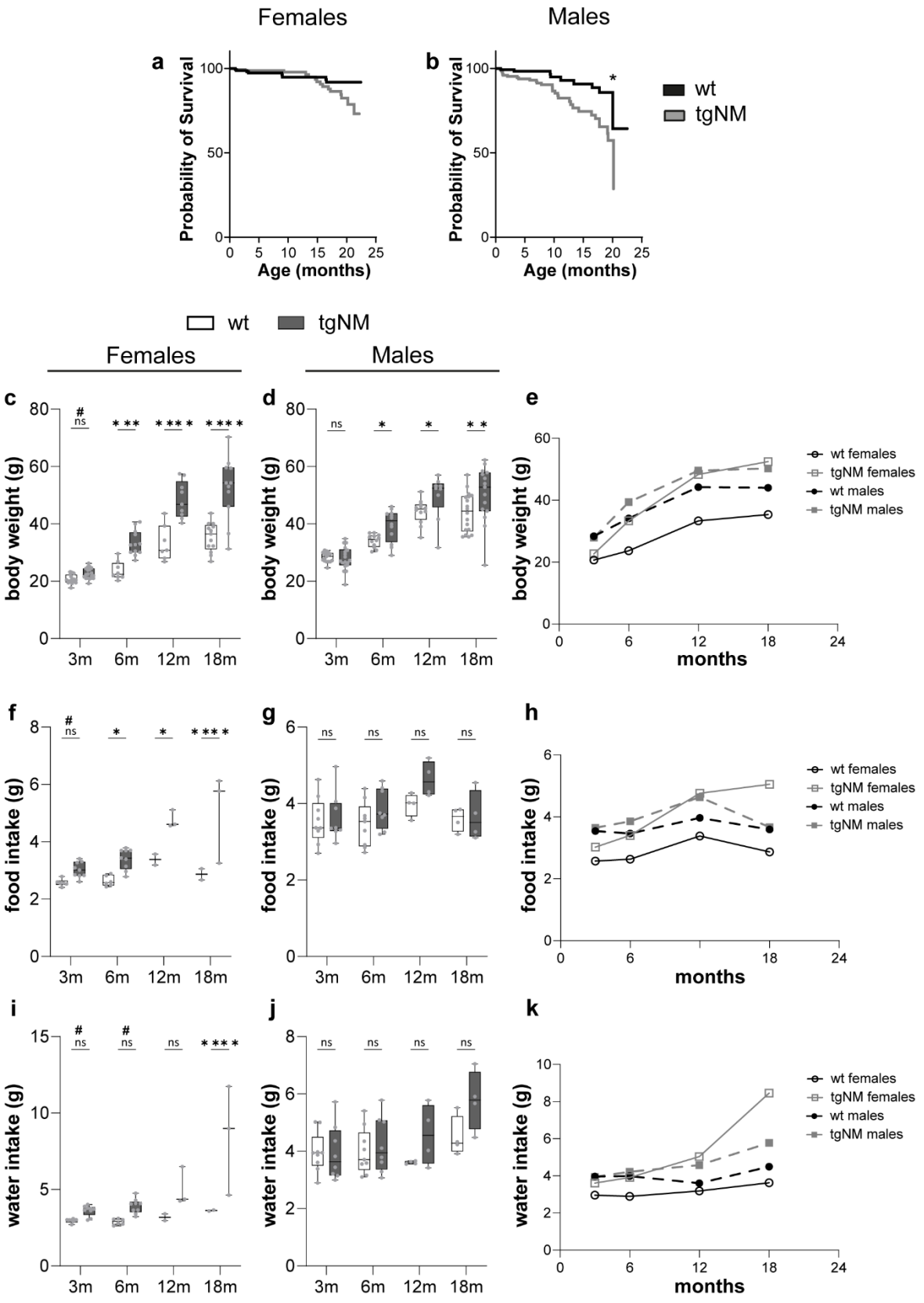

Figure 14. TgNM basal colony characterization. a-b) Survival analysis of tgNM **(a)** females and **(b)** males compared with their wt littermates. Animals used for experimental purposes were considered censored and natural deaths were considered as events. F: p≤0.1815, Log-rank (Mantel-Cox) (HR=1.779, 95%CI of ratio 0.7856 to 4.031) test and

Gehan-Breslow-Wilcoxon (HR=1.747, 95%CI of ratio 0.7706 to 3.961) test [n=153 (wt), n=156 (tgNM)]. M: p≤0.0019, Log-rank (Mantel-Cox) (HR=1.779, 95%CI of ratio 1.629 to 5.723) test and Gehan-Breslow-Wilcoxon (HR=2.726, 95%CI of ratio 1.449 to 5.128) test [n=125 (wt), n=146 (tgNM)]. **c-e)** Body weight of tgNM **(c)** females and **(d)** males compared to wt littermates at 3, 6, 12 and 18 m. *p≤0.05 compared to age-matched wt ((Uncorrected Fisher's LSD test). #p≤0.05 compared to age-matched wt (Mann-Whitney test). 3m [F: n=16(wt), n=19(tgNM); M: n=17(wt), n=18(tgNM)], 6m [F: n=8(wt), n=12(tgNM); M: n=12(wt), n=12(tgNM)], 12m [F: n=7(wt), n=9(tgNM); M: n=12(wt), n=9(tgNM)], 18m [F: n=13(wt), n=11(tgNM); M: n=18(wt), n=15(tgNM)]. **f-h)** Food intake of **(f)** females and **(g)** males compared to wt littermates at 3, 6, 12 and 18 m. **i-k)** Water intake of **(i)** females and **(j)** males compared to wt littermates at 3, 6, 12 and 18 m. *p≤0.05 compared to age-matched wt ((Uncorrected Fisher's LSD test). #p≤0.05 compared to age-matched wt (Mann-Whitney test). 3 & 6m [F: n=22/N=6 cages(wt), n=32/N=9 cages(tgNM); M: n=24/N=9 cages(wt), n=25/N=8 cages(tgNM)], 12m [F: n=7/N=2 cages(wt), n=9/N=3 cages(tgNM); M: n=12/N=3 cages(wt), n=10/N=4 cages(tgNM)], 18m [F: n=7/N=2 cages(wt), n=5/N=3 cages(tgNM); M: n=11/N=3 cages(wt), n=7/N=4 cages(tgNM)].

At the time of euthanasia, peripheral organs were evaluated in both wt and tgNM mice. At 6 m of age, tgNM females exhibited increased weights of several organs, including the GI tract, stomach, heart, kidneys, adrenal glands, liver, pancreas, inguinal white adipose tissue (WAT), gonadal WAT, renal WAT and brown adipose tissue (BAT) (Figure 15 a-m). In contrast, tgNM males at 6 m of age showed increased weights only in inguinal WAT, gonadal WAT, renal WAT and BAT (Figure 16 a-m). By 18 m of age, tgNM females continued to exhibit increased weights in the previously mentioned organs compared to wt littermates, with additional increases observed in the cecum. However, there were no significant differences in inguinal, gonadal and renal WAT's weight (Figure 15 a-m). Meanwhile, tgNM males at 18 m showed increased heart weight and decreased gonadal WAT weight compared to their wt counterparts (Figure 16 a-m). When comparing the age effect in tgNM females, we observed that the stomach, heart, kidneys, adrenal glands and BAT significantly increased their weight over time in tgNM females (Figure 15 b, d, e, f, m). In tgNM males, we observed increased over time weight only in the stomach and liver (Figure 16 b, g).

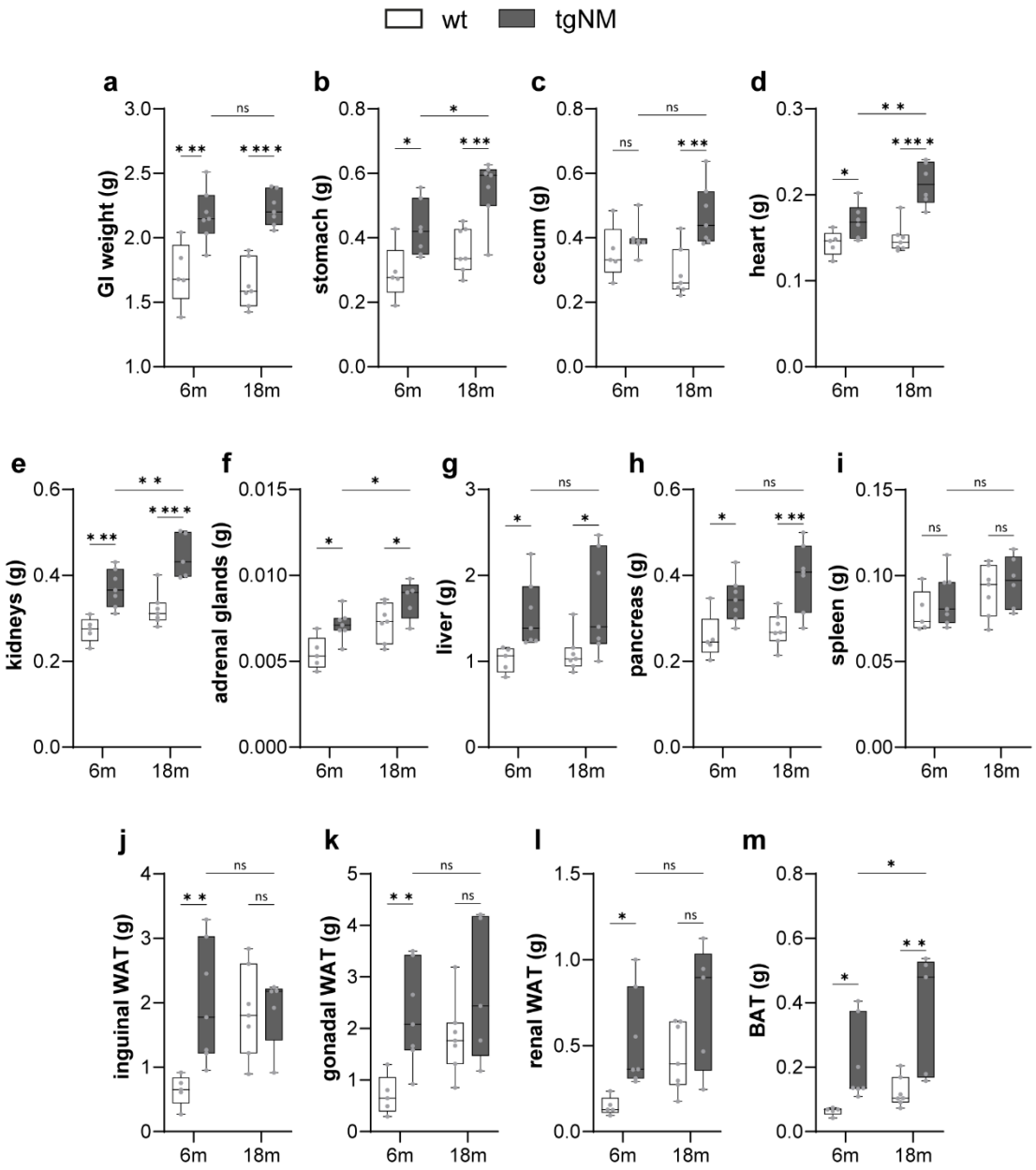

Figure 15. Females' peripheral organs weight characterization. a-m) Peripheral organ's weight (GI, stomach, cecum, heart, kidneys, adrenal glands, liver, pancreas, spleen, inguinal WAT, gonadal WAT, renal WAT and BAT) of wt and tgNM females compared with their wt littermates at 6m and 18m. *p≤0.05 compared to age-matched wt (Uncorrected Fisher's LSD test). 6m [n=5(wt), n=7(tgNM)], 18m [n=7(wt), n=5(tgNM)].

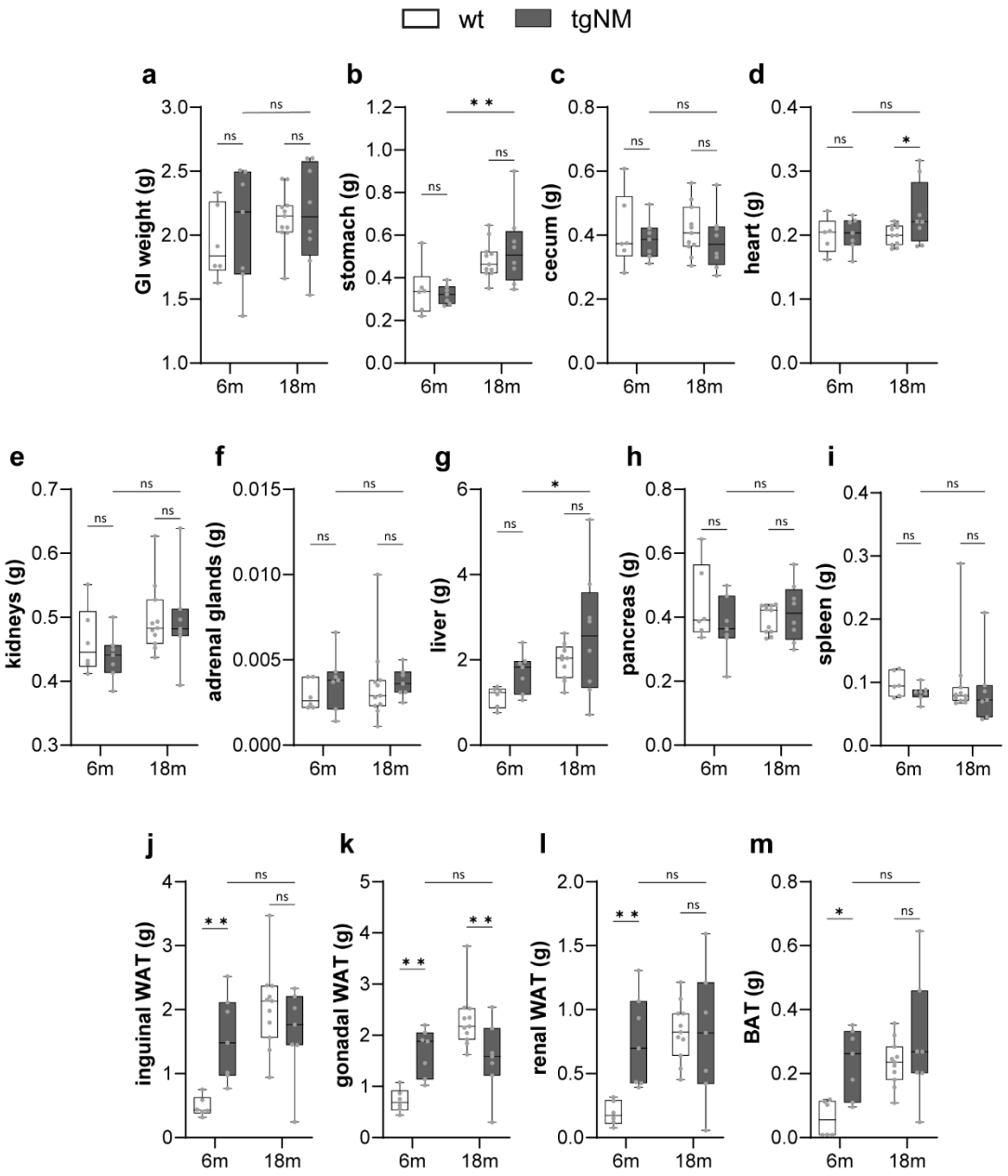

Figure 16. Males' peripheral organs weight characterization. a-m) Peripheral organ's weight (GI, stomach, cecum, heart, kidneys, adrenal glands, liver, pancreas, inguinal WAT, gonadal WAT, renal WAT and BAT) of wt and tgNM males compared with their wt littermates at 6m and 18m. *p≤0.05 compared to age-matched wt (Uncorrected Fisher's LSD test). 6m [n=6(wt), n=7(tgNM)], 18m [n=11(wt), n=7(tgNM)].

1.2 Sensorimotor behavioral assessment

The sensorimotor capacities of tgNM mice at different time points (3 m, 6 m, 12 m, and 18 m) were evaluated in correspondence with the progressive NM accumulation in the primary affected nuclei of the model, specifically the SNpc, VTA, and LC.

Female tgNM mice exhibited impaired motor balance and coordination as early as 3 m, demonstrated by their increased time crossing the beam compared to wt counterparts (Figure 17 a). This difference was not observed in males, where both genotypes required similar times to cross the beam at all ages (Figure 17 b). Additionally, we evaluated the mice's ability to grip and navigate a pole to descend to their home cage using the Pole Test Consistent with previous findings, 6 m old tgNM females exhibited impaired locomotion, requiring more time to maneuver themselves atop the pole and descend (Figure 17 c). This impairment was not observed in tgNM males (Figure 17 d). Furthermore, the Marble Burying Test revealed impaired burying behavior in tgNM females, indicated by a reduced number of buried marbles (Figure 17 e), but again no differences were reported in tgNM males compared to wt littermates (Figure 17 f). However, the Grip Strength Test did not reveal any alterations in forepaw strength in either sex at any evaluated time point (Figure 17 g, h).

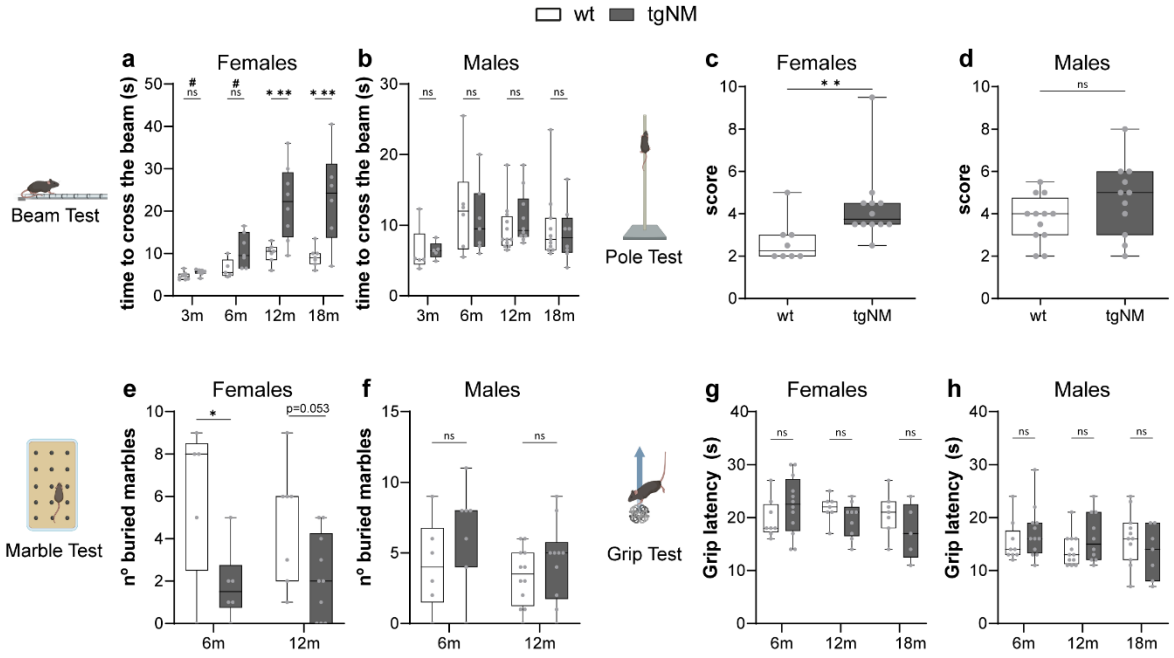

Figure 17. Motor behavioral characterization. a) Females and **b)** Males Beam test; Average time to cross the beam after two trials at 3, 6, 12 and 18 m. #p≤0.05 compared to age-matched wt (Mann-Whitney test). *p≤0.05 compared to age-matched wt (Uncorrected Fisher's LSD test). 3 m [F: n=8(wt), n=7(tgNM); M: n=5(wt), n=5(tgNM)], 6 m [F: n=5(wt), n=7(tgNM); M: n=6(wt), n=7(tgNM)], 12 m [F: n=7(wt), n=8(tgNM); M: n=12(wt), n=10(tgNM)], 18 m [F: n=7(wt), n=6(tgNM); M: n=11(wt), n=8(tgNM)]. **c)** Females and **d)** Males Pole test; Score average after two trials at 6 m. *p≤0.05 compared to age-matched wt (Mann-Whitney test). 6 m [F: n=8(wt), n=12(tgNM); M: n=12(wt), n=10(tgNM)]. **e)** Females and **f)** Males Marble burying test. Nº of buried marbles in 10 min at 6 m and 12 m. *p≤0.05 compared to age-matched wt (Uncorrected Fisher's LSD). 6 m [F: n=5(wt), n=7(tgNM); M: n=6(wt), n=7(tgNM)], 12 m [F: n=7(wt), n=10(tgNM); M: n=12(wt), n=10(tgNM)]. **g)** Females and **h)** Males Grip test; Quantification of grip latency time at 6 m, 12 m and 18 m. Uncorrected Fisher's LSD test, compared tgNM to age-matched wt, not significant. 6 m [F: n=8(wt), n=12(tgNM); M: n=9(wt), n=12(tgNM)], 12 m [F: n=7(wt), n=9(tgNM); M: n=12(wt), n=10(tgNM)], 18 m [F: n=7(wt), n=5(tgNM); M: n=11(wt), n=7(tgNM)].

To assess olfactory discrimination, we tested tgNM mice's ability to detect a lemon essence starting at 6 m. The results indicated impaired olfactory capacity in tgNM females compared to wt littermates at 18 m old (Figure 18 a). No differences were detected in tgNM males at any time point (Figure 18 b). In the step-down test, tgNM males presented altered memory consolidation of an aversive stimulus since 6 m old, (Figure 18 d). However, tgNM females showed impaired memory consolidation at 18 m old (Figure 18 c), as previously reported by our group (Laguna et al., 2024). Considering the potential presence of depressive-like behavior reported previously by our group, we evaluated the total immobilization time and the latency to surrender and using the Tail Suspension Test. We observed significantly increased immobilization time in tgNM females at 6 m, however this significance was not observed at older time points (Figure 18 e). No significant differences in immobilization time were observed in tgNM males at any time point (Figure 18 f). Moreover, no significant changes were detected in the latency to surrender in tgNM females (Figure 18 g). However, at 12 m, tgNM males present significantly reduced time to surrender compared to their wt counterparts (Figure 18 h). A significant reduction in vocalizations was recorded in tgNM mice, both females and males, starting at 3 m (Figure 18 I, j), a phenotype linked to early pre-motor symptoms such as cranial sensorimotor deficits in α-synuclein tg mice (Grant et al., 2014).

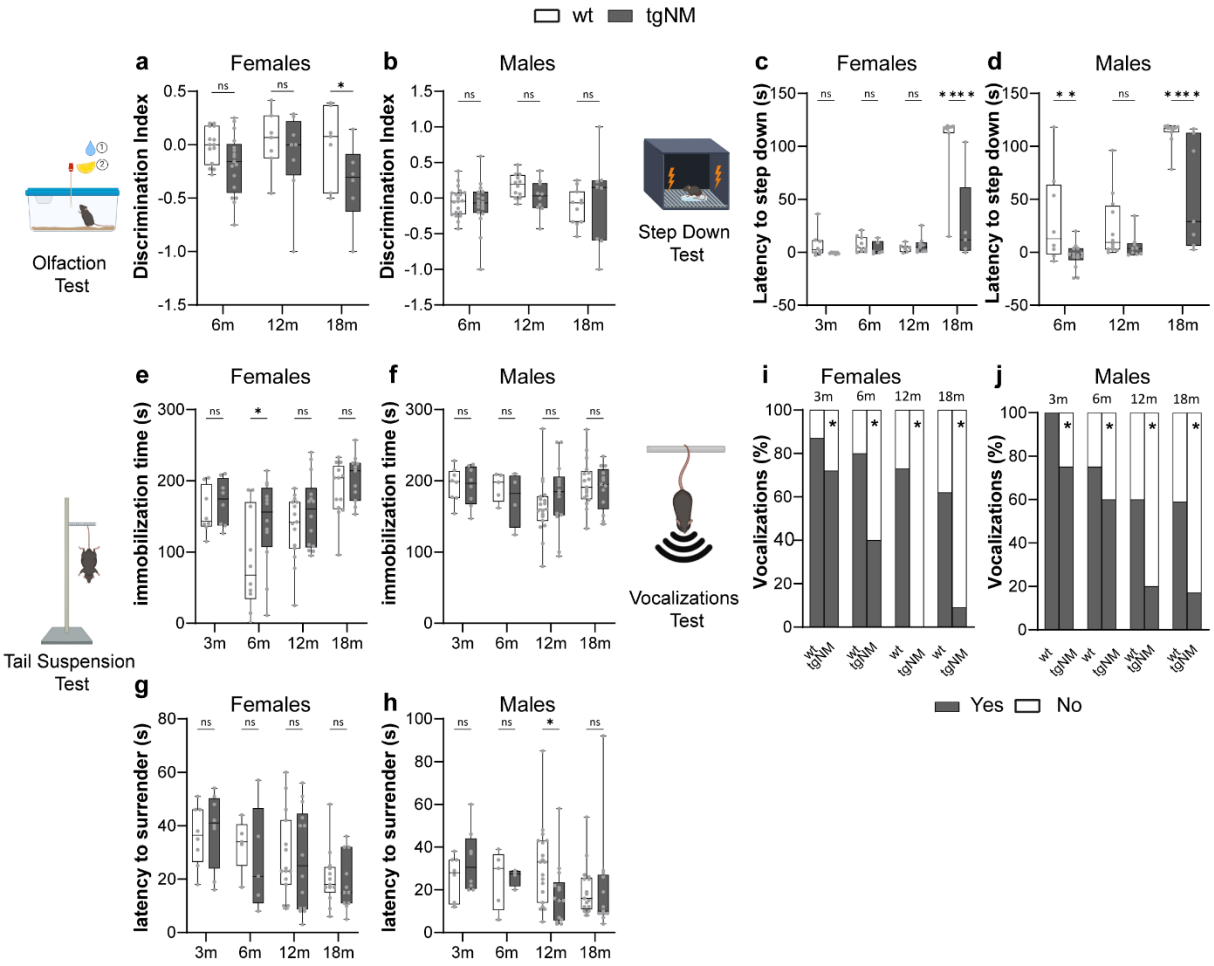

Figure 18. Olfactory and emotional behavioral characterization. a) Females and **b)** Males Olfaction test. Quantification of the DI (time on lemon vs time on water) at 6 m, 12 m and 18 m. *p≤0.05 compared to age-matched wt (Uncorrected Fisher's LSD test). 6 m [F: n=14(wt), n=17(tgNM); M: n=20(wt), n=18(tgNM)], 12 m [F: n=7(wt), n=9(tgNM); M: n=12(wt), n=10(tgNM)], 18 m [F: n=7(wt), n=6(tgNM); M: n=11(wt), n=8(tgNM)]. **c)** Females and **d)** Males Step down test; quantification of the latency to step down the platform on the second day without electric shock at 3 m (only females), 6 m, 12 m and 18 m. *p≤0.05 compared to age-matched wt (Uncorrected Fisher's LSD test). 3m [F: n=8(wt), n=7(tgNM)], 6 m [F: n=10(wt), n=6(tgNM); M: n=8(wt), n=14(tgNM)], 12 m [F: n=7(wt), n=9(tgNM); M: n=12(wt), n=9(tgNM)], 18 m [F: n=7(wt), n=5(tgNM); M: n=11(wt), n=7(tgNM)]. **e, g)** Females and **f, h)** Males Tail suspension test; quantification of the immobilization time and the latency to surrender at 3 m, 6 m, 12 m and 18 m. *p≤0.05 compared to age-matched wt (Uncorrected Fisher's LSD test). 3 m [F: n=8(wt), n=8(tgNM); M: n=8(wt), n=8(tgNM)], 6 m [F: n=5(wt), n=5(tgNM); M: n=5(wt), n=4(tgNM)], 12 m [F: n=15(wt), n=14(tgNM); M: n=19(wt), n=14(tgNM)], 18 m [F: n=13(wt), n=11(tgNM); M: n=17(wt), n=13(tgNM)]. **i)** Females and **j)** Males Vocalizations test; quantification of vocalizations at 3 m, 6 m, 12 m and 18 m. *p≤0.05 compared to age-matched wt (Mann Whitney test). 3 m [F: n=8(wt), n=8(tgNM); M: n=5(wt), n=5(tgNM)], 6 m [F: n=5(wt), n=5(tgNM); M: n=5(wt), n=4(tgNM)], 12 m [F: n=11(wt), n=9(tgNM); M: n=10(wt), n=10(tgNM)], 18 m [F: n=13(wt), n=11(tgNM); M: n=17(wt), n=18(tgNM)].

Overall, our results demonstrate that progressive NM production and accumulation in SNpc, VTA and LC from tgNM mice housed without coprophagy between genotypes, is associated with PD-like sensorimotor deficits as reported in Laguna, et al., 2024 for mice housed without considering coprophagy between genotypes. We showed previously that these changes occur in the absence of neurodegeneration, thereby modeling prodromal/early PD stages (Laguna et al., 2024). Remarkably, most of the studied sensorimotor capacities were impaired exclusively in tgNM female mice and not in their male littermates.

1.3 GI function assessment

Alterations in the DVC of tgNM mice were reported by Laguna et al. 2024, including a decrease in pigmented TH-positive cells, an increase in eNM debris, microglial activation and the presence of LB-like inclusions. Following the characterization of the behavioral phenotype in both wt and tgNM mice, we proceeded to assess the GI phenotype of tgNM animals at the same key time points (3 m, 6 m, 12 m and 18 m). This approach allowed us to investigate whether these neurodegenerative changes in the DVC correlate with or potentially contribute to any observed alterations in GI function over time.

1.3.1 GI function assessment in vivo

We started by analyzing GI functionality through the evaluation of total intestinal transit time, which was measured by the time a red dye administered by oral gavage traversed the GI tract and was excreted in feces. By 6 m, tgNM females exhibited a reduced intestinal transit time compared to their wt littermates when the time to produce a red fecal pellet was normalized by GI length (Figure 19 a). However, no changes were observed in tgNM males at any time point (Figure 19 b).

Given that increased transit time can influence pellet expulsion and knowing that colonic propulsion and defecation are regulated by CNS inputs (Corsetti et al., 2019), we subsequently measured the total fecal

output. TgNM females presented increased defecation within one-hour period as early as 3 m (Figure 19 c), while no changes were observed in the number of fecal pellets in tgNM males at any time point (Figure 19 d). However, the total transportation capacity of the small intestine, evaluated as propulsion rate, showed no differences in tgNM females at 18 m (Figure 19 e). Conversely, 18 m tgNM male mice presented increased small intestine transport compared to wt littermates (Figure 19 f).

Stool consistency was initially assessed using the Bristol stool chart, with both tgNM and wt animals displaying similar stool shapes and consistency at 6 and 18 m, categorized as types 3 and 4 (Figure 19 g). Nonetheless, fecal pellets from tgNM females contained increased water content starting at 3 m compared to wt females (Figure 19 h). TgNM males also showed increased fecal water content beginning at 6 m of age (Figure 19 i).

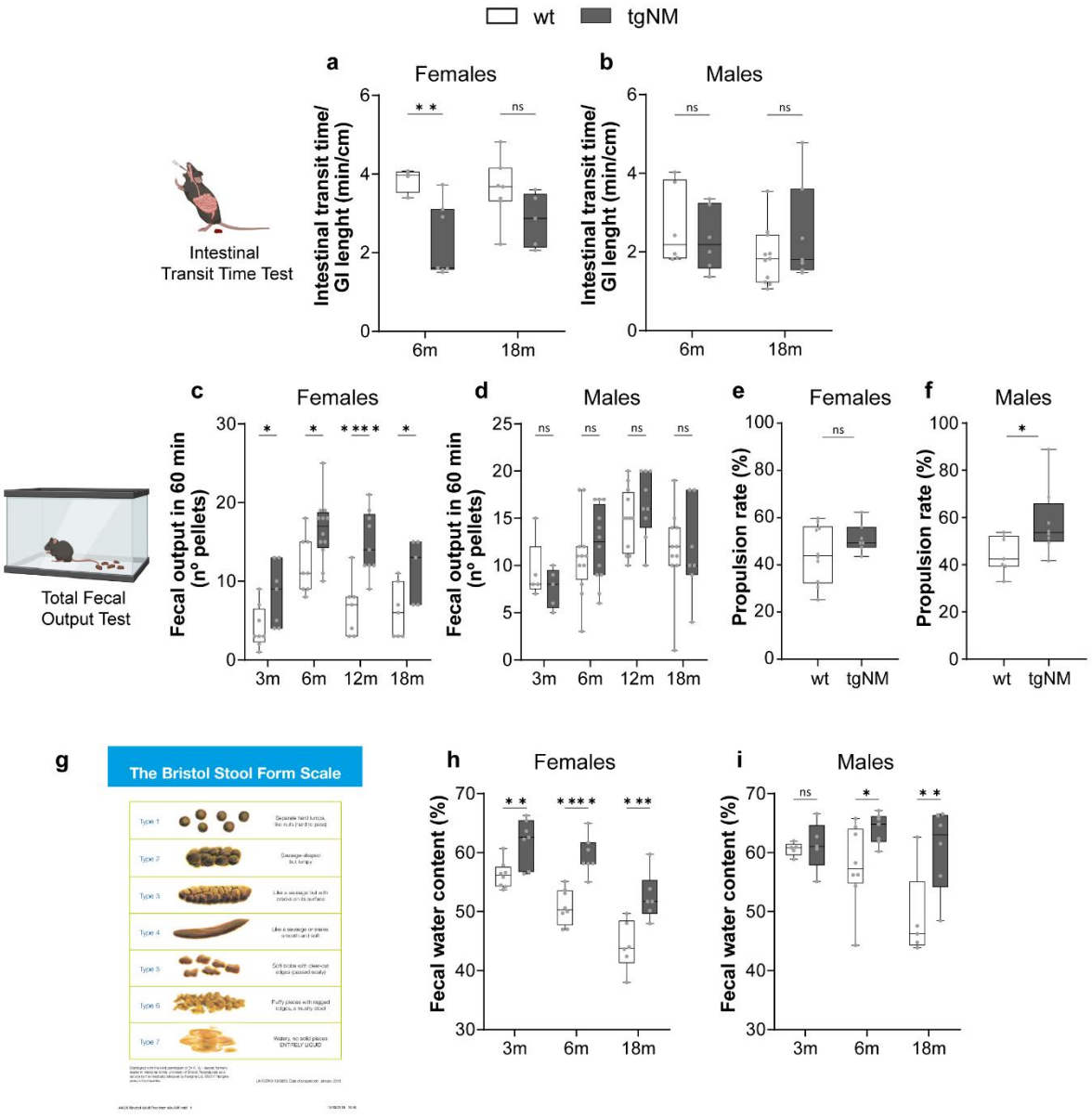

Figure 19. GI behavioral characterization. a) Females and **b)** Males Total intestinal transit time; Time to produce a red pellet divided by the GI tract length (min/cm) at 6 and 18 m. *p≤0.05 compared to age-matched wt (Uncorrected Fisher's LSD test). 6 m [F: n=4(wt), n=7(tgNM); M: n=6(wt), n=6(tgNM)], 18 m [F: n=7(wt), n=5(tgNM); M: n=11(wt), n=7(tgNM)]. **c)** Females and **d)** Males Total fecal output; nº of fecal pellets produced in 1 h at 3, 6, 12 and 18 m. *p≤0.05 compared to age-matched wt (Uncorrected Fisher's LSD). 3 m [F: n=8(wt), n=7(tgNM); M: n=5(wt), n=5(tgNM)], 6 m [F: n=8(wt), n=12(tgNM); M: n=12(wt), n=12(tgNM)], 12 m [F: n=7(wt), n=9(tgNM); M: n=12(wt), n=9(tgNM)], 18 m [F: n=7 (wt), n=5(tgNM); M: n=11(wt), n=7(tgNM)]. **e)** Females and **f)** Males Propulsion rate; total transportation capacity of the small intestine measured in % at 18 m. *p≤0.05 compared to age-matched wt (Mann-Whitney test). 18 m [F: n=10(wt), n=7(tgNM); M: n=7(wt), n=8(tgNM)]. **g)** Bristol Scale adapted from (Lewis & Heaton, 1997). **h)** Females and **i)** Males Fecal water content in % measured from collected pellets for a period of 10 min at 3, 6 and 18 m. *p≤0.05 compared to age-matched wt (Uncorrected Fisher's LSD). 3 m [F: n=8(wt), n=7(tgNM); M: n=5(wt), n=5(tgNM)], 6 m [F: n=8(wt), n=7(tgNM); M: n=8(wt), n=7(tgNM)], 18 m [F: n=6 (wt), n=6(tgNM); M: n=5(wt), n=6(tgNM)].

When studying their gut anatomy, tgNM females presented longer GI tracts as early as 6 m (Figure 20 a). Specifically, measurements of the small intestine (from pylorus to cecum) and colon indicated extended lengths in tgNM females at 18 m (Figure 20 b, c). No significant anatomical differences were observed in tgNM males compared to their wt counterparts at any time point (Figure 20 d, e, f).

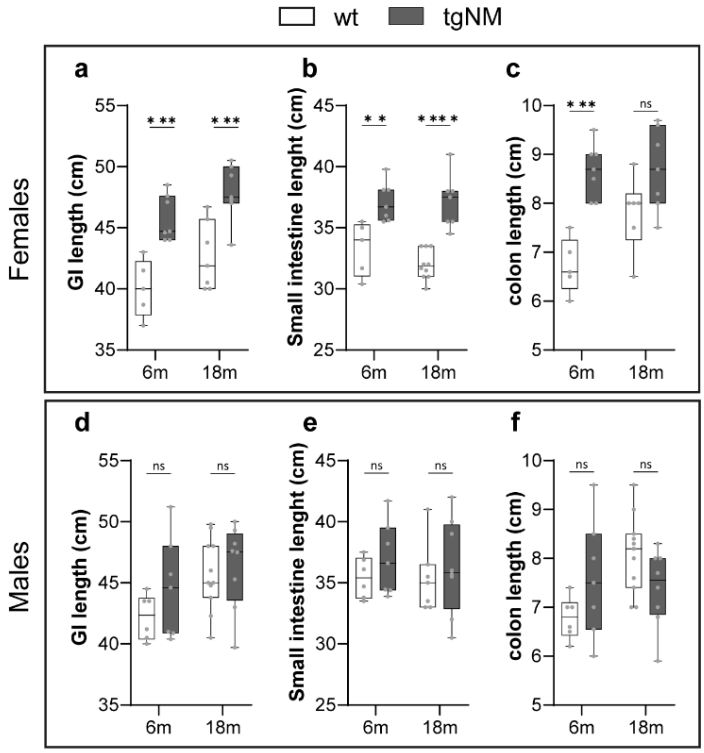

Figure 20. GI measurements. a-f) GI length, small intestine length and colon length at 6 and 18 m of females **(a, b, c)** and males **(d, e, f)** in cm. *p≤0.05 compared to age matched wt (Uncorrected Fisher's LSD). GI length: 6 m [F: n=5(wt), n=7(tgNM); M: n=6(wt), n=7(tgNM)], 18 m [F: n=7 (wt), n=7(tgNM); M: n=11(wt), n=8(tgNM)]; Small intestine length: 6 m [F: n=5(wt), n=7(tgNM); M: n=6(wt), n=7(tgNM)], 18 m [F: n=10 (wt), n=7(tgNM); M: n=7(wt), n=8(tgNM)]; Colon length: 6 m [F: n=5(wt), n=7(tgNM); M: n=6(wt), n=7(tgNM)], 18 m [F: n=6 (wt), n=7(tgNM); M: n=11(wt), n=8(tgNM)].

In summary, our model does not exhibit gross signs of constipation, despite constipation being a common GI symptom in PD patients (Xu et al., 2022). Notably, while DVC neurodegeneration in this model has been reported to begin around 8-12 m of age, tgNM females display altered GI function compared to wt littermates as early as 3 m. This suggests that GI dysfunction in tgNM females may appear before DVC neuronal loss.

1.3.2 Gut motility assessment *ex vivo*

Gut motility is regulated by a complex interplay of both central and peripheral reflexes, along with descending modulation from the brain-gut axis (Kellow et al., 2006). Effective communication between different regions of the GI tract is maintained through the longitudinal transmission of myogenic and neurogenic signals, which coordinate smooth muscle contractions and ensure efficient intestinal transit. To better understand the GI function of tgNM females, we specifically explored their gut motility, aiming to characterize any alterations that may explain the observed results.

First, we studied the myogenic activity of the circular and longitudinal muscle layers in the proximal colon of 6 m old tgNM females by assessing tone (mg), frequency (contractions/min), and amplitude (mg) (Figure 21 a). No significant differences were observed in the spontaneous phasic contractions between tgNM females and their wt littermates (Figure 21 b, c, d, e, f, g).

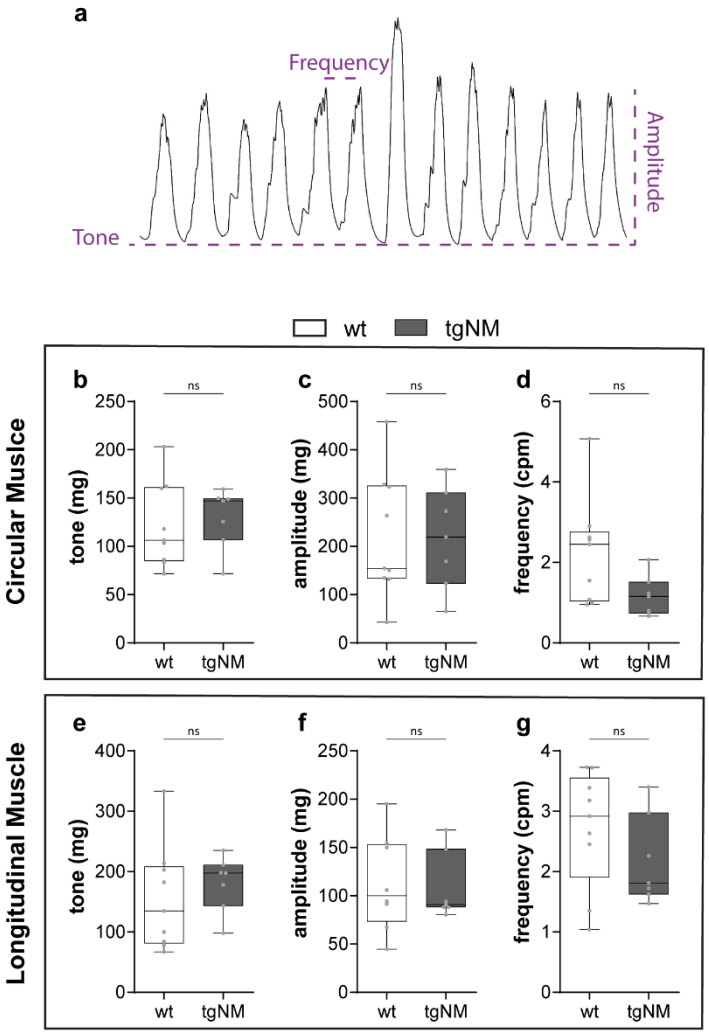

Figure 21. Myogenic activity from the circular and longitudinal colonic muscle. a) Recording representation showing spontaneous phasic contractions. **b-d)** Myogenic basal activity measurements (tone, amplitude and frequency) of the circular colonic muscle. Mann Whitney tests tgNM compared to age-matched wt not significant. 6 m [F: N=9(wt) n=36, N=7(tgNM) n=27]. **e-g)** Myogenic basal activity measurements (tone, amplitude and frequency) of the longitudinal colonic muscle. Mann Whitney tests tgNM compared to age-matched wt not significant. 6 m [F: N=8(wt) n=29, N=7(tgNM) n=26].

Next, we assessed the neural-mediated excitatory response under non-nitrergic and non-purinergic (NNNP) conditions by blocking the main inhibitory neurotransmitters. When EFS was applied at increasing voltages (Figure 22 a), no EFS-induced contractions were observed (data not shown), likely due to experimental limitations rather than impairment in cholinergic response. Consequently, we further examined excitatory neurotransmission by adding different CCH concentrations to achieve the 100% of cholinergic contractile response. The muscarinic agonist increased the frequency of contractions in both circular and longitudinal muscle layers, yet the contractile response did not differ significantly between tgNM females and wt littermates (Figure 22 b, c).

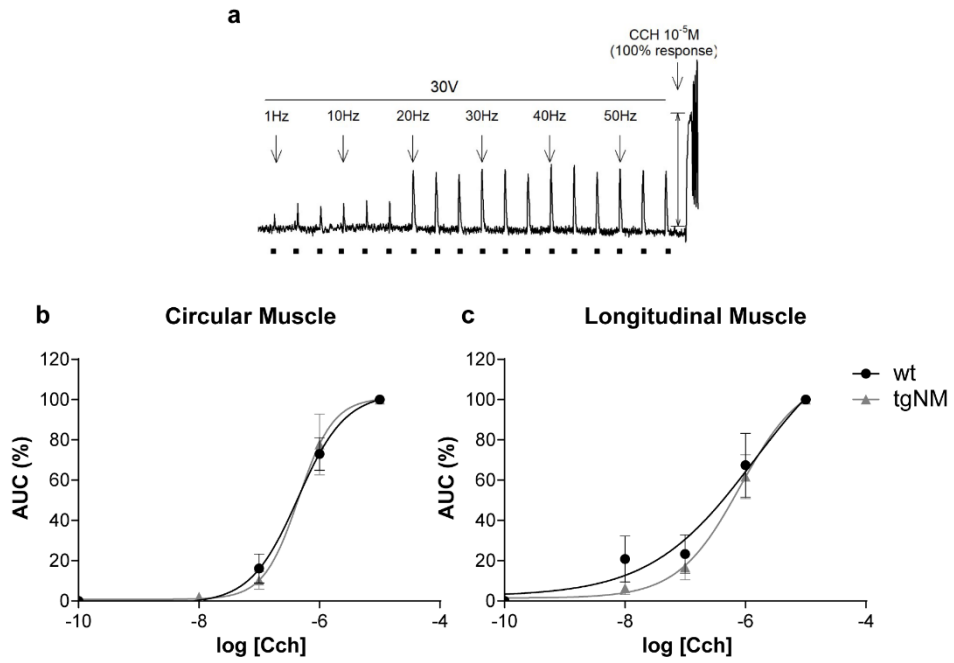

Figure 22. Neural-mediated excitatory responses in the circular and longitudinal muscle. a) Recording representation showing the protocol of EFS in NNNP conditions and CCH-induced contractions. **b)** Change in AUC during CCH addition in the circular colonic muscle. Data were normalized to Basal AUC (Basal activity = 100 ± SEM). Šídák's multiple comparisons test tgNM compared to age-matched wt not significant. 6 m [F: N=7(wt) n=9, N=6(tgNM) n=8]. **c)** Change in AUC during CCH addition in the longitudinal colonic muscle. Data were normalized to Basal AUC (Basal activity = 100 ± SEM). Šídák's multiple comparisons test tgNM compared to age-matched wt not significant. 6 m [F: N=6(wt) n=6, N=4(tgNM) n=4].

We then investigated neural-mediated inhibitory responses under NANC conditions by blocking the main excitatory neurotransmitters. EFS application induced relaxation (on-response) followed by a contraction (off-response) due to smooth muscle depolarization post-stimulus. Both relaxation and off-contraction were voltage-dependent (Figure 23 a). Under NANC conditions, these responses are typically inhibited by incubating tissues with L-NNA (1nM) and MRS2179 (10 µM) (Gallego et al., 2008), indicating that the on-response and off-response are associated with the release of NO and adenosine triphosphate (ATP) by inhibitory neurons (Traserra et al., 2024). However, we found no differences in the neural-mediated inhibitory response, as both relaxation and off-contraction were similar in the circular and longitudinal colonic muscles of tgNM females compared to wt littermates (Figure 23 b, c).

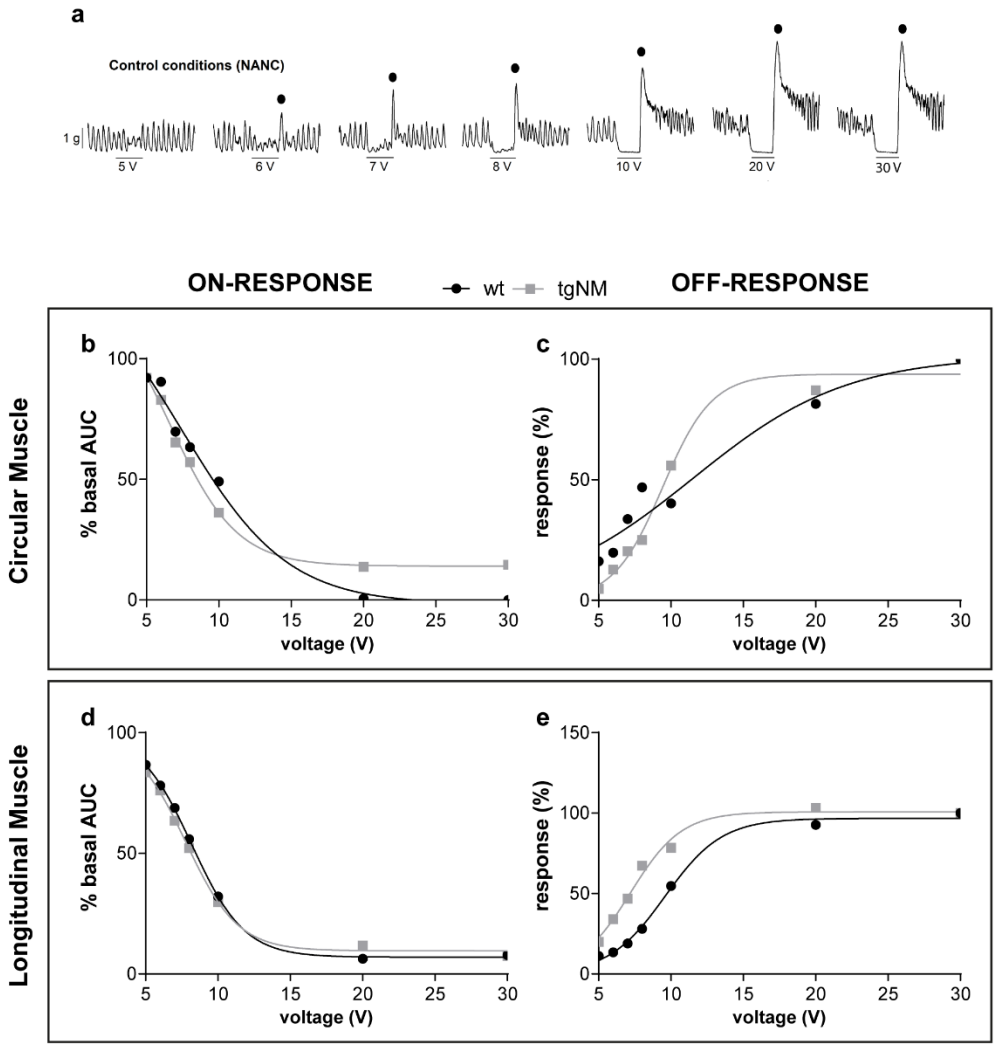

Figure 23. Neural-mediated inhibitory responses in the circular and longitudinal muscle. a) Recording representation showing the protocol of EFS in NANC conditions. **b, c)** Change in AUC during EFS (on-response) and after EFS (off-response) in the circular colonic muscle. Data were normalized to Basal AUC (Basal activity = 100 ± SEM). Šídák's multiple comparisons test tgNM compared to age-matched wt not significant. 6 m [F: N=8(wt) n=13, N=6(tgNM) n=12]. **d, e)** Change in AUC during EFS (on-response) and after EFS (off-response) in the longitudinal colonic muscle. Data were normalized to Basal AUC (Basal activity = 100 ± SEM). Šídák's multiple comparisons test tgNM compared to age-matched wt not significant. 6 m [F: N=8(wt) n=13, N=7(tgNM) n=18].

In summary, these results demonstrate that neuromuscular function, along with cholinergic and nitrergic activities, remain intact in the colonic muscles of 6 m old tgNM females, with no significant alterations in excitatory or inhibitory responses.

1.3.3 Expression of GI motility neuromodulators

To further investigate potential neuromodulatory changes regulating GI motility (Blin et al., 2023), we aimed to determine the expression of two key enzymes, ChAT and nNOS, that are critical for the synthesis

of ACh and NO, respectively. Therefore, we examined the expression of ChAT and nNOS in the myenteric plexus of duodenal and colonic samples from 18 m old tgNM and wt females (Figure 24 a, b).

Our analysis revealed that the number of Hu-positive cells, as a general marker of neurons, was unchanged in both the duodenum and the proximal colon myenteric plexuses from tgNM females compared to wt littermates (Figure 24 c, f), indicating no general neuronal loss in these regions. Additionally, we observed no significant differences in the proportion of ChAT and nNOS-positive neurons between tgNM and wt females in either the duodenum or proximal colon (Figure 24 d, e, g, h), suggesting that cholinergic and nitrergic neuronal populations remain stable in these regions. Parallel stereological cell counts of ChAT-positive neurons in the DVC further demonstrated no decrease in tgNM mice at any time point analyzed (Laguna et al., 2024).

These findings indicate that, at 18 m, tgNM females do not exhibit alterations in the expression of ChAT or nNOS in the myenteric plexus of the duodenum or colon, supporting preserved cholinergic and nitrergic functions in these regions.

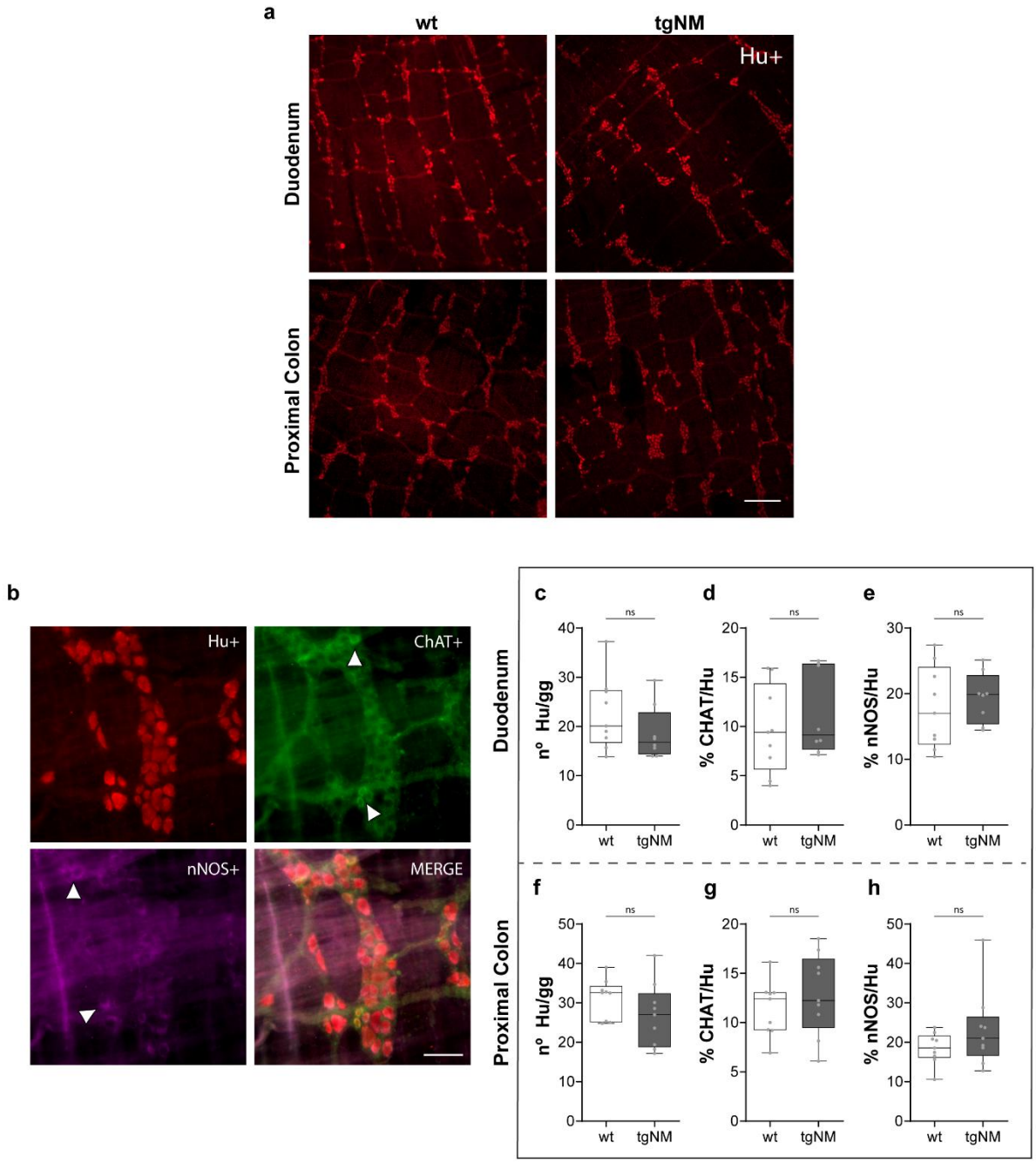

Figure 24. Characterization of the enteric neuronal phenotype. a) Myenteric plexus of duodenal and proximal colon representative images showing Hu-positive neurons (red) from wt and tgNM females at 18 m. Scale bar represent 200 µm. **b)** Representative images from the myenteric plexus of a proximal colon section of an 18 m old wt female at higher magnification. Immunolabeled by Hu (red), ChAT (green) and nNOS (purple). Scale bar represents 50 µm. White arrows point out ChAT-positive and nNOS-positive neurons. **c)** Quantification of Hu-positive neurons per ganglion (gg) in duodenum and **f)** proximal colon myenteric plexus of tgNM and wt females at 18 m. **d)** Quantification of the proportion of ChAT-positive neurons per Hu-positive neurons per ganglion (% ChAT+/Hu+) of duodenum and **g)** proximal colon myenteric plexus of tgNM and wt females at 18 m. **e)** Quantification of the proportion of nNOS-positive neurons per Hu-positive neurons per ganglion (% nNOS+/Hu+) of duodenum and **h)** proximal colon myenteric plexus of tgNM and wt females at 18 m. Mann Whitney tests tgNM compared to age-matched wt not significant. [D: n=9(wt), n=8(tgNM), C: n=9(wt), n=9(tgNM)].

1.3.4 Assessment of neurotransmitter levels

The ENS innervates the GI tract via a complex network of sensory, motor and interneurons playing a critical role in coordinating gut function and homeostasis (Corsetti et al., 2019; Mertz, 2002). Neurotransmitters such as ACh, DA, NE and 5-HT are essential for regulating processes including blood flow, gut motility, nutrient absorption, GI immunity, and microbiome interactions (Mittal et al., 2017). To further explore the impact of these neurotransmitters, we characterized key medullary-related neurotransmitter systems in the same duodenal and proximal colon samples from 6 m and 18 m old animals using UPLC-MS/MS.

1.3.4.1 The cholinergic system

The cholinergic system is crucial for regulating intestinal motility by influencing smooth muscle cells, and it also plays a key role in mediating neuroimmune communication with the CNS (Jonge, 2013). This system is composed of ACh, cholinergic receptors, ChAT enzyme, and acetylcholinesterase (AChE) enzyme (Uwada et al., 2023). While ACh is predominantly found in the GI tract, it has also been detected in non-neural cells and microbial communities, underscoring its diverse functional roles in gut physiology (Halder & Lal, 2021).

Although our previous analyses did not reveal significant differences in the number of ChAT-positive neurons, we detected reduced levels of ACh in the duodenum at 18 m, as well as in the proximal colon at both 6 m and 18 m in tgNM females (Figure 25 b). In contrast, tgNM males showed no significant differences in ACh levels compared to their wt littermates at any time point or in any sample type (Figure 25 c).

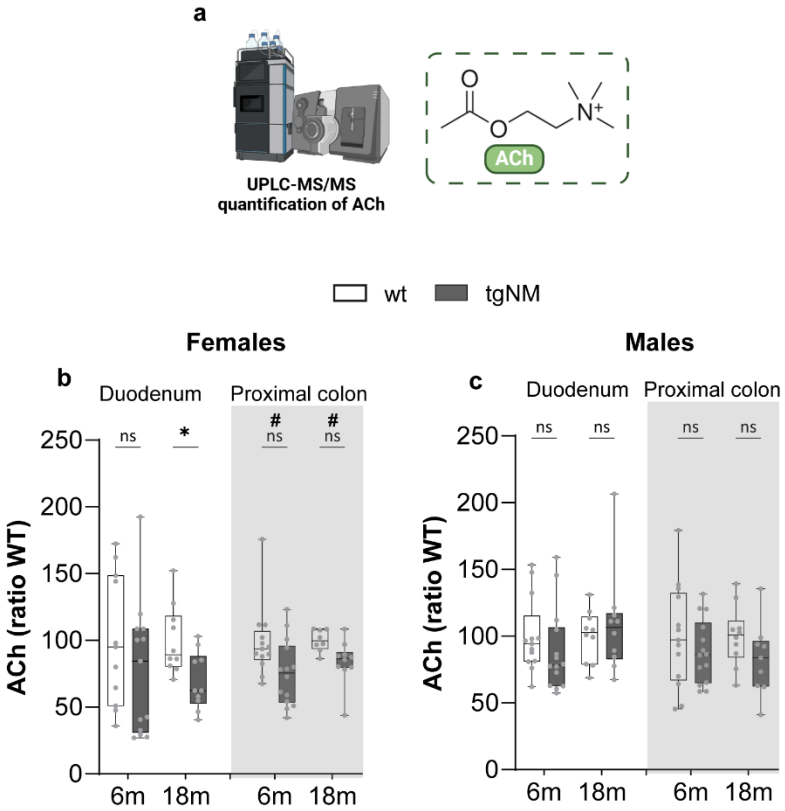

Figure 25. Levels of ACh in the duodenum and proximal colon. a) Schematic simplified representation of quantification of ACh molecules. **b, c)** UPLC-MS/MS measurements of ACh in duodenum and proximal colon homogenates of female and male mice at 6 m and 18 m. Groups are normalized to their age-matched wt. *p≤0.05 compared to age-matched wt (Uncorrected Fisher's LSD). #p≤0.05 compared to age-matched wt (Mann-Whitney test). 6 m [F&M: D&C: n=13(wt), n=14(tgNM)]. 18 m [F&M: D&C: n=10(wt), n=10(tgNM)].

1.3.4.2 The dopaminergic system

The dopaminergic system plays a crucial role in the physiology and physiopathology of the GI tract. DA is one of catecholamine neurotransmitters that regulate GI motility, primarily through the activation of DA receptors (DRs) located throughout the GI tract. DA can be synthesized and released by enteric neurons, as well as by non-neuronal sources, such as stomach epithelial cells, cells within the lamina propria, immune cells and even gut bacteria (Eisenhofer et al., 1997; Mittal et al., 2017). Additionally, DA is crucial in regulating immune function to maintain gut homeostasis and protect the GI mucosal barrier (Serio & Zizzo, 2023). Disruptions in this dopaminergic system may contribute to the onset or exacerbation of GI disorders (Matt & Gaskill, 2019). DA synthesis begins with the conversion of L-Tyrosine into L-DOPA by TH, and L-DOPA then serves as the precursor for DA. DA can subsequently be metabolized into NE by DBH (DA-beta-hydroxylase) enzyme (Figure 26 a). NE, an autonomic neurotransmitter and potent vasoactive agent, influences intestinal absorption and secretion (Yeo et al., 1988).

In tgNM females, NE levels were reduced in both the duodenum and proximal colon at 6 m (Figure 26 d), despite elevated DA levels in these regions (Figure 26 c) and increased L-DOPA in the proximal colon (Figure 26 b). This might be the result of either a decrease in the ability to synthesize and store the transmitter or result from an enhanced rate of utilization. By 18 m, no significant changes in metabolite levels were observed in the duodenum. However, in the proximal colon, a decline in L-DOPA levels (Figure 26 a), along with a trend toward reduced DA (Figure 26 b), likely contributed to the observed significant decrease in NE levels (Figure 26 d).

In tgNM males, NE levels remained stable across all samples at both time points (Figure 26 g). At 6 m, L-DOPA levels were reduced in the duodenum (Figure 26 e), but this did not affect DA concentrations (Figure 26 f). No changes in metabolite levels were observed in the proximal colon at this time point. By 18 m, L-DOPA levels were increased in both the duodenum and proximal colon (Figure 26 e), correlating with an increase in DA levels in the proximal colon, although DA remained unchanged in the duodenum (Figure 26 f). These findings suggest a reduced capability to convert L-DOPA to DA in the duodenum leading to increased L-DOPA levels without significantly altering DA or NE concentrations.

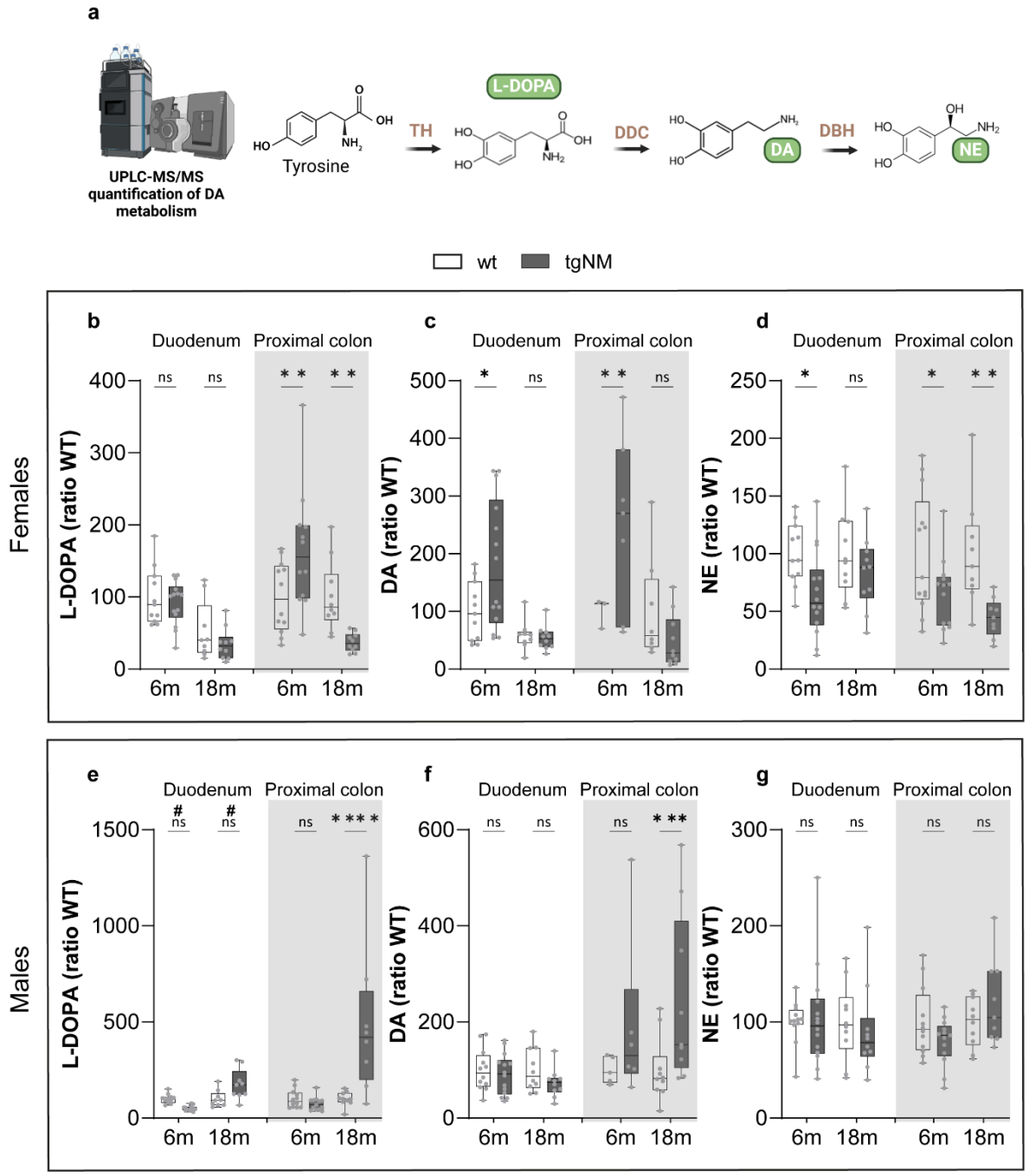

Figure 26. Levels of neurotransmitters in the duodenum and proximal colon. a) Schematic simplified representation of DA metabolism. In green are the measured metabolites (L-DOPA, DA and NE). In orange there are the rate limiting enzymes: TH (tyrosine hydroxylase), DDC (L-DOPA decarboxylase) and DBH (DA-beta-hydroxylase). **b-g)** UPLC-MS/MS measurements of DA and its metabolites in duodenum and proximal colon homogenates of female **(b, c, d)** and male **(e, f, g)** mice at 6 m and 18 m. Groups are normalized to their age-matched wt. *p≤0.05 compared to age-matched wt (Uncorrected Fisher's LSD). #p≤0.05 compared to age-matched wt (Mann-Whitney test). 6 m [F&M: D&C: n=13(wt), n=14(tgNM)]. 18 m [F&M: D&C: n=10(wt), n=10(tgNM)].

1.3.4.3 The serotonergic system

Trp is an essential amino acid and a precursor to several physiologically essential compounds, including 5-HT, melatonin and Kyn (Guzel & Mirowska-Guzel, 2022). Approximately 1–2% of Trp is metabolized into 5-HT and melatonin, while around 95% is metabolized through the Kyn pathway (N. Liu et al., 2021). EEC cells in the gut are the primary source of 5-HT, producing about 95% of the body's total 5-HT, within the remaining 5% synthesized in other peripheral tissues and the CNS (Martin et al., 2017). The synthesis and release of 5-HT by EEC cells are modulated by gut microbiota, particularly through the production of SCFAs. EEC cells respond to chemical and mechanical stimuli, as well as signals from gut microbiota, to release 5-HT, which increases GI motility, activates nociceptive pain neurons, and influences CNS activity (Gershon & Liu, 2007; Spohn & Mawe, 2017). Within the intestinal mucosa, 5-HT plays a dual role, exerting either pro- or anti-inflammatory effects depending on its receptor interactions (Rapalli et al., 2016; Spohn & Mawe, 2017). Beyond its role in gut physiology, 5-HT also impacts metabolic homeostasis, affecting functions in pancreatic islets, the liver and adipose tissue (Figure 27 a).

In tgNM females, no major significant alterations in Trp or 5-HT levels were detected at either time point in any of the samples (Figure 27 b, c). However, at 6 m, Kyn levels were elevated in the proximal colon, while at 18 m, a reduction in Kyn levels was observed in the duodenum (Figure 27 e).

In tgNM males, Trp and 5-HT levels remained unchanged at 6 m (Figure 27 f, g), although there was a reduction in Kyn levels in the proximal colon (Figure 27 i). Additionally, increased 5-HIAA levels were detected in the duodenum, while a decrease was noted in the proximal colon (Figure 27 h). This suggests that the deamination of 5-HT into 5-HIAA may vary between tissues, reflecting region-specific differences in 5-HT metabolism. At 18 m, both Trp and 5-HT levels were elevated in the proximal colon (Figure 27 f, g), while 5-HIAA levels remained unchanged (Figure 27 h).

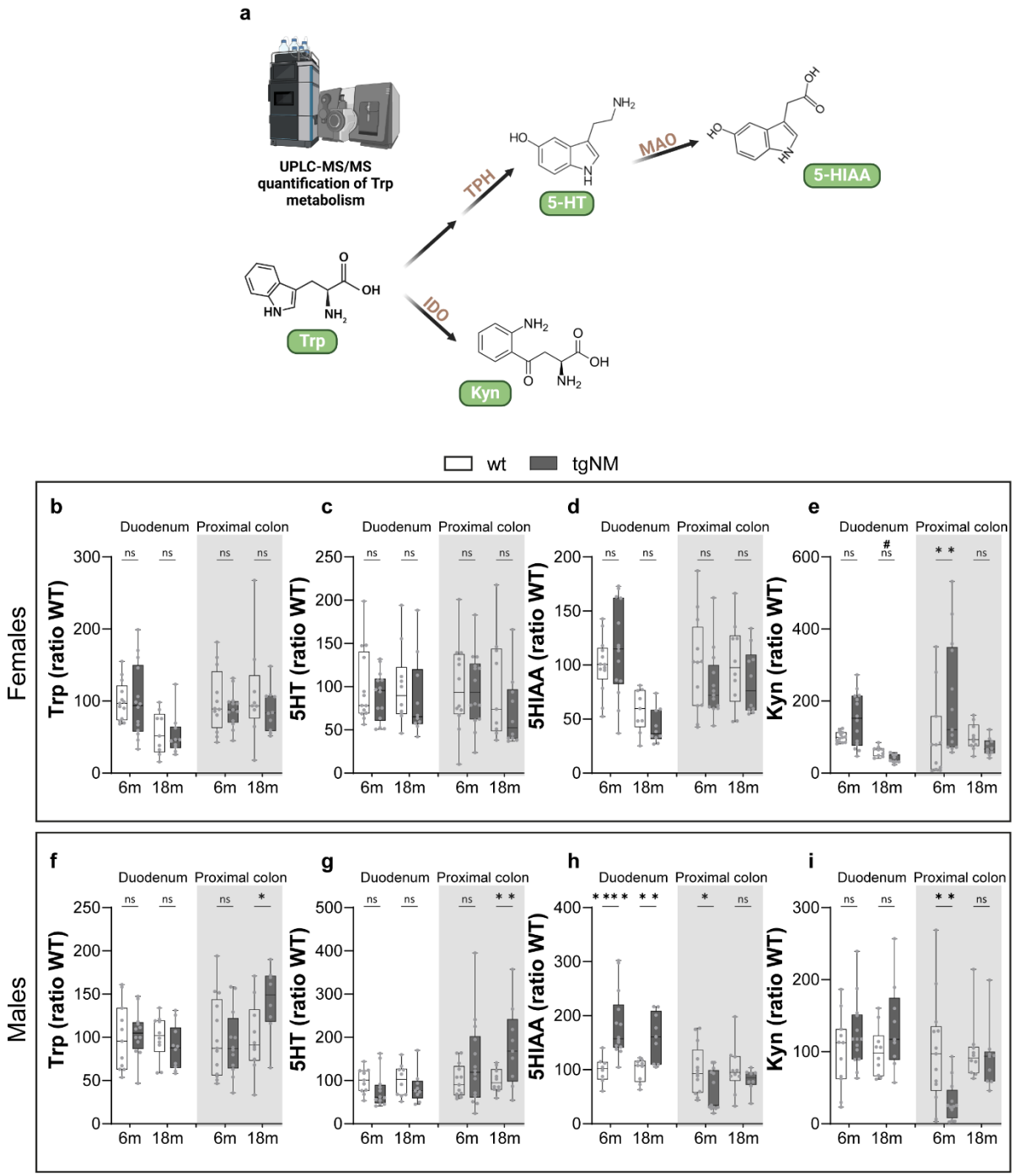

Figure 27. Levels of neurotransmitters in the duodenum and proximal colon. a) Schematic simplified representation of Trp metabolism. In green are the measured metabolites (Trp, 5-HT, Kyn and 5-HIAA). In orange are the rate limiting enzymes: TPH (tryptophan hydroxylase), IDO (indoleamine 2,3-dioxygenase) and MAO (monoamine oxidase). **b-i)** UPLC-MS/MS measurements of 5-HT and its metabolites in duodenum and proximal colon homogenates of female **(b, c, d, e)** and male (**f, g, h, i)** mice at 6 m and 18 m. Groups are normalized to their age-matched wt. *p≤0.05 compared to age-matched wt (Uncorrected Fisher's LSD). #p≤0.05 compared to age-matched wt (Mann-Whitney test). 6 m [F&M: D&C: n=13(wt), n=14(tgNM)]. 18 m [F&M: D&C: n=10(wt), n=10(tgNM)].

In summary, the assessment of neurotransmitter dynamics in the duodenum and proximal colon of tgNM and wt mice revealed notable alterations. In females, significant changes were detected in the cholinergic

and dopaminergic systems at both time points, while in males, the serotonergic system showed alterations primarily at old ages. These findings suggest a dysregulation in neurotransmitter synthesis and metabolism, potentially contributing to impaired gut function and inflammation, with a more pronounced effect observed in tgNM females.

1.4 Transcriptional profiling of duodenum samples in tgNM mice

To gain insight into the pathophysiology underlying the GI symptoms exhibited by tgNM mice before the onset of dopaminergic cell degeneration in the SN, we conducted a transcriptomic microarray analysis to identify DEGs and associated pathways that may underline or contribute to the observed GI phenotype in duodenal samples from tgNM mice at 6 m of age. This approach allowed us to explore early molecular changes that might precede neurodegeneration, providing a deeper understanding of how alterations in the gut environment could potentially influence disease progression in this model.

1.4.1 Differential expression analysis (DEA)

DEA across sexes and genotypes was performed by the Statistics and Bioinformatics Unit at Vall d'Hebron Research Institute (UEB-VHIR). They used the statistical programming language "R" and specialized libraries from the Bioconductor Project tailored for microarray data analysis (Gentleman et al., 2005).To identify statistically significant DEGs, a threshold of a raw p-value ≤0.01 and an absolute logarithmic FC greater than 0.6 was applied, corresponding approximately to a 1.5-fold up/down-regulation on a linear scale. The analysis revealed a higher number of DEGs in females than in males. Specifically, tgNM females exhibited 75 genes with altered expression compared to their wt counterparts, whereas tgNM males showed 46 genes with altered expression compared to their wt littermates (Annex Table 1 and Annex Table 2). The top ten most significant DEGs for each comparison between genotypes are described in (Table 10 and Table 11).

Table 10. DEGs in tgNM females compared to wt littermates in the duodenum. Top ten most significant DEGs, including a brief description and the statistics for each gene. All identified DEGs are provided in Annex Data Table 1.

Gene Symbol	Name	Description	logFC	P.Value	adj.P.Val
Ccdc190	Coiled-Coil Domain Containing 190	Protein coding gene	-0,77933071	2,755E-05	0,55314196
Ppp1r26	Protein phosphatase-1, regulatory subunit 26	Predicted to enable protein phosphatase inhibitor activity	0,98553885	9,0759E-05	0,691166
Parvb	Parvin beta	Predicted to enable actin binding activity.	0,87017876	0,00010327	0,691166
Klk9	Kallikrein related-peptidase 9	Predicted to be active in secretory granule	-1,03696555	0,00018717	0,78837558

Bhmt	Betaine-homocysteine methyltransferase	Enables betaine-homocysteine S-methyltransferase activity	-1,00909704	0,00019813	0,78837558
Crmp1	Collapsin response mediator protein 1	Forms part of the collapsin response mediator protein family	-1,02691638	0,00024871	0,78837558
Ptgis	Prostaglandin I2 (prostacyclin) synthase	Predicted to enable heme binding activity and prostaglandin-I synthase activity	0,84643482	0,00033552	0,78837558
Rgr	Retinal G protein coupled receptor	The gene is a member of the opsin family of G-protein coupled receptors	-0,64983305	0,00040731	0,78837558
Gpihbp1	GPI-anchored HDL-binding protein 1	Enables lipase binding activity; lipoprotein particle binding activity; and protein transporter activity	0,76970073	0,00041843	0,78837558
Sohlh1	Spermatogenesis and oogenesis specific basic helix-loop-helix 1	Involved in oocyte differentiation; positive regulation of transcription by RNA polymerase II; and spermatogenesis	-0,78841069	0,00059501	0,91896458

Table 11. DEGs in tgNM males compared to wt littermates in the duodenum. Top ten most significant DEGs, including a brief description and the statistics for each gene. All identified DEGs are provided in Annex Data Table 2.

Gene Symbol	Name	Description	logFC	P.Value	adj.P.Val
Ccdc87	Coiled-coil domain containing 87	Involved in positive regulation of acrosome reaction and positive regulation of fertilization	1,072145945	7,46684E-05	0,999908741
Amh	anti-Mullerian hormone	Plays an important role in several reproductive functions	0,86746924	0,000128562	0,999908741
4933421I07Rik	RIKEN cDNA 4933421I07 gene	Restricted expression towards testis	0,842733629	0,000228561	0,999908741
Zfp846	Zinc finger protein 846	Predicted to be involved in regulation of transcription by RNA polymerase II	0,623236931	0,000564385	0,999908741
Olfr1087	olfactory receptor family 8 subfamily K member 3B	Part of the olfactory receptor gene family involved in the olfactory system	1,009354445	0,000802284	0,999908741
Olfr347	olfactory receptor family 1 subfamily J member 18	Part of the olfactory receptor gene family involved in the olfactory system	0,620620223	0,000981172	0,999908741
Pak3	p21 (RAC1) activated kinase 3	Involved in axon genesis and dendritic spine morphogenesis	-0,884459001	0,001109786	0,999908741

Klre1	Killer cell lectin-like receptor family E member 1	Enables identical protein binding activity and transmembrane signaling receptor activity	0,732003393	0,001187748	0,999908741
Lrp1b	Low density lipoprotein-related protein 1B	Putative tumor suppressor and a member of the low-density lipoprotein (LDL) receptor family	-0,655797156	0,001690779	0,999908741
A530053G22Rik	RIKEN cDNA A530053G22 gene		-0,640807498	0,001790989	0,999908741

1.4.2 Shared DEGs across genotypes and sexes

To determine the extent of gene overlap among genotypes, a multiple comparisons analysis was conducted and visualized through a Venn diagram. Under the same statistical criteria as previously applied, only the Gad2 gene showed changes in both tgNM females and males compared to their respective wt littermates (Figure 28 c). Additionally, we employed the same statistical criteria to analyze gene overlap among sexes. This analysis revealed 13 genes that were commonly altered in both wt and tgNM females compared to the respective males (Figure 28 d). Conversely, 122 genes were specifically altered in wt females compared to wt males, and 108 genes were specific to tgNM females compared to tgNM males (Figure 28 d). We next examined common patterns of gene regulation between genotypes and sexes using unsupervised clustering techniques. The resulting heatmaps revealed a distinct clustering of gene expression profiles between genotypes and sex conditions (Figure 28 e, f).

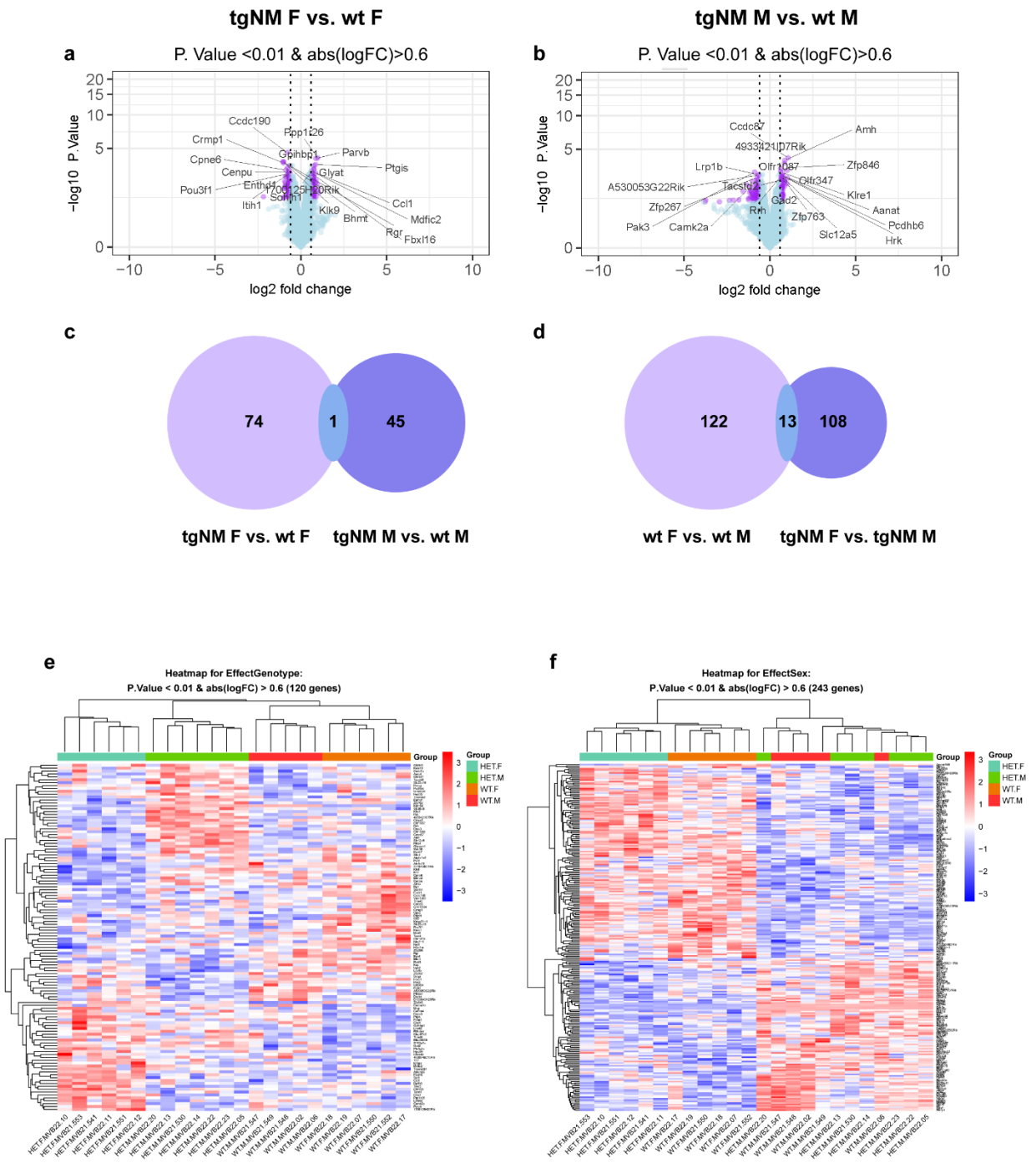

Figure 28. DEA between tgNM and wt mice. a, b) Volcano plots showing statistically significant (raw p value ≤0.01, FC>|1.5|), purple dots. Gene symbols are shown for the most significant genes. **c)** Venn diagram showing the overlap between DEGs identified in "effect of genotype" (right) **d)** Venn diagram showing the overlap between DEGs identified in "effect of sex" (left). **e)** Heatmap for multiple comparison of "effect of genotype". **f)** Heatmap for multiple comparison of "effect of sex".

1.4.3 Gene set enrichment analysis (GSEA)

Following the DEA in tgNM and wt mice, we aimed to further investigate the molecular mechanisms underlying the observed phenotypic differences in the GI tract of tgNM mice by performing a GSEA (Subramanian et al., 2005) to identify biologically significant pathways and processes associated with the DEGs. This analysis was conducted using Gene Ontology (GO) and the Reactome Pathway Knowledge databases (Fabregat et al., 2018). Enriched GO and Reactome terms were selected with an adjusted p-value ≤0.15.

The GSEA analysis with the GO database revealed statistically significant pathways in both sexes. Among the top 15 enriched biological pathways identified in females (Figure 29 a) and in males (Figure 29 b), immune response-related pathways and metabolism-related pathways were notably enriched among the downregulated genes in both sexes. In males, no activated pathways were significantly enriched, while in females, pathways related to synaptic vesicle, zymogen activation and calcium concentration were significantly enriched.

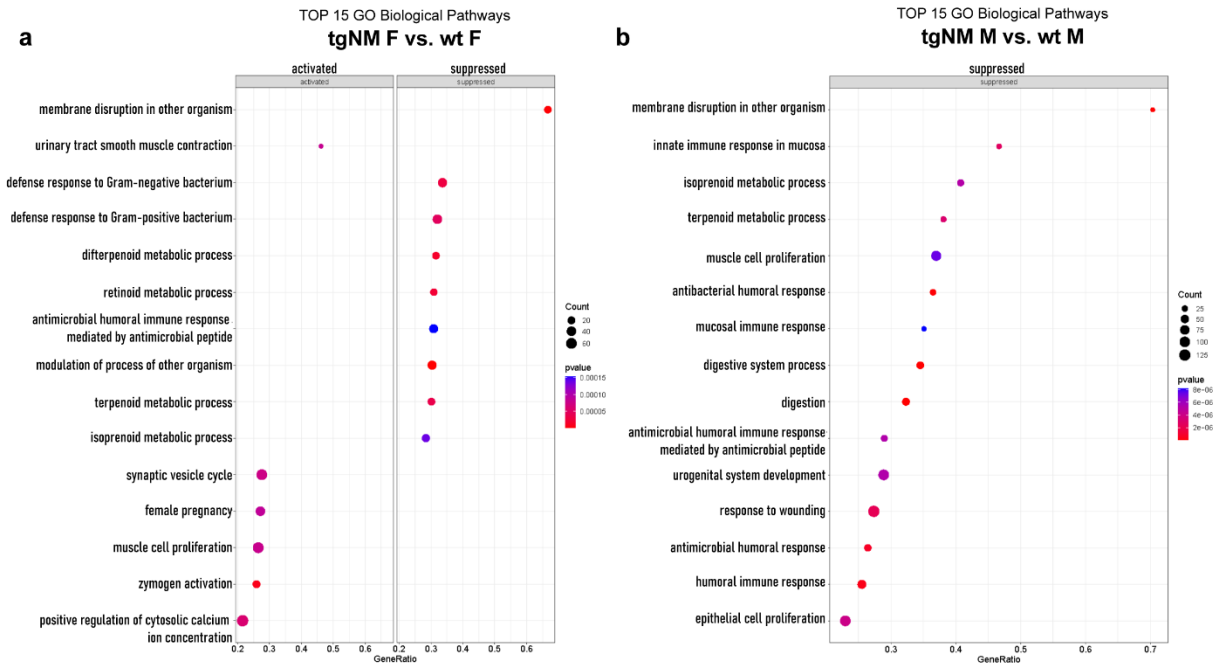

Figure 29. Gene set enrichment analysis with GO database. a-b) Top 15 GO biological pathways (adj. p value <0.15) enriched in tgNM and wt **(a)** females and **(b)** males.

GSEA analysis with the Reactome database also revealed statistically significant pathways in both sexes. In females, some of the biological pathways enriched among the downregulated genes were common with the GO terms, including pathways associated with the immune system, metabolism and digestion, and the cell cycle (Figure 30 a). In males, most of the biological pathways enriched among the downregulated genes were metabolic and digestion-related pathways (Figure 30 b). Altogether, these

findings suggest that the observed phenotypic differences in the GI tract may be linked to alterations in immune system function and metabolism.

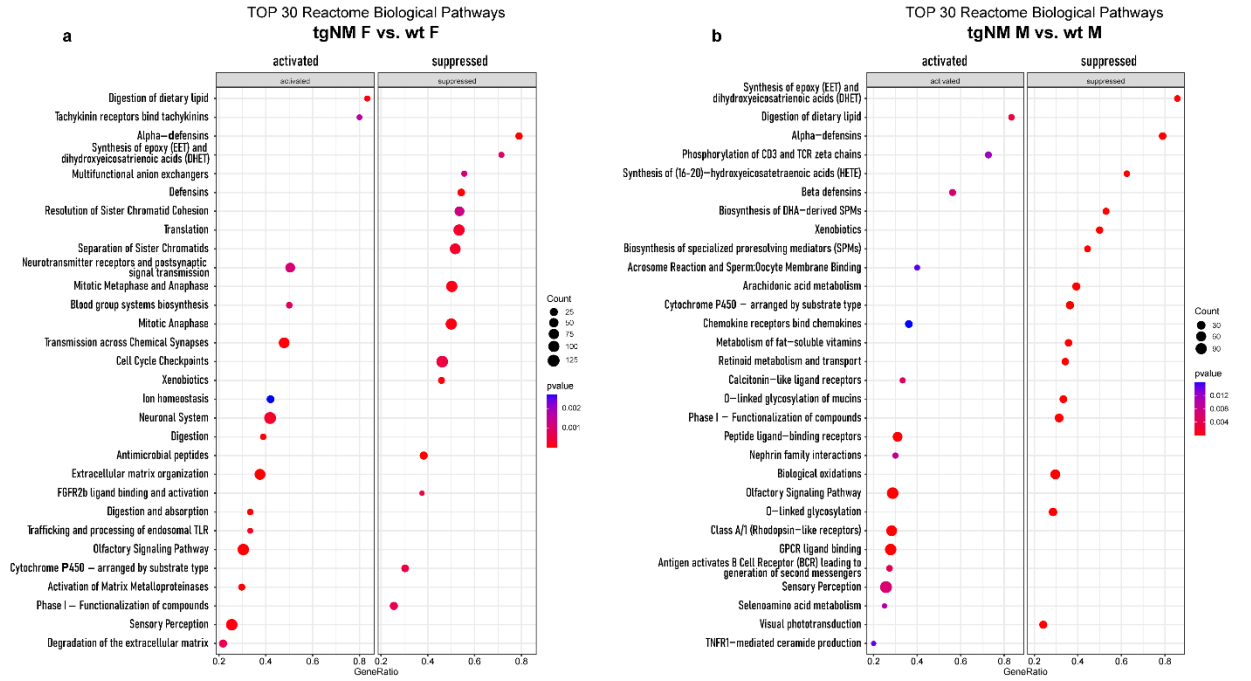

Figure 30. Gene set enrichment analysis with Reactome database. a-b) Top 30 Reactome biological pathways (adj. p value <0.15) enriched in tgNM and wt **(a)** females and **(b)** males.

1.5 GI permeability and inflammation

Intestinal inflammation, gut barrier impairment, and alterations in tight junction proteins are increasingly recognized as contributing factors in the pathogenesis of PD. Emerging evidence suggests that chronic intestinal inflammation may disrupt the gut barrier, leading to increased intestinal permeability, commonly referred to as "leaky gut" (Forsyth et al., 2011; Perez-Pardo et al., 2018). In line with this, our microarray analysis of duodenal samples revealed several altered pathways associated with immune system activity. Consequently, we aimed to further characterize the peripheral inflammatory profile in the GI tract of tgNM mice to better understand how immune-related changes may contribute to the gut dysfunction and potentially influence PD-like pathology in this model.

1.5.1 Changes in the cytokine expression profile in duodenal and proximal colon samples

To characterize the inflammatory profile, we quantified the expression of several cytokines, including IL-6, IL-10, IL-1b, TNF-α and INF-γ, in duodenal and proximal colon samples from 6 m and 18 m wt and tgNM mice. Using RT-qPCR, we found no significant changes in cytokine levels at 6 m in either sex (Figure 31 a, b, d), except for elevated INF-γ levels in the proximal colon of tgNM females (Figure 31 c). At 18 m,

elevated INF-γ levels were again observed in the proximal colon of tgNM females (Figure 31 g). In contrast, tgNM females at this age exhibited reduced IL-10 and INF-γ levels in the duodenum (Figure 31 e). In tgNM males, we observed increased IL-10 levels in the duodenum (Figure 31 f) and reduced TNF-α levels in the proximal colon at 18 m (Figure 31 h).

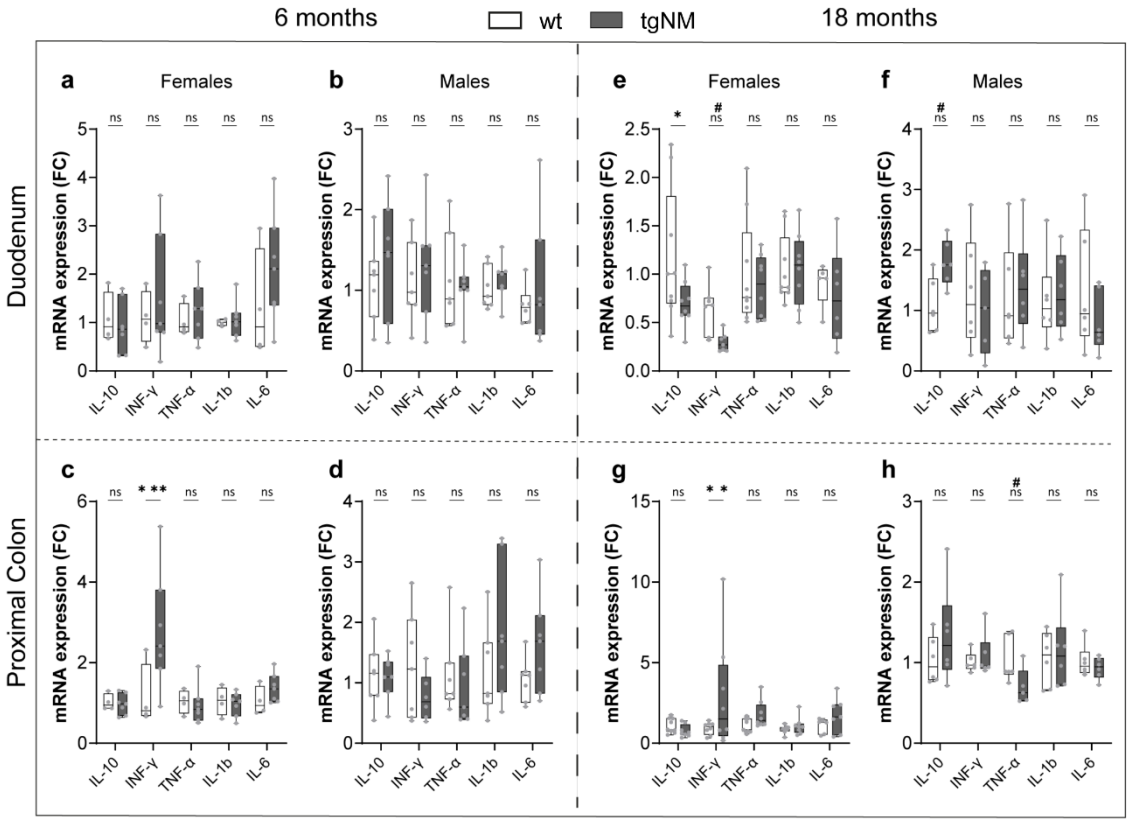

Figure 31. Cytokine expression in duodenum and proximal colon samples. a-d) Expression of cytokine levels in duodenum and proximal colon samples of 6 m tgNM and wt **(a, c)** females and **(b, d)** males by RT-qPCR using the comparative method normalized to wt (FC). *p≤0.05 compared to age-matched wt (Uncorrected Fisher's LSD). 6 m [F-D: n=4(wt), n=7(tgNM), F-C: n=4(wt), n=7(tgNM); M-D: n=7(wt), n=7(tgNM), M-C: n=7(wt), n=7(tgNM)]. **e-h)** Expression of cytokines levels in duodenum and proximal colon samples of 18 m tgNM and wt **(e, g)** females and **(f, h)** males by RT-qPCR using the comparative method normalized to wt (FC). *p≤0.05 compared to age-matched wt (Uncorrected Fisher's LSD). #p≤0.05 compared to age-matched wt (Mann-Whitney test). 18 m [F-D: n=9(wt), n=8(tgNM), F-C: n=9(wt), n=8(tgNM); M-D: n=6(wt), n=6(tgNM), M-C: n=6(wt), n=6(tgNM)].

1.5.2 Changes in inflammatory markers expression in duodenal and proximal colon samples

We next examined the expression of additional inflammatory markers, including s100b, GFAP, Toll-like receptor 2 and 4 (TLR-2 and TLR-4), in the same duodenal and proximal colon samples. Notably, we observed elevated TLR-4 levels in the duodenum of 6 m tgNM males (Figure 32 b), while no other significant changes were detected in duodenal samples for either sex across all time points (Figure 32 a,

e, f). In the proximal colon, 6 m old tgNM females presented significantly reduced S100b expression (Figure 32 c), although this reduction was no longer significant at 18 m (Figure 32 g). Additionally, tgNM males exhibited reduced TLR-2 levels in the proximal colon at 6 m (Figure 32 d) but this reduction was absent at 18 m (Figure 32 h).

S100b, primarily expressed by EG cells, has been reported to have decreased in the feces of patients with IBD (Di Liddo et al., 2020), highlighting its potential as a marker for gut inflammation. Alongside S100b, calprotectin (S100A9/S100A8), another member of the S100b protein family, plays a key role in activating the innate immunity (Ayling & Kok, 2018; Inciarte-Mundo et al., 2022) and has emerged as a potential biomarker for intestinal inflammation, particularly in the context of PD, given its established role in IBD (Aho et al., 2021; Hor et al., 2021a; Mulak et al., 2019). To investigate whether calprotectin could reflect inflammatory changes in this mouse model, we assessed fecal calprotectin levels in both sexes at 6, 12 and 18 m using ELISA. However, no significant changes in fecal calprotectin levels were detected at any time point for either sex (Figure 32 i, j).

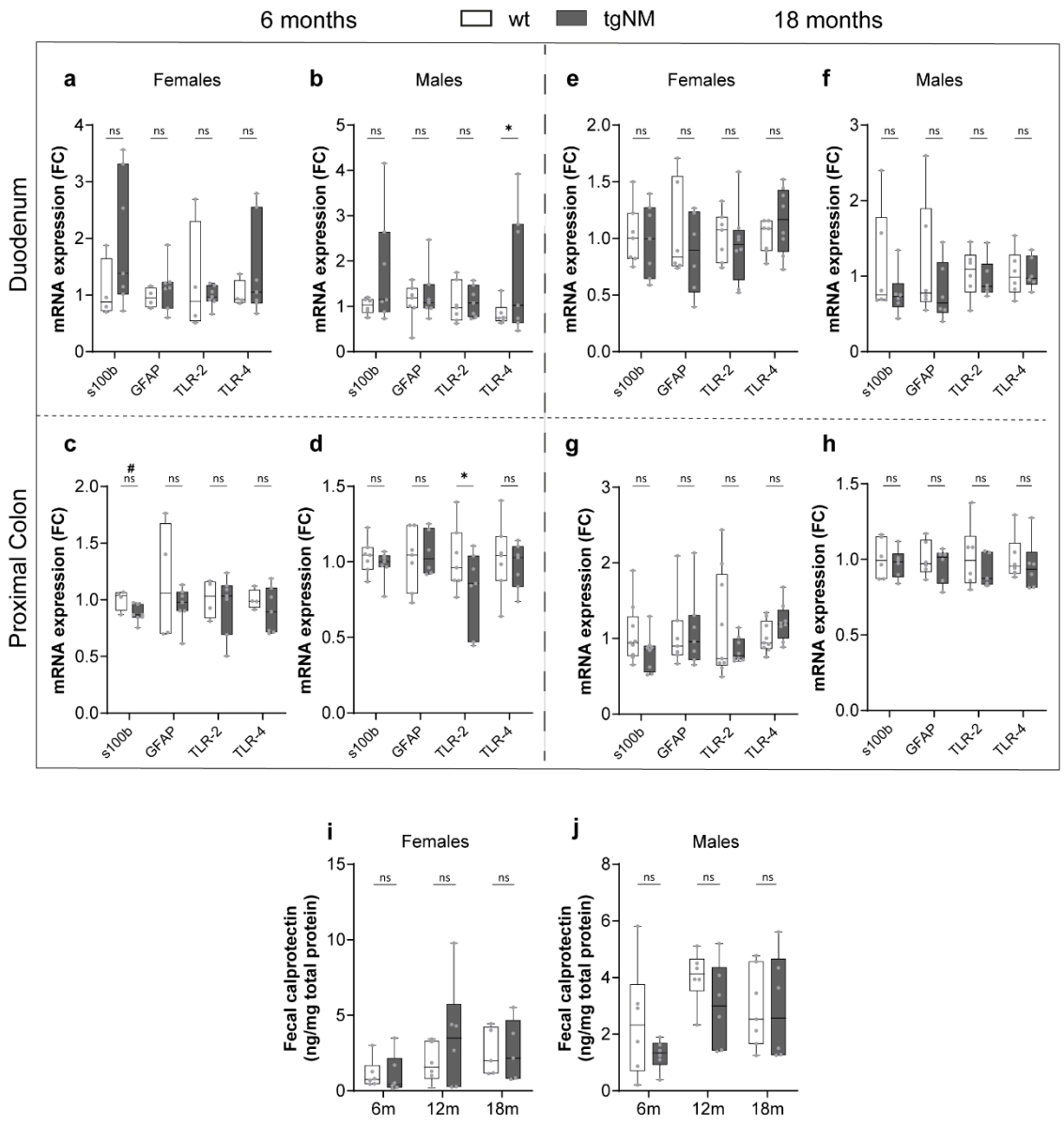

Figure 32. Inflammatory markers expression in duodenum and proximal colon samples. a-d) Expression of inflammatory markers levels in duodenum and proximal colon samples of 6 m tgNM and wt **(a, c)** females and **(b, d)** males by RT-qPCR using the comparative method normalized to wt (FC). *p≤0.05 compared to age-matched wt (Uncorrected Fisher's LSD). #p≤0.05 compared to age-matched wt (Mann-Whitney test). 6 m [F-D: n=4(wt), n=7(tgNM), F-C: n=4(wt), n=7(tgNM); M-D: n=7(wt), n=7(tgNM), M-C: n=7(wt), n=7(tgNM)]. **e-h)** Expression of inflammatory markers levels in duodenum and proximal colon samples of 18 m tgNM and wt **(e, g)** females and **(f, h)** males by RT-qPCR using the comparative method normalized to wt (FC). Uncorrected Fisher's LSD test tgNM compared to age-matched wt not significant. 18 m [F-D: n=9(wt), n=8(tgNM), F-C: n=9(wt), n=8(tgNM); M-D: n=6(wt), n=6(tgNM), M-C: n=6(wt), n=6(tgNM)]. **i-j)** Fecal calprotectin levels normalized to total fecal protein (ng/mg total protein) measured by ELISA in **(i)** females and **(j)** males at 6, 12 and 18 m. Uncorrected Fisher's LSD test tgNM compared to age-matched wt not significant. 6 m [F&M: n=6(wt), n=6(tgNM)], 12 m [F&M: n=6(wt), n=6(tgNM)], 18 m [F: n=5(wt), n=5(tgNM), M: n=7(wt), n=6(tgNM)].

Additionally, we assessed the protein levels of other neuropathological markers including TAU and α-synuclein, together with TH and GFAP in duodenal and proximal colon samples from both wt and tgNM

females at 18 m to further explore the presence of pathological changes in the GI tract. In the duodenum, we observed elevated levels of TH and GFAP, along with a trend toward increased α-synuclein expression (FIG 33 a, b). Conversely, in the proximal colon, α-synuclein levels were significantly increased, while TH expression was reduced (FIG 33 c, d). TAU protein levels remained unchanged in both tissues. These findings suggest that α-synuclein accumulation in the GI tract may contribute to the functional GI alterations observed in tgNM mice.

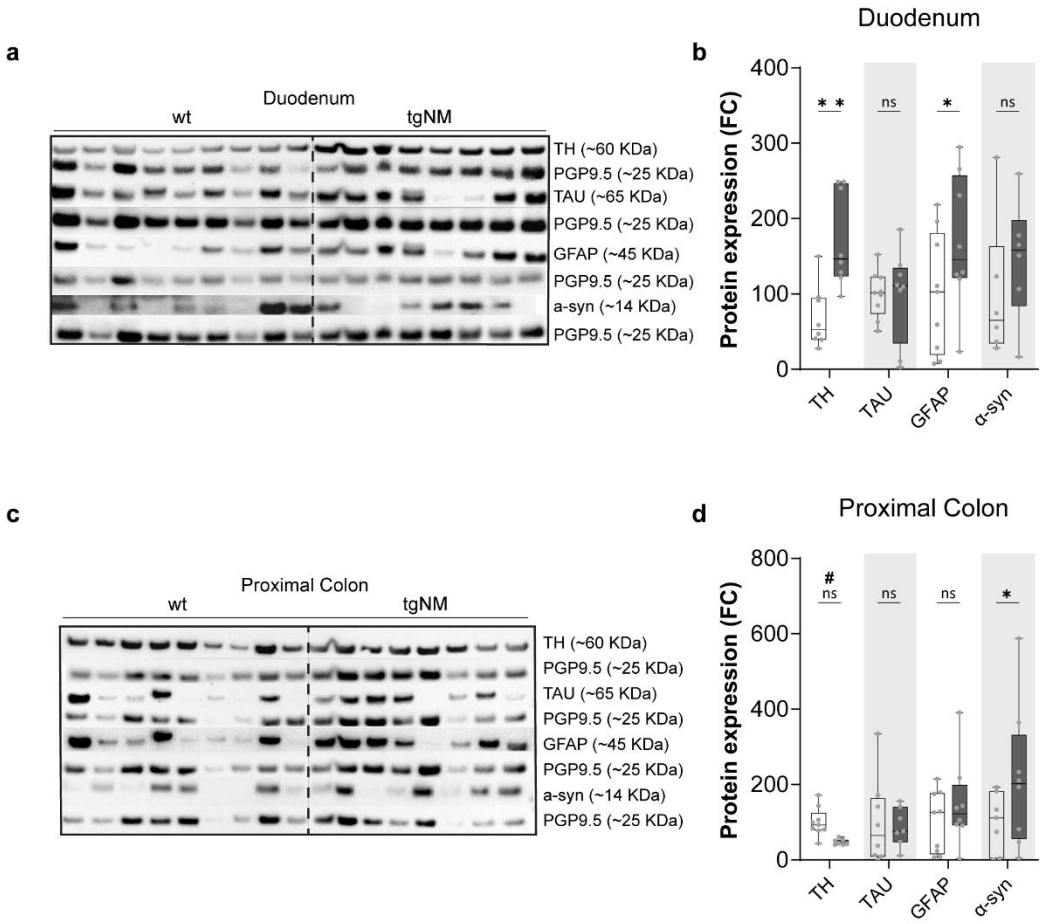

Figure 33. Protein levels of pathological markers in duodenum and proximal colon samples. a, c) Representative WB membranes from the main proteins assessed in the duodenum and the proximal colon from wt and tgNM females at 18 m. **b, d)** Protein quantification normalized to PGP9.5. *p≤0.05 compared to age-matched wt (Uncorrected Fisher's LSD). #p≤0.05 compared to age-matched wt (Mann-Whitney test). 18 m [D: n=8(wt), n=8(tgNM), C: n=9(wt), n=7(tgNM)].

1.5.3 Altered TJs proteins expression levels in duodenal and proximal colon samples

As previously mentioned, disruption of the gut barrier allows microbial products and toxins to translocate into the systemic circulation, exacerbating systemic and neuro-inflammation (Di Tommaso et al., 2021;

Forsyth et al., 2011). TJs proteins are critical for maintaining intestinal barrier integrity. Alterations in the expression and localization of these proteins have been observed in PD patients, indicating compromised gut barrier function. Notably, studies have demonstrated decreased expression of occludin in the colonic mucosa (Clairembault et al., 2015) and increased levels of ZO-1 in fecal samples of PD patients, correlating with increased intestinal permeability and inflammation (Dumitrescu et al., 2021).

To further explore these findings, we assessed the expression of three TJs proteins (ZO-2, claudin-2 and occludin) using RT-qPCR in duodenal and proximal colon samples. At 6 m, tgNM females exhibited significantly elevated expression of ZO-2 and claudin-2 in the duodenum (Figure 34 a) while occludin levels were increased in the proximal colon (Figure 34 c). In contrast, no significant changes were detected in the duodenum and proximal colon of 6 m old tgNM males (Figure 34 b, d). By 18 m, tgNM females continued to exhibit elevated claudin-2 expression in the duodenum (Figure 34 e), along with increased ZO-2 and occludin expression in the proximal colon (Figure 34 g). In tgNM males at 18 m, we observed increased ZO-2 and occludin expression in the duodenum (Figure 34 f) along with elevated claudin-2 levels in the proximal colon (Figure 34 h).

To complement these findings, we analyzed ZO-1 and occludin protein levels in the duodenum and proximal colon of 18 m old tgNM females by WB (Figure 34 I, j). Results indicated increased ZO-1 levels in both the duodenum and proximal colon, while occludin levels were elevated only in the duodenum (Figure 34 k, l).

The elevated levels of ZO-1, ZO-2, claudin-2, and occludin suggest alterations in tight junction dynamics, potentially leading to impaired barrier integrity. This compromised barrier function could facilitate increased permeability, allowing microbial products to translocate into systemic circulation and potentially triggering systemic inflammation associated with PD-like pathology in this model.

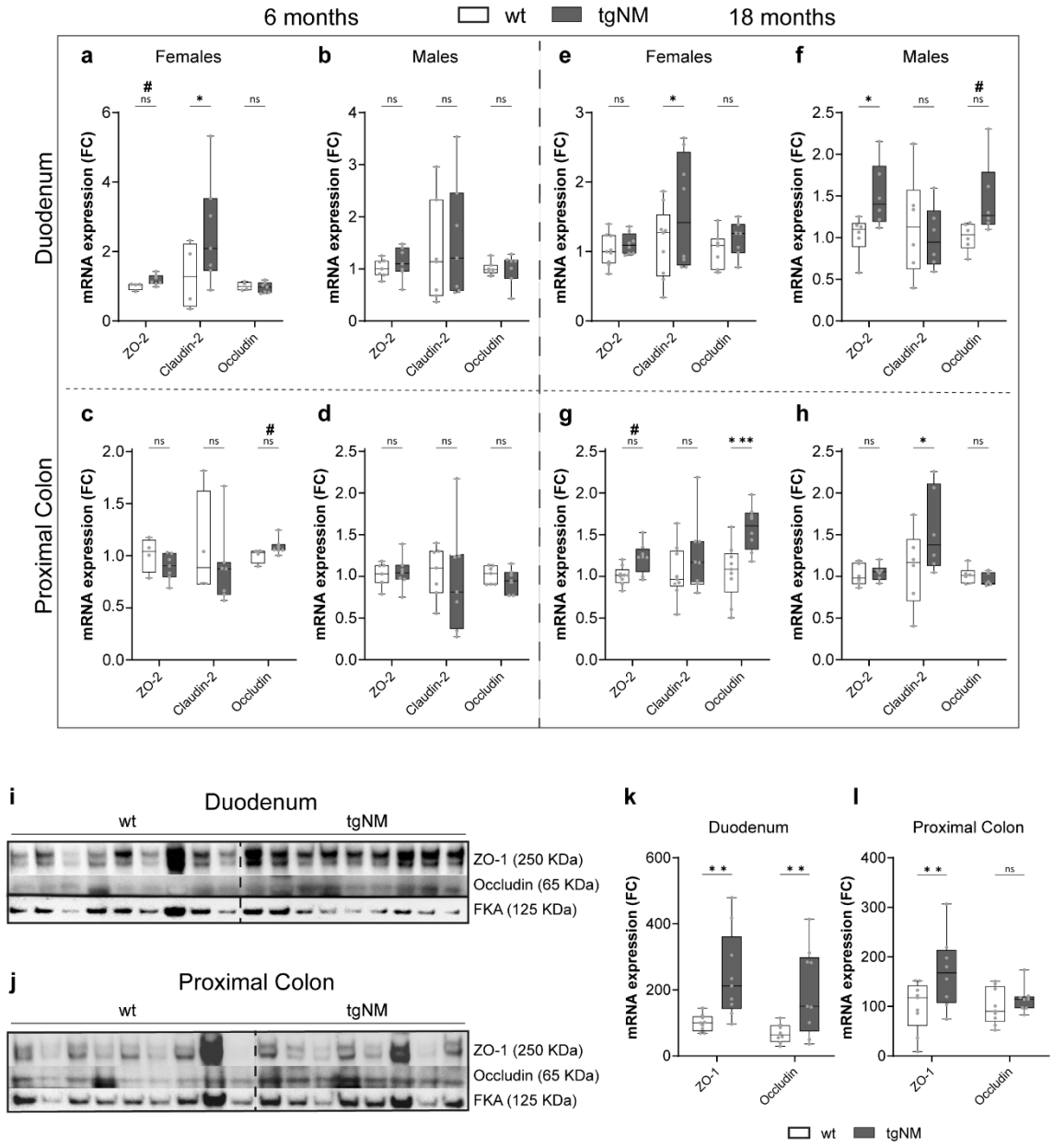

Figure 34. TJs expression in duodenum and proximal colon samples. **a-d)** Expression of ZO-2, claudin-2 and occludin mRNA levels in duodenum and proximal colon samples of 6 m tgNM and wt **(a, c)** females and **(b, d)** males by RT-qPCR using the comparative method normalized to wt (FC). **e-h)** Expression of ZO-2, claudin-2 and occludin mRNA levels in duodenum and proximal colon samples of 18 m tgNM and wt **(e, g)** females and **(f, h)** males by RT-qPCR using the comparative method normalized to wt (FC). *p≤0.05 compared to age-matched wt (Uncorrected Fisher's LSD). #p≤0.05 compared to age-matched wt (Mann-Whitney test). 6 m [F-D: n=4(wt), n=7(tgNM), F-C: n=4(wt), n=7(tgNM); M-D: n=7(wt), n=7(tgNM), M-C: n=7(wt), n=7(tgNM)]. 18 m [F-D: n=9(wt), n=8(tgNM), F-C: n=9(wt), n=8(tgNM); M-D: n=6(wt), n=6(tgNM), M-C: n=6(wt), n=6(tgNM)]. **i-j)** Representative WB membranes of ZO-1 and occludin proteins in **i)** duodenum and **j)** proximal colon samples from tgNM and wt females at 18 m. Immunoblot densitometry was normalized to FKA expression levels. Kilodaltons, KDa; *p≤0.05 compared to age-matched wt (Uncorrected Fisher's LSD). 18 m [D: n=9(wt), n=9(tgNM); C: n=9(wt), n=8(tgNM)].

1.5.4 *In vivo* and *ex vivo* gut permeability assessment

To validate our previous findings, we initially assessed gut permeability *in vivo* by measuring serum levels of 4-kDa fluorescein isothiocyanate-conjugated (FITC) dextran 1 h after oral gavage administration in wt and tgNM mice at different ages. Significantly elevated serum FITC-dextran levels were detected in tgNM females at both 6 and 18 m, but not at 3 m (Figure 35 a), indicating increased gut permeability with age in this group. No significant changes in FITC-dextran levels were detected in tgNM males at any time point (Figure 35 b).

To confirm that our measurements reflected overall gut permeability across the entire GI tract, rather than just small intestine permeability, we extended the interval to 2.5 h post-administration to allow the FITC-dextran to traverse through the full GI length. This extended analysis supported our initial findings, with a significant increase in FITC-dextran passage in 18 m tgNM females (Figure 35 c) reinforcing the presence of increased gut permeability and compromised gut barrier integrity in tgNM females. Consistent with the 1 h interval results, no differences in gut permeability were detected in tgNM males (Figure 35 d).

To complement these *in* vivo findings, we then focused specifically on assessing colonic mucosal permeability. For this purpose, we dissected the mucosal segments from the colon of 6 m old wt and tgNM females and mounted them in Ussing chambers for *ex vivo* analysis. Using this set up, we measured the passage of 4-kDa FITC-dextran across the tissue as an indicator of colonic permeability. The results showed a trend toward increased colonic mucosal permeability in tgNM females, although this difference was not statistically significant (Figure 35 e). To ensure viability in the Ussing chambers, we added forskolin at a defined concentration to the serosal side of the tissue and monitored the short-circuit current (Isc) response. The observed changes in Isc confirmed the viability of the mounted tissue samples, supporting the reliability of our permeability measurements (data not shown).

These combined *in vivo* and *ex vivo* findings indicate a potential increase in gut permeability in tgNM females, with age-dependent effects observed along the GI tract.

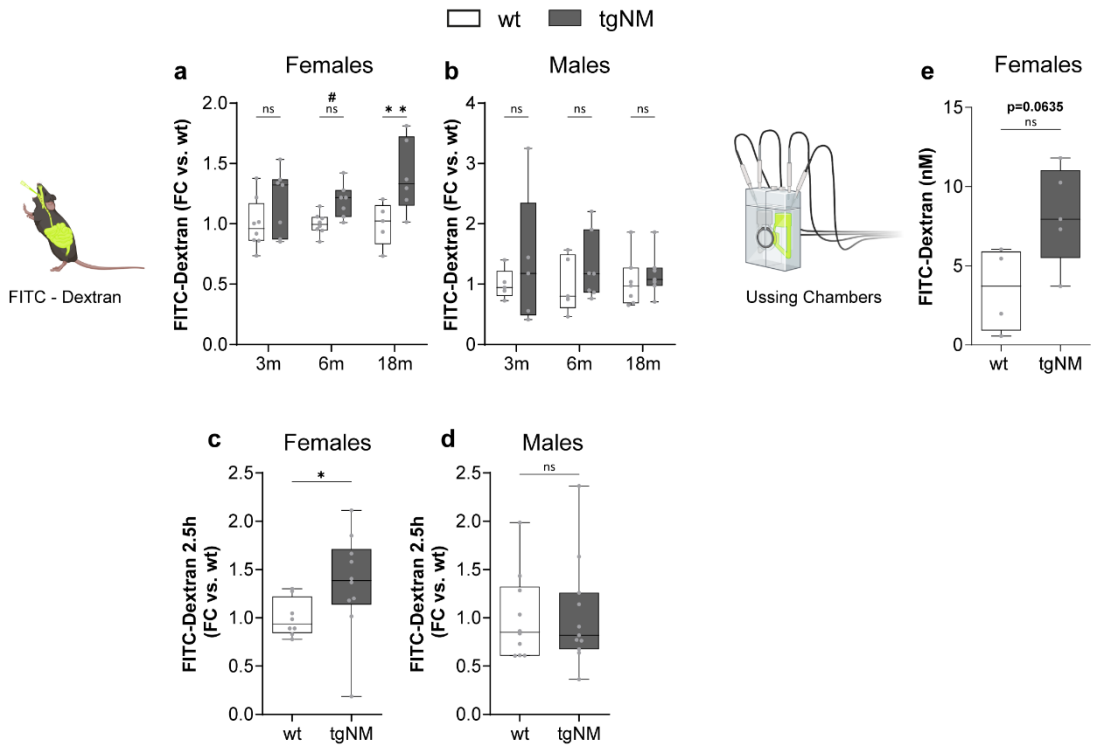

Figure 35.Gut permeability measurements in wt and tgNM mice. a-b) FITC-Dx serum levels after 1 h administration at 3, 6 and 18 m of wt and tgNM **(a)** females and **(b)** males normalized to their wt littermates. *p≤0.05 compared to age-matched wt (Uncorrected Fisher's LSD). #p≤0.05 compared to age-matched wt (Mann-Whitney test). 3 m [F: n=8(wt), n=7(tgNM)]; M: n=5(wt), n=5(tgNM)], 6 m [F: n=8(wt), n=7(tgNM); M: n=5(wt), n=7(tgNM)], 18 m [F: n=5(wt), n=6(tgNM); M: n=7(wt), n=7(tgNM)]. **c-d)** FITC-Dx serum levels after 2.5 h administration at 18 m of tgNM **(c)** females and **(d)** males normalized to their wt counterparts. *p≤0.05 compared to age-matched wt (Mann-Whitney test). 18 m [F: n=8(wt), n=10(tgNM), M: n=10(wt), n=11(tgNM)]. **e)** FITC-dextran levels (nM) after Ussing chambers experiment of tgNM females compared to wt littermates at 6 m. p=0.0635 compared to age-matched wt (Mann-Whitney test). 6 m [n=4(wt), n=5(tgNM)].

1.5.5 Gut barrier disruption increases the levels of peripheral cytokines

Given the observed increase in gut permeability, we hypothesized that this disruption of the gut barrier could lead to elevated levels of inflammatory cytokines in the periphery. The gut barrier acts as a selective barrier, preventing pathogens and inflammatory mediators from entering systemic circulation. However, when this barrier is compromised microbial products and antigens can translocate, potentially triggering immune responses and elevating cytokine levels in the bloodstream (Di Vincenzo et al., 2024). To investigate whether gut barrier disruption was associated with systemic inflammation, we analyzed serum and fecal samples by ELISA to profile their inflammatory cytokines at different time points.

At 3 m, tgNM females exhibited elevated serum levels of IL-1a and IL-6 (Figure 36 a), although no significant changes were observed in their fecal cytokine levels (Figure 37 a). In contrast, tgNM males did not show alterations in serum cytokine levels at 3 m (Figure 36 b), but TNF-α and MCP-1 levels were elevated in their feces (Figure 37 b). By 6 m, tgNM females displayed increased serum levels of TNF-α, IL-

10, IL-27, INF-β and GM-CSF (Figure 36 c), alongside elevated IL-6 levels in their feces (Figure 37 c). In tgNM males, increased serum levels of IL-23, IL-27 and INF-β were observed, accompanied by reduced IL-6 levels (Figure 36 d) while IL-12p70 levels were elevated in their feces (Figure 37 d). At 18 m, the only significant change in tgNM females was an increase in serum IL-23 levels (Figure 36 e) whereas tgNM males exhibited increased serum levels of IL-12p70 and IL-6 (Figure 36 f). No significant changes were detected in the fecal cytokine profile of tgNM females at this age (Figure 37 e). Conversely, tgNM males at 18 m presented elevated fecal levels of IL-23, TNF- α, IL-10, IL-17a, INF-β ad GM-CSF (Figure 37 f).

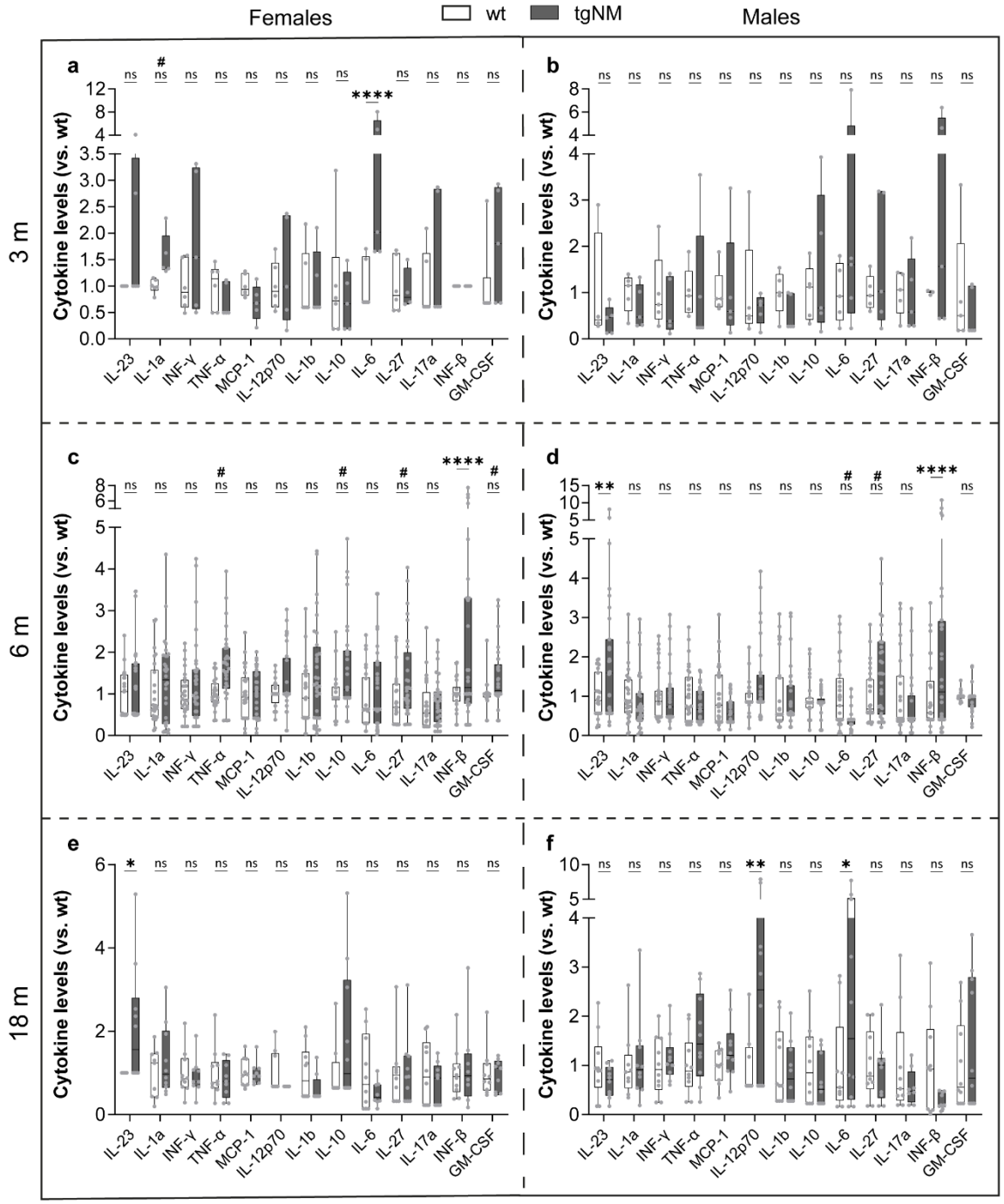

Figure 36. Serum cytokine profile in wt and tgNM mice. a, c, e) Cytokine levels profile in serum samples at 3, 6 and 18 m of tgNM females normalized to wt females. 3 m [n=6(wt), n=5(tgNM)], 6 m [n=26(wt), n=32(tgNM)], 18 m [n=10(wt), n=10(tgNM)]. **b, d, f)** Cytokine levels profile in serum samples at 3, 6 and 18 m of tgNM males normalized to wt males. 3 m [n=5(wt), n=5(tgNM)], 6 m [n=30(wt), n=31(tgNM)], 18 m [n=10(wt), n=10(tgNM)]. *p≤0.05 compared to wt-matched (Uncorrected Fisher's LSD). #p≤0.05 compared to wt-matched (Mann-Whitney test).

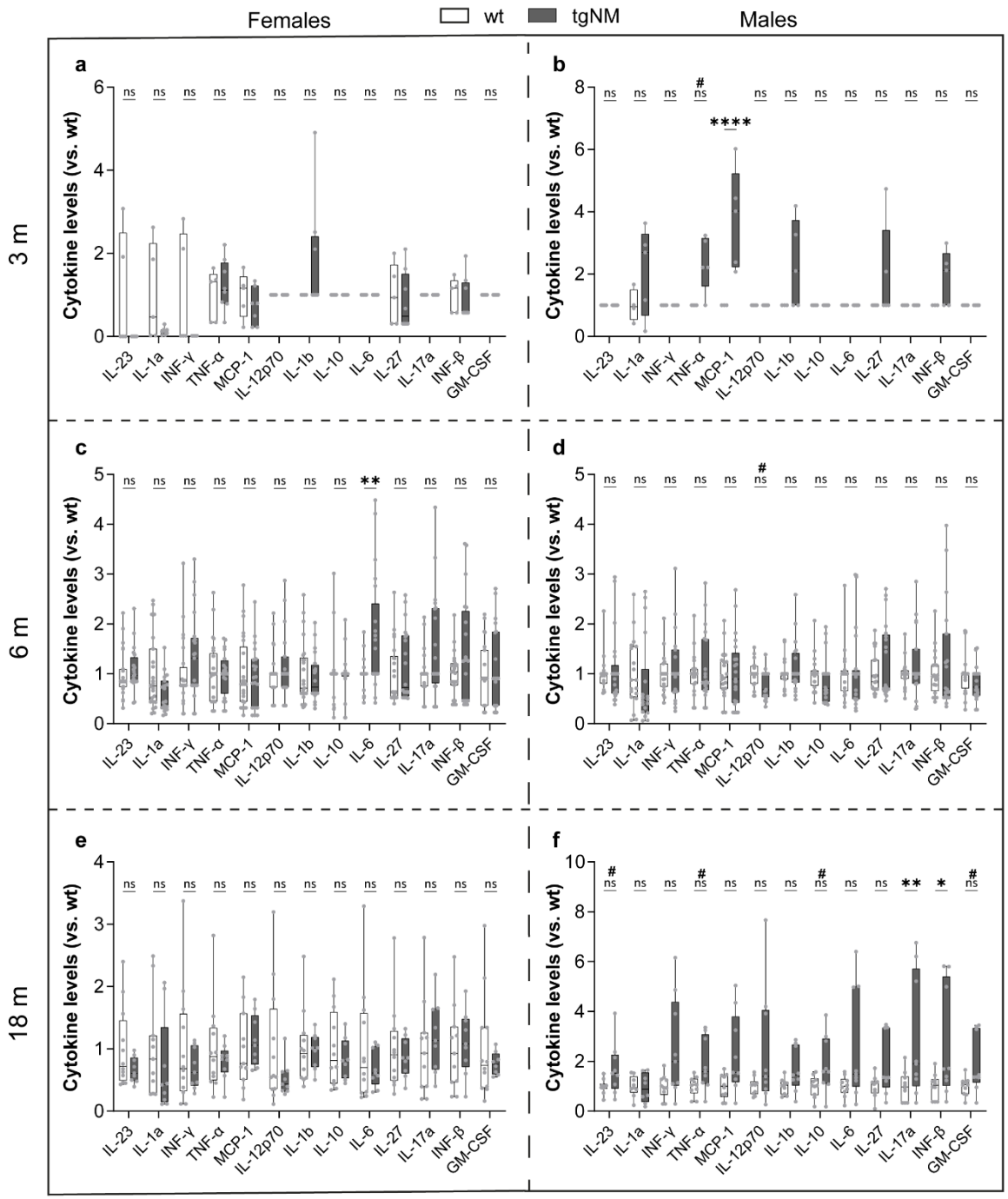

Figure 37. Fecal cytokine profile in wt and tgNM mice. a, c, e) Cytokine levels profile in fecal samples at 3, 6 and 18 m of tgNM females normalized to wt females 3 m [n=5(wt), n=8(tgNM)], 6 m [n=25(wt), n=21(tgNM)], 18 m [n=12(wt), n=9(tgNM)]. **b, d, f)** Cytokine levels profile in fecal samples at 3, 6 and 18 m of tgNM males normalized to

wt males. 3 m [n=4(wt), n=5(tgNM)], 6 m [n=20(wt), n=21(tgNM)], 18 m [n=10(wt), n=9(tgNM)]. *p≤0.05 compared to wt-matched (Uncorrected Fisher's LSD). #p≤0.05 compared to wt-matched (Mann-Whitney test).

1.6 GI permeability and altered metabolism

The microarray analysis also revealed significant alterations in the metabolic and digestive processes in the duodenal samples of tgNM mice. These alterations may be associated with the observed gut barrier disruption, potentially impacting nutrient absorption and digestion. To assess this possibility, we performed a comprehensive metabolomic study on fecal samples of tgNM mice at 6 and 18 m of age, as well as serum samples at 18 m, to identify potential changes in PD-relevant cellular pathways, particularly in those related to energy metabolism.

At 6 m, tgNM females exhibited reduced levels of several metabolites (low molecular weight multimers (LMWM)) in their feces. Specifically, essential amino acids such as lysine, threonine, phenylalanine, methionine, valine and isoleucine were significantly reduced. Additionally, conditionally essential amino acids like glycine and tyrosine, among other metabolites, were also decreased (Figure 38 a). Conversely, tgNM males only displayed increased levels of succinate and aspartate in their feces compared to wt littermates (Figure 38 b). Analysis of SCFAs revealed no significant changes in acetate, propionate, butyrate and isobutyrate levels when compared to wt littermates in females and males (Figure 38 c, d).

We next evaluated the metabolic and lipid profiles at 18 m of age of feces and serum samples from the same animals. Contrary to observations at 6 m, tgNM females at 18 m presented increased levels in their feces of essential and conditionally essential amino acids, along with other metabolites (Figure 38 e). Notably, SCFAs, which are typically reduced in fecal samples of PD patients (Unger et al., 2016), were found to be increased in the feces of tgNM females at 18 m compared to wt littermates. Specifically, elevated levels of acetate, propionate, butyrate, isobutyrate and valerate were observed (Figure 38 j). In contrast, no significant differences were observed in the metabolic profile of tgNM males (Figure 38 f). neither in the SCFAs levels (Figure 38 k).

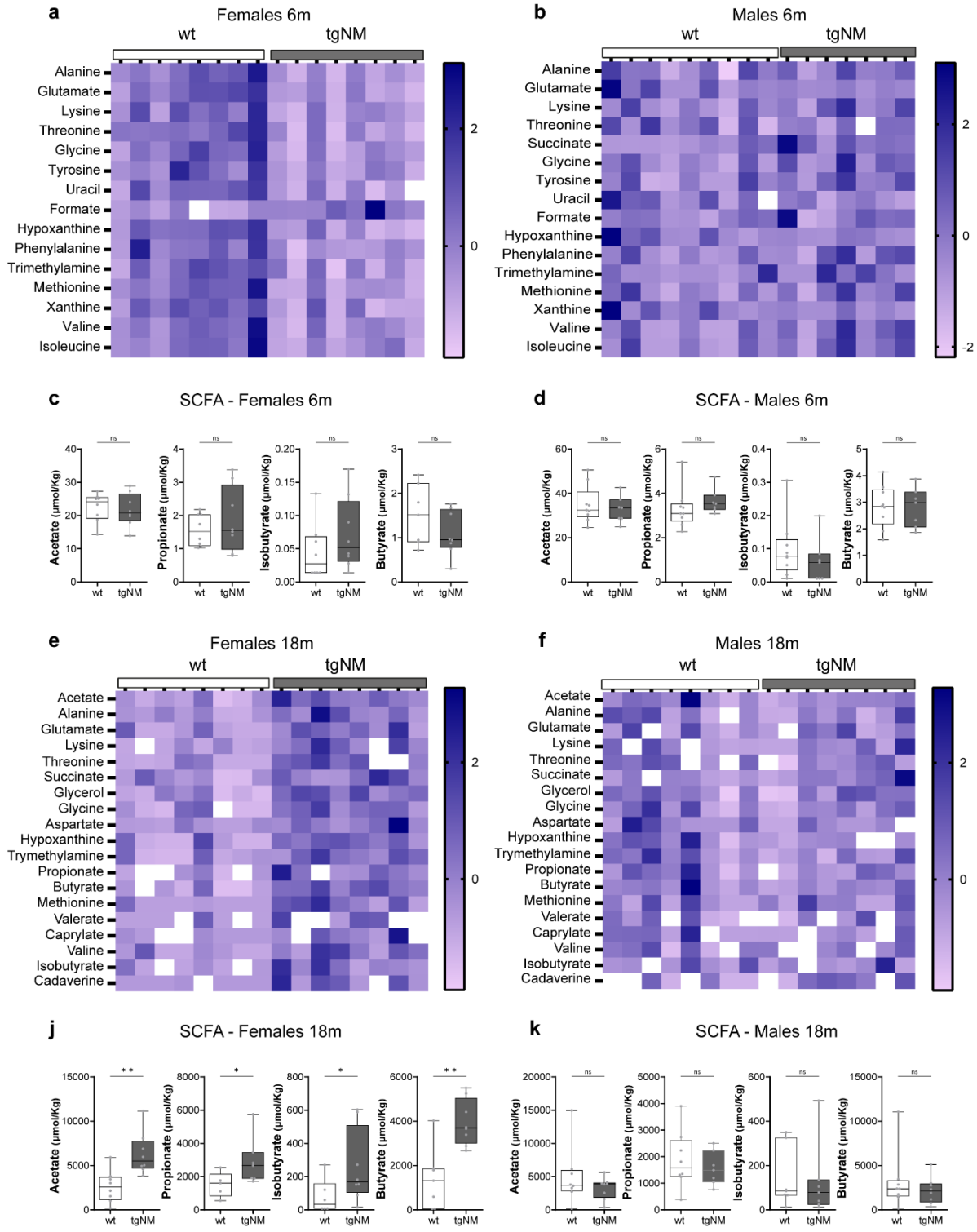

Figure 38. Fecal metabolomics in wt and tgNM mice. a-b) Metabolite levels of LMWM profile in 6 m tgNM compared to wt (µmol/Kg) **(a)** females and **(b)** males. **c-d)** SCFAs levels in 6 m tgNM compared to wt **(c)** females and **(d)** males. *p≤0.05 compared to age-matched wt (Mann-Whitney test). 6 m [F: n=8(wt), n=8(tgNM), M: n=9(wt), n=7(tgNM)]. **e-f)** Metabolite levels of LMWM profile in 18 m tgNM compared to wt (µmol/Kg) **(e)** females and **(f)** males. **j-k)** SCFAs levels in 18 m tgNM compared to wt **(j)** females and **(k)** males. *p≤0.05 compared to age-matched wt (Mann-Whitney test). 18 m [F: n=8(wt), n=8(tgNM), M: n=8(wt), n=8(tgNM)].

For the serum samples, we evaluated the metabolic, lipid, glycoprotein and lipoprotein profiles. At 18 m, the LMWM profile of tgNM females revealed reduced levels of glycine and histidine, alongside increased levels of creatine (Figure 39 a, c). Contrarily, no significant differences were detected in males (Figure 39 b). Notably, SCFAs could not be detected in serum samples in both sexes.

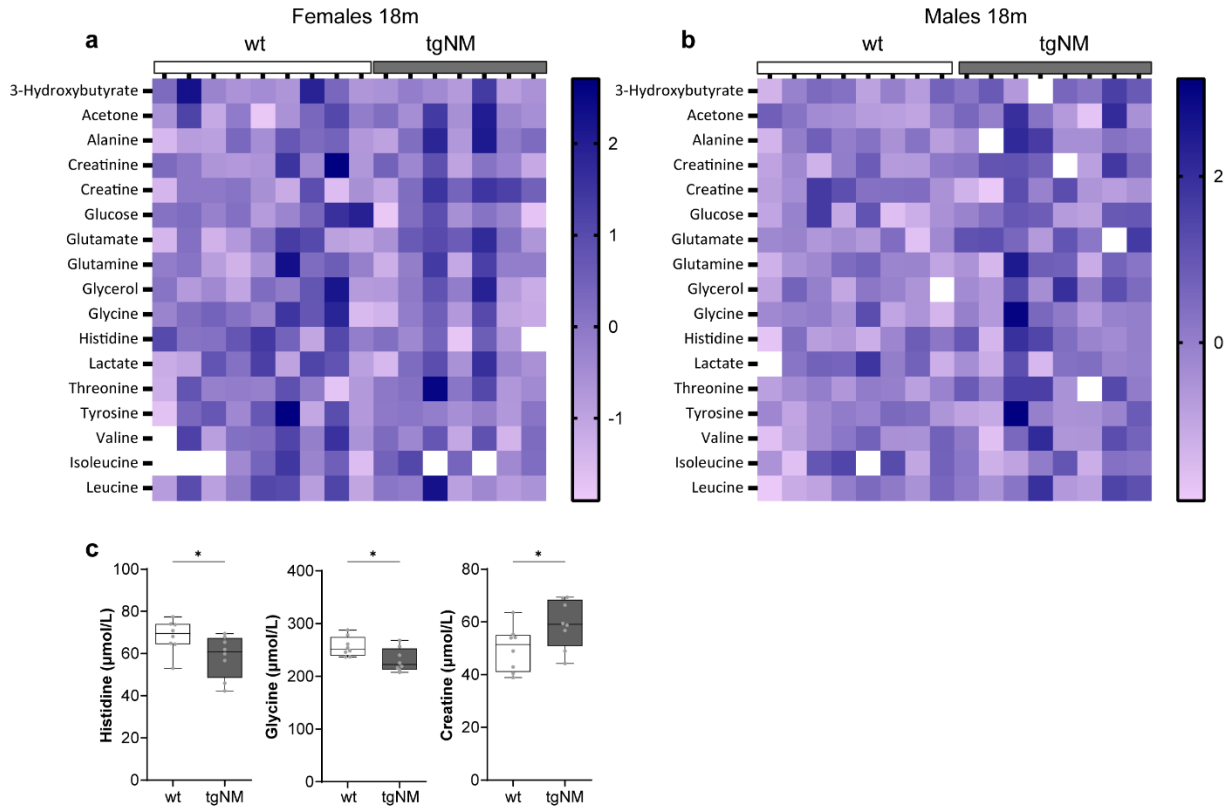

Figure 39. Serum LMWM profile in wt and tgNM mice. a-b) Metabolite levels of the LMWM profile in 18 m tgNM compared to wt (µmol/L) **(a)** females and **(b)** males. **c)** Significantly altered metabolites in females. *p≤0.05 compared to age-matched wt (Mann-Whitney test). [F&M: n=8(wt), n=8(tgNM)].

The lipid profile in our study revealed significant elevations in glycerophospholipids (PL), sphingomyelin (SM), and lysophosphatidylcholine (LPC). In addition, we observed increased levels of polyunsaturated fatty acids (PUFAs), notably an elevated combined content of omega-6 and omega-7 fatty acids, as well as omega-3 fatty acids, including a rise in the sum of arachidonic acid (ARA) and eicosapentaenoic acid (EPA) (ARA+EPA) (Figure 40 a, c). In contrast, no significant alterations in the lipid profile were detected in tgNM males relative to their wt littermates at 18 m (Figure 40 b).

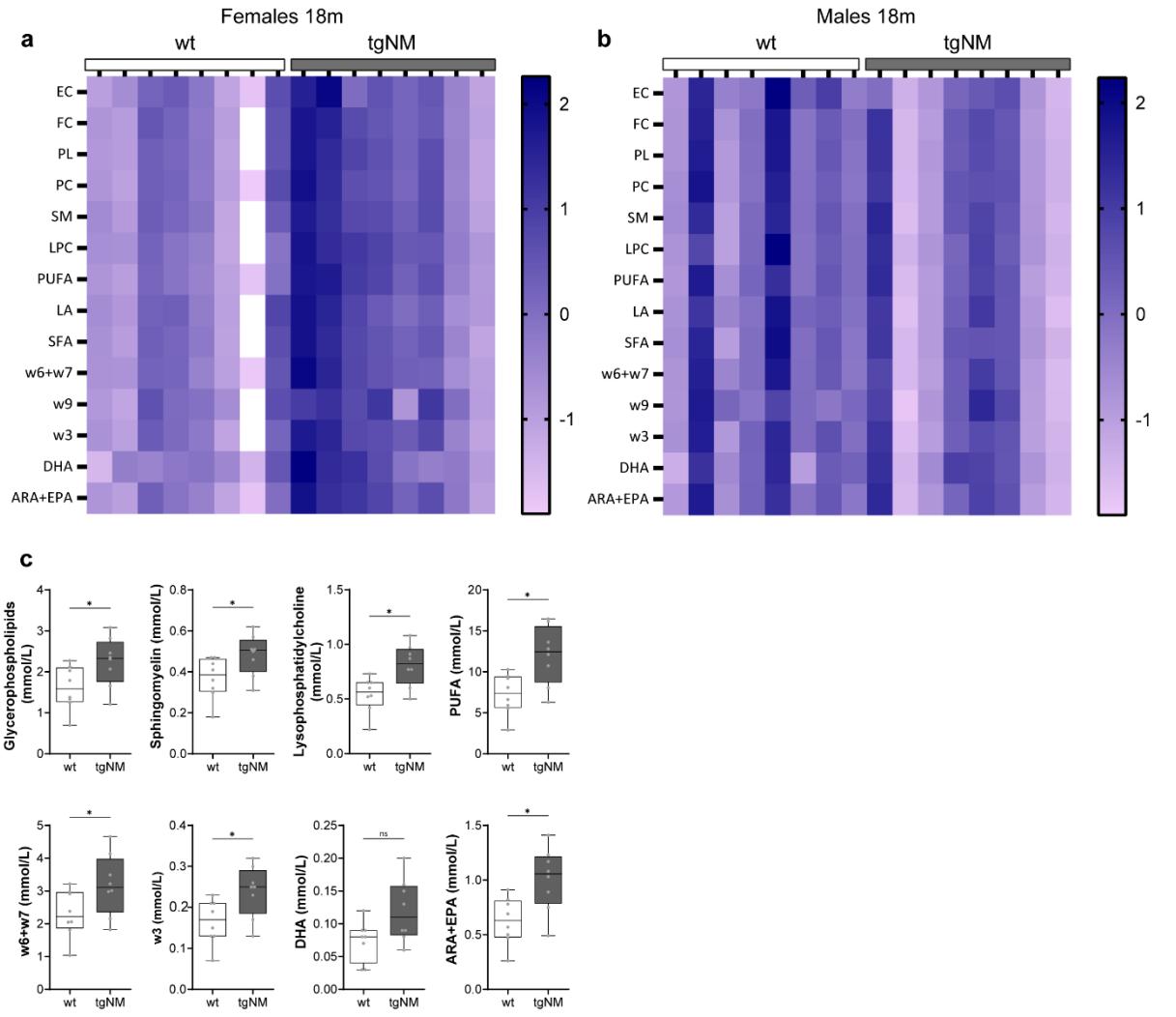

Figure 40. Serum lipid profile in wt and tgNM mice. a-b) Metabolite levels of the lipid profile in 18 m tgNM compared to wt (mmol/L) **(a)** females and **(b)** males. **c)** Significantly altered metabolites in females. *p≤0.05 compared to age-matched wt (Mann-Whitney test). [F&M: n=8(wt), n=8(tgNM)].

The lipoprotein profile showed significantly increased levels of HDL-C and reduced levels of very low-density lipoprotein (VLDL) particles, specifically large and small ones in tgNM females (Figure 41 a, c). In 18 m tgNM males, we only observed reduced levels of VLDL-C (Figure 41 b, d).

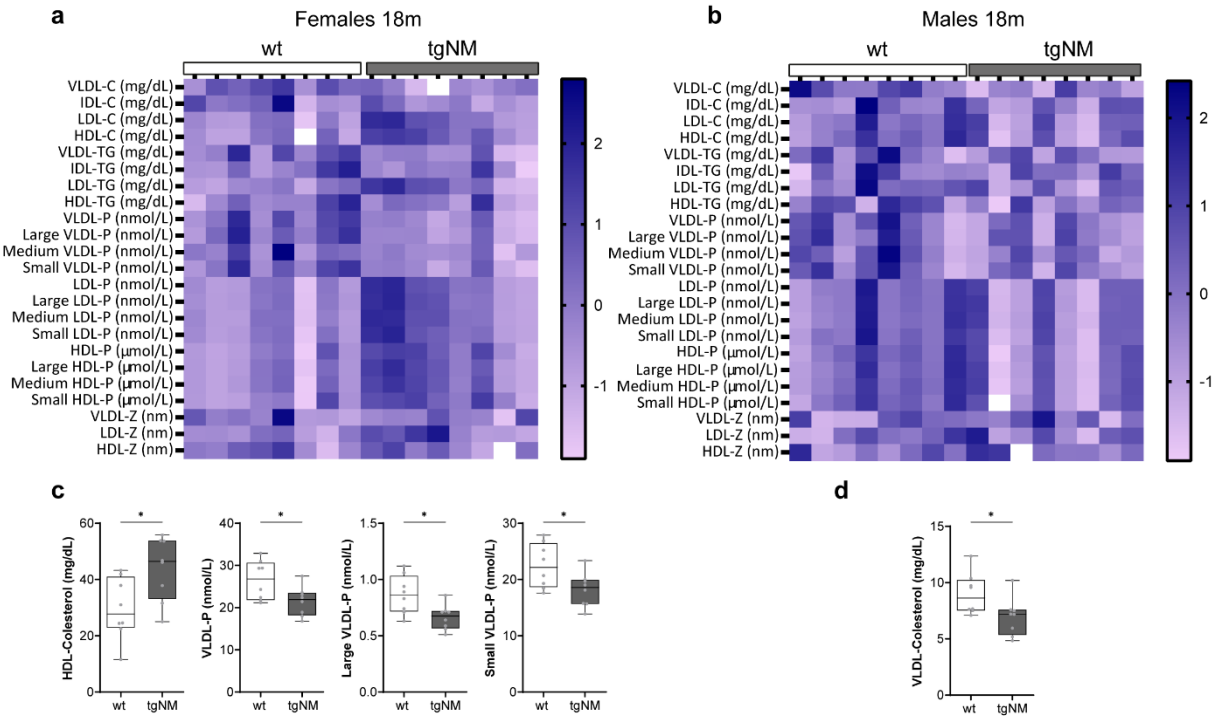

Figure 41. Serum lipoprotein profile in wt and tgNM mice. a-b) Metabolite levels of the lipoprotein profile in 18 m tgNM compared to wt (µmol/Kg) **(a)** females and **(b)** males. **c)** Significantly altered metabolites in females. **d)** Significantly altered metabolite in males. *p≤0.05 compared to age-matched wt (Mann-Whitney test). [F&M: n=8(wt), n=8(tgNM)].

Finally, the glycoprotein profile revealed increased serum levels of glycoprotein-A (Glyc-A) and B (Glyc-B), as well as an increased height-to-width (H/W) ratio of Glyc-B in tgNM females (Figure 42 a, c) and no significant changes in tgNM males were detected (Figure 42 b).

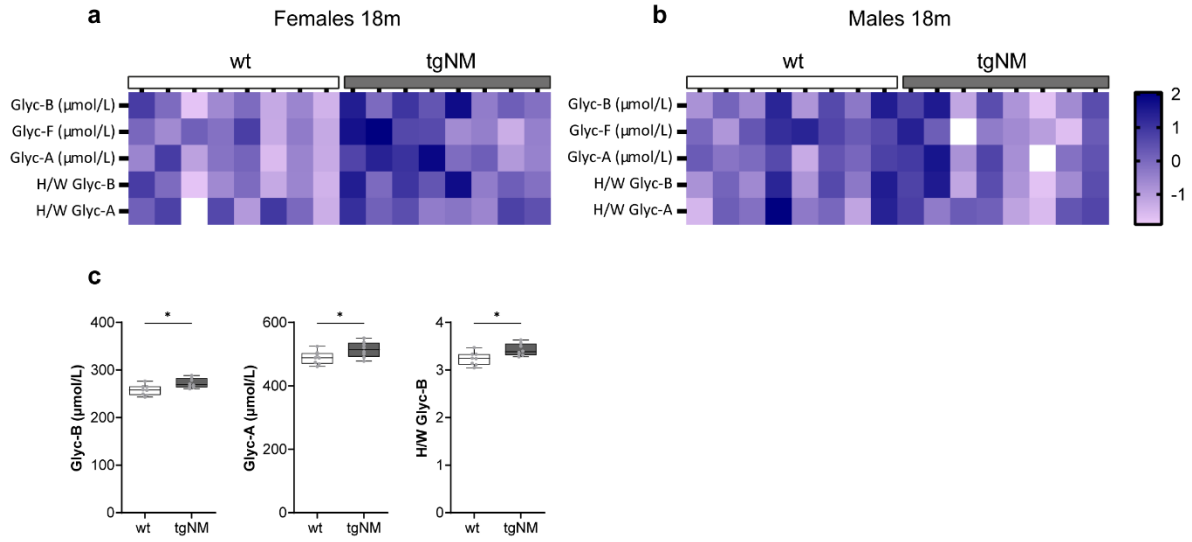

Figure 42. Serum glycoproteic profile in wt and tgNM mice. a-b) Metabolite levels of the glycoprotein profile in 18 m tgNM compared to wt (µmol/Kg) **(a)** females and **(b)** males. **c)** Significantly altered metabolites in females. *p≤0.05 compared to age-matched wt (Mann-Whitney test). [F&M: n=8(wt), n=8(tgNM)].

Altogether, these findings show a significant sex and age dependent alterations in metabolic and lipid profiles in tgNM mice, suggesting a systemic impact of gut barrier disruption on metabolic homeostasis. Most of the changes were observed in females, while males presented minimal changes.

1.7 Fecal gut microbiota characterization

To better understand the complex interactions between GI function, immune responses and metabolic shifts in tgNM mice, we analyzed the composition of the gut microbiome by 16S rRNA sequencing on fecal samples. Initially, samples were collected from both female and male mice at 6 m. However, as subsequent analyses revealed more pronounced phenotype in females, we expanded our sampling to include females' feces at 1, 3, 6, and 18 m. The 16S rRNA sequencing and all the associated bioinformatic analysis were performed by Microomics Systems S.L.

1.7.1 α-diversity

Measurements of α-diversity were used to study the diversity within a single sample. The metrics used were richness, that are the number of different phylotypes present in a community (observed Operational Taxonomic Units (OTUs)), and evenness, that reflects the relative abundance of these species, considering the number and the abundance of phylotypes in a community. In the first and second analysis, both richness and evenness were not significant between tgNM animals and their wt littermates at any time point (Figure 43 a-d, Figure 44 a, b), indicating similar variety and abundance of microbial species in their GI tracts. However, we observed that the number of observed OTUs is decreased in tgNM females at 18 m compared to 3 m, and the evenness is decreased in both wt and tgNM females at 18 m compared with wt and tgNM at 3 m respectively (Figure 44 a-b). These observations suggest that aging contributes to shifts in gut microbial diversity.

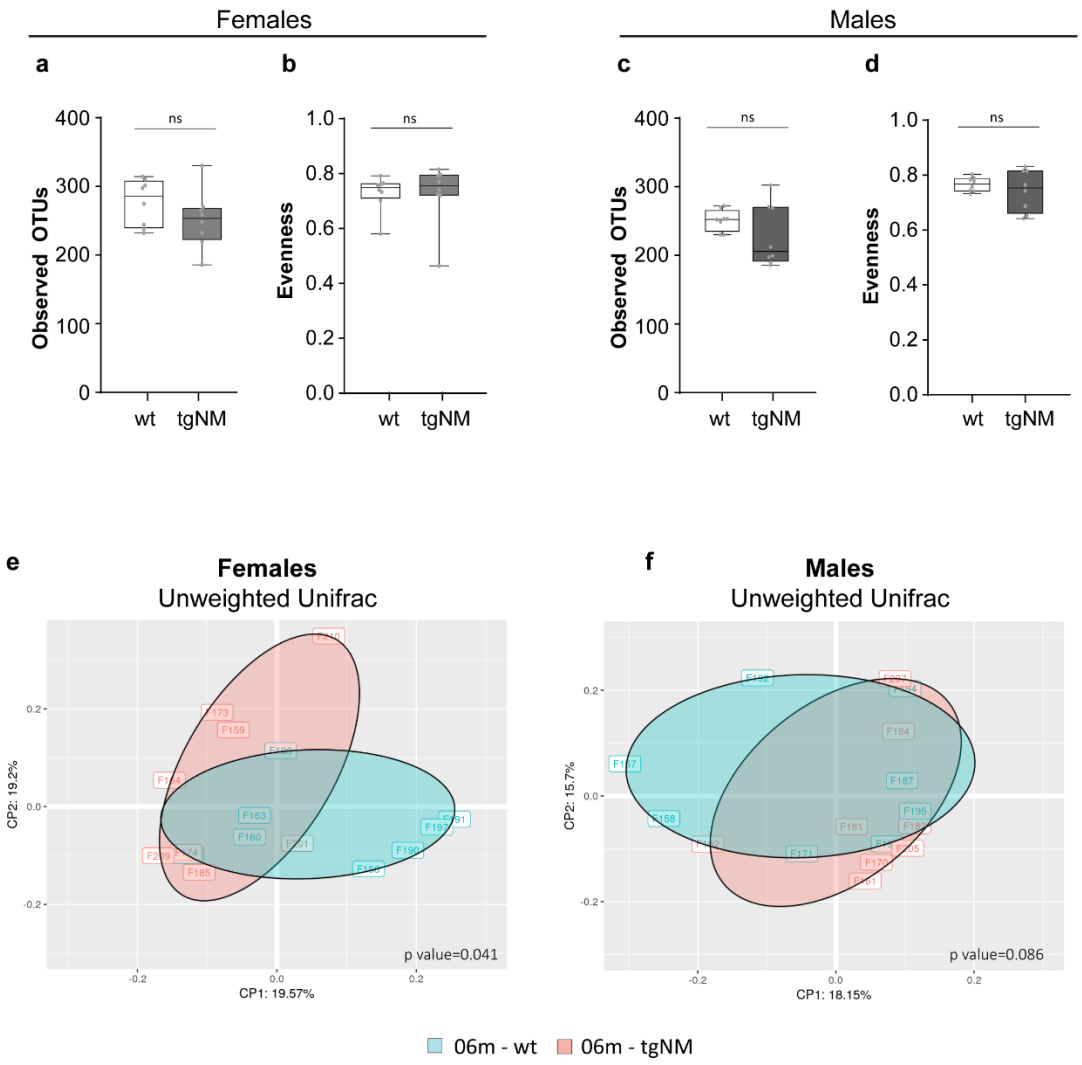

Figure 43. Fecal α-diversity boxplots and β-diversity PCoA plots in tgNM and wt mice. **a, c)** Number of different phylotypes present in a community (Observed OTUs) at 6 m in tgNM **(a)** females and **(c)** males compared to their wt. **b, d)** Given as the Pielou's evenness index, quantification of how equal the community is numerically. Mann Whitney tests tgNM compared to age-matched wt not significant. **e-f)** Unweighted UniFrac PCoA plots at 6 m in **(e)** female and **(f)** male mice. It only considers the presence or absence of OTUs *p≤0.05 Pairwise PERMANOVA analysis tgNM compared to wt. Females **p value = 0.041*,** males p value=0.086 ns. 6 m F&M [n=8(wt), n=8 (tgNM)].

1.7.2 β-diversity

β-diversity was used to analyze the variations in microbial community composition across different groups. This was quantified using PERMANOVA applied to the Unweighted UniFrac distance, which considers the presence or absence of OTUs. In tgNM males at 6 m, PCoA revealed no significant differences in β-diversity compared to their wt littermates (Figure 43 f). Conversely, tgNM females exhibited significant differences in β-diversity compared to their wt counterparts at both analysis at 6 m (Figure 43 e, Figure 44 c) and at 18 m (Figure 44 c). Notably, at 3 m a non-significant trend was observed (Table 12), suggesting that changes in gut microbiota may precede the behavioral alterations observed at

6 m, while no differences were evident at 1 m (Figure 44 c). These findings indicate that the divergence in gut microbiota composition between tgNM and wt females becomes more pronounced after 3 m of age.

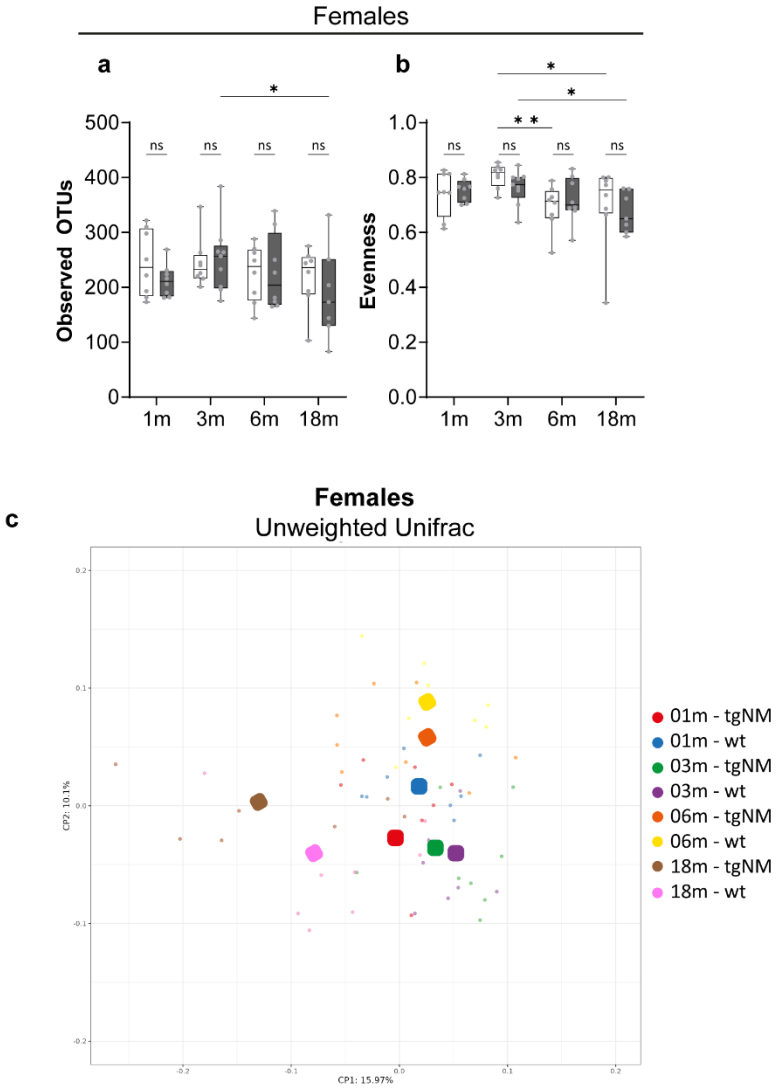

Table 12. Pairwise Permanova Analysis for Unweighted Unifrac in females. Main comparisons are highlighted in dark purple (*p value≤0.05).

	tgNM – 01m	tgNM – 03m	tgNM – 06m	tgNM – 18m
wt - 01m	0,235	0,0047	0,0015	0,0015
wt – 03m	0,0015	0,0622	0,0015	0,0015
wt – 06m	0,0024	0,0015	0,0146*	0,0015
wt – 18m	0,0024	0,0015	0,0015	0,0452*

Figure 44. Fecal α-diversity boxplots and β-diversity PCoA plot in tgNM and wt females at different time points. **a)** Number of different phylotypes present in a community (Observed OTUs) at 1, 3, 6, 18 m in tgNM females compared to age-matched wt and compared to genotype-matched at other time points. **b)** Given as the Pielou's evenness index, quantification of how equal the community is numerically. *p≤0.05 compared age-matched wt and compared to genotype-matched at other time points (Uncorrected Fisher's LSD). **c)** Unweighted UniFrac PCoA plots

at 1, 3, 6, 18 m in female mice. It only considers the presence or absence of OTUs. *p≤0.05 compared to wt (Pairwise PERMANOVA analysis) p values appear in Table 12. 1 & 6 m [n=8(wt), n=8 (tgNM)]; 3 m [n=8(wt), n=9 (tgNM)]; 18 m [n=8(wt), n=7 (tgNM)].

1.7.3 Taxonomic profile

We next characterized the differential abundance of taxa using the Negative Binomial Model (NBM), a statistical approach commonly applied to count data in microbiome studies due to its ability to account for overdispersion. When comparing tgNM females and males to their wt counterparts at 6 m, we observed that tgNM females presented a greater number of differentially abundant taxa than tgNM males. Specifically, at the genus level, 17 taxa were significantly altered in females compared to only 9 in males (Table 13, Table 14). Notably, tgNM females presented an increased relative abundance of the genera *Akkermansia* and a decreased abundance of *Roseburia*, whereas tgNM males presented reduced relative abundance of *Desulfovibrio* and *Lanchospiraceae*.

Table 13. Number of differentially abundant taxa identified as significant by the Kruskal-Wallis test in tgNM vs wt females. The table presents the number of differentially abundant taxa (p value≤0.05) at various taxonomic levels (i.e. phylum, class, order, family, genus and species) at the time point studied (6 m).

	Nº of differentially abundant taxa
Taxa level	Time point
	6m
Phylum	2 (Patescibacteria, Verrucomicrobiota)
Class	3
Order	7
Family	8 (Atopobiaceae, Eggerthellaceae, Acholeplasmataceae, RF39, Monoglobaceae, Clostridia_uncultured, Saccharimonadaceae, Akkermansiaceae)
Genus	17 (Coriobacteriaceae_UCG-002, Enterorhabdus, Anaeroplasma, Stoquefichus, Faecalibaculum, Turicibacter, RF39, Roseburia, [Eubacterium]_ventriosum_group, [Eubacterium]_xylanophilum_group, Monoglobus, UCG-005, Incertae_Sedis, Ruminococcus, Clostridia_uncultured, Candidatus_Saccharimonas, Akkermansia)
Species	25

Table 14. Number of differentially abundant taxa identified as significant by the Kruskal-Wallis test in tgNM vs wt males. The table presents the number of differentially abundant taxa (p value≤0.05) at various taxonomic levels (i.e. phylum, class, order, family, genus and species) at the time point studied (6 m).

	Nº of differentially abundant taxa
Taxa level	Time point
	6m
Phylum	2 (Desulfobacterota, Firmicutes)
Class	1
Order	3
Family	3 (Desulfovibrionaceae, Clostridia_UCG-014, coprostanoligenes_group)
Genus	9 (Alloprevotella, Desulfovibrio, Turicibacter, Christensenellaceae_R-7_group, Clostridia_UCG-014, Lachnospiraceae, Lachnospiraceae-uncultured, Ruminococcus, [Eubacterium]_coprostanoligenes_group)
Species	14

Next, we assessed genotype differences and temporal dynamics in tgNM females compared to wt by analyzing their taxonomic profiles at 1, 3, 6 and 18 m (Table 15). Our analysis indicates a progressive increase in the number of differentially abundant taxa between genotypes with age. Notably, at the genus level at 6 m, we again observed decreased *Roseburia* abundance consistent with our earlier findings, although no significant changes in *Akkermansia* were detected this time. By 18 m, there was a reduction in the relative abundance of *Alistipes* and *Prevotellaceae UCG-001*, together with an increase in *Bififobacterium*, among others.

We next evaluated the aging effects within each genotype. We found that wt females exhibited a higher number of differentially abundant genera at young ages. Specifically, 17 genera were different between 3 and 1 m, but this difference gradually decreased to 8 and 10 genera by 6 and 18 m, respectively, compared to 1 m. Conversely, tgNM females displayed an increasing number of differentially abundant taxa with age, rising from 5 genera at 3 m, to 13 and 18 genera at 6 and 18 m, respectively, compared to 1 m (Table 16).

Overall, these findings reveal distinct shifts in the gut microbiota between tgNM and wt mice, with changes being more pronounced in females. Notably, the genotype effect on the number of differentially abundant taxa increases over time. Additionally, aging seems to affect the gut microbiota of wt and tgNM females in a different pattern. In wt females, differences are more pronounced at younger ages, whereas in tgNM females, the differences become increasingly pronounced over time, suggesting a potential link with age-dependent NM accumulation.

Table 15. Number of differentially abundant taxa identified as significant using the NBM in tgNM vs wt females (Genotype effect). The table presents the number of differentially abundant taxa (p value≤0.05) at various taxonomic levels (i.e. phylum, class, order, family, genus and species) across each studied time point (1, 3, 6 and 18 m).

Number of differentially abundant taxa				
Taxa level	Time point			
	1m	3m	6m	18m
Phylum	1 (Patescibacteria)	3 (Actinobacteriota, Cyanobacteria, Proteobacteria)	2 (Actinobacteriota, Bacteroidota)	4 (Actinobacteriota, Bacteroidota, Cyanobacteria, Proteobacteria)
Class	1	3	2	7
Order	1	5	3	8
Family	1 (Saccharimonada-ceae)	7 (Atopobiaceae, Eggerthellaceae, Gastranaerophilales, Erysipelatoclostridia-ceae, RF39, Anaerovoracaceae, Sutterellaceae)	3 (Muribaculaceae, Monoglobaceae, [Eubacterium]_coprostanoligenes_group	10 (Bifidobacteriaceae, Atopobiaceae, Muribaculaceae, Rikenellaceae, Gastranaerophilales, Clostridia_vadinBB60_group, Oscillospiraceae, Ruminococcaceae, uncultured, Sutterellaceae)
Genus	5 (Rikenellaceae_RC9_gut_group, Lachnoclostridium, Harryflintia, Paludicola, Candidatus_Saccharimonas)	8 (Coriobacteriaceae_UCG-002, Enterorhabdus, Gastranaerophilales, Erysipelatoclostridium, Faecalibaculum, RF39, Incertae_Sedis, Parasutterella)	9 (Muribaculaceae, Faecalibaculum, Roseburia, [Eubacterium]_xylanophilum_group, Lachnospiraceae-uncultured, Monoglobus, Butyricicoccus, Incertae_Sedis, [Eubacterium]_coprostanoligenes_group)	21 (Bifidobacterium, Coriobacteriaceae_UCG-002, Muribaculaceae, Prevotellaceae_UCG-001, Alistipes, Rikenellaceae_RC9_gut_group, Gastranaerophilales, Bilophila, Dubosiella, Faecalibaculum, Turicibacter, Erysipelotrichaceae-uncultured, Christensenellaceae-uncultured, Clostridia_vadinBB60_group, Marvinbryantia, Oscillibacter, Oscillospiraceae-uncultured, Incertae_Sedis, Rhodospirillales-uncultured, Parasutterella)
Species	9	8	13	28

Table 16. Number of differentially abundant taxa identified as significant using the NBM in tgNM and wt females (Age effect). The table presents the number of differentially abundant taxa (p value≤0.05) at the genus level across each studied time point (1, 3, 6 and 18 m) for wt and tgNM females.

Number of differentially abundant taxa						
Taxa level	wt			tgNM		
	Time point			Time point		
	1m vs 3m	1 m vs 6m	1m vs 18 m	1m vs 3m	1 m vs 6m	1m vs 18 m
Genus	17	8	10	5	13	18

1.8 The neuroendocrine gut-brain axis characterization

During the characterization of tgNM mice, we observed that tgNM animals, specifically tgNM females, presented increased body weight (Figure 14 c), expanded adipose tissue (Figure 15 j-m) and elevated food and water intake (Figure 14 f, i). These observations suggest that tgNM mice may experience endocrine and/or metabolic disturbances; to explore this further, we investigated the neuroendocrine gut-brain axis. This bidirectional communication network connects the GI tract with the CNS through an intricate set of hormones, neuropeptides and other signaling molecules that play several roles in regulating physiological and behavioral processes. Nutrient-related signals reach the CNS via spinal, vagal, and endocrine pathways. Among these, endocrine signaling involves the release of gut-derived peptides into the systemic circulation, which act on key brain regions, including the DVC and the hypothalamus. This complex signaling pathway not only regulates appetite and metabolism but also modulates emotional and stress-related responses, highlighting its influence on both central and peripheral functions (Gruber et al., 2024; Mayer, 2011). However, the functional consequences of NM accumulation in the hypothalamus and its possible neurodegeneration have not been assessed previously (Laguna et al., 2024).

1.8.1 The hypothalamus in tgNM mice

Previously, we demonstrated that NM accumulation leads to the degeneration of NM-laden neurons in the DVC and that NM accumulates in the hypothalamus of tgNM mice (Laguna et al., 2024). In human studies, the presence of LBs in the hypothalamus has been associated with autonomic and endocrine dysfunctions commonly observed in PD patients (Sandyk et al., 1987). Moreover, recent studies have provided evidence of microstructural alterations in the hypothalamus of PD patients during early neurodegenerative stages (C. Zhou et al., 2024).

To evaluate potential alterations in the hypothalamus, we analyzed the expression levels of key genes involved in its function by RT-qPCR. We first assessed the expression levels of L-amino acid decarboxylase (AADC) and TH to assess the potential disruption in DA synthesis in the hypothalamus of tgNM mice. At

18 m, tgNM females exhibited a significant reduction in both AADC and TH expression compared to wt littermates (Figure 45 a), suggesting a decline in DA synthesis. In contrast, 18 m tgNM males showed a significant increase in AADC expression and a trend toward elevated TH levels (Figure 45 b). At 6 m, no significant changes were detected in either AADC or TH expression for any sex, suggesting that alterations in DA metabolism may appear later with the progression of NM accumulation.

In the arcuate (ARC) nucleus, anorexigenic neurons secrete proopiomelanocortin (POMC) and cocaine- and amphetamine-regulated transcript (CART) neuropeptides to suppress appetite. Orexigenic neurons within the same nucleus, which express neuropeptide Y (NPY) and agouti-related peptide (AgRP), stimulate appetite. We assessed the expression of these markers to identify possible alterations that could explain the altered feeding behavior observed in tgNM mice. At 6 m, tgNM males displayed reduced POMC expression compared to wt littermates, but this reduction was no longer observed at 18 m (Figure 45 b). No significant changes were detected in the expression levels of CART or NPY at any time point for either sex. NPY-positive neurons project to the lateral hypothalamic area (LHA), where they enhance the production and release of other orexigenic peptides such as melanin-concentrating hormone (MCH) and orexin-A (ORX-A). However, no significant differences were observed in the expression levels of these peptides or related circuits at any time point in either sex (Figure 45 a, b). These results may indicate that while the hypothalamic circuitry involved in feeding behaviour and energy regulation remains largely intact, age- and sex-specific vulnerabilities in DA metabolism might contribute to the metabolic phenotypes observed in tgNM mice.

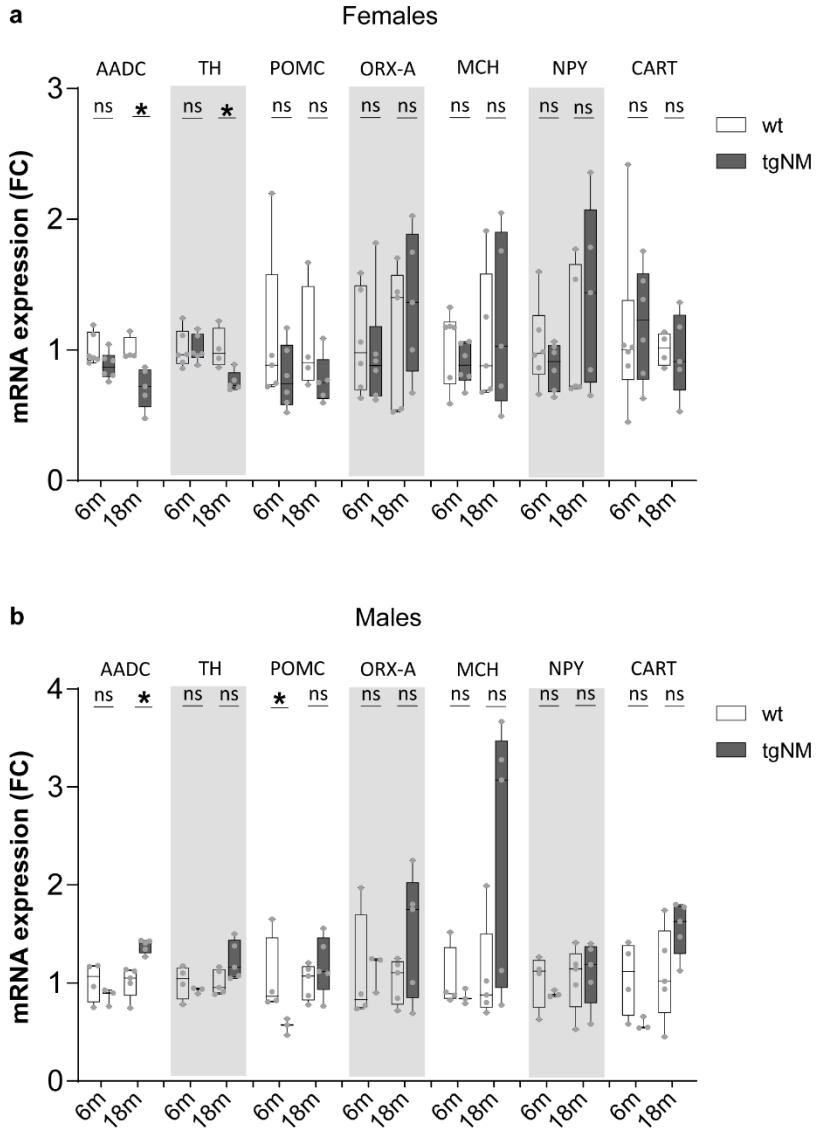

Figure 45. Enzymes and neuropeptides expression in the hypothalamus of wt and tgNM mice. a-b) Expression levels in the hypothalamus of 6 and 18 m old **(a)** females and **(b)** males. Groups are normalized to their age-matched wt. *p≤0.05 compared to age-matched (Uncorrected Fisher's LSD). 6 m [F: n=5-6(wt), n=6(tgNM); M: n=4(wt), n=3(tgNM)], 18 m [F: n=4-5(wt), n=5(tgNM); M: n=5(wt), n=5(tgNM)].

1.8.1.1 Gut peptides and hormones characterization in tgNM animals.

We next characterized key metabolic hormones involved in various pathways, including the satiety signaling pathway, by measuring levels of ghrelin, GLP-1 active, glucagon, insulin, leptin, peptide YY (PYY) and amylin by a multiplex ELISA. At 6 m, tgNM females presented significantly elevated serum levels of GLP-1, leptin and PYY compared to wt littermates (Figure 46 a). TgNM males showed increased levels of leptin and insulin (Figure 46 b). However, by 18 m, only insulin levels remained elevated in tgNM females compared to wt littermates (Figure 46 c), with no significant hormonal changes observed in tgNM males

(Figure 46 d). Despite the increase in leptin, a key component of the satiety signaling pathway, tgNM females continued to exhibit increased food intake, adipose tissue accumulation and increased body weight after 6 m. These findings suggest the possibility that tgNM females have developed leptin resistance, leading to persistent hunger despite high energy reserves. Additionally, the elevated levels of gut-derived peptides GLP-1 and PYY, which are normally released after meals to promote satiety, suggest a compensatory response to the increased food intake. However, if the downstream signaling pathways are impaired, these peptides become less effective at inducing satiety, further contributing to the observed overeating behavior in these animals.

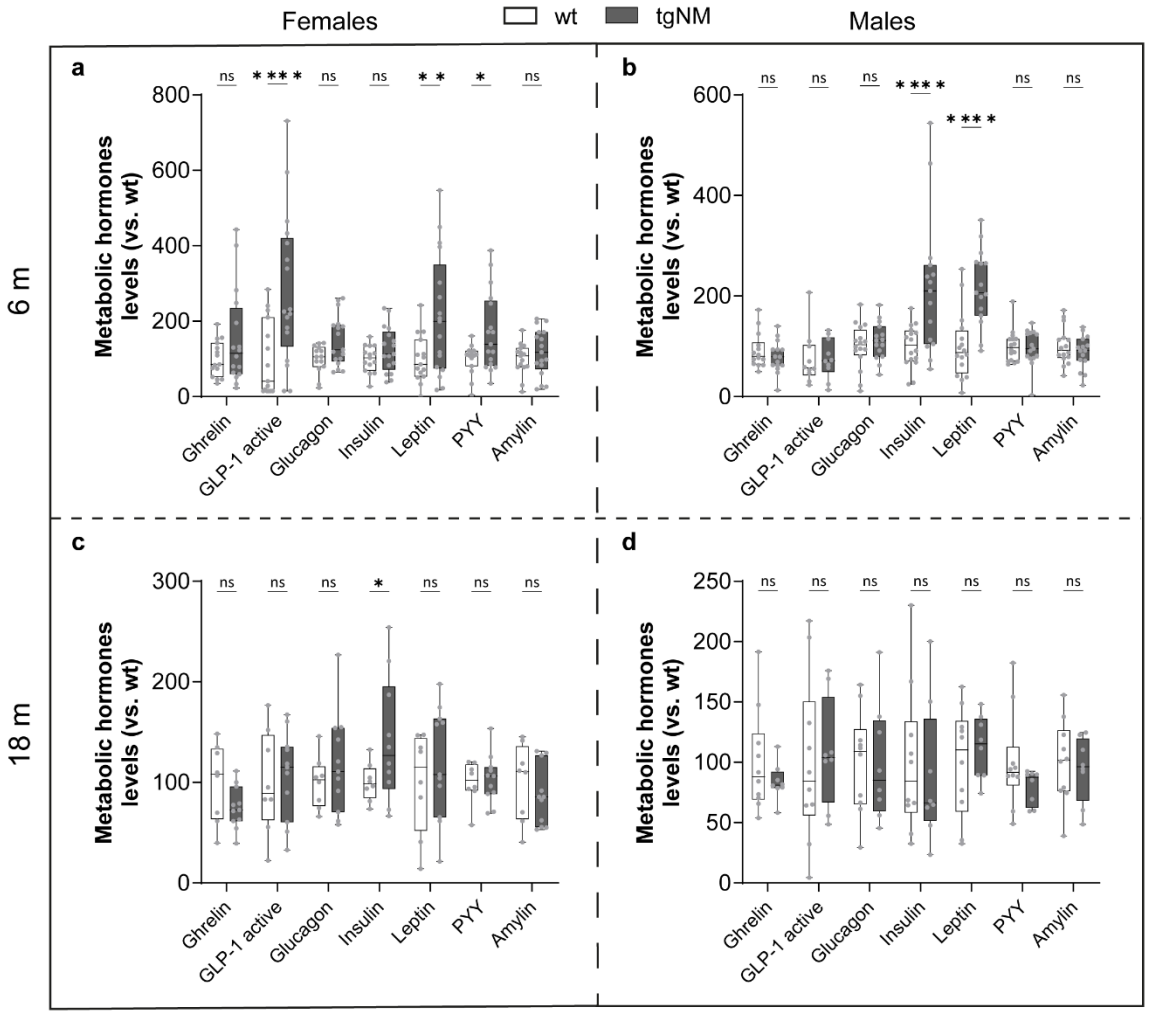

Figure 46. Serum metabolic hormones profile in wt and tgNM mice. a, c) Levels in tgNM females at 6 and 18 m normalized to wt females. *p≤0.05 compared to wt-matched (Uncorrected Fisher's LSD). 6 m [n=15(wt), n=17(tgNM)], 18 m [n=8(wt), n=11(tgNM)]. **b, d)** Levels in tgNM males at 6 and 18 m normalized to wt males. *p≤0.05 compared to wt-matched (Uncorrected Fisher's LSD). 6 m [n=16(wt), n=15(tgNM)], 18 m [n=10(wt), n=8(tgNM)].

1.8.2 The HPA axis in tgNM mice

We next assessed the HPA axis, given its critical role in stress responses and its potential influence on gut motility (J. A. Rusch et al., 2023). To explore this pathway, we measured serum corticosterone levels at 6 and 18 m by ELISA.

Results show that tgNM females did not exhibit any significant differences in the corticosterone levels at any time point compared to their wt littermates (Figure 47 a). In contrast, tgNM males displayed elevated corticosterone levels at 6 m, but by 18 m, these levels were significantly reduced relative to wt littermates (Figure 47 b). This data suggests that the levels of hormones in the HPA axis is not altered in tgNM mice.

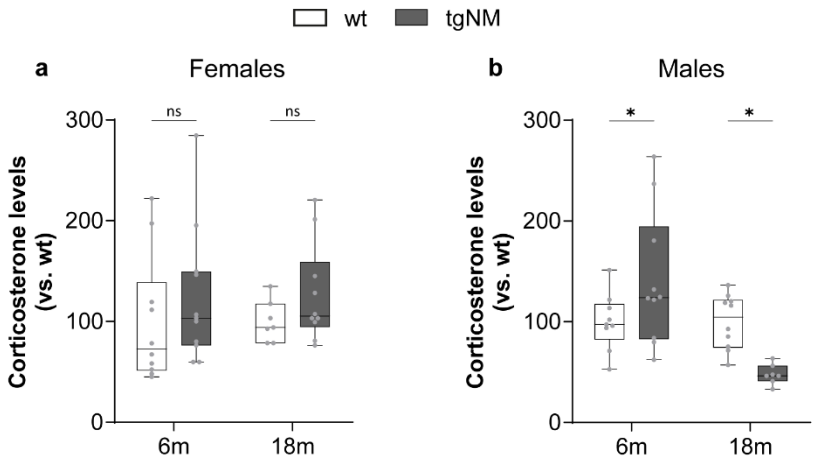

Figure 47. Serum corticosterone levels in wt and tgNM mice. a) Levels in tgNM females at 6 and 18 m normalized to wt females. Uncorrected Fisher's LSD test tgNM compared to age-matched wt not significant. 6 m [n=11(wt), n=11(tgNM)], 18 m [n=8(wt), n=11(tgNM)]. **b)** Levels in tgNM males at 6 and 18 m normalized to wt males. *p≤0.05 compared to wt-matched (Uncorrected Fisher's LSD). 6 m [n=10(wt), n=11(tgNM)], 18 m [n=10(wt), n=8(tgNM)].

1.8.3 Hypothalamic-pituitary-gonadal axis characterization

To assess potential hypothalamic-pituitary axis dysfunction and its systemic effects in tgNM mice, we analyzed serum levels of key pituitary hormones including ACTH, FSH, GH, PRL, TSH and LH at 6 and 18 m by ELISA.

At 6 m, tgNM females exhibited significantly reduced levels of PRL and LH compared to their wt littermates (Figure 48 a). However, by 18 m, these females exhibited elevated levels of PRL and GH, while FSH, TSH and LH levels were notably decreased (Figure 46 c). The increase in PRL and GH may indicate compensatory mechanisms or age-related changes in neuroendocrine function, potentially linked to the progressive accumulation of NM within the hypothalamus. Conversely, the concurrent reduction in FSH, TSH, and LH suggests a further dysregulation of the hypothalamic-pituitary-gonadal and hypothalamic-

pituitary-thyroid axes, possibly contributing to altered reproductive and metabolic outcomes in these aged tgNM females. In tgNM males, significant increases in GH, PRL, TSH and LH levels were observed at 6 m compared to their wt counterparts (Figure 48 b). However, by 18 m, these hormonal differences were no longer apparent (Figure 48 d).

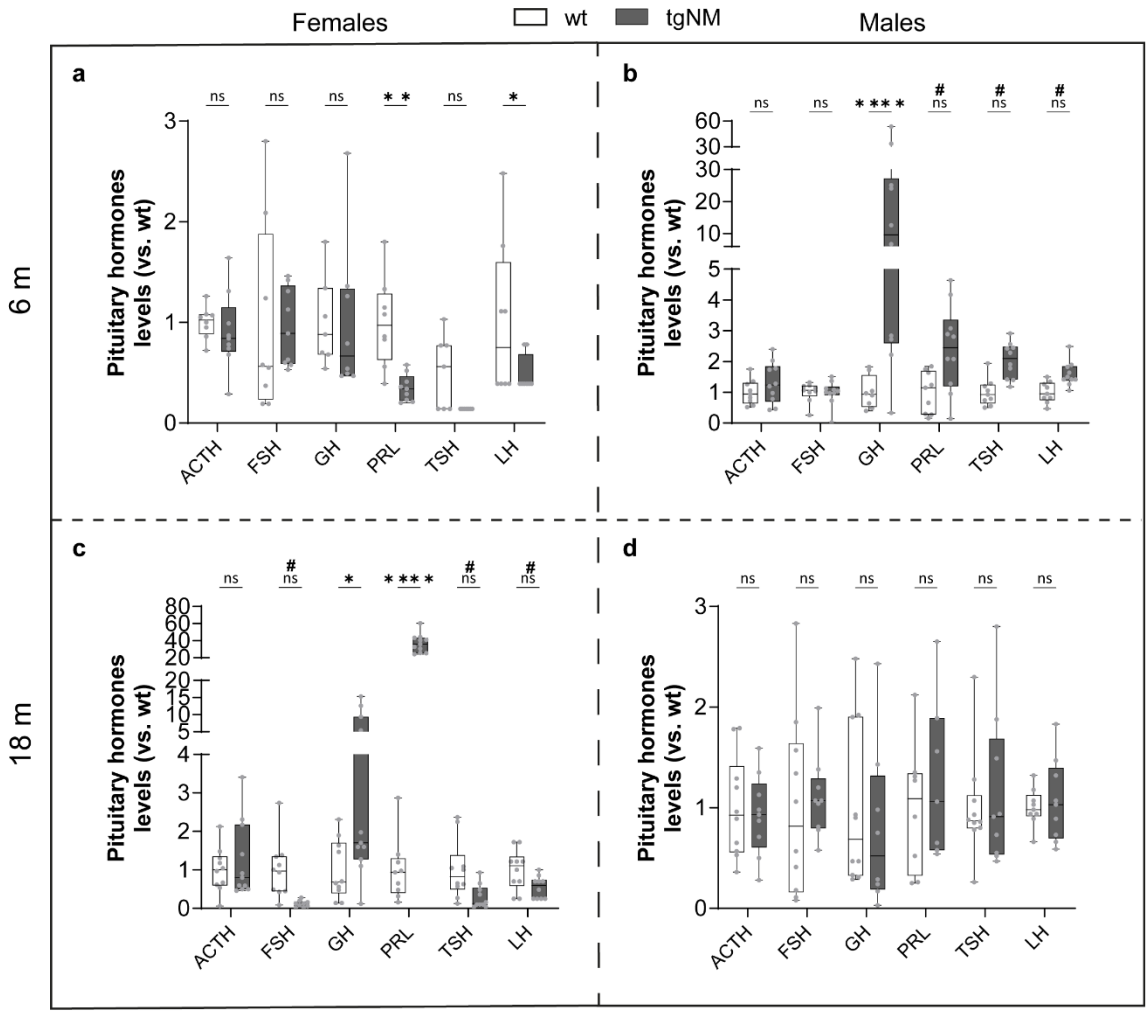

Figure 48. Serum pituitary hormones in wt and tgNM mice. a, c) Levels in tgNM females at 6 and 18 m normalized to wt females. *p≤0.05 compared to wt-matched (Uncorrected Fisher's LSD). #p≤0.05 compared to wt-matched (Mann-Whitney test). 6 m [n=8(wt), n=9(tgNM)], 18 m [n=10(wt), n=11(tgNM)]. **b, d)** Levels in tgNM males at 6 and 18 m normalized to wt males. *p≤0.05 compared to wt-matched (Uncorrected Fisher's LSD). #p≤0.05 compared to wt-matched (Mann-Whitney test). 6 m [n=9(wt), n=10(tgNM)], 18 m [n=10(wt), n=9(tgNM)].

Given the observed alterations in pituitary hormones levels and the consistent sexual dimorphism observed in our experiments, we next measured the serum levels of estradiol and testosterone in tgNM mice. In tgNM females, estradiol levels were reduced as early as 3 m and continued to decrease over time in both wt and tgNM females, with significantly lower estradiol levels detected at 18 m compared to wt littermates at this time point (Figure 49 a). This age-dependent decline in estradiol was also observed in tgNM males, with significantly lower estradiol levels detected at 18 m compared to wt littermates (Figure

49 b). Regarding testosterone, tgNM females showed an increase at 3 m; however, this elevation was not sustained at older ages. Instead, testosterone levels progressively decreased in both genotypes over time (Figure 49 c). In tgNM males, no significant increase in testosterone was observed, but wt males exhibited elevated testosterone levels at 6 m (Figure 49 d).

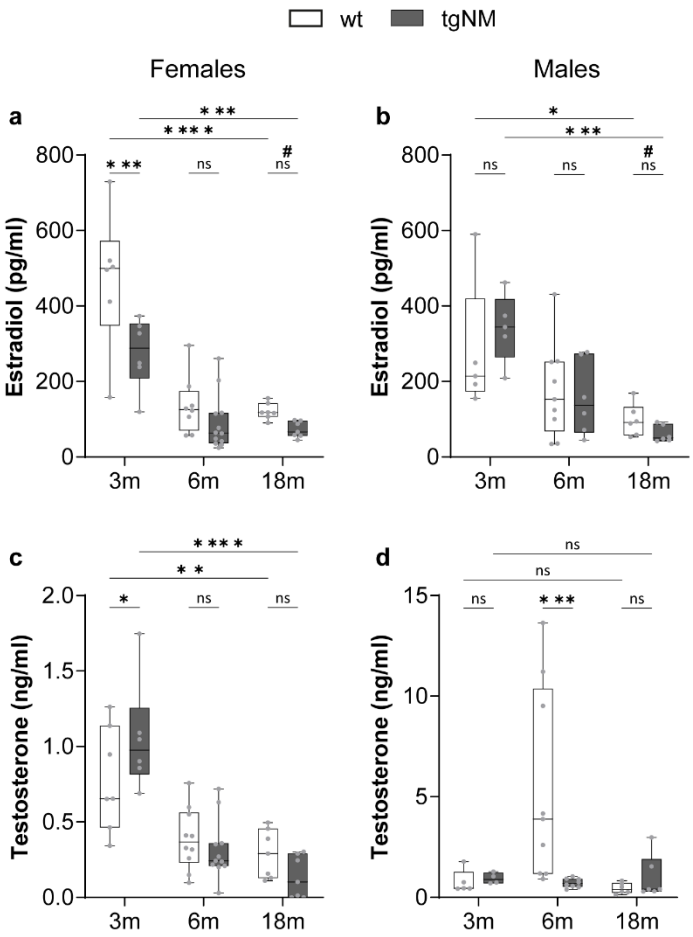

Figure 49. Sexual hormones characterization in wt and tgNM animals. a-b) Estradiol levels in serum samples at 3, 6 and 18 m of wt and tgNM females **(a)** and males **(b)**. *p≤0.05 compared to genotype or age-matched (Tukey's multiple comparisons test); #p≤0.05 compared to age-matched (Mann-Whitney test). 3 m [F: n=6(wt), n=6(tgNM); M: n=5(wt), n=5(tgNM)], 6 m [F: n=8(wt), n=12(tgNM); M: n=9(wt), n=6(tgNM)], 18 m [F: n=7(wt), n=7(tgNM); M: n=6(wt), n=6(tgNM)]. **c-d)** Testosterone levels in serum samples at 3, 6 and 18 m of wt and tgNM females **(c)** and males **(d)**. *p≤0.05 compared to genotype or age-matched (Tukey's multiple comparisons test). 3 m [F: n=7(wt), n=6(tgNM); M: n=5(wt), n=4(tgNM)], 6 m [F: n=10(wt), n=11(tgNM); M: n=9(wt), n=8(tgNM)], 18 m [F: n=7(wt), n=7(tgNM); M: n=6(wt), n=6(tgNM)].

2 CHAPTER 2. Determine if gut microbiota modulation by a HFD exacerbates the manifestation of both motor and non-motor symptoms in tgNM mice.

After the basal characterization of tgNM mice presented in Chapter 1, this chapter aimed to explore the potential interactions between diet, gut microbiota and the manifestation of the parkinsonian phenotype observed in tgNM mice.

The findings from Chapter 1 support a model in which alterations in gut microbiome and gut barrier dysfunction generate a pro-inflammatory environment in the gut that may contribute to neuropathological changes and neuroinflammation in the brain through the vagal and neuroendocrine pathways. To rigorously test this hypothesis, we decided to use a HFD paradigm known to induce alterations in gut microbiota composition and promote inflammation (Dang et al., 2023; K. A. Kim et al., 2012; Moreira et al., 2012; Rohr et al., 2020). Specifically, we aimed to determine whether modulation of the gut microbiota through a HFD could exacerbate the PD-like phenotype observed in these mice.

We designed an experiment involving wt and tgNM female and male mice. Starting at 2 m of age, both wt and tgNM animals were fed a CHOW diet or a HFD for a period of 5 m, after which they were euthanized. We choose this time frame because, according to the findings from Laguna *et. al* 2024, it corresponds to an early prodromal stage with minor behavioral alterations and with a TH phenotypic loss in catecholaminergic neurons from the SNpc, VTA and DVC, but without an overt cell loss (Laguna et al., 2024).

2.1 HFD produce changes in gut microbiota composition

First, we assessed if feeding with HFD could modulate gut microbiota composition in these mice, as reported in other models. To this end, we performed 16S RNA sequencing on fecal samples collected from both CHOW-fed and HFD-fed female and male mice at 6 m of age. This analysis allowed us to profile the bacterial communities and determine the impact of dietary intervention on gut microbiota diversity and composition. This methodology and all the bioinformatic analysis were performed by Microomics Systems S.L.

2.1.1 α-diversity

α-diversity was assessed to evaluate both the richness and evenness of the fecal microbiota in the study groups. No significant effects of HFD were detected on either genotype or sex with respect to the observed OTUs (Figure 50 a, c), suggesting that the overall microbial species count remained relatively stable despite dietary intervention. However, notable shifts were observed in the relative abundances of

taxa in HFD-fed tgNM animals compared to their CHOW-fed counterparts (Figure 50 b, d). Additionally, HFD-fed wt males exhibited alterations in microbial evenness compared to their CHOW-fed littermates (Figure 50 d) suggesting that while the total number of species was unaffected by HFD, dietary changes impacted the distribution of microbial taxa within these groups making them more balanced.

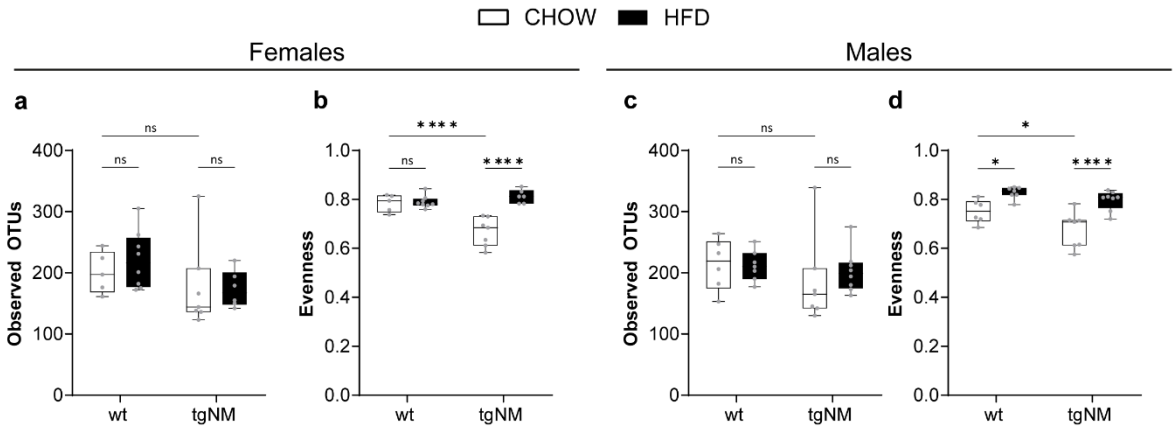

Figure 50. Fecal α-diversity boxplots in tgNM and wt mice fed with CHOW and HFD. a) Number of different phylotypes present in a community (Observed OTUs) at 6 m in tgNM and wt HFD-fed females compared to CHOW-fed littermates. **b)** Given as the Pielou's evenness index, quantification of how equal the community is numerically. *p≤0.05 compared to wt (Uncorrected Fisher's LSD). 6 m [CHOW: n=5 (wt), n=7 (tgNM); HFD: n=8 (wt), n=6 (tgNM)]. **c)** Number of different phylotypes present in a community (Observed OTUs) at 6 m in tgNM and wt HFD-fed males compared to CHOW-fed littermates. **d)** Given as the Pielou's evenness index, quantification of how equal the community is numerically. *p≤0.05 compared to wt (Uncorrected Fisher's LSD). 6 m [CHOW: n=6 (wt), n=7 (tgNM); HFD: n=7 (wt), n=8 (tgNM)].

2.1.2 β-diversity

Next, we analyzed the β-diversity of the gut microbiota to evaluate differences in microbial community composition among the groups. This was quantified using PERMANOVA on the Unweighted UniFrac distance, which accounts for phylogenetic dissimilarities between samples based on the presence or absence of OTUs. PCoA plots revealed distinct clustering patterns. As observed in Chapter 1, β-diversity was significantly different between tgNM and wt females in CHOW conditions and this difference was maintained in HFD conditions. Notably, HFD-fed females exhibited significant shifts in β-diversity compared to their CHOW-fed counterparts in both genotypes (Figure 51 a). In contrast, as observed in Chapter 1, tgNM males did not show significant β-diversity differences compared to their wt counterparts under CHOW conditions. However, under HFD conditions, both wt and tgNM males demonstrated significant alterations in microbial community composition compared to their CHOW-fed counterparts (Figure 51 b).

Overall, these findings suggest that dietary intervention with HFD induces significant alterations in gut microbiota composition in both genotypes and sexes, highlighting the critical role of diet in modulating gut microbiota composition.

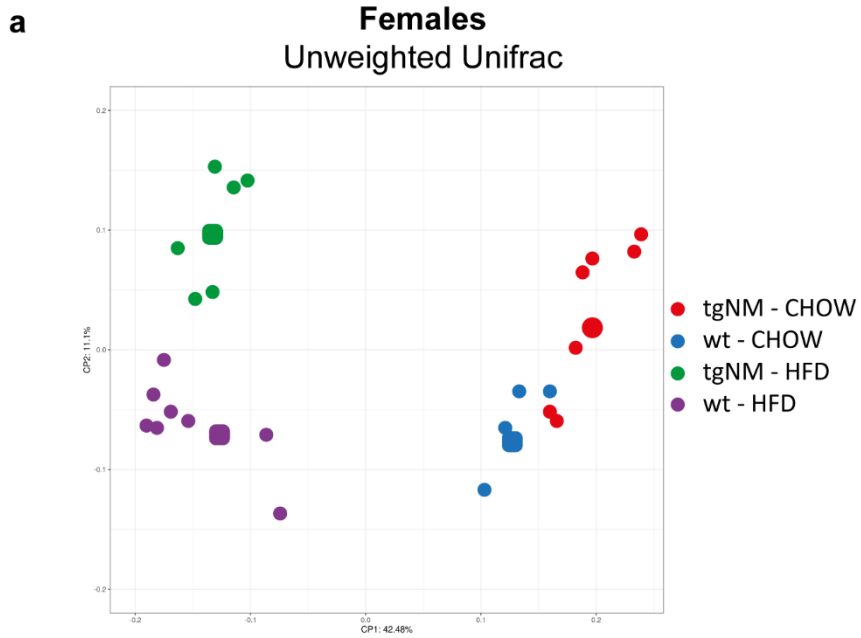

Table 17. Pairwise Permanova Analysis for Unweighted Unifrac in females at 6 m old.

	tgNM - CHOW	wt - CHOW	tgNM – HFD
wt - CHOW	0,004*		
tgNM – HFD	0,0015*	0,0036	
wt – HFD	0,0015	0,0015*	0,0015*

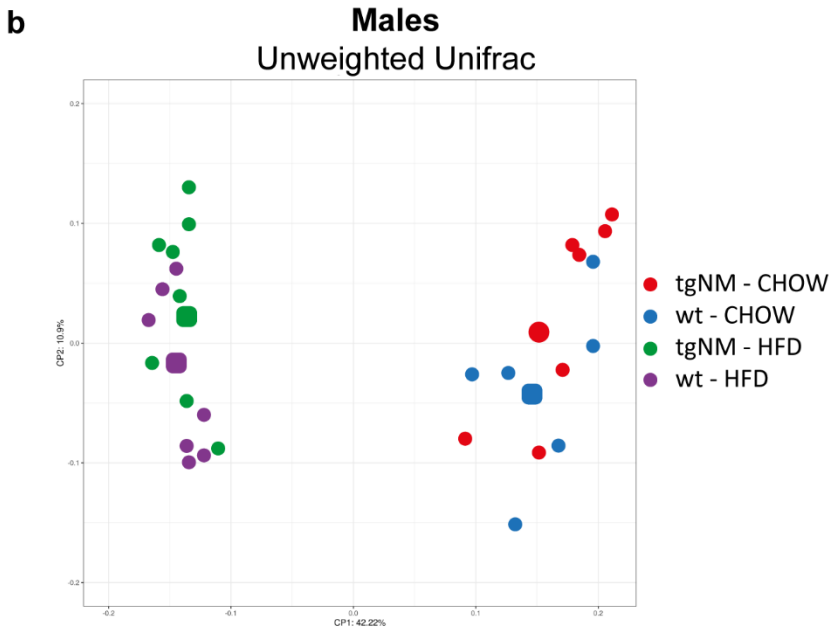

Table 18. Pairwise Permanova Analysis for Unweighted Unifrac in males at 6 m old.

	tgNM - CHOW	wt - CHOW	tgNM – HFD
wt - CHOW	0,127		
tgNM – HFD	0,003*	0,003	
wt – HFD	0,003	0,003*	0,0156*

Figure 51. Fecal β-diversity PCoA plots in tgNM and wt mice fed with CHOW and HFD. a) Females Unweighted UniFrac PCoA plot at 6 m for visualization of microbial communities' structure. Each dot represents one sample, distances between dots represent the ecological distances between samples. b) Males Unweighted UniFrac PCoA plot at 6 m for visualization of microbial communities' structure. Each dot represents one sample, distances between dots represent the ecological distances between samples. *p≤0.05 compared to CHOW-fed equivalent genotype and to CHOW-fed wt (Unweighted Unifrac – Pairwise Permanova analysis) p values are represented in table 17 and table 18. 6 m [F: CHOW n=5(wt), n=7(tgNM), HFD n=8(wt), n=6(tgNM); M: CHOW n=6(wt), n=7(tgNM), HFD n=7(wt), n=8(tgNM)].

2.1.3 Taxonomic profile

Next, we obtained the taxonomic profiles of the fecal samples by analyzing the differential abundance of taxa using the NBM.

We observed that HFD-fed wt females exhibited 33 significantly different genera compared to their CHOW-fed counterparts, while HFD-fed tgNM females showed 34 significant changes (Table 19). In wt females, the HFD was associated with an increased relative abundance of *Alistipes* and *Blautia* and a decreased abundance of *Lactobacillus and Muribaculaceae*, among others. In contrast, HFD-fed tgNM females displayed elevated levels of *Bacteroides*, *Alistipes*, and *Blautia*, along with reduced *Lactobacillus* and *Muribaculaceae* levels.

In male mice, HFD-fed wt animals presented 24 significantly altered genera compared to CHOW-fed, whereas HFD-fed tgNM males had 27 differentially abundant genera (Table 20). Notably, in wt males, HFD increased the relative abundance of *Alistipes* and *Blautia* while decreasing *Bifidobacterium, Muribaculaceae* and *Desulfovibrio*, among others. Similarly, in tgNM males, the HFD group showed increased levels of *Bacteroides*, *Alistipes*, and *Blautia* while reduced *Muribaculaceae*.

Table 19. Number of differentially abundant taxa identified as significant by the NBM in HFD vs CHOW-fed tgNM and wt females. The table presents the number of differentially abundant taxa at various taxonomic levels (e.g. phylum, class, order, family, genus and species) at the studied time point (6 m).

Nº of significant differentially abundant taxa between CHOW and HFD		
Taxa level	wt	tgNM
Phylum	4 (Actinobacteriota, Patescibacteria, Deferribacterota, Proteobacteria)	3 (Patescibacteria, Proteobacteria, Firmicutes)
Class	6 (Actinobacteria, Coriobacteriia, Saccharimonadia, Deferribacteres, Bacilli, Gammaproteobacteria)	5 (Actinobacteria, Saccharimonadia, Gammaproteobacteria, Bacilli, Coriobacteriia,
Order	8	10
Family	13 (Atopobiaceae, Marinifilaceae, Muribaculaceae, Prevotellaceae, Rikenellaceae, Deferribacteraceae, Lactobacillaceae, Streptococcaceae, Oscillospiraceae, Peptococcaceae, Sutterellaceae, Enterobacteriaceae)	18 (Atopobiaceae, Bacteroidaceae, Marinifilaceae, Muribaculaceae, Rikenellaceae, Tannerellaceae, Lactobacillaceae, Streptococcaceae, Clostridia_UCG-014, Clostridiaceae, Butyricicoccaceae, Oscillospiraceae, UCG-010, Peptococcaceae, Anaerovoracaceae, Saccharimonadaceae, Sutterellaceae, Enterobacteriaceae)
Genus	33 (Coriobacteriaceae_UCG-002, Odoribacter, Muribaculaceae, Alloprevotella, Prevotellaceae_UCG-001, Alistipes, Rikenella, Rikenellaceae_RC9_gut_group, Mucispirillum, Bilophila, Dubosiella, Faecalibaculum, Lactobacillus, Lachnospiraceae-A2, ASF356, NK4A136_group Blautia, Lachnoclostridium, Tuzzerella, xylanophilum_group, Colidextribacter, Oscillibacter, Anaerotruncus, Harryflintia, Ruminococcaceae-uncultured, Oscillospiraceae-uncultured, Peptococcus, Peptococcaceae-uncultured, Candidatus_Saccharimonas, Parasutterella, Escherichia-Shigella	34 (Coriobacteriaceae_UCG-002, Bacteroides, Odoribacter, Muribaculaceae, Alistipes, Rikenella, Rikenellaceae_RC9_gut_group, Parabacteroides, Bilophila, Lactobacillus, Streptococcus, Christensenellaceae-uncultured, Clostridia_UCG-014, Clostridium_sensu_stricto_1, Blautia, Lachnoclostridium, Lachnospiraceae_FCS020_group, Lachnospiraceae_NK4A136_group, xylanophilum_group, Lachnospiraceae-uncultured, Colidextribacter, NK4A214_group, Oscillibacter, Oscillospiraceae-uncultured, Anaerotruncus, Harryflintia, Ruminococcaceae-uncultured, UCG-010, Peptococcaceae-uncultured, Candidatus_Saccharimonas, Parasutterella, Escherichia-Shigella
Species	42	38

Table 20. Number of differentially abundant taxa identified as significant by the NBM in HFD vs CHOW-fed tgNM and wt males. The table presents the number of differentially abundant taxa at various taxonomic levels (e.g. phylum, class, order, family, genus and species) at the studied time point (6 m).

Nº of significant differentially abundant taxa between CHOW and HFD		
Taxa level	wt	tgNM
Phylum	1 (proteobacteria)	1 (pastescibacteria)
Class	3 (Actinobacteria, Coriobacteriia, Gammaproteobacteria)	2 (Saccharimonadia, Clostridia)
Order	6	7
Family	11 (Bifidobacteriaceae, Atopobiaceae, Marinifilaceae, Muribaculaceae, Prevotellaceae, Rikenellaceae, Streptococcaceae, RF39, Clostridia_UCG-014, Oscillospiraceae, Enterobacteriaceae)	16 (Atopobiaceae, Bacteroidaceae, Marinifilaceae, Muribaculaceae, Prevotellaceae, Rikenellaceae, Tannerellaceae, Streptococcaceae, Clostridia_UCG-014, Lachnospiraceae, Oscillospiraceae, Ruminococcaceae, UCG-010, Saccharimonadaceae, Sutterellaceae, Enterobacteriaceae)
Genus	24 (Bifidobacterium, Coriobacteriaceae_UCG-002, Odoribacter, Muribaculaceae, Alloprevotella, Alistipes, Rikenella, Desulfovibrio, RF39, Christensenellaceae-uncultured, Clostridia_UCG-014, Blautia, Lachnoclostridium, Lachnospiraceae_NK4A136_group, Lachnospiraceae_UCG-006, Tuzzerella, Colidextribacter, Intestinimonas, NK4A214_group, Ruminococcaceae-uncultured, Peptococcus, Escherichia-Shigella)	27 (Coriobacteriaceae_UCG-002, Bacteroides, Odoribacter, Muribaculaceae, Alloprevotella, Alistipes, Rikenella, Rikenellaceae_RC9_gut_group, Parabacteroides, Christensenellaceae-uncultured, Clostridia_UCG-014, Blautia, Lachnoclostridium , xylanophilum_group, Lachnospiraceae-uncultured, UCG-009, Colidextribacter, NK4A214_group, Oscillospiraceae-uncultured, Anaerotruncus, Ruminococcaceae-uncultured, UCG-010, Peptococcus, Candidatus_Saccharimonas, Parasutterella, Escherichia-Shigella)
Species	34	43

2.2 HFD-fed animals basal characterization

After confirming that HFD intake alters gut microbiota composition, we aimed to assess its broader effects on various physiological parameters. This section focuses on the baseline characterization of HFD-fed animals, including their body weight, anatomical changes, and food and water intake behaviors.

2.2.1 Longitudinal characterization of body weight, food and water intake

Body weight, as well as food and water intake, was monitored weekly from 2 m of age over the course of 4 m on both animals fed with a HFD or CHOW diet. Results indicated a significant increase in body weight in both genotypes and sexes on HFD (Figure 52 a, b, c, d), with HFD-fed tgNM females showing a particularly pronounced increase compared to HFD-fed tgNM males (Figure 52 m). Analysis of food intake revealed no significant differences among HFD-fed females (Figure 52 e, f); however, HFD-fed males

showed a reduction in food intake relative to their CHOW-fed counterparts (Figure 52 g, h). When comparing both sexes, in CHOW conditions, tgNM males had increased food intake than tgNM females, however this difference is no longer observed in HFD conditions (Figure 52 n). In terms of water intake, HFD-fed tgNM females consumed significantly more water than CHOW-fed females (Figure 52 i, j), while HFD-fed males drank less water than CHOW-fed males (Figure 52 k, l). Comparing both sexes, in HFD conditions, tgNM males consumed less water than tgNM females (Figure 52 o). These findings suggest that HFD has sex-specific effects on food and water consumption behaviors in tgNM and wt mice, potentially linked to differential metabolic demands or compensatory mechanisms. In addition, the results suggest that the mechanisms regulating food and water intake are functional in males from both genotypes while the circuit of feeding regulation seems impaired in tgNM females.

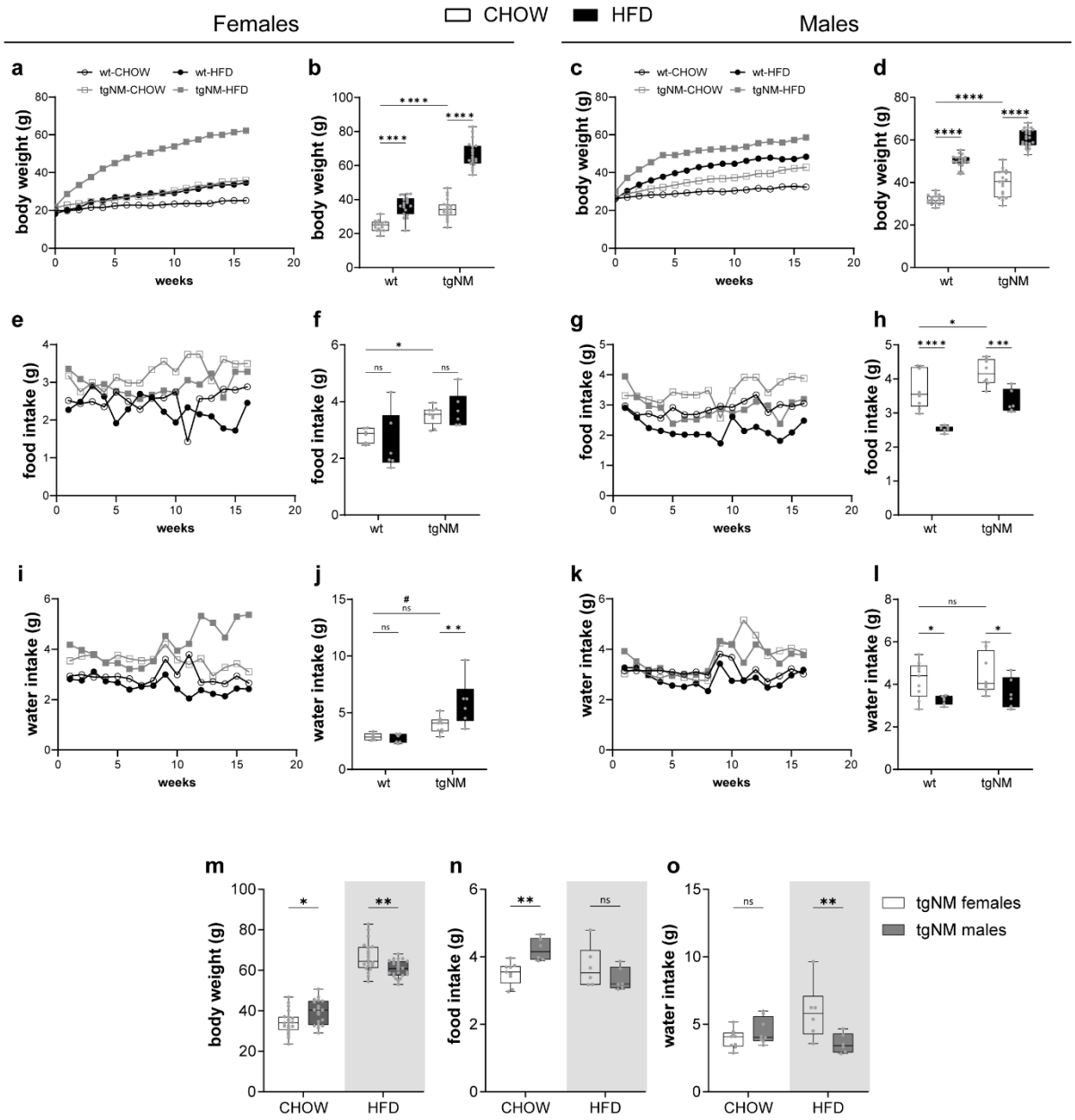

Figure 52. HFD impacts body weight, food and water intake. a, c) Body weight over 16 weeks of CHOW and HFD-fed **(a)** females and **(c)** males for both genotypes. **b, d)** Body weight at 6 m, after 4 m of HFD or CHOW feeding of **(b)** females and **(d)** males. **e, g)** Food intake over 16 weeks of CHOW and HFD-fed **(e)** females and **(g)** males for both genotypes. **f, h)** Food intake at 6 m, after 4 m of HFD or CHOW feeding of **(f)** females and **(h)** males. **i, k)** Water intake over 16 weeks of CHOW and HFD-fed **(i)** females and **(k)** males for both genotypes. **j, l)** Water intake at 6 m, after 4 m of HFD or CHOW feeding of **(j)** females and **(l)** males. *p≤0.05 compared to CHOW-fed equivalent genotype and to CHOW-wt (Uncorrected Fisher's LSD). **m, n, o)** Comparison between tgNM females and males fed with CHOW or HFD for body weight, food intake and water intake. *p≤0.05 compared to tgNM females' equivalent diet (Uncorrected Fisher's LSD). [F: CHOW n=15(wt) N=6 cages, n=20(tgNM)N=9 cages, HFD n=19(wt) N= 6 cages, n=20(tgNM) N= 6 cages; M: CHOW n=19(wt) N= 9 cages, n=19(tgNM) N=8 cages, HFD n=21(wt) N= 6 cages, n=24(tgNM) N=6 cages].

2.2.2 Effect of HFD on the peripheral organ's anatomy

At the time of euthanasia, peripheral organs were weighed in both CHOW and HFD-fed animals. At 7-8 m of age, HFD-fed wt females exhibited increased weights of several organs including the kidneys, adrenal glands, pancreas, inguinal WAT, gonadal WAT, renal WAT and BAT, compared to CHOW-fed wt females (Figure 53 c, e, f, h, j, k, l, m). In HFD-tgNM females, the organ weight differences were even more pronounced, with significantly increased weights observed in the GI tract, heart, kidneys, adrenal glands, liver, pancreas, spleen, inguinal WAT, gonadal WAT, renal WAT and BAT compared to their CHOW-fed tgNM littermates (Figure 53 a, d, e, f, g, h, I, j, k, l, m). In contrast, HFD-fed wt males at 7-8 m showed increased weights only in the liver, inguinal WAT, gonadal WAT, renal WAT and BAT compared to CHOW-fed wt counterparts (Figure 54 g, j, k, l, m). Similarly, HFD-fed tgNM males exhibited increased weights in the liver, pancreas, spleen, inguinal WAT and renal WAT compared to CHOW-fed tgNM littermates (Figure 54 g, h, i, j, l). We observed that both HFD-fed wt and tgNM females and males presented reduced cecum weight compared to their CHOW-fed littermates. Overall, these findings support the conclusion that HFD feeding increases body weight primarily through adipose tissue expansion in males. In contrast, females exhibited a more pronounced weight gain that exceeded the levels observed in Chapter 1. This increase was not limited to adipose tissue but also included significant gains in the weight of other organs, suggesting a concurrent rise in lean body mass.

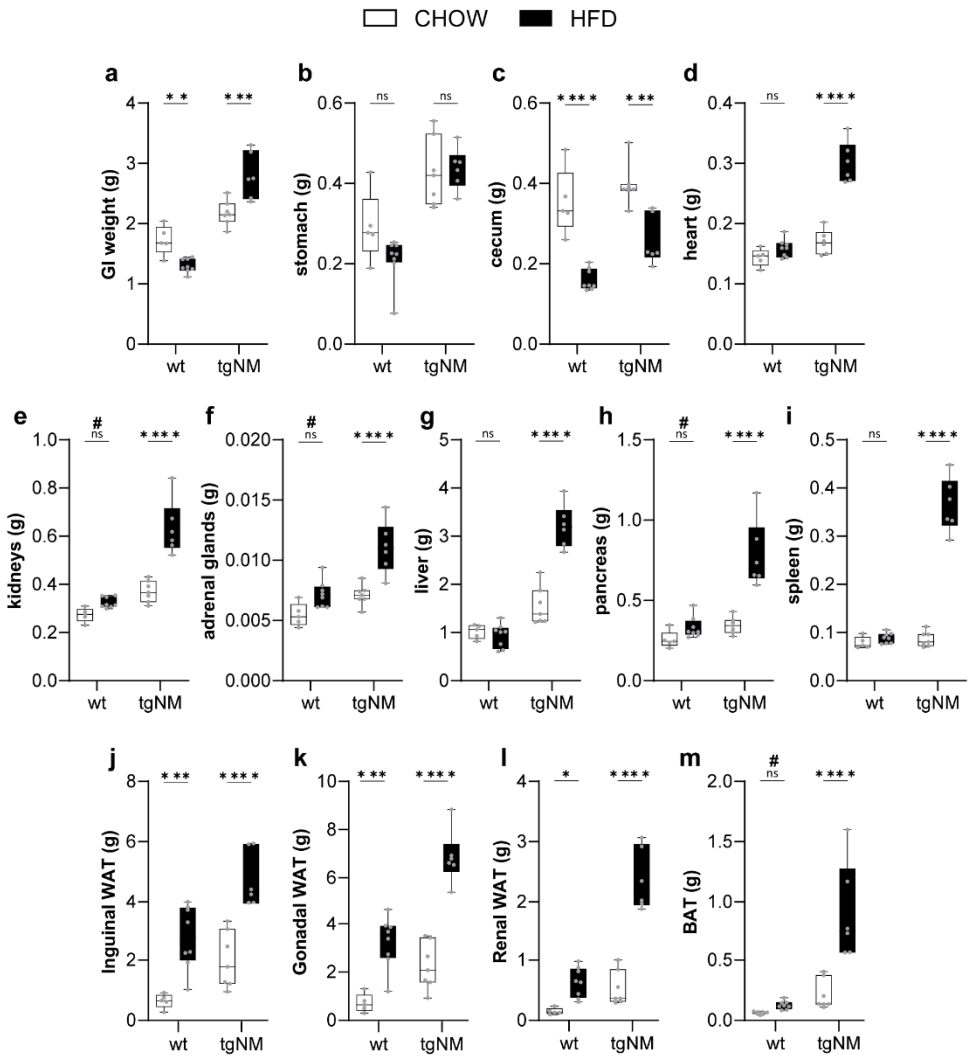

Figure 53. Females' peripheral organs weight characterization. a-m) Peripheral organ's weight (GI, stomach, cecum, heart, kidneys, adrenal glands, liver, pancreas, spleen, inguinal WAT, gonadal WAT, renal WAT and BAT) of wt and tgNM females fed with CHOW or HFD, compared with their CHOW littermates at 7-8 m. *p≤0.05 compared to CHOW-fed equivalent genotype (Uncorrected Fisher's LSD test). 7-8 m [CHOW: n=5(wt), n=7(tgNM)]; HFD: n=8(wt), n=6(tgNM)].

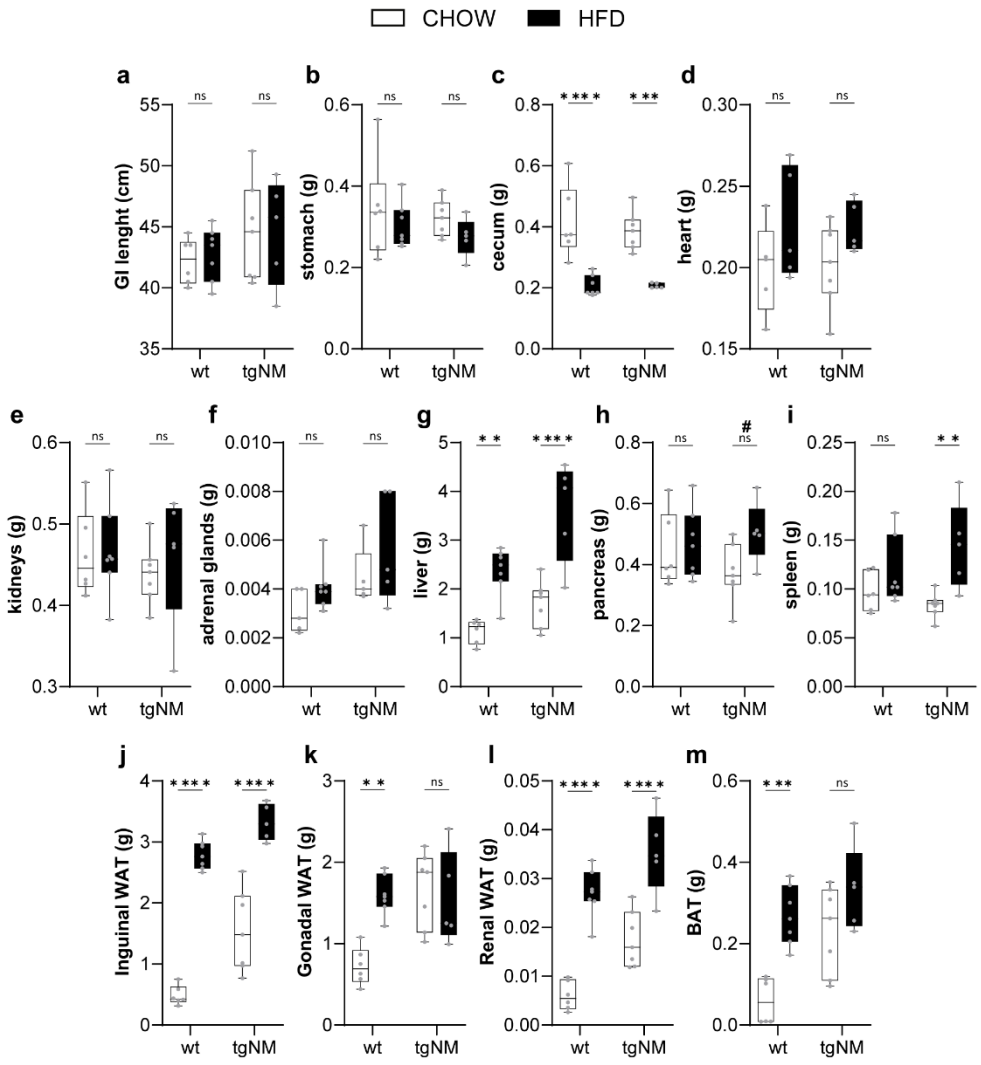

Figure 54. Males' peripheral organs weight characterization. a-m) Peripheral organ's weight (GI, stomach, cecum, heart, kidneys, adrenal glands, liver, pancreas, spleen, inguinal WAT, gonadal WAT, renal WAT and BAT) of wt and tgNM males fed with CHOW or HFD, compared with their CHOW littermates at 7-8 m. *p≤0.05 compared to CHOW-fed equivalent genotype (Uncorrected Fisher's LSD test). 7-8 m [CHOW: n=6(wt), n=7(tgNM)]; HFD: n=7(wt), n=5(tgNM)].

2.3 Sensorimotor behavioral assessment

To further explore the impact of HFD on the sensorimotor abilities of wt and tgNM mice, we conducted a series of tests consistent with those described in Chapter 1. By repeating this battery of assessments, our goal was to determine whether feeding with HFD exacerbates sensorimotor impairments in these animals at young ages.

HFD-fed wt and tgNM mice exhibited impaired motor balance and coordination, as evidenced by their increased time to cross the beam compared to their CHOW-fed counterparts (Figure 55 a, b). In the Grip Strength Test, HFD-fed wt females exhibited diminished forepaw strength, while no significant alterations

in forepaw strength were observed in tgNM females or males (Figure 55 c, d). The Marble Burying Test revealed impaired burying behavior in HFD-fed tgNM animals, as indicated by a reduced number of buried marbles, while no differences were detected in HFD-fed wt animals (Figure 55 e, f).

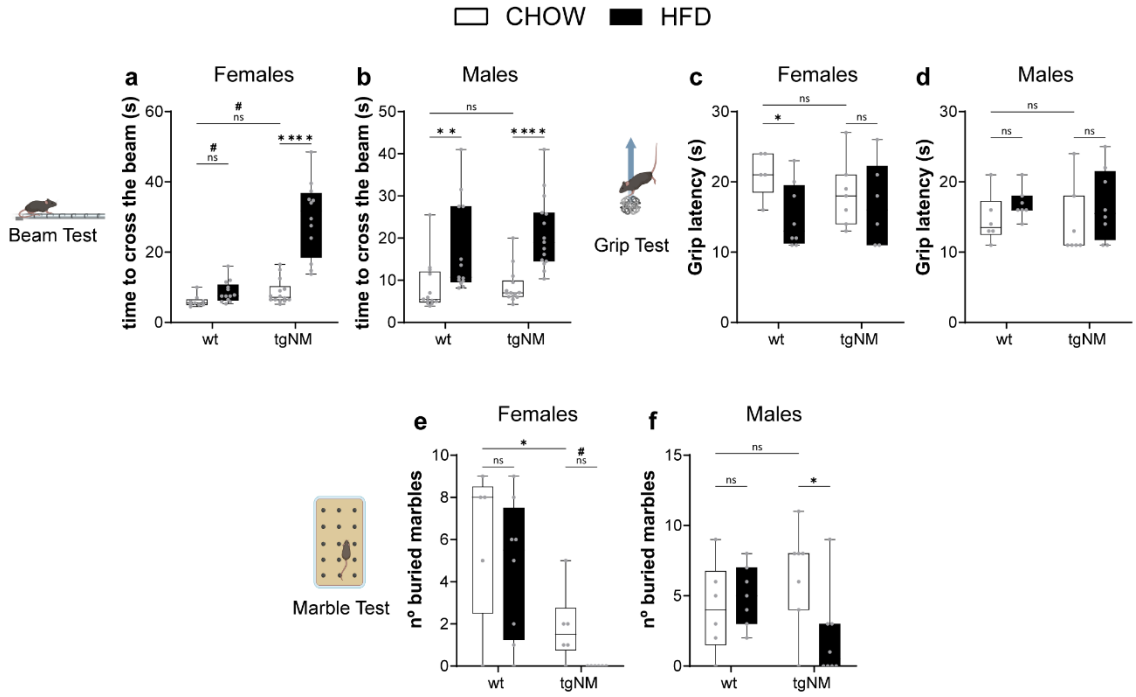

Figure 55. Motor behavioral characterization. a) Females and **b)** Males Beam test; Average time to cross the beam after two trials. *p≤0.05 compared to CHOW-fed genotype (Uncorrected Fisher's LSD). #p≤0.05 compared to CHOW-fed wt (Mann-Whitney test). 6 m [F: CHOW n=9(wt), n=14(tgNM), HFD n=13(wt), n=12(tgNM); M: CHOW n=12(wt), n=14(tgNM), HFD n=13(wt), n=15(tgNM)]. **c)** Females and **d)** Males Grip test; Quantification of grip latency time. *p≤0.05 compared to CHOW-fed equivalent genotype (Uncorrected Fisher's LSD). 6 m [F: CHOW n=5(wt), n=7(tgNM), HFD n=8(wt), n=6(tgNM); M: CHOW n=6(wt), n=7(tgNM), HFD n=7(wt), n=8(tgNM)]. **e)** Females and **f)** Males Marble burying test. Nº of buried marbles in 10 min. *p≤0.05 compared to CHOW-fed equivalent genotype (Uncorrected Fisher's LSD). #p≤0.05 compared to CHOW-fed tgNM (Mann-Whitney test). 6 m [F: CHOW n=5(wt), n=6(tgNM), HFD n=8(wt), n=6(tgNM); M: CHOW n=6(wt), n=7(tgNM), HFD n=7(wt), n=8(tgNM)].

Olfactory discrimination, assessed by testing the ability to detect lemon essence, was not significantly affected by HFD in either wt or tgNM mice, regardless of sex (Figure 56 a, b). Additionally, HFD-fed tgNM animals exhibited a significant reduction in vocalizations, contrasting with HFD-fed wt animals, which did not show a reduction (Figure 56 c, d). We also assessed whether HFD could induce depressive-like behavior using the Tail Suspension Test. HFD-fed wt females exhibited a decreased latency to surrender compared to CHOW-fed littermates (Figure 56 e), suggesting a tendency toward passive behavior associated with behavioral despair or depressive-like states (Steru et al., 1985). Conversely, HFD-fed wt males showed an increased latency to surrender compared to CHOW-fed counterparts (Figure 56 f). Regarding total immobilization time, HFD-fed wt females remained immobile for longer durations than

CHOW-fed littermates, whereas HFD did not increase immobilization time in either tgNM females or males (Figure 56 g, h).

Overall, these results suggest that feeding with HFD exacerbates the motor impairment of both tgNM females and males together with their vocalization ability. Although, no other sensorimotor capacity is affected.

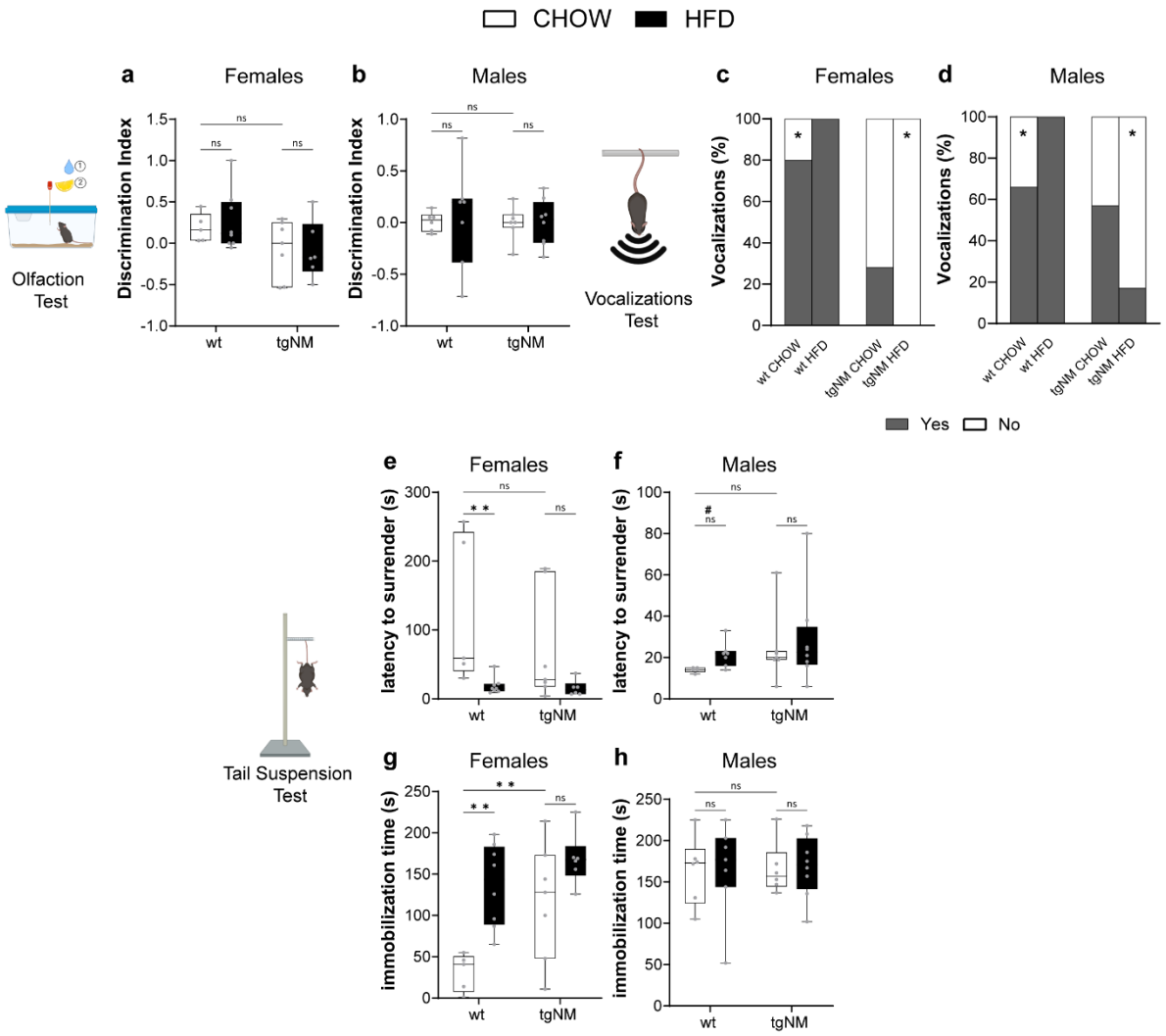

Figure 56. Olfactory and emotional behavioral characterization. a) Females and **b)** Males Olfaction test. Quantification of the DI (time on lemon vs time on water). *p≤0.05 compared to CHOW-fed equivalent genotype (Uncorrected Fisher's LSD). 6 m [F: CHOW n=5(wt), n=7(tgNM), HFD n=8(wt), n=6(tgNM); M: CHOW n=6(wt), n=7(tgNM), HFD n=7(wt), n=8(tgNM)]. **c)** Females and **d)** Males Vocalizations test; quantification of vocalizations. *p≤0.05 compared to CHOW-fed equivalent genotype (Fisher's exact test). 6 m [F: CHOW n=5(wt), n=7(tgNM), HFD n=8(wt), n=6(tgNM); M: CHOW n=6(wt), n=7(tgNM), HFD n=7(wt), n=8(tgNM)]. **e, g)** Females and **f,h)** Males Tail suspension test; quantification of the latency to surrender and the total immobilization time. *p≤0.05 compared to CHOW-fed equivalent genotype (Uncorrected Fisher's LSD). 6 m [F: CHOW n=5(wt), n=7(tgNM), HFD n=8(wt), n=6(tgNM); M: CHOW n=6(wt), n=7(tgNM), HFD n=7(wt), n=8(tgNM)].

2.4 Effect of HFD in GI assessments

Following the behavioral phenotypic characterization, we proceeded to evaluate the impact of HFD on the GI phenotype of both wt and tgNM animals. This section explores how HFD influences various aspects of GI function and morphology, specifically through measurements of intestinal motility, fecal water content, gut anatomy, neurotransmission, gut permeability and inflammatory markers. By examining these parameters, we aimed to better understand how HFD impacts gut physiology and inflammation in wt and tgNM animals.

2.4.1 Effects of HFD on the intestinal motility and fecal water content

Our initial assessment focused on total intestinal transit time, which we found to be unaffected by HFD in either sex when normalized by GI length compared to their CHOW-fed counterparts (Figure 57 a.b). Subsequently, we measured total fecal output and found that HFD increased the number of defecations within a one-hour period of tgNM females and wt males (Figure 57 c, d). Analysis of stool water content revealed a decrease in moisture in HFD-fed tgNM females compared to CHOW-fed littermates (Figure 57 e). No differences were observed in males (Figure 57 f).

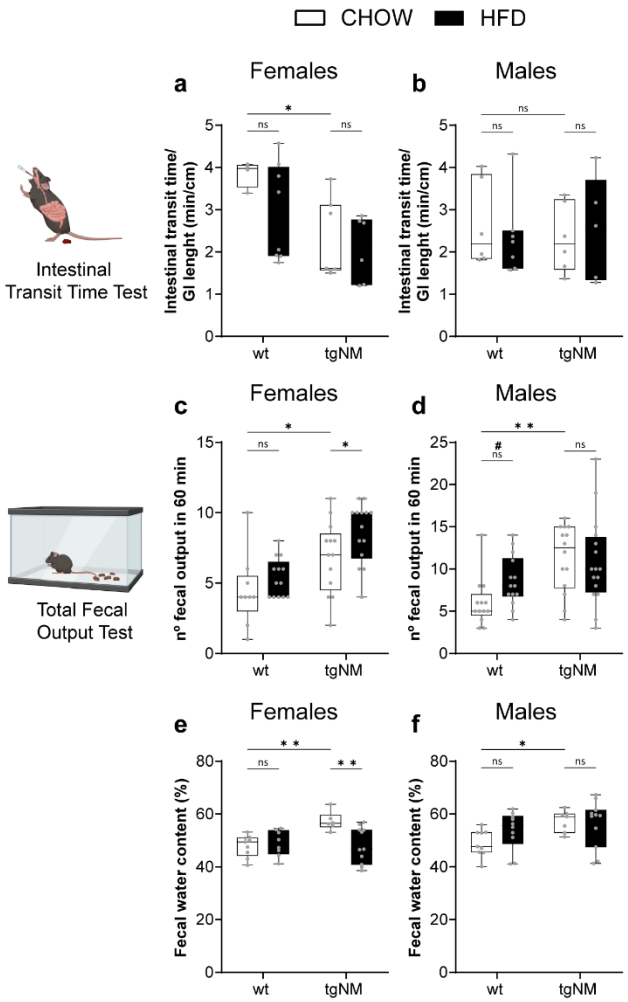

Figure 57. GI behavioral characterization. a) Females and **b)** Males Total intestinal transit time; Time to produce a red pellet divided by the GI tract length (min/cm). *p≤0.05 compared to CHOW-fed equivalent genotype (Uncorrected Fisher's LSD). 6 m [F: CHOW n=4(wt), n=7(tgNM), HFD n=8(wt), n=6(tgNM); M: CHOW n=6(wt), n=6(tgNM), HFD n=7(wt), n=5(tgNM)]. **c)** Females and **d)** Males Total fecal output; nº of fecal pellets produced in 1 h. *p≤0.05 compared to CHOW-fed equivalent genotype (Uncorrected Fisher's LSD), #p≤0.05 compared to CHOW-fed genotype (Mann-Whitney test). 6 m [F: CHOW n=9(wt), n=14(tgNM), HFD n=13(wt), n=14(tgNM); M: CHOW n=13(wt), n=14(tgNM), HFD n=14(wt), n=16(tgNM)]. **e)** Females and **f)** Males Fecal water content in % measured from collected pellets for a period of 10 min. *p≤0.05 compared to CHOW-fed equivalent genotype (Uncorrected Fisher's LSD). 6 m [F: CHOW n=9(wt), n=6(tgNM), HFD n=8(wt), n=11(tgNM); M: CHOW n=9(wt), n=7(tgNM), HFD n=10(wt), n=11(tgNM)].

2.4.2 Effects of HFD on gut anatomy

Upon examining gut anatomy, HFD-fed tgNM females displayed an increased GI tract length relative to CHOW-fed tgNM females (Figure 58 a). Specifically, the small intestine (from the pylorus to the cecum) was elongated in HFD-fed tgNM females (Figure 58 b), while the colon length remained unchanged (Figure 58 c). No significant anatomical differences were observed in HFD-fed males compared to CHOW-fed males in any genotype (Figure 58 d, e, f).

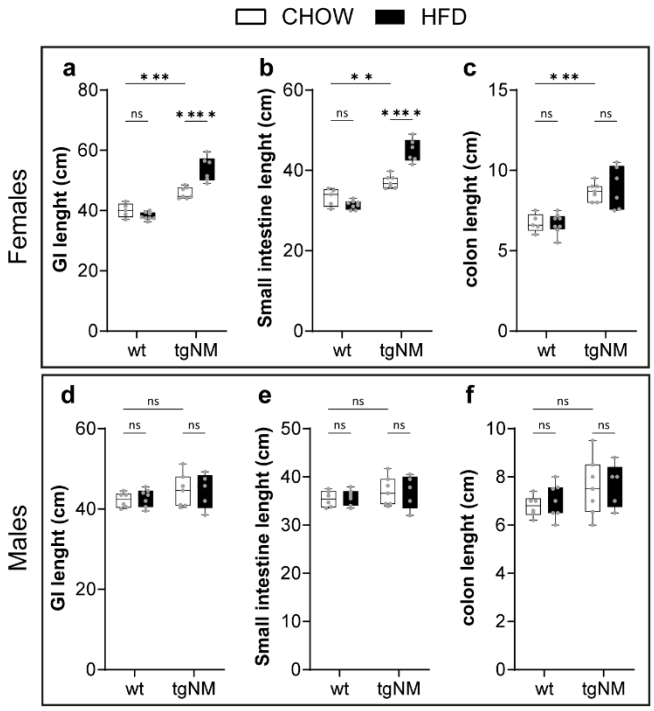

Figure 58. GI tract measurement. a-f) GI tract, small intestine and colon length in cm of female **(a, b, c)** and male **(d, e, f)** mice. *p≤0.05 compared to CHOW-fed equivalent genotype (Uncorrected Fisher's LSD). GI length: 6 m [F: CHOW n=5(wt), n=7(tgNM), HFD n=8(wt), n=6(tgNM); M: CHOW n=6(wt), n=7(tgNM), HFD n=7(wt), n=5(tgNM)]; Small intestine length: 6 m [F: CHOW n=5(wt), n=7(tgNM), HFD n=8(wt), n=6(tgNM); M: CHOW n=6(wt), n=7(tgNM), HFD n=7(wt), n=5(tgNM)] Colon length: 6 m [F: CHOW n=5(wt), n=7(tgNM), HFD n=8(wt), n=6(tgNM); M: CHOW n=6(wt), n=7(tgNM), HFD n=7(wt), n=5(tgNM)].

In summary, our findings indicate that feeding with HFD exacerbated most of the sex-specific changes observed in tgNM animals during Chapter 1, which were more pronounced in tgNM females than in males.

2.4.3 Effect of HFD on the gut neurotransmitter levels

In Chapter 1, we measured key medullary-related neurotransmitters and their metabolites in duodenal and proximal colon samples at 6 m using UPLC-MS/MS. Results revealed significant dysregulation in neurotransmitter synthesis and metabolism, particularly in tgNM females. Given these previous findings and the observed alterations in intestinal motility (specifically the increased defecation frequency in HFD-fed tgNM mice), we aimed to investigate whether HFD further affects the levels of neurotransmitters in the same duodenal and colon samples from both wt and tgNM mice. This would allow us to explore the potential link between dietary stress, neurotransmitter alteration and impaired gut function in our model.

2.4.3.1 Cholinergic system

In wt females, HFD significantly increased ACh levels in the proximal colon. Conversely, tgNM females presented a significant reduction in ACh levels in the duodenum under HFD, with no changes detected in the proximal colon (Figure 59 a). In males, HFD reduced ACh levels in the duodenum of wt and tgNM animals. Additionally, HFD also reduced ACh levels of wt males in the proximal colon (Figure 59 b). These data highlight a predominant effect of HFD in reducing ACh levels in the gut in both genotypes.

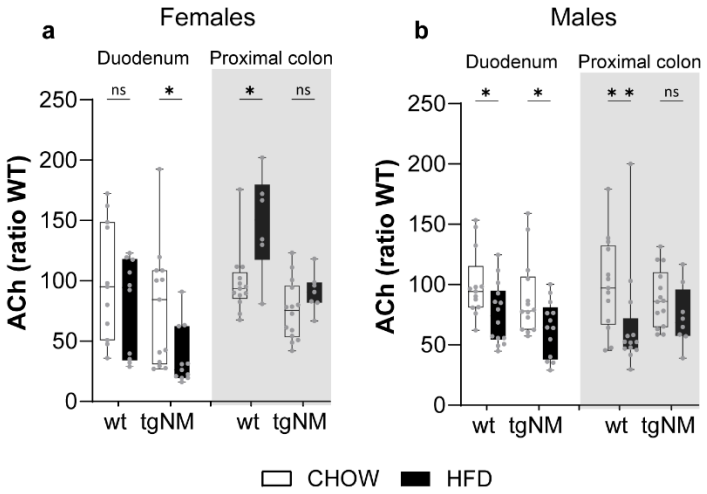

Figure 59. Levels of ACh in the duodenum and proximal colon. a-b) UPLC-MS/MS measurements of ACh in duodenum and proximal colon homogenates of female **(a)** and male **(b)** mice fed with CHOW or HFD. Groups are normalized to their CHOW-fed wt. *p≤0.05 compared to CHOW-fed equivalent genotype (Uncorrected Fisher's LSD). 7-8 m [F: CHOW D&C: n=13(wt), n=14(tgNM), HFD D&C: n=10(wt), n=11(tgNM)]. 7-8 m [M: CHOW D&C: n=13(wt), n=14(tgNM), HFD D&C: n=14(wt), n=13(tgNM)].

2.4.3.2 Dopaminergic system

In HFD-fed wt females, we detected a significant increase in L-DOPA levels in the duodenum, accompanied by a trend toward elevated DA levels, while NE levels remained unchanged. In contrast, HFD-fed tgNM females showed a significant reduction in NE levels, likely attributable to the observed decrease in DA levels and a trend toward reduced L-DOPA in the duodenum. In the proximal colon, NE levels were elevated in HFD-fed wt females compared to their CHOW-fed littermates, despite no observed changes in precursor levels. Notably, HFD did not affect neurotransmitter levels in the proximal colon of tgNM females (Figure 60 a, b, c). These results highlight a tissue-specific response to HFD in the regulation of catecholamine neurotransmitters.

In HFD-fed wt males, we observed reductions in both L-DOPA and DA levels in the duodenum, with a tendency to reduced NE levels. Conversely, HFD-fed tgNM males presented reduced NE levels without alterations in L-DOPA or DA. In the proximal colon, DA levels were elevated in HFD-fed wt animals, with

no changes in L-DOPA or NE. In contrast, HFD-fed tgNM males displayed increased NE levels, accompanied by elevated L-DOPA and a trend toward higher DA levels (Figure 60 d, e, f).

These data highlight complex sex-specific differential metabolic responses between wt and tgNM mice under HFD conditions.

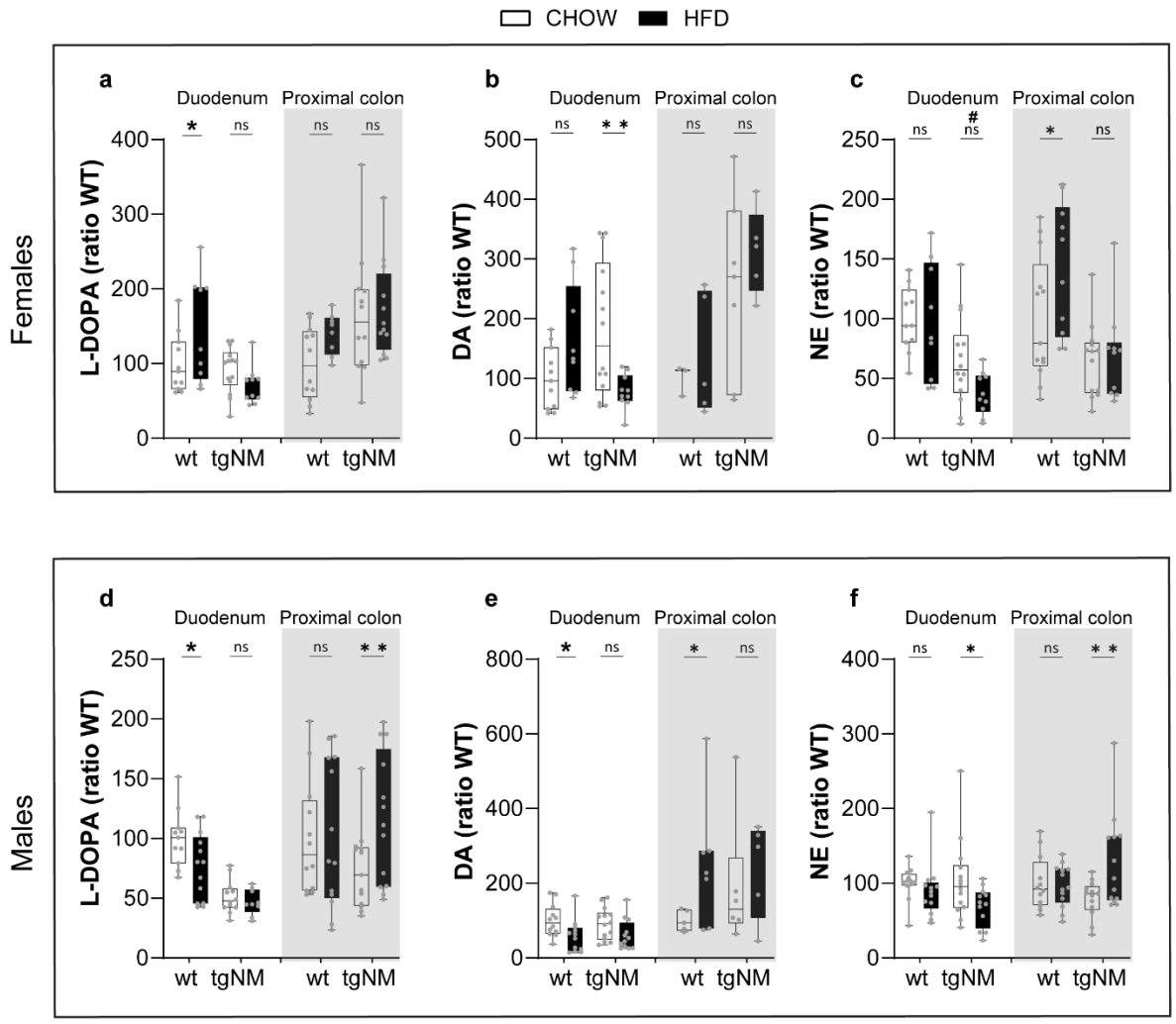

Figure 60. Levels of neurotransmitters in the duodenum and proximal colon. a-f) UPLC-MS/MS measurements of L-DOPA, DA and NE in duodenum and proximal colon homogenates of female **(a, b, c)** and male **(d, e, f)** mice fed with CHOW or HFD. Groups are normalized to their CHOW-fed wt. *p≤0.05 compared to CHOW-fed equivalent genotype (Uncorrected Fisher's LSD). #p≤0.05 compared to CHOW-fed equivalent genotype (Mann-Whitney test). 7-8 m [F: CHOW D&C: n=13(wt), n=14(tgNM), HFD D&C: n=10(wt), n=11(tgNM)]. 7-8 m [M: CHOW D&C: n=13(wt), n=14(tgNM), HFD D&C: n=14(wt), n=13(tgNM)].

2.4.3.3 Serotonergic system

In HFD-fed wt females, Trp levels were elevated in the duodenum along with increased 5-HIAA levels, while 5-HT and Kyn remained stable, suggesting an upregulation of 5-HT metabolism into 5-HIAA. In contrast, HFD-fed tgNM females displayed reduced levels of both 5-HIAA and Kyn levels, while stable Trp and 5-HT levels. In the proximal colon of HFD-fed wt females, Trp levels were similarly increased, accompanied by elevated 5-HT, 5-HIAA and Kyn levels. However, HFD-fed tgNM females showed no significant alterations in Trp metabolism (Figure 61 a, b, c, d).

In HFD-fed wt males, Trp levels were elevated in the duodenum, accompanied by increased 5-HIAA levels, while 5-HT remained unchanged, suggesting, as seen in HFD-fed wt females, an upregulation of 5-HT metabolism. In contrast, HFD-fed tgNM males exhibited a trend toward decreased Trp levels, accompanied by reduced Kyn levels, with stable 5-HT levels. In the proximal colon of HFD-fed wt males, no changes were observed in Trp or 5-HT levels, but both 5-HIAA and Kyn levels were decreased, suggesting reduced Trp metabolism into Kyn as well as reduced 5-HT metabolism into 5-HIAA. Conversely, HFD-fed tgNM males showed no significant alterations in Trp metabolism (Figure 61 e, f, g, h).

These data highlight differential metabolic responses between wt and tgNM females and males under HFD conditions.

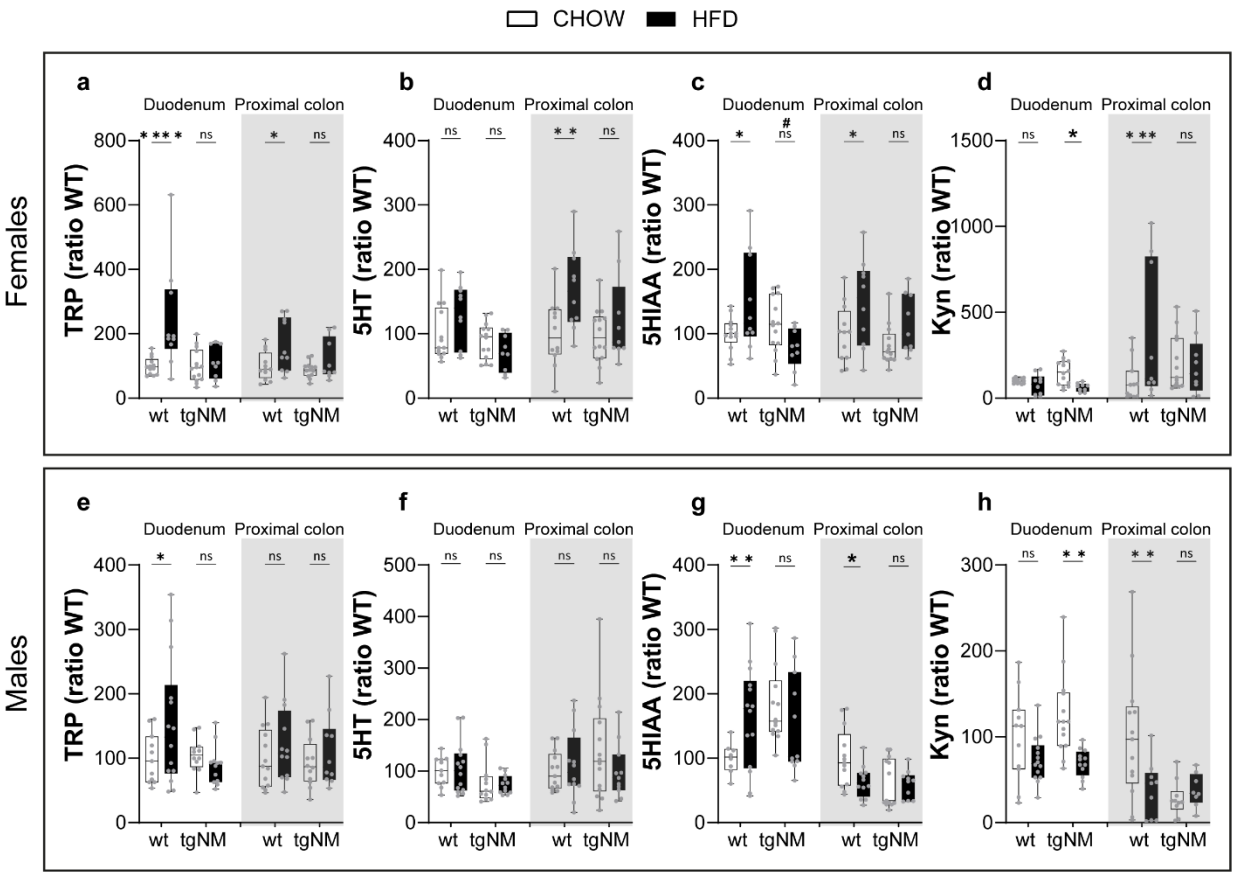

Figure 61. Levels of neurotransmitters in the duodenum and proximal colon. a-h) UPLC-MS/MS measurements of Trp, 5-HT, 5-HIAA and Kyn in duodenum and proximal colon homogenates of female **(a, b, c, d)** and male **(e, f, g, h)** mice fed with CHOW or HFD. Groups are normalized to their CHOW-fed wt. *p≤0.05 compared to CHOW-fed equivalent genotype (Uncorrected Fisher's LSD). #p≤0.05 compared to CHOW-fed equivalent genotype (Mann-Whitney test). 7-8 m [F: CHOW D&C: n=13(wt), n=14(tgNM), HFD D&C: n=10(wt), n=11(tgNM)]. 7-8 m [M: CHOW D&C: n=13(wt), n=14(tgNM), HFD D&C: n=14(wt), n=13(tgNM)].

In summary, the evaluation of neurotransmitter dynamics in the duodenum and proximal colon of HFD-fed tgNM and wt mice revealed significant alterations. In wt females, HFD impacted the cholinergic, dopaminergic and serotonergic systems, while in tgNM females, HFD exacerbated reductions in ACh, DA and NE levels particularly in the duodenum. Interestingly, no major changes were noted in the serotonergic system for tgNM females. These findings suggest that HFD has a deleterious effect on neurotransmitter regulation, with a more pronounced impact on the small intestine, particularly in tgNM females. In males, HFD notably affected the cholinergic system in both genotypes and mildly influenced the dopaminergic and serotonergic systems.

2.4.4 Effect of HFD on gut permeability

Emerging evidence suggests that excessive dietary fat consumption can differentially enhance intestinal permeability. Components of the intestinal barrier system including the mucus layer, IECs, TJs proteins, immune cells, and gut microbiota, are particularly susceptible to external factors such as dietary fats (Rohr et al., 2020). Therefore, we investigated the impact of HFD on the integrity of the gut barrier in our tgNM mice.

To assess gut permeability *in vivo*, we quantified serum levels of 4-kDa FITC-Dx 1 h post-oral gavage administration. Elevated serum concentrations of FITC-Dx were observed in HFD-fed tgNM mice compared to their CHOW-fed counterparts, indicating increased intestinal permeability in both sexes (Figure 62 a, b). To further validate these results, we examined the expression levels of TJs proteins ZO-2, claudin-2, and occludin using RT-qPCR in duodenal and proximal colon tissues. In the duodenum, HFD-fed wt females presented increased levels of claudin-2 compared to CHOW-fed counterparts. No significant changes were detected in tgNM female mice fed with HFD (Figure 62 c). In wt males, HFD feeding resulted in a significant upregulation of ZO-2 and occludin expression relative to their CHOW-fed counterparts. TgNM males fed with HFD only presented increased levels of occludin (Figure 62 d). In the proximal colon, we again observed changes only in HFD-fed wt females, that presented reduced levels of ZO-2 and claudin-2 (Figure 62 e). In males, no significant changes were observed (Figure 62 f).

Altogether, our results indicate that HFD further compromises the intestinal barrier integrity in tgNM mice as shown by increased permeability in both females and males. The expression of these specific TJs shows regional differences and does not appear consistently altered in HFD-fed tgNM mice.

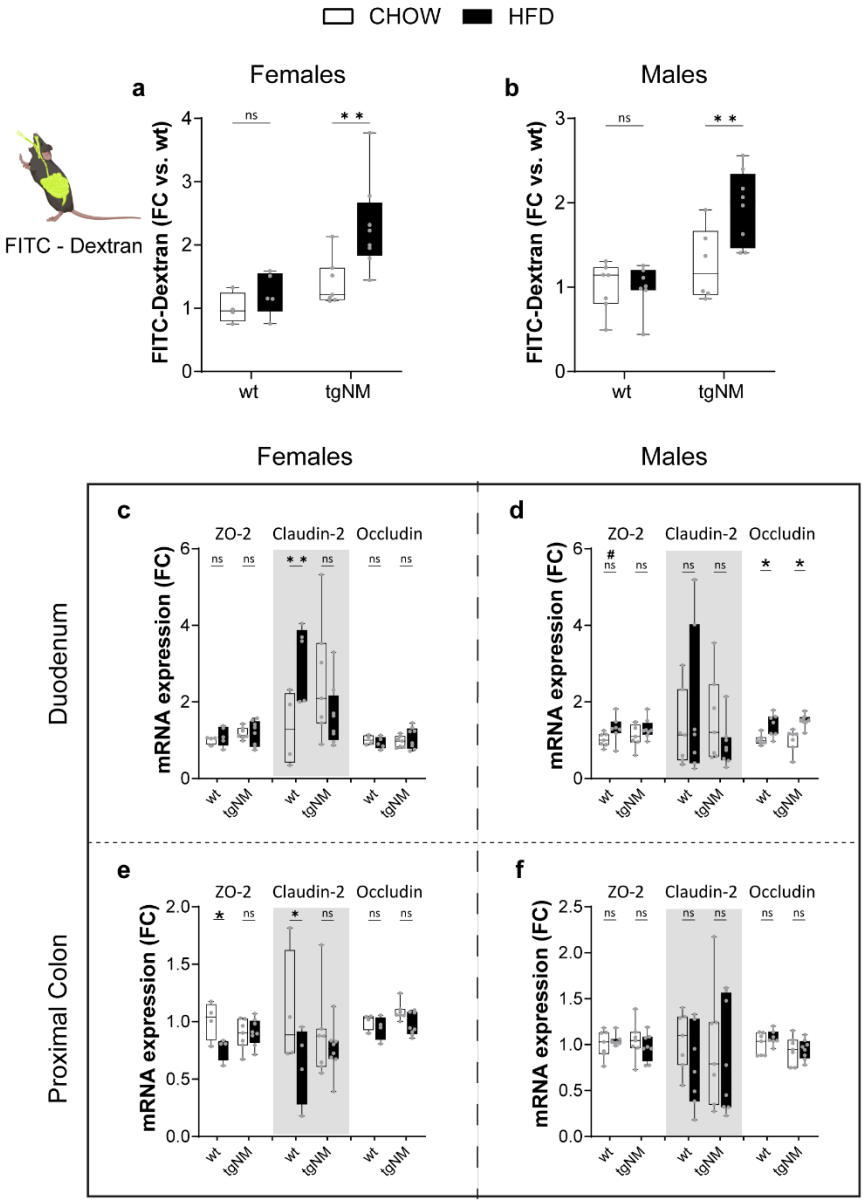

Figure 62. Gut permeability assessment and TJs expression. a) Females and **b)** males FITC-Dx serum levels after 1 h administration. Groups are normalized to their CHOW-fed wt. 7-8 m [F: CHOW n=4(wt), n=7(tgNM), HFD n=5(wt), n=8(tgNM); M: CHOW n=7(wt), n=6(tgNM), HFD n=7(wt), n=8(tgNM)]. **c)** Females and **d)** males expression of ZO-2, claudin-2 and occludin levels in duodenum samples by RT-qPCR using the comparative method normalized to CHOW-fed wt (FC). **e)** Females and **f)** males expression of ZO-2, claudin-2 and occludin protein levels in proximal colon samples by RT-qPCR using the comparative method normalized to CHOW-fed wt (FC). *p≤0.05 compared to CHOW-fed equivalent genotype (Uncorrected Fisher's LSD). #p≤0.05 compared to CHOW-fed (Mann-Whitney test). 7-8 m [F: CHOW n=4(wt), n=7(tgNM), HFD n=4(wt), n=8(tgNM); M: CHOW n=7(wt), n=6(tgNM), HFD n=7(wt), n=8(tgNM)].

2.4.5 Effect of HFD in the expression of inflammatory markers within the GI tract

Alterations in the intestinal barrier are known to allow translocation of substances such as LPS, lipopeptides and fatty acids, which can interact with TLR-2 and TLR-4, triggering systemic inflammatory responses (Sepehri et al., 2016; Velloso et al., 2015). To further investigate these interactions, we assessed the expression of different inflammatory markers, including s100B, GFAP, TLR-2, and TLR-4, in the same tissue samples.

In the duodenum, HFD-fed tgNM females exhibited significantly reduced expression levels of GFAP, TLR-2 and TLR-4 compared to their CHOW-fed littermates. In contrast, HFD-fed wt females only presented increased levels of s100b compared to their CHOW-fed wt counterparts (Figure 63 a). In male mice, HFD-fed tgNM males similarly displayed decreased levels of GFAP and TLR-4, while no significant changes in inflammatory markers expression were observed in HFD-fed wt males (Figure 63 b). In the proximal colon samples, HFD-fed wt and tgNM females both exhibited increased s100B expression compared to their CHOW-fed counterparts (Figure 63 c). Similarly, HFD-fed wt males also showed increased s100B levels compared to CHOW-fed wt males. However, in tgNM males, HFD resulted in decreased GFAP expression in the proximal colon, similarly as in the duodenum (Figure 63 d).

Based on existing literature, we hypothesized that HFD-fed tgNM mice would present elevated levels of TLR-2 and TLR-4 due to their obesity and increased gut permeability (Hausmann et al., 2002; Jialal et al., 2014; Rohr et al., 2020; Velloso et al., 2015). Obesity is frequently associated with increased LPS levels, because of HFD-induced gut permeability, which promotes systemic inflammation (Hersoug et al., 2018; Rohr et al., 2020; K. Wang et al., 2024). However, the reduced levels of GFAP, TLR-2, and TLR-4 in tgNM mice indicate a potentially dysregulated inflammatory response in tgNM mice under HFD. It suggests an atypical response to HFD-induced metabolic stress, which may reflect altered glial and immune activity in the intestinal microenvironment.

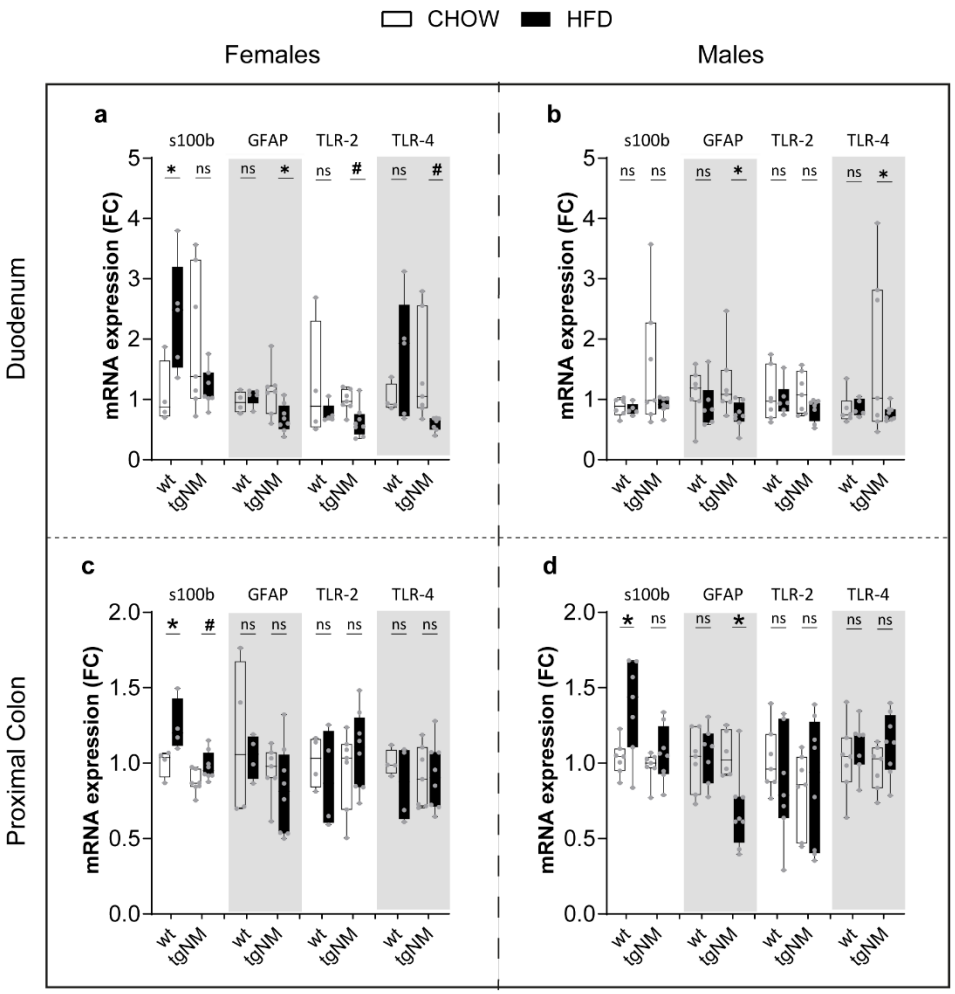

Figure 63. Inflammatory markers expression in duodenum and proximal colon samples. a) Females and **b)** males expression of s100b, GFAP, TLR-2 and TLR-4 levels in duodenum samples by RT-qPCR using the comparative method normalized to CHOW-fed wt (FC). 7-8 m [F: CHOW n=4(wt), n=7(tgNM), HFD n=5(wt), n=8(tgNM); M: CHOW n=7(wt), n=7(tgNM), HFD n=6(wt), n=8(tgNM)]. **c)** Females and **d)** males expression of s100b, GFAP, TLR-2 and TLR-4 levels in proximal colon samples by RT-qPCR using the comparative method normalized to CHOW-fed wt (FC). *p≤0.05 compared to CHOW-fed equivalent genotype (Uncorrected Fisher's LSD). #p≤0.05 compared to CHOW-fed (Mann-Whitney test). 7-8 m [F: CHOW n=4(wt), n=7(tgNM), HFD n=4(wt), n=8(tgNM); M: CHOW n=7(wt), n=7(tgNM), HFD n=7(wt), n=8(tgNM)].

To further validate the hypothesis that HFD increases gut permeability and exacerbates intestinal inflammation, we analyzed the inflammatory cytokine profile in duodenal and proximal colon samples. Using RT-qPCR, we assessed the expression levels of different cytokines including IL-10, INF-γ, TNF-α, IL-1b and IL-6.

In the duodenum, both HFD-fed wt and tgNM females exhibited reduced INF-γ levels. Additionally, HFD-fed tgNM females showed further reductions in TNF-α and IL-6 levels compared to their CHOW-fed littermates (Figure 64 a). In males, a significant reduction in INF-γ levels was observed exclusively in HFD-fed wt animals, with no significant changes detected in other cytokines (Figure 64 b). In the proximal

colon, a similar trend was noted, with reduced INF-γ levels in HFD-fed tgNM females (Figure 64 c). In contrast, HFD-fed wt males displayed increased IL-6 levels in the proximal colon compared to CHOW-fed wt males (Figure 64 d). No other significant changes in cytokine expression were detected in either sex or genotype.

In summary, HFD-fed tgNM females exhibited a consistent decrease in pro-inflammatory cytokines (INF-γ, TNF-α, and IL-6), while HFD-fed wt males showed an increase in IL-6 in the proximal colon. These findings align with the reductions in inflammatory markers reported in the previous section, reinforcing the notion of an atypical inflammatory response to HFD-induced metabolic stress in tgNM mice.

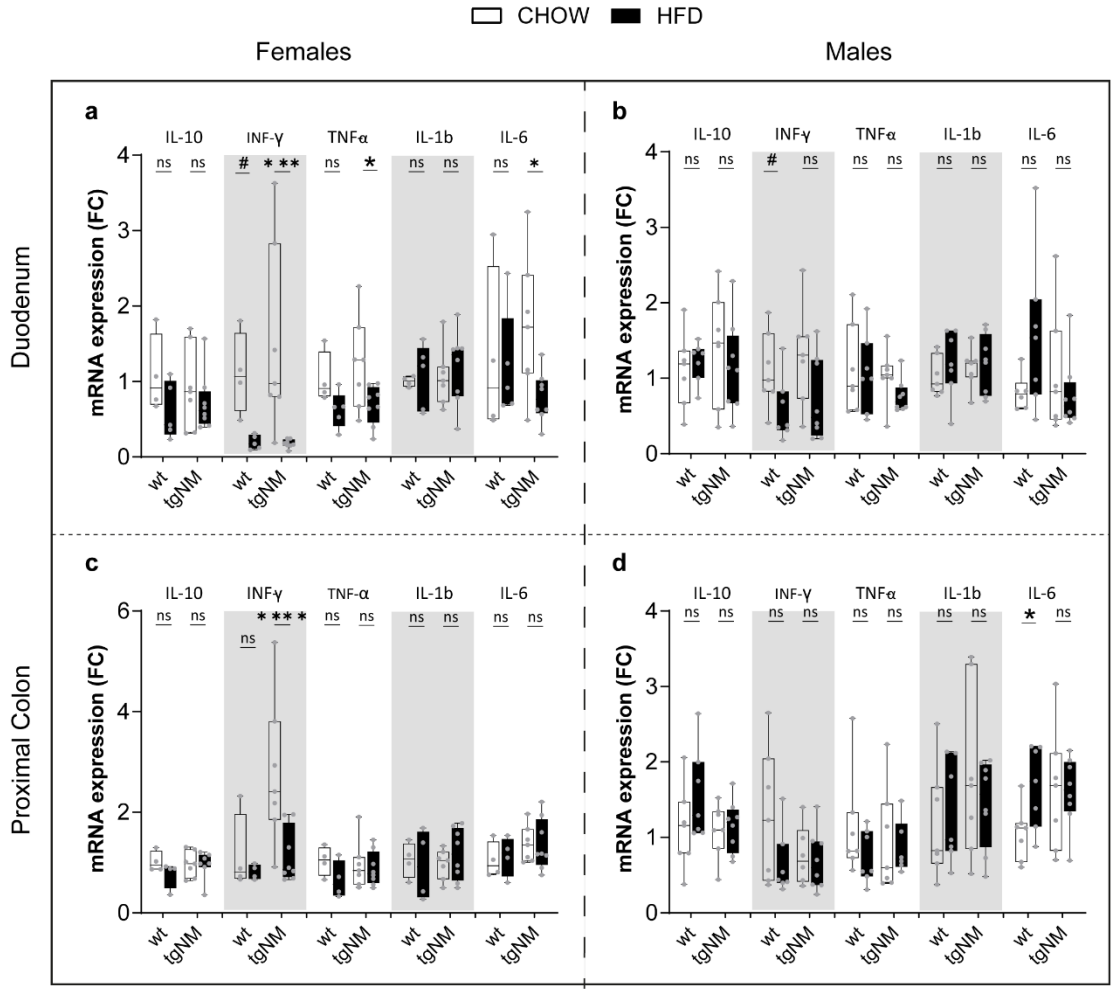

Figure 64. Inflammatory cytokines expression in duodenum and proximal colon samples. a) Females and **b)** males expression of inflammatory cytokine levels in duodenum samples by RT-qPCR using the comparative method normalized to CHOW-fed wt (FC). **c)** Females and **d)** males expression of inflammatory cytokine levels in duodenum samples by RT-qPCR using the comparative method normalized to CHOW-fed wt (FC). *p≤0.05 compared to CHOW-fed equivalent genotype (Uncorrected Fisher's LSD). #p≤0.05 compared to CHOW-fed (Mann-Whitney test). 7-8 m [F: CHOW n=4(wt), n=7(tgNM), HFD n=5(wt), n=8(tgNM); M: CHOW n=7(wt), n=7(tgNM), HFD n=7(wt), n=8(tgNM)].

2.4.6 Effect of HFD in peripheral inflammation

We next investigated the systemic inflammatory response to HFD. We analyzed serum and fecal samples by ELISA to characterize the peripheral inflammatory profile. Levels of IL-23, IL-1a, INF-γ, TNF-α, MCP-1, IL-12p70, IL-1b, IL-10, IL-6, IL-27, IL-17a, INF-β and GM-CSF were quantified.

In tgNM females, HFD feeding resulted in significantly elevated serum levels of IL-23, INF-γ, IL-12p70, IL-10, IL-27 and GM-CSF compared to their CHOW-fed littermates (Figure 65 a). Conversely, HFD-fed wt females exhibited a more modest systemic inflammatory response, with increased levels of TNF-α, IL-12p70 and IL-17a (Figure 65 a). In males, HFD induced a less pronounced pro-inflammatory effect. In HFD-fed tgNM males, serum levels of MCP-1 and IL-17a were elevated, whereas in HFD-fed wt males, increased levels of IL-23 and INF-β were observed (Figure 65 b).

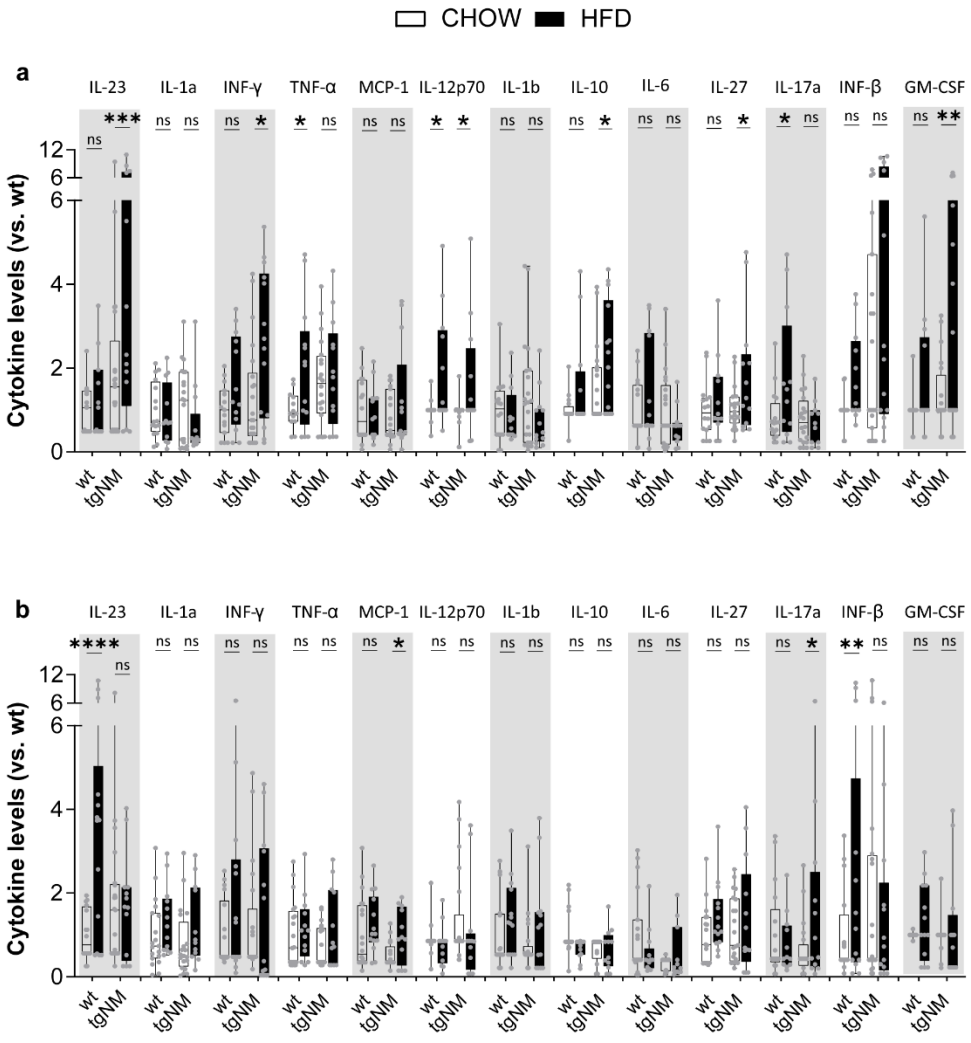

Figure 65. Inflammatory cytokine profile in serum samples. a) Females and **b)** males expression of diverse cytokine levels in fecal samples. Groups are normalized to their CHOW-fed wt. *p≤0.05 compared to CHOW-fed equivalent genotype (Uncorrected Fisher's LSD). 6 m [F: CHOW n=16(wt), n=22(tgNM), HFD n=13(wt), n=14(tgNM); M: CHOW n=20(wt), n=21(tgNM), HFD n=14(wt), n=13(tgNM)].

In fecal samples, HFD-fed wt females showed significantly elevated IL-23, IL-1a, INF-γ, TNF-α, MCP-1, IL-1b, IL-10, IL-6, IL-27 and INF-β compared to their CHOW-fed wt littermates. Meanwhile, HFD-fed tgNM females presented increased levels of IL-1a, INF-γ, MCP-1, IL-1b, IL-27, IL-17a and INF-β (Figure 66 a). HFD-fed wt males presented significantly elevated levels of IL-23, IL-1a, INF-γ, TNF-α, IL-27 and INF-β. In contrast, HFD-fed tgNM males displayed a more modest fecal inflammatory response, with increased levels of IL-1a, IL-1b and IL-27 (Figure 66 b).

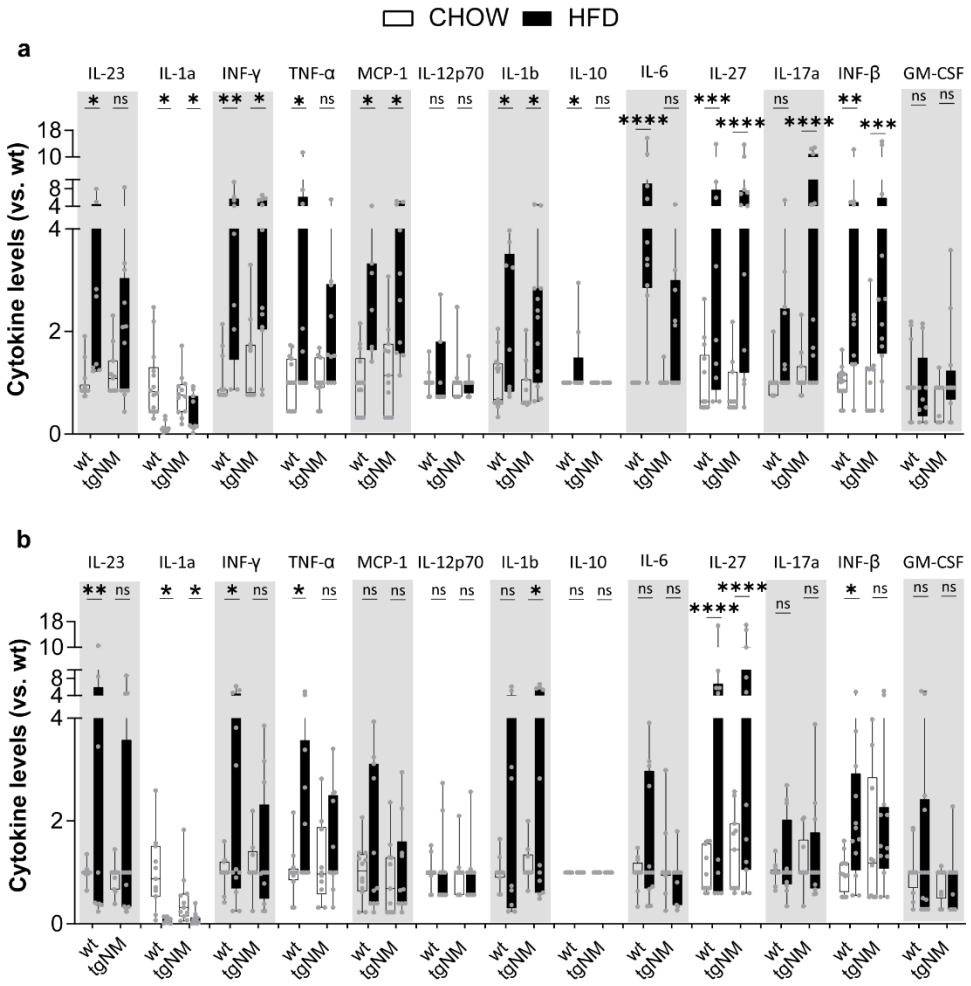

Figure 66. Inflammatory cytokine profile in fecal samples. a) Females and **b)** males expression of diverse cytokine levels in fecal samples. Groups are normalized to their CHOW-fed wt. *p≤0.05 compared to CHOW-fed equivalent genotype (Uncorrected Fisher's LSD). 6 m [F: CHOW n=15(wt), n=12(tgNM), HFD n=11(wt), n=12(tgNM); M: CHOW n=12 (wt), n=11(tgNM), HFD n=12(wt), n=13(tgNM)].

In summary, HFD-fed females exhibited a robust inflammatory response across both serum and fecal profiles, characterized by elevated levels of several cytokines, indicating heightened systemic inflammation. In HFD-fed males, the inflammatory response comprised changes in less cytokines. Overall, the increased peripheral inflammatory response after HFD feeding was consistent in both sexes and

genotypes confirming our initial hypothesis of exacerbated intestinal inflammation as a consequence of HFD-induced increased gut permeability, despite the controversial results obtained by RT-qPCR in the expression of inflammatory markers.

2.5 Neuroendocrine gut-brain axis characterization

In this section, we explored the neuroendocrine gut-brain axis to investigate the impact of HFD on the interplay between metabolic dysregulation and neuronal signaling in both wt and tgNM mice. During the initial characterization of tgNM mice in Chapter 1, we identified marked signs of metabolic dysregulation, particularly in tgNM females, who exhibited increased food and water intake along with greater body weight and adipose tissue mass compared to their wt counterparts. Following HFD intervention, these metabolic impairments were further exacerbated, with HFD-fed tgNM females exhibiting a significant body weight gain and adipose tissue accumulation, together with increase in water consumption. In this section we aimed to better understand how HFD influences this complex neuroendocrine axis and to explore potential alterations in the signaling pathways that may contribute to the pathophysiology of PD.

2.5.1 Effect of HFD in the expression levels of key enzymes, hormones and neuropeptides in the hypothalamus

We assessed the potential impact of HFD on the hypothalamic regulation of energy homeostasis by analyzing the expression levels of key genes involved in DA metabolism and feeding/energy expenditure by RT-qPCR.

In females, no significant changes were detected in the expression levels of enzymes, hormones and neuropeptides in HFD-fed wt or tgNM animals at 6 m (Figure 67 a). In HFD-fed wt males, we only observed reduced levels of POMC (Figure 67 b). However, HFD-fed tgNM males presented increased expression levels of MCH, POMC, OXYTOCIN and TH in comparison to their CHOW-fed counterparts (Figure 67 b). These data suggest that HFD may influence both anorexigenic and orexigenic pathways in tgNM males, altering the hypothalamic regulation of appetite and energy homeostasis. Surprisingly, tgNM females did not show major differences as we would expect considering the severe phenotype they present in terms of body weight and food/water intake.

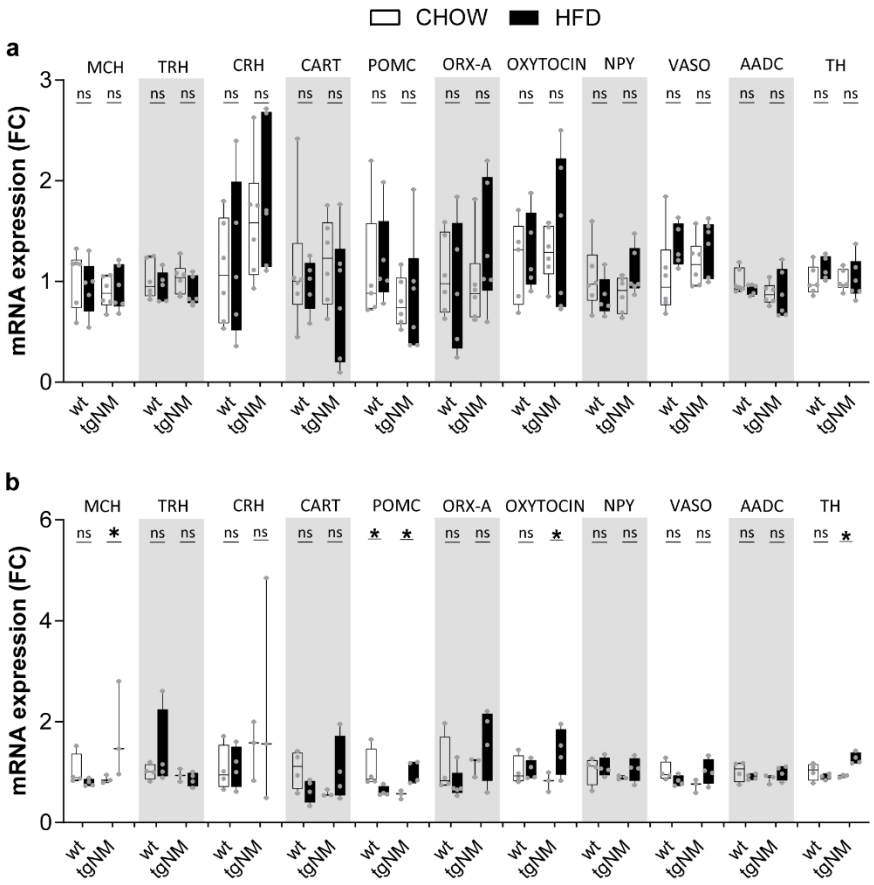

Figure 67. Hormones, neuropeptides and enzymes expression profile in the hypothalamus. a) Females and **b)** males expression of different hormones, neuropeptides and enzymes in the hypothalamus samples by RT-qPCR using the comparative method normalized to CHOW-fed wt (FC). *p≤0.05 compared to CHOW-fed equivalent genotype (Uncorrected Fisher's LSD test). 7-8 m [F: CHOW n=5-6(wt), n=6(tgNM), HFD n=5(wt), n=6(tgNM); M: CHOW n=4(wt), n=3(tgNM), HFD n=4-5(wt), n=3-4(tgNM)].

2.5.2 Effect of HFD in the metabolic hormonal profile

We next measured the serum levels of several key metabolic hormones involved in satiety, appetite regulation and energy homeostasis by multiplex ELISA, including ghrelin, active GLP-1, glucagon, leptin, insulin, PYY and amylin.

In HFD-fed wt females, significant increases were observed in ghrelin, GLP-1 active, glucagon, leptin and amylin levels compared to their CHOW-fed counterparts (Figure 68 a). In contrast, HFD-fed tgNM females exhibited a different hormonal profile, characterized by significantly elevated levels of insulin and leptin, but no significant changes in other metabolic hormones (Figure 68 a). HFD-fed wt males showed a hormonal pattern similar to that of HFD-fed tgNM females, with significantly increased levels of insulin and leptin (Figure 68 b). In HFD-fed tgNM males, however, we observed more hormonal changes, with

significantly increased levels of ghrelin, GLP-1 active, glucagon, insulin, leptin, PYY, and amylin (Figure 68 b).

These results suggest that tgNM females seem particularly vulnerable to metabolic stress, showing a limited hormonal response after HFD feeding. In contrast, tgNM males display a more dynamic hormonal response to HFD.

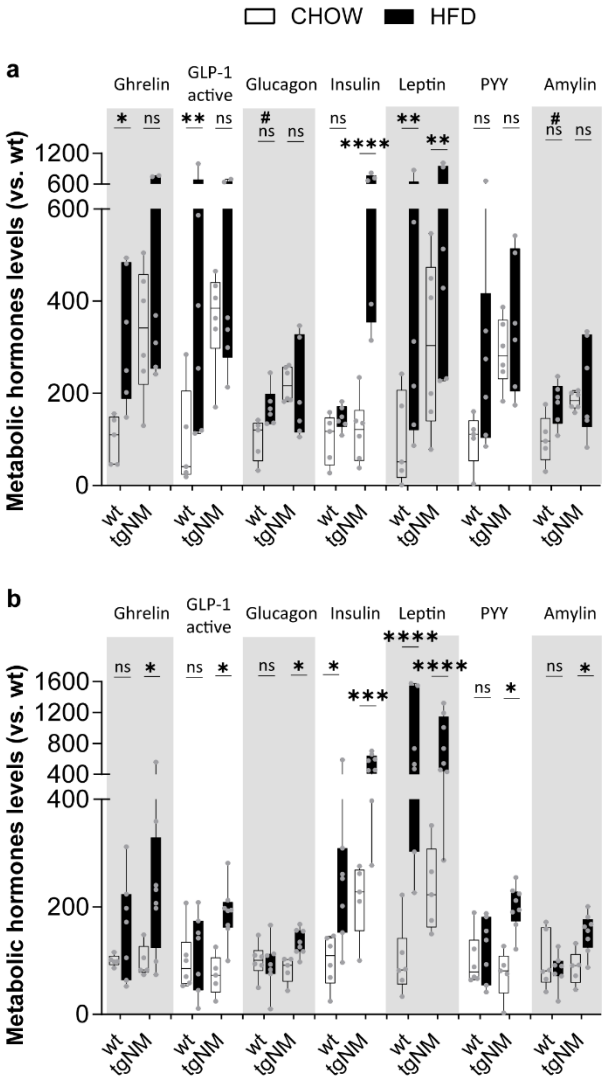

Figure 68. Metabolic hormones profile in serum samples. a) Metabolic hormones levels in serum samples of females and **b)** males fed with CHOW or HFD. Groups are normalized to their CHOW-fed wt. *p≤0.05 compared to CHOW-fed equivalent genotype (Uncorrected Fisher's LSD test). #p≤0.05 compared to CHOW-fed equivalent genotype (Mann-Whitney test).6 m [F: CHOW n=5(wt), n=6(tgNM), HFD n=6(wt), n=6(tgNM); M: CHOW n=6 (wt), n=5(tgNM), HFD n=7(wt), n=8(tgNM)].

2.5.3 Effect of HFD in glucose metabolism

To further investigate the observed differences in metabolic hormone regulation, we conducted a GTT to assess how effectively tgNM mice manage glucose levels under dietary stress. Given the pronounced metabolic dysregulation in HFD-fed tgNM females, this test aimed to determine whether these metabolic impairments translated into altered glucose tolerance compared to their CHOW-fed counterparts.

Our results showed that HFD-fed wt females and males presented a higher AUC in the GTT compared to CHOW-fed littermates (Figure 69 a, b, c, d), indicating impaired glucose tolerance. Surprisingly, HFD-fed tgNM males displayed glucose clearance rates comparable to CHOW-fed wt animals (Figure 69 c, d), while HFD-fed tgNM females demonstrated improved glucose tolerance, although not significant, as reflected by a lower AUC in the GTT compared to CHOW-fed wt females (Figure 69 a, b). These findings were unexpected, especially given the previous observations of obesity, peripheral inflammation and hormonal dysregulation in HFD-fed tgNM mice, which would typically predict impaired glucose handling (Martyn et al., 2008; Montgomery et al., 2013a).

To further explore these results, we measured basal blood glucose levels. HFD-fed wt animals displayed significantly higher basal glucose levels compared to CHOW-fed wt counterparts (Figure 69 e, f). Intriguingly, HFD-fed tgNM females presented significantly lower basal glucose levels than CHOW-fed tgNM females (Figure 69 e), while HFD-fed tgNM males presented the same basal blood glucose levels as their CHOW-fed counterparts (Figure 69 f). Additionally, we assessed urinary glucose levels and creatinine excretion. Results showed increased urinary glucose levels in both HFD-fed tgNM animals and HFD-fed wt males, but not in HFD-fed wt females (Figure 69 g,h). These results seem to indicate a complex metabolic adaptation in HFD-fed tgNM animals that allow for efficient glucose regulation despite the pronounced obesity.

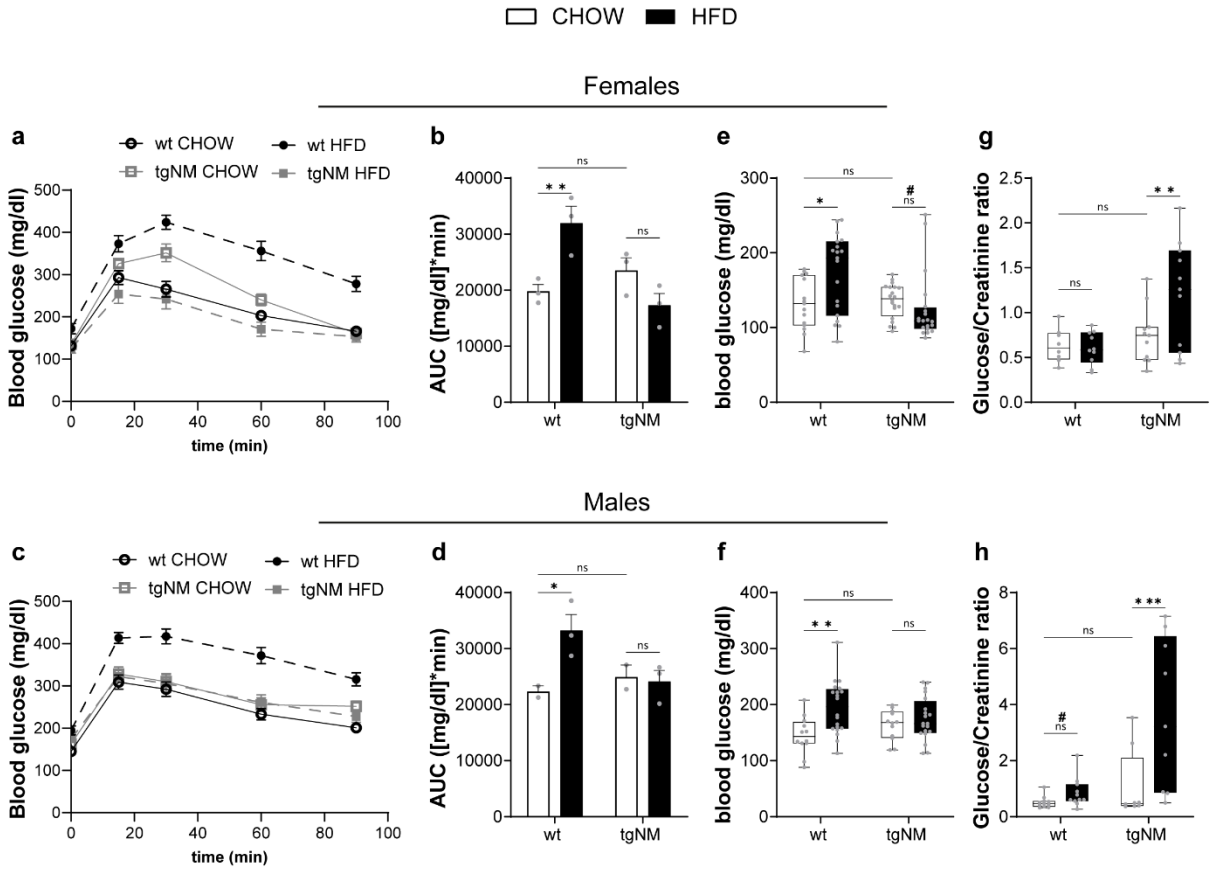

Figure 69. Glucose metabolism. a) Females and **c)** males GTT measurements. Representation of the mean values of 3 independent experiments. **b)** Females and **d)** males AUC of GTTs. Mean values of 3 independent experiments. [F: CHOW n=15(wt), n=20(tgNM), HFD n=19(wt), n=20(tgNM); M: CHOW n=12 (wt), n=12(tgNM), HFD n=20(wt), n=20(tgNM)]. **e)** Females and **f)** males blood glucose basal levels after 5-6 h fasting. [F: CHOW n=15(wt), n=20(tgNM), HFD n=19(wt), n=20(tgNM); M: CHOW n=12 (wt), n=12(tgNM), HFD n=20(wt), n=20(tgNM)]. **g)** Females and **h)** males urinary glucose/creatinine ratio measurements in urine samples. [F: CHOW n=8(wt), n=11(tgNM), HFD n=10(wt), n=11(tgNM); M: CHOW n=11 (wt), n=8(tgNM), HFD n=11(wt), n=9(tgNM)]. *p≤0.05 compared to CHOW-fed equivalent genotype (Uncorrected Fisher's LSD test). #p≤0.05 compared to CHOW-fed equivalent genotype (Mann-Whitney test).

2.6 Effect of HFD on renal function

Next, we aimed to determine whether the metabolic dysregulation observed in tgNM mice, translated into significant alterations in renal function. It is known that metabolic syndrome is associated with increased risk of chronic kidney disease (CKD) (J. Chen et al., 2004). Moreover, obesity often induces structural, hemodynamic and metabolic alterations in the kidneys, many of which are likely compensatory mechanisms responding to increased systemic metabolic demands (Tsuboi et al., 2017). Moreover, recent epidemiological studies have reported an increased risk for PD in patients with CKD (Meléndez-Flores & Estrada-Bellmann, 2021). Thus, in collaboration with the Nephrology and kidney transplantation group at

VHIR, we aimed to determine whether the metabolic dysregulation observed in tgNM mice, translated into significant alterations in renal function.

Our analysis showed a significant increase in kidney weight in wt and tgNM females fed with HFD (Figure 70 a) compared to their CHOW-fed counterparts, though no significant changes were observed in HFD-fed male mice (Figure 70 c). This increase in kidney weight may be associated with an elevated body mass index, as suggested in previous studies (Mandal et al., 2012a). Animal studies have further shown that kidney hypertrophy commonly precedes hyperfiltration (Bak et al., 2000). Therefore, we measured the GFR to assess kidney function. Both HFD-fed wt and tgNM females and males exhibited increased GFR compared to their CHOW-fed littermates, indicating that HFD induced glomerular hyperfiltration (Figure 70 b, d). Hyperfiltration is generally considered an early marker that may precede albuminuria and/or a decline in renal function, potentially leading to progressive nephron damage through elevated glomerular hydrostatic pressure (Tonneijck et al., 2017). However, no significant changes in albuminuria (albumin/creatinine ratio, ACR) were detected in HFD-fed tgNM or wt mice urine samples (Figure 70 e, f). These results suggest that while hyperfiltration is present, it has not yet progressed to albuminuria or significant renal impairment.

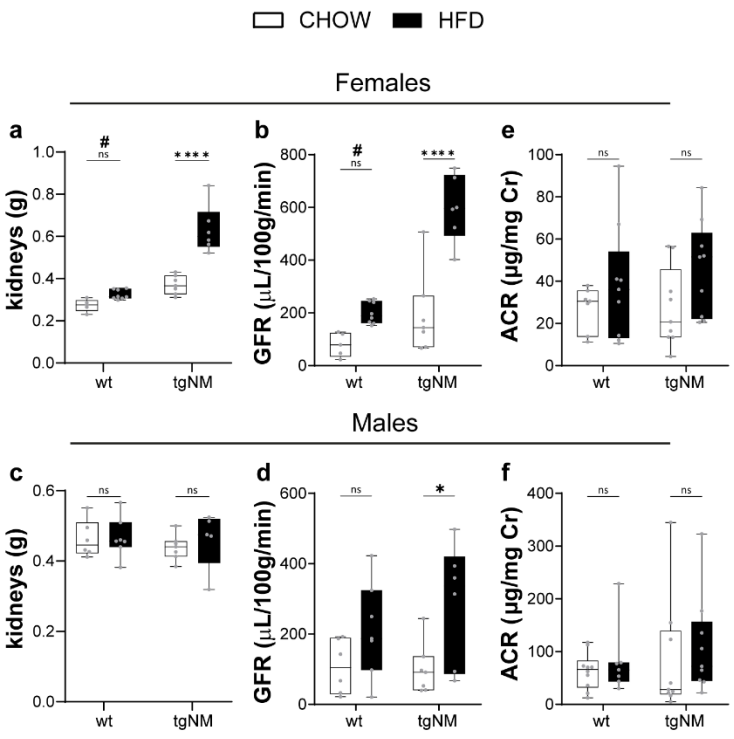

Figure 70. Assessment of renal function. a) Females and **c)** males kidneys weight. [F: CHOW n=5(wt), n=7(tgNM), HFD n=8(wt), n=6(tgNM); M: CHOW n=6 (wt), n=7(tgNM), HFD n=7(wt), n=5(tgNM)]. **b)** Females and **d)** males GFR. [F: CHOW n=5(wt), n=7(tgNM), HFD n=8(wt), n=6(tgNM); M: CHOW n=6 (wt), n=7(tgNM), HFD n=7(wt), n=6(tgNM)]. **e)** Females and **f)** males Urinary ACR in urine samples. [F: CHOW n=7(wt), n=9(tgNM), HFD n=9(wt), n=9(tgNM); M: CHOW n=10 (wt), n=9(tgNM), HFD n=7(wt), n=9(tgNM)]. *p≤0.05 compared to CHOW-fed equivalent genotype (Uncorrected Fisher's LSD test). #p≤0.05 compared to CHOW-fed equivalent genotype (Mann-Whitney test).

We further analyzed podocyte density by calculating the number of podocytes per glomerular tuft area. In females, we observed a reduced podocyte-to-tuft area ratio in CHOW-fed tgNM mice compared to wt littermates, though HFD did not impact this ratio in either genotype (Figure 71 a). In males, HFD-fed tgNM mice presented a reduced podocyte-to-tuft area ratio compared to CHOW-fed littermates. These reductions, likely reflect changes in podocyte density associated with glomerular tuft enlargement rather than actual podocyte cell loss, given the absence of albuminuria (Figure 71 c). Unexpectedly, glomerular tuft area analysis showed distinctive patterns. CHOW-fed tgNM females had an increased tuft area compared to CHOW-fed wt littermates, yet HFD induced a significant reduction in tuft area in tgNM females compared their CHOW-fed counterparts (Figure 71 b). This suggests that, despite these females presented obesity and hyperfiltration due to HFD, tgNM females' glomerular structure does not exhibit the typical hypertrophic adaptation, a surprising finding since hyperfiltration and obesity are usually associated with increased glomerular size (Tsuboi et al., 2017). In contrast, HFD-fed tgNM males displayed an increase in tuft area compared to their CHOW-fed littermates, consistent with the effects of hyperfiltration (Figure 71 d).

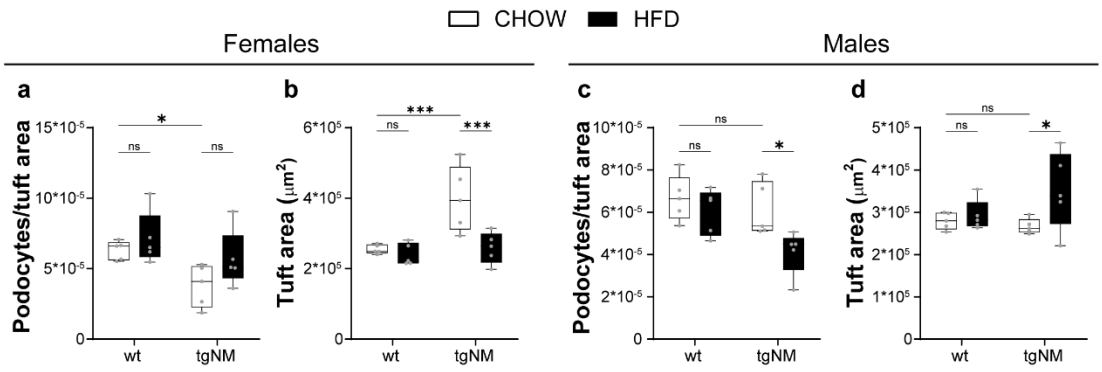

Figure 71. Assessment of renal function. a) Females and **c)** males kidneys weight. [F: CHOW n=5(wt), n=7(tgNM), HFD n=8(wt), n=6(tgNM); M: CHOW n=6 (wt), n=7(tgNM), HFD n=7(wt), n=5(tgNM)]. **b)** Females and **d)** males Urinary ACR in urine samples. [F: CHOW n=7(wt), n=9(tgNM), HFD n=9(wt), n=9(tgNM); M: CHOW n=10 (wt), n=9(tgNM), HFD n=7(wt), n=9(tgNM)]. e) Females and f) males GFR. [F: CHOW n=5(wt), n=7(tgNM), HFD n=8(wt), n=6(tgNM); M: CHOW n=6 (wt), n=7(tgNM), HFD n=7(wt), n=6(tgNM)].*p≤0.05 compared to CHOW-fed equivalent genotype (Uncorrected Fisher's LSD test). #p≤0.05 compared to CHOW-fed equivalent genotype (Mann-Whitney test).

2.7 Brain characterization

In our previous study, we characterized the consequences of NM accumulation in key catecholaminergic brain nuclei, specifically in the SNpc and VTA of the midbrain, the LC in the brainstem and the medullary neuronal groups from the DVC in tgNM mice at different ages (Laguna et al., 2024). Building on these findings, we aimed at exploring if feeding with HFD could contribute to the pathophysiology of PD and if

modify the course of the brain neurodegenerative process observed in tgNM mice. Given that HFD induces gut microbiota alterations, exacerbates peripheral inflammation and leads to metabolic dysfunction in tgNM mice, as demonstrated in the previous sections, we hypothesized that HFD feeding may also accelerate neurodegeneration and exacerbate the PD-like phenotype observed in the brains of tgNM mice. We did not consider a possible effect on the LC since the extent of neurodegeneration in this region is already very significant at early stages in tgNM mice (Laguna et al., 2024).

2.7.1 Effects of HFD on dopaminergic dysfunction in the SNpc and VTA of adult tgNM mice

To evaluate the impact of HFD on dopaminergic dysfunction, we first assessed the expression of TH in striatal fibers by OD in inmmunostained histological sections. However, no differences were found in either sex or genotype under CHOW or HFD conditions at this age (Figure 72 b, c). We next performed stereological cell counts of TH-positive cells, total DA neurons (TH-positive cells, TH-positive-NM-positive cells and TH-negative-NM-positive cells) and eNM granules in the SNpc and VTA. In the SNpc, no significant changes were observed in the number of TH-positive neurons, total DA neurons, or eNM granules in both HFD-fed wt and tgNM females compared to their CHOW-fed littermates (Figure 72 d, e, f). Similarly, in males, no significant differences were detected in TH-positive or total DA neurons across genotypes under HFD (Figure 72 g, h). However, HFD-fed tgNM males exhibited a significant reduction in the number of eNM granules compared to their CHOW-fed littermates (Figure 72 i). In the VTA, again no significant changes were observed in the number of TH-positive or total DA neurons in both HFD-fed wt and tgNM females compared to their CHOW-littermates (Figure 72 j, k). However, HFD-fed tgNM females showed an increase in the number of eNM granules compared to CHOW-fed counterparts (Figure 72 l). Similarly, HFD-fed wt and tgNM males did not present any significant change in the number of TH-positive neurons, DA neurons, nor in the number of eNM granules, compared to their CHOW-fed littermates (Figure 72 m, n, o).

The previous results on the number of eNM granules prompted s to perform a direct comparison between sexes and we observed sex-specific differences under HFD. In the SNpc, HFD-fed tgNM males had significantly fewer eNM granules compared to HFD-fed tgNM females (Figure 72 p). In the VTA, under CHOW conditions, tgNM males exhibited more eNM granules than tgNM females. However, under HFD, tgNM females increased their eNM granules number to match that of tgNM males (Figure 72 r). Afterwards, we assessed intracellular NM accumulation by OD in both nuclei. In the SNpc, CHOW-fed tgNM males exhibited higher intracellular NM levels than tgNM females. However, under HFD, tgNM females surpassed the intracellular NM levels of tgNM males (Figure 72 q). A similar pattern was observed in the VTA, where CHOW-fed tgNM males had greater intracellular NM levels than tgNM females.

However, under HFD, tgNM females increased their intracellular NM levels to match that of tgNM males (Figure 72 s).

In summary, HFD-fed tgNM mice did not exhibit overt dopaminergic cell death in SNpc or VTA. However, an increased presence of eNM debris was detected in HFD-fed tgNM females, which originates from degenerating neurons and is typically observed in PD and aged postmortem brains (Beach et al., 2007; Ishikawa, 1998; Korzhevskii et al., 2021). This was accompanied by elevated intracellular NM levels compared to CHOW-fed females, suggesting that HFD-fed tgNM females might be closer to the pathogenic threshold of NM levels that induce neurodegeneration as early as 7-8 m of age. In contrast, these deleterious effects were not observed in tgNM males, where eNM granules decreased, and intracellular NM levels remained stable under HFD. These findings highlight a sex-specific vulnerability to HFD-induced dopaminergic dysfunction in adult tgNM mice.

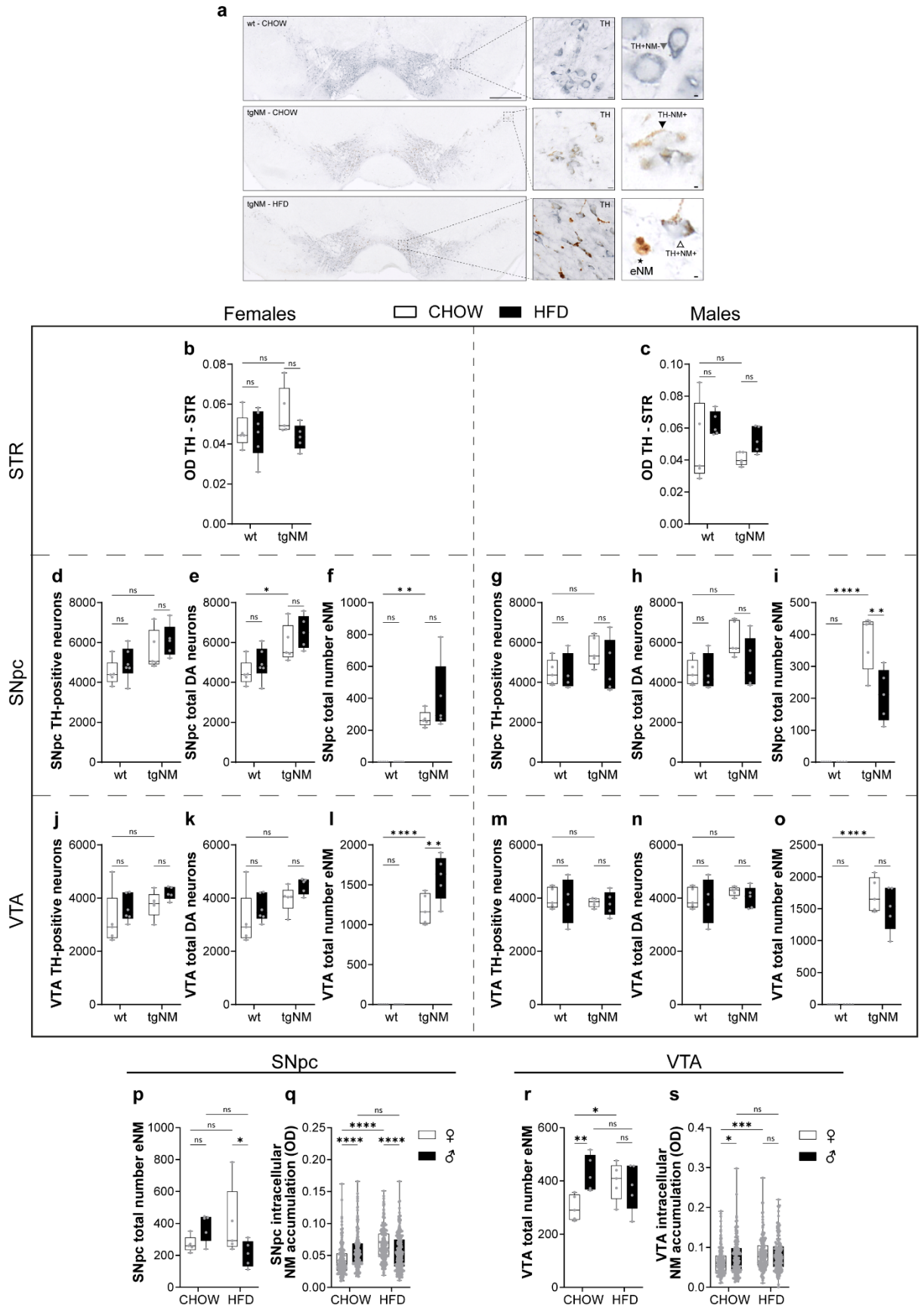
a
wt - CHOW
TH
TH+NM-
tgNM - CHOW
TH
TH-NM+
tgNM - HFD
TH
△ TH+NM+
★ eNM
Females
CHOW
HFD
Males
STR
SNpc
VTA
b
c
OD TH - STR
d
e
f
g
h
i
SNpc TH-positive neurons
SNpc total DA neurons
SNpc total number eNM
j
k
l
m
n
o
VTA TH-positive neurons
VTA total DA neurons
VTA total number eNM
wt
tgNM
ns
SNpc
VTA
p
q
r
s
SNpc total number eNM
SNpc intracellular NM accumulation (OD)
VTA total number eNM
VTA intracellular NM accumulation (OD)
CHOW
HFD
♀
♂

Figure 72. Effect of HFD in the dopaminergic dysfunction in the SNpc and VTA of tgNM mice. a) SNpc and VTA representative sections inmmunostained for TH in blue, NM appears as brown. Higher magnification of TH-positive-NM-negative neurons (grey arrowhead), TH-negative-NM-positive neurons (black arrowhead), TH-positive-NM-positive neurons (white arrowhead) and eNM granules (star) from wt and tgNM mice. Scale bars 500 µm / 10 µm. **b)** Females and **c)** males quantification of striatal TH by OD after immunostaining. d, e, f) Females and g, h, i) males stereological cell counts of SNpc TH-positive neurons, total DA neurons (TH-positive-NM-negative & TH-positive-NM-positive & TH-negative-NM-positive) and eNM granules fed with CHOW or HFD. Wt total DA neurons are the same as TH-positive neurons but are represented for comparison. **j, k, l)** Females and **m, n, o)** males stereological cell counts of VTA TH-positive neurons, total DA neurons (TH-positive-NM-negative & TH-positive-NM-positive & TH-negative-NM-positive) and eNM granules fed with CHOW or HFD. Wt total DA neurons are the same as TH-positive neurons but are represented for comparison. *p≤0.05 compared to CHOW-fed equivalent genotype and to CHOW-fed wt (Uncorrected Fisher's LSD test). [F&M: CHOW: n=5 (wt & tgNM); HFD n=4-6 (wt & tgNM)]. **p)** SNpc and **r)** VTA total number of eNM granules of tgNM female and male mice fed with CHOW or HFD. **q)** SNpc and **s)** VTA quantification of intracellular NM by OD of tgNM female and male mice fed with CHOW or HFD. *p≤0.05 compared to CHOW-fed or HFD-fed contrary sex and to CHOW-fed counterparts (Uncorrected Fisher's LSD test). [F&M: CHOW&HFD n=5(tgNM); SNpc (N=200) & VTA (N=150)].

2.7.2 Effects of HFD on DA metabolism and oxidation in the SNpc and VTA of adult tgNM mice

In the previous section, we observed that HFD increased intracellular NM levels in tgNM females, reaching or even exceeding those observed in tgNM males within the SNpc and VTA. To better understand the consequences of these changes, we performed UPLC-MS/MS analysis in midbrain dissected tissue to assess DA metabolism and oxidation levels in these nuclei. Specifically, we quantified L-DOPA, DA, and its metabolites NE and 3-MT. Additionally, we evaluated the rate of non-encapsulated DA oxidation into NM precursors by measuring the AC levels and free and protein-bound 5-SCD and 5-SCDA levels (Figure 73).

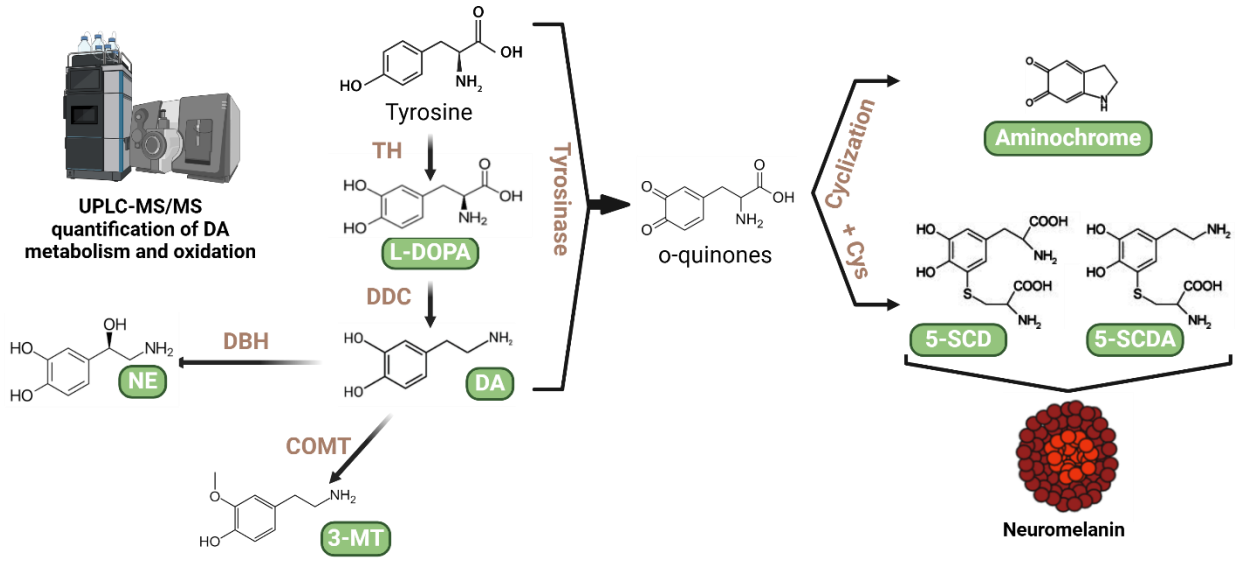

Figure 73. UPLC-MS/MS quantification of DA metabolism and catechol oxidation. Schematic simplified representation of DA is synthesized in the cytoplasm from L-DOPA by DDC. Both cytosolic DA and L-DOPA can be oxidized either spontaneously or by TYR to produce o-quinones. These, in turn generate AC, 5-SCD and 5-SCDA, which will act as precursors of the melanic components of NM. In green are marked the measured metabolites and in orange are the enzymes involved: TH (tyrosine hydroxylase), DDC (L-DOPA decarboxylase), DBH (DA-beta-hydroxylase) and COMT (catechol-O-methyltransferase).

In wt females, HFD increased the levels of L-DOPA, which consequently elevated DA and its metabolites NE and 3-MT (Figure 74 a, b, c, d). However, as wt animals present very low levels of TYR expression in the brain, the levels of 5-SCD and 5-SCDA remained barely detectable, as expected. In contrast, HFD-fed tgNM females presented similar levels of L-DOPA, DA, NE and 3-MT compared to their CHOW-fed counterparts (Figure 74 a, b, c, d). Notably, HFD-fed tgNM females exhibited an increased rate of L-DOPA oxidation, leading to elevated 5-SCD levels (Figure 75 a, c). This finding may explain why L-DOPA and DA levels did not increase in response to HFD, as observed in wt females. Additionally, this could account for the unaltered DA oxidation index in HFD-fed tgNM females (Figure 75 b, d). In males, no significant changes in DA metabolism or oxidation were detected after HFD in either wt or tgNM groups compared to their CHOW-fed littermates (Figure 74 e, f, g, h and Figure 75 e, f, g, h). Levels of AC were undetectable in any sample (data not shown) due to methodological problems.

These results are consistent with the intracellular NM levels measured in the SNpc and VTA, where HFD had no effect on NM accumulation in males while HFD-fed tgNM females showed increased intracellular NM levels in alignment with their elevated oxidation index.

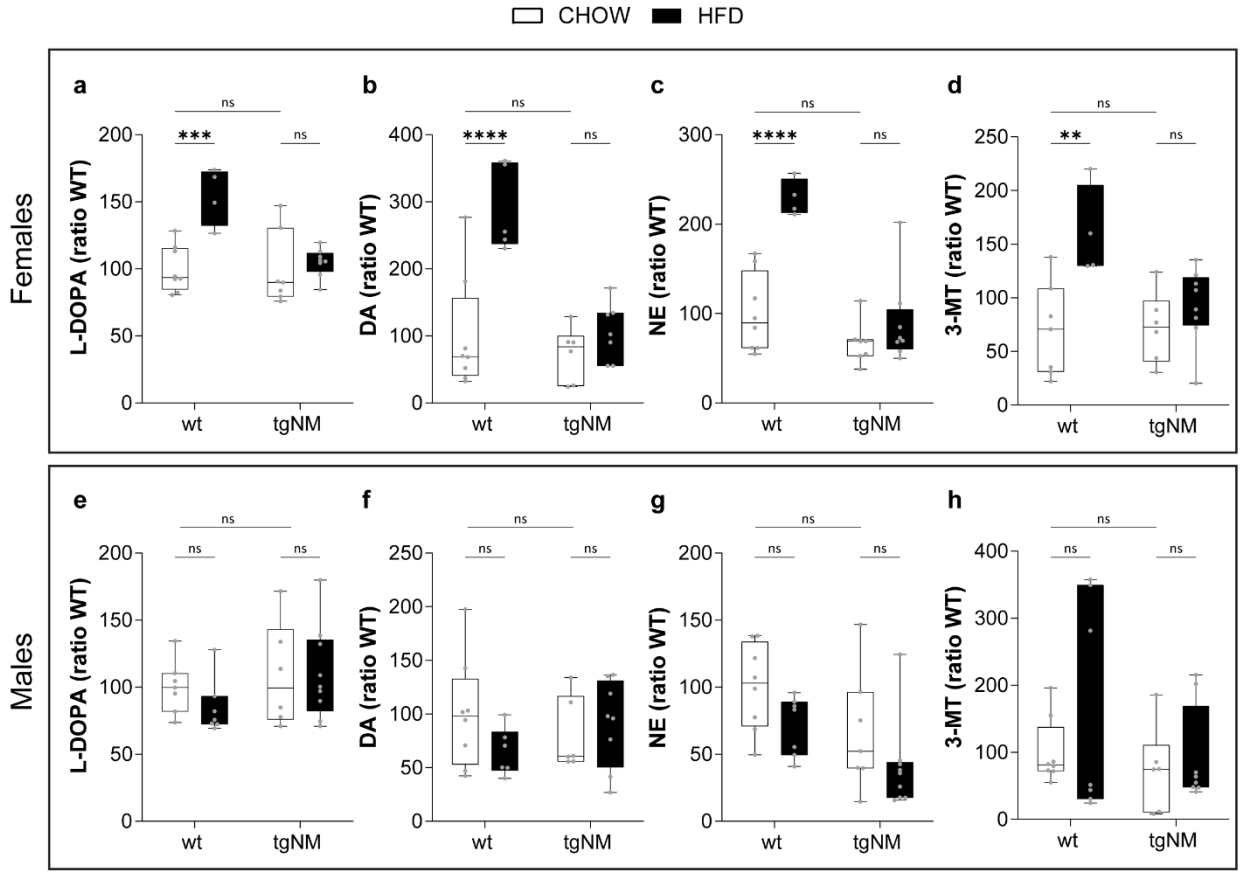

Figure 74. UPLC-MS/MS quantification of DA metabolism. a-d) UPLC-MS/MS measurements of L-DOPA, DA, NE and 3-MT midbrain homogenates of female and **e-h)** male mice fed with CHOW or HFD. Groups are normalized to their CHOW-fed wt. *p≤0.05 compared to CHOW-fed equivalent genotype (Uncorrected Fisher's LSD). 7-8 m [F: CHOW: n=8(wt), n=4-5(tgNM), HFD: n=6-7(wt), n=7-8(tgNM)]. 7-8 m [M: CHOW: n=7-8(wt), n=6-7(tgNM), HFD: n=6-7(wt), n=8-9(tgNM)].

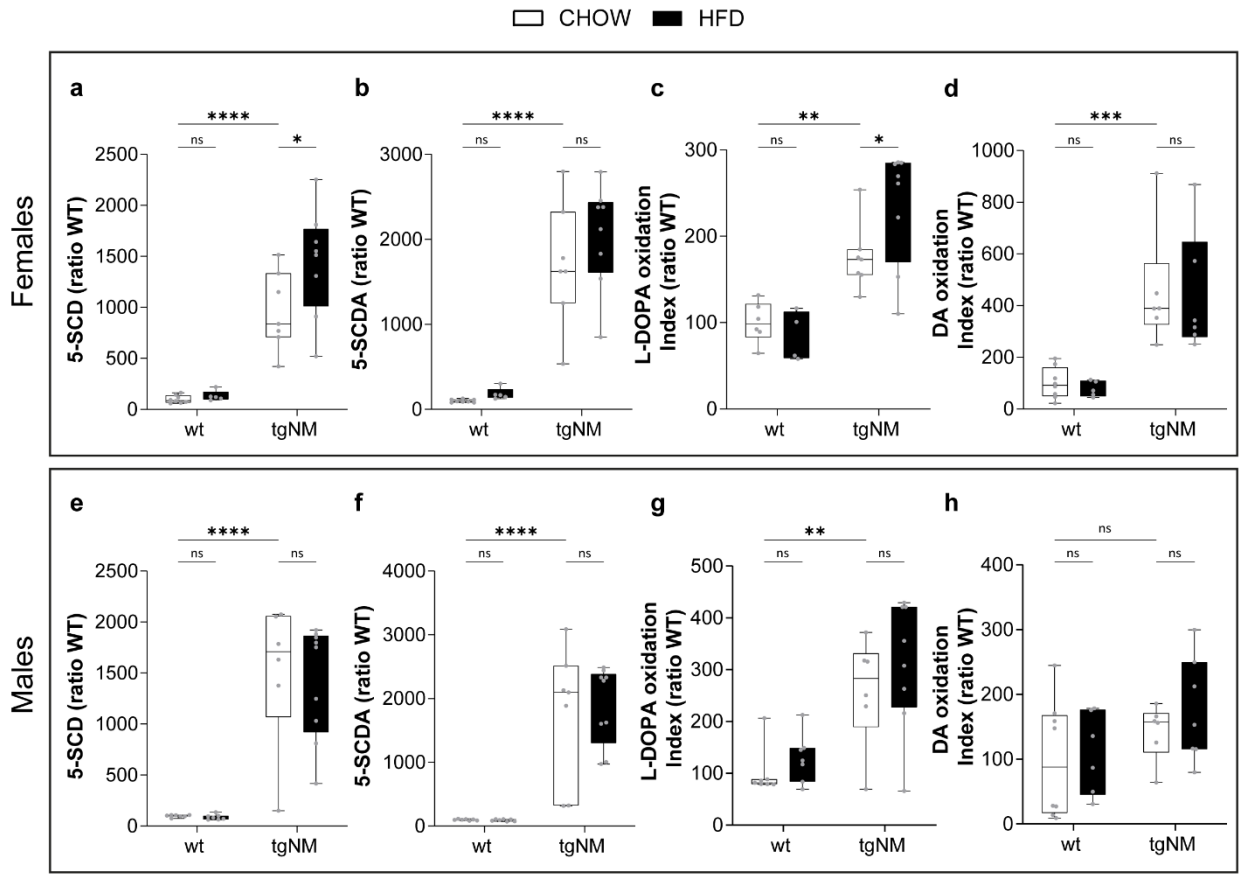

Figure 75. UPLC-MS/MS quantification of catechol oxidation. a-d) UPLC-MS/MS measurements of 5-SCD, 5-SCDA, L-DOPA oxidation index and DA oxidation index of midbrain homogenates of female and **e-h)** male mice fed with CHOW or HFD. Groups are normalized to their CHOW-fed wt. *p≤0.05 compared to CHOW-fed equivalent genotype (Uncorrected Fisher's LSD). 7-8 m [F: CHOW: n=8(wt), n=4-5(tgNM), HFD: n=6-7(wt), n=7-8(tgNM)]. 7-8 m [M: CHOW: n=7-8(wt), n=6-7(tgNM), HFD: n=6-7(wt), n=8-9(tgNM)].

2.7.3 Effects of HFD on PD-like neuropathological alterations and neuroinflammation in the SNpc and VTA of adult tgNM mice

Neuropathologically, we have previously reported that NM-containing neurons in the SNpc and VTA of tgNM mice exhibit intracellular inclusion bodies, including cytoplasmatic LB-like inclusions and nuclear MB-like inclusions, resembling those typically seen in PD and aged human brains (Laguna et al., 2024). Both LB-like and MB-like inclusions in tgNM mice are immunopositively for p62 (Figure 76 a, f), a ubiquitin-binding protein commonly associated with neuropathological inclusions and is restricted to melanized neurons and rarely observed in wt mice.

In the SNpc, HFD did not significantly affect the number of LB-like or MB-like inclusions of either tgNM or wt females and males (Figure 76 b, d, g, i). In the VTA, HFD-fed tgNM females presented a slight but not statistically significant increase in the number of LB-like inclusions compared to their CHOW-fed

counterparts (Figure 76 c) and did not present changes in the number of MB-like inclusions (Figure 76 h). No significant changes were observed in the VTA of HFD-fed tgNM males for LB-like or MB-like inclusions (Figure 76 e, j).

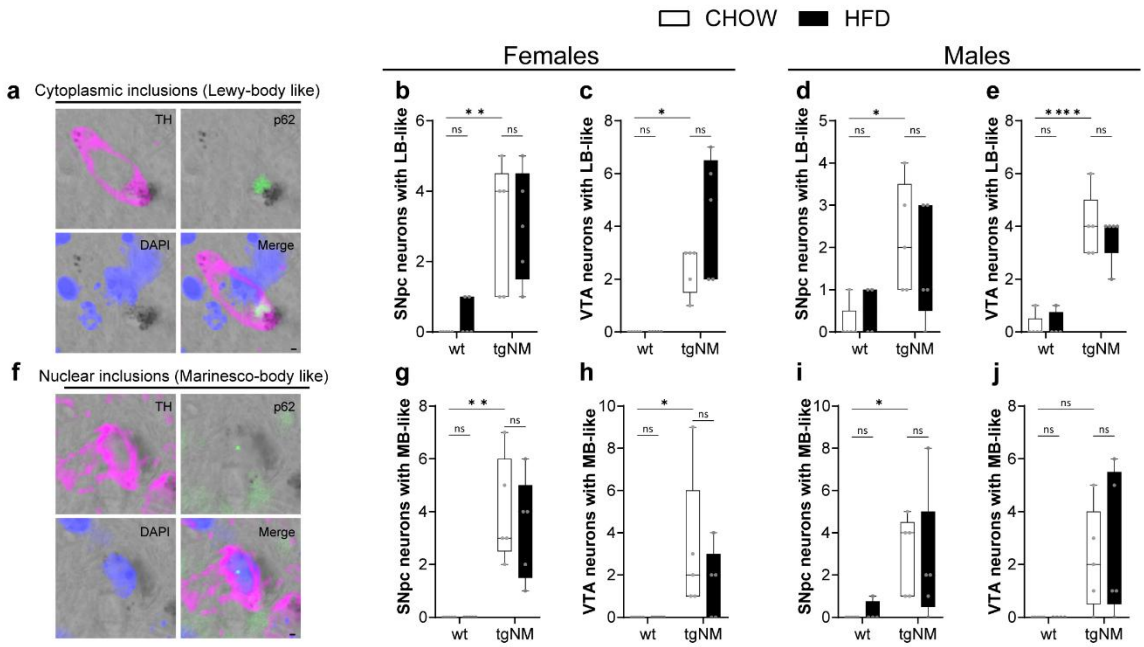

Figure 76. Effect of HFD on the PD-like neuropathological alterations in the SNpc and VTA of tgNM mice. a, f) Representative images of SNpc from tgNM mice exhibiting NM-laden neurons with LB-like and MB-like detected by IF with TH (pink), p62 (green), nuclei are stained with DAPI (blue) and NM appears as dark grey. Scale bar 2 µm. **b)** Females and **d)** males quantification of NM-laden neurons in the SNpc with p62-positive total cytoplasmatic LB-like inclusions, fed with CHOW or HFD. **c)** Females and **e)** males quantification of NM-laden neurons in the SNpc with p62-positive total nuclear MB-like inclusions, fed with CHOW or HFD. **g)** Females and **i)** males quantification of NM-laden neurons in the VTA with p62-positive total cytoplasmatic LB-like inclusions, fed with CHOW or HFD. **h)** Females and **j)** males quantification of NM-laden neurons in the VTA with p62-positive total nuclear MB-like inclusions, fed with CHOW or HFD. *p≤0.05 compared to CHOW-fed equivalent genotype and to CHOW-fed wt (Uncorrected Fisher's LSD test). [F&M: CHOW&HFD n=4-5(wt & tgNM)].

In addition to these neuropathological changes, HFD-fed tgNM females also presented neuroinflammatory alterations in the SNpc and VTA compared to their CHOW-fed littermates, characterized by increased numbers of phagocytic CD68-positive cells (Figure 77 b, c) and ameboid-reactive-like Iba1-positive microglial cells (Figure 77 g, h). These inflammatory changes were not observed in the SNpc or VTA of HFD-fed tgNM males when compared to their CHOW-fed littermates (Figure 77 d, e, i, j).

These findings, combined with the increased eNM granules and intracellular NM accumulation observed in HFD-fed tgNM females, males us hypothesize that inclusion-containing neurons may be those that are

more prone to degeneration and that these neuropathological features trigger the activation of phagocytic microglia, as shown by the CD68-inmmunostaining.

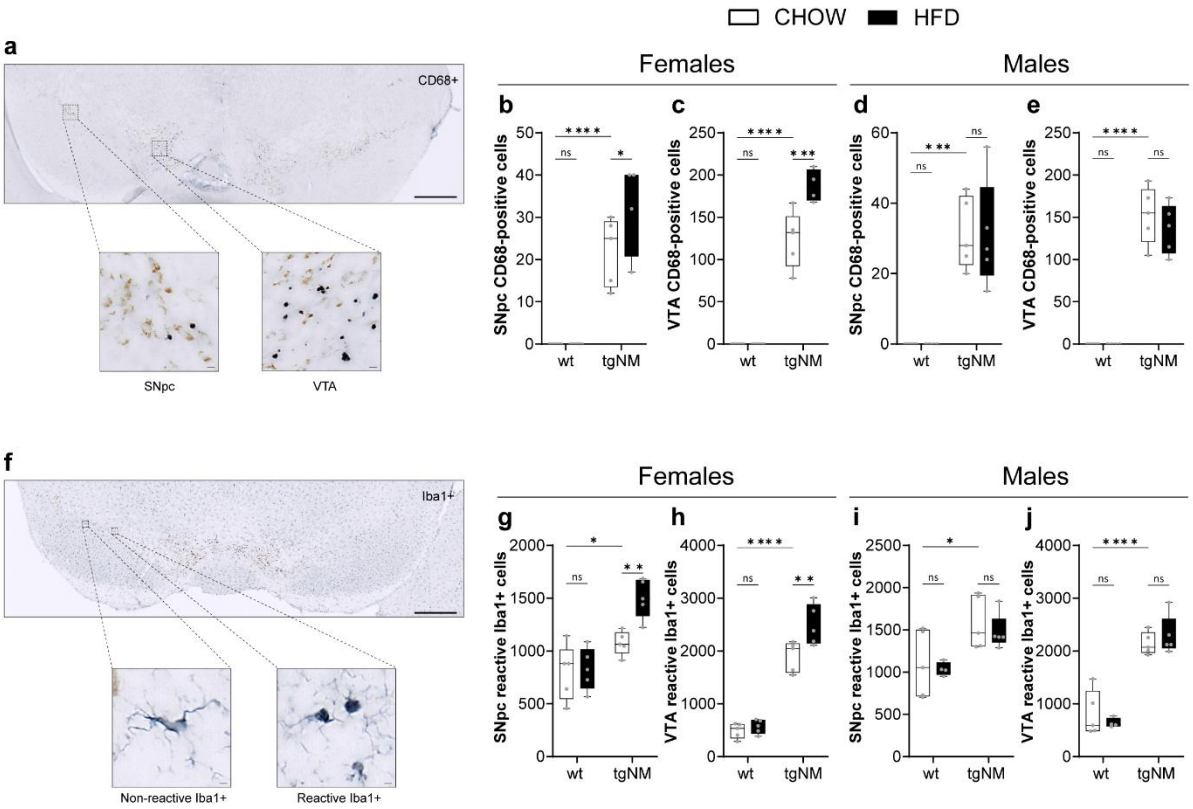

Figure 77. Effect of HFD in the neuroinflammation in the SNpc and VTA of tgNM mice. a) Representative image of SNpc and VTA from tgNM mice exhibiting CD68-positive cells (blue) and NM in brown. Scale bar 500 µm / 10 µm. **b)** Females and **d)** males quantification of CD68-positive cells in the SNpc, fed with CHOW or HFD. **c)** Females and **e)** males quantification of CD68-positive cells in the VTA, fed with CHOW or HFD. *p≤0.05 compared to CHOW-fed equivalent genotype and to CHOW-fed wt (Uncorrected Fisher's LSD test). [F&M: CHOW&HFD n=4-5(wt&tgNM)]. **f)** Representative image of SNpc and VTA from tgNM mice exhibiting Non-reactive and Reactive Iba1-positive cells (blue) and NM in brown. Scale bar 500 µm / 2 µm. **g)** Females and **i)** males quantification of Reactive Iba1-positive cells in the SNpc, fed with CHOW or HFD. **h)** Females and **j)** males quantification of Reactive Iba1-positive cells in the VTA, fed with CHOW or HFD. *p≤0.05 compared to CHOW-fed equivalent genotype and to CHOW-fed wt (Uncorrected Fisher's LSD test). [F&M: CHOW&HFD n=4-5(wt&tgNM)].

2.7.4 Effects of HFD on dopaminergic and cholinergic dysfunction in the DVC of adult tgNM mice

To investigate the effects of HFD in dopaminergic dysfunction in the DVC, we performed dopaminergic and cholinergic stereological cell counts in wt and tgNM mice fed with CHOW or HFD.

In HFD-fed tgNM females, stereological analysis revealed no significant changes in the number of TH-positive neurons or total DA neurons in the DVC compared to CHOW-fed counterparts (Figure 78 b, c). However, the number of analyzed animals for the CHOW-fed tgNM females' group was notably low and we are currently running an additional experiment with a larger sample size to confirm the observations.

In males, we observed an unexpected increase in TH-positive neurons and total DA neurons in HFD-fed wt males compared to CHOW-fed littermates, whereas no changes were observed in their HFD-fed tgNM counterparts compared to the CHOW-fed group (Figure 78 d, e). We next analyzed ChAT-positive neurons, and we observed that both HFD-fed tgNM females and males exhibited an increase in the number of ChAT-positive neurons in the DVC compared to their CHOW-fed counterparts (Figure 78 g, h). Similar to the results observed in the VTA, HFD-fed tgNM females presented an increased number of eNM granules in the DVC (Figure 78 j), accompanied by elevated intracellular NM levels (Figure 78 m) in comparison to their CHOW-fed littermates. Conversely, HFD-fed tgNM males did not present changes in eNM granules (FIG 78 k) and exhibited reduced intracellular NM accumulation compared to their CHOW-fed littermates (Figure 78 m). When comparing the number of eNM granules between sexes, preliminary observations because of low sample size for CHOW-fed tgNM females, suggest that under CHOW conditions, tgNM males have a higher number of eNM compared to tgNM females. However, under HFD, tgNM females appear to increase their eNM granules count to match that of tgNM males (Figure 78 l). Similarly, in terms of intracellular NM levels, CHOW-fed tgNM males exhibited higher levels than tgNM females. This sex-specific difference disappeared under HFD, as tgNM females increased their intracellular NM levels to match those of tgNM males (Figure 78 m).

In summary, HFD-fed tgNM mice did not exhibit overt dopaminergic cell death in the DVC. However, the increased presence of eNM granules and elevated intracellular NM levels in HFD-fed tgNM females suggest that HFD exacerbates neurodegenerative processes in the DVC as early as 7-8 m of age. In contrast, tgNM males appear to be less affected, as their eNM granule counts remained stable, and their intracellular NM levels even decreased under HFD. Although, as mentioned before, we are currently increasing the sample size in order to confirm the observations.

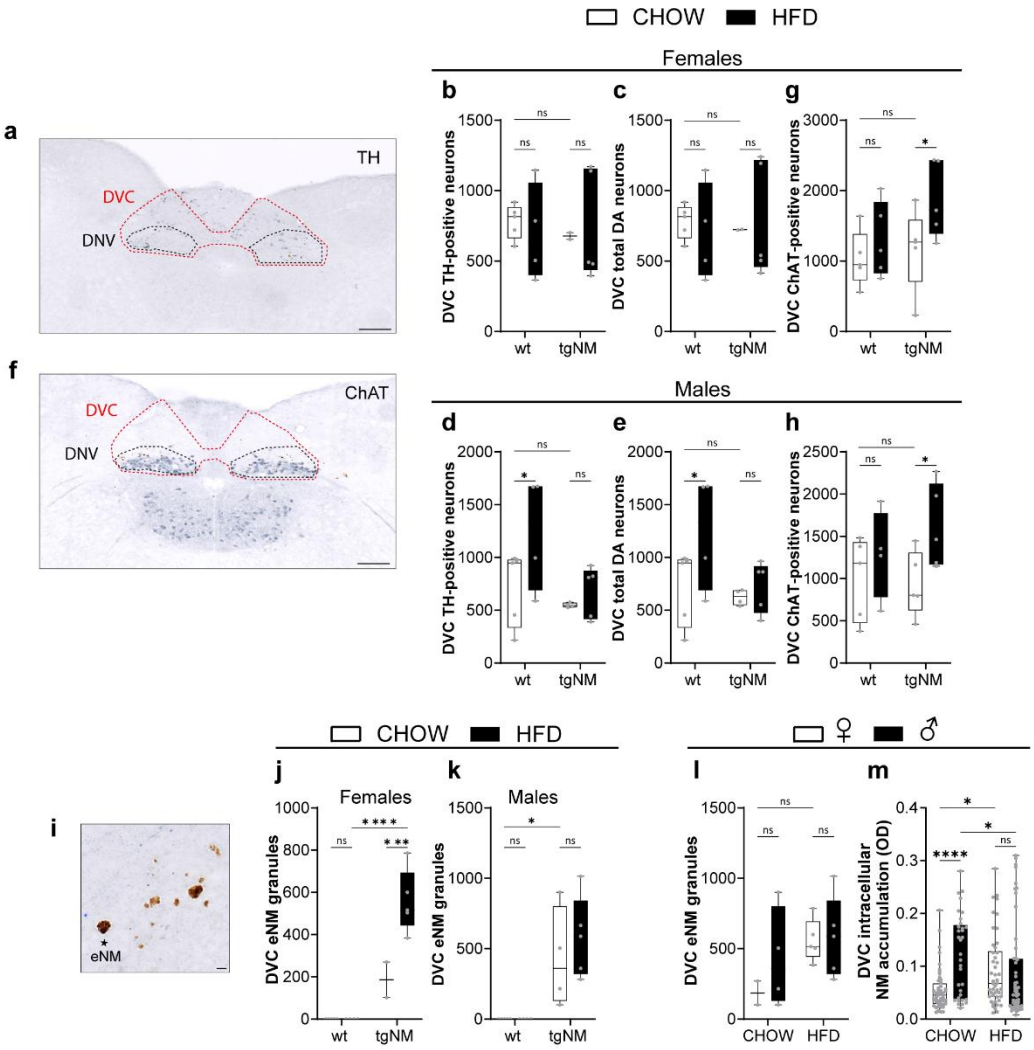

Figure 78. Effect of HFD on the dopaminergic dysfunction in DVC of tgNM mice. a) Medullary section is inmmunostained for TH (blue) and NM in brown. Scale bar 200 µm**. b, c)** Females and **d, e)** males stereological cell counts of TH-positive and total DA neurons in DVC sections, fed with CHOW or HFD. **f)** Medullary section inmmunostained for ChAT (blue) and NM in brown. Scale bar 200 µm**. g)** Females and **h)** males stereological cell count of ChAT-positive cells in DVC sections, fed with CHOW or HFD**. i)** Higher magnification of TH inmmunostained DVC section showing eNM granules in tgNM mice. Scale bar 10 µm. **j)** Females and **k)** males stereological quantification of the number of eNM granules in DVC sections, fed with CHOW or HFD. *p≤0.05 compared to CHOW-fed equivalent genotype and to CHOW-fed wt (Uncorrected Fisher's LSD test). [F: CHOW n=5(wt), n=2(tgNM); HFD n=4(wt), n=5(tgNM); M: CHOW n=5(wt), n=4-5(tgNM); HFD n=4(wt), n=5(tgNM)]. **l)** DVC total number of eNM granules of tgNM female and male mice fed with CHOW or HFD. **m)** DVC quantification of intracellular NM by OD of tgNM female and male mice fed with CHOW or HFD. *p≤0.05 compared to CHOW-fed or HFD-fed contrary sex and to CHOW-fed counterparts (Uncorrected Fisher's LSD test). [F: CHOW n=4(wt), n=2(tgNM) N=48; HFD n=4(wt), n=5(tgNM)N=46; M: CHOW n=5(wt), n=4(tgNM) N=33; HFD n=4(wt), n=5(tgNM) N=53].

2.7.5 Effects of HFD on PD-like neuropathological alterations and neuroinflammation in the DVC of young tgNM mice

We next assessed NM-containing neurons in DVC sections from tgNM mice to see if HFD feeding might have exacerbated the PD-like neuropathological features of tgNM mice. In tgNM females, HFD induced a significant increase in the number of LB-like inclusions compared to their CHOW-fed littermates (Figure 79 b). However, no such significant changes were observed HFD-fed tgNM males (Figure 79 c). Additionally, no MB-like inclusions were detected in any of the groups (data not shown). HFD-fed tgNM females also exhibited neuroinflammatory changes in the DVC, characterized by an increase in the number of phagocytic CD68-positive cells (Figure 79 e), along with a slight, but not statistically significant, increase in ameboid-reactive-like Iba1-positive microglial cells (Figure 79 h). In contrast, HFD-fed tgNM males showed only a mild increase in these inflammatory markers compared to their CHOW-fed littermates, though these changes were not statistically significant (Figure 79 f, i).

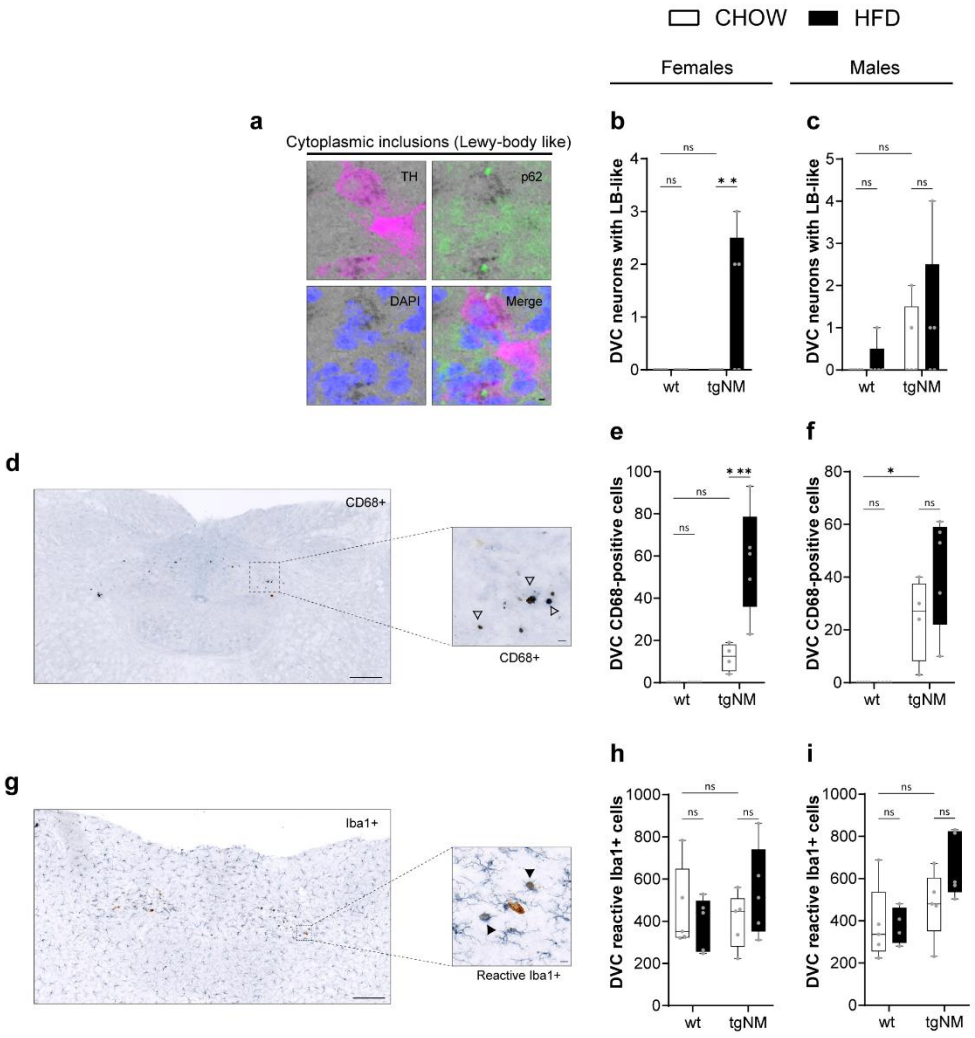

Figure 79. Effect of HFD on the PD-like neuropathological alterations in the DVC of tgNM mice. **a)** Representative image of a cytoplasmic LB-like inclusion in a TH-positive neuron detected by IF with TH (pink), p62 (green), the nuclei stained with DAPI (blue) and NM appears as dark grey. Scale bar 5 µm. **b)** Females and **c)** males quantification of NM-laden neurons in the DVC with p62-positive total cytoplasmatic LB-like inclusions, fed with CHOW or HFD. [F&M CHOW&HFD (n=5)]. **d)** Medullary section of tgNM mice inmmunostained for CD68-positive (blue), NM appears in brown. Scale bar 200 µm / 10 µm. **e)** Females and **f)** males quantification of CD68-positive cells in DVC sections, fed with CHOW or HFD. [F: CHOW n=5(wt), n=4(tgNM); HFD n=5(wt), n=5(tgNM); M: CHOW n=5(wt), n=4(tgNM); HFD n=4(wt), n=5(tgNM)]. **g)** Medullary section of tgNM mice inmmunostained for Iba1-positive (blue), NM appears in brown. Scale bar 200 µm / 10 µm. **h)** Females and **i)** males quantification of reactive Iba1-positive cells in DVC sections, fed with CHOW or HFD. [F: CHOW&HFD n=5(wt), n=5(tgNM); M: CHOW n=5(wt), n=5(tgNM); HFD n=4(wt), n=5(tgNM)]. *p≤0.05 compared to CHOW-fed equivalent genotype and to CHOW-fed wt (Uncorrected Fisher's LSD test).

In summary, HFD-fed tgNM mice did not exhibit overt cell death in SNpc, VTA or DVC regions. However, an increased presence of eNM granules, which originate from degenerating neurons and are commonly observed in PD and aged postmortem brains (Beach et al., 2007; Ishikawa, 1998; Korzhevskii et al., 2021), was evident in HFD-fed tgNM females in all these brain areas. This neuropathological change was accompanied by elevated intracellular NM levels, which we have previously shown that set the threshold for the initiation of PD (Carballo-Carbajal et al., 2019), suggesting that feeding with a HFD accelerates the neurodegenerative process in tgNM females. In contrast, tgNM males were less affected by HFD, where eNM granules and intracellular NM levels remained stable or even decreased under HFD conditions. Beyond the neuropathological changes, HFD also induced increased microglial activation and phagocytic activity in tgNM females, which was not observed in tgNM males. These findings highlight a sex-specific vulnerability to HFD-induced catecholaminergic dysfunction and neuroinflammation.

3 CHAPTER 3. Determine if rejuvenation of the gut microbiota by FMT can slow down the manifestation of PD-like symptoms in tgNM mice.

In Chapter 1, we characterized the motor and non-motor symptoms of tgNM mice and observed that tgNM females exhibited a more pronounced PD-like phenotype compared to tgNM males. In Chapter 2, we demonstrated that HFD modulated the gut microbiota and exacerbated PD-like symptoms in tgNM mice, with tgNM females being particularly affected. Importantly, we showed that HFD exacerbated PD-like neuropathology in tgNM females as early as 7-8 m of age, highlighting a sex-specific vulnerability. Building on these findings, in Chapter 3 we aimed to further explore the potential interactions between the gut-brain axis in tgNM mice for therapeutic development. Specifically, we assessed whether rejuvenation of the gut microbiota through FMT from young (3 m old), healthy wt animals could mitigate the PD-like symptoms observed in tgNM mice. Thus, aiming to evaluate the therapeutic potential of FMT in attenuating PD-like symptoms, providing insights into the role of gut microbiota modulation in PD.

Given the pronounced vulnerability of tgNM females, as demonstrated in previous chapters, this experiment focused exclusively on wt and tgNM females. Starting at 12 m of age, female mice were subjected to a three-day ABX treatment to deplete the host gut microbiota, thereby maximizing the potential for engraftment of the donor microbiota. Following this depletion, the animals received either FMT or PBS 1X treatment once a week for 6 m (Methods 1.4.4) till euthanasia at 18 m of age.

3.1 Modulation of host gut microbiota by FMT engraftment

First, we assessed if FMT from young, healthy wt mice donors modulated the host gut microbiota composition in wt and tgNM females. To this end, we performed 16S rRNA sequencing on fecal samples collected from PBS-treated and FMT-treated females at 18 m of age.

3.1.1 α-diversity

Measurements of α-diversity were used to study the diversity within a single sample. The metrics used were richness, that are the number of different phylotypes present in a community, and evenness, that reflects the relative abundance of these species, considering the number and the abundance of phylotypes in a community. No significant effects of FMT were detected regarding the richness (Figure 80 a) suggesting that the overall microbial species count remained stable despite ABX depletion followed by FMT intervention. However, a reduction in the relative abundances of taxa was observed in FMT-treated wt females compared to their PBS-treated counterparts (Figure 80 b).

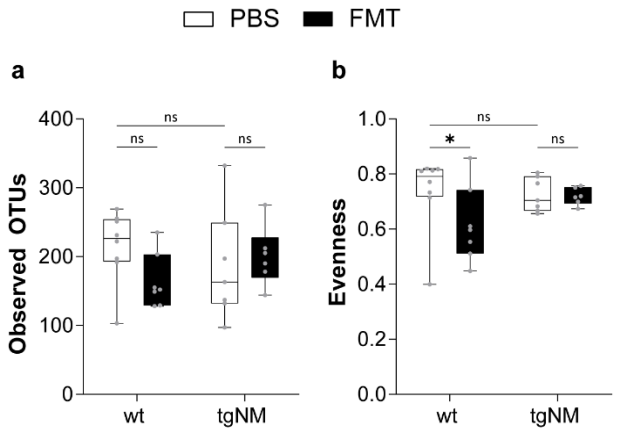

Figure 80. Fecal α-diversity boxplots of wt and tgNM females treated with PBS or FMT. a) Number of different phylotypes present in a community (Observed OTUs) at 18 m in wt and tgNM females treated with PBS or FMT. **b)** Given as the Pielou's evenness index, quantification of how equal the community is numerically at 18 m in wt and tgNM females treated with PBS or FMT. *p≤0.05 compared to PBS-treated equivalent genotype and to PBS-treated wt (Uncorrected Fisher's LSD). 18 m [PBS: n=8(wt), n=7 (tgNM); FMT: n=7(wt), n=6(tgNM)].

3.1.2 β-diversity

Next, we analyzed β-diversity to evaluate the differences in microbial community composition among the groups. β-diversity was quantified using PERMANOVA on the Unweighted UniFrac distance, and clustering patterns were visualized through PCoA plots. FTM-treated wt females presented a distinct β-diversity compared to PBS-treated wt females, suggesting successful microbial engraftment in these animals. In contrast, FMT-treated tgNM females did not exhibited significant shifts in β-diversity compared to PBS-treated tgNM females, indicating that factors other than FMT treatment may be influencing gut microbiota composition in these tgNM animals (Figure 81 a). Interestingly, FMT-treated tgNM females also presented significantly different β-diversity compared to FMT-treated wt females, further suggesting that an intrinsic factor, likely associated to the tgNM genotype, is influencing the microbial community composition in tgNM females, preventing it from aligning with the microbial profile observed in FMT-treated wt females.

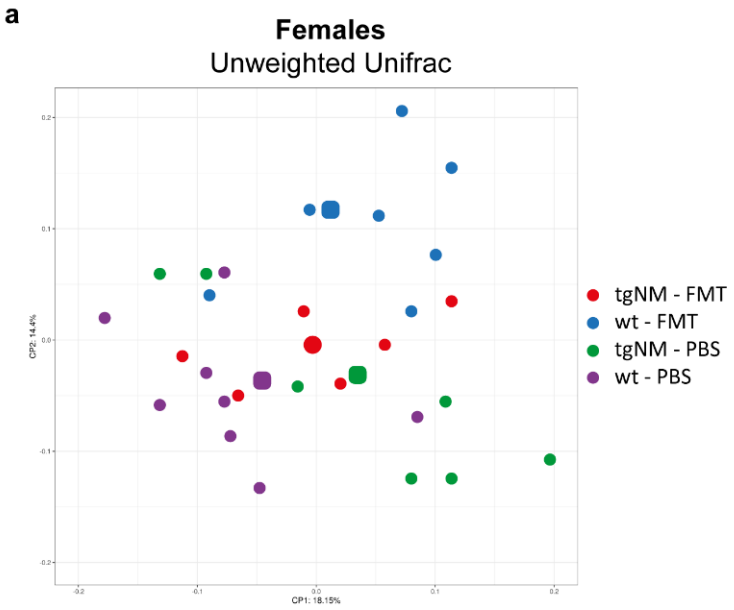

Table 21. Pairwise Permanova Analysis for Unweighted Unifrac in females at 18 m old.

	tgNM - FMT	wt - FMT	tgNM – PBS
wt – FMT	0,024*		
tgNM – PBS	0,114	0,01	
wt – PBS	0,009	0,006*	0,03*

Figure 81. Fecal β-diversity PCoA plot of wt and tgNM females treated with PBS or FMT. a) PCoA plots for visualization of microbial communities' structure. Each dot represents one sample, distances between dots represent the ecological distances between samples. *p≤0.05 compared to PBS-treated equivalent genotype and to PBS-treated wt (Unweighted Unifrac – Pairwise Permanova analysis), p values are represented in Table 21. 18 m [PBS: n=8(wt), n=7(tgNM); FMT: n=7(wt), n=6(tgNM)].

3.1.2.1 Taxonomic profile

We next obtained the taxonomic profiles of the fecal samples by analyzing the differential abundance of taxa using the NBM. At the genus level, FMT-treated wt females exhibited 11 significantly different taxa compared to their PBS-treated littermates, while FMT-treated tgNM females presented 9 significantly different taxa compared to their PBS-treated littermates (Table 22). However, if we look into which genus is changed, only changes in Dubosiella, Faecalibaculum and Erysipelotrichaceae-uncultured are common for both genotypes. These findings further support that something linked with the genotype more than just FMT, influences the microbial community composition in tgNM females.

Table 22. Number of differentially abundant taxa identified as significant by the NBM in FMT vs PBS-treated tgNM and wt females. The table presents the number of differentially abundant taxa at various taxonomic levels (e.g. phylum, class, order, family, genus and species) at the studied time point (18 m).

Taxa level	wt	tgNM
Phylum	3 (Proteobacteria, Firmicutes, Bacteroidota)	2 (Desulfobacterota, Actinobacteriota)
Class	3 (Bacteroidia, Bacilli, Gammaproteobacteria)	2 (Actinobacteria, Desulfovibrionia)
Order	4	6
Family	6 (Muribaculaceae, Rikenellaceae, Lactobacillaceae, Sutterellaceae, Eubacterium_coprostanoligenes group, Clostridia_UCG-014)	7 (Christensenellaceae, Enterobacteriaceae, Bifidobacteriaceae, Monoglobaceae, Erysipelatoclostridiaceae, Desulfovibrionaceae, Erysipelotrichaceae)
Genus	11 (Parasutterella, Dubosiella, Faecalibaculum, Lactobacillus, Muribaculaceae, Rikenellaceae_RC9_gut group, Muribaculum, Eubacterium_coprostanoligenes group, Clostridia_UCG-014, Eubacterium_ventriosum group, Erysipelotrichaceae-uncultured)	9 (Faecalibaculum, Escherichia-Shigella, Dubosiella, Desulfovibrio, Bifidobacterium, Monoglobus, Erysipelotrichaceae-uncultured, Ruminococcaceae, Alistipes)
Species	17	12

3.2 Body weight follow-up

Body weight was monitored weekly over the course of the 6 m experiment to evaluate the health status of the animals during the treatment.

At baseline, FMT-treated tgNM females displayed significantly lower body weight compared to their PBS-treated tgNM littermates. This difference persisted throughout the treatment period indicating that FMT treatment did not have any effect in the body weight of tgNM females. Similarly, FMT treatment did not affect body weight of wt females (Figure 82 a, b), suggesting that FMT intervention did not significantly influence weight regulation.

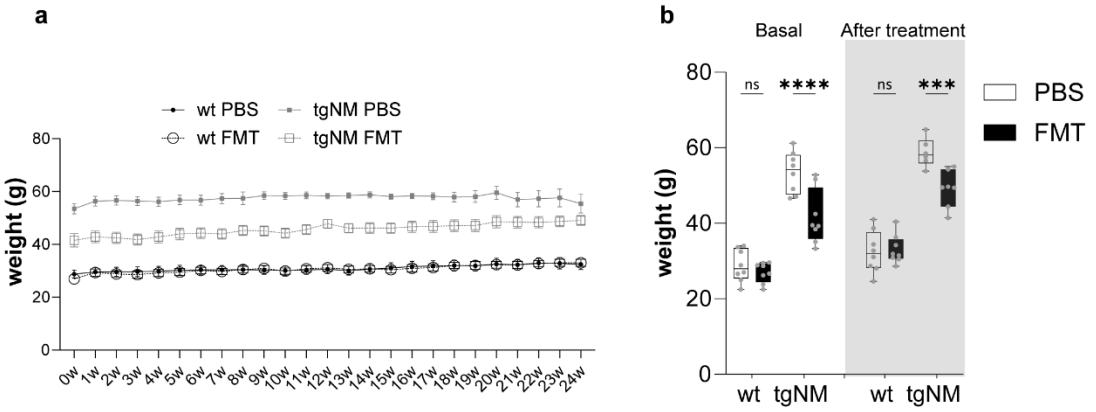

Figure 82. FMT impacts body weight. a) Body weight over 24 weeks (6 m) of PBS and FMT-treated wt and tgNM females. **b)** Body weight at basal time 12 m and after treatment time 18 m of PBS or FMT treatment. 12 m (PBS: n=8(wt), n=8(tgNM); FMT: n=8(wt), n=8(tgNM)) 18 m [PBS: n=8(wt), n=6(tgNM); FMT: n=8(wt), n=7(tgNM)].

3.3 Effect of FMT treatment on motor behavior and GI functions

We next evaluated the impact of FMT treatment on motor capacities and GI function in wt and tgNM females. Using the beam test to assess motor coordination and balance, we found that FMT treatment did not significantly affect motor performance in wt females at any time point during the experiment. In contrast, in basal conditions, tgNM females treated with FMT demonstrated better motor performance as evidenced by significantly reduced time to cross the beam compared to their PBS-treated littermates. This improvement persisted after 2 m of treatment. However, after 6 m of treatment, no significant differences in motor performance were observed between the two groups. These results suggest that FMT did not have a beneficial effect on motor behavior in tgNM females, as the initial improvement observed at baseline was no longer evident after 6 m. Moreover, FMT had no relevant impact on motor behavior in wt females at any time point (Figure 83 a).

In parallel, we assessed total fecal output and observed that FMT treatment had no effect on wt females at any time point. In tgNM females, FMT appeared to reduce the nº of defecations after 2 m of treatment, suggesting a potential short-term impact on GI motility. However, this reduction was not sustained, as the number of defecations increased after 6 m of treatment, resembling those of the PBS-treated tgNM group (Figure 83 b). This suggest that any initial effects of FMT on fecal output in tgNM females were temporary and did not persist with prolonged treatment.

Moreover, we evaluated gut barrier permeability *in vivo* by measuring serum levels of FITC-dextran 1 h after oral gavage administration. In wt females, FMT-treatment resulted in significantly reduced levels of FITC-dextran after 2 m of treatment, indicating a possible improvement in gut barrier integrity. Although this reduction persisted after 6 m of treatment, it was no longer statistically significant. In contrast, FMT-

treated tgNM females did not exhibit any changes in serum FITC-dextran levels compared to their PBS-treated littermates at any time point (Figure 83 c), suggesting that FMT did not influence gut permeability in tgNM females.

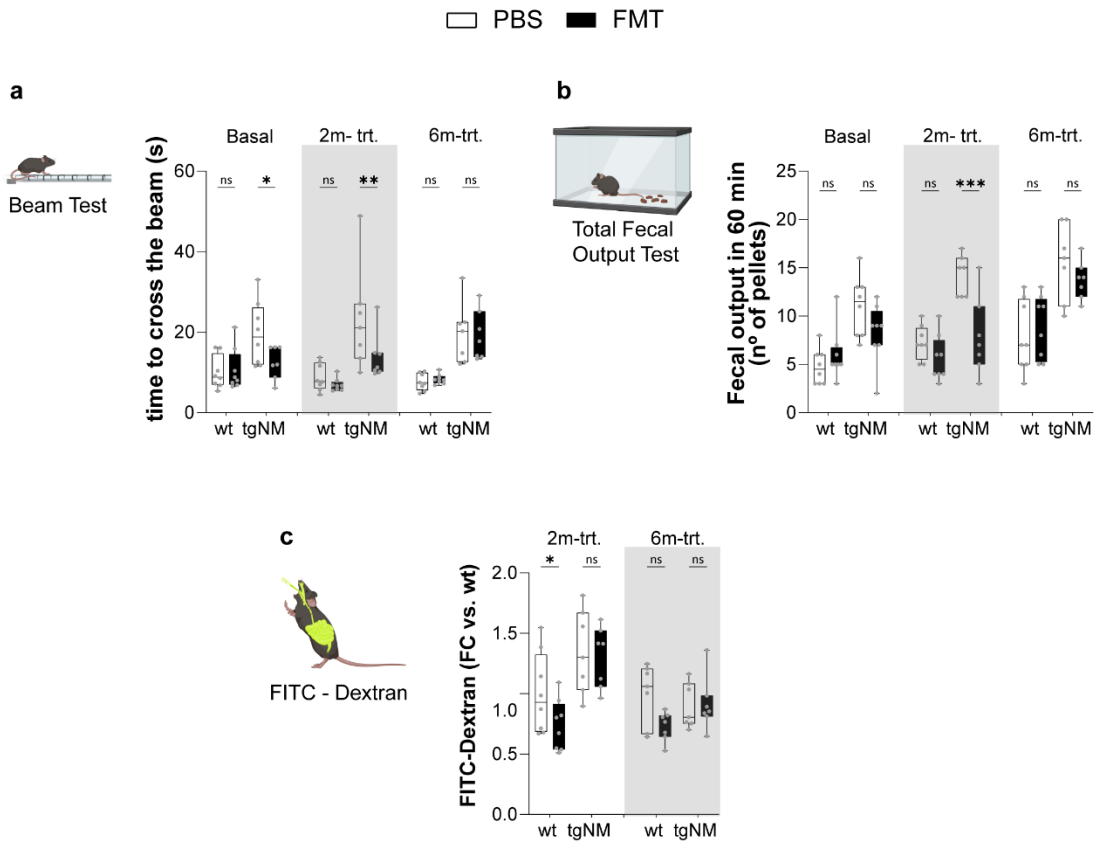

Figure 83. Motor and GI functions assessment after FMT treatment. a) Beam test; Average time to cross the beam after two trials at basal conditions (12 m), 2 m after treatment (14 m) and 6 m after treatment (18 m). **b)** Total fecal output; nº of fecal pellets produced in 1 h trials at basal conditions (12 m), 2 m after treatment (14 m) and 6 m after treatment (18 m). **c)** FITC-Dx serum levels after 1 h administration at 2 m after treatment (14 m) and 6 m after treatment (18 m). Groups are normalized to their PBS-treated wt group for each time point. *p≤0.05 compared to genotype-matched PBS-treated (Uncorrected Fisher's LSD). 12, 14, 18 m [PBS n=8(wt), n=7-8(tgNM), FMT n=7-8(wt), n=7-8(tgNM)].

Finally, at the time of euthanasia, the GI tracts of the females were evaluated. In wt females, FMT treatment did not result in any significant changes in GI weight or length. However, in tgNM females, FMT treatment was associated with a lighter and shorter GI tract compared to their PBS-treated littermates. This reduction in GI size was specifically attributed to a shorter small intestine and colon, suggesting that FMT may have influenced GI morphology in tgNM females (Figure 84 a, b, c, d).

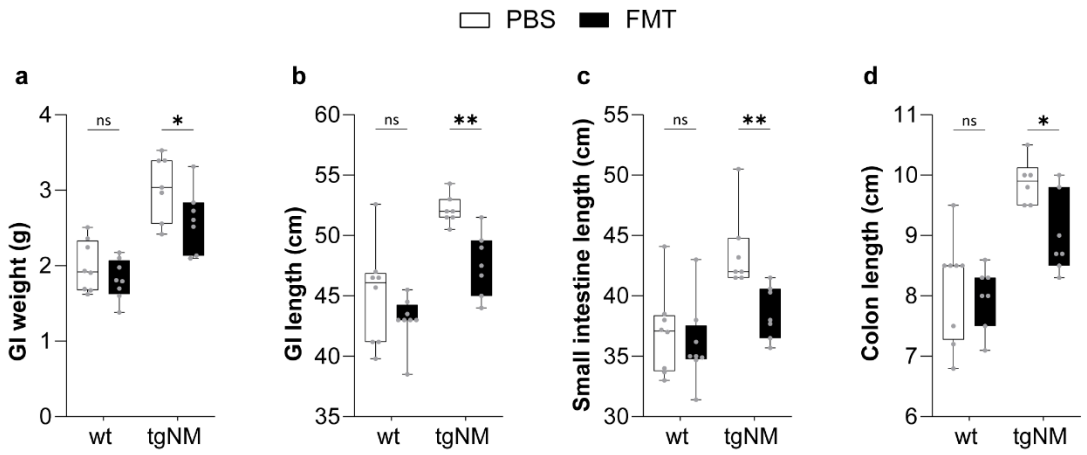

Figure 84. GI tract characterization. a) GI tract weight. **b)** GI tract length. **c)** Small intestine length. **d)** Colon length of wt and tgNM females after 6 m treatment of PBS or FMT. *p≤0.05 compared to genotype-matched PBS-treated (Uncorrected Fisher's LSD). 18 m [PBS n=8(wt), n=7(tgNM), FMT n=8(wt), n=7(tgNM)].

Altogether, these findings suggest that FMT treatment from young wt donors into adult tgNM females did not produce any persistent beneficial effects. However, the success of microbial engraftment remains uncertain. While it seems that FMT successfully altered gut microbial composition in wt females, no significant differences were observed between PBS-treated and FMT-treated tgNM females, suggesting that host genotype may have a stronger influence on gut microbiota composition than the FMT intervention itself. Additionally, intrinsic variability within the tgNM batch selected for FMT treatment may have influenced the results. These FMT-treated tgNM females initially exhibited better motor performance and differences in body weight compared to the PBS-treated tgNM group, potentially confounding the interpretation of the results. Further studies are needed to refine experimental approaches and elucidate the factors influencing FMT efficacy in this model.

DISCUSSION

1 CHAPTER 1. Characterization of behavioral and GI alterations linked to age-dependent intracellular NM accumulation in mice.

In Chapter 1, we conducted a comprehensive characterization of both behavioral and GI alterations in our tgNM mouse model, a novel and physiologically relevant tool for investigating the early pathophysiological events in PD. This model mimics the progressive, age-dependent intracellular accumulation of NM in catecholaminergic neurons (Laguna et al., 2024). Building on our earlier findings that NM accumulates across key catecholaminergic regions, we now show that this accumulation is closely linked to a range of prodromal PD-like features, including early sensorimotor deficits, GI dysmotility, intestinal inflammation, disruption of gut barrier integrity, and significant shifts in both gut microbiota composition and fecal metabolomic profiles. These alterations are accompanied by changes in peripheral and central neuroendocrine signaling, as well as lipid and amino acid metabolism. Notably, many of these phenotypes manifest in a sex-dependent manner, with tgNM females showing an increased vulnerability to metabolic, GI, and hormonal disruptions compared to males. Together, these findings emphasize the multifactorial nature of early PD and highlights the tgNM model for exploring the interactions between NM accumulation, gut-brain axis dysfunction, systemic metabolism, and sex-specific disease progression.

1.1 Sensorimotor and behavioral phenotype

Initially, our analysis confirmed early-onset sensorimotor deficits in tgNM mice, specifically in females, which exhibited motor and balance alterations as early as 3 m of age. This is particularly notable given that, in human PD, such symptoms typically appear in prodromal stages, prior to the significant loss of dopaminergic neurons in the SNpc (Gaenslen et al., 2011; Hustad & Aasly, 2020; E. D. Louis & Bennett, 2007). Interestingly, these early motor deficits were absent in tgNM males, indicating a distinct sex-dependent vulnerability that needs further investigation. In addition to motor deficits, tgNM female mice exhibited significant non-motor symptoms, including emotional disturbances and olfactory impairments, however they were detectable at 18 m of age. The early appearance of reduced audible vocalizations in both tgNM males and females at 3 m suggests shared early neurobiological alterations despite clear divergence in other sensorimotor capacities. Such vocalization impairments could correspond with hypophonia, a common non-motor symptom in PD patients, characterized by decreased speech volume and pith fluctuation (Arnold et al., 2013; Dashtipour et al., 2018). These results also align with early cranial sensorimotor deficits observed in α-synuclein transgenic mice (Grant et al., 2014).

1.2 GI function and morphology

Previously, we demonstrated age-related neurodegeneration in pigmented TH-positive neurons within the DVC in tgNM mice aged 8–12 m, primarily attributed to phenotypic downregulation rather than actual neuronal loss. This reduction was accompanied by the extensive presence of eNM granules and notable microglial activation (Laguna et al., 2024). Given the critical role of the DNV in innervating GI regions, we conducted a detailed characterization of GI function and morphology.

Our findings reveal significant alterations in GI functionality in tgNM females, evidenced by reduced intestinal transit time, increased fecal output, and elevated fecal moisture levels, appearing as early as 3 m of age. Remarkably, these functional alterations precede any observable catecholaminergic neuronal loss in the DVC. The accelerated transit time likely correlates with the increased nº of fecal depositions observed. Elevated fecal moisture could result from factors such as increased gut motility or stress-induced modulation of intestinal secretion, as higher stool moisture generally implies increased stool volume, stimulating colonic propulsion and expulsion (Babygirija et al., 2011). To further explore potential causes, we assessed GI tract morphology, discovering unexpected structural alterations characterized by extended small intestine and colon lengths in tgNM females already at 6 m. These morphological changes initially seemed counterintuitive, as one might anticipate shorter GI lengths associated with faster transit. Despite pronounced GI dysfunction, tgNM mice did not exhibit constipation, contrasting markedly with the typical clinical presentation observed in PD patients (Abbott et al., 2001; Pfeiffer, 2003). Notably, none of the previously studied PD mouse models, including those using MPTP or rotenone, have reported similar GI functional changes (Perez-Pardo et al., 2017; Z. Zhao et al., 2021). For instance, MPTP mouse models typically present increased intestinal transit and reduced stool frequency and fecal moisture (Ellett et al., 2016; N. R. Han et al., 2021b; Lai et al., 2018; Natale et al., 2010; Sampath et al., 2019), while rotenone-based studies have different results, often reporting either reductions in GI parameters or no significant changes at all (Miyazaki et al., 2020; Morais et al., 2018; Tasselli et al., 2013). Notably, previous studies primarily utilized male mice, which could explain discrepancies with our current findings involving female tgNM mice. Additionally, methodological variations across these studies, such as differences in mouse age, dosing regimens, and experimental duration, make direct comparisons challenging.

In genetic and transgenic PD mouse models, such as TLR-4 KO, Thy1-α-synuclein Line 61, MitoPark, $SNCA^{G51D}$ KI and PrP human A53T-α-synuclein models, increased intestinal transit times, reduced fecal pellet production, diminished fecal moisture, and shorter colon lengths were commonly reported (Cuvelier et al., 2018; Ghaisas et al., 2019; Hallett et al., 2012; Kim et al., 2024; Perez-Pardo et al., 2018; Rota et al., 2019; Sampson et al., 2016; Wang et al., 2012). The divergence between these findings and our tgNM model results might partly be explained by the elevated food and water intake observed in tgNM females starting at 3 m of age. A feature that was not observed in the previous mentioned mouse

models. Typically, assessments of fecal pellet output assume similar distal colonic contents under basal conditions. However, increased food consumption in tgNM females likely elevates the fecal content, thereby possibly influencing our observed outcomes.

1.3 Neuromodulatory systems and neurotransmitters alterations

The ENS plays a crucial role in regulating motility, blood flow and secretion, but it also communicates with the endocrine and immune system and the microbiome through the complex combined activity of diverse enteric neuron types (Furness, 2012). Although the ENS operates independently of the CNS, it communicates with it via parasympathetic input from the DNV and sympathetic inputs from para- and prevertebral ganglia to maintain gut homeostasis (Wachsmuth et al., 2022). The myenteric plexus, responsible for controlling GI motility, contains neurons producing ACh, NO, VIP and catecholamines (Annerino et al., 2012). The submucosal plexus is comprised of a series of ganglia and connecting fibers and these neurons control secretory functions, absorption and blood flow (Sharkey & Mawe, 2022). Neural pathways connecting the gut to the brain fall into three categories: vagal, spinal thoracolumbar, and spinal lumbosacral, each of which carries afferent and efferent signals (Figure 84) (Furness et al., 2014). However, it is not clear whether GI dysfunction in PD has a central origin or an intrinsic origin at the level of the ENS. Moreover, it is not clear whether single or multiple neurotransmitters are involved in the control of smooth muscle contractility and gut motility or how these change in relation to PD.

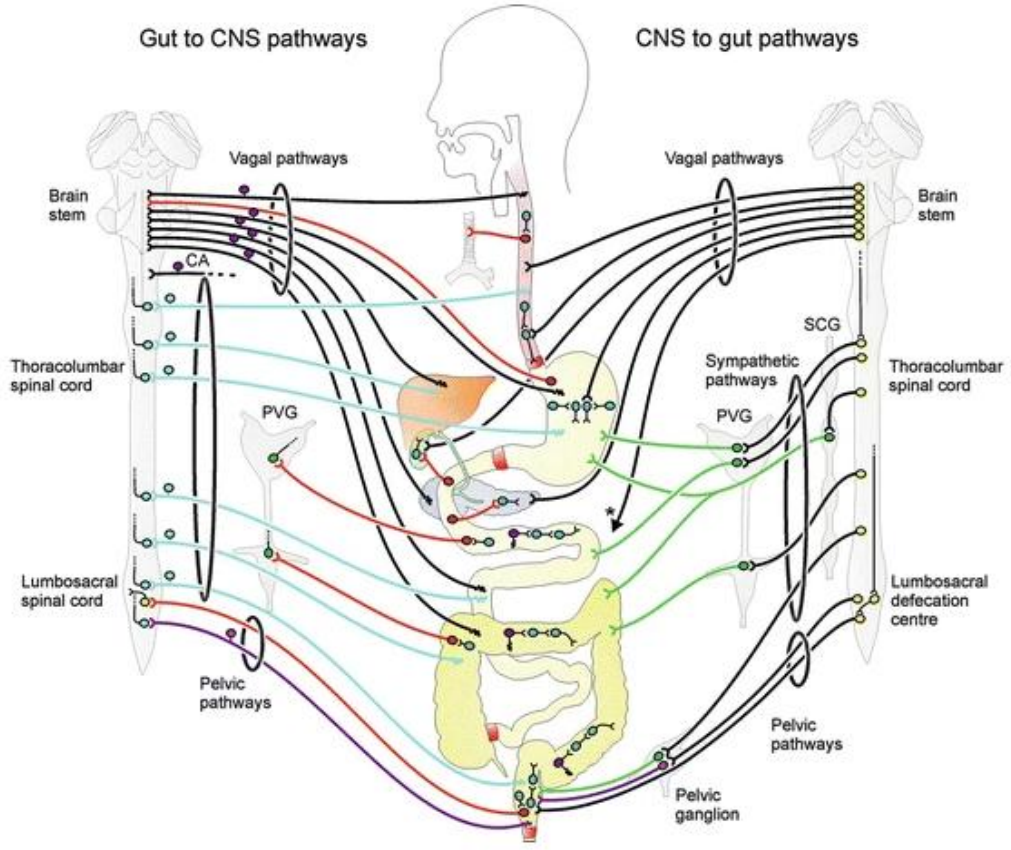

Figure 85. The innervation of the GI tract. The innervation of the GI tract involves complex neural circuits connecting the ENS, the CNS, and the sympathetic ganglia, as well as direct connections among various GI organs. In the schema: Left side. Neural pathways from the ENS project outward to other organs and the CNS. For example, intestinofugal neurons (shown in red) transmit signals from the gut to the CNS, sympathetic ganglia, gallbladder, pancreas, and trachea. Additionally, extrinsic primary afferent neurons carry sensory information from the gut, following spinal and vagal nerve routes. Center. The small and large intestines contain complete ENS reflex circuits. These circuits are composed of motor neurons and interneurons (blue) responsible for controlling motility, and intrinsic sensory neurons (purple) that relay local sensory information within the gut. Right Side. Pathways originating in the CNS reach the ENS and GI effector tissues through vagal, sympathetic, and pelvic pathways. Vagal medullary and pelvic spinal outflows include pre-enteric neurons, those whose axons project into enteric ganglia. Moreover, many gut-projecting sympathetic neurons with cell bodies in the prevertebral ganglia (PVG, shown in green) also serve as pre-enteric neurons. Additional connections include cervical afferents (CA), which link the esophagus to the cervical spinal cord and the sympathetic chain ganglia (SCG). This integrated network ensures that both local reflexes within the gut and central neural inputs coordinate GI function. Adapted from (Furness et al., 2014).

We hypothesized that the differences in propulsive activities observed in tgNM females could be due to altered myenteric neuronal function or muscular layer activity. However, we did not detect differences in spontaneous myogenic activity of both colonic circular and longitudinal muscle layers. Moreover, both excitatory and inhibitory neural pathways also appeared preserved in the colon of tgNM females at 6 m old. The total number of myenteric neurons or specific neuronal populations such as cholinergic or nitrergic neurons, were also spared at 18 m in the myenteric plexus of duodenum and proximal colon of tgNM females, aligning with the preserved *ex vivo* neural-mediated responses observed in our study. These results are consistent with analyses in PD patients, that generally show no differences in total myenteric neuron counts or neurochemical phenotypes in either the myenteric or submucosal plexus (Annerino et al., 2012; Corbillé et al., 2014; Desmet et al., 2017). However, one study found a significant decrease in submucosal neuronal density in colonic biopsies, but the proportion of TH-positive neurons was not evaluated (Lebouvier et al., 2010). These findings conflict with a study that reported fewer dopaminergic neurons in the colonic myenteric plexus. However the study used DA IHC, which is not a reliable marker for these cells. When the same researchers instead used TH IHC, they found no differences between PD and controls (Singaram et al., 1995). Such observations indicate that neuropathology and neuronal loss within the DNV, rather than myenteric plexus or submucosal plexus damage themselves, might drive PD-associated GI dysfunction.

Interestingly, despite unchanged myenteric neuron counts, female tgNM mice exhibited significant reduction of ACh levels in the duodenum at 6 m and in the proximal colon at both 6 and 18 m. A deficit in cholinergic signaling would usually be expected to diminish smooth-muscle contractility and slow intestinal transit; however, our *in vivo* gut motility tests demonstrated accelerated GI transit. This discrepancy suggests that intrinsic enteric neurons remain functionally intact, whereas extrinsic parasympathetic vagal innervation to the gut may be selectively compromised. Although ChAT-positive

neuron counts in the DVC were unchanged (Laguna et al., 2024), this finding does not exclude selective dysfunction of vagal efferent projections. Interestingly, PET studies have revealed a reduction in GI AChE density in early PD patients, indicating signs of parasympathetic denervation of the gut (Fedorova et al., 2017; Gjerløff et al., 2015). Complementing these findings, recent high-resolution ultrasound assessments have demonstrated structural atrophy of the vagus nerve in PD patients, which correlates with measures of autonomic dysfunction, although GI symptoms were not explicitly included in patient selection (Huckemann et al., 2023). Together, these data implicate vagal degeneration as an early feature of PD that likely contributes to enteric dysregulation. Accordingly, future studies in tgNM mice should therefore characterize the anatomical integrity and synaptic function of vagal efferent fibers to the gut to elucidate the pathophysiological basis driving their GI dysmotility.

Concurrently, we observed a marked elevation in DA levels alongside a significant reduction in NE concentrations in both duodenal and proximal colonic tissues at 6 m. Enteric dopaminergic neurons express TH and DAT, but lack DBH expression, confirming their ability to synthesize DA without converting it into NE (Anlauf et al., 2003; Z. S. Li et al., 2004). Therefore, the observed decrease in NE is unlikely to result from intrinsic enteric neuron dysfunction and more likely reflects a disruption of extrinsic adrenergic innervation. The LC represents the major source of NE in the brain, and it's the second major area affected in PD (Giguère et al., 2018). In tgNM mice, NM begins to accumulate early within LC neurons, leading to considerable degeneration of the noradrenergic system as early as 3 m of age, which includes the loss of NE neurons and reduced NE levels in both the LC and the PFC (Laguna et al., 2024). The LC has connections to the DNV and the nucleus ambiguous, enabling it to influence both sympathetic and parasympathetic outputs, which subsequently regulate the GI system. As a result, degeneration of the LC likely plays a role in the diminished NE levels observed in the GI tract and may also contribute to the autonomic dysfunction observed in tgNM mice.

DA typically acts as an inhibitory modulator of intestinal motility via activation of D1-like (D1 and D5) and D2-like (D2, D3, D4) receptors. D1-like receptors signaling reduces cholinergic neurotransmission through nitrergic and purinergic pathways, thereby decreasing ACh release (Auteri et al., 2016; Zhi et al., 2006; Zizzo et al., 2010). Paradoxically, our tgNM model exhibited increased GI motility despite elevated DA and reduced ACh, indicating that the net effect of dopaminergic signaling on gut transit is complex. To better clarify the modulatory role of DA in GI motility in this tgNM model, future experiments should assess the expression levels of dopaminergic receptors in the GI tract of tgNM mice. Moreover, performing detailed pharmacological studies to assess the functionality of these receptors would be valuable, particularly given the central role of dopaminergic dysfunction in PD.

1.4 Transcriptomic characterization of duodenal samples

In the duodenum of tgNM compared to wt females, we identified 75 DEGs. Notably, none of these DEGs intersected with pathways directly implicated in neurodegeneration, and there is currently no strong or consistent evidence linking most of these genes to PD pathophysiology. However, several genes exhibit potential roles in GI and immune functions. In the following sections, we discuss these candidates in the context of GI physiology.

1.4.1 GI-related genes in females

Ptgis (Prostaglandin I_2 Synthase) catalyzes the formation of prostacyclin (PGI_2), a potent vasodilator and inflammatory mediator (Stitham et al., 2011). Upregulation of Ptgis in tgNM females may impact GI function through its multifaceted role in metabolic regulation, immune responses and cancer progression (Ding et al., 2023). Dysregulated prostacyclin production can, therefore, affect both local and systemic immune responses.

Glyat (Glycine-N-Acyltransferase) is involved in glycine conjugation pathways essential for detoxification (Lino Cardenas et al., 2010). Glyat is upregulated in tgNM females. Efficient detoxification in the gut is critical for protecting the mucosal barrier against both endogenous metabolites and xenobiotics compounds.

Bhmt (Betaine-Homocysteine S-Methyltransferase) plays a key role in the methionine cycle, facilitating methylation processes and homocysteine metabolism. Its downregulation in tgNM females could reduce the conversion of homocysteine to methionine, potentially leading to elevated homocysteine levels, a condition associated with increased oxidative stress and inflammation, as observed in IBD (Romagnuolo et al., 2001; J. Wang et al., 2024).

Pla2g2c (Phospholipase A_2, Group IIC) is a member of the secretory phospholipase A_2 family. Pla2g2c exhibits tissue-specific expression and distinct structural features that influence its secretion, enzymatic activity, and receptor interactions. Its upregulation in tgNM females may contribute to chronic inflammation (Cormier, 2023). Notably, studies in mice have shown that related family members, such as Pla2g2a, influence gut microbiota through expression in intestinal Paneth cells, thereby affecting immunity and cancer risk (M. Murakami et al., 2015).

1.4.2 Immune-related genes in females

Ccl1 (C-C Motif Chemokine Ligand 1) is a chemokine that mediates immune cell chemotaxis through its receptor CCR8, playing a critical role in restoring mucosal homeostasis following intestinal epithelial damage. Upregulated in tgNM females, Ccl1 is primarily produced by macrophages during DSS-induced colitis (Kang et al., 2021).

Lilrb4a (Leukocyte Immunoglobulin-Like Receptor, Subfamily B, Member 4A) is expressed on a range of immune cells, including myeloid cells, dendritic cells and macrophages. Lilrb4a is essential for maintaining immune homeostasis. Its upregulation in tgNM females indicates its potential contribution on modulating mucosal immunity (X. Wang et al., 2025).

Tarm1 (T Cell-Interacting, Activating Receptor on Myeloid Cells 1) is predominantly expressed in monocytes and neutrophils (Radjabova et al., 2015). It is upregulated in tgNM females. Given its association with inflammatory conditions and significant expression in macrophages, Tarm1 may contribute to the regulation of immune responses during intestinal inflammation (K. Zhang et al., 2024).

Bpifb6 (BPI Fold Containing Family B Member 6) is proposed to be secreted into the extracellular space where it may function in signal transduction and receptor activity, or as an antimicrobial peptide within the innate immune system. Its upregulation in tgNM females, along with its localization in the endoplasmic reticulum where it influences vesicle trafficking and Golgi morphology, suggests a role in modulating inflammatory responses (Bell et al., 2024).

Slfn1 (Schlafen 1) is a member of the Schlafen family. It is implicated in cell growth regulation and T-cell activation and differentiation. Its downregulation in tgNM females may affect T-cell mediated immune responses (U. Jo & Pommier, 2022; Mavrommatis et al., 2013).

Tlr7 (Toll-Like Receptor 7) is primarily expressed by plasmacytoid dendritic cells. It detects single-stranded RNA viruses and initiates cascades leading to type I interferon and pro-inflammatory cytokine production. Upregulation of Tlr7 in tgNM females highlights the contribution of innate immune defenses (Hamade et al., 2024).

In the duodenum of tgNM compared to wt males, 46 DEGs were identified. Similar to the females, none of these genes were directly linked to PD pathogenesis. Instead, most DEGs are associated with fundamental biological processes such as metabolism, cytoskeletal dynamics or neuronal development. However, we found two genes clearly associated with the immune system:

Klre1 (Killer cell lectin-like receptor subfamily E member 1). Is a novel natural killer (NK) receptor, predominantly expressed in lymphoid tissues and immune cells (Y. Han et al., 2004). It appears upregulated in tgNM males, suggesting a role in modulating immune responses.

Glycam1 (Glycosylation-dependent cell adhesion molecule 1) is a mucin-like glycoprotein, expressed by lymph node endothelial cells (Dowbenko et al., 1993). It's also upregulated in tgNM males, highlighting its potential involvement in immune cell adhesion and mucosal immunity.

1.4.3 Altered biological pathways in the duodenum

Because genes function interdependently within complex regulatory networks, we applied GSEA to our duodenal transcriptomic data to capture broader pathway-level changes. In tgNM females, GO analysis revealed that upregulated pathways primarily involved calcium regulation, ion transport, and tissue/organ

development, among other functions. Conversely, downregulated pathways involved the immune system, including host defense mechanisms, pathogen recognition, and antigen processing/presentation. Another prominent cluster of downregulated pathways was related to metabolism, encompassing the synthesis, modification, or breakdown of small molecules (e.g., retinoids or isoprenoids) and the detoxification of potentially harmful substances. In tgNM males, most pathways were downregulated, with a significant proportion linked to metabolism, immune responses, and organ/tissue development. Only five pathways were found to be upregulated, and these again were related to metabolism and immune function. Analysis via Reactome supported these observations. In tgNM females, upregulated pathways involved metabolism, immunity, and other physiological or organismal functions, whereas downregulated pathways were again dominated by metabolic and immune processes, alongside fundamental cellular events. A similar trend emerged in tgNM males, where the majority of pathways were downregulated, mainly metabolism and immune-related, and among the few that were upregulated, one notably pertained to digestion and dietary lipids.

These findings indicate that both immune and metabolic pathways experience significant transcriptional changes. The observed downregulation of immune-related pathways suggests a compromised or modulated host defense capacity that may impair gut barrier integrity, leading to low-grade inflammation and promote an altered microbial environment, which in turn may affect local GI function and contribute to systemic inflammation, which is increasingly recognized as a contributing factor in PD (Rolli-Derkinderen et al., 2020). Meanwhile, alterations in metabolic pathways, especially those involving lipid metabolism and detoxification processes, could affect nutrient absorption and systemic energy homeostasis. Moreover, the upregulation of pathways related to calcium/ion transport and tissue development, may represent compensatory or adaptive mechanisms aiming to maintain or restore intestinal function under pathological conditions. To identify potential therapeutic targets within these transcriptomic datasets, future studies should validate the key altered biological pathways at both the transcript and protein levels in the duodenum. Additionally, performing the same analysis in the colon could provide us a more comprehensive understanding of GI alterations in tgNM mice and help us to clarify the molecular signatures across different innervated regions.

Notably, the different expression profiles observed between tgNM females and males further support the hypothesis that sex-specific molecular responses in the duodenum could explain the distinct GI phenotypes. In the following sections, we will discuss the translational implications of these expression profiles and their potential relevance to early PD pathogenesis.

1.5 Gut barrier dysfunction, inflammation and microbiota interactions

The intestinal barrier, primarily composed of the gut epithelium and its protective mucus layer, is essential for maintaining GI homeostasis. It selectively regulates nutrients, electrolytes, and water absorption from

the intestinal lumen into systemic circulation, while simultaneously providing robust protection against pathogenic microorganisms and harmful substances (Farhadi et al., 2003; Kelly et al., 2015). Structurally, barrier integrity depends on multiple interconnected components, notably the mucus layer covering a monolayer of epithelial cells tightly linked by specialized intercellular junctions known as TJs. These TJs include several key proteins, including ZO-1, ZO-2, occludin, JAMs, and various claudins, which collectively maintain barrier integrity and tightly regulate permeability (Dörfel & Huber, 2012).

In our tgNM model, specifically in tgNM females, we observed significant alterations in gut barrier integrity, as evidenced by increased gut permeability and altered expression profiles of key TJs proteins. Specifically, increased claudin-2 expression was detected in the duodenum of both young and old tgNM females, likely contributing to enhanced intestinal permeability observed in these mice. Claudin-2 is known to form pore-like channels within the epithelial barrier, thereby facilitating increased paracellular permeability (T. Suzuki, 2013). Moreover, increased claudin-2 expression has been reported in biopsies of Ulcerative colitis (UC) patients, which is a chronic inflammatory condition affecting the colon and the rectum (Heller et al., 2005). Concurrently, elevated ZO-2 expression levels in the duodenum at 6 m and in the proximal colon at 18 m, along with increased ZO-1 protein levels at 18 m in both the duodenum and proximal colon, suggest compensatory cellular mechanisms attempting to restore or reinforce TJs structures in response to barrier disruption. ZO proteins primarily function as scaffold molecules, anchoring transmembrane TJs proteins to the actin cytoskeleton, thus contributing to both structural stability and functional adaptability (Figure 86) (T. Suzuki, 2013).

In the context of PD, intestinal barrier dysfunction has received growing attention, although the available evidence remains preliminary. To date, only a few studies have demonstrated increased colonic permeability in PD patients, assessed using urinary excretion assays following oral ingestion of different sugars. Alterations in the excretion of mannitol and lactulose reflect changes in small intestine permeability, whereas variations in sucralose or chromium-labeled EDTA excretion indicate colonic permeability alterations (Forsyth et al., 2011; Menozzi et al., 2021; Perez-Pardo et al., 2018; Shaikh et al., 2015). Due to limited sample sizes, these studies remain preliminary, highlighting the need for larger, independent studies to unequivocally confirm intestinal barrier dysfunction in PD patients (Van Ijzendoorn & Derkinderen, 2019).

Contrarily to our observations, Perez-Pardo et al. (2018) reported reduced colonic ZO-1 levels in PD patients (Perez-Pardo et al., 2018). In contrast, Clairembault et al. (2015) did not find differences in ZO-1 levels between PD patients and HC, although they observed reduced occludin expression. Interestingly, despite these molecular alterations, functional assessments of barrier integrity measuring para- and transcellular permeability via Ussing chambers, did not show significant differences between groups. These findings suggest that molecular level alterations in TJs composition may occur without overt functional impairment, allowing the intestinal barrier to maintain basic functionality despite structural

modifications (Clairembault et al., 2015). Furthermore, other PD-related studies have reported increased fecal ZO protein levels (Aho et al., 2021; Dumitrescu et al., 2021; Schwiertz et al., 2018), whereas Mulak et al. (2019) reported no significant differences (Mulak et al., 2019). However, these studies could not directly link altered fecal TJs protein levels to increased intestinal permeability. Consequently, altered TJs protein levels in feces should be considered as potential biomarkers, and further studies measuring intestinal permeability are needed in PD patients.

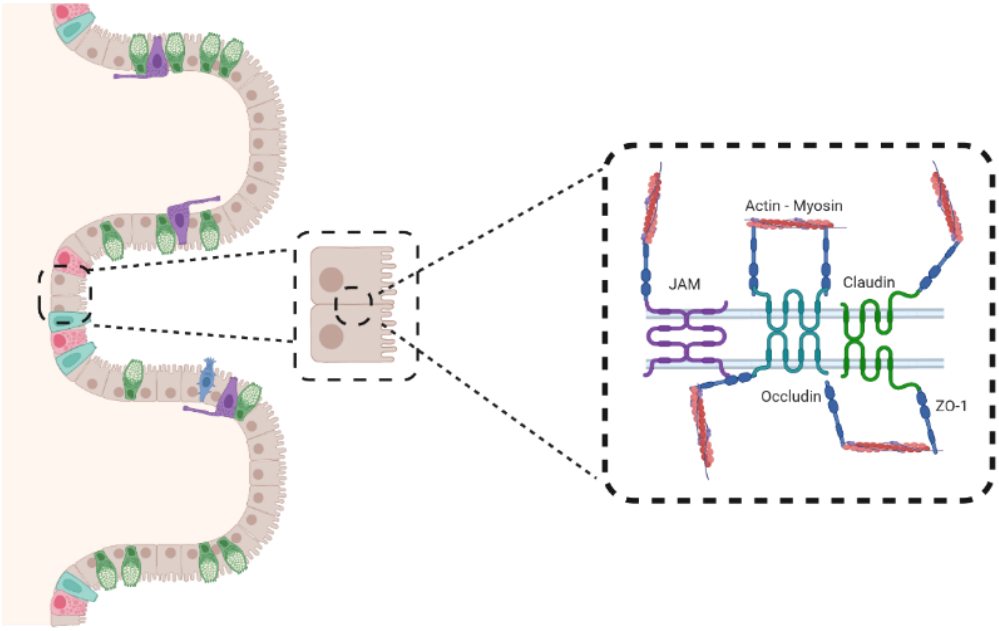

Figure 86. Simplified schematic representation of tight junctions. The intercellular spaces between intestinal enterocytes are sealed by different complexes including tight junction's complexes. These junctions consist of transmembrane proteins, including occludin, claudins and JAMs, as well as intracellular scaffold proteins such as ZO proteins, which anchor the transmembrane components to the actin cytoskeleton, maintaining barrier integrity (T. Suzuki, 2013). Created in https://BioRender.com.

In addition to our observations regarding TJs and intestinal barrier functionality, we also identified significant alterations in cytokine expression and secretion, particularly at 6 m of age in tgNM females. Specifically, serum levels of TNF-α, IL-10, IL-17, INF-β and GM-CSF were notably elevated, alongside increased fecal levels of IL-6 and increased expression levels of INF-γ in the proximal colon. Among these cytokines, TNF-α and IFN-γ are well-characterized as pro-inflammatory mediators known to disrupt intestinal epithelial barrier integrity, with previous studies linking their upregulation to barrier dysfunction observed in IBD (Barbaro et al., 2016; Langer et al., 2019; Neurath, 2014). Moreover, these cytokines directly modulate TJs functionality, affecting intestinal permeability and potentially contributing to chronic inflammation (Bruewer et al., 2003, 2005; Capaldo & Nusrat, 2008; Madara & Stafford, 1989). An

elevated number of studies suggest a significant association between PD and IBD, reporting increased risk of developing PD in individuals with IBD (Bialecka et al., 2007; H. X. Li et al., 2023; Villumsen et al., 2019; Weimers et al., 2019; F. Zhu et al., 2019b; Y. Zhu et al., 2022). Supporting this epidemiological link, shared genetic factors, particularly common alleles in the leucine-rich repeat kinase 2 (LRRK2) gene, have been identified in both PD and Crohn's disease patients (Hui et al., 2018). A systematic review and meta-analysis indicated that IBD patients receiving chronic anti-inflammatory treatment with anti-TNF-α biologics had a 78% reduced probability of developing PD compared to untreated patients, providing additional evidence that chronic inflammation contributes to PD pathogenesis (S. Park et al., 2019). Consistent with these findings, elevated levels of pro-inflammatory mediators, including IL-1α, IL-1B, CXCL8 and CRP (C-reactive protein), have been detected in fecal samples from PD patients (Houser et al., 2018). Additionally, serum analyses have demonstrated increased IL-6 and TNF-α alongside reduced CXCL8 in PD patients compared to HC (Aho et al., 2021; Fu et al., 2023). A recent comprehensive systematic review and meta-analysis further reported increased levels of inflammatory markers such as IL-6, TNF-α, IL-1β, MCP-1 and CRP in both CSF and peripheral blood samples from PD patients (Y. Qu et al., 2023). Elevated pro-inflammatory cytokine profiles have also been reported in colonic biopsies from PD patients (Devos et al., 2013; Perez-Pardo et al., 2018). Although we did not detect altered levels of calprotectin in out tgNM mice, increased levels of fecal calprotectin have been reported in PD cohorts, further reinforcing the presence of GI inflammation as a characteristic feature of PD pathology (Dumitrescu et al., 2021; Hor et al., 2021b; Mulak et al., 2019; Schwiertz et al., 2018). Robust evidence supports the presence of GI inflammation in PD patients, however, the relationship between inflammatory markers in the gut and systemic circulation remains incompletely understood. Additionally, inflammatory profiles are different among PD patients, thus further research it is still necessary to better correlate specific inflammatory patterns with clinical manifestations and disease progression (Di Lazzaro et al., 2024; Rolli-Derkinderen et al., 2020).

Despite methodological differences and variations in patient populations, several studies examining fecal microbiota in PD consistently report significant alterations in gut microbiome composition compared to HC. In our study, we initially characterized the fecal microbiota of tgNM females and males at 6 m. Despite our relatively limited sample size, we detected significant differences in microbiota β-diversity in tgNM females compared to their wt counterparts, whereas such differences were not observed in males. This observation aligns closely with the sex-dependent phenotypic differences repeatedly observed throughout our study, further strengthening the distinct microbial composition associated with tgNM females. Notably, tgNM females exhibited an increased abundance of the family Verrucomicrobiota and the genera *Akkermansia*, together with decreased levels of *Roseburia* genera. Interestingly, these microbial changes closely resemble some of the most consistently reported microbiota alterations in human PD patients (Table 3, Introduction). *Akkermansia*, a mucin-degrading bacterial genus, is usually

considered beneficial for human physiology (Cani et al., 2022) due to its ability to stimulate mucin production, reinforce gut epithelial integrity (Reunanen et al., 2015), and regulate immunological responses (Derrien et al., 2011; Ottman et al., 2017). Additionally, protective effects of *Akkermansia* have been reported in various neurological and metabolic contexts, including ALS (Blacher et al., 2019), reversal of HFD-induced metabolic disorders (Everard et al., 2013), and alleviation of cognitive impairment and amyloid pathology in AD models (He et al., 2022; Ou et al., 2020). However, in the context of PD, *Akkermansia* has been associated with disease onset and progression (Nishiwaki et al., 2020), suggesting a dual role that is likely influenced by the local intestinal environment. Rotenone and paraquat PD mouse models also reported increased levels of *Akkermansia* in their feces (K. Wang et al., 2022; Z. Zhao et al., 2021). Supporting this complexity, *Akkermansia muciniphila* relative abundance was found elevated in mice fed fiber-free diets compared to a fiber-rich diets, resulting in decreased mucus-layer thickness and increased susceptibility to intestinal pathogens (Desai et al., 2016; Schmit et al., 2023). Additionally, an in vitro study showed that under mucin-free conditions, *Akkermansia muciniphila* could induce intracellular calcium release in EECs cells (Amorim Neto et al., 2022). These findings suggest that environmental factors, such as nutrient availability and mucosal composition, critically modulate the interactions between *Akkermansia*, and likely other bacterial species, and host tissues. Furthermore, *Roseburia* is a butyrate-producing bacterium involved in metabolic reprogramming, immune modulation, and maintenance of the gut barrier (K. Nie et al., 2021). Reduced *Roseburia* abundance has also been reported in patients with Chron's disease and UC (Machiels et al., 2014; Shen et al., 2018). Experimental studies have further demonstrated *Roseburia's* ability to suppress Chron's disease pathogenesis through induction of anti-inflammatory responses in mouse models (Shen et al., 2018). In the context of PD, reduced *Roseburia* relative abundance has been correlated with poorer clinical outcomes, including worsening motor, non-motor and cognitive symptoms (Cilia et al., 2020).

Next, when we assessed longitudinal changes in the fecal microbiota composition in female mice to determine potential age-related effects, we found that bacterial relative abundances declined with age in both wt and tgNM females. These findings are consistent with previous findings indicating that aging, the main risk factor of PD, significantly impacts gut microbial composition and diversity (Dinan et al., 2017; Ghosh et al., 2022). Interestingly, microbial diversity in wt females became increasingly homogeneous over time, suggesting and age-dependent stabilization of the gut microbiota. In contrast, microbiota diversity in tgNM females progressively diverged with age. We suggest that NM-accumulation in these females over time influences and/or disrupts gut microbial homeostasis, resulting in increasingly pronounced microbial differences as tgNM females age.

When assessing genotype-related microbial diversity, we observed significant differences emerging at 6 m between tgNM and wt females, with the number of differentially abundant taxa increasing progressively over time. At 18 m, we detected a reduction in the relative abundance of *Alistipes*, which

contrasts with the increased abundance typically reported in fecal samples from PD patients. Conversely, the observed reduction in *Prevotellaceae* accompanied by increased *Bifidobacterium* closely aligned with microbial alterations previously reported in PD (Table 3, introduction). Notably, common probiotics such as *Bifidobacterium* and *Lactobacillus*, that are generally considered beneficial due to their positive effects on immune regulation and resistance to pathogen colonization (K. Hou et al., 2022), are found significantly increased in PD patients (Table 3, Introduction). Elevated *Bifidobacterium* and *Lactobacillus* and loss of SCFAs producing bacteria have also been observed in IBD (W. Wang et al., 2014). Further studies should investigate whether the increased presence of *Akkermansia*, *Bifidobacterium* and *Lactobacillus* in PD are beneficial, potentially acting as a compensatory mechanism to overcome dysbiosis, or if, alternatively, they play a detrimental role in disease progression. It is important to note that bacterial function is likely to be strain specific, and different strains of the same species might exert opposing effects. Therefore, inferring potential roles of bacteria in PD based on current knowledge at the genus and species level may not be sufficiently informative (Tan et al., 2022; van der Maden et al., 2025).

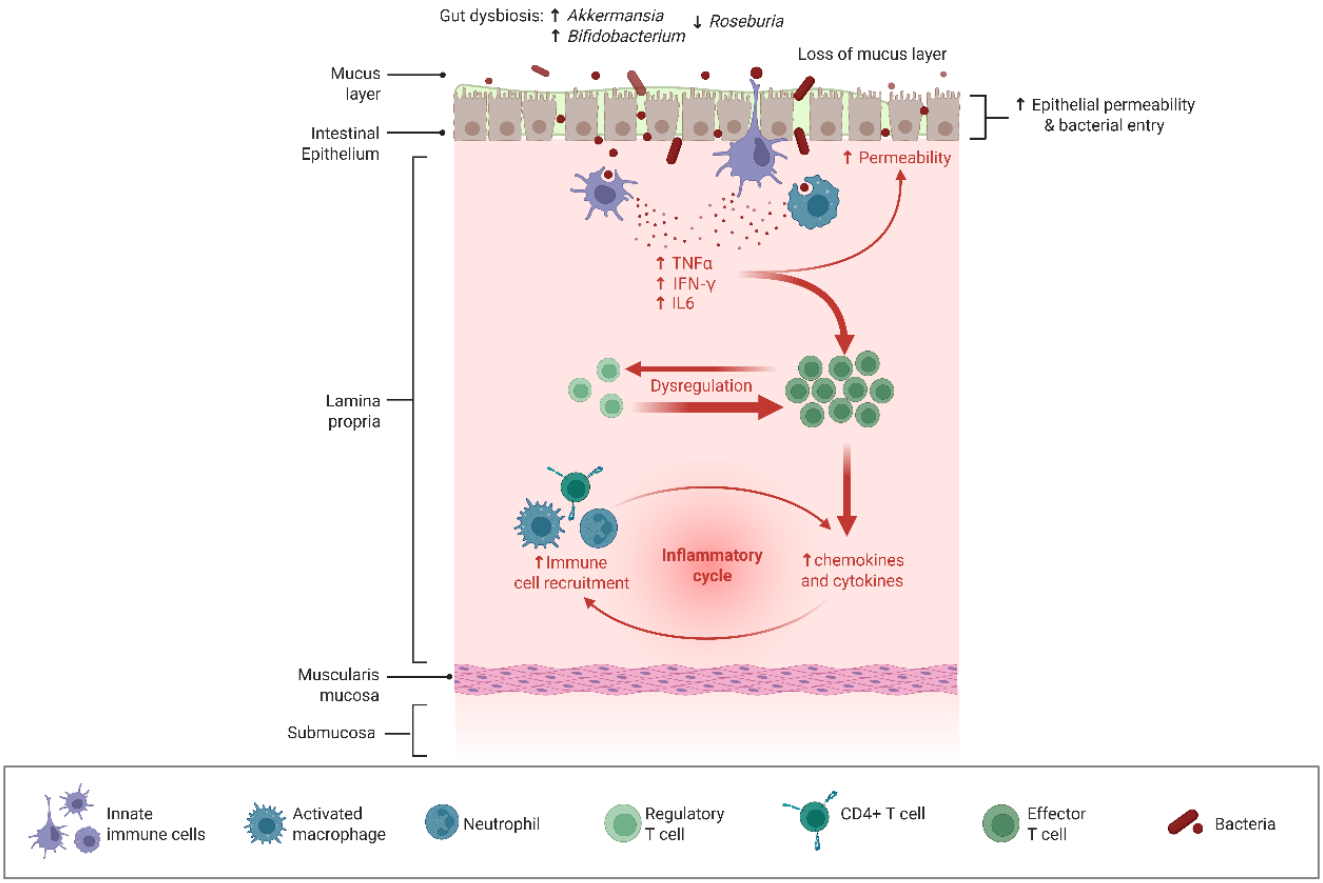

Figure 87. Gut Inflammatory manifestations in PD. Schematic representation of the inflammatory changes identified in the gut of PD patients and reproduced in tgNM mice. Intestinal dysbiosis disrupts the mucus layer and compromises gut permeability, which in turn triggers local immune responses. The resulting low-grade inflammation, combined with increased permeability, promotes the release of pro-inflammatory cytokines into the

circulation. These cytokines activate both innate and adaptive immune responses, creating a self-perpetuating cycle of systemic inflammation. Created in https://BioRender.com.

1.6 Metabolic and lipidomic alterations

In our microarray analysis, we identified significant alterations in several metabolic pathways, particularly those involved in lipid metabolism and detoxification processes, potentially affecting nutrient absorption and systemic energy homeostasis. These findings align with the observed impaired gut barrier integrity and altered gut microbiota composition in tgNM females. Consistently, we observed marked alterations in the fecal metabolic and lipidomic profiles of tgNM females at both 6 and 18 m.

At 6 m, tgNM females displayed reduced fecal concentrations of several amino acids, including branched-chain amino acids (BCAAs) such as isoleucine and valine, as well as aromatic amino acids (AAAs), including tyrosine and phenylalanine, both crucial precursors for DA biosynthesis pathways. Interestingly, by 18 m, the fecal amino acid profile shifted significantly, showing overall increased amino acid levels, with valine being the only significantly elevated BCAAs at this later age. This shift may reflect the observed age-dependent changes in gut microbiota composition or function that impact amino acid metabolism. Despite these fecal alterations, serum amino acid concentrations did not differ significantly between tgNM and wt females at 18 m.

Several human studies have investigated metabolomic profiles in PD patients across different biological samples, including CSF, blood, and urine (Engelborghs et al., 2003; Figura et al., 2018; Hirayama et al., 2016; Iwasaki et al., 1992; Molina et al., 1997; Nagesh Babu et al., 2018; Socha et al., 2019; Y. Zhang et al., 2022). However, the results from these studies are heterogeneous regarding the amino acid profiles. Some studies reported higher BCAAs concentrations in serum samples from PD patients (Nagesh Babu et al., 2018), while others reported reduced levels (Molina et al., 1997; Y. Zhang et al., 2022), and still others detected changes in CSF but not in serum (Wuolikainen et al., 2016). Similarly, fecal metabolomic data from PD patients remains limited and inconsistent. For instance, some studies observed increased fecal levels of BCAAs and AAAs, while others reported significant reductions (Vascellari et al., 2020; Yan et al., 2021; Y. Zhang et al., 2022). This variability could arise from methodological differences, variations in disease stage, dietary factors and microbiota composition. Indeed, impaired GI function and microbial dysbiosis in PD patients, as well as in our tgNM females, might disrupt amino acid absorption and metabolism, leading to altered amino acid availability.

Microbial metabolism of amino acids significantly contributes to producing metabolic end-products, such as SCFAs, primarily acetate, propionate, and butyrate (Den Besten et al., 2013). SCFAs have anti-inflammatory properties, partly through their inhibitory effect on histone deacetylases, promoting anti-inflammatory cytokine production and suppressing pro-inflammatory cytokines (P. Louis et al., 2014).

Interestingly, although at 6 m tgNM females showed a decreased relative abundance of *Roseburia*, a known butyrate-producing bacteria (Nishiwaki et al., 2022), and increased *Akkermansia* abundance, which degrades mucins to produce SCFAs, fecal SCFAs concentrations did not differ significantly between tgNM and wt females. However, by 18 m, fecal SCFAs levels significantly increased in tgNM females. These findings contrast with observations in PD patients, where decreased fecal butyrate and overall SCFAs are frequently reported and associated with intestinal inflammation, altered gut microbiota, poor cognitive outcomes, and lower body mass index (Aho et al., 2021; Tan, Chong, et al., 2021; Unger et al., 2016). Notably, other studies, such as Vascellari *et al.* (2020), reported no significant changes in fecal SCFAs in PD patients.

Additionally, accumulating evidence strongly links PD pathogenesis with disruptions in lipid metabolism, involving alterations in fatty acids, glycerolipids, glycerophospholipids, sphingolipids, ceramides, sphingomyelins, sterols, and lipoproteins (Xicoy et al., 2019, 2021). In line with these findings, tgNM females presented different alterations in serum lipid profiles, notably increased levels of glycerophospholipids. It is important to consider that glycerophospholipids represent diverse lipid subclasses with distinct biological functions. A recent study reported increased serum glycerophospholipid concentrations in PD patients, linking these lipid alterations specifically to bacterial taxa, including *Akkermansia* and *Roseburia* (Pereira et al., 2022), thus supporting the involvement of microbiota-host interactions in PD-associated lipid dysregulation.

We also identified elevated serum sphingomyelin levels in tgNM females. Increased sphingomyelin concentrations have previously been associated with genetic forms of PD, particularly those involving GBA mutations (Guedes et al., 2017; Xicoy et al., 2021). Additionally, our data showed increased PUFAs in the serum of tgNM females. However, existing literature on PUFAs in PD remains controversial, with studies reporting inconsistent associations between PUFA levels and PD risk (Xicoy et al., 2019; D. Yoo et al., 2021).

Lipids are transported in circulation bound to apolipoproteins, forming complexes known as lipoproteins. Intriguingly, our tgNM females exhibited increased levels of HDL-C, contrasting with findings from human PD studies, which report lower HDL-C concentrations in PD patients compared to HCs (Guo et al., 2015). Finally, we detected elevated serum concentration of GlycA and GlycB in tgNM females, along with an increased GlycB area (H/W ratio). Higher GlycA and GlycB levels have been previously linked to obesity, insulin resistance, abdominal fat accumulation and systemic inflammation (Amigó et al., 2021; Lorenzo et al., 2017). Importantly, both GlycA area and GlycB area have been identified as robust inflammatory biomarkers, independently of obesity status (Fuertes-Martín et al., 2019). Elevated GlycB area measurements have specifically been associated with enhanced inflammatory states in PD patients, particularly those with advanced neurological manifestations (Laguna et al., 2021).

1.7 Neuroendocrine and hormonal dysfunction

Non-motor symptoms in PD extend beyond GI disturbances and include a wide range of systemic features. This broader spectrum reflects a complex etiology involving both neuroendocrine and metabolic dysregulation. The hypothalamus plays a central role in the regulation of energy balance, metabolism, stress responses, circadian rhythms and reproductive function. Increasing evidence points to early hypothalamic involvement in PD, with hormonal alterations contributing to non-motor symptoms and systemic comorbidities (Mulak, 2020). In our tgNM model, we observed clear signs of neuroendocrine disruption, particularly in females, which appear to be closely linked to the metabolic and GI phenotypes previously described.

The hypothalamus integrates orexigenic and anorexigenic signals from the periphery and the CNS to maintain energy balance. Multiple hypothalamic nuclei are involved in this regulation, transmitting information to brain regions involved in reward and motivation (Volkow et al., 2011). While traditional homeostatic centers in the hypothalamus and brainstem regulate food intake and body weight, corticolimbic areas contribute to the emotional and hedonic aspects of eating behavior. In this context, disruptions in hormonal or neurotransmitter signaling can impair the balance between homeostatic and hedonic regulation, promoting maladaptive eating behaviors and contributing to the development of metabolic dysregulation (De Pablo-Fernández et al., 2017; Mulak, 2020; Stuber et al., 2025).

In the initial characterization, we observed that tgNM females presented increased body weight along with increased food and water intake as early as 3 m. Interestingly, despite these dysregulations, the expression of key hypothalamic neuropeptides involved in appetite control remained unchanged at both 6 m and 18 m. However, consistent with NM accumulation within the catecholaminergic neurons in the hypothalamus (Laguna et al., 2024), we observed reduced expression levels of AADC and TH at 18 m in tgNM females, suggesting impaired dopaminergic signaling at later stages. DA, together with other neurotransmitters and neuropeptides, plays a critical role in maintaining homeostatic energy balance. Thus, dopaminergic dysfunction in the hypothalamus likely contributes to the altered metabolic phenotype observed in tgNM females. Beyond its homeostatic role, DA also encodes the hedonic value of food and facilitates reward-based learning by associating environmental cues with pleasurable outcomes, adding further complexity to the interpretation of feeding behavior and energy regulation in tgNM females. To better understand the mechanisms underlying these phenotypes, our group is currently characterizing the structure and function of dopaminergic circuits within the hypothalamus of tgNM mice.

Supporting the metabolic dysregulation, we detected increased serum levels of the metabolic hormones leptin, PYY and active GLP-1 in tgNM females at 6 m. By 18 m, however, only insulin levels remained elevated. In parallel, increased body weight in tgNM females was partly attributable to increased WAT mass. Since adipocytes are the primary source of leptin, this increase in WAT likely explains the elevated

circulating leptin levels, as leptin secretion correlates with fat mass (Picó et al., 2021). Leptin also plays a key role in energy expenditure by activating the sympathetic nervous system in BAT, promoting thermogenesis and increasing energy expenditure (Rahmouni, 2010). However, preliminary indirect calorimetry data in our tgNM mice indicates that energy expenditure is comparable to that of their wt counterparts, which suggest a potential impairment in leptin signaling (ongoing collaboration with Dr. Rubén Nogueiras from the Molecular Metabolism group. Department of Physiology, CiMUS, University of Santiago de Compostela. CIBER Fisiopatología de la Obesidad y Nutrición (CIBEROBN)).

In humans, obesity is frequently associated with hyperleptinemia, yet this condition often fails to reduce food intake or increase energy expenditure, pointing to leptin resistance (Chrysafi et al., 2020). A similar mechanism may be happening in tgNM females, where elevated leptin levels fail to elicit appropriate metabolic responses, contributing to sustained weight gain and increased adiposity. Several factors might explain this impaired leptin responsiveness. One possibility is reduced leptin transport across the BBB, which would limit its central action. Alternatively, even if leptin reaches its target, there might be defects in downstream signaling. Under normal conditions, leptin binds to receptors in the arcuate nucleus (ARC) of the hypothalamus, activating POMC-expressing neurons while inhibiting NPY/AGRP-expressing neurons. Activation of POMC neurons leads to the production of α- and β -melanocyte stimulating hormones (α-MSH and β-MSH), which act on melanocortin 4 receptors (MC4Rs) in key hypothalamic and corticolimbic areas, suppressing food intake and reducing the motivational drive to seek food (Balthasar et al., 2004; Friedman, 2019; Sadaf Farooqi et al., 2007). Impairment in leptin signaling cascade could reduce leptin's anorexigenic effects, leading to hyperphagia, which promotes the development of metabolic dysfunction and obesity, contributing to the observed phenotype in tgNM females.

In PD patients, body weight fluctuations are commonly observed during disease progression. Some studies report an initial increase in fat mass during the early stages of PD, likely due to reduced physical activity following diagnosis (Lindskov et al., 2016; Vikdahl et al., 2014). At later stages, however, weight loss is more frequently observed, often attributed to increased energy expenditure (Levi et al., 1990; Tan et al., 2018). Other contributing factors include dysphagia, delayed gastric emptying, impaired nutrient absorption, constipation, gut dysbiosis, and diminished olfactory and gustatory function (Bachmann & Trenkwalde, 2006; Breasail et al., 2022; Sharma & Vassallo, 2014). Cognitive decline in advanced stages may further reduce the drive to eat and drink (De Lucia et al., 2020; Jung et al., 2021). Despite the metabolic relevance of leptin, data on its levels in PD patients remain scarce and inconclusive. A recent meta-analysis including six studies (198 PD patients vs. 182 HC) reported no significant differences in circulating leptin levels between groups (Rahnemayan et al., 2021). However, the analysis was limited by a lack of control for key confounding factors such as BMI, disease stage, and medication use. Thus, further research is needed to clarify the role of leptin signaling in PD pathophysiology and to determine whether leptin resistance plays a broader role in non-motor metabolic symptoms.

Despite blood samples being collected under fasting conditions, tgNM females showed elevated levels of the gut-derived peptides PYY and GLP-1 at 6 m. Both hormones are secreted by enteroendocrine L cells in the intestinal mucosa in response to nutrient stimulation and play well-established roles in promoting satiety and reducing food intake (A. De Silva et al., 2011). PYY acts through both peripheral and central mechanisms. Peripherally, it binds to Y_2 receptors on vagal afferent fibers in the GI tract, transmitting signals to the NTS and ultimately to the hypothalamus (Koda et al., 2005). Within the ARC of the hypothalamus, PYY stimulates anorexigenic POMC neurons and inhibits orexigenic NPY neurons, contributing to appetite suppression and energy balance (Batterham et al., 2002). However, the physiological role of PYY in regulating appetite in PD remains poorly understood (Siervo et al., 2024).

GLP-1 exerts a broad range of metabolic effects, including appetite suppression and regulation of blood glucose levels, through both central and peripheral pathways (D'Alessio, 2016; Nauck et al., 2021). Centrally, GLP-1 acts on hypothalamic receptors by stimulating anorexigenic POMC/CART neurons and inhibiting orexigenic NPY/AgRP neurons, thereby promoting satiety and reducing food intake (Secher et al., 2014). In parallel, recent evidence suggests that the anorexigenic effects of intestinal GLP-1 are also mediated through vagal afferent pathways that activate catecholaminergic neurons in the AP, which project to the NTS (Yamamoto et al., 2003). These NTS catecholaminergic neurons, in turn, send projections to key hypothalamic regions involved in the regulation of feeding behavior, such as the PVN and ARC (Krieger, 2020; Nauck et al., 2021). In our model, the accumulation of NM within NTS catecholaminergic neurons may impair their function, potentially disrupting the transmission of vagal GLP-1 signals to the hypothalamus. This impaired gut-brain communication could contribute to the persistent hyperphagia observed in tgNM females, despite elevated circulating levels of GLP-1.

By 18 m, tgNM females exhibited elevated insulin levels, a change that may reflect the progression of metabolic dysfunction first detected at earlier stages. At 6 m, these animals already presented signs of hyperphagia, increased adiposity, and elevated levels of satiety hormones such as leptin, PYY and GLP-1. The increase in insulin levels at 18 m may indicate a shift toward insulin resistance, a condition commonly associated with obesity and chronic metabolic stress. This is particularly relevant because epidemiological studies show that individuals with type 2 diabetes mellitus (T2D) have an increased risk of developing PD (Cullinane et al., 2023). T2D appears to facilitate neurodegeneration through impaired insulin signaling in the brain, as well as through chronic systemic inflammation and hyperglycemia (Bassil et al., 2022; Donath & Shoelson, 2011). Interestingly, the use of GLP-1 receptor agonists in diabetic patients has been associated with reduced prevalence of PD (Brauer et al., 2020). There is increasing evidence that activation of GLP-1 receptors exerts neuroprotective effects in various experimental models of PD, thus GLP-1 agonists are being tested as disease-modifying treatments in clinical trials for AD and PD. However, the underlying mechanisms of action remain unclear (Glotfelty et al., 2020; Kalinderi et al., 2024; Meissner et al., 2024). Together, these observations suggest that the hyperinsulinemia observed in aged tgNM

females may be a downstream consequence of early GLP-1 dysregulation and could represent an important mechanistic link between peripheral metabolic alterations and PD-related neurodegenerative processes.

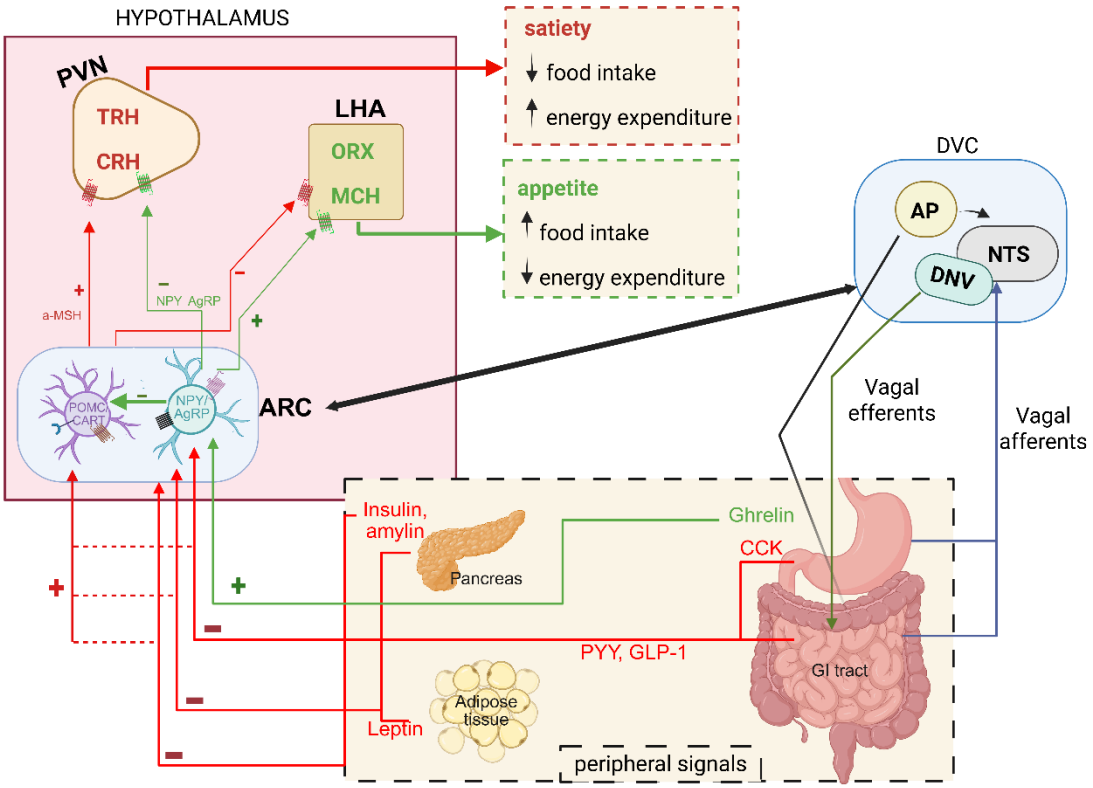

Figure 88. The role of gut hormones and hypothalamic circuits in food intake and energy expenditure regulation. Appetite and energy balance are regulated by a complex network of neuronal pathways involving reciprocal connections between the hypothalamus, brainstem, and higher cortical regions. Peripheral signals, including gut-derived hormones, convey information about nutrient status through both neural (e.g., vagal) and endocrine routes. These signals influence key hypothalamic circuits, such as the orexigenic NPY/AgRP and anorexigenic POMC/CART neurons within ARC, which project to areas like the PVN and LHA to regulate food intake and energy expenditure. The brainstem also integrates visceral signals via the DVC, which includes the NTS, AP and DNV, and sends projections to the hypothalamus. Together, these circuits coordinate metabolic responses including appetite suppression, thermogenesis, and glucose homeostasis. Anorexigenic pathways are shown in red; orexigenic pathways in green. ARC, arcuate nucleus; NPY/AgRP, neuropeptide Y and agouti-related peptide; POMC/CART, pro-opiomelanocortin and cocaine- and amphetamine-regulated transcript; PVN, paraventricular nucleus; LHA, lateral hypothalamic area; DVC, dorsal vagal complex; DNV, dorsal motor nucleus of the vagus; NTS, nucleus tractus solitarius; AP, area postrema; GI tract, gastrointestinal tract; TRH, thyrotropin-releasing hormone; CRH, corticotropin-releasing hormone; MCH, melanin-concentrating hormone; GLP-1, glucagon-like peptide-1; CCK, cholecystokinin; PP, pancreatic polypeptide; PYY, peptide YY; ORX, orexin. Created with Biorender.com. Adapted from (K. Suzuki et al., 2010).

1.8 Sex differences and implications

One of the most striking observations in our tgNM model is the clear sexual dimorphism across multiple physiological domains, including motor and non-motor behavior, GI function, metabolism and neuroendocrine function. Female tgNM mice consistently exhibited more pronounced alterations compared to their male counterparts, suggesting an increased vulnerability to NM-associated neuronal dysfunction. While sex differences are not uncommon in PD, they manifest in complex and sometimes paradoxical ways. Epidemiological studies show that men are approximately twice as likely to develop PD compared to women; however, women often experience faster disease progression, higher mortality and more sever non-motor symptoms (Cerri et al., 2019b; Martinez-Martin et al., 2012). Recent work from our lab has shown that males have higher levels of intracellular NM than females, regardless of PD diagnosis, which may contribute to the higher incidence of PD observed in men (Guillard-Sirieix, C., *in preparation*).

Sexual dimorphism is largely shaped by differences in endogenous and exogenous sex steroid levels. Our analysis of the hypothalamic-pituitary-gonadal axis revealed that tgNM females exhibited early and progressive hormonal disruption. Estradiol levels were significantly reduced as early as 3 m of age and continued to decline with age, reaching significantly lower levels compared to wt females by 18 m. This estrogen deficiency could be a key contributor to the increased susceptibility of tgNM females to metabolic, endocrine and possibly to dopaminergic dysfunction, given the known neuroprotective, anti-inflammatory, and regulatory roles of estrogens in brain homeostasis (Y. H. Lee et al., 2019; Villa et al., 2016). Consistent with this, we also observed reduced levels of LH and FSH in aged tgNM females, suggesting impaired gonadotropin-releasing hormone (GnRH) signaling from the ARC of the hypothalamus (Marques et al., 2024). Moreover, pituitary hormone profiling revealed additional sex-specific differences.

Overall, our findings demonstrate a clear sexual dimorphism in the tgNM model, with females exhibiting more pronounced disruptions in neuroendocrine signaling, metabolic regulation, and behavioral function. Importantly, both tgNM males and females carry the same transgene and express NM in the same catecholaminergic nuclei, yet the downstream consequences differ markedly between sexes. Moreover, we also reported in Chapter 2 that tgNM males at 6 m presented increased intracellular NM levels compared to tgNM females. This suggests that NM accumulation alone is not sufficient to explain the observed phenotypes. Instead, sex-specific intrinsic factors, such as differences in hormonal environment, neuroendocrine sensitivity, gut microbiota composition and low-grade inflammation, are likely to modulate vulnerability to NM-associated dysfunction. These observations emphasize that sex-specific biological factors can shape disease vulnerability and progression, reinforcing the importance of analyzing

male and female subjects separately in preclinical models, and supporting the need for personalized therapeutic strategies in PD.

1.9 Summary

Overall, our findings reveal that gut barrier dysfunction, intestinal inflammation, and microbiota dysbiosis contribute to PD pathophysiology in a humanized tgNM mouse modelling the prodromal phase of the disease. We showed that the intestinal barrier is compromised in tgNM females, leading to increased permeability and greater exposure of the systemic immune system to luminal antigens. This disruption can trigger a cascade of immune responses and low-grade inflammation, which in turn can further impair barrier function by altering TJs protein expression, creating a self-perpetuating cycle of gut dysfunction. These alterations were accompanied by significant changes in gut microbiota composition and microbial metabolite profiles, as well as systemic metabolic and neuroendocrine imbalances. Importantly, many of these phenotypes appeared prior to detectable dopaminergic neurodegeneration in the SNpc, supporting the idea that GI and metabolic alterations may actively contribute to disease onset and progression.

The tgNM model is particularly valuable because, unlike toxin-induced or α-synuclein overexpression models, it uniquely mimics the endogenous, age-dependent NM accumulation observed in the human brain. As a result, the phenotypic alterations in tgNM mice closely resemble the prodromal stage of human PD, providing understanding into early disease mechanisms without confounding factors such as acute neurotoxicity or artificial protein expression. This physiological model facilitates detailed assessment of the gut-brain axis and helps clarify early pathogenic events and the contribution of peripheral organ dysfunction to PD pathology. Moreover, the tgNM model represents a powerful tool to evaluate therapeutic strategies targeting peripheral mechanisms, opening new avenues to potentially modify disease progression.

Moreover, the tgNM model demonstrates a clear sexual dimorphism, reinforcing the importance of incorporating sex as a biological variable in mechanistic and therapeutic research. Although further studies are needed to fully elucidate the causal relationships between gut and brain alterations, our data highlight the gut microbiota, intestinal barrier integrity, and peripheral metabolic pathways as promising targets for early intervention strategies in PD.

2 CHAPTER 2. Determine if gut microbiota modulation by a HFD exacerbates the manifestation of both motor and non-motor symptoms in tgNM mice.

In Chapter 2, we assessed how chronic HFD feeding modifies or exacerbates the phenotype of tgNM mice described in Chapter 1. The results from our study show that HFD changed the gut microbiota and induced a clear metabolic stress in tgNM mice. We report that HFD exacerbated intestinal barrier permeability, promoted a systemic pro-inflammatory state, impaired the metabolic and neuroendocrine systems, as well as it produced neuroinflammation and neuropathological changes in the CNS. Notably, HFD exacerbated NM accumulation and neuroinflammation in key catecholaminergic brain areas. Moreover, we continue to observe that many of these phenotypes were manifested in a sex-dependent manner, with tgNM females being more vulnerable to metabolic stress. Together, these findings highlight how environmental factors such as diet can induce changes in the gut microbiota and exacerbate the onset and progression of PD-like pathology in a preclinical model of PD-like tgNM mice.

2.1 Gut microbiota, barrier integrity, and inflammation

It is well established that HFD feeding alters gut microbiota composition (Murphy et al., 2015), and our results in the tgNM model confirm this effect. Notably, shifts in gut microbial taxa are linked to the development of obesity and metabolic syndrome. The gut microbiota exerts endocrine functions through the production of metabolites, such as SCFAs, that influence host energy metabolism, gut barrier integrity, other organs and immune responses (Bäckhed et al., 2004, 2007; Den Besten et al., 2013; Tremaroli & Bäckhed, 2012). Studies have shown that transplant of gut microbiota from conventional mice into adult germ-free mice, produced increase in body fat and that microbiota transplantation from HFD-fed mice donors to lean germ-free recipients was sufficient to induce increased adiposity, highlighting the causal role of microbial communities in metabolic regulation (Bäckhed et al., 2004; Turnbaugh et al., 2008).

In our study, we observed that HFD-induced increase in specific bacterial taxa, notably the genera *Bacteroides*, *Alistipes*, and *Blautia.* Both *Bacteroides* and *Alistipes* are gram-negative bacteria and have been previously linked to diet-induced obesity and metabolic syndrome (Lu et al., 2016; Singh et al., 2020). While *Bacteroides* and *Alistipes* are generally beneficial symbiotic bacteria under physiological conditions, their expansion under HFD could reflect an adaptive advantage in the altered intestinal environment, with possible consequences for host metabolism and inflammation (B. J. Parker et al., 2020; A. G. Wexler & Goodman, 2017; H. M. Wexler, 2007). In contrast, the consistent increase in *Blautia* across all HFD-fed groups might represent a compensatory or adaptive response aiming to preserve metabolic homeostasis. *Blautia* is often associated with beneficial functions such as SCFAs production. Supporting this hypothesis,

human studies have reported an inverse correlation between *Blautia* abundance and visceral fat accumulation (Ozato et al., 2019), indicating a potential role for *Blautia* in mitigating obesity-related metabolic dysfunction. Additionally, another study demonstrated that *Blautia* supplementation can reduce lipid accumulation and ameliorate hyperlipidemia in HFD-fed mice (W. Xu et al., 2023). However, despite its potential benefits, the increased abundance of *Blautia* alone did not prevent weight gain or metabolic dysregulation in our tgNM animals, suggesting that its role might be limited or insufficient to counteract the broader HFD-induced changes.

Parallelly, we observed that HFD-induced decrease in other bacteria such as *Muribaculaceae* and *Lactobacillus*. *Muribaculaceae,* a butyrate-producing bacteria, was reduced in all HFD-fed groups (Mamun et al., 2025) while Lactobacillus was only decreased in HFD-fed females. We also observed reduced abundance of *Lactobacillus* only in HFD-fed females. *Lactobacillus* has been reported to maintain gut barrier integrity, alleviate metabolic disorders by regulating oxidative stress and inflammatory pathways (Rastogi & Singh, 2022). However, as previously discussed with the genera *Bifidobacterium,* the beneficial effect of *Lactobacillus* depends on the strain. Not all of them have the ability to reduce the body weight or exert anti-obesity effects (Stojanov et al., 2020; van der Maden et al., 2025).

The consistent increased abundance of *Blautia,* an acetate-producer genus (Ye et al., 2023), alongside reduced *Muribaculaceae,* a known butyrate producer, suggests that HFD-induced microbial shifts may have opposing influences on SCFAs profiles. While we did not directly measure SCFAs concentrations in this study, the microbial patterns observed suggest an imbalanced SCFAs profile that could contribute to impaired epithelial barrier function. Nevertheless, the relationship between SCFAs production and obesity is still debated. While some studies report increased fecal SCFAs in obese humans and rodents (Rahat-Rozenbloom et al., 2014; Schwiertz et al., 2010; Turnbaugh et al., 2006), others, including recent systematic reviews, indicate that HFD, obesity and metabolic syndrome are commonly associated with reduced SCFAs levels (Ilyés et al., 2022). Therefore, it would be interesting to quantify SCFAs levels in feces and serum of HFD-fed tgNM mice in future studies to better understand these functional dynamics.

Importantly, despite clear microbiota alterations, we only observed significantly increased gut permeability in HFD-fed tgNM mice from both sexes, but not in their wt counterparts. Increased gut permeability is typically associated with altered expression or localization of TJs (Nascimento et al., 2021). However, in our study, the duodenal and proximal colon expression levels of key TJs proteins were not specifically altered in tgNM mice under HFD. Future studies should evaluate TJs expression and localization histologically, to determine whether subtle or regional alterations might explain the observed barrier dysfunction. Moreover, assessing potential morphological disruptions on the intestinal epithelium could also help us clarify this increased permeability.

Compromised intestinal barrier integrity not only disrupts nutrient absorption and epithelial homeostasis but also allows the translocation of microbial components into systemic circulation causing low-grade

systemic inflammation (Cândido et al., 2018). Unexpectedly, despite observing increased gut permeability, we observed a significant reduction in duodenal inflammatory markers in tgNM mice after HFD, including decreased expression of GFAP, TLR-2 and TLR-4, as well as reduced levels of pro-inflammatory cytokines such as IFN-γ, TNF-α, and IL-6, especially in HFD-fed tgNM females. Although HFD is associated with increased inflammation, some studies reported that HFD may impair TLR-2-mediated immune responses (Amar et al., 2007; Q. Zhou et al., 2009), which could explain these unexpected findings. Despite the reduced local intestinal inflammation in the duodenum, HFD-fed tgNM mice presented elevated fecal inflammatory cytokines compared to CHOW-fed mice, suggesting ongoing immune activation likely related to microbial alterations and/or barrier dysfunction. Importantly, metabolic organs, such as the adipose tissue and the liver, are known to induce inflammatory responses under dietary challenges and obesity (Bae et al., 2023; Hersoug et al., 2018; Y. S. Lee et al., 2018; Zatterale et al., 2020). Indeed, the elevated serum inflammatory profile, especially in HFD-fed tgNM females, suggests that systemic inflammation might also originate from metabolically stressed tissues rather than from gut mucosal inflammation alone.

2.2 Sensorimotor and behavioral phenotype

As described in Chapter 1, the tgNM model presented early-onset sensorimotor deficits, specifically in females, with motor and balance impairments as early as 3 m of age. In the current chapter, we investigated whether these impairments were exacerbated by chronic HFD consumption. Indeed, all HFD-fed mice, irrespective of genotype and sex, presented significant impairments in motor coordination, as evidenced by the beam test. Notably, HFD-fed tgNM females exhibited the most pronounced deficits, presenting the longest crossing times among all experimental groups. This observation indicates that dietary intervention significantly worsened the intrinsic motor coordination deficits observed in tgNM females. Interestingly, tgNM males did not previously display detectable motor deficits even at advanced ages under CHOW conditions. However, following HFD, motor coordination deficits appeared as early as 6 m. Assessing sensorimotor functions in obese mice was challenging, as increased body weight itself may confound motor performance results. Although we used a wider beam for the beam test, we cannot entirely exclude the influence of elevated body weight on the observed motor coordination impairments. However, impaired burying behavior was also significantly affected in both male and female tgNM mice fed with HFD, but not in HFD-fed wt animals, suggesting that the observed motor deficits are not only attributable to increased body weight. Although, no changes were observed in olfactory capacity, neither in depressive-like behaviors, HFD worsened the capacity to vocalize of tgNM animals in both females and males.

2.3 GI function and morphology

Despite chronic feeding with HFD, we did not observe significant changes in intestinal transit time in any of the experimental groups. Nevertheless, specific alterations were evident in the GI function of HFD-fed tgNM females. These females presented an increased fecal output accompanied by decreased fecal water content, a pattern that was absent in their wt counterparts and tgNM males fed with HFD. Opposite to our results, different studies have reported that HFD reduced fecal output and increased intestinal transit time, together with smaller fecal pellets and reduced fecal water content, thus showing constipation (Anitha et al., 2016; Beraldi et al., 2020; Mukai et al., 2020; Pei et al., 2023). The complex metabolic and neuroendocrine phenotype we have described for tgNM females suggests that other factors related to host-genotype interactions are contributing to GI function in tgNM females and might explain this discrepancy.

We did not assess the possible intestinal neurodegeneration after HFD feeding, however other studies have reported the loss of myenteric neurons in the small intestine and the colon (Anitha et al., 2016; Beraldi et al., 2015, 2020; Reichardt et al., 2017; Stenkamp-Strahm et al., 2013; Voss et al., 2013). Moreover, another study also reported morphological changes in the myenteric neuronal populations of the small intestine, together with morphological changes of the intestinal wall and mucosal cells (Soares et al., 2015).

Despite not detecting phenotypic changes in gut motility, we found substantial alterations in key neurotransmitters involved in gut motility within the duodenum. Specifically, in HFD-fed tgNM females, DA, NE and ACh were significantly reduced, whereas 5-HT levels remained unchanged. Notably, these neurotransmitters changes were not evident in the proximal colon of HFD-fed tgNM females, indicating regional specificity within the GI tract. The observed reduction in DA and NE in tgNM females could partly result from decreased levels of their precursor, L-DOPA, although these reductions did not reach statistical significance, thus suggesting impaired catecholaminergic metabolism or synthesis under HFD. The pronounced decrease in ACh observed in HFD-fed tgNM females surpasses the reductions previously observed under CHOW conditions at 18 m, suggesting a possible exacerbation of impaired cholinergic vagal signaling by HFD. Together with this, HFD-fed tgNM males also presented decreased levels of ACh in the duodenum. This observation was also reported by another study, showing that HFD feeding significantly reduced cholinergic neuromuscular contractions (Pei et al., 2023). Also, decreased vagus nerve activity in the context of obesity has been reported (Pavlov & Tracey, 2012). Altogether, our findings indicate impaired neurotransmission in the gut of HFD-fed tgNM mice.

Furthermore, the morphological changes of the gut previously described in Chapter 1 were further amplified by HFD in tgNM females. Specifically, we observed a marked elongation of the small intestine exclusively in HFD-fed tgNM females, a morphological adaptation not detected in any other group. The

elongation of the gut supports the idea that GI phenotypic plasticity helps animals meet energetic demands and compensate for poorer food quality (Chapman & McLean, 2023). Intriguingly, all HFD-fed groups showed reduced cecum weights, a finding consistent with previous studies reporting cecal weight reductions in C57BL/6J mice fed with HFD, which was attributed to diet-induced shifts in gut microbiota composition (Fujisaka et al., 2018).

Despite the absence of detectable changes in total intestinal transit time, stable food intake, and reductions in neurotransmitters typically implicated in gut motility, the paradoxically increased fecal output in HFD-fed tgNM females needs further examination. Moreover, it was clear that reduction in neurotransmitters was not the only factor to explain the morphological changes and increased fecal output as HFD-fed tgNM males did not present any morphological change or GI impairment.

2.4 Metabolic dysregulation and inflammation

Metabolic syndrome is generally characterized by obesity, hypertension, dyslipidemia and insulin resistance, collectively increasing the risk for cardiovascular and metabolic diseases (Grundy et al., 2005). Although obesity alone does not constitute metabolic syndrome, it plays a central role by promoting a state of chronic low-grade inflammation, which has been widely implicated in the pathogenesis of metabolic dysfunction (Amar et al., 2007; Grundy et al., 2005; Hotamisligil, 2006; K. A. Kim et al., 2012; Q. Zhou et al., 2009). Within the context of this thesis, a recent systematic review and meta-analysis of 11 studies found that individuals with metabolic syndrome exhibit a significantly higher incidence of PD, with abdominal obesity, overweight and general obesity emerging as specific risk factors within this population (A. P. da S. Souza et al., 2021b). Moreover, another study reported that diabetes mellitus increases the risk of developing PD, and PD patients suffering diabetes present a more aggressive phenotype (Pagano et al., 2018). These findings support the importance of metabolic health in modulating susceptibility to neurodegenerative diseases.

In this context, HFD-fed tgNM mice developed a phenotype consistent with metabolic syndrome, particularly in females. TgNM females surpassed the body weight of HFD-fed tgNM males, reversing the sex differences observed under CHOW conditions, where tgNM males weighed more. However, tgNM females exhibited increased leptin and insulin levels without increased food intake, suggesting central leptin and insulin resistance driving excessive weight gain independent of hyperphagia. Despite hormonal signals indicating energy sufficiency, they accumulated disproportionately large amounts of WAT and BAT, surpassing even that of tgNM males. These observations suggest a potential impairment in hypothalamic pathways regulating energy expenditure and thermogenesis, possibly due to neurodegeneration within these key metabolic nuclei. In contrast, tgNM males exhibited a broader endocrine response, including increased ghrelin, GLP-1, glucagon, insulin, PYY, amylin, and leptin, alongside reduced food intake. Despite hypophagia, they still gained weight and accumulated adipose tissue, although to a lesser extent than

tgNM females. This suggests that, unlike females, tgNM males may retain or even amplify satiety signaling while developing obesity through mechanisms such as altered lipid metabolism or reduced energy expenditure. However, when assessing the hypothalamic expression profile of key hormones, neuropeptides and enzymes at 6 m, we found no differences between HFD-fed and CHOW-fed wt and tgNM females. While males showed some significant changes, these results have to be interpreted cautiously due to limited sample size and thus require further validation and the usage of alternative techniques like ELISA. Also, as previously detailed in Chapter 1, tgNM females presented clear signs of neuroendocrine disruption, closely linked to their metabolic phenotype.

As mentioned previously, HFD-fed tgNM mice, especially tgNM females, exhibited a marked and substantial increase in adipose tissue mass. Adipose tissue expansion, particularly via hypertrophy, is a metabolically active and inflammatory process (Richard et al., 2020). Enlarged adipocytes become metabolically dysfunctional and secrete increased levels of pro-inflammatory adipokines such as TNF-α, IL-6, and leptin, while decreasing the production of anti-inflammatory factors such adiponectin (J. Jo et al., 2009; Skurk et al., 2007). This shift in adipokine balance promotes local inflammatory environment, which promotes macrophage infiltration and the recruitment of other immune cells into adipose tissue, establishing a state of chronic low-grade inflammation (Burhans et al., 2019). This inflammatory state contributes to systemic insulin resistance and type 2 diabetes (Kahn & Flier, 2000; Mohallem & Aryal, 2020; Nieto-Vazquez et al., 2008; Zatterale et al., 2020), and may also contribute to central inflammation that exacerbates neurodegenerative vulnerability. Ongoing studies directed to assess inflammation in the adipose tissue of tgNM mice will further strengthen this point.

Different studies have identified hypothalamic inflammation, particularly within the ARC, as a key mediator linking dietary excess to metabolic disruption (C. T. De Souza et al., 2005; Grundy et al., 2005; Thaler et al., 2011; Valdearcos et al., 2014, 2015). Remarkably, in contrast to peripheral tissues where inflammation typically develops gradually from weeks to months in response to dietary challenges, hypothalamic inflammatory markers can become elevated within just 24 hours of initial HFD exposure in rodent models, even before weight gain. Thus, indicating that hypothalamic inflammation is not simply a downstream effect of obesity, but may serve as an early trigger of metabolic dysregulation (Thaler et al., 2011). Such hypothalamic neuroinflammation directly impairs insulin and leptin signaling pathways, disrupting their anorexigenic actions leading to increased food intake and further metabolic imbalance (C. T. De Souza et al., 2005; Thaler et al., 2011; Valdearcos et al., 2015). However, in our study, this relationship between hypothalamic inflammation leading to hyperphagia was not fully recapitulated. Additional experiments are ongoing to further characterize the hypothalamus of tgNM mice, first to confirm the hypothesis that there is hypothalamic inflammation, and second, to assess the expression of insulin and leptin receptors, as its disruption possibly leads to the altered integration of peripheral metabolic signals.

2.5 Metabolic dysregulation and renal function

Further complicating the metabolic phenotype of the tgNM model, we observed paradoxical metabolic responses in glucose homeostasis following chronic HFD. While HFD-fed wt mice predictably exhibited impaired glucose tolerance and elevated basal glucose levels, which are hallmarks of diet-induced insulin resistance (Montgomery et al., 2013b), HFD-fed tgNM mice, despite exhibiting obesity and increased circulating insulin levels, maintained or even improved glucose tolerance, particularly in females. Moreover, basal blood glucose levels were lower in HFD-fed tgNM females and remained unchanged in tgNM males, in contrast to the hyperglycemia observed in their HFD-fed wt counterparts. These findings suggest that tgNM mice may use alternative, potentially protective mechanisms to preserve systemic glucose balance despite underlying metabolic stress. Supporting this interpretation, we observed glycosuria, significantly elevated urinary glucose excretion in both HFD-fed tgNM females and males, and effect that was less pronounced in HFD-fed wt animals. Glycosuria may act as a physiological compensatory mechanism in tgNM mice, facilitating enhanced glucose clearance and thereby preventing hyperglycemia despite obesity-induced insulin resistance. A similar phenomenon has been reported in ARC POMC-deficient (Arc*Pomc*$^{-/-}$) mice, which also showed improved glucose tolerance and normoglycemia despite severe obesity and insulin resistance. In that study, enhanced glycosuria was identified as the key factor of improved glucose clearance (Chhabra et al., 2016). Mechanistically, the authors demonstrated that NE, released via sympathetic innervation, upregulates the glucose transporter GLUT2 in renal proximal tubules. Reduced NE signaling, via renal denervation or hypothalamic POMC deficiency downregulates GLUT2 expression, thereby limiting glucose reabsorption and increasing urinary glucose excretion (Chhabra et al., 2016, 2017). GLUT2 is a major glucose transporter located on the basolateral membrane of epithelial cells in the liver, kidney, and intestine, playing a central role in glucose homeostasis (de Souza Cordeiro et al., 2022). Given that tgNM mice show early and progressive loss of NE in both the brain and gut, as shown in Chapter 1, and that we also have previously reported reduced NE levels in the heart (Laguna et al., 2024), it is likely that similar processes are occurring in the kidneys. Degeneration in catecholaminergic neurons may lead to reduced central and peripheral sympathetic signaling, including impaired renal sympathetic innervation. Reduced renal sympathetic signaling may impair release of NE and consequently decrease GLUT2-mediated glucose reabsorption, thus promoting glycosuria. If this hypothesis is true, it would suggest that the preservation of glucose tolerance in tgNM mice may paradoxically be a consequence of neurodegenerative processes impairing normal renal sympathetic innervation and glucose management. However, this interpretation should be validated and thus, further studies should assess the expression levels of GLUT2 in renal tissue, quantify the levels of NE and assess structural integrity of renal sympathetic innervation in tgNM mice.

Another hypothesis, not mutually exclusive, is that hypothalamic POMC neurons may be dysfunctional or degenerating in our model. While we did not observe changes in POMC gene expression in the hypothalamus of HFD-fed mice, we cannot exclude the possibility of functional impairment, especially in the context of likely hypothalamic inflammation due to HFD (Valdearcos et al., 2015). As discussed before, additional analyses of hypothalamic inflammation and POMC neuronal integrity are ongoing in the group to address these issues.

Obesity is associated with increased kidney mass and glomerular hypertrophy, even in the absence of kidney disease (Hoy et al., 2010; Kasiske & Napier, 1985; Mandal et al., 2012b; Samuel et al., n.d.; Van Der Heijden et al., 2015). In line with this, renal morphological adaptations in HFD-fed tgNM mice were also observed. Both wt and tgNM females exhibited kidney hypertrophy following HFD, but this effect was significantly more pronounced in tgNM females. Interestingly, HFD-fed males, regardless of the genotype, did not show any significant changes in kidney weight. However, HFD-fed tgNM males presented increased glomerular area and reduced podocyte numbers. These observations have been already reported in other studies showing that glomerular enlargement under hypertrophic stress produces podocytes loss before the onset of detectable albuminuria (Fukuda et al., 2012; Martínez-Montoro et al., 2022; Minakawa et al., 2019). Surprisingly, HFD-fed tgNM females presented reduced glomerular area and preserved podocyte density, returning to values comparable to CHOW-fed wt counterparts.

Functionally, both HFD-fed tgNM females and males exhibited increased GFR, suggesting an early adaptation to obesity and insulin resistance and indicating a risk for developing CKD (Basolo et al., 2023; Chagnac et al., 2000, 2003; Henegar et al., 2001; Naderpoor et al., 2017). Despite these functional and morphological changes, ACR remained unchanged across all groups. This suggests that, at the time of the assessment, renal adaptations remain compensatory rather than pathological, however they can represent a preclinical stage of kidney dysfunction.

Growing evidence implicates CKD as a risk factor for neurodegeneration. Multiple cross-sectional studies report an increase incidence of PD in individuals with CKD or end-stage renal disease (ESRD) (M. J. Kwon et al., 2023; Nam et al., 2019; I. K. Wang et al., 2014). CKD is related to abnormal involuntary movements due to damaged basal ganglia and cortical structures (Safarpour et al., 2021) and CKD-neuropathology is thought to result from neuroinflammation, mitochondrial dysfunction, increased oxidative stress and impaired BBB (Bobot et al., 2020; Chagas et al., 2025; DENG et al., 2001; W. Jing et al., 2018; Mazumder et al., 2019). Additionally, elevated levels of uremic toxins have been recently identified in the CSF and plasma of PD patients, suggesting a possible mechanistic link between renal dysfunction and PD pathogenesis (Sankowski et al., 2020).

2.6 Metabolic dysregulation, brain catecholaminergic dysfunction and neuroinflammation

As previously discussed, increasing number of epidemiological studies highlight obesity and metabolic syndrome as critical environmental risk factors for the onset and progression of neurodegenerative disorders, including PD (J. Chen et al., 2014; Cullinane et al., 2023; Hao et al., 2016; W. Huang et al., 2024; L. Y. Li et al., 2023; Pagano et al., 2018; K. Y. Park et al., 2022; A. P. da S. Souza et al., 2021b; S. J. Spencer et al., 2017). Our findings further support this evidence and show that metabolic stress induced by a feeding with a HFD significantly modulates NM accumulation dynamics and exacerbates neuropathological vulnerability, particularly in a sex-dependent manner.

Interestingly, despite chronic metabolic stress, we did not observe overt neuronal loss or significant changes in TH expression across key catecholaminergic nuclei, including the SNpc, VTA and DVC, in tgNM mice fed with HFD for 4 m. A recent study in rats fed with HFD for 25 weeks, reported reduced TH protein levels only in the VTA, but no changes were observed in the SNpc, although they did not perform stereological counting to assess the number of the neurons (Bittencourt et al., 2022). Despite no significant TH-positive cell loss, we identified significant diet-dependent alterations in NM accumulation patterns, suggesting that metabolic dysregulation influenced NM metabolism, leading to neuronal dysfunction rather than neuronal death at this time point.

A previous study from our group showed that accumulation of NM above a specific threshold is associated with a general impairment of cellular proteostasis, leading to the formation of PD-like intracellular inclusions, and mitochondrial function that initially leads to neuronal dysfunction and ultimately to neuronal loss (Figure 89) (Carballo-Carbajal et al., 2019). In this study, the obtained results suggest that chronic metabolic challenges through HFD, may accelerate this pathological process in tgNM females by exacerbating intracellular NM accumulation and increasing neuroinflammation. Although we did not detect overt neuronal loss at 6 m, continued HFD feeding may eventually lead to significant catecholaminergic neurons loss.

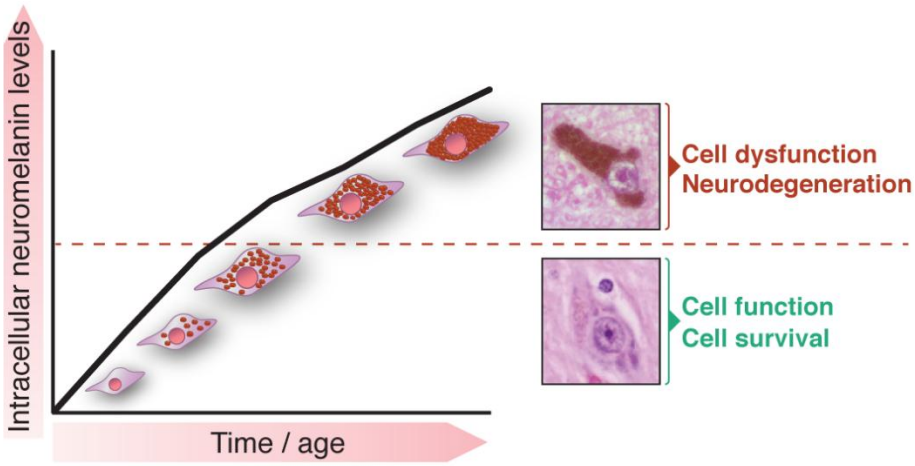

Figure 89. Schematic representation of NM accumulation. NM accumulation above a pathogenic threshold triggers cell dysfunction and neurodegeneration (Carballo-Carbajal et al., 2019).

We observed that HFD feeding induced a pronounced sex-specific divergence in both intracellular and extracellular NM accumulation. Under CHOW conditions, tgNM males exhibited higher levels of intracellular and extracellular NM compared to tgNM females. However, following HFD feeding, tgNM females reached the same intracellular NM levels as tgNM males in the VTA and DVC and even surpassed the observed NM levels of tgNM males in the SNpc. These observations suggest different sex-dependent molecular adaptations or vulnerabilities to metabolic stress. These findings align with recent data from our group demonstrating higher intracellular NM accumulation and increased eNM debris in males compared to females, both in healthy and PD postmortem human brains, suggesting a sex-specific baseline vulnerability for neurodegeneration even in the absence of overt PD pathology (Guillard Sirieix, C. *et. al. in preparation*). NM-containing neurons are particularly susceptible to neurodegeneration due to multiple intrinsic factors, particularly in PD (Carballo-Carbajal et al., 2019; E. Hirsch et al., 1988; Kastner et al., 1992; Mann & Yates, 1983): i) elevated oxidative stress, ii) high metabolic demands, iii) long and extensively arborized axons, iv) excessive iron loads, v) unique electrophysiological properties such as calcium-dependent pacemaking and vi) DA-derived oxidative toxicity (Figure 90) (Giguère et al., 2018; Sulzer & Surmeier, 2013). These properties impose high levels of oxidative stress, making NM-containing neurons probably more vulnerable to additional metabolic challenges.

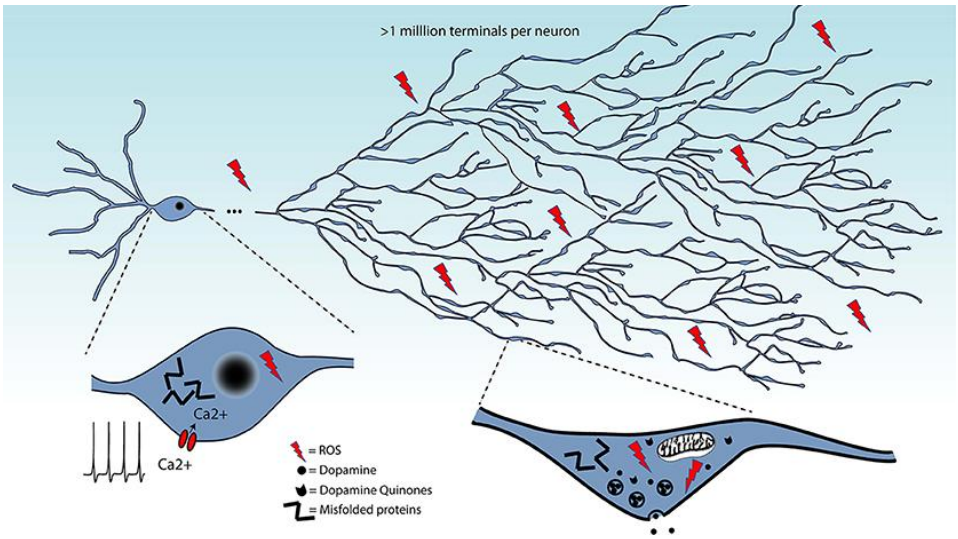

Figure 90. Schematic representation of the selective vulnerability of neuronal populations in PD. Including the large axonal arborization, their electrophysiological properties including calcium-dependent pacemaking, high levels of oxidant stress, pathological protein aggregation and reactive DA quinones. Retrieved from (Giguère et al., 2018). ROS, reactive oxygen species, Ca2+, Calcium.

NM is naturally accumulating with aging, and is hypothesized to possess antioxidant properties, effectively scavenging free radicals and sequestering cytotoxic DA metabolites such as quinones and semiquinones, as well as reactive metals and environmental toxins (Double et al., 2003; Gerlach et al., 2003; Karlsson & Lindquist, 2016; Zecca et al., 2003, 2008; Zucca et al., 2014b). Under physiological conditions, NM synthesis likely represents an adaptive protective mechanism aiming to reduce oxidative stress and reduce dopaminergic neuronal toxicity. Consistent with this idea, the observed NM accumulation together with elevated L-DOPA oxidation, specifically in HFD-fed tgNM females, might be an initial protective response against HFD-induced metabolic stress. However, exacerbated NM production and accumulation is likely to surpass the proposed beneficial threshold, potentially contributing to neuronal dysfunction and neuronal damage, as previous reported by our group (Carballo-Carbajal et al., 2019). Indeed, we found significantly increased eNM debris in HFD-fed tgNM females, suggesting an early-stage degenerative process. The presence of eNM is commonly observed in aging and PD postmortem brains and suggests the presence of dying neurons (Beach et al., 2007; Korzhevskii et al., 2021; William Langston et al., 1983). Moreover, eNM debris may act as pro-inflammatory signals, triggering microglial activation and sustained oxidative stress (Beach et al., 2007; Carballo-Carbajal et al., 2019; Moreno-García et al., 2021; Oberländer et al., 2011). Consistently, we observed increased neuroinflammation in HFD-fed tgNM females, characterized by increased phagocytic CD68+ and reactive Iba1+ microglial cells within the SNpc, VTA and DVC brain areas. In contrast, HFD-fed tgNM males did not exhibit increased quinone accumulation, intracellular NM alterations, or increased microglial activation compared to CHOW-fed

tgNM males. Intriguingly, HFD-fed tgNM males even presented reduced eNM debris in the SNpc, suggesting effective microglial phagocytosis and clearance or reduced cell death.

Despite limited numbers for certain analyses, specially in the DVC, preliminary findings showed that HFD-fed tgNM mice presented increased ChAT-positive cholinergic neurons in the DVC. This observation needs further validation through increased sample sizes to assess whether cholinergic modulation represents a compensatory mechanism or a response to altered vagal function associated with metabolic stress. Despite this observation, we previously discussed that ACh levels in the duodenum were reduced in both HFD-fed tgNM females and males. It would be interesting to further characterize the parasympathetic vagal innervation to better understand how metabolic peripheral challenges affected the CNS.

2.7 Summary

Overall, our findings demonstrate that chronic dietary stress induced by HFD significantly disturbs peripheral metabolic homeostasis and CNS functions in tgNM mice. We observed that HFD alters gut microbiota composition, increases gut permeability, and exacerbates existing impairments in intestinal barrier integrity. These changes probably facilitate the translocation of microbial products, triggering systemic inflammation, which as described in Chapter 1, could further compromise intestinal barrier function, creating a self-perpetuating cycle of gut dysfunction. Such peripheral metabolic dysregulation was also accompanied by endocrine imbalances and dysfunction in metabolically active organs, likely contributing to chronic inflammation and increased oxidative stress. Importantly, our data indicates that metabolic alterations induced by HFD accelerate NM accumulation in key catecholaminergic nuclei, and increase neuroinflammatory responses, particularly affecting female tgNM mice. These neuropathological changes reinforce the idea that dietary factors influence brain physiology and susceptibility to neurodegeneration. Additionally, we suggest that neurodegenerative processes initiated by metabolic stress may reciprocally exacerbate peripheral metabolic dysfunction through disrupted brain-organ communication. Moreover, these results suggest that individuals with unknown susceptibilities, genetic or environmental, might increase their risk of developing PD if exposed to additional metabolic challenges. Finally, consistent with observations from Chapter 1, the pronounced sexual dimorphism persisted under dietary metabolic stress, emphasizing sex-specific vulnerabilities and adaptive responses in this tgNM model. Altogether, our findings emphasize the complex interaction between metabolic dysregulation, systemic inflammation and central neurodegeneration, supporting the utility of the tgNM model for future investigations.

3 CHAPTER 3. Determine if rejuvenation of the gut microbiota by FMT can slow down the manifestation of PD-like symptoms in tgNM mice.

In Chapter 3, we explored the therapeutic potential of rejuvenating gut microbiota by treating old tgNM females with FMT from young, wt, healthy female donors. This intervention aimed to mitigate their PD-like features by restoring a more youthful microbial composition without modifying dietary inputs. Despite successful microbial shifts in wt recipients, our findings revealed that FMT did not produce any persistent beneficial effects in tgNM females. These results, although negative in outcome, provide new insight into the challenges of microbiota-targeted interventions in the context of aging and neurodegeneration. They suggest that the gut-brain axis may be less responsive or even resistant to microbial modulation once aging and neurodegenerative processes are present.

3.1 Effects of FMT on gut microbiota composition and barrier function

In recent years, the gut microbiota has emerged as a key modulator of host immunity, metabolism and behavior (Cryan et al., 2019; Dinan et al., 2017; Fransen et al., 2017; Heintz & Mair, 2014; Morais et al., 2020; Nicholson et al., 2012; Rooks & Garrett, 2016). Aging, one of the main risk factors for PD, is associated with substantial changes in microbial diversity and composition, which are influenced by intrinsic biological processes as well as lifestyle factors (Ghosh et al., 2022; Pellanda et al., 2021). Recent studies report that microbiota transplantation from young donors into aged individuals can ameliorate age-associated phenotypes, improving systemic health (Boehme et al., 2021; A. Parker et al., 2022; Smith et al., 2017). However, it remains unclear if these beneficial microbiota-mediated effects translate into therapeutic strategies for age-related neurodegenerative diseases like PD.

Our study tried to further assess this question by evaluating the potential of FMT, from young healthy wt donors, to restore gut microbiota homeostasis and reduce and/or reverse the PD-like phenotype of old tgNM females. Despite successful microbiota engraftment in wt females, evidenced by a significant shift in β-diversity, FMT-treated tgNM females did not show similar microbiota changes. Their microbiota remained statistically indistinguishable from PBS-treated tgNM controls and significantly different from their FMT-treated wt counterparts. These findings suggest that intrinsic host factors, likely associated with genotype or existing pathology, can be critical barriers to successful engraft donor microbiota in tgNM females. It seems that the pathological gut environment in aged tgNM females may favor specific resilient bacterial populations, limiting colonization or long-term persistence of donor microbiota. A previous study reported that FMT-treatment produced the largest microbiome changes during the first week, after which the community often reverted toward the recipient's original microbiome (A. Parker et al., 2022). Given

that our intervention lasted for 6 m with weekly FMT doses, and even so failed to achieve durable engraftment in tgNM females, it raises important questions about how persistent host factors, possibly driven by neurodegenerative signals or systemic inflammation, could influence microbial colonization stability. Moreover, future studies should assess whether more aggressive or repeated interventions are needed to overcome this problem.

At the genus level, FMT treatment reduced the abundance of *Bifidobacterium* in tgNM females, aligning with our earlier observations in Chapter 1 and clinical findings that report elevated *Bifidobacterium* in PD patients (Table 3, Introduction). Thus, this reduction could potentially represent a beneficial modification. However, we concurrently observed increases in *Lactobacillus*, *Allistpes* and *Desulfovibrio* in FMT-treated tgNM females, genera similarly reported elevated in PD cohorts. These changes suggest that even beneficial donor microbiota might selectively enrich disease-associated taxa in a compromised host environment, ultimately neutralizing therapeutic efficacy.

In line with the microbiota analysis, functional assessments showed no improvement in gut barrier integrity, GI function, or motor performance in FMT-treated tgNM females. Interestingly, while FMT-treated wt showed improved gut permeability, this benefit was absent in tgNM females. The observed reduction in GI tract length in FMT-treated tgNM females remains challenging to interpret due to inherent variability and the obvious absence of baseline measures for this parameter in this specific cohort. Indeed, subtle pre-treatment behavioral and physiological differences among tgNM females, such as their slightly better motor performance and lower fecal output, highlight the importance of carefully monitoring baseline phenotypes before interventions. These baseline differences might partially explain the lack of responsiveness of the FMT treatment.

Our findings also reveal critical technical limitations and conceptual considerations that future studies must address. It remains unclear whether the ABX pre-treatment efficiently depleted the endogenous microbiota in the treated animals. ABX treatment duration, type, dosage, and host microbiota resilience significantly influence microbiota depletion efficacy (Gheorghe et al., 2021; Hibbing et al., 2009; Willing et al., 2011). Without confirming microbiota depletion by sequencing immediately post-ABX treatment, it remains unclear whether insufficient microbiota depletion may have compromised successful FMT engraftment. Moreover, different ABX regimens or prolonged ABX exposure might be necessary to ensure effective depletion in genetically predisposed or aged animal models that exhibit inherently resilient microbial communities.

Moreover, even when the same donor microbiota was introduced to both wt and tgNM mice, only wt females exhibited changes in gut microbiota and functional improvements. Ongoing CNS-driven pathological signals, may create a hostile gut environment in tgNM mice that limits donor microbiota engraftment and persistence. Thus, even microbiota-targeted therapies might be ineffective without simultaneously addressing the central neurodegenerative processes.

Finally, this exploratory study highlights the limitations and complexities associated with microbiota-targeted therapies in the context of neurodegenerative disorders. Beyond gut microbiota profiling, ideally future studies should include analysis of systemic and peripheral immune responses, metabolomics and lipidomic assessments, and detailed characterization of neuronal health. Our findings illustrate significant host-genotype barriers to microbiota engraftment and therapeutic benefit in aged tgNM females, emphasizing the need for integrated, multimodal strategies that simultaneously target central neurodegenerative processes, systemic inflammation, and gut dysbiosis to effectively address the complex pathophysiology of PD.

CONCLUSIONS

1 CHAPTER 1. Characterization of behavioral and GI alterations linked to age-dependent intracellular NM accumulation in mice.

1. Human-like NM accumulation in catecholaminergic brain nuclei induces early sensorimotor and GI dysfunctions before dopaminergic neuronal loss in the SNpc and VTA.
2. Gut microbiota dysbiosis, gut barrier impairment, low-grade intestinal and systemic inflammation, and metabolic alterations emerge at young ages, especially in tgNM females, supporting early peripheral contributions to the progression of PD pathology.
3. GI dysfunctions are primarily associated with disrupted extrinsic vagal regulation rather than intrinsic enteric neuronal loss.
4. TgNM mice present a strong sexual dimorphism across different parameters, with TgNM females showing stronger sensorimotor deficits, GI dysfunction and neuroendocrine and metabolic dysregulations than tgNM males.
5. The tgNM mouse model recapitulates key prodromal PD features and represents a relevant tool to assess gut-brain axis dysfunction, systemic metabolic impairment, and sex-specific PD mechanisms.

2 CHAPTER 2. Determine if gut microbiota modulation by a HFD exacerbates the manifestation of both motor and non-motor symptoms in tgNM mice.

1. Chronic HFD feeding alters gut microbiota, increases gut permeability and exacerbates systemic inflammation and metabolic dysfunction in tgNM mice.
2. Gut microbiota changes under HFD are linked to impaired gut barrier function and systemic immune activation.
3. HFD-fed tgNM females show stronger endocrine, adipose tissue, renal and behavioral alterations compared to tgNM males.
4. Peripheral metabolic stress exacerbates early PD-like neuropathology independently of dopaminergic neuronal loss.
5. HFD accelerates NM accumulation and neuroinflammation in key catecholaminergic brain regions, especially in tgNM females.
6. Peripheral metabolic dysfunction and neurodegeneration interact bidirectionally, indicating impaired brain-organ communication in tgNM mice.
7. The tgNM model under HFD demonstrates how environmental factors like diet can modulate PD onset and progression.

3 **CHAPTER 3.** Determine if rejuvenation of the gut microbiota by FMT can slow down the manifestation of PD-like symptoms in tgNM mice.

1. FMT from young healthy wt females rejuvenated the gut microbiota composition of aged wt females but failed to induce lasting microbiota changes, improve gut barrier function, GI physiology or motor performance in aged tgNM females.
2. Intrinsic host factors such as genotype, aging and existing pathology limited successful microbial engraftment in tgNM females.
3. ABX pre-treatment and FMT protocols need optimization to achieve effective host microbiota depletion and donor colonization.
4. Microbiota-targeted therapies alone may be insufficient once CNS-driven pathology is established, thus future strategies should combine microbiota modulation with interventions targeting central and systemic inflammation.

BIBLIOGRAPHY

Abbott, R. D., Petrovitch, H., White, L. R., Masaki, K. H., Tanner, C. M., Curb, J. D., Grandinetti, A., Blanchette, P. L., Popper, J. S., & Ross, G. W. (2001). Frequency of bowel movements and the future risk of Parkinson's disease. *Neurology*, *57*(3), 456–462. https://doi.org/10.1212/WNL.57.3.456

Abbruzzese, G., Barone, P., Lopiano, L., & Stocchi, F. (2021). The Current Evidence for the Use of Safinamide for the Treatment of Parkinson's Disease. *Drug Design, Development and Therapy*, *15*, 2507–2517. https://doi.org/10.2147/DDDT.S302673

Abdelmotilib, H., Maltbie, T., Delic, V., Liu, Z., Hu, X., Fraser, K. B., Moehle, M. S., Stoyka, L., Anabtawi, N., Krendelchtchikova, V., Volpicelli-Daley, L. A., & West, A. (2017). α-Synuclein Fibril-induced Inclusion Spread in Rats and Mice Correlates with Dopaminergic Neurodegeneration. *Neurobiology of Disease*, *105*, 84. https://doi.org/10.1016/J.NBD.2017.05.014

Adams-Carr, K. L., Bestwick, J. P., Shribman, S., Lees, A., Schrag, A., & Noyce, A. J. (2016). Constipation preceding Parkinson's disease: A systematic review and meta-analysis. In *Journal of Neurology, Neurosurgery and Psychiatry* (Vol. 87, Issue 7, pp. 710–716). BMJ Publishing Group. https://doi.org/10.1136/jnnp-2015-311680

Adler, C. H., & Beach, T. G. (2016). Neuropathological basis of nonmotor manifestations of Parkinson's disease. *Movement Disorders*, *31*(8), 1114–1119. https://doi.org/10.1002/MDS.26605

Aho, V. T. E., Houser, M. C., Pereira, P. A. B., Chang, J., Rudi, K., Paulin, L., Hertzberg, V., Auvinen, P., Tansey, M. G., & Scheperjans, F. (2021). Relationships of gut microbiota, short-chain fatty acids, inflammation, and the gut barrier in Parkinson's disease. *Molecular Neurodegeneration*, *16*(1), 1–14. https://doi.org/10.1186/S13024-021-00427-6/FIGURES/7

Aho, V. T. E., Pereira, P. A. B., Voutilainen, S., Paulin, L., Pekkonen, E., Auvinen, P., & Scheperjans, F. (2019). Gut microbiota in Parkinson's disease: Temporal stability and relations to disease progression. *EBioMedicine*, *44*, 691–707. https://doi.org/10.1016/j.ebiom.2019.05.064

Al-Asmakh, M., & Hedin, L. (2015). Microbiota and the control of blood-tissue barriers. *Tissue Barriers*, *3*(3), 1–7. https://doi.org/10.1080/21688370.2015.1039691

Alcalay, R. N., Gu, Y., Mejia-Santana, H., Cote, L., Marder, K. S., & Scarmeas, N. (2012). The association between Mediterranean diet adherence and Parkinson's disease. *Movement Disorders*, *27*(6), 771–774. https://doi.org/10.1002/mds.24918

Amar, S., Zhou, Q., Shaik-Dasthagirisaheb, Y., & Leeman, S. (2007). Diet-induced obesity in mice causes changes in immune responses and bone loss manifested by bacterial challenge. *Proceedings of the National Academy of Sciences of the United States of America*, *104*(51), 20466–20471. https://doi.org/10.1073/PNAS.0710335105/ASSET/77B44E8C-953D-470C-9024-03176D497596/ASSETS/GRAPHIC/ZPQ0510787250008.JPEG

Amigó, N., Fuertes-Martín, R., Malo, A. I., Plana, N., Ibarretxe, D., Girona, J., Correig, X., & Masana, L. (2021). Glycoprotein Profile Measured by a1 H-Nuclear Magnetic Resonance Based on Approach in Patients with Diabetes: A New Robust Method to Assess Inflammation. *Life*, *11*(12), 1407. https://doi.org/10.3390/LIFE11121407/S1

Amorim Neto, D. P., Bosque, B. P., Pereira de Godoy, J. V., Rodrigues, P. V., Meneses, D. D., Tostes, K., Costa Tonoli, C. C., Faustino de Carvalho, H., González-Billault, C., & de Castro Fonseca, M. (2022). Akkermansia muciniphila induces mitochondrial calcium overload and α -synuclein aggregation in an enteroendocrine cell line. *IScience*, *25*(3), 103908. https://doi.org/10.1016/J.ISCI.2022.103908

Andersen, K. B., Krishnamurthy, A., Just, M. K., Van Den Berge, N., Skjærbæk, C., Horsager, J., Knudsen, K., Vogel, J. W., Toledo, J. B., Attems, J., Polvikoski, T., Saito, Y., Murayama, S., & Borghammer, P. (2025). Sympathetic and parasympathetic subtypes of body-first Lewy body disease observed in postmortem tissue from prediagnostic individuals. *Nature Neuroscience 2025*, 1–12. https://doi.org/10.1038/s41593-025-01910-9

Anderson, M. J., & Walsh, D. C. I. (2013). PERMANOVA, ANOSIM, and the Mantel test in the face of heterogeneous dispersions: What null hypothesis are you testing? *Ecological Monographs*, *83*(4), 557–574. https://doi.org/10.1890/12-2010.1

Anitha, M., Reichardt, F., Tabatabavakili, S., Nezami, B. G., Chassaing, B., Mwangi, S., Vijay-Kumar, M., Gewirtz, A., & Srinivasan, S. (2016). Intestinal dysbiosis contributes to the delayed gastrointestinal transit in high-fat diet fed mice. *Cellular and Molecular Gastroenterology and Hepatology*, *2*(3), 328–339. https://doi.org/10.1016/J.JCMGH.2015.12.008

Anlauf, M., Schäfer, M. K. H., Eiden, L., & Weihe, E. (2003). Chemical coding of the human gastrointestinal nervous system: Cholinergic, VIPergic, and catecholaminergic phenotypes. *Journal of Comparative Neurology*, *459*(1), 90–111. https://doi.org/10.1002/CNE.10599

Annerino, D. M., Arshad, S., Taylor, G. M., Adler, C. H., Beach, T. G., & Greene, J. G. (2012). Parkinson's disease is not associated with gastrointestinal myenteric ganglion neuron loss. *Acta Neuropathologica*, *124*(5), 665. https://doi.org/10.1007/S00401-012-1040-2

Antonini, A., Moro, E., Godeiro, C., & Reichmann, H. (2018). Medical and surgical management of advanced Parkinson's disease. *Movement Disorders*, *33*(6), 900–908. https://doi.org/10.1002/MDS.27340

Antonini, A., Pahwa, R., Odin, P., Isaacson, S. H., Merola, A., Wang, L., Kandukuri, P. L., Alobaidi, A., Yan, C. H., Bao, Y., Zadikoff, C., Parra, J. C., Bergmann, L., & Chaudhuri, K. R. (2022). Comparative Effectiveness of Device-Aided Therapies on Quality of Life and Off-Time in Advanced Parkinson's Disease: A Systematic Review and Bayesian Network Meta-analysis. *CNS Drugs*, *36*(12), 1269–1283. https://doi.org/10.1007/S40263-022-00963-9/FIGURES/5

Arai, K., Kato, N., Kashiwado, K. I., & Hattori, T. (2000). Pure autonomic failure in association with human α-synucleinopathy. *Neuroscience Letters*, *296*(2–3), 171–173. https://doi.org/10.1016/S0304-3940(00)01623-2

Arnold, C., Gehrig, J., Gispert, S., Seifried, C., & Kell, C. A. (2013). Pathomechanisms and compensatory efforts related to Parkinsonian speech. *NeuroImage : Clinical*, *4*, 82. https://doi.org/10.1016/J.NICL.2013.10.016

Arotcarena, M. L., Dovero, S., Prigent, A., Bourdenx, M., Camus, S., Porras, G., Thiolat, M. L., Tasselli, M., Aubert, P., Kruse, N., Mollenhauer, B., Damas, I. T., Estrada, C., Garcia-Carrillo, N., Vaikath, N. N.,

El-Agnaf, O. M. A., Herrero, M. T., Vila, M., Obeso, J. A., … Bezard, E. (2020). Bidirectional gut-to-brain and brain-to-gut propagation of synucleinopathy in non-human primates. *Brain*, *143*(5), 1462–1475. https://doi.org/10.1093/brain/awaa096

Ascherio, A., & Schwarzschild, M. A. (2016). The epidemiology of Parkinson's disease: risk factors and prevention. *The Lancet Neurology*, *15*(12), 1257–1272. https://doi.org/10.1016/S1474-4422(16)30230-7

Auteri, M., Zizzo, M. G., Amato, A., & Serio, R. (2016). Dopamine induces inhibitory effects on the circular muscle contractility of mouse distal colon via D1- and D2-like receptors. *Journal of Physiology and Biochemistry*, *73*(3), 395–404. https://doi.org/10.1007/S13105-017-0566-0/FIGURES/5

Ayling, R. M., & Kok, K. (2018). Fecal Calprotectin. *Advances in Clinical Chemistry*, *87*, 161–190. https://doi.org/10.1016/BS.ACC.2018.07.005

Babygirija, R., Bülbül, M., Cerjak, D., Ludwig, K., & Takahashi, T. (2011). Sustained acceleration of colonic transit following chronic homotypic stress in oxytocin knockout mice. *Neuroscience Letters*, *495*(1), 77–81. https://doi.org/10.1016/J.NEULET.2011.03.045

Bachmann, C. G., & Trenkwalde, C. (2006). Body weight in patients with Parkinson's disease. *Movement Disorders*, *21*(11), 1824–1830. https://doi.org/10.1002/MDS.21068

Bäckhed, F., Ding, H., Wang, T., Hooper, L. V., Gou, Y. K., Nagy, A., Semenkovich, C. F., & Gordon, J. I. (2004). The gut microbiota as an environmental factor that regulates fat storage. *Proceedings of the National Academy of Sciences of the United States of America*, *101*(44), 15718. https://doi.org/10.1073/PNAS.0407076101

Bäckhed, F., Manchester, J. K., Semenkovich, C. F., & Gordon, J. I. (2007). Mechanisms underlying the resistance to diet-induced obesity in germ-free mice. *Proceedings of the National Academy of Sciences of the United States of America*, *104*(3), 979. https://doi.org/10.1073/PNAS.0605374104

Bae, H. R., Shin, S. K., Yoo, J. H., Kim, S., Young, H. A., & Kwon, E. Y. (2023). Chronic inflammation in high-fat diet-fed mice: Unveiling the early pathogenic connection between liver and adipose tissue. *Journal of Autoimmunity*, *139*, 103091. https://doi.org/10.1016/J.JAUT.2023.103091

Bak, M., Thomsen, K., Christiansen, T., & Flyvbjerg, A. (2000). Renal enlargement precedes renal hyperfiltration in early experimental diabetes in rats. *Journal of the American Society of Nephrology : JASN*, *11*(7), 1287–1292. https://doi.org/10.1681/ASN.V1171287

Bakken, J. S., Borody, T., Brandt, L. J., Brill, J. V., Demarco, D. C., Franzos, M. A., Kelly, C., Khoruts, A., Louie, T., Martinelli, L. P., Moore, T. A., Russell, G., & Surawicz, C. (2011). Treating clostridium difficile infection with fecal microbiota transplantation. *Clinical Gastroenterology and Hepatology*, *9*(12), 1044–1049. https://doi.org/10.1016/j.cgh.2011.08.014

Balthasar, N., Coppari, R., McMinn, J., Liu, S. M., Lee, C. E., Tang, V., Kenny, C. D., McGovern, R. A., Chua, S. C., Elmquist, J. K., & Lowell, B. B. (2004). Leptin receptor signaling in POMC neurons is required for normal body weight homeostasis. *Neuron*, *42*(6), 983–991.

https://doi.org/10.1016/J.NEURON.2004.06.004/ASSET/7A142191-8635-4A28-A614-02E9804D81C8/MAIN.ASSETS/GR5.GIF

Barbaro, M. R., Di Sabatino, A., Cremon, C., Giuffrida, P., Fiorentino, M., Altimari, A., Bellacosa, L., Stanghellini, V., & Barbara, G. (2016). Interferon-γ is increased in the gut of patients with irritable bowel syndrome and modulates serotonin metabolism. *American Journal of Physiology - Gastrointestinal and Liver Physiology*, *310*(6), G439–G447. https://doi.org/10.1152/AJPGI.00368.2015/ASSET/IMAGES/LARGE/ZH30061670550005.JPEG

Barichella, M., Pacchetti, C., Bolliri, C., Cassani, E., Iorio, L., Pusani, C., Pinelli, G., Privitera, G., Cesari, I., Faierman, S. A., Caccialanza, R., Pezzoli, G., & Cereda, E. (2016). Probiotics and prebiotic fiber for constipation associated with Parkinson disease. *Neurology*, *87*(12), 1274–1280. https://doi.org/10.1212/WNL.0000000000003127

Barichella, M., Severgnini, M., Cilia, R., Cassani, E., Bolliri, C., Caronni, S., Ferri, V., Cancello, R., Ceccarani, C., Faierman, S., Pinelli, G., De Bellis, G., Zecca, L., Cereda, E., Consolandi, C., & Pezzoli, G. (2019). Unraveling gut microbiota in Parkinson's disease and atypical parkinsonism. *Movement Disorders*, *34*(3), 396–405. https://doi.org/10.1002/mds.27581

Barrilero, R., Gil, M., Amigó, N., Dias, C. B., Wood, L. G., Garg, M. L., Ribalta, J., Heras, M., Vinaixa, M., & Correig, X. (2018). LipSpin: A New Bioinformatics Tool for Quantitative 1H NMR Lipid Profiling. *Analytical Chemistry*, *90*(3), 2031–2040. https://doi.org/10.1021/ACS.ANALCHEM.7B04148/SUPPL_FILE/AC7B04148_SI_001.PDF

Basolo, A., Salvetti, G., Giannese, D., Genzano, S. B., Ceccarini, G., Giannini, R., Sotgia, G., Fierabracci, P., Piaggi, P., & Santini, F. (2023). Obesity, Hyperfiltration, and Early Kidney Damage: A New Formula for the Estimation of Creatinine Clearance. *The Journal of Clinical Endocrinology and Metabolism*, *108*(12), 3280. https://doi.org/10.1210/CLINEM/DGAD330

Bassil, F., Delamarre, A., Canron, M. H., Dutheil, N., Vital, A., Négrier-Leibreich, M. L., Bezard, E., Fernagut, P. O., & Meissner, W. G. (2022). Impaired brain insulin signalling in Parkinson's disease. *Neuropathology and Applied Neurobiology*, *48*(1), e12760. https://doi.org/10.1111/NAN.12760

Batterham, R. L., Cowley, M. A., Small, C. J., Herzog, H., Cohen, M. A., Dakin, C. L., Wren, A. M., Brynes, A. E., Low, M. J., Ghatei, M. A., Cone, R. D., & Bloom, S. R. (2002). Gut hormone PYY3-36 physiologically inhibits food intake. *Nature 2002 418:6898*, *418*(6898), 650–654. https://doi.org/10.1038/nature00887

Beach, T. G., Adler, C. H., Sue, L. I., Vedders, L., Lue, L. F., White, C. L., Akiyama, H., Caviness, J. N., Shill, H. A., Sabbagh, M. N., & Walker, D. G. (2010). Multi-organ distribution of phosphorylated α-synuclein histopathology in subjects with Lewy body disorders. *Acta Neuropathologica*, *119*(6), 689–702. https://doi.org/10.1007/S00401-010-0664-3/TABLES/7

Beach, T. G., Sue, L. I., Walker, D. G., Lue, L. F., Connor, D. J., Caviness, J. N., Sabbagh, M. N., & Adler, C. H. (2007). Marked microglial reaction in normal aging human substantia nigra: Correlation with extraneuronal neuromelanin pigment deposits. *Acta Neuropathologica*, *114*(4), 419–424. https://doi.org/10.1007/S00401-007-0250-5/METRICS

Beach, T. G., Walker, D. G., Sue, L. I., Newell, A., Adler, C. C., & Joyce, J. N. (2004). Substantia Nigra Marinesco Bodies Are Associated with Decreased Striatal Expression of Dopaminergic Markers. *Journal of Neuropathology and Experimental Neurology*, *63*(4), 329–337. https://doi.org/10.1093/JNEN/63.4.329

Bedarf, J. R., Hildebrand, F., Coelho, L. P., Sunagawa, S., Bahram, M., Goeser, F., Bork, P., & Wüllner, U. (2017). Functional implications of microbial and viral gut metagenome changes in early stage L-DOPA-naïve Parkinson's disease patients. *Genome Medicine*, *9*(1), 39. https://doi.org/10.1186/s13073-017-0428-y

Bedarf, J. R., Romano, S., Heinzmann, S. S., Duncan, A., Traka, M. H., Ng, D., Segovia-Lizano, D., Simon, M.-C., Narbad, A., Wüllner, U., & Hildebrand, F. (2024). A prebiotic diet intervention can restore faecal short chain fatty acids in Parkinson's Disease yet fails to restore the gut microbiome homeostasis. *MedRxiv*, 2024.09.09.24313184. https://doi.org/10.1101/2024.09.09.24313184

Bell, D., Bell, A. H., Weber, R. S., & Hanna, E. Y. (2024). Intestinal-Type Adenocarcinoma in Head and Neck: Dissecting Oncogenic Gene Alterations Through Whole Transcriptome and Exome Analysis. *Modern Pathology*, *37*(1), 100372. https://doi.org/10.1016/J.MODPAT.2023.100372

Ben-Shlomo, Y., Darweesh, S., Llibre-Guerra, J., Marras, C., San Luciano, M., & Tanner, C. (2024). The epidemiology of Parkinson's disease. *The Lancet*, *403*(10423), 283–292. https://doi.org/10.1016/S0140-6736(23)01419-8

Beraldi, E. J., Borges, S. C., de Almeida, F. L. A., dos Santos, A., Saad, M. J. A., & Buttow, N. C. (2020). Colonic neuronal loss and delayed motility induced by high-fat diet occur independently of changes in the major groups of microbiota in Swiss mice. *Neurogastroenterology & Motility*, *32*(2), e13745. https://doi.org/10.1111/NMO.13745

Beraldi, E. J., Soares, A., Borges, S. C., de Souza, A. C. da S., Natali, M. R. M., Bazotte, R. B., & Buttow, N. C. (2015). High-fat diet promotes neuronal loss in the myenteric plexus of the large intestine in mice. *Digestive Diseases and Sciences*, *60*(4), 841–849. https://doi.org/10.1007/S10620-014-3402-1

Béreau, M., Fleury, V., Bouthour, W., Castrioto, A., Lhommée, E., & Krack, P. (2018). Hyperdopaminergic behavioral spectrum in Parkinson's disease: A review. *Revue Neurologique*, *174*(9), 653–663. https://doi.org/10.1016/J.NEUROL.2018.07.005

Berg, D., Borghammer, P., Fereshtehnejad, S. M., Heinzel, S., Horsager, J., Schaeffer, E., & Postuma, R. B. (2021). Prodromal Parkinson disease subtypes — key to understanding heterogeneity. *Nature Reviews Neurology 2021 17:6*, *17*(6), 349–361. https://doi.org/10.1038/s41582-021-00486-9

Berry, C., La Vecchia, C., & Nicotera, P. (2010). Paraquat and Parkinson's disease. *Cell Death & Differentiation 2010 17:7*, *17*(7), 1115–1125. https://doi.org/10.1038/cdd.2009.217

Betarbet, R., Sherer, T. B., MacKenzie, G., Garcia-Osuna, M., Panov, A. V., & Greenamyre, J. T. (2000). Chronic systemic pesticide exposure reproduces features of Parkinson's disease. *Nature Neuroscience 2000 3:12*, *3*(12), 1301–1306. https://doi.org/10.1038/81834

Bezard, E., & Przedborski, S. (2011). A tale on animal models of Parkinson's disease. *Movement Disorders*, *26*(6), 993–1002. https://doi.org/10.1002/MDS.23696

Bialecka, M., Kurzawski, M., Klodowska-Duda, G., Opala, G., Juzwiak, S., Kurzawski, G., Tan, E. K., & Drozdzik, M. (2007). CARD15 variants in patients with sporadic Parkinson's disease. *Neuroscience Research*, *57*(3), 473–476. https://doi.org/10.1016/J.NEURES.2006.11.012

Bido, S., Muggeo, S., Massimino, L., Marzi, M. J., Giannelli, S. G., Melacini, E., Nannoni, M., Gambarè, D., Bellini, E., Ordazzo, G., Rossi, G., Maffezzini, C., Iannelli, A., Luoni, M., Bagicaluppi, M., Gregori, S., Nicassio, F., & Broccoli, V. (2021). Microglia-specific overexpression of α-synuclein leads to severe dopaminergic neurodegeneration by phagocytic exhaustion and oxidative toxicity. *Nature Communications 2021 12:1*, *12*(1), 1–15. https://doi.org/10.1038/s41467-021-26519-x

Bisaglia, M. (2022). Mediterranean Diet and Parkinson's Disease. *International Journal of Molecular Sciences*, *24*(1), 42. https://doi.org/10.3390/IJMS24010042

Bittencourt, A., Brum, P. O., Ribeiro, C. T., Gasparotto, J., Bortolin, R. C., de Vargas, A. R., Heimfarth, L., de Almeida, R. F., Moreira, J. C. F., de Oliveira, J., & Gelain, D. P. (2022). High fat diet-induced obesity causes a reduction in brain tyrosine hydroxylase levels and non-motor features in rats through metabolic dysfunction, neuroinflammation and oxidative stress. *Nutritional Neuroscience*, *25*(5), 1026–1040. https://doi.org/10.1080/1028415X.2020.1831261

Blacher, E., Bashiardes, S., Shapiro, H., Rothschild, D., Mor, U., Dori-Bachash, M., Kleimeyer, C., Moresi, C., Harnik, Y., Zur, M., Zabari, M., Brik, R. B. Z., Kviatcovsky, D., Zmora, N., Cohen, Y., Bar, N., Levi, I., Amar, N., Mehlman, T., … Elinav, E. (2019). Potential roles of gut microbiome and metabolites in modulating ALS in mice. *Nature 2019 572:7770*, *572*(7770), 474–480. https://doi.org/10.1038/s41586-019-1443-5

Blake, M. R., Raker, J. M., & Whelan, K. (2016). Validity and reliability of the Bristol Stool Form Scale in healthy adults and patients with diarrhoea-predominant irritable bowel syndrome. *Alimentary Pharmacology & Therapeutics*, *44*(7), 693–703. https://doi.org/10.1111/APT.13746

Blesa, J., & Przedborski, S. (2014). Parkinson's disease: Animal models and dopaminergic cell vulnerability. *Frontiers in Neuroanatomy*, *8*(DEC), 123289. https://doi.org/10.3389/FNANA.2014.00155/BIBTEX

Blin, J., Gautier, C., Aubert, P., Durand, T., Oullier, T., Aymeric, L., Naveilhan, P., Masson, D., Neunlist, M., & Bach-Ngohou, K. (2023). Psychological stress induces an increase in cholinergic enteric neuromuscular pathways mediated by glucocorticoid receptors. *Frontiers in Neuroscience*, *17*, 1100473. https://doi.org/10.3389/FNINS.2023.1100473/BIBTEX

Block, M. L., Zecca, L., & Hong, J. S. (2007). Microglia-mediated neurotoxicity: uncovering the molecular mechanisms. *Nature Reviews Neuroscience 2007 8:1*, *8*(1), 57–69. https://doi.org/10.1038/nrn2038

Blocq, P., Marinesco, G., & Mott, F. W. (1893). *Sur un cas de tremblement parkinsonien hémiplégique : symptomatique d'une tumeur du pédoncule cérébral.* (G. Masson).

Bloem, B. R., & Boonstra, T. A. (2023). The inadequacy of current pesticide regulations for protecting brain health: the case of glyphosate and Parkinson's disease. *The Lancet Planetary Health*, *7*(12), e948–e949. https://doi.org/10.1016/S2542-5196(23)00255-3

Bobot, M., Thomas, L., Moyon, A., Fernandez, S., McKay, N., Balasse, L., Garrigue, P., Brige, P., Chopinet, S., Poitevin, S., Cérini, C., Brunet, P., Dignat-George, F., Burtey, S., Guillet, B., & Hache, G. (2020). Uremic toxic blood-brain barrier disruption mediated by AhR activation leads to cognitive impairment during experimental renal dysfunction. *Journal of the American Society of Nephrology*, *31*(7), 1509–1521. https://doi.org/10.1681/ASN.2019070728

Boehme, M., Guzzetta, K. E., Bastiaanssen, T. F. S., van de Wouw, M., Moloney, G. M., Gual-Grau, A., Spichak, S., Olavarría-Ramírez, L., Fitzgerald, P., Morillas, E., Ritz, N. L., Jaggar, M., Cowan, C. S. M., Crispie, F., Donoso, F., Halitzki, E., Neto, M. C., Sichetti, M., Golubeva, A. V., … Cryan, J. F. (2021). Microbiota from young mice counteracts selective age-associated behavioral deficits. *Nature Aging 2021 1:8*, *1*(8), 666–676. https://doi.org/10.1038/s43587-021-00093-9

Bolyen, E., Rideout, J. R., Dillon, M. R., Bokulich, N. A., Abnet, C. C., Al-Ghalith, G. A., Alexander, H., Alm, E. J., Arumugam, M., Asnicar, F., Bai, Y., Bisanz, J. E., Bittinger, K., Brejnrod, A., Brislawn, C. J., Brown, C. T., Callahan, B. J., Caraballo-Rodríguez, A. M., Chase, J., … Caporaso, J. G. (2019). Reproducible, interactive, scalable and extensible microbiome data science using QIIME 2. *Nature Biotechnology 2019 37:8*, *37*(8), 852–857. https://doi.org/10.1038/s41587-019-0209-9

Bonaz, B., Bazin, T., & Pellissier, S. (2018). The vagus nerve at the interface of the microbiota-gut-brain axis. In *Frontiers in Neuroscience* (Vol. 12, Issue FEB, p. 49). Frontiers Media S.A. https://doi.org/10.3389/fnins.2018.00049

Bonaz, B., Sinniger, V., & Pellissier, S. (2017). The vagus nerve in the neuro-immune axis: Implications in the pathology of the gastrointestinal tract. *Frontiers in Immunology*, *8*(NOV), 293876. https://doi.org/10.3389/FIMMU.2017.01452/BIBTEX

Boncuk Ulaş, S., Güzey Aras, Y., Irmak Gözükara, S., Acar, T., & Acar, B. A. (2023). Correlates of Zonulin and Claudin-5, markers of intestinal and brain endothelial permeability, in Parkinson's Disease: A pilot study. *Parkinsonism and Related Disorders*, *110*. https://doi.org/10.1016/j.parkreldis.2023.105361

Borghammer, P. (2018). How does parkinson's disease begin? Perspectives on neuroanatomical pathways, prions, and histology. *Movement Disorders*, *33*(1), 48–57. https://doi.org/10.1002/mds.27138

Borghammer, P. (2021). The α-Synuclein Origin and Connectome Model (SOC Model) of Parkinson's Disease: Explaining Motor Asymmetry, Non-Motor Phenotypes, and Cognitive Decline. *Journal of Parkinson's Disease*, *11*(2), 455–474. https://doi.org/10.3233/JPD-202481/ASSET/IMAGES/10.3233_JPD-202481-FIG6.JPG

Borghammer, P. (2023). The brain-first vs. body-first model of Parkinson's disease with comparison to alternative models. *Journal of Neural Transmission 2023 130:6*, *130*(6), 737–753. https://doi.org/10.1007/S00702-023-02633-6

Borghammer, P., Just, M. K., Horsager, J., Skjærbæk, C., Raunio, A., Kok, E. H., Savola, S., Murayama, S., Saito, Y., Myllykangas, L., & Van Den Berge, N. (2022). A postmortem study suggests a revision of the dual-hit hypothesis of Parkinson's disease. *Npj Parkinson's Disease 2022 8:1*, *8*(1), 1–11. https://doi.org/10.1038/s41531-022-00436-2

Borghammer, P., & Van Den Berge, N. (2019). Brain-First versus Gut-First Parkinson's Disease: A Hypothesis. *Journal of Parkinson's Disease*, *9*(s2), S281–S295. https://doi.org/10.3233/JPD-191721

Braak, H., Del Tredici, K., Rüb, U., De Vos, R. A. I., Jansen Steur, E. N. H., & Braak, E. (2003). Staging of brain pathology related to sporadic Parkinson's disease. *Neurobiology of Aging*, *24*(2), 197–211. https://doi.org/10.1016/S0197-4580(02)00065-9

Braak, H., Rüb, U., Gai, W. P., & Del Tredici, K. (2003). Idiopathic Parkinson's disease: Possible routes by which vulnerable neuronal types may be subject to neuroinvasion by an unknown pathogen. *Journal of Neural Transmission*, *110*(5), 517–536. https://doi.org/10.1007/s00702-002-0808-2

Brauer, R., Wei, L., Ma, T., Athauda, D., Girges, C., Vijiaratnam, N., Auld, G., Whittlesea, C., Wong, I., & Foltynie, T. (2020). Diabetes medications and risk of Parkinson's disease: a cohort study of patients with diabetes. *Brain : A Journal of Neurology*, *143*(10), 3067–3076. https://doi.org/10.1093/BRAIN/AWAA262

Breasail, M. O., Smith, M. D., Tenison, E., Henderson, E. J., & Lithander, F. E. (2022). Parkinson's disease: the nutrition perspective. *Proceedings of the Nutrition Society*, *81*(1), 12–26. https://doi.org/10.1017/S0029665121003645

Brochard, V., Combadière, B., Prigent, A., Laouar, Y., Perrin, A., Beray-Berthat, V., Bonduelle, O., Alvarez-Fischer, D., Callebert, J., Launay, J. M., Duyckaerts, C., Flavell, R. A., Hirsch, E. C., & Hunot, S. (2009). Infiltration of CD4+ lymphocytes into the brain contributes to neurodegeneration in a mouse model of Parkinson disease. *The Journal of Clinical Investigation*, *119*(1), 182–192. https://doi.org/10.1172/JCI36470

Brodacki, B., Staszewski, J., Toczyłowska, B., Kozłowska, E., Drela, N., Chalimoniuk, M., & Stepien, A. (2008). Serum interleukin (IL-2, IL-10, IL-6, IL-4), TNFα, and INFγ concentrations are elevated in patients with atypical and idiopathic parkinsonism. *Neuroscience Letters*, *441*(2), 158–162. https://doi.org/10.1016/J.NEULET.2008.06.040

Brooks, M. E., Kristensen, K., van Benthem, K. J., Magnusson, A., Berg, C. W., Nielsen, A., Skaug, H. J., Mächler, M., & Bolker, B. M. (2017). glmmTMB balances speed and flexibility among packages for zero-inflated generalized linear mixed modeling. *R Journal*, *9*(2), 378–400. https://doi.org/10.32614/RJ-2017-066

Brouwer, M., Huss, A., van der Mark, M., Nijssen, P. C. G., Mulleners, W. M., Sas, A. M. G., van Laar, T., de Snoo, G. R., Kromhout, H., & Vermeulen, R. C. H. (2017). Environmental exposure to pesticides and the risk of Parkinson's disease in the Netherlands. *Environment International*, *107*, 100–110. https://doi.org/10.1016/J.ENVINT.2017.07.001

Browning, K. N., & Travagli, R. A. (2014). Central Nervous System Control of Gastrointestinal Motility and Secretion and Modulation of Gastrointestinal Functions. *Comprehensive Physiology*, *4*(4), 1339. https://doi.org/10.1002/CPHY.C130055

Bruewer, M., Luegering, A., Kucharzik, T., Parkos, C. A., Madara, J. L., Hopkins, A. M., & Nusrat, A. (2003). Proinflammatory Cytokines Disrupt Epithelial Barrier Function by Apoptosis-Independent Mechanisms. *The Journal of Immunology*, *171*(11), 6164–6172. https://doi.org/10.4049/JIMMUNOL.171.11.6164

Bruewer, M., Utech, M., Ivanov, A. I., Hopkins, A. M., Parkos, C. A., & Nusrat, A. (2005). Interferon-γ induces internalization of epithelial tight junction proteins via a macropinocytosis-like process. *The FASEB Journal*, *19*(8), 923–933. https://doi.org/10.1096/FJ.04-3260COM

Bruggeman, A., Vandendriessche, C., Hamerlinck, H., De Looze, D., Tate, D. J., Vuylsteke, M., De Commer, L., Devolder, L., Raes, J., Verhasselt, B., Laukens, D., Vandenbroucke, R. E., & Santens, P. (2024). Safety and efficacy of faecal microbiota transplantation in patients with mild to moderate Parkinson's disease (GUT-PARFECT): a double-blind, placebo-controlled, randomised, phase 2 trial. *EClinicalMedicine*, *71*. https://doi.org/10.1016/j.eclinm.2024.102563

Burhans, M. S., Hagman, D. K., Kuzma, J. N., Schmidt, K. A., & Kratz, M. (2019). Contribution of Adipose Tissue Inflammation to the Development of Type 2 Diabetes Mellitus. *Comprehensive Physiology*, *9*(1), 1–58. https://doi.org/10.1002/CPHY.C170040

Bush, W. D., Garguilo, J., Zucca, F. A., Albertini, A., Zecca, L., Edwards, G. S., Nemanich, R. J., & Simon, J. D. (2006). The surface oxidation potential of human neuromelanin reveals a spherical architecture with a pheomelanin core and a eumelanin surface. *Proceedings of the National Academy of Sciences of the United States of America*, *103*(40), 14785–14789. https://doi.org/10.1073/PNAS.0604010103/ASSET/2650CC78-ADD1-4198-9380-7266659B85B3/ASSETS/GRAPHIC/ZPQ04006-3608-M02.JPEG

Butkovich, L. M., Houser, M. C., Chalermpalanupap, T., Porter-Stransky, K. A., Iannitelli, A. F., Boles, J. S., Lloyd, G. M., Coomes, A. S., Eidson, L. N., De Sousa Rodrigues, M. E., Oliver, D. L., Kelly, S. D., Chang, J., Bengoa-Vergniory, N., Wade-Martins, R., Giasson, B. I., Joers, V., Weinshenker, D., & Tansey, M. G. (2020). Transgenic Mice Expressing Human α-Synuclein in Noradrenergic Neurons Develop Locus Ceruleus Pathology and Nonmotor Features of Parkinson's Disease. *The Journal of Neuroscience*, *40*(39), 7559. https://doi.org/10.1523/JNEUROSCI.1468-19.2020

Calabrese, V., Santoro, A., Monti, D., Crupi, R., Di Paola, R., Latteri, S., Cuzzocrea, S., Zappia, M., Giordano, J., Calabrese, E. J., & Franceschi, C. (2018). Aging and Parkinson's Disease: Inflammaging, neuroinflammation and biological remodeling as key factors in pathogenesis. *Free Radical Biology and Medicine*, *115*, 80–91. https://doi.org/10.1016/J.FREERADBIOMED.2017.10.379

Calabresi, P., Mechelli, A., Natale, G., Volpicelli-Daley, L., Di Lazzaro, G., & Ghiglieri, V. (2023). Alpha-synuclein in Parkinson's disease and other synucleinopathies: from overt neurodegeneration back to early synaptic dysfunction. *Cell Death & Disease 2023 14:3*, *14*(3), 1–16. https://doi.org/10.1038/s41419-023-05672-9

Callahan, B. J., McMurdie, P. J., Rosen, M. J., Han, A. W., Johnson, A. J. A., & Holmes, S. P. (2016). DADA2: High-resolution sample inference from Illumina amplicon data. *Nature Methods 2016 13:7*, *13*(7), 581–583. https://doi.org/10.1038/nmeth.3869

Camargo, S. M. R., & Verrey, F. (2014). The Molecular Mechanism of Intestinal Levodopa Absorption and Its Possible Implications for the Treatment of Parkinson's Disease. *Article in Journal of Pharmacology and Experimental Therapeutics*. https://doi.org/10.1124/jpet.114.216317

Cândido, T. L. N., Bressan, J., & Alfenas, R. de C. G. (2018). Dysbiosis and metabolic endotoxemia induced by high-fat diet. *Nutricion Hospitalaria*, *35*(6), 1432–1440. https://doi.org/10.20960/NH.1792

Cani, P. D., Depommier, C., Derrien, M., Everard, A., & de Vos, W. M. (2022). Akkermansia muciniphila: paradigm for next-generation beneficial microorganisms. *Nature Reviews Gastroenterology & Hepatology 2022 19:10*, *19*(10), 625–637. https://doi.org/10.1038/s41575-022-00631-9

Cantu-Jungles, T. M., Rasmussen, H. E., & Hamaker, B. R. (2019). Potential of prebiotic butyrogenic fibers in Parkinson's disease. In *Frontiers in Neurology* (Vol. 10, Issue JUN, p. 663). Frontiers Media S.A. https://doi.org/10.3389/fneur.2019.00663

Capaldo, C. T., & Nusrat, A. (2008). Cytokine regulation of tight junctions. *Biochimica et Biophysica Acta*, *1788*(4), 864. https://doi.org/10.1016/J.BBAMEM.2008.08.027

Carabotti, M., Scirocco, A., Maselli, M. A., & Severi, C. (2015). The gut-brain axis: Interactions between enteric microbiota, central and enteric nervous systems. *Annals of Gastroenterology*, *28*(2), 203–209. www.annalsgastro.gr

Carballo-Carbajal, I., Laguna, A., Romero-Giménez, J., Cuadros, T., Bové, J., Martinez-Vicente, M., Parent, A., Gonzalez-Sepulveda, M., Peñuelas, N., Torra, A., Rodríguez-Galván, B., Ballabio, A., Hasegawa, T., Bortolozzi, A., Gelpi, E., & Vila, M. (2019). Brain tyrosinase overexpression implicates age-dependent neuromelanin production in Parkinson's disease pathogenesis. *Nature Communications*, *10*(1), 973. https://doi.org/10.1038/s41467-019-08858-y

Caruso, R., Ono, M., Bunker, M. E., Núñez, G., & Inohara, N. (2019). Dynamic and Asymmetric Changes of the Microbial Communities after Cohousing in Laboratory Mice. *Cell Reports*, *27*(11), 3401-3412.e3. https://doi.org/10.1016/J.CELREP.2019.05.042

Cerri, S., Mus, L., & Blandini, F. (2019a). Parkinson's Disease in Women and Men: What's the Difference? *Journal of Parkinson's Disease*, *9*(3), 501–515. https://doi.org/10.3233/JPD-191683

Cerri, S., Mus, L., & Blandini, F. (2019b). Parkinson's Disease in Women and Men: What's the Difference? *Journal of Parkinson's Disease*, *9*(3), 501. https://doi.org/10.3233/JPD-191683

Chade, A. R., Kasten, M., & Tanner, C. M. (2006). Nongenetic causes of Parkinson's disease. *Journal of Neural Transmission, Supplement*, *70*, 147–151. https://doi.org/10.1007/978-3-211-45295-0_23

Chagas, Y. W., Vaz de Castro, P. A. S., & Simões-e-Silva, A. C. (2025). Neuroinflammation in kidney disease and dialysis. *Behavioural Brain Research*, *483*, 115465. https://doi.org/10.1016/J.BBR.2025.115465

Chagnac, A., Weinstein, T., Herman, M., Hirsh, J., Gafter, U., & Ori, Y. (2003). The effects of weight loss on renal function in patients with severe obesity. *Journal of the American Society of Nephrology : JASN*, *14*(6), 1480–1486. https://doi.org/10.1097/01.ASN.0000068462.38661.89

Chagnac, A., Weinstein, T., Korzets, A., Ramadan, E., Hirsch, J., & Gafter, U. (2000). Glomerular hemodynamics in severe obesity. *American Journal of Physiology - Renal Physiology*, *278*(5 47-5). https://doi.org/10.1152/AJPRENAL.2000.278.5.F817/ASSET/IMAGES/LARGE/AFLU20504003BX.JPEG

Challis, C., Hori, A., Sampson, T. R., Yoo, B. B., Challis, R. C., Hamilton, A. M., Mazmanian, S. K., Volpicelli-Daley, L. A., & Gradinaru, V. (2020). Gut-seeded α-synuclein fibrils promote gut dysfunction and brain pathology specifically in aged mice. *Nature Neuroscience*, *23*(3), 327–336. https://doi.org/10.1038/s41593-020-0589-7

Chapman, O. S., & McLean, B. S. (2023). Seasonal and sex-specific changes in the gastrointestinal tracts of Peromyscus maniculatus. *Journal of Mammalogy*, *104*(6), 1364–1376. https://doi.org/10.1093/JMAMMAL/GYAD086

Charcot, J.-M. (1872). Leçons sur les maladies du système nerveux faites à la Salpêtrières. In *A Delahaye, Paris* (Issue De la paralysie agitante. In Oeuvres Complètes (t 1)).

Chaudhuri, K. R., Healy, D. G., & Schapira, A. H. V. (2006). Non-motor symptoms of Parkinson's disease: diagnosis and management. *The Lancet Neurology*, *5*(3), 235–245. https://doi.org/10.1016/S1474-4422(06)70373-8

Chen, H., Jacobs, E., Schwarzschild, M. A., McCullough, M. L., Calle, E. E., Thun, M. J., & Ascherio, A. (2005). Nonsteroidal antiinflammatory drug use and the risk for Parkinson's disease. *Annals of Neurology*, *58*(6), 963–967. https://doi.org/10.1002/ANA.20682

Chen, J., Guan, Z., Wang, L., Song, G., Ma, B., & Wang, Y. (2014). Meta-Analysis: Overweight, Obesity, and Parkinson's Disease. *International Journal of Endocrinology*, *2014*, 203930. https://doi.org/10.1155/2014/203930

Chen, J., Muntner, P., Hamm, L. L., Jones, D. W., Batuman, V., Fonseca, V., Whelton, P. K., & He, J. (2004). The Metabolic Syndrome and Chronic Kidney Disease in U.S. Adults. *Annals of Internal Medicine*, *140*(3). https://doi.org/10.7326/0003-4819-140-3-200402030-00007

Chen, S. G., Stribinskis, V., Rane, M. J., Demuth, D. R., Gozal, E., Roberts, A. M., Jagadapillai, R., Liu, R., Choe, K., Shivakumar, B., Son, F., Jin, S., Kerber, R., Adame, A., Masliah, E., & Friedland, R. P. (2016). Exposure to the Functional Bacterial Amyloid Protein Curli Enhances Alpha-Synuclein Aggregation in Aged Fischer 344 Rats and Caenorhabditis elegans. *Scientific Reports*, *6*(1), 1–10. https://doi.org/10.1038/srep34477

Chen, S. J., Chen, C. C., Liao, H. Y., Lin, Y. T., Wu, Y. W., Liou, J. M., Wu, M. S., Kuo, C. H., & Lin, C. H. (2022). Association of Fecal and Plasma Levels of Short-Chain Fatty Acids with Gut Microbiota and Clinical Severity in Patients with Parkinson Disease. *Neurology*, *98*(8), E848–E858. https://doi.org/10.1212/WNL.0000000000013225/ASSET/A5D7B1FA-45C5-4663-89B3-6707FA7B28DB/ASSETS/GRAPHIC/11TTU1.JPEG

Chen, Y., Sun, X., Lin, Y., Zhang, Z., Gao, Y., & Wu, I. X. Y. (2021). Non-Genetic Risk Factors for Parkinson's Disease: An Overview of 46 Systematic Reviews. *Journal of Parkinson's Disease*, *11*(3), 919–935. https://doi.org/10.3233/JPD-202521/ASSET/IMAGES/10.3233_JPD-202521-FIG2.JPG

Chernova, V. O., Terveer, E. M., van Prehn, J., Kuijper, E. J., Keller, J. J., van der Meulen-de Jong, A. E., Bauer, M. P., van Hilten, J. J., & Contarino, M. F. (2023). Fecal microbiota transplantation for Parkinson's disease using levodopa - carbidopa intestinal gel percutaneous endoscopic gastro-jejeunal tube. *Parkinsonism & Related Disorders*, *111*. https://doi.org/10.1016/J.PARKRELDIS.2023.105410

Chhabra, K. H., Adams, J. M., Fagel, B., Lam, D. D., Qi, N., Rubinstein, M., & Low, M. J. (2016). Hypothalamic POMC Deficiency Improves Glucose Tolerance Despite Insulin Resistance by Increasing Glycosuria. *Diabetes*, *65*(3), 660–672. https://doi.org/10.2337/DB15-0804

Chhabra, K. H., Morgan, D. A., Tooke, B. P., Adams, J. M., Rahmouni, K., & Low, M. J. (2017). Reduced renal sympathetic nerve activity contributes to elevated glycosuria and improved glucose tolerance in hypothalamus-specific Pomc knockout mice. *Molecular Metabolism*, *6*(10), 1274–1285. https://doi.org/10.1016/J.MOLMET.2017.07.005

Choong, C. J., & Mochizuki, H. (2022). Neuropathology of α-synuclein in Parkinson's disease. *Neuropathology*, *42*(2), 93–103. https://doi.org/10.1111/NEUP.12812

Chrysafi, P., Perakakis, N., Farr, O. M., Stefanakis, K., Peradze, N., Sala-Vila, A., & Mantzoros, C. S. (2020). Leptin alters energy intake and fat mass but not energy expenditure in lean subjects. *Nature Communications 2020 11:1*, *11*(1), 1–15. https://doi.org/10.1038/s41467-020-18885-9

Chung, Y. C., Shin, W. H., Baek, J. Y., Cho, E. J., Baik, H. H., Kim, S. R., Won, S. Y., & Jin, B. K. (2016). CB2 receptor activation prevents glial-derived neurotoxic mediator production, BBB leakage and peripheral immune cell infiltration and rescues dopamine neurons in the MPTP model of Parkinson's disease. *Experimental & Molecular Medicine 2016 48:1*, *48*(1), e205–e205. https://doi.org/10.1038/emm.2015.100

Cilia, R., Piatti, M., Cereda, E., Bolliri, C., Caronni, S., Ferri, V., Cassani, E., Bonvegna, S., Ferrarese, C., Zecchinelli, A. L., Barichella, M., & Pezzoli, G. (2020). Does Gut Microbiota Influence the Course of Parkinson's Disease? A 3-Year Prospective Exploratory Study in de novo Patients. *Journal of Parkinson's Disease*, *Preprint*(Preprint), 1–12. https://doi.org/10.3233/jpd-202297

Cirstea, M. S., Yu, A. C., Golz, E., Sundvick, K., Kliger, D., Radisavljevic, N., Foulger, L. H., Mackenzie, M., Huan, T., Brett Finlay, B., & Appel-Cresswell, S. (2020). Microbiota Composition and Metabolism Are Associated With Gut Function in Parkinson's Disease. *Movement Disorders*, mds.28052. https://doi.org/10.1002/mds.28052

Claesson, M. J., Cusack, S., O'Sullivan, O., Greene-Diniz, R., De Weerd, H., Flannery, E., Marchesi, J. R., Falush, D., Dinan, T., Fitzgerald, G., Stanton, C., Van Sinderen, D., O'Connor, M., Harnedy, N., O'Connor, K., Henry, C., O'Mahony, D., Fitzgerald, A. P., Shanahan, F., … O'Toole, P. W. (2011). Composition, variability, and temporal stability of the intestinal microbiota of the elderly. *Proceedings of the National Academy of Sciences of the United States of America*, *108*(SUPPL. 1), 4586–4591. https://doi.org/10.1073/pnas.1000097107

Clairembault, T., Leclair-Visonneau, L., Coron, E., Bourreille, A., Le Dily, S., Vavasseur, F., Heymann, M. F., Neunlist, M., & Derkinderen, P. (2015). Structural alterations of the intestinal epithelial barrier in Parkinson's disease. *Acta Neuropathologica Communications*, *3*, 12. https://doi.org/10.1186/s40478-015-0196-0

Constantinescu, M. (2016). The Enteric Nervous System. . *Gastroenterology*, 23–38.

Corbillé, A. G., Coron, E., Neunlist, M., Derkinderen, P., & Lebouvier, T. (2014). Appraisal of the dopaminergic and noradrenergic innervation of the submucosal plexus in PD. *Journal of Parkinson's Disease*, *4*(4), 571–576. https://doi.org/10.3233/JPD-140422

Cormier, R. (2023). Role of phospholipase A2s in gastrointestinal cancer. *Phospholipases in Physiology and Pathology: Volumes 1-7*, *3*, 125–144. https://doi.org/10.1016/B978-0-323-95697-0.00011-X

Corsetti, M., Costa, M., Bassotti, G., Bharucha, A. E., Borrelli, O., Dinning, P., Di Lorenzo, C., Huizinga, J. D., Jimenez, M., Rao, S., Spiller, R., Spencer, N. J., Lentle, R., Pannemans, J., Thys, A., Benninga, M., & Tack, J. (2019). First translational consensus on terminology and definitions of colonic motility in animals and humans studied by manometric and other techniques. *Nature Reviews Gastroenterology & Hepatology 2019 16:9*, *16*(9), 559–579. https://doi.org/10.1038/s41575-019-0167-1

Cribari-Neto, F., & Zeileis, A. (2010). Beta Regression in *R*. *Journal of Statistical Software*, *34*(2), 1–24. https://doi.org/10.18637/jss.v034.i02

Cryan, J. F., O'riordan, K. J., Cowan, C. S. M., Sandhu, K. V., Bastiaanssen, T. F. S., Boehme, M., Codagnone, M. G., Cussotto, S., Fulling, C., Golubeva, A. V., Guzzetta, K. E., Jaggar, M., Long-Smith, C. M., Lyte, J. M., Martin, J. A., Molinero-Perez, A., Moloney, G., Morelli, E., Morillas, E., … Dinan, T. G. (2019). The microbiota-gut-brain axis. *Physiological Reviews*, *99*(4), 1877–2013. https://doi.org/10.1152/physrev.00018.2018

Cullinane, P. W., de Pablo Fernandez, E., König, A., Outeiro, T. F., Jaunmuktane, Z., & Warner, T. T. (2023). Type 2 Diabetes and Parkinson's Disease: A Focused Review of Current Concepts. *Movement Disorders*, *38*(2), 162–177. https://doi.org/10.1002/MDS.29298

Cuvelier, E., Méquinion, M., Leghay, C., Sibran, W., Stievenard, A., Sarchione, A., Bonte, M. A., Vanbesien-Mailliot, C., Viltart, O., Saitoski, K., Caron, E., Labarthe, A., Comptdaer, T., Semaille, P., Carrié, H., Mutez, E., Gressier, B., Destée, A., Chartier-Harlin, M. C., & Belarbi, K. (2018). Overexpression of Wild-Type Human Alpha-Synuclein Causes Metabolism Abnormalities in Thy1-aSYN Transgenic Mice. *Frontiers in Molecular Neuroscience*, *11*, 379807. https://doi.org/10.3389/FNMOL.2018.00321/BIBTEX

D'Alessio, D. (2016). Is GLP-1 a hormone: Whether and When? *Journal of Diabetes Investigation*, *7*, 50–55. https://doi.org/10.1111/JDI.12466

D'Amato, R. J., Lipman, Z. P., & Snyder, S. H. (1986). Selectivity of the Parkinsonian Neurotoxin MPTP: Toxic Metabolite MPP+ Binds to Neuromelanin. *Science*, *231*(4741), 987–989. https://doi.org/10.1126/SCIENCE.3080808

Dang, Y., Ma, C., Chen, K., Chen, Y., Jiang, M., Hu, K., Li, L., Zeng, Z., & Zhang, H. (2023). The Effects of a High-Fat Diet on Inflammatory Bowel Disease. *Biomolecules 2023, Vol. 13, Page 905*, *13*(6), 905. https://doi.org/10.3390/BIOM13060905

Dashtipour, K., Tafreshi, A., Lee, J., & Crawley, B. (2018). Speech Disorders in Parkinson's Disease: Pathophysiology, Medical Management and Surgical Approaches. *Neurodegenerative Disease Management*, *8*(5), 337–348. https://doi.org/10.2217/NMT-2018-0021

Dautan, D., Paslawski, W., Montejo, S., Doyon, D., Marangiu, R., Kaplitt, M. G., Chen, R., Dawson, V. L., Zhang, X., Dawson, T. M., & Svenningsson, P. (2024). Gut-Initiated Alpha Synuclein Fibrils Drive Parkinson's Disease Phenotypes: Temporal Mapping of non-Motor Symptoms and REM Sleep Behavior Disorder. *BioRxiv : The Preprint Server for Biology*. https://doi.org/10.1101/2024.04.22.590542

Dawson, T. M., Golde, T. E., & Lagier-Tourenne, C. (2018). Animal models of neurodegenerative diseases. *Nature Neuroscience 2018 21:10*, *21*(10), 1370–1379. https://doi.org/10.1038/s41593-018-0236-8

d'Azyr, F. V. (1786). *Traite d'anatomie et de physiologie* (Didot, Vol. 1).

De Lau, L. M. L., Bornebroek, M., Witteman, J. C. M., Hofman, A., Koudstaal, P. J., & Breteler, M. M. B. (2005). Dietary fatty acids and the risk of Parkinson disease: The Rotterdam Study. *Neurology*, *64*(12), 2040–2045. https://doi.org/10.1212/01.WNL.0000166038.67153.9F

De Lucia, N., Peluso, S., Esposito, M., Masi, A., Saccà, F., Bruzzese, D., De Michele, G., & De Rosa, A. (2020). Frontal defect contribution to decreasing of body mass index in Parkinson's disease patients. *Journal of Clinical Neuroscience*, *72*, 229–232. https://doi.org/10.1016/j.jocn.2019.11.034

De Pablo-Fernández, E., Breen, D. P., Bouloux, P. M., Barker, R. A., Foltynie, T., & Warner, T. T. (2017). Neuroendocrine abnormalities in Parkinson's disease. *Journal of Neurology, Neurosurgery & Psychiatry*, *88*(2), 176–185. https://doi.org/10.1136/JNNP-2016-314601

De Silva, A., Salem, V., Long, C. J., Makwana, A., Newbould, R. D., Rabiner, E. A., Ghatei, M. A., Bloom, S. R., Matthews, P. M., Beaver, J. D., & Dhillo, W. S. (2011). The Gut Hormones PYY3-36 and GLP-17-36 amide Reduce Food Intake and Modulate Brain Activity in Appetite Centers in Humans. *Cell Metabolism*, *14*(5), 700–706. https://doi.org/10.1016/J.CMET.2011.09.010

De Souza, C. T., Araujo, E. P., Bordin, S., Ashimine, R., Zollner, R. L., Boschero, A. C., Saad, M. J. A., & Velloso, L. A. (2005). Consumption of a Fat-Rich Diet Activates a Proinflammatory Response and Induces Insulin Resistance in the Hypothalamus. *Endocrinology*, *146*(10), 4192–4199. https://doi.org/10.1210/EN.2004-1520

de Souza Cordeiro, L. M., Bainbridge, L., Devisetty, N., McDougal, D. H., Peters, D. J. M., & Chhabra, K. H. (2022). Loss of function of renal Glut2 reverses hyperglycaemia and normalises body weight in mouse models of diabetes and obesity. *Diabetologia*, *65*(6), 1032. https://doi.org/10.1007/S00125-022-05676-8

Del Rey, N. L. G., Quiroga-Varela, A., Garbayo, E., Carballo-Carbajal, I., Fernández-Santiago, R., Monje, M. H. G., Trigo-Damas, I., Blanco-Prieto, M. J., & Blesa, J. (2018). Advances in parkinson's disease: 200

years later. *Frontiers in Neuroanatomy*, *12*, 425800. https://doi.org/10.3389/FNANA.2018.00113/BIBTEX

Demailly, A., Moreau, C., & Devos, D. (2024). Effectiveness of Continuous Dopaminergic Therapies in Parkinson's Disease: A Review of L-DOPA Pharmacokinetics/Pharmacodynamics. *Journal of Parkinson's Disease*, *14*(5), 925–939. https://doi.org/10.3233/JPD-230372/ASSET/IMAGES/10.3233_JPD-230372-IMG1.JPG

Den Besten, G., Van Eunen, K., Groen, A. K., Venema, K., Reijngoud, D. J., & Bakker, B. M. (2013). The role of short-chain fatty acids in the interplay between diet, gut microbiota, and host energy metabolism. *Journal of Lipid Research*, *54*(9), 2325. https://doi.org/10.1194/JLR.R036012

Den hartog jager, W. A., & Bethlem, J. (1960). THE DISTRIBUTION OF LEWY BODIES IN THE CENTRAL AND AUTONOMIC NERVOUS SYSTEMS IN IDIOPATHIC PARALYSIS AGITANS. *Journal of Neurology, Neurosurgery, and Psychiatry*, *23*(4), 283. https://doi.org/10.1136/JNNP.23.4.283

DENG, G., VAZIRI, N. D., JABBARI, B., NI, Z., & YAN, X.-X. (2001). Increased Tyrosine Nitration of the Brain in Chronic Renal Insufficiency. *Journal of the American Society of Nephrology*, *12*(9), 1892–1899. https://doi.org/10.1681/ASN.V1291892

Derrien, M., Van Baarlen, P., Hooiveld, G., Norin, E., Müller, M., & de Vos, W. M. (2011). Modulation of mucosal immune response, tolerance, and proliferation in mice colonized by the mucin-degrader Akkermansia muciniphila. *Frontiers in Microbiology*, *2*(AUG), 10940. https://doi.org/10.3389/FMICB.2011.00166/BIBTEX

Desai, M. S., Seekatz, A. M., Koropatkin, N. M., Kamada, N., Hickey, C. A., Wolter, M., Pudlo, N. A., Kitamoto, S., Terrapon, N., Muller, A., Young, V. B., Henrissat, B., Wilmes, P., Stappenbeck, T. S., Núñez, G., & Martens, E. C. (2016). A Dietary Fiber-Deprived Gut Microbiota Degrades the Colonic Mucus Barrier and Enhances Pathogen Susceptibility. *Cell*, *167*(5), 1339-1353.e21. https://doi.org/10.1016/J.CELL.2016.10.043/ATTACHMENT/44648B92-C9AB-4773-9950-347AF836AAF8/MMC7.XLSX

Desmet, A. S., Cirillo, C., Tack, J., Vandenberghe, W., & Berghe, P. Vanden. (2017). Live calcium and mitochondrial imaging in the enteric nervous system of parkinson patients and controls. *ELife*, *6*. https://doi.org/10.7554/ELIFE.26850

Devos, D., Lebouvier, T., Lardeux, B., Biraud, M., Rouaud, T., Pouclet, H., Coron, E., Bruley des Varannes, S., Naveilhan, P., Nguyen, J. M., Neunlist, M., & Derkinderen, P. (2013). Colonic inflammation in Parkinson's disease. *Neurobiology of Disease*, *50*(1), 42–48. https://doi.org/10.1016/j.nbd.2012.09.007

Di Lazzaro, G., Picca, A., Boldrini, S., Bove, F., Marzetti, E., Petracca, M., Piano, C., Bentivoglio, A. R., & Calabresi, P. (2024). Differential profiles of serum cytokines in Parkinson's disease according to disease duration. *Neurobiology of Disease*, *190*, 106371. https://doi.org/10.1016/J.NBD.2023.106371

Di Liddo, R., Piccione, M., Schrenk, S., Dal Magro, C., Cosma, C., Padoan, A., Contran, N., Scapellato, M. L., Pagetta, A., Romano Spica, V., Conconi, M. T., Parnigotto, P. P., D'Incà, R., & Michetti, F. (2020).

S100B as a new fecal biomarker of inflammatory bowel diseases. *European Review for Medical and Pharmacological Sciences*, *24*(1), 323–332. https://doi.org/10.26355/EURREV_202001_19929

Di Tommaso, N., Gasbarrini, A., & Ponziani, F. R. (2021). Intestinal Barrier in Human Health and Disease. *International Journal of Environmental Research and Public Health 2021, Vol. 18, Page 12836*, *18*(23), 12836. https://doi.org/10.3390/IJERPH182312836

Di Vincenzo, F., Del Gaudio, A., Petito, V., Lopetuso, L. R., & Scaldaferri, F. (2024). Gut microbiota, intestinal permeability, and systemic inflammation: a narrative review. *Internal and Emergency Medicine*, *19*(2), 275–293. https://doi.org/10.1007/S11739-023-03374-W/FIGURES/2

Dickson, D. W. (2012). Parkinson's Disease and Parkinsonism: Neuropathology. *Cold Spring Harbor Perspectives in Medicine*, *2*(8), a009258. https://doi.org/10.1101/CSHPERSPECT.A009258

Dinan, T. G., Cryan, J. F., Dinan, T. G., Cryan, J. F., & Physiol, J. (2017). Gut instincts: microbiota as a key regulator of brain development, ageing and neurodegeneration. *The Authors. The Journal of Physiology C*, *595*, 489–503. https://doi.org/10.1113/JP273106

Ding, H., Wang, K. yun, Chen, S. yang, Guo, K. W., & Qiu, W. hong. (2023). Validating the role of PTGIS gene in colorectal cancer by bioinformatics analysis and in vitro experiments. *Scientific Reports 2023 13:1*, *13*(1), 1–13. https://doi.org/10.1038/s41598-023-43289-2

Dodiya, H. B., Forsyth, C. B., Voigt, R. M., Engen, P. A., Patel, J., Shaikh, M., Green, S. J., Naqib, A., Roy, A., Kordower, J. H., Pahan, K., Shannon, K. M., & Keshavarzian, A. (2020). Chronic stress-induced gut dysfunction exacerbates Parkinson's disease phenotype and pathology in a rotenone-induced mouse model of Parkinson's disease. *Neurobiology of Disease*, *135*, 104352. https://doi.org/10.1016/J.NBD.2018.12.012

Doherty, K. M., Silveira-Moriyama, L., Parkkinen, L., Healy, D. G., Farrell, M., Mencacci, N. E., Ahmed, Z., Brett, F. M., Hardy, J., Quinn, N., Counihan, T. J., Lynch, T., Fox, Z. V., Revesz, T., Lees, A. J., & Holton, J. L. (2013). Parkin Disease: A Clinicopathologic Entity? *JAMA Neurology*, *70*(5), 571–579. https://doi.org/10.1001/JAMANEUROL.2013.172

Donath, M. Y., & Shoelson, S. E. (2011). Type 2 diabetes as an inflammatory disease. *Nature Reviews Immunology 2011 11:2*, *11*(2), 98–107. https://doi.org/10.1038/nri2925

Dörfel, M. J., & Huber, O. (2012). Modulation of Tight Junction Structure and Function by Kinases and Phosphatases Targeting Occludin. *BioMed Research International*, *2012*(1), 807356. https://doi.org/10.1155/2012/807356

Double, K. L., Gerlach, M., Schünemann, V., Trautwein, A. X., Zecca, L., Gallorini, M., Youdim, M. B. H., Riederer, P., & Ben-Shachar, D. (2003). Iron-binding characteristics of neuromelanin of the human substantia nigra. *Biochemical Pharmacology*, *66*(3), 489–494. https://doi.org/10.1016/S0006-2952(03)00293-4

Dovonou, A., Bolduc, C., Soto Linan, V., Gora, C., Peralta, M. R., & Lévesque, M. (2023). Animal models of Parkinson's disease: bridging the gap between disease hallmarks and research questions. *Translational Neurodegeneration 2023 12:1*, *12*(1), 1–25. https://doi.org/10.1186/S40035-023-00368-8

Dowbenko, D., Kikuta, A., Fennie, C., Gillett, N., & Lasky, L. A. (1993). Glycosylation-dependent cell adhesion molecule 1 (GlyCAM 1) mucin is expressed by lactating mammary gland epithelial cells and is present in milk. *Journal of Clinical Investigation*, *92*(2), 952. https://doi.org/10.1172/JCI116671

Duan, W. X., Wang, F., Liu, J. Y., & Liu, C. F. (2023). Relationship Between Short-chain Fatty Acids and Parkinson's Disease: A Review from Pathology to Clinic. *Neuroscience Bulletin 2023 40:4*, *40*(4), 500–516. https://doi.org/10.1007/S12264-023-01123-9

Dumitrescu, L., Marta, D., Dănău, A., Lefter, A., Tulbă, D., Cozma, L., Manole, E., Gherghiceanu, M., Ceafalan, L. C., & Popescu, B. O. (2021). Serum and Fecal Markers of Intestinal Inflammation and Intestinal Barrier Permeability Are Elevated in Parkinson's Disease. *Frontiers in Neuroscience*, *15*, 689723. https://doi.org/10.3389/FNINS.2021.689723/BIBTEX

Dutta, S. K., Verma, S., Jain, V., Surapaneni, B. K., Vinayek, R., Phillips, L., & Nair, P. P. (2019). Parkinson's disease: The emerging role of gut dysbiosis, antibiotics, probiotics, and fecal microbiota transplantation. In *Journal of Neurogastroenterology and Motility* (Vol. 25, Issue 3, pp. 363–376). Korean Society of Neurogastroenterology and Motility. https://doi.org/10.5056/jnm19044

Eadie, M. J., & Tyrer, J. H. (1965a). ALIMENTARY DISORDER IN PARKINSONISM. *Australasian Annals of Medicine*, *14*(1), 13–22. https://doi.org/10.1111/IMJ.1965.14.1.13

Eadie, M. J., & Tyrer, J. H. (1965b). RADIOLOGICAL ABNORMALITIES OF THE UPPER PART OF THE ALIMENTARY TRACT IN PARKINSONISM. *Australasian Annals of Medicine*, *14*(1), 23–27. https://doi.org/10.1111/IMJ.1965.14.1.23

Eisenhofer, G., Aneman, Å., Friberg, P., Hooper, D., Fåndriks, L., Lonroth, H., Hunyady, B., & Mezey, E. (1997). Substantial Production of Dopamine in the Human Gastrointestinal Tract. *The Journal of Clinical Endocrinology & Metabolism*, *82*(11), 3864–3871. https://doi.org/10.1210/JCEM.82.11.4339

Ellett, L. J., Hung, L. W., Munckton, R., Sherratt, N. A., Culvenor, J., Grubman, A., Furness, J. B., White, A. R., Finkelstein, D. I., Barnham, K. J., & Lawson, V. A. (2016). Restoration of intestinal function in an MPTP model of Parkinson's Disease. *Scientific Reports 2016 6:1*, *6*(1), 1–11. https://doi.org/10.1038/srep30269

Engelborghs, S., Marescau, B., & De Deyn, P. P. (2003). Amino acids and biogenic amines in cerebrospinal fluid of patients with Parkinson's disease. *Neurochemical Research*, *28*(8), 1145–1150. https://doi.org/10.1023/A:1024255208563/METRICS

Engelen, M., Vanna, R., Bellei, C., Zucca, F. A., Wakamatsu, K., Monzani, E., Ito, S., Casella, L., & Zecca, L. (2012). Neuromelanins of Human Brain Have Soluble and Insoluble Components with Dolichols Attached to the Melanic Structure. *PLOS ONE*, *7*(11), e48490. https://doi.org/10.1371/JOURNAL.PONE.0048490

Erny, D., De Angelis, A. L. H., Jaitin, D., Wieghofer, P., Staszewski, O., David, E., Keren-Shaul, H., Mahlakoiv, T., Jakobshagen, K., Buch, T., Schwierzeck, V., Utermöhlen, O., Chun, E., Garrett, W. S., Mccoy, K. D., Diefenbach, A., Staeheli, P., Stecher, B., Amit, I., & Prinz, M. (2015). Host microbiota

constantly control maturation and function of microglia in the CNS. *Nature Neuroscience*, *18*(7), 965–977. https://doi.org/10.1038/nn.4030

Evancho, A., Do, M., Fortenberry, D., Billings, R., Sartayev, A., & Tyler, W. J. (2024). Vagus nerve stimulation in Parkinson's disease: a scoping review of animal studies and human subjects research. *Npj Parkinson's Disease 2024 10:1*, *10*(1), 1–16. https://doi.org/10.1038/s41531-024-00803-1

Everard, A., Belzer, C., Geurts, L., Ouwerkerk, J. P., Druart, C., Bindels, L. B., Guiot, Y., Derrien, M., Muccioli, G. G., Delzenne, N. M., De Vos, W. M., & Cani, P. D. (2013). Cross-talk between Akkermansia muciniphila and intestinal epithelium controls diet-induced obesity. *Proceedings of the National Academy of Sciences of the United States of America*, *110*(22), 9066–9071. https://doi.org/10.1073/PNAS.1219451110/-/DCSUPPLEMENTAL

Fabregat, A., Jupe, S., Matthews, L., Sidiropoulos, K., Gillespie, M., Garapati, P., Haw, R., Jassal, B., Korninger, F., May, B., Milacic, M., Roca, C. D., Rothfels, K., Sevilla, C., Shamovsky, V., Shorser, S., Varusai, T., Viteri, G., Weiser, J., … D'Eustachio, P. (2018). The Reactome Pathway Knowledgebase. *Nucleic Acids Research*, *46*(D1), D649–D655. https://doi.org/10.1093/NAR/GKX1132

Fahn, S. (2015). The medical treatment of Parkinson disease from James Parkinson to George Cotzias. *Movement Disorders*, *30*(1), 4–18. https://doi.org/10.1002/MDS.26102

Farhadi, A., Banan, A., Fields, J., & Keshavarzian, A. (2003). Intestinal barrier: An interface between health and disease. *Journal of Gastroenterology and Hepatology*, *18*(5), 479–497. https://doi.org/10.1046/J.1440-1746.2003.03032.X

Fasano, A., Visanji, N. P., Liu, L. W. C., Lang, A. E., & Pfeiffer, R. F. (2015). Gastrointestinal dysfunction in Parkinson's disease. In *The Lancet Neurology* (Vol. 14, Issue 6, pp. 625–639). Lancet Publishing Group. https://doi.org/10.1016/S1474-4422(15)00007-1

Fedorova, T. D., Seidelin, L. B., Knudsen, K., Schacht, A. C., Geday, J., Pavese, N., Brooks, D. J., & Borghammer, P. (2017). Decreased intestinal acetylcholinesterase in early Parkinson disease. *Neurology*, *88*(8), 775–781. https://doi.org/10.1212/WNL.0000000000003633

Fedorow, H., Halliday, G. M., Rickert, C. H., Gerlach, M., Riederer, P., & Double, K. L. (2006). Evidence for specific phases in the development of human neuromelanin. *Neurobiology of Aging*, *27*(3), 506–512. https://doi.org/10.1016/J.NEUROBIOLAGING.2005.02.015

Fénelon, G., & Walusinski, O. (2021). The landmark contributions of Paul Blocq, Georges Marinesco, and Édouard Brissaud in Parkinson's disease. *Revue Neurologique*, *177*(10), 1214–1220. https://doi.org/10.1016/J.NEUROL.2021.02.386

Fernández-Santiago, R., Carballo-Carbajal, I., Castellano, G., Torrent, R., Richaud, Y., Sánchez-Danés, A., Vilarrasa-Blasi, R., Sánchez-Pla, A., Mosquera, J. L., Soriano, J., López-Barneo, J., Canals, J. M., Alberch, J., Raya, Á., Vila, M., Consiglio, A., Martín-Subero, J. I., Ezquerra, M., & Tolosa, E. (2015). Aberrant epigenome in iPSC -derived dopaminergic neurons from Parkinson's disease patients . *EMBO Molecular Medicine*, *7*(12), 1529–1546.

https://doi.org/10.15252/EMMM.201505439/SUPPL_FILE/EMMM201505439.REVIEWER_COMMENTS.PDF

Ferreira, J. J., Poewe, W., Rascol, O., Stocchi, F., Antonini, A., Moreira, J., Guimarães, B., Rocha, J. F., & Soares-da-Silva, P. (2022). Effect of Opicapone on Levodopa Pharmacokinetics in Patients with Fluctuating Parkinson's Disease. *Movement Disorders*, *37*(11), 2272–2283. https://doi.org/10.1002/MDS.29193

Figura, M., Kuśmierska, K., Bucior, E., Szlufik, S., Koziorowski, D., Jamrozik, Z., & Janik, P. (2018). Serum amino acid profile in patients with Parkinson's disease. *PLoS ONE*, *13*(1), e0191670. https://doi.org/10.1371/JOURNAL.PONE.0191670

Fischer, D. L., Gombash, S. E., Kemp, C. J., Manfredsson, F. P., Polinski, N. K., Duffy, M. F., & Sortwell, C. E. (2016). Viral Vector-Based Modeling of Neurodegenerative Disorders: Parkinson's Disease. *Methods in Molecular Biology*, *1382*, 367–382. https://doi.org/10.1007/978-1-4939-3271-9_26

Fleming, M. A., Ehsan, L., Moore, S. R., & Levin, D. E. (2020). The Enteric Nervous System and Its Emerging Role as a Therapeutic Target. *Gastroenterology Research and Practice*, *2020*, 8024171. https://doi.org/10.1155/2020/8024171

FOLCH, J., LEES, M., & SLOANE STANLEY, G. H. (1957). A SIMPLE METHOD FOR THE ISOLATION AND PURIFICATION OF TOTAL LIPIDES FROM ANIMAL TISSUES. *Journal of Biological Chemistry*, *226*(1), 497–509. https://doi.org/10.1016/S0021-9258(18)64849-5

Forstenpointner, J., Maallo, A. M. S., Elman, I., Holmes, S., Freeman, R., Baron, R., & Borsook, D. (2022). The solitary nucleus connectivity to key autonomic regions in humans. *European Journal of Neuroscience*, *56*(2), 3938–3966. https://doi.org/10.1111/EJN.15691

Forsyth, C. B., Shannon, K. M., Kordower, J. H., Voigt, R. M., Shaikh, M., Jaglin, J. A., Estes, J. D., Dodiya, H. B., & Keshavarzian, A. (2011). Increased intestinal permeability correlates with sigmoid mucosa alpha-synuclein staining and endotoxin exposure markers in early Parkinson's disease. *PLoS ONE*, *6*(12). https://doi.org/10.1371/journal.pone.0028032

Fortea, M., Albert-Bayo, M., Abril-Gil, M., Ganda Mall, J. P., Serra-Ruiz, X., Henao-Paez, A., Expósito, E., González-Castro, A. M., Guagnozzi, D., Lobo, B., Alonso-Cotoner, C., & Santos, J. (2021). Present and Future Therapeutic Approaches to Barrier Dysfunction. *Frontiers in Nutrition*, *8*, 718093. https://doi.org/10.3389/FNUT.2021.718093/BIBTEX

Franceschi, C., Bonafè, M., Valesin, S., Oliveri, F., De luca, M., Ottaviani, E., & De Benedictis, G. (2006). Inflamm-aging: An Evolutionary Perspective on Immunosenescence. *Annals of the New York Academy of Sciences*, *908*(1), 244–254. https://doi.org/10.1111/j.1749-6632.2000.tb06651.x

Francisco Pan-Montojo, A., Anichtchik, O., Dening, Y., Knels, L., Pursche, S., Jung, R., Jackson, S., Gille, G., Spillantini, M. G., Reichmann, H., Funk, R. H. W., & Pan-Montojo, F. J. (2010). Progression of Parkinson's disease pathology is reproduced by intragastric administration of rotenone in mice. *Nature Precedings 2010*, 1–1. https://doi.org/10.1038/npre.2010.3352.3

Fransen, F., van Beek, A. A., Borghuis, T., El Aidy, S., Hugenholtz, F., van der Gaast - de Jongh, C., Savelkoul, H. F. J., de Jonge, M. I., Boekschoten, M. V., Smidt, H., Faas, M. M., & de Vos, P. (2017).

Aged gut microbiota contributes to systemical inflammaging after transfer to germ-free mice. *Frontiers in Immunology*, *8*(NOV), 293898. https://doi.org/10.3389/FIMMU.2017.01385/BIBTEX

Frazzitta, G., Ferrazzoli, D., Folini, A., Palamara, G., & Maestri, R. (2019). Severe Constipation in Parkinson's Disease and in Parkinsonisms: Prevalence and Affecting Factors. *Frontiers in Neurology*, *10*(JUN), 621. https://doi.org/10.3389/fneur.2019.00621

Friedman, J. M. (2019). Leptin and the endocrine control of energy balance. *Nature Metabolism 2019 1:8*, *1*(8), 754–764. https://doi.org/10.1038/S42255-019-0095-Y

Fu, J., Chen, S., Liu, J., Yang, J., Ou, R., Zhang, L., Chen, X., & Shang, H. (2023). Serum inflammatory cytokines levels and the correlation analyses in Parkinson's disease. *Frontiers in Cell and Developmental Biology*, *11*, 1104393. https://doi.org/10.3389/FCELL.2023.1104393/BIBTEX

Fuertes-Martín, R., Moncayo, S., Insenser, M., Martínez-García, M. Á., Luque-Ramírez, M., Grau, N. A., Blanchar, X. C., & Escobar-Morreale, H. F. (2019). Glycoprotein A and B Height-to-Width Ratios as Obesity-Independent Novel Biomarkers of Low-Grade Chronic Inflammation in Women with Polycystic Ovary Syndrome (PCOS). *Journal of Proteome Research*, *18*(11), 4038–4045. https://doi.org/10.1021/ACS.JPROTEOME.9B00528/ASSET/IMAGES/LARGE/PR9B00528_0001.JPEG

Fukuda, A., Chowdhury, M. A., Venkatareddy, M. P., Wang, S. Q., Nishizono, R., Suzuki, T., Wickman, L. T., Wiggins, J. E., Muchayi, T., Fingar, D., Shedden, K. A., Inoki, K., & Wigg, R. C. (2012). Growth-dependent podocyte failure causes glomerulosclerosis. *Journal of the American Society of Nephrology : JASN*, *23*(8), 1351–1363. https://doi.org/10.1681/ASN.2012030271

Funayama, M., Nishioka, K., Li, Y., & Hattori, N. (2022). Molecular genetics of Parkinson's disease: Contributions and global trends. *Journal of Human Genetics 2022 68:3*, *68*(3), 125–130. https://doi.org/10.1038/s10038-022-01058-5

Furness, J. B. (2000). Types of neurons in the enteric nervous system. *Journal of the Autonomic Nervous System*, *81*(1–3), 87–96. https://doi.org/10.1016/S0165-1838(00)00127-2

Furness, J. B. (2012). The enteric nervous system and neurogastroenterology. *Nature Reviews Gastroenterology & Hepatology 2012 9:5*, *9*(5), 286–294. https://doi.org/10.1038/nrgastro.2012.32

Furness, J. B., Callaghan, B. P., Rivera, L. R., & Cho, H. J. (2014). The enteric nervous system and gastrointestinal innervation: Integrated local and central control. *Advances in Experimental Medicine and Biology*, *817*, 39–71. https://doi.org/10.1007/978-1-4939-0897-4_3/FIGURES/7

Gaenslen, A., Swid, I., Liepelt-Scarfone, I., Godau, J., & Berg, D. (2011). The Patients' Perception of Prodromal Symptoms Before the Initial Diagnosis of Parkinson's Disease. *Movement Disorders*, *26*(4), 653. https://doi.org/10.1002/MDS.23499

Galiano-Landeira, J., Torra, A., Vila, M., & Bové, J. (2020). CD8 T cell nigral infiltration precedes synucleinopathy in early stages of Parkinson's disease. *Brain*, *143*(12), 3717–3733. https://doi.org/10.1093/BRAIN/AWAA269

Gallego, D., Gil, V., Aleu, J., Aulí, M., Clavé, P., & Jiménez, M. (2008). Purinergic and nitrergic junction potential in the human colon. *American Journal of Physiology - Gastrointestinal and Liver*

Physiology, *295*(3), 522–533. https://doi.org/10.1152/AJPGI.00510.2007/ASSET/IMAGES/LARGE/ZH30080851710009.JPEG

Galvin, J. E., Lee, V. M. Y., & Trojanowski, J. Q. (2001). Synucleinopathies: Clinical and Pathological Implications. *Archives of Neurology*, *58*(2), 186–190. https://doi.org/10.1001/ARCHNEUR.58.2.186

Gao, C., Jiang, J., Tan, Y., & Chen, S. (2023). Microglia in neurodegenerative diseases: mechanism and potential therapeutic targets. *Signal Transduction and Targeted Therapy 2023 8:1*, *8*(1), 1–37. https://doi.org/10.1038/s41392-023-01588-0

Gardener, H., & Caunca, M. R. (2018). Mediterranean Diet in Preventing Neurodegenerative Diseases. *Current Nutrition Reports*, *7*(1), 10–20. https://doi.org/10.1007/s13668-018-0222-5

Gaspar, P., Berger, B., Gay, M., Hamon, M., Cesselin, F., Vigny, A., Javoy-Agid, F., & Agid, Y. (1983). Tyrosine hydroxylase and methionine-enkephalin in the human mesencephalon: Immunocytochemical localization and relationships. *Journal of the Neurological Sciences*, *58*(2), 247–267. https://doi.org/10.1016/0022-510X(83)90221-6

Gentleman, R., Carey, V. J., Huber, W., Irizarry, R. A., & Dudoit, S. (2005). Bioinformatics and Computational Biology Solutions Using R and Bioconductor. *Springer New York*. https://doi.org/10.1007/0-387-29362-0

Gerhard, A., Pavese, N., Hotton, G., Turkheimer, F., Es, M., Hammers, A., Eggert, K., Oertel, W., Banati, R. B., & Brooks, D. J. (2006). In vivo imaging of microglial activation with [11C](R)-PK11195 PET in idiopathic Parkinson's disease. *Neurobiology of Disease*, *21*(2), 404–412. https://doi.org/10.1016/J.NBD.2005.08.002

Gerlach, M., Double, K. L., Ben-Shachar, D., Zecca, L., Youdim, M. B. H., & Riederer, P. (2003). Neuromelanin and its interaction with iron as a potential risk factor for dopaminergic neurodegeneration underlying Parkinson's disease. *Neurotoxicity Research*, *5*(1–2), 35–43. https://doi.org/10.1007/BF03033371

Gershon, M. D., & Liu, M. T. (2007). Serotonin and neuroprotection in functional bowel disorders. *Neurogastroenterology & Motility*, *19*(SUPPL.2), 19–24. https://doi.org/10.1111/J.1365-2982.2007.00962.X

Gheorghe, C. E., Ritz, N. L., Martin, J. A., Wardill, H. R., Cryan, J. F., & Clarke, G. (2021). Investigating causality with fecal microbiota transplantation in rodents: applications, recommendations and pitfalls. *Gut Microbes*, *13*(1). https://doi.org/10.1080/19490976.2021.1941711

Ghosh, T. S., Shanahan, F., & O'Toole, P. W. (2022). The gut microbiome as a modulator of healthy ageing. *Nature Reviews Gastroenterology & Hepatology 2022 19:9*, *19*(9), 565–584. https://doi.org/10.1038/s41575-022-00605-x

Gibson, G. R., & Roberfroid, M. B. (1995). Dietary Modulation of the Human Colonic Microbiota: Introducing the Concept of Prebiotics. *The Journal of Nutrition*, *125*(6), 1401–1412. https://doi.org/10.1093/jn/125.6.1401

Giguère, N., Nanni, S. B., & Trudeau, L. E. (2018). On cell loss and selective vulnerability of neuronal populations in Parkinson's disease. *Frontiers in Neurology*, *9*(JUN), 383041. https://doi.org/10.3389/FNEUR.2018.00455/BIBTEX

Gjerløff, T., Fedorova, T., Knudsen, K., Munk, O. L., Nahimi, A., Jacobsen, S., Danielsen, E. H., Terkelsen, A. J., Hansen, J., Pavese, N., Brooks, D. J., & Borghammer, P. (2015). Imaging acetylcholinesterase density in peripheral organs in Parkinson's disease with 11C-donepezil PET. *Brain*, *138*(3), 653–663. https://doi.org/10.1093/BRAIN/AWU369

Goetz, C. G. (2011). The History of Parkinson's Disease: Early Clinical Descriptions and Neurological Therapies. *Cold Spring Harbor Perspectives in Medicine*, *1*(1), a008862. https://doi.org/10.1101/CSHPERSPECT.A008862

Gómez, J., Brezmes, J., Mallol, R., Rodríguez, M. A., Vinaixa, M., Salek, R. M., Correig, X., & Cañellas, N. (2014). Dolphin: A tool for automatic targeted metabolite profiling using 1D and 2D 1 H-NMR data. *Analytical and Bioanalytical Chemistry*, *406*(30), 7967–7976. https://doi.org/10.1007/S00216-014-8225-6/TABLES/2

González-Bosch, C., Boorman, E., Zunszain, P. A., & Mann, G. E. (2021). Short-chain fatty acids as modulators of redox signaling in health and disease. *Redox Biology*, *47*, 102165. https://doi.org/10.1016/J.REDOX.2021.102165

Gonzalez-Sepulveda, M., Compte, J., Cuadros, T., Nicolau, A., Guillard-Sirieix, C., Peñuelas, N., Lorente-Picon, M., Parent, A., Romero-Gimenez, J., Cladera-Sastre, J. M., Laguna, A., & Vila, M. (2023). In vivo reduction of age-dependent neuromelanin accumulation mitigates features of Parkinson's disease. *Brain*, *146*(3), 1040–1052. https://doi.org/10.1093/BRAIN/AWAC445

Gonzalez-Sepulveda, M., Laguna, A., Carballo-Carbajal, I., Galiano-Landeira, J., Romero-Gimenez, J., Cuadros, T., Parent, A., Peñuelas, N., Compte, J., Nicolau, A., Guillard-Sirieix, C., Xicoy, H., Kobayashi, J., & Vila, M. (2020). Validation of a reversed phase UPLC-MS/MS method to determine dopamine metabolites and oxidation intermediates in neuronal differentiated SH-SY5Y cells and brain tissue. *ACS Chemical Neuroscience*, *11*(17), 2679–2687. https://doi.org/10.1021/acschemneuro.0c00336

Goto, Y. (2019). Epithelial cells as a transmitter of signals from commensal bacteria and host immune cells. *Frontiers in Immunology*, *10*(AUG), 458627. https://doi.org/10.3389/FIMMU.2019.02057/PDF

Grant, L. M., Richter, F., Miller, J. E., White, S. A., Fox, C. M., Zhu, C., Chesselet, M. F., & Ciucci, M. R. (2014). Vocalization deficits in mice over-expressing alpha-synuclein, a model of pre-manifest Parkinson's disease. *Behavioral Neuroscience*, *128*(2), 110. https://doi.org/10.1037/A0035965

Greggio, E., Bergantino, E., Carter, D., Ahmad, R., Costin, G. E., Hearing, V. J., Clarimon, J., Singleton, A., Eerola, J., Hellström, O., Tienari, P. J., Miller, D. W., Beilina, A., Bubacco, L., & Cookson, M. R. (2005). Tyrosinase exacerbates dopamine toxicity but is not genetically associated with Parkinson's disease. *Journal of Neurochemistry*, *93*(1), 246–256. https://doi.org/10.1111/J.1471-4159.2005.03019.X

Groiss, S. J., Wojtecki, L., Sudmeyer, M., & Schnitzler, A. (2009). Review: Deep brain stimulation in Parkinson's disease. *Http://Dx.Doi.Org/10.1177/1756285609339382*, *2*(6), 379–391. https://doi.org/10.1177/1756285609339382

Gruber, T., Lechner, F., Krieger, J. P., & García-Cáceres, C. (2024). Neuroendocrine gut–brain signaling in obesity. *Trends in Endocrinology and Metabolism*, *0*(0). https://doi.org/10.1016/J.TEM.2024.05.002/ASSET/1F1F02ED-EA8F-4ADB-BDDA-0F7B9638CF67/MAIN.ASSETS/GR2.JPG

Grundmann, D., Loris, E., Maas-Omlor, S., Huang, W., Scheller, A., Kirchhoff, F., & Schäfer, K. H. (2019). Enteric Glia: S100, GFAP, and Beyond. *The Anatomical Record*, *302*(8), 1333–1344. https://doi.org/10.1002/AR.24128

Grundy, S. M., Cleeman, J. I., Daniels, S. R., Donato, K. A., Eckel, R. H., Franklin, B. A., Gordon, D. J., Krauss, R. M., Savage, P. J., Smith, S. C., Spertus, J. A., & Costa, F. (2005). Diagnosis and Management of the Metabolic Syndrome. *Circulation*, *112*(17), 2735–2752. https://doi.org/10.1161/CIRCULATIONAHA.105.169404

Guedes, L. C., Chan, R. B., Gomes, M. A., Conceição, V. A., Machado, R. B., Soares, T., Xu, Y., Gaspar, P., Carriço, J. A., Alcalay, R. N., Ferreira, J. J., Outeiro, T. F., & Miltenberger-Miltenyi, G. (2017). Serum lipid alterations in GBA-associated Parkinson's disease. *Parkinsonism & Related Disorders*, *44*, 58–65. https://doi.org/10.1016/J.PARKRELDIS.2017.08.026

Guo, X., Song, W., Chen, K., Chen, X. P., Zheng, Z., Cao, B., Huang, R., Zhao, B., Wu, Y., & Shang, H. F. (2015). The serum lipid profile of Parkinson's disease patients: a study from China. *International Journal of Neuroscience*, *125*(11), 838–844. https://doi.org/10.3109/00207454.2014.979288

Guzel, T., & Mirowska-Guzel, D. (2022). The Role of Serotonin Neurotransmission in Gastrointestinal Tract and Pharmacotherapy. *Molecules 2022, Vol. 27, Page 1680*, *27*(5), 1680. https://doi.org/10.3390/MOLECULES27051680

Haikal, C., Chen, Q. Q., & Li, J. Y. (2019). Microbiome changes: An indicator of Parkinson's disease? In *Translational Neurodegeneration* (Vol. 8, Issue 1, p. 38). BioMed Central Ltd. https://doi.org/10.1186/s40035-019-0175-7

Halder, N., & Lal, G. (2021). Cholinergic System and Its Therapeutic Importance in Inflammation and Autoimmunity. *Frontiers in Immunology*, *12*, 660342. https://doi.org/10.3389/FIMMU.2021.660342/BIBTEX

Hall, D. A., Voigt, R. M., Cantu-Jungles, T. M., Hamaker, B., Engen, P. A., Shaikh, M., Raeisi, S., Green, S. J., Naqib, A., Forsyth, C. B., Chen, T., Manfready, R., Ouyang, B., Rasmussen, H. E., Sedghi, S., Goetz, C. G., & Keshavarzian, A. (2023). An open label, non-randomized study assessing a prebiotic fiber intervention in a small cohort of Parkinson's disease participants. *Nature Communications 2023 14:1*, *14*(1), 1–14. https://doi.org/10.1038/s41467-023-36497-x

Hallett, P. J., McLean, J. R., Kartunen, A., Langston, J. W., & Isacson, O. (2012). Alpha-synuclein overexpressing transgenic mice show internal organ pathology and autonomic deficits. *Neurobiology of Disease*, *47*(2), 258–267. https://doi.org/10.1016/J.NBD.2012.04.009

Halliday, G., McCann, H., & Shepherd, C. (2012). Evaluation of the Braak hypothesis: how far can it explain the pathogenesis of Parkinson's disease? *Expert Review of Neurotherapeutics*, *12*(6), 673–686. https://doi.org/10.1586/ERN.12.47

Hamade, H., Tsuda, M., Oshima, N., Stamps, D. T., Wong, M. H., Stamps, J. T., Thomas, L. S., Salumbides, B. C., Jin, C., Nunnelee, J. S., Dhall, D., Targan, S. R., & Michelsen, K. S. (2024). Toll-like receptor 7 protects against intestinal inflammation and restricts the development of colonic tissue-resident memory CD8+ T cells. *Frontiers in Immunology*, *15*, 1465175. https://doi.org/10.3389/FIMMU.2024.1465175

Hamaker, B. R., & Tuncil, Y. E. (2014). A perspective on the complexity of dietary fiber structures and their potential effect on the gut microbiota. In *Journal of Molecular Biology* (Vol. 426, Issue 23, pp. 3838–3850). Academic Press. https://doi.org/10.1016/j.jmb.2014.07.028

Han, N. R., Kim, Y. K., Ahn, S., Hwang, T. Y., Lee, H., & Park, H. J. (2021). A Comprehensive Phenotype of Non-motor Impairments and Distribution of Alpha-Synuclein Deposition in Parkinsonism-Induced Mice by a Combination Injection of MPTP and Probenecid. *Frontiers in Aging Neuroscience*, *12*, 599045. https://doi.org/10.3389/FNAGI.2020.599045/BIBTEX

Han, Y., Zhang, M., Li, N., Chen, T., Zhang, Y., Wan, T., & Cao, X. (2004). KLRL1, a novel killer cell lectinlike receptor, inhibits natural killer cell cytotoxicity. *Blood*, *104*(9), 2858–2866. https://doi.org/10.1182/BLOOD-2004-03-0878

Hantikainen, E., Roos, E., Bellocco, R., D'Antonio, A., Grotta, A., Adami, H. O., Ye, W., Trolle Lagerros, Y., & Bonn, S. (2022). Dietary fat intake and risk of Parkinson disease: results from the Swedish National March Cohort. *European Journal of Epidemiology*, *1*, 1–11. https://doi.org/10.1007/S10654-022-00863-8/TABLES/3

Hao, S., Dey, A., Yu, X., & Stranahan, A. M. (2016). Dietary obesity reversibly induces synaptic stripping by microglia and impairs hippocampal plasticity. *Brain, Behavior, and Immunity*, *51*, 230–239. https://doi.org/10.1016/J.BBI.2015.08.023

Hasegawa, S., Goto, S., Tsuji, H., Okuno, T., Asahara, T., Nomoto, K., Shibata, A., Fujisawa, Y., Minato, T., Okamoto, A., Ohno, K., & Hirayama, M. (2015). Intestinal dysbiosis and lowered serum lipopolysaccharide-binding protein in Parkinson's disease. *PLoS ONE*, *10*(11). https://doi.org/10.1371/journal.pone.0142164

Hausmann, M., Kiessling, S., Mestermann, S., Webb, G., Spöttl, T., Andus, T., Schölmerich, J., Herfarth, H., Ray, K., Falk, W., & Rogler, G. (2002). Toll-like receptors 2 and 4 are up-regulated during intestinal inflammation. *Gastroenterology*, *122*(7), 1987–2000. https://doi.org/10.1053/gast.2002.33662

Hawkes, C. H., Del Tredici, K., & Braak, H. (2007). Parkinson's disease: A dual-hit hypothesis. In *Neuropathology and Applied Neurobiology* (Vol. 33, Issue 6, pp. 599–614). https://doi.org/10.1111/j.1365-2990.2007.00874.x

Hawkes, C. H., Del Tredici, K., & Braak, H. (2009). Parkinson's Disease. *Annals of the New York Academy of Sciences*, *1170*(1), 615–622. https://doi.org/10.1111/J.1749-6632.2009.04365.X

He, X., Yan, C., Zhao, S., Zhao, Y., Huang, R., & Li, Y. (2022). The preventive effects of probiotic Akkermansia muciniphila on D-galactose/AlCl3 mediated Alzheimer's disease-like rats. *Experimental Gerontology*, *170*, 111959. https://doi.org/10.1016/J.EXGER.2022.111959

Heel, K. A., McCauley, R. D., Papadimitriou, J. M., & Hall, J. C. (1997). REVIEW: Peyer's patches. *Journal of Gastroenterology and Hepatology*, *12*(2), 122–136. https://doi.org/10.1111/J.1440-1746.1997.TB00395.X

Heintz, C., & Mair, W. (2014). You are what you host: Microbiome modulation of the aging process. In *Cell* (Vol. 156, Issue 3, pp. 408–411). NIH Public Access. https://doi.org/10.1016/j.cell.2014.01.025

Heintz-Buschart, A., Pandey, U., Wicke, T., Sixel-Döring, F., Janzen, A., Sittig-Wiegand, E., Trenkwalder, C., Oertel, W. H., Mollenhauer, B., & Wilmes, P. (2018). The nasal and gut microbiome in Parkinson's disease and idiopathic rapid eye movement sleep behavior disorder. *Movement Disorders*, *33*(1), 88–98. https://doi.org/10.1002/mds.27105

Heinzel, S., Aho, V. T. E., Suenkel, U., von Thaler, A., Schulte, C., Deuschle, C., Paulin, L., Hantunen, S., Brockmann, K., Eschweiler, G. W., Maetzler, W., Berg, D., Auvinen, P., & Scheperjans, F. (2020). Gut Microbiome Signatures of Risk and Prodromal Markers of Parkinson Disease. *Annals of Neurology*, *88*(2), 320–331. https://doi.org/10.1002/ana.25788

Heinzel, S., Berg, D., Gasser, T., Chen, H., Yao, C., Postuma, R. B., Postuma Cochairs, R. B., Adler, C. H., Bloem, B., Chan, P., Deuschl, G., Dubois, B., Goetz, C. G., Halliday, G. M., Hardy, J., Lang, A. E., Litvan, I., Marek, K., Obeso, J., … Stern, M. (2019). Update of the MDS research criteria for prodromal Parkinson's disease. *Movement Disorders*, *34*(10), 1464–1470. https://doi.org/10.1002/MDS.27802

Heller, F., Florian, P., Bojarski, C., Richter, J., Christ, M., Hillenbrand, B., Mankertz, J., Gitter, A. H., Bürgel, N., Fromm, M., Zeitz, M., Fuss, I., Strober, W., & Schulzke, J. D. (2005). Interleukin-13 is the key effector Th2 cytokine in ulcerative colitis that affects epithelial tight junctions, apoptosis, and cell restitution. *Gastroenterology*, *129*(2), 550–564. https://doi.org/10.1016/j.gastro.2005.05.002

Henegar, J. R., Bigler, S. A., Henegar, L. K., Tyagi, S. C., & Hall, J. E. (2001). Functional and structural changes in the kidney in the early stages of obesity. *Journal of the American Society of Nephrology*, *12*(6), 1211–1217. https://doi.org/10.1681/ASN.V1261211

Hens, J., Vanderwinden, J. M., De Laet, M. H., Scheuermann, D. W., & Timmermans, J. P. (2001). Morphological and neurochemical identification of enteric neurones with mucosal projections in the human small intestine. *Journal of Neurochemistry*, *76*(2), 464–471. https://doi.org/10.1046/J.1471-4159.2001.00032.X

Hersoug, L. G., Møller, P., & Loft, S. (2018). Role of microbiota-derived lipopolysaccharide in adipose tissue inflammation, adipocyte size and pyroptosis during obesity. *Nutrition Research Reviews*, *31*(2), 153–163. https://doi.org/10.1017/S0954422417000269

Hibbing, M. E., Fuqua, C., Parsek, M. R., & Peterson, S. B. (2009). Bacterial competition: surviving and thriving in the microbial jungle. *Nature Reviews Microbiology 2009 8:1*, *8*(1), 15–25. https://doi.org/10.1038/nrmicro2259

Hill-Burns, E. M., Debelius, J. W., Morton, J. T., Wissemann, W. T., Lewis, M. R., Wallen, Z. D., Peddada, S. D., Factor, S. A., Molho, E., Zabetian, C. P., Knight, R., & Payami, H. (2017). Parkinson's disease and Parkinson's disease medications have distinct signatures of the gut microbiome. *Movement Disorders*, *32*(5), 739–749. https://doi.org/10.1002/mds.26942

Hirayama, M., Tsunoda, M., Yamamoto, M., Tsuda, T., & Ohno, K. (2016). Serum tyrosine-to-phenylalanine ratio is low in Parkinson's disease. *Journal of Parkinson's Disease*, *6*(2), 423–431. https://doi.org/10.3233/JPD-150736/ASSET/37231DF8-A944-4ECB-84C0-E6E087F97676/ASSETS/GRAPHIC/10.3233_JPD-150736-FIG4.JPG

Hirsch, E. C., Vyas, S., & Hunot, S. (2012). Neuroinflammation in Parkinson's disease. *Parkinsonism & Related Disorders*, *18*(SUPPL. 1), S210–S212. https://doi.org/10.1016/S1353-8020(11)70065-7

Hirsch, E., Graybiel, A. M., & Agid, Y. A. (1988). Melanized dopaminergic neurons are differentially susceptible to degeneration in Parkinson's disease. *Nature*, *334*(6180), 345–348. https://doi.org/10.1038/334345a0

Holdorff, B. (2019). Centenary of Tretiakoff's thesis on the morphology of Parkinson's disease, evolved on the grounds of encephalitis lethargica pathology. *Journal of the History of the Neurosciences*, *28*(4), 387–398. https://doi.org/10.1080/0964704X.2019.1622361

Holmqvist, S., Chutna, O., Bousset, L., Aldrin-Kirk, P., Li, W., Björklund, T., Wang, Z. Y., Roybon, L., Melki, R., & Li, J. Y. (2014). Direct evidence of Parkinson pathology spread from the gastrointestinal tract to the brain in rats. *Acta Neuropathologica*, *128*(6), 805–820. https://doi.org/10.1007/s00401-014-1343-6

Hopfner, F., Künstner, A., Müller, S. H., Künzel, S., Zeuner, K. E., Margraf, N. G., Deuschl, G., Baines, J. F., & Kuhlenbäumer, G. (2017). Gut microbiota in Parkinson disease in a northern German cohort. *Brain Research*, *1667*, 41–45. https://doi.org/10.1016/j.brainres.2017.04.019

Hor, J. W., Lim, S. Y., Khor, E. S., Chong, K. K., Song, S. L., Ibrahim, N. M., Teh, C. S. J., Chong, C. W., Hilmi, I. N., & Tan, A. H. (2021a). Fecal Calprotectin in Parkinson's Disease and Multiple System Atrophy. *Journal of Movement Disorders*, *15*(2), 106–114. https://doi.org/10.14802/JMD.21085

Hor, J. W., Lim, S. Y., Khor, E. S., Chong, K. K., Song, S. L., Ibrahim, N. M., Teh, C. S. J., Chong, C. W., Hilmi, I. N., & Tan, A. H. (2021b). Fecal Calprotectin in Parkinson's Disease and Multiple System Atrophy. *Journal of Movement Disorders*, *15*(2), 106–114. https://doi.org/10.14802/JMD.21085

Horsager, J., Andersen, K. B., Knudsen, K., Skjærbæk, C., Fedorova, T. D., Okkels, N., Schaeffer, E., Bonkat, S. K., Geday, J., Otto, M., Sommerauer, M., Danielsen, E. H., Bech, E., Kraft, J., Munk, O. L., Hansen, S. D., Pavese, N., Göder, R., Brooks, D. J., … Borghammer, P. (2020). Brain-first versus body-first Parkinson's disease: a multimodal imaging case-control study. *Brain*, *143*(10), 3077–3088. https://doi.org/10.1093/BRAIN/AWAA238

Horsager, J., & Borghammer, P. (2024). Brain-first vs. body-first Parkinson's disease: An update on recent evidence. *Parkinsonism & Related Disorders*, *122*, 106101. https://doi.org/10.1016/J.PARKRELDIS.2024.106101

Hotamisligil, G. S. (2006). Inflammation and metabolic disorders. *Nature 2006 444:7121*, *444*(7121), 860–867. https://doi.org/10.1038/nature05485

Hou, K., Wu, Z. X., Chen, X. Y., Wang, J. Q., Zhang, D., Xiao, C., Zhu, D., Koya, J. B., Wei, L., Li, J., & Chen, Z. S. (2022). Microbiota in health and diseases. *Signal Transduction and Targeted Therapy 2022 7:1*, *7*(1), 1–28. https://doi.org/10.1038/s41392-022-00974-4

Hou, S.-M., Hsia, C.-W., Tsai, C.-L., Hsia, C.-H., Jayakumar, T., Velusamy, M., & Sheu, J.-R. (2022). Gut microenvironmental changes as a potential trigger in Parkinson's disease through the gut–brain axis. *Journal of Biomedical Science 2022 29:1*, *29*(1), 1–18. https://doi.org/10.1186/S12929-022-00839-6

Houser, M. C., Chang, J., Factor, S. A., Molho, E. S., Zabetian, C. P., Hill-Burns, E. M., Payami, H., Hertzberg, V. S., & Tansey, M. G. (2018). Stool Immune Profiles Evince Gastrointestinal Inflammation in Parkinson's Disease. *Movement Disorders*, *33*(5), 793–804. https://doi.org/10.1002/mds.27326

Houser, M. C., & Tansey, M. G. (2017). The gut-brain axis: is intestinal inflammation a silent driver of Parkinson's disease pathogenesis? *Npj Parkinson's Disease*, *3*(1). https://doi.org/10.1038/s41531-016-0002-0

Hoy, W. E., Hughson, M. D., Zimanyi, M., Samuel, T., Douglas-Denton, R., Holden, L., Mott, S., & Bertram, J. F. (2010). Distribution of volumes of individual glomeruli in kidneys at autopsy: association with age, nephron number, birth weight and body mass index. *Clinical Nephrology*, *74 Suppl 1*(SUPPL.1), S105-12. https://doi.org/10.5414/CNP74S105

Huang, H., Xu, H., Luo, Q., He, J., Li, M., Chen, H., Tang, W., Nie, Y., & Zhou, Y. (2019). Fecal microbiota transplantation to treat Parkinson's disease with constipation: A case report. *Medicine*, *98*(26), e16163. https://doi.org/10.1097/MD.0000000000016163

Huang, W., Xiao, Y., Zhang, L., & Liu, H. (2024). Association between a body shape index and Parkinson's disease: A large cross-sectional study from NHANES. *Heliyon*, *10*(4), e26557. https://doi.org/10.1016/J.HELIYON.2024.E26557

Hubble, J. P., Cao, T., Hassanein, R. E. S., Neuberger, J. S., & Roller, W. C. (1993). Risk factors for Parkinson's disease. *Neurology*, *43*(9), 1693–1693. https://doi.org/10.1212/WNL.43.9.1693

Huckemann, S., Mueller, K., Averdunk, P., Kühn, E., Hilker, L., Kools, S., Scholz, L., Bulut, Y., Brünger, J., Fiegert, S., Grüter, T., Fisse, A. L., Motte, J., Yoon, M. S., Gold, R., Schneider-Gold, C., Tönges, L., & Pitarokoili, K. (2023). Vagal cross-sectional area correlates with parasympathetic dysfunction in Parkinson's disease. *Brain Communications*, *5*(1). https://doi.org/10.1093/BRAINCOMMS/FCAD006

Hughes, A. J., Daniel, S. E., Kilford, L., & Lees, A. J. (1992). Accuracy of clinical diagnosis of idiopathic Parkinson's disease: a clinico-pathological study of 100 cases. *Journal of Neurology, Neurosurgery, and Psychiatry*, *55*(3), 181. https://doi.org/10.1136/JNNP.55.3.181

Hui, K. Y., Fernandez-Hernandez, H., Hu, J., Schaffner, A., Pankratz, N., Hsu, N. Y., Chuang, L. S., Carmi, S., Villaverde, N., Li, X., Rivas, M., Levine, A. P., Bao, X., Labrias, P. R., Haritunians, T., Ruane, D., Gettler, K., Chen, E., Li, D., … Peter, I. (2018). Functional variants in the LRRK2 gene confer shared

effects on risk for Crohn's disease and Parkinson's disease. *Science Translational Medicine*, *10*(423). https://doi.org/10.1126/SCITRANSLMED.AAI7795

Hustad, E., & Aasly, J. O. (2020). Clinical and Imaging Markers of Prodromal Parkinson's Disease. *Frontiers in Neurology*, *11*, 520289. https://doi.org/10.3389/FNEUR.2020.00395/XML/NLM

Hutkins, R. W., Krumbeck, J. A., Bindels, L. B., Cani, P. D., Fahey, G., Goh, Y. J., Hamaker, B., Martens, E. C., Mills, D. A., Rastal, R. A., Vaughan, E., & Sanders, M. E. (2016). Prebiotics: Why definitions matter. In *Current Opinion in Biotechnology* (Vol. 37, pp. 1–7). Elsevier Ltd. https://doi.org/10.1016/j.copbio.2015.09.001

Ilyés, T., Silaghi, C. N., & Crăciun, A. M. (2022). Diet-Related Changes of Short-Chain Fatty Acids in Blood and Feces in Obesity and Metabolic Syndrome. *Biology*, *11*(11), 1556. https://doi.org/10.3390/BIOLOGY11111556

Imamura, K., Hishikawa, N., Sawada, M., Nagatsu, T., Yoshida, M., & Hashizume, Y. (2003). Distribution of major histocompatibility complex class II-positive microglia and cytokine profile of Parkinson's disease brains. *Acta Neuropathologica*, *106*(6), 518–526. https://doi.org/10.1007/S00401-003-0766-2/FIGURES/6

Impellizzeri, D., Siracusa, R., Amico, R. D. ', Khan, E., Hasan, I., & Haque, M. E. (2023). Parkinson's Disease: Exploring Different Animal Model Systems. *International Journal of Molecular Sciences 2023, Vol. 24, Page 9088*, *24*(10), 9088. https://doi.org/10.3390/IJMS24109088

Inciarte-Mundo, J., Frade-Sosa, B., & Sanmartí, R. (2022). From bench to bedside: Calprotectin (S100A8/S100A9) as a biomarker in rheumatoid arthritis. *Frontiers in Immunology*, *13*, 1001025. https://doi.org/10.3389/FIMMU.2022.1001025/BIBTEX

Irizarry, R. A., Hobbs, B., Collin, F., Beazer-Barclay, Y. D., Antonellis, K. J., Scherf, U., & Speed, T. P. (2003). Exploration, normalization, and summaries of high density oligonucleotide array probe level data. *Biostatistics*, *4*(2), 249–264. https://doi.org/10.1093/BIOSTATISTICS/4.2.249

Ishikawa, A. (1998). Clinical and neuropathological aspects of autosomal recessive juvenile parkinsonism. *Journal of Neurology, Supplement*, *245*(3), P4–P9. https://doi.org/10.1007/PL00007745/METRICS

Ito, S., & Wakamatsu, K. (2008). Chemistry of Mixed Melanogenesis—Pivotal Roles of Dopaquinone†. *Photochemistry and Photobiology*, *84*(3), 582–592. https://doi.org/10.1111/J.1751-1097.2007.00238.X

Iwasaki, Y., Ikeda, K., Shiojima, T., & Kinoshita, M. (1992). Increased plasma concentrations of aspartate, glutamate and glycine in Parkinson's disease. *Neuroscience Letters*, *145*(2), 175–177. https://doi.org/10.1016/0304-3940(92)90015-Y

Jackson, A., Forsyth, C. B., Shaikh, M., Voigt, R. M., Engen, P. A., Ramirez, V., & Keshavarzian, A. (2019). Diet in Parkinson's Disease: Critical Role for the Microbiome. In *Frontiers in Neurology* (Vol. 10). Frontiers Media S.A. https://doi.org/10.3389/fneur.2019.01245

Jialal, I., Kaur, H., & Devaraj, S. (2014). Toll-like Receptor Status in Obesity and Metabolic Syndrome: A Translational Perspective. *The Journal of Clinical Endocrinology & Metabolism*, *99*(1), 39–48. https://doi.org/10.1210/JC.2013-3092

Jing, L., Hou, L., Zhang, D., Li, S., Ruan, Z., Zhang, X., Hong, J. S., & Wang, Q. (2021). Microglial Activation Mediates Noradrenergic Locus Coeruleus Neurodegeneration via Complement Receptor 3 in a Rotenone-Induced Parkinson's Disease Mouse Model. *Journal of Inflammation Research*, *14*, 1341–1356. https://doi.org/10.2147/JIR.S299927

Jing, W., Jabbari, B., & Vaziri, N. D. (2018). Uremia induces upregulation of cerebral tissue oxidative/inflammatory cascade, down-regulation of Nrf2 pathway and disruption of blood brain barrier. *American Journal of Translational Research*, *10*(7), 2137. https://pmc.ncbi.nlm.nih.gov/articles/PMC6079125/

Jo, J., Gavrilova, O., Pack, S., Jou, W., Mullen, S., Sumner, A. E., Cushman, S. W., & Periwal, V. (2009). Hypertrophy and/or Hyperplasia: Dynamics of Adipose Tissue Growth. *PLoS Computational Biology*, *5*(3), e1000324. https://doi.org/10.1371/JOURNAL.PCBI.1000324

Jo, U., & Pommier, Y. (2022). Structural, molecular, and functional insights into Schlafen proteins. *Experimental & Molecular Medicine 2022 54:6*, *54*(6), 730–738. https://doi.org/10.1038/s12276-022-00794-0

Joers, V., Tansey, M. G., Mulas, G., & Carta, A. R. (2017). Microglial phenotypes in Parkinson's disease and animal models of the disease. *Progress in Neurobiology*, *155*, 57–75. https://doi.org/10.1016/J.PNEUROBIO.2016.04.006

Jonge, W. J. de. (2013). The Gut's Little Brain in Control of Intestinal Immunity. *International Scholarly Research Notices*, *2013*(1), 630159. https://doi.org/10.1155/2013/630159

Jost, W. H. (2010). Gastrointestinal dysfunction in Parkinson's Disease. *Journal of the Neurological Sciences*, *289*(1), 69–73. https://doi.org/10.1016/J.JNS.2009.08.020

Jung, D., De Gagne, J. C., Lee, H., & Lee, M. (2021). Factors associated with eating performance in older adults with dementia in long-term care facilities: a cross-sectional study. *BMC Geriatrics*, *21*(1), 1–7. https://doi.org/10.1186/S12877-021-02315-6/TABLES/2

Kahn, B. B., & Flier, J. S. (2000). Obesity and insulin resistance. *Journal of Clinical Investigation*, *106*(4), 473. https://doi.org/10.1172/JCI10842

Kalaitzakis, M. E., Graeber, M. B., Gentleman, S. M., & Pearce, R. K. B. (2008). The dorsal motor nucleus of the vagus is not an obligatory trigger site of Parkinson's disease: a critical analysis of α-synuclein staging. *Neuropathology and Applied Neurobiology*, *34*(3), 284–295. https://doi.org/10.1111/J.1365-2990.2007.00923.X

Kalia, L. V., Brotchie, J. M., & Fox, S. H. (2013). Novel nondopaminergic targets for motor features of Parkinson's disease: Review of recent trials. *Movement Disorders*, *28*(2), 131–144. https://doi.org/10.1002/MDS.25273

Kang, L., Schmalzl, A., Leupold, T., Gonzalez-Acera, M., Atreya, R., Neurath, M. F., Becker, C., & Wirtz, S. (2021). CCR8 Signaling via CCL1 Regulates Responses of Intestinal IFN-γ Producing Innate Lymphoid Cells and Protects From Experimental Colitis. *Frontiers in Immunology*, *11*, 609400. https://doi.org/10.3389/FIMMU.2020.609400/BIBTEX

Karampetsou, M., Ardah, M. T., Semitekolou, M., Polissidis, A., Samiotaki, M., Kalomoiri, M., Majbour, N., Xanthou, G., El-Agnaf, O. M. A., & Vekrellis, K. (2017). Phosphorylated exogenous alpha-synuclein fibrils exacerbate pathology and induce neuronal dysfunction in mice. *Scientific Reports*, *7*(1), 16533. https://doi.org/10.1038/S41598-017-15813-8

Karlsson, O., & Lindquist, N. G. (2016). Melanin and neuromelanin binding of drugs and chemicals: toxicological implications. *Archives of Toxicology*, *90*(8), 1883–1891. https://doi.org/10.1007/S00204-016-1757-0

Kasiske, B. L., & Napier, J. (1985). Glomerular Sclerosis in Patients with Massive Obesity. *American Journal of Nephrology*, *5*(1), 45–50. https://doi.org/10.1159/000166902

Kastner, A., Hirsch, E. C., Lejeune, O., Javoy-Agid, F., Rascol, O., & Agid, Y. (1992). Is the vulnerability of neurons in the substantia nigra of patients with Parkinson's disease related to their neuromelanin content? *Journal of Neurochemistry*, *59*(3), 1080–1089. https://doi.org/10.1111/J.1471-4159.1992.TB08350.X

Katoh, K., & Standley, D. M. (2013). MAFFT Multiple Sequence Alignment Software Version 7: Improvements in Performance and Usability. *Molecular Biology and Evolution*, *30*(4), 772–780. https://doi.org/10.1093/MOLBEV/MST010

Kazanova, A., Sung, J., Oliveira, N., Gavino, C., Recinto, S., Bessaiah, H., Pei, J., Burns, L., Miller, W., Brouillard-Galipeau, M., Zhu, L., Guerra, L., Elemeery, M. N., MacDonald, A., Lanoix, J., Thibault, P., McBride, H., Desjardins, M., Stratton, J. A., … Gruenheid, S. (2024). Modeling gene-environment interactions in Parkinson's Disease: Helicobacter pylori infection of Pink1−/− mice induces CD8 T cell-dependent motor and cognitive dysfunction. *BioRxiv*, 2024.02.25.580545. https://doi.org/10.1101/2024.02.25.580545

Kechagia, M., Basoulis, D., Konstantopoulou, S., Dimitriadi, D., Gyftopoulou, K., Skarmoutsou, N., & Fakiri, E. M. (2013). Health Benefints of Probiotics: A Review. *ISRN Nutrition*, *2013*.

Kellow, J. E., Azpiroz, F., Delvaux, M., Gebhart, G. F., Mertz, H. R., Quigley, E. M. M., & Smout, A. J. P. M. (2006). Applied Principles of Neurogastroenterology: Physiology/Motility Sensation. *Gastroenterology*, *130*(5), 1412–1420. https://doi.org/10.1053/j.gastro.2005.08.061

Kelly, J. R., Kennedy, P. J., Cryan, J. F., Dinan, T. G., Clarke, G., & Hyland, N. P. (2015). Breaking down the barriers: The gut microbiome, intestinal permeability and stress-related psychiatric disorders. *Frontiers in Cellular Neuroscience*, *9*(OCT), 166028. https://doi.org/10.3389/FNCEL.2015.00392/PDF

Keshavarzian, A., Green, S. J., Engen, P. A., Voigt, R. M., Naqib, A., Forsyth, C. B., Mutlu, E., & Shannon, K. M. (2015). Colonic bacterial composition in Parkinson's disease. *Movement Disorders*, *30*(10), 1351–1360. https://doi.org/10.1002/mds.26307

Khan, A. F., Adewale, Q., Lin, S. J., Baumeister, T. R., Zeighami, Y., Carbonell, F., Palomero-Gallagher, N., & Iturria-Medina, Y. (2023). Patient-specific models link neurotransmitter receptor mechanisms with motor and visuospatial axes of Parkinson's disease. *Nature Communications 2023 14:1*, *14*(1), 1–17. https://doi.org/10.1038/s41467-023-41677-w

Kim, K. A., Gu, W., Lee, I. A., Joh, E. H., & Kim, D. H. (2012). High Fat Diet-Induced Gut Microbiota Exacerbates Inflammation and Obesity in Mice via the TLR4 Signaling Pathway. *PLOS ONE*, *7*(10), e47713. https://doi.org/10.1371/JOURNAL.PONE.0047713

Kim, S. (2019). Transneuronal propagation of pathologic alpha-Synuclein from the gut to the brain models Parkinson's disease. *Neuron.*, *103*, 627–641.

Kim, S., Kwon, S.-H., Kam, T.-I., Dawson, V. L., Dawson, T. M., & Ko, H. S. (2019). Transneuronal Propagation of Pathologic α-Synuclein from the Gut to the Brain Models Parkinson's Disease. *Neuron*, *103*, 627-641.e7. https://doi.org/10.1016/j.neuron.2019.05.035

Knudsen, K., Fedorova, T. D., Horsager, J., Andersen, K. B., Skjærbæk, C., Berg, D., Schaeffer, E., Brooks, D. J., Pavese, N., Van Den Berge, N., & Borghammer, P. (2021). Asymmetric Dopaminergic Dysfunction in Brain-First versus Body-First Parkinson's Disease Subtypes. *Journal of Parkinson's Disease*, *11*(4), 1677–1687. https://doi.org/10.3233/JPD-212761

Ko, T. H., Lee, Y. H., Chan, L., Tsai, K. W. K., Hong, C. T., & Lo, W. L. (2023). Magnetic Resonance–Guided focused ultrasound surgery for Parkinson's disease: A mini-review and comparison between deep brain stimulation. *Parkinsonism & Related Disorders*, *111*, 105431. https://doi.org/10.1016/J.PARKRELDIS.2023.105431

Koda, S., Date, Y., Murakami, N., Shimbara, T., Hanada, T., Toshinai, K., Niijima, A., Furuya, M., Inomata, N., Osuye, K., & Nakazato, M. (2005). The Role of the Vagal Nerve in Peripheral PYY3–36-Induced Feeding Reduction in Rats. *Endocrinology*, *146*(5), 2369–2375. https://doi.org/10.1210/EN.2004-1266

Körner, A., & Pawelek, J. (1982). Mammalian Tyrosinase Catalyzes Three Reactions in the Biosynthesis of Melanin. *Science*, *217*(4565), 1163–1165. https://doi.org/10.1126/SCIENCE.6810464

Korzhevskii, D. E., Kirik, O. V., Guselnikova, V. V., Tsyba, D. L., Fedorova, E. A., & Grigorev, I. P. (2021). Changes in cytoplasmic and extracellular neuromelanin in human substantia nigra with normal aging. *European Journal of Histochemistry*, *65*(s1). https://doi.org/10.4081/ejh.2021.3283

Krainc, T., Monje, M. H. G., Kinsinger, M., Bustos, B. I., & Lubbe, S. J. (2023). Melanin and Neuromelanin: Linking Skin Pigmentation and Parkinson's Disease. *Movement Disorders*, *38*(2), 185–195. https://doi.org/10.1002/MDS.29260

Krieger, J. P. (2020). Intestinal glucagon-like peptide-1 effects on food intake: Physiological relevance and emerging mechanisms. *Peptides*, *131*, 170342. https://doi.org/10.1016/J.PEPTIDES.2020.170342

Kuai, X. yi, Yao, X. han, Xu, L. juan, Zhou, Y. qing, Zhang, L. ping, Liu, Y., Pei, S. fang, & Zhou, C. li. (2021). Evaluation of fecal microbiota transplantation in Parkinson's disease patients with constipation. *Microbial Cell Factories*, *20*(1). https://doi.org/10.1186/S12934-021-01589-0

Kupsky, W. J., Grimes, M. M., Sweeting, J., Bertsch, R., & Cote, L. J. (1987). Parkinson's disease and megacolon: Concentric hyaline inclusions (lewy bodies) in enteric ganglion cells. *Neurology*, *37*(7), 1253–1255. https://doi.org/10.1212/WNL.37.7.1253

Kwon, D., Paul, K. C., Yu, Y., Zhang, K., Folle, A. D., Wu, J., Bronstein, J. M., & Ritz, B. (2024). Traffic-related air pollution and Parkinson's disease in central California. *Environmental Research*, *240*(Pt 1). https://doi.org/10.1016/J.ENVRES.2023.117434

Kwon, D., Zhang, K., Paul, K. C., Folle, A. D., Del Rosario, I., Jacobs, J. P., Keener, A. M., Bronstein, J. M., & Ritz, B. (2024). Diet and the gut microbiome in patients with Parkinson's disease. *Npj Parkinson's Disease 2024 10:1*, *10*(1), 1–9. https://doi.org/10.1038/s41531-024-00681-7

Kwon, M. J., Kim, J. K., Kim, J. H., Kim, J. H., Kim, M. J., Kim, N. Y., Choi, H. G., & Kim, E. S. (2023). Exploring the Link between Chronic Kidney Disease and Parkinson's Disease: Insights from a Longitudinal Study Using a National Health Screening Cohort. *Nutrients*, *15*(14). https://doi.org/10.3390/NU15143205

Laguna, A., Peñuelas, N., Gonzalez-Sepulveda, M., Nicolau, A., Arthaud, S., Guillard-Sirieix, C., Lorente-Picón, M., Compte, J., Miquel-Rio, L., Xicoy, H., Liu, J., Parent, A., Cuadros, T., Romero-Giménez, J., Pujol, G., Giménez-Llort, L., Fort, P., Bortolozzi, A., Carballo-Carbajal, I., & Vila, M. (2024). Modelling human neuronal catecholaminergic pigmentation in rodents recapitulates age-related neurodegenerative deficits. *Nature Communications 2024 15:1*, *15*(1), 1–18. https://doi.org/10.1038/s41467-024-53168-7

Laguna, A., Xicoy, H., Tolosa, E., Serradell, M., Vilas, D., Gaig, C., Fernández, M., Yanes, O., Santamaria, J., Amigó, N., Iranzo, A., & Vila, M. (2021). Serum metabolic biomarkers for synucleinopathy conversion in isolated REM sleep behavior disorder. *Npj Parkinson's Disease 2021 7:1*, *7*(1), 1–8. https://doi.org/10.1038/s41531-021-00184-9

Lai, F., Jiang, R., Xie, W., Liu, X., Tang, Y., Xiao, H., Gao, J., Jia, Y., & Bai, Q. (2018). Intestinal Pathology and Gut Microbiota Alterations in a Methyl-4-phenyl-1,2,3,6-tetrahydropyridine (MPTP) Mouse Model of Parkinson's Disease. *Neurochemical Research*, *43*(10), 1986–1999. https://doi.org/10.1007/S11064-018-2620-X/FIGURES/9

Langer, V., Vivi, E., Regensburger, D., Winkler, T. H., Waldner, M. J., Rath, T., Schmid, B., Skottke, L., Lee, S., Jeon, N. L., Wohlfahrt, T., Kramer, V., Tripal, P., Schumann, M., Kersting, S., Handtrack, C., Geppert, C. I., Suchowski, K., Adams, R. H., … Stürzl, M. (2019). IFN-γ drives inflammatory bowel disease pathogenesis through VE-cadherin–directed vascular barrier disruption. *The Journal of Clinical Investigation*, *129*(11), 4691. https://doi.org/10.1172/JCI124884

Lawson, V. A., Furness, J. B., Klemm, H. M., Pontell, L., Chan, E., Hill, A. F., & Chiocchetti, R. (2010). The brain to gut pathway: A possible route of prion transmission. *Gut*, *59*(12), 1643–1651. https://doi.org/10.1136/gut.2010.222620

Le, W., Wu, J., & Tang, Y. (2016). Protective microglia and their regulation in Parkinson's disease. *Frontiers in Molecular Neuroscience*, *9*(SEP2016), 218961. https://doi.org/10.3389/FNMOL.2016.00089/BIBTEX

Lebouvier, T., Neunlist, M., des Varannes, S. B., Coron, E., Drouard, A., N'Guyen, J. M., Chaumette, T., Tasselli, M., Paillusson, S., Flamand, M., Galmiche, J. P., Damier, P., & Derkinderen, P. (2010). Colonic Biopsies to Assess the Neuropathology of Parkinson's Disease and Its Relationship with Symptoms. *PLoS ONE*, *5*(9), e12728. https://doi.org/10.1371/JOURNAL.PONE.0012728

Leclair-Visonneau, L., Clairembault, T., Coron, E., Le DIly, S., Vavasseur, F., Dalichampt, M., Péreón, Y., Neunlist, M., & Derkinderen, P. (2017). REM sleep behavior disorder is related to enteric neuropathology in Parkinson disease. *Neurology*, *89*(15), 1612–1618. https://doi.org/10.1212/WNL.0000000000004496

Leclair-Visonneau, L., Neunlist, M., Derkinderen, P., & Lebouvier, T. (2020). The gut in Parkinson's disease: Bottom-up, top-down, or neither? In *Neurogastroenterology and Motility* (Vol. 32, Issue 1). Blackwell Publishing Ltd. https://doi.org/10.1111/nmo.13777

Lee, H. S., Lobbestael, E., Vermeire, S., Sabino, J., & Cleynen, I. (2021). Inflammatory bowel disease and Parkinson's disease: common pathophysiological links. *Gut*, *70*(2), 408–417. https://doi.org/10.1136/GUTJNL-2020-322429

Lee, Y. H., Cha, J., Chung, S. J., Yoo, H. S., Sohn, Y. H., Ye, B. S., & Lee, P. H. (2019). Beneficial effect of estrogen on nigrostriatal dopaminergic neurons in drug-naïve postmenopausal Parkinson's disease. *Scientific Reports 2019 9:1*, *9*(1), 1–9. https://doi.org/10.1038/s41598-019-47026-6

Lee, Y. S., Wollam, J., & Olefsky, J. M. (2018). An Integrated View of Immunometabolism. *Cell*, *172*(1–2), 22. https://doi.org/10.1016/J.CELL.2017.12.025

Levi, S., Cox, M., Lugon, M., Hodkinson, M., & Tomkins, A. (1990). Increased energy expenditure in Parkinson's disease. *BMJ : British Medical Journal*, *301*(6763), 1256. https://doi.org/10.1136/BMJ.301.6763.1256

Lewis, S. J., & Heaton, K. W. (1997). Stool Form Scale as a Useful Guide to Intestinal Transit Time. *Scandinavian Journal of Gastroenterology*, *32*(9), 920–924. https://doi.org/10.3109/00365529709011203

Lewy, F. H. (1942). The diseases of the basal ganglia. . *Res Publ Ass Nerv Ment Dis, 21*, 1–20.

Lewy FH. (1912). Paralysis agitans. In Lewandowsky M (Ed.), *Pathologische Anatomie. Handbuch der Neurologie* (Neurol. II, Vol. 3, pp. 920–933). Springer.

Li, C., Cui, L., Yang, Y., Miao, J., Zhao, X., Zhang, J., Cui, G., & Zhang, Y. (2019). Gut microbiota differs between parkinson's disease patients and healthy controls in northeast China. *Frontiers in Molecular Neuroscience*, *12*. https://doi.org/10.3389/fnmol.2019.00171

Li, F., Wang, P., Chen, Z., Sui, X., Xie, X., & Zhang, J. (2019). Alteration of the fecal microbiota in North-Eastern Han Chinese population with sporadic Parkinson's disease. In *Neuroscience Letters* (Vol. 707). Elsevier Ireland Ltd. https://doi.org/10.1016/j.neulet.2019.134297

Li, H. X., Zhang, C., Zhang, K., Liu, Y. Z., Peng, X. X., & Zong, Q. (2023). Inflammatory bowel disease and risk of Parkinson's disease: evidence from a meta-analysis of 14 studies involving more than 13.4 million individuals. *Frontiers in Medicine*, *10*. https://doi.org/10.3389/FMED.2023.1137366

Li, L. Y., Liu, S. F., Zhuang, J. L., Li, M. M., Huang, Z. P., Chen, Y. H., Chen, X. R., Chen, C. N., Lin, S., & Ye, L. C. (2023). Recent research progress on metabolic syndrome and risk of Parkinson's disease. *Reviews in the Neurosciences*, *34*(7), 719–735. https://doi.org/10.1515/REVNEURO-2022-0093/XML

Li, W., Wu, X., Hu, X., Wang, T., Liang, S., Duan, Y., Jin, F., & Qin, B. (2017). Structural changes of gut microbiota in Parkinson's disease and its correlation with clinical features. *Sci China Life Sci*, *60*(11), 1223–1233. https://doi.org/10.1007/s11427-016-9001-4

Li, Z. S., Pham, T. D., Tamir, H., Chen, J. J., & Gershon, M. D. (2004). Enteric Dopaminergic Neurons: Definition, Developmental Lineage, and Effects of Extrinsic Denervation. *Journal of Neuroscience*, *24*(6), 1330–1339. https://doi.org/10.1523/JNEUROSCI.3982-03.2004

Liddle, R. A. (2018). Parkinson's Disease from the Gut. *Brain Research*, *1693*(Pt B), 201. https://doi.org/10.1016/J.BRAINRES.2018.01.010

Lim, S.-Y., Ahmad-Annuar, A., Lohmann, P. K., Lange, L. M., Bahr, N., Klein, C., Phd, S., Mata, I., Lee, ;, Chian, K., Lim, S.-Y., Tan, A. H., Ahmad-Annuar, A., Okubadejo, N. U., Lohmann, K., Morris, H. R., Toh, T. S., Tay, Y. W., Lange, L. M., … Klein, C. (2024). Uncovering the genetic basis of Parkinson's disease globally: from discoveries to the clinic. *Personal View Lancet Neurol*, *23*, 1267–1280. https://doi.org/10.1016/S1474-4422(24)00378-8

Lin, A., Zheng, W., He, Y., Tang, W., Wei, X., He, R., Huang, W., Su, Y., Huang, Y., Zhou, H., & Xie, H. (2018). Gut microbiota in patients with Parkinson's disease in southern China. *Parkinsonism and Related Disorders*, *53*, 82–88. https://doi.org/10.1016/j.parkreldis.2018.05.007

Lin, C. H., Chen, C. C., Chiang, H. L., Liou, J. M., Chang, C. M., Lu, T. P., Chuang, E. Y., Tai, Y. C., Cheng, C., Lin, H. Y., & Wu, M. S. (2019). Altered gut microbiota and inflammatory cytokine responses in patients with Parkinson's disease. *Journal of Neuroinflammation*, *16*(1). https://doi.org/10.1186/s12974-019-1528-y

Lindquist, N. G., Larsson, B. S., & Lydén-Sokolowski, A. (1988). Autoradiography of [14C]paraquat or [14C]diquat in frogs and mice: Accumulation in neuromelanin. *Neuroscience Letters*, *93*(1), 1–6. https://doi.org/10.1016/0304-3940(88)90002-X

Lindskov, S., Sjöberg, K., Hagell, P., & Westergren, A. (2016). Weight stability in Parkinson's disease. *Nutritional Neuroscience*, *19*(1), 11–20. https://doi.org/10.1179/1476830515Y.0000000044

Lino Cardenas, C. L., Bourgine, J., Cauffiez, C., Allorge, D., Lo-Guidice, J. M., Broly, F., & Chevalier, D. (2010). Genetic polymorphisms of Glycine N-acyltransferase (GLYAT) in a French Caucasian population. *Xenobiotica*, *40*(12), 853–861. https://doi.org/10.3109/00498254.2010.519407

Lionnet, A., Leclair-Visonneau, L., Neunlist, M., Murayama, S., Takao, M., Adler, C. H., Derkinderen, P., & Beach, T. G. (2018). Does Parkinson's disease start in the gut? In *Acta Neuropathologica* (Vol. 135, Issue 1). Springer Verlag. https://doi.org/10.1007/s00401-017-1777-8

Liu, B., Fang, F., Pedersen, N. L., Tillander, A., Ludvigsson, J. F., Ekbom, A., Svenningsson, P., Chen, H., & Karin, W. (2017). Vagotomy and Parkinson disease A Swedish register-based matched-cohort study). *Neurology*, *88*(21), 1996–2002. https://doi.org/10.1212/WNL.0000000000003961

Liu, L., & Zhu, G. (2018). Gut–Brain Axis and Mood Disorder. *Frontiers in Psychiatry*, *9*(MAY), 223. https://doi.org/10.3389/fpsyt.2018.00223

Liu, N., Sun, S., Wang, P., Sun, Y., Hu, Q., & Wang, X. (2021). The Mechanism of Secretion and Metabolism of Gut-Derived 5-Hydroxytryptamine. *International Journal of Molecular Sciences 2021, Vol. 22, Page 7931*, *22*(15), 7931. https://doi.org/10.3390/IJMS22157931

Lloyd-Price, J., Abu-Ali, G., & Huttenhower, C. (2016). The healthy human microbiome. In *Genome Medicine* (Vol. 8, Issue 1). BioMed Central Ltd. https://doi.org/10.1186/s13073-016-0307-y

Lorente-picón, M., & Laguna, A. (2021). New Avenues for Parkinson's Disease Therapeutics: Disease-Modifying Strategies Based on the Gut Microbiota. *Biomolecules 2021, Vol. 11, Page 433*, *11*(3), 433. https://doi.org/10.3390/BIOM11030433

Lorenzo, C., Festa, A., Hanley, A. J., Rewers, M. J., Escalante, A., & Haffner, S. M. (2017). Novel Protein Glycan–Derived Markers of Systemic Inflammation and C-Reactive Protein in Relation to Glycemia, Insulin Resistance, and Insulin Secretion. *Diabetes Care*, *40*(3), 375–382. https://doi.org/10.2337/DC16-1569

Louis, E. D., & Bennett, D. A. (2007). Mild Parkinsonian signs: An overview of an emerging concept. *Movement Disorders*, *22*(12), 1681–1688. https://doi.org/10.1002/MDS.21433

Louis, P., Hold, G. L., & Flint, H. J. (2014). The gut microbiota, bacterial metabolites and colorectal cancer. *Nature Reviews Microbiology 2014 12:10*, *12*(10), 661–672. https://doi.org/10.1038/nrmicro3344

Lu, Y., Fan, C., Li, P., Lu, Y., Chang, X., & Qi, K. (2016). Short Chain Fatty Acids Prevent High-fat-diet-induced Obesity in Mice by Regulating G Protein-coupled Receptors and Gut Microbiota. *Scientific Reports 2016 6:1*, *6*(1), 1–13. https://doi.org/10.1038/srep37589

Luk, K. C., Kehm, V. M., Zhang, B., O'Brien, P., Trojanowski, J. Q., & Lee, V. M. Y. (2012). Intracerebral inoculation of pathological α-synuclein initiates a rapidly progressive neurodegenerative α-synucleinopathy in mice. *The Journal of Experimental Medicine*, *209*(5), 975. https://doi.org/10.1084/JEM.20112457

Lundblad, M., Picconi, B., Lindgren, H., & Cenci, M. A. (2004). A model of l-DOPA-induced dyskinesia in 6-hydroxydopamine lesioned mice: relation to motor and cellular parameters of nigrostriatal function. *Neurobiology of Disease*, *16*(1), 110–123. https://doi.org/10.1016/J.NBD.2004.01.007

Ma, K., Xiong, N., Shen, Y., Han, C., Liu, L., Zhang, G., Wang, L., Guo, S., Guo, X., Xia, Y., Wan, F., Huang, J., Lin, Z., & Wang, T. (2018). Weight Loss and Malnutrition in Patients with Parkinson's Disease: Current Knowledge and Future Prospects. *Frontiers in Aging Neuroscience*, *10*(JAN). https://doi.org/10.3389/FNAGI.2018.00001

Machiels, K., Joossens, M., Sabino, J., De Preter, V., Arijs, I., Eeckhaut, V., Ballet, V., Claes, K., Van Immerseel, F., Verbeke, K., Ferrante, M., Verhaegen, J., Rutgeerts, P., & Vermeire, S. (2014). A decrease of the butyrate-producing species Roseburia hominis and Faecalibacterium prausnitzii defines dysbiosis in patients with ulcerative colitis. *Gut*, *63*(8), 1275–1283. https://doi.org/10.1136/GUTJNL-2013-304833

Madara, J. L., & Stafford, J. (1989). Interferon-gamma directly affects barrier function of cultured intestinal epithelial monolayers. *The Journal of Clinical Investigation*, *83*(2), 724–727. https://doi.org/10.1172/JCI113938

Makki, K., Deehan, E. C., Walter, J., & Bäckhed, F. (2018). The Impact of Dietary Fiber on Gut Microbiota in Host Health and Disease. In *Cell Host and Microbe* (Vol. 23, Issue 6, pp. 705–715). Cell Press. https://doi.org/10.1016/j.chom.2018.05.012

Mamun, M. A. Al, Rakib, A., Mandal, M., & Singh, U. P. (2025). Impact of a High-Fat Diet on the Gut Microbiome: A Comprehensive Study of Microbial and Metabolite Shifts During Obesity. *Cells 2025, Vol. 14, Page 463*, *14*(6), 463. https://doi.org/10.3390/CELLS14060463

Mandal, R., Loeffler, A. G., Salamat, S., & Fritsch, M. K. (2012a). Organ Weight Changes Associated With Body Mass Index Determined From a Medical Autopsy Population. *American Journal of Forensic Medicine and Pathology*, *33*(4), 382–389. https://doi.org/10.1097/PAF.0B013E3182518E5F

Mandal, R., Loeffler, A. G., Salamat, S., & Fritsch, M. K. (2012b). Organ Weight Changes Associated With Body Mass Index Determined From a Medical Autopsy Population. *American Journal of Forensic Medicine and Pathology*, *33*(4), 382–389. https://doi.org/10.1097/PAF.0B013E3182518E5F

Manfredsson, F. P., Luk, K. C., Benskey, M. J., Gezer, A., Garcia, J., Kuhn, N. C., Sandoval, I. M., Patterson, J. R., O'Mara, A., Yonkers, R., & Kordower, J. H. (2018). Induction of alpha-synuclein pathology in the enteric nervous system of the rat and non-human primate results in gastrointestinal dysmotility and transient CNS pathology. *Neurobiology of Disease*, *112*, 106–118. https://doi.org/10.1016/j.nbd.2018.01.008

Mann, D. M. A., & Yates, P. O. (1983). Possible role of neuromelanin in the pathogenesis of Parkinson's disease. *Mechanisms of Ageing and Development*, *21*(2), 193–203. https://doi.org/10.1016/0047-6374(83)90074-X

Marano, M., Anzini, G., Saltarocchi, L., Ricciuti, R., Capone, F., Tan, H., Torrecillos, F., Lanzone, J., & Di Lazzaro, V. (2024). Left Vagus Stimulation Modulates Contralateral Subthalamic β Power Improving the Gait in Parkinson's Disease. *Movement Disorders*, *39*(2), 424–428. https://doi.org/10.1002/MDS.29690

Marques, P., Lages, A. D. S., Skorupskaite, K., Rozario, K. S., Anderson, R. A., & George, J. T. (2024). Physiology of GnRH and Gonadotrophin Secretion. *Endotext*. https://www.ncbi.nlm.nih.gov/books/NBK279070/

Marras, C., Beck, J. C., Bower, J. H., Roberts, E., Ritz, B., Ross, G. W., Abbott, R. D., Savica, R., Van Den Eeden, S. K., Willis, A. W., & Tanner, C. (2018). Prevalence of Parkinson's disease across North America. *Npj Parkinson's Disease*, *4*(1). https://doi.org/10.1038/S41531-018-0058-0

Marras, C., Fereshtehnejad, S. M., Berg, D., Bohnen, N. I., Dujardin, K., Erro, R., Espay, A. J., Halliday, G., Van Hilten, J. J., Hu, M. T., Jeon, B., Klein, C., Leentjens, A. F. G., Mollenhauer, B., Postuma, R. B., Rodríguez-Violante, M., Simuni, T., Weintraub, D., Lawton, M., & Mestre, T. A. (2024). Transitioning from Subtyping to Precision Medicine in Parkinson's Disease: A Purpose-Driven Approach. *Movement Disorders*, *39*(3), 462–471. https://doi.org/10.1002/MDS.29708

Marsden, C. D. (1961). Pigmentation in the nucleus substantiae nigrae of mammals. *Journal of Anatomy*, *95*(Pt 2), 256. https://pmc.ncbi.nlm.nih.gov/articles/PMC1244469/

Martin, A. M., Young, R. L., Leong, L., Rogers, G. B., Spencer, N. J., Jessup, C. F., & Keating, D. J. (2017). The Diverse Metabolic Roles of Peripheral Serotonin. *Endocrinology*, *158*(5), 1049–1063. https://doi.org/10.1210/EN.2016-1839

Martinez-Martin, P., Pecurariu, C. F., Odin, P., Van Hilten, J. J., Antonini, A., Rojo-Abuin, J. M., Borges, V., Trenkwalder, C., Aarsland, D., Brooks, D. J., & Chaudhuri, K. R. (2012). Gender-related differences in the burden of non-motor symptoms in Parkinson's disease. *Journal of Neurology*, *259*(8), 1639–1647. https://doi.org/10.1007/S00415-011-6392-3/TABLES/4

Martínez-Montoro, J. I., Morales, E., Cornejo-Pareja, I., Tinahones, F. J., & Fernández-García, J. C. (2022). Obesity-related glomerulopathy: Current approaches and future perspectives. *Obesity Reviews*, *23*(7), e13450. https://doi.org/10.1111/OBR.13450

Martyn, J. A. J., Kaneki, M., & Yasuhara, S. (2008). Obesity-Induced Insulin Resistance and Hyperglycemia: Etiological Factors and Molecular Mechanisms. *Anesthesiology*, *109*(1), 137. https://doi.org/10.1097/ALN.0B013E3181799D45

Masini, D., Plewnia, C., Bertho, M., Scalbert, N., Caggiano, V., & Fisone, G. (2021). A guide to the generation of a 6-hydroxydopamine mouse model of Parkinson's disease for the study of non-motor symptoms. *Biomedicines*, *9*(6), 598. https://doi.org/10.3390/BIOMEDICINES9060598/S1

Matheoud, D., Cannon, T., Voisin, A., Penttinen, A. M., Ramet, L., Fahmy, A. M., Ducrot, C., Laplante, A., Bourque, M. J., Zhu, L., Cayrol, R., Le Campion, A., McBride, H. M., Gruenheid, S., Trudeau, L. E., & Desjardins, M. (2019). Intestinal infection triggers Parkinson's disease-like symptoms in Pink1 −/− mice. In *Nature* (Vol. 571, Issue 7766, pp. 565–569). Nature Publishing Group. https://doi.org/10.1038/s41586-019-1405-y

Matt, S. M., & Gaskill, P. J. (2019). Where Is Dopamine and how do Immune Cells See it?: Dopamine-Mediated Immune Cell Function in Health and Disease. *Journal of Neuroimmune Pharmacology 2019 15:1*, *15*(1), 114–164. https://doi.org/10.1007/S11481-019-09851-4

Mavrommatis, E., Fish, E. N., & Platanias, L. C. (2013). The Schlafen Family of Proteins and Their Regulation by Interferons. *Journal of Interferon & Cytokine Research*, *33*(4), 206. https://doi.org/10.1089/JIR.2012.0133

Mayer, E. A. (2011). Gut feelings: the emerging biology of gut–brain communication. *Nature Reviews Neuroscience 2011 12:8*, *12*(8), 453–466. https://doi.org/10.1038/nrn3071

Mazumder, M. K., Paul, R., Bhattacharya, P., & Borah, A. (2019). Neurological sequel of chronic kidney disease: From diminished Acetylcholinesterase activity to mitochondrial dysfunctions, oxidative stress and inflammation in mice brain. *Scientific Reports 2019 9:1*, *9*(1), 1–22. https://doi.org/10.1038/s41598-018-37935-3

McCormack, A. L., Thiruchelvam, M., Manning-Bog, A. B., Thiffault, C., Langston, J. W., Cory-Slechta, D. A., & Di Monte, D. A. (2002). Environmental Risk Factors and Parkinson's Disease: Selective

Degeneration of Nigral Dopaminergic Neurons Caused by the Herbicide Paraquat. *Neurobiology of Disease*, *10*(2), 119–127. https://doi.org/10.1006/NBDI.2002.0507

McFleder, R. L., Makhotkina, A., Groh, J., Keber, U., Imdahl, F., Peña Mosca, J., Peteranderl, A., Wu, J., Tabuchi, S., Hoffmann, J., Karl, A. K., Pagenstecher, A., Vogel, J., Beilhack, A., Koprich, J. B., Brotchie, J. M., Saliba, A. E., Volkmann, J., & Ip, C. W. (2023). Brain-to-gut trafficking of alpha-synuclein by CD11c+ cells in a mouse model of Parkinson's disease. *Nature Communications 2023 14:1*, *14*(1), 1–13. https://doi.org/10.1038/s41467-023-43224-z

McGeer, P. L., Itagaki, S., Boyes, B. E., & McGeer, E. G. (1988). Reactive microglia are positive for HLA-DR in the: Substantia nigra of Parkinson's and Alzheimer's disease brains. *Neurology*, *38*(8), 1285–1291. https://doi.org/10.1212/WNL.38.8.1285

Mehanna, R., Smilowska, K., Fleisher, J., Post, B., Hatano, T., Pimentel Piemonte, M. E., Kumar, K. R., McConvey, V., Zhang, B., Tan, E. K., Savica, R., Tan, E. K., Mehanna, R., Smilowska, K., Marras, C., Ross, O., Fleisher, J., McConvey, V., Wu, Y. R., … Salari, M. (2022). Age Cutoff for Early-Onset Parkinson's Disease: Recommendations from the International Parkinson and Movement Disorder Society Task Force on Early Onset Parkinson's Disease. *Movement Disorders Clinical Practice*, *9*(7), 869–878. https://doi.org/10.1002/MDC3.13523

Meissner, W. G., Remy, P., Giordana, C., Maltête, D., Derkinderen, P., Houéto, J.-L., Anheim, M., Benatru, I., Boraud, T., Brefel-Courbon, C., Carrière, N., Catala, H., Colin, O., Corvol, J.-C., Damier, P., Dellapina, E., Devos, D., Drapier, S., Fabbri, M., … Rascol, O. (2024). Trial of Lixisenatide in Early Parkinson's Disease. *New England Journal of Medicine*, *390*(13), 1176–1185. https://doi.org/10.1056/NEJMOA2312323/SUPPL_FILE/NEJMOA2312323_DATA-SHARING.PDF

Meléndez-Flores, J. D., & Estrada-Bellmann, I. (2021). Linking chronic kidney disease and Parkinson's disease: a literature review. *Metabolic Brain Disease*, *36*(1), 1–12. https://doi.org/10.1007/S11011-020-00623-1/TABLES/2

Menozzi, E., Macnaughtan, J., & Schapira, A. H. V. (2021). The gut-brain axis and Parkinson disease: clinical and pathogenetic relevance. *Annals of Medicine*, *53*(1), 611–625. https://doi.org/10.1080/07853890.2021.1890330

Mertz, H. (2002). Role of the brain and sensory pathways in gastrointestinal sensory disorders in humans. *Gut*, *51*(suppl 1), i29–i33. https://doi.org/10.1136/GUT.51.SUPPL_1.I29

Mestre, T. A., Fereshtehnejad, S. M., Berg, D., Bohnen, N. I., Dujardin, K., Erro, R., Espay, A. J., Halliday, G., Van Hilten, J. J., Hu, M. T., Jeon, B., Klein, C., Leentjens, A. F. G., Marinus, J., Mollenhauer, B., Postuma, R., Rajalingam, R., Rodríguez-Violante, M., Simuni, T., … Marras, C. (2021). Parkinson's Disease Subtypes: Critical Appraisal and Recommendations. *Journal of Parkinson's Disease*, *11*(2), 395. https://doi.org/10.3233/JPD-202472

Minakawa, A., Fukuda, A., Sato, Y., Kikuchi, M., Kitamura, K., Wiggins, R. C., & Fujimoto, S. (2019). Podocyte hypertrophic stress and detachment precedes hyperglycemia or albuminuria in a rat model of obesity and type2 diabetes-associated nephropathy. *Scientific Reports 2019 9:1*, *9*(1), 1–15. https://doi.org/10.1038/s41598-019-54692-z

Miranda, M., Botti, D., Bonfigli, A., Ventura, T., & Arcadi, A. (1984). Tyrosinase-like activity in normal human substantia nigra. *General Pharmacology: The Vascular System*, *15*(6), 541–544. https://doi.org/10.1016/0306-3623(84)90212-X

Mittal, R., Debs, L. H., Patel, A. P., Nguyen, D., Patel, K., O'Connor, G., Grati, M., Mittal, J., Yan, D., Eshraghi, A. A., Deo, S. K., Daunert, S., & Liu, X. Z. (2017). Neurotransmitters: The Critical Modulators Regulating Gut–Brain Axis. *Journal of Cellular Physiology*, *232*(9), 2359–2372. https://doi.org/10.1002/JCP.25518

Miyake, Y., Sasaki, S., Tanaka, K., Fukushima, W., Kiyohara, C., Tsuboi, Y., Yamada, T., Oeda, T., Miki, T., Kawamura, N., Sakae, N., Fukuyama, H., Hirota, Y., & Nagai, M. (2010). Dietary fat intake and risk of Parkinson's disease: A case-control study in Japan. *Journal of the Neurological Sciences*, *288*(1–2), 117–122. https://doi.org/10.1016/j.jns.2009.09.021

Miyazaki, I., Isooka, N., Imafuku, F., Sun, J., Kikuoka, R., Furukawa, C., & Asanuma, M. (2020). Chronic Systemic Exposure to Low-Dose Rotenone Induced Central and Peripheral Neuropathology and Motor Deficits in Mice: Reproducible Animal Model of Parkinson's Disease. *International Journal of Molecular Sciences 2020, Vol. 21, Page 3254*, *21*(9), 3254. https://doi.org/10.3390/IJMS21093254

Mohallem, R., & Aryal, U. K. (2020). Regulators of TNFα mediated insulin resistance elucidated by quantitative proteomics. *Scientific Reports 2020 10:1*, *10*(1), 1–15. https://doi.org/10.1038/s41598-020-77914-1

Molina, J. A., Jiménez-Jiménez, F. J., Gómez, P., Vargas, C., Navarro, J. A., Ortí-Pareja, M., Gasalla, T., Benito-León, J., Bermejo, F., & Arenas, J. (1997). Decreased cerebrospinal fluid levels of neutral and basic amino acids in patients with Parkinson's disease. *Journal of the Neurological Sciences*, *150*(2), 123–127. https://doi.org/10.1016/S0022-510X(97)00069-5

Montgomery, M. K., Hallahan, N. L., Brown, S. H., Liu, M., Mitchell, T. W., Cooney, G. J., & Turner, N. (2013a). Mouse strain-dependent variation in obesity and glucose homeostasis in response to high-fat feeding. *Diabetologia*, *56*(5), 1129–1139. https://doi.org/10.1007/S00125-013-2846-8/FIGURES/6

Montgomery, M. K., Hallahan, N. L., Brown, S. H., Liu, M., Mitchell, T. W., Cooney, G. J., & Turner, N. (2013b). Mouse strain-dependent variation in obesity and glucose homeostasis in response to high-fat feeding. *Diabetologia*, *56*(5), 1129–1139. https://doi.org/10.1007/S00125-013-2846-8/FIGURES/6

Morais, L. H., Hara, D. B., Bicca, M. A., Poli, A., & Takahashi, R. N. (2018). Early signs of colonic inflammation, intestinal dysfunction, and olfactory impairments in the rotenone-induced mouse model of Parkinson's disease. *Behavioural Pharmacology*, *29*, 199–210. https://doi.org/10.1097/FBP.0000000000000389

Morais, L. H., Schreiber, H. L., & Mazmanian, S. K. (2020). The gut microbiota–brain axis in behaviour and brain disorders. In *Nature Reviews Microbiology* (pp. 1–15). Nature Research. https://doi.org/10.1038/s41579-020-00460-0

Moreira, A. P. B., Texeira, T. F. S., Ferreira, A. B., Do Carmo Gouveia Peluzio, M., & De Cássia Gonçalves Alfenas, R. (2012). Influence of a high-fat diet on gut microbiota, intestinal permeability and metabolic endotoxaemia. *British Journal of Nutrition*, *108*(5), 801–809. https://doi.org/10.1017/S0007114512001213

Moreno-García, A., Kun, A., Calero, M., & Calero, O. (2021). The Neuromelanin Paradox and Its Dual Role in Oxidative Stress and Neurodegeneration. *Antioxidants*, *10*(1), 124. https://doi.org/10.3390/ANTIOX10010124

Morris, R., Yarnall, A. J., Hunter, H., Taylor, J. P., Baker, M. R., & Rochester, L. (2019). Noninvasive vagus nerve stimulation to target gait impairment in Parkinson's disease. *Movement Disorders*, *34*(6), 918–919. https://doi.org/10.1002/MDS.27664

Mukai, R., Handa, O., Naito, Y., Takayama, S., Suyama, Y., Ushiroda, C., Majima, A., Hirai, Y., Mizushima, K., Okayama, T., Katada, K., Kamada, K., Uchiyama, K., Ishikawa, T., Takagi, T., & Itoh, Y. (2020). High-Fat Diet Causes Constipation in Mice via Decreasing Colonic Mucus. *Digestive Diseases and Sciences*, *65*(8), 2246–2253. https://doi.org/10.1007/S10620-019-05954-3/FIGURES/4

Mulak, A. (2018). A controversy on the role of short-chain fatty acids in the pathogenesis of Parkinson's disease. *Movement Disorders*, *33*(3), 398–401. https://doi.org/10.1002/mds.27304

Mulak, A. (2020). An overview of the neuroendocrine system in Parkinson's disease: what is the impact on diagnosis and treatment? *Expert Review of Neurotherapeutics*, *20*(2), 127–135. https://doi.org/10.1080/14737175.2020.1701437

Mulak, A., Koszewicz, M., Panek-Jeziorna, M., Koziorowska-Gawron, E., & Budrewicz, S. (2019). Fecal calprotectin as a marker of the gut immune system activation is elevated in parkinson's disease. *Frontiers in Neuroscience*, *13*(SEP). https://doi.org/10.3389/fnins.2019.00992

Murakami, K., Wakamatsu, K., Nakanishi, Y., Takahashi, H., Sugiyama, S., & Ito, S. (2008). Serum Levels of Pigmentation Markers Are Elevated in Patients Undergoing Hemodialysis. *Blood Purification*, *25*(5–6), 483–489. https://doi.org/10.1159/000112516

Murakami, M., Sato, H., Miki, Y., Yamamoto, K., & Taketomi, Y. (2015). A new era of secreted phospholipase A2. *Journal of Lipid Research*, *56*(7), 1248–1261. https://doi.org/10.1194/JLR.R058123

Murphy, E. A., Velazquez, K. T., & Herbert, K. M. (2015). Influence of high-fat diet on gut microbiota: A driving force for chronic disease risk. *Current Opinion in Clinical Nutrition and Metabolic Care*, *18*(5), 515–520. https://doi.org/10.1097/MCO.0000000000000209

Naderpoor, N., Lyons, J. G., Mousa, A., Ranasinha, S., De Courten, M. P. J. D., Soldatos, G., & De Courten, B. D. (2017). Higher glomerular filtration rate is related to insulin resistance but not to obesity in a predominantly obese non-diabetic cohort. *Scientific Reports*, *7*, 45522. https://doi.org/10.1038/SREP45522

Nagatsu, T., Mogi, M., Ichinose, H., & Togari, A. (2000). Changes in cytokines and neurotrophins in Parkinson's disease. *Journal of Neural Transmission, Supplement*, *60*, 277–290. https://doi.org/10.1007/978-3-7091-6301-6_19

Nagatsu, T., Nakashima, A., Watanabe, H., Ito, S., Wakamatsu, K., Zucca, F. A., Zecca, L., Youdim, M., Wulf, M., Riederer, P., & Dijkstra, J. M. (2023). The role of tyrosine hydroxylase as a key player in neuromelanin synthesis and the association of neuromelanin with Parkinson's disease. *Journal of Neural Transmission 2023 130:5*, *130*(5), 611–625. https://doi.org/10.1007/S00702-023-02617-6

Nagatsu, T., & Sawada, M. (2005). Inflammatory Process in Parkinsons Disease: Role for Cytokines. *Current Pharmaceutical Design*, *11*(8), 999–1016. https://doi.org/10.2174/1381612053381620

Nagesh Babu, G., Gupta, M., Paliwal, V. K., Singh, S., Chatterji, T., & Roy, R. (2018). Serum metabolomics study in a group of Parkinson's disease patients from northern India. *Clinica Chimica Acta*, *480*, 214–219. https://doi.org/10.1016/J.CCA.2018.02.022

Nagpal, R., Mainali, R., Ahmadi, S., Wang, S., Singh, R., Kavanagh, K., Kitzman, D. W., Kushugulova, A., Marotta, F., & Yadav, H. (2018). Gut microbiome and aging: Physiological and mechanistic insights. In *Nutrition and Healthy Aging* (Vol. 4, Issue 4, pp. 267–285). IOS Press. https://doi.org/10.3233/NHA-170030

Nam, G. E., Kim, N. H., Han, K., Choi, K. M., Chung, H. S., Kim, J. W., Han, B., Cho, S. J., Jung, S. J., Yu, J. H., Park, Y. G., & Kim, S. M. (2019). Chronic renal dysfunction, proteinuria, and risk of Parkinson's disease in the elderly. *Movement Disorders*, *34*(8), 1184–1191. https://doi.org/10.1002/MDS.27704

Nascimento, J. C., Matheus, V. A., Oliveira, R. B., Tada, S. F. S., & Collares-Buzato, C. B. (2021). High-Fat Diet Induces Disruption of the Tight Junction-Mediated Paracellular Barrier in the Proximal Small Intestine Before the Onset of Type 2 Diabetes and Endotoxemia. *Digestive Diseases and Sciences*, *66*(10), 3359–3374. https://doi.org/10.1007/S10620-020-06664-X/FIGURES/9

Natale, G., Kastsiushenka, O., Fulceri, F., Ruggieri, S., Paparelli, A., & Fornai, F. (2010). MPTP-induced parkinsonism extends to a subclass of TH-positive neurons in the gut. *Brain Research*, *1355*, 195–206. https://doi.org/10.1016/J.BRAINRES.2010.07.076

Nauck, M. A., Quast, D. R., Wefers, J., & Pfeiffer, A. F. H. (2021). The evolving story of incretins (GIP and GLP-1) in metabolic and cardiovascular disease: A pathophysiological update. *Diabetes, Obesity and Metabolism*, *23*(S3), 5–29. https://doi.org/10.1111/DOM.14496

Neurath, M. F. (2014). Cytokines in inflammatory bowel disease. *Nature Reviews Immunology 2014 14:5*, *14*(5), 329–342. https://doi.org/10.1038/nri3661

Nicholson, J. K., Holmes, E., Kinross, J., Burcelin, R., Gibson, G., Jia, W., & Pettersson, S. (2012). Host-gut microbiota metabolic interactions. *Science*, *336*(6086), 1262–1267. https://doi.org/10.1126/SCIENCE.1223813/ASSET/6CB4C145-E6AE-4557-86F1-2BDD196B2064/ASSETS/GRAPHIC/336_1262_F1.JPEG

Nie, K., Ma, K., Luo, W., Shen, Z., Yang, Z., Xiao, M., Tong, T., Yang, Y., & Wang, X. (2021). Roseburia intestinalis: A Beneficial Gut Organism From the Discoveries in Genus and Species. *Frontiers in Cellular and Infection Microbiology*, *11*, 757718. https://doi.org/10.3389/FCIMB.2021.757718/PDF

Nie, S., Jing, Z., Wang, J., Deng, Y., Zhang, Y., Ye, Z., & Ge, Y. (2023). The link between increased Desulfovibrio and disease severity in Parkinson's disease. *Applied Microbiology and Biotechnology*, *107*(9), 3033–3045. https://doi.org/10.1007/S00253-023-12489-1/FIGURES/5

Nieto-Vazquez, I., Fernández-Veledo, S., Krämer, D. K., Vila-Bedmar, R., Garcia-Guerra, L., & Lorenzo, M. (2008). Insulin resistance associated to obesity: the link TNF-alpha. *Archives Of Physiology And Biochemistry*, *114*(3), 183–194. https://doi.org/10.1080/13813450802181047

Nishiwaki, H., Hamaguchi, T., Ito, M., Ishida, T., Maeda, T., Kashihara, K., Tsuboi, Y., Ueyama, J., Shimamura, T., Mori, H., Kurokawa, K., Katsuno, M., Hirayama, M., & Ohno, K. (2020). Short-Chain Fatty Acid-Producing Gut Microbiota Is Decreased in Parkinson's Disease but Not in Rapid-Eye-Movement Sleep Behavior Disorder. *MSystems*, *5*(6). https://doi.org/10.1128/msystems.00797-20

Nishiwaki, H., Ito, M., Hamaguchi, T., Maeda, T., Kashihara, K., Tsuboi, Y., Ueyama, J., Yoshida, T., Hanada, H., Takeuchi, I., Katsuno, M., Hirayama, M., & Ohno, K. (2022). Short chain fatty acids-producing and mucin-degrading intestinal bacteria predict the progression of early Parkinson's disease. *Npj Parkinson's Disease 2022 8:1*, *8*(1), 1–12. https://doi.org/10.1038/s41531-022-00328-5

Oberländer, U., Pletinckx, K., Döhler, A., Müller, N., Lutz, M. B., Arzberger, T., Riederer, P., Gerlach, M., Koutsilieri, E., & Scheller, C. (2011). Neuromelanin is an immune stimulator for dendritic cells in vitro. *BMC Neuroscience*, *12*(1), 1–9. https://doi.org/10.1186/1471-2202-12-116/FIGURES/5

Obeso, J. A., Stamelou, M., Goetz, C. G., Poewe, W., Lang, A. E., Weintraub, D., Burn, D., Halliday, G. M., Bezard, E., Przedborski, S., Lehericy, S., Brooks, D. J., Rothwell, J. C., Hallett, M., DeLong, M. R., Marras, C., Tanner, C. M., Ross, G. W., Langston, J. W., … Stoessl, A. J. (2017). Past, present, and future of Parkinson's disease: A special essay on the 200th Anniversary of the Shaking Palsy. *Movement Disorders*, *32*(9), 1264–1310. https://doi.org/10.1002/MDS.27115

Odamaki, T., Kato, K., Sugahara, H., Hashikura, N., Takahashi, S., Xiao, J. Z., Abe, F., & Osawa, R. (2016). Age-related changes in gut microbiota composition from newborn to centenarian: A cross-sectional study. *BMC Microbiology*, *16*(1). https://doi.org/10.1186/s12866-016-0708-5

O'Donovan, S. M., Crowley, E. K., Brown, J. R. M., O'Sullivan, O., O'Leary, O. F., Timmons, S., Nolan, Y. M., Clarke, D. J., Hyland, N. P., Joyce, S. A., Sullivan, A. M., & O'Neill, C. (2020). Nigral overexpression of α-synuclein in a rat Parkinson's disease model indicates alterations in the enteric nervous system and the gut microbiome. *Neurogastroenterology and Motility*, *32*(1). https://doi.org/10.1111/nmo.13726

Ottman, N., Reunanen, J., Meijerink, M., Pietila, T. E., Kainulainen, V., Klievink, J., Huuskonen, L., Aalvink, S., Skurnik, M., Boeren, S., Satokari, R., Mercenier, A., Palva, A., Smidt, H., De Vos, W. M., & Belzer, C. (2017). Pili-like proteins of Akkermansia muciniphila modulate host immune responses and gut barrier function. *PLOS ONE*, *12*(3), e0173004. https://doi.org/10.1371/JOURNAL.PONE.0173004

Ou, Z., Deng, L., Lu, Z., Wu, F., Liu, W., Huang, D., & Peng, Y. (2020). Protective effects of Akkermansia muciniphila on cognitive deficits and amyloid pathology in a mouse model of Alzheimer's disease. *Nutrition & Diabetes 2020 10:1*, *10*(1), 1–10. https://doi.org/10.1038/s41387-020-0115-8

Ou, Z., Pan, J., Tang, S., Duan, D., Yu, D., Nong, H., & Wang, Z. (2021). Global Trends in the Incidence, Prevalence, and Years Lived With Disability of Parkinson's Disease in 204 Countries/Territories From 1990 to 2019. *Frontiers in Public Health*, *9*, 776847. https://doi.org/10.3389/FPUBH.2021.776847/BIBTEX

Ouchi, Y., Yoshikawa, E., Sekine, Y., Futatsubashi, M., Kanno, T., Ogusu, T., & Torizuka, T. (2005). Microglial activation and dopamine terminal loss in early Parkinson's disease. *Annals of Neurology*, *57*(2), 168–175. https://doi.org/10.1002/ANA.20338

Pagano, G., Polychronis, S., Wilson, H., Giordano, B., Ferrara, N., Niccolini, F., & Politis, M. (2018). Diabetes mellitus and Parkinson disease. *Neurology*, *90*(19), E1654–E1662. https://doi.org/10.1212/WNL.0000000000005475

Palavra, N. C., Lubomski, M., Flood, V. M., Davis, R. L., & Sue, C. M. (2021). Increased Added Sugar Consumption Is Common in Parkinson's Disease. *Frontiers in Nutrition*, *8*. https://doi.org/10.3389/FNUT.2021.628845

Pan, L., Li, C., Meng, L., Tian, Y., He, M., Yuan, X., Zhang, G., Zhang, Z., Xiong, J., Chen, G., & Zhang, Z. (2022). Tau accelerates α-synuclein aggregation and spreading in Parkinson's disease. *Brain*, *145*(10), 3454–3471. https://doi.org/10.1093/BRAIN/AWAC171

Parashar, A., & Udayabanu, M. (2017). Gut microbiota: Implications in Parkinson's disease. In *Parkinsonism and Related Disorders* (Vol. 38, pp. 1–7). Elsevier Ltd. https://doi.org/10.1016/j.parkreldis.2017.02.002

Park, J. M., Lee, S. C., Ham, C., & Kim, Y. W. (2023). Effect of probiotic supplementation on gastrointestinal motility, inflammation, motor, non-motor symptoms and mental health in Parkinson's disease: a meta-analysis of randomized controlled trials. *Gut Pathogens*, *15*(1), 9. https://doi.org/10.1186/S13099-023-00536-1

Park, K. Y., Nam, G. E., Han, K., Park, H. K., & Hwang, H. S. (2022). Waist circumference and risk of Parkinson's disease. *Npj Parkinson's Disease 2022 8:1*, *8*(1), 1–8. https://doi.org/10.1038/s41531-022-00353-4

Park, S., Kim, J., Chun, J., Han, K., Soh, H., Kang, E. A., Lee, H. J., Im, J. P., & Kim, J. S. (2019). Patients with Inflammatory Bowel Disease Are at an Increased Risk of Parkinson's Disease: A South Korean Nationwide Population-Based Study. *Journal of Clinical Medicine*, *8*(8), 1191. https://doi.org/10.3390/JCM8081191

Parker, A., Romano, S., Ansorge, R., Aboelnour, A., Le Gall, G., Savva, G. M., Pontifex, M. G., Telatin, A., Baker, D., Jones, E., Vauzour, D., Rudder, S., Blackshaw, L. A., Jeffery, G., & Carding, S. R. (2022). Fecal microbiota transfer between young and aged mice reverses hallmarks of the aging gut, eye, and brain. *Microbiome*, *10*(1), 68. https://doi.org/10.1186/S40168-022-01243-W

Parker, B. J., Wearsch, P. A., Veloo, A. C. M., & Rodriguez-Palacios, A. (2020). The Genus Alistipes: Gut Bacteria With Emerging Implications to Inflammation, Cancer, and Mental Health. *Frontiers in Immunology*, *11*, 522172. https://doi.org/10.3389/FIMMU.2020.00906/BIBTEX

Parkinson, J. (1817). An Essay on the Shaking Palsy. *Https://Doi.Org/10.1176/Jnp.14.2.223*, *14*(2). https://doi.org/10.1176/JNP.14.2.223

Pasternak, A., Szura, M., Gil, K., & Matyja, A. (2016). Interstitial cells of Cajal — systematic review. *Folia Morphologica*, *75*(3), 281–286. https://doi.org/10.5603/FM.A2016.0002

Paumier, K. L., Luk, K. C., Manfredsson, F. P., Kanaan, N. M., Lipton, J. W., Collier, T. J., Steece-Collier, K., Kemp, C. J., Celano, S., Schulz, E., Sandoval, I. M., Fleming, S., Dirr, E., Polinski, N. K., Trojanowski, J. Q., Lee, V. M., & Sortwell, C. E. (2015). Intrastriatal injection of pre-formed mouse α-synuclein fibrils into rats triggers α-synuclein pathology and bilateral nigrostriatal degeneration. *Neurobiology of Disease*, *82*, 185–199. https://doi.org/10.1016/J.NBD.2015.06.003

Pavlov, V. A., & Tracey, K. J. (2012). The vagus nerve and the inflammatory reflex - Linking immunity and metabolism. *Nature Reviews Endocrinology*, *8*(12), 743–754. https://doi.org/10.1038/NRENDO.2012.189

Pei, Y., Wang, R., Chen, W., Yi, S., Huang, C., Liang, S., Cao, H., Xu, Y., & Tan, B. (2023). Impaired colonic motility in high-glycemic diet-induced diabetic mice is associated with disrupted gut microbiota and neuromuscular function. *Endocrine Connections*, *12*(9). https://doi.org/10.1530/EC-23-0078

Pellanda, P., Ghosh, T. S., & O'Toole, P. W. (2021). Understanding the impact of age-related changes in the gut microbiome on chronic diseases and the prospect of elderly-specific dietary interventions. *Current Opinion in Biotechnology*, *70*, 48–55. https://doi.org/10.1016/J.COPBIO.2020.11.001

Pereira, P. A. B., Trivedi, D. K., Silverman, J., Duru, I. C., Paulin, L., Auvinen, P., & Scheperjans, F. (2022). Multiomics implicate gut microbiota in altered lipid and energy metabolism in Parkinson's disease. *Npj Parkinson's Disease 2022 8:1*, *8*(1), 1–17. https://doi.org/10.1038/s41531-022-00300-3

Perez-Pardo, P., de Jong, E. M., Broersen, L. M., van Wijk, N., Attali, A., Garssen, J., & Kraneveld, A. D. (2017). Promising Effects of Neurorestorative Diets on Motor, Cognitive, and Gastrointestinal Dysfunction after Symptom Development in a Mouse Model of Parkinson's Disease. *Frontiers in Aging Neuroscience*, *9*(MAR), 57. https://doi.org/10.3389/fnagi.2017.00057

Perez-Pardo, P., Dodiya, H. B., Engen, P. A., Forsyth, C. B., Huschens, A. M., Shaikh, M., Voigt, R. M., Naqib, A., Green, S. J., Kordower, J. H., Shannon, K. M., Garssen, J., Kraneveld, A. D., & Keshavarzian, A. (2018). Role of TLR4 in the gut-brain axis in Parkinson's disease: A translational study from men to mice. *Gut*, *68*(5). https://doi.org/10.1136/gutjnl-2018-316844

Petrov, V. A., Saltykova, I. V., Zhukova, I. A., Alifirova, V. M., Zhukova, N. G., Dorofeeva, Y. B., Tyakht, A. V., Kovarsky, B. A., Alekseev, D. G., Kostryukova, E. S., Mironova, Y. S., Izhboldina, O. P., Nikitina, M. A., Perevozchikova, T. V., Fait, E. A., Babenko, V. V., Vakhitova, M. T., Govorun, V. M., & Sazonov, A. E. (2017). Analysis of gut microbiota in patients with parkinson's disease. *Bulletin of Experimental Biology and Medicine*, *162*(6), 734–737. https://doi.org/10.1007/s10517-017-3700-7

Picó, C., Palou, M., Pomar, C. A., Rodríguez, A. M., & Palou, A. (2021). Leptin as a key regulator of the adipose organ. *Reviews in Endocrine and Metabolic Disorders 2021 23:1*, *23*(1), 13–30. https://doi.org/10.1007/S11154-021-09687-5

Pietrucci, D., Cerroni, R., Unida, V., Farcomeni, A., Pierantozzi, M., Mercuri, N. B., Biocca, S., Stefani, A., & Desideri, A. (2019). Dysbiosis of gut microbiota in a selected population of Parkinson's patients. *Parkinsonism and Related Disorders*, *65*, 124–130. https://doi.org/10.1016/j.parkreldis.2019.06.003

Poewe, W., Seppi, K., Tanner, C. M., Halliday, G. M., Brundin, P., Volkmann, J., Schrag, A. E., & Lang, A. E. (2017). Parkinson disease. *Nature Reviews Disease Primers 2017 3:1*, *3*(1), 1–21. https://doi.org/10.1038/nrdp.2017.13

Polymeropoulos, M. H., Lavedan, C., Leroy, E., Ide, S. E., Dehejia, A., Dutra, A., Pike, B., Root, H., Rubenstein, J., Boyer, R., Stenroos, E. S., Chandrasekharappa, S., Athanassiadou, A., Papapetropoulos, T., Johnson, W. G., Lazzarini, A. M., Duvoisin, R. C., Di Iorio, G., Golbe, L. I., & Nussbaum, R. L. (1997). Mutation in the alpha-synuclein gene identified in families with Parkinson's disease. *Science (New York, N.Y.)*, *276*(5321), 2045–2047. http://www.ncbi.nlm.nih.gov/pubmed/9197268

Postuma, R. B., Iranzo, A., Hu, M., Högl, B., Boeve, B. F., Manni, R., Oertel, W. H., Arnulf, I., Ferini-Strambi, L., Puligheddu, M., Antelmi, E., Cochen De Cock, V., Arnaldi, D., Mollenhauer, B., Videnovic, A., Sonka, K., Jung, K. Y., Kunz, D., Dauvilliers, Y., … Pelletier, A. (2019). Risk and predictors of dementia and parkinsonism in idiopathic REM sleep behaviour disorder: a multicentre study. *Brain*, *142*(3), 744–759. https://doi.org/10.1093/BRAIN/AWZ030

Price, M. N., Dehal, P. S., & Arkin, A. P. (2009). FastTree: Computing Large Minimum Evolution Trees with Profiles instead of a Distance Matrix. *Molecular Biology and Evolution*, *26*(7), 1641–1650. https://doi.org/10.1093/MOLBEV/MSP077

Pringsheim, T., Day, G. S., Smith, D. B., Rae-Grant, A., Licking, N., Armstrong, M. J., De Bie, R. M. A., Roze, E., Miyasaki, J. M., Hauser, R. A., Espay, A. J., Martello, J. P., Gurwell, J. A., Billinghurst, L., Sullivan, K., Fitts, M. S., Cothros, N., Hall, D. A., Rafferty, M., … Lang, A. E. (2021). Dopaminergic therapy for motor symptoms in early Parkinson disease practice Guideline summary. *Neurology*, *97*(20), 942–957. https://doi.org/10.1212/WNL.0000000000012868/ASSET/7AB20B3F-6554-4259-8B15-D593F8836964/ASSETS/GRAPHIC/12TTU1.GIF

Prota, G. (2000). Melanins, Melanogenesis and Melanocytes: Looking at Their Functional Significance from the Chemist's Viewpoint. *Pigment Cell Research*, *13*(4), 283–293. https://doi.org/10.1034/J.1600-0749.2000.130412.X

Pruesse, E., Quast, C., Knittel, K., Fuchs, B. M., Ludwig, W., Peplies, J., & Glöckner, F. O. (2007). SILVA: a comprehensive online resource for quality checked and aligned ribosomal RNA sequence data compatible with ARB. *Nucleic Acids Research*, *35*(21), 7188–7196. https://doi.org/10.1093/NAR/GKM864

Przedborski, S., Tieu, K., Perier, C., & Vila, M. (2004). MPTP as a mitochondrial neurotoxic model of Parkinson's disease. *Journal of Bioenergetics and Biomembranes*, *36*(4 SPEC.ISS.), 375–379. https://doi.org/10.1023/B:JOBB.0000041771.66775.D5/METRICS

Pyatha, S., Kim, H., Lee, D., & Kim, K. (2022). Association between Heavy Metal Exposure and Parkinson's Disease: A Review of the Mechanisms Related to Oxidative Stress. *Antioxidants*, *11*(12), 2467. https://doi.org/10.3390/ANTIOX11122467

Qian, E., & Huang, Y. (2019). Subtyping of Parkinson's Disease - Where Are We Up To? *Aging and Disease*, *10*(5), 1130. https://doi.org/10.14336/AD.2019.0112

Qian, Y., Yang, X., Xu, S., Huang, P., Li, B., Du, J., He, Y., Su, B., Xu, L. M., Wang, L., Huang, R., Chen, S., & Xiao, Q. (2020). Gut metagenomics-derived genes as potential biomarkers of Parkinson's disease. *Brain*, *143*(8), 2474–2489. https://doi.org/10.1093/brain/awaa201

Qu, Y., Li, J., Qin, Q., Wang, D., Zhao, J., An, K., Mao, Z., Min, Z., Xiong, Y., Li, J., & Xue, Z. (2023). A systematic review and meta-analysis of inflammatory biomarkers in Parkinson's disease. *Npj Parkinson's Disease 2023 9:1*, *9*(1), 1–14. https://doi.org/10.1038/s41531-023-00449-5

Qu, Z. D., Thacker, M., Castelucci, P., Bagyánszki, M., Epstein, M. L., & Furness, J. B. (2008). Immunohistochemical analysis of neuron types in the mouse small intestine. *Cell and Tissue Research*, *334*(2), 147–161. https://doi.org/10.1007/S00441-008-0684-7/TABLES/3

Radjabova, V., Mastroeni, P., Skjødt, K., Zaccone, P., de Bono, B., Goodall, J. C., Chilvers, E. R., Juss, J. K., Jones, D. C., Trowsdale, J., & Barrow, A. D. (2015). TARM1 Is a Novel Leukocyte Receptor Complex–Encoded ITAM Receptor That Costimulates Proinflammatory Cytokine Secretion by Macrophages and Neutrophils. *The Journal of Immunology*, *195*(7), 3149–3159. https://doi.org/10.4049/JIMMUNOL.1401847

Rahat-Rozenbloom, S., Fernandes, J., Gloor, G. B., & Wolever, T. M. S. (2014). Evidence for greater production of colonic short-chain fatty acids in overweight than lean humans. *International Journal of Obesity 2014 38:12*, *38*(12), 1525–1531. https://doi.org/10.1038/ijo.2014.46

Rahmouni, K. (2010). Leptin-Induced Sympathetic Nerve Activation: Signaling Mechanisms and Cardiovascular Consequences in Obesity. *Current Hypertension Reviews*, *6*(2), 104. https://doi.org/10.2174/157340210791170994

Rahnemayan, S., Mirghafourvand, M., Fathalizadeh, A., Faramarzi, E., Reyhanifard, A., Mahmoodpoor, A., & Sanaie, S. (2021). Leptin levels in patients with Parkinson's disease: A systematic review and meta-analysis. *Clinical Nutrition ESPEN*, *41*, 104–109. https://doi.org/10.1016/j.clnesp.2020.11.001

Rajkovaca Latic, I., Popovic, Z., Mijatovic, K., Sahinovic, I., Pekic, V., Vucic, D., Cosic, V., Miskic, B., & Tomic, S. (2024). Association of intestinal inflammation and permeability markers with clinical manifestations of Parkinson's disease. *Parkinsonism & Related Disorders*, *123*, 106948. https://doi.org/10.1016/J.PARKRELDIS.2024.106948

Rapalli, A., Bertoni, S., Arcaro, V., Saccani, F., Grandi, A., Vivo, V., Cantoni, A. M., & Barocelli, E. (2016). Dual role of endogenous serotonin in 2,4,6-trinitrobenzene sulfonic acid-induced colitis. *Frontiers in Pharmacology*, *7*(MAR), 187228. https://doi.org/10.3389/FPHAR.2016.00068/BIBTEX

Rascol, O., Fabbri, M., & Poewe, W. (2021). Amantadine in the treatment of Parkinson's disease and other movement disorders. *The Lancet Neurology*, *20*(12), 1048–1056.

https://doi.org/10.1016/S1474-4422(21)00249-0/ASSET/831AB10E-5E6A-42EA-8B7E-97C016B4CB0D/MAIN.ASSETS/GR2.SML

Rastogi, S., & Singh, A. (2022). Gut microbiome and human health: Exploring how the probiotic genus Lactobacillus modulate immune responses. *Frontiers in Pharmacology*, *13*, 1042189. https://doi.org/10.3389/FPHAR.2022.1042189/XML/NLM

Raunio, A., Kaivola, K., Tuimala, J., Kero, M., Oinas, M., Polvikoski, T., Paetau, A., Tienari, P. J., & Myllykangas, L. (2019). Lewy-related pathology exhibits two anatomically and genetically distinct progression patterns: a population-based study of Finns aged 85. *Acta Neuropathologica*, *138*(5), 771–782. https://doi.org/10.1007/S00401-019-02071-3

Ray Dorsey, E., Elbaz, A., Nichols, E., Abd-Allah, F., Abdelalim, A., Adsuar, J. C., Ansha, M. G., Brayne, C., Choi, J. Y. J., Collado-Mateo, D., Dahodwala, N., Do, H. P., Edessa, D., Endres, M., Fereshtehnejad, S. M., Foreman, K. J., Gankpe, F. G., Gupta, R., Hankey, G. J., … Murray, C. J. L. (2018). Global, regional, and national burden of Parkinson's disease, 1990–2016: a systematic analysis for the Global Burden of Disease Study 2016. *The Lancet Neurology*, *17*(11), 939–953. https://doi.org/10.1016/S1474-4422(18)30295-3

Reale, M., Iarlori, C., Thomas, A., Gambi, D., Perfetti, B., Di Nicola, M., & Onofrj, M. (2009). Peripheral cytokines profile in Parkinson's disease. *Brain, Behavior, and Immunity*, *23*(1), 55–63. https://doi.org/10.1016/J.BBI.2008.07.003

Reeve, A., Simcox, E., & Turnbull, D. (2014). Ageing and Parkinson's disease: Why is advancing age the biggest risk factor? *Ageing Research Reviews*, *14*(100), 19. https://doi.org/10.1016/J.ARR.2014.01.004

Reichardt, F., Chassaing, B., Nezami, B. G., Li, G., Tabatabavakili, S., Mwangi, S., Uppal, K., Liang, B., Vijay-Kumar, M., Jones, D., Gewirtz, A. T., & Srinivasan, S. (2017). Western diet induces colonic nitrergic myenteric neuropathy and dysmotility in mice via saturated fatty acid- and lipopolysaccharide-induced TLR4 signalling. *The Journal of Physiology*, *595*(5), 1831–1846. https://doi.org/10.1113/JP273269

Rekdal, V. M., Bess, E. N., Bisanz, J. E., Turnbaugh, P. J., & Balskus, E. P. (2019). Discovery and inhibition of an interspecies gut bacterial pathway for Levodopa metabolism. *Science*, *364*(6445). https://doi.org/10.1126/science.aau6323

Reunanen, J., Kainulainen, V., Huuskonen, L., Ottman, N., Belzer, C., Huhtinen, H., de Vos, W. M., & Satokaria, R. (2015). Akkermansia muciniphila Adheres to Enterocytes and Strengthens the Integrity of the Epithelial Cell Layer. *Applied and Environmental Microbiology*, *81*(11), 3655–3662. https://doi.org/10.1128/AEM.04050-14

Rey, N. L., Bousset, L., George, S., Madaj, Z., Meyerdirk, L., Schulz, E., Steiner, J. A., Melki, R., & Brundin, P. (2019). α-Synuclein conformational strains spread, seed and target neuronal cells differentially after injection into the olfactory bulb. *Acta Neuropathologica Communications*, *7*(1), 1–18. https://doi.org/10.1186/S40478-019-0859-3/TABLES/1

Rey, N. L., George, S., Steiner, J. A., Madaj, Z., Luk, K. C., Trojanowski, J. Q., Lee, V. M. Y., & Brundin, P. (2018). Spread of aggregates after olfactory bulb injection of α-synuclein fibrils is associated with early neuronal loss and is reduced long term. *Acta Neuropathologica*, *135*(1), 65–83. https://doi.org/10.1007/S00401-017-1792-9/FIGURES/6

Richard, A. J., White, U., Elks, C. M., & Stephens, J. M. (2020). Adipose Tissue: Physiology to Metabolic Dysfunction. *Endotext*. https://www.ncbi.nlm.nih.gov/books/NBK555602/

Richardson, J. R., Quan, Y., Sherer, T. B., Greenamyre, J. T., & Miller, G. W. (2005). Paraquat Neurotoxicity is Distinct from that of MPTP and Rotenone. *Toxicological Sciences*, *88*(1), 193–201. https://doi.org/10.1093/TOXSCI/KFI304

Rivest, J., Barclay, C. L., & Suchowersky, O. (1999). COMT Inhibitors in Parkinson's Disease. *Canadian Journal of Neurological Sciences*, *26*(S2), S34–S38. https://doi.org/10.1017/S031716710000007X

Rohr, M. W., Narasimhulu, C. A., Rudeski-Rohr, T. A., & Parthasarathy, S. (2020). Negative Effects of a High-Fat Diet on Intestinal Permeability: A Review. *Advances in Nutrition*, *11*(1), 77–91. https://doi.org/10.1093/ADVANCES/NMZ061

Rolli-Derkinderen, M., Leclair-Visonneau, L., Bourreille, A., Coron, E., Neunlist, M., & Derkinderen, P. (2020). Is Parkinson's disease a chronic low-grade inflammatory bowel disease? *Journal of Neurology*, *267*(8), 2207–2213. https://doi.org/10.1007/S00415-019-09321-0/FIGURES/2

Romagnuolo, J., Fedorak, R. N., Dias, V. C., Bamforth, F., & Teltscher, M. (2001). Hyperhomocysteinemia and inflammatory bowel disease: prevalence and predictors in a cross-sectional study. *The American Journal of Gastroenterology*, *96*(7), 2143–2149. https://doi.org/10.1111/J.1572-0241.2001.03950.X

Romano, S., Savva, G. M., Bedarf, J. R., Charles, I. G., Hildebrand, F., & Narbad, A. (2021). Meta-analysis of the Parkinson's disease gut microbiome suggests alterations linked to intestinal inflammation. *Npj Parkinson's Disease 2021 7:1*, *7*(1), 1–13. https://doi.org/10.1038/s41531-021-00156-z

Rooks, M. G., & Garrett, W. S. (2016). Gut microbiota, metabolites and host immunity. In *Nature Reviews Immunology* (Vol. 16, Issue 6, pp. 341–352). Nature Publishing Group. https://doi.org/10.1038/nri.2016.42

Rose, K. N., Schwarzschild, M. A., & Gomperts, S. N. (2024). Clearing the Smoke: What Protects Smokers from Parkinson's Disease? *Movement Disorders*, *39*(2), 267–272. https://doi.org/10.1002/MDS.29707

Rusch, C., Flanagan, R., Suh, H., & Subramanian, I. (2023). To restrict or not to restrict? Practical considerations for optimizing dietary protein interactions on levodopa absorption in Parkinson's disease. *Npj Parkinson's Disease 2023 9:1*, *9*(1), 1–8. https://doi.org/10.1038/s41531-023-00541-w

Rusch, J. A., Layden, B. T., & Dugas, L. R. (2023). Signalling cognition: the gut microbiota and hypothalamic-pituitary-adrenal axis. *Frontiers in Endocrinology*, *14*. https://doi.org/10.3389/FENDO.2023.1130689

Sadaf Farooqi, I., Bullmore, E., Keogh, J., Gillard, J., O'Rahilly, S., & Fletcher, P. C. (2007). Leptin regulates striatal regions and human eating behavior. *Science*, *317*(5843), 1355. https://doi.org/10.1126/SCIENCE.1144599/SUPPL_FILE/FAROOQI.SOM.PDF

Safarpour, Y., Vaziri, N. D., & Jabbari, B. (2021). Movement Disorders in Chronic Kidney Disease – A Descriptive Review. *Journal of Stroke and Cerebrovascular Diseases*, *30*(9). https://doi.org/10.1016/j.jstrokecerebrovasdis.2020.105408

Sampath, C., Kalpana, R., Ansah, T., Charlton, C., Hale, A., Channon, K. M., Srinivasan, S., & Gangula, P. R. (2019). Impairment of Nrf2- and Nitrergic-Mediated Gastrointestinal Motility in an MPTP Mouse Model of Parkinson's Disease. *Digestive Diseases and Sciences*, *64*(12), 3502–3517. https://doi.org/10.1007/S10620-019-05693-5/FIGURES/12

Sampson, T. R., Debelius, J. W., Thron, T., Janssen, S., Shastri, G. G., Ilhan, Z. E., Challis, C., Schretter, C. E., Rocha, S., Gradinaru, V., Chesselet, M. F., Keshavarzian, A., Shannon, K. M., Krajmalnik-Brown, R., Wittung-Stafshede, P., Knight, R., & Mazmanian, S. K. (2016). Gut Microbiota Regulate Motor Deficits and Neuroinflammation in a Model of Parkinson's Disease. *Cell*, *167*(6), 1469-1480.e12. https://doi.org/10.1016/j.cell.2016.11.018

Samuel, T., Hoy, W., … R. D.-D.-J. of the, & 2005, undefined. (n.d.). Determinants of glomerular volume in different cortical zones of the human kidney. *Journals.Lww.ComT Samuel, WE Hoy, R Douglas-Denton, MD Hughson, JF BertramJournal of the American Society of Nephrology, 2005•journals.Lww.Com*. Retrieved April 19, 2025, from https://journals.lww.com/JASN/fulltext/2005/10000/Determinants_of_Glomerular_Volume_in_Different.36.aspx

Sandyk, R., Iacono, R. P., & Bamford, C. R. (1987). The hypothalamus in Parkinson Disease. *The Italian Journal of Neurological Sciences*, *8*(3), 227–234. https://doi.org/10.1007/BF02337479

Sankowski, B., Księżarczyk, K., Raćkowska, E., Szlufik, S., Koziorowski, D., & Giebułtowicz, J. (2020). Higher cerebrospinal fluid to plasma ratio of p-cresol sulfate and indoxyl sulfate in patients with Parkinson's disease. *Clinica Chimica Acta*, *501*, 165–173. https://doi.org/10.1016/J.CCA.2019.10.038

Sasselli, V., Pachnis, V., & Burns, A. J. (2012). The enteric nervous system. *Developmental Biology*, *366*(1), 64–73. https://doi.org/10.1016/J.YDBIO.2012.01.012

Sawchenko, P. E. (1983). Central connections of the sensory and motor nuclei of the vagus nerve. *Journal of the Autonomic Nervous System*, *9*(1), 13–26. https://doi.org/10.1016/0165-1838(83)90129-7

Schenck, C. H., Boeve, B. F., & Mahowald, M. W. (2013). Delayed emergence of a parkinsonian disorder or dementia in 81% of older men initially diagnosed with idiopathic rapid eye movement sleep behavior disorder: a 16-year update on a previously reported series. *Sleep Medicine*, *14*(8), 744–748. https://doi.org/10.1016/J.SLEEP.2012.10.009

Scheperjans, F., Aho, V., Pereira, P. A. B., Koskinen, K., Paulin, L., Pekkonen, E., Haapaniemi, E., Kaakkola, S., Eerola-Rautio, J., Pohja, M., Kinnunen, E., Murros, K., & Auvinen, P. (2015). Gut microbiota are

related to Parkinson's disease and clinical phenotype. *Movement Disorders*, *30*(3), 350–358. https://doi.org/10.1002/mds.26069

Scheperjans, F., Derkinderen, P., & Borghammer, P. (2018). The gut and Parkinson's disease: Hype or hope? In *Journal of Parkinson's Disease* (Vol. 8, Issue s1, pp. S31–S39). IOS Press. https://doi.org/10.3233/JPD-181477

Scheperjans, F., Levo, R., Bosch, B., Lääperi, M., Pereira, P. A. B., Smolander, O. P., Aho, V. T. E., Vetkas, N., Toivio, L., Kainulainen, V., Fedorova, T. D., Lahtinen, P., Ortiz, R., Kaasinen, V., Satokari, R., & Arkkila, P. (2024). Fecal Microbiota Transplantation for Treatment of Parkinson Disease: A Randomized Clinical Trial. *JAMA Neurology*, *81*(9), 925–938. https://doi.org/10.1001/JAMANEUROL.2024.2305

Schmit, K. J., Garcia, P., Sciortino, A., Mittelbronn, M., Buttini, M., & Wilmes Correspondence, P. (2023). *Fiber deprivation and microbiome-borne curli shift gut bacterial populations and accelerate disease in a mouse model of Parkinson's disease*. https://doi.org/10.1016/j.celrep.2023.113071

Schreiber, A., Shulhevich, Y., Geraci, S., Hesser, J., Stsepankou, D., Neudecker, S., Koenig, S., Heinrich, R., Hoecklin, F., Pill, J., Friedemann, J., Schweda, F., Gretz, N., & Schock-Kusch, D. (2012). Transcutaneous measurement of renal function in conscious mice. *American Journal of Physiology - Renal Physiology*, *303*(5), 783–788. https://doi.org/10.1152/AJPRENAL.00279.2012/ASSET/IMAGES/LARGE/ZH20161266730004.JPEG

Schwiertz, A., Spiegel, J., Dillmann, U., Grundmann, D., Bürmann, J., Faßbender, K., Schäfer, K. H., & Unger, M. M. (2018). Fecal markers of intestinal inflammation and intestinal permeability are elevated in Parkinson's disease. *Parkinsonism and Related Disorders*, *50*, 104–107. https://doi.org/10.1016/j.parkreldis.2018.02.022

Schwiertz, A., Taras, D., Schäfer, K., Beijer, S., Bos, N. A., Donus, C., & Hardt, P. D. (2010). Microbiota and SCFA in Lean and Overweight Healthy Subjects. *Obesity*, *18*(1), 190–195. https://doi.org/10.1038/OBY.2009.167

Secher, A., Jelsing, J., Baquero, A. F., Hecksher-Sørensen, J., Cowley, M. A., Dalbøge, L. S., Hansen, G., Grove, K. L., Pyke, C., Raun, K., Schäfer, L., Tang-Christensen, M., Verma, S., Witgen, B. M., Vrang, N., & Knudsen, L. B. (2014). The arcuate nucleus mediates GLP-1 receptor agonist liraglutide-dependent weight loss. *The Journal of Clinical Investigation*, *124*(10), 4473–4488. https://doi.org/10.1172/JCI75276

Seethaler, B., Nguyen, N. K., Basrai, M., Kiechle, M., Walter, J., Delzenne, N. M., & Bischoff, S. C. (2022). Short-chain fatty acids are key mediators of the favorable effects of the Mediterranean diet on intestinal barrier integrity: data from the randomized controlled LIBRE trial. *The American Journal of Clinical Nutrition*, *116*(4), 928–942. https://doi.org/10.1093/AJCN/NQAC175

Segal, A., Zlotnik, Y., Moyal-Atias, K., Abuhasira, R., & Ifergane, G. (2021). Fecal microbiota transplant as a potential treatment for Parkinson's disease – A case series. *Clinical Neurology and Neurosurgery*, *207*, 106791. https://doi.org/10.1016/J.CLINEURO.2021.106791

Sepehri, Z., Kiani, Z., Nasiri, A. A., & Kohan, F. (2016). Toll-like receptor 2 and type 2 diabetes. *Cellular and Molecular Biology Letters*, *21*(1), 1–9. https://doi.org/10.1186/S11658-016-0002-4/FIGURES/2

Seppi, K., Ray Chaudhuri, K., Coelho, M., Fox, S. H., Katzenschlager, R., Perez Lloret, S., Weintraub, D., Sampaio, C., Chahine, L., Hametner, E. M., Heim, B., Lim, S. Y., Poewe, W., & Djamshidian-Tehrani, A. (2019). Update on treatments for nonmotor symptoms of Parkinson's disease—an evidence-based medicine review. *Movement Disorders*, *34*(2), 180–198. https://doi.org/10.1002/MDS.27602

Serio, R., & Zizzo, M. G. (2023). The multiple roles of dopamine receptor activation in the modulation of gastrointestinal motility and mucosal function. *Autonomic Neuroscience*, *244*, 103041. https://doi.org/10.1016/J.AUTNEU.2022.103041

Shaikh, M., Rajan, K., Forsyth, C. B., Voigt, R. M., & Keshavarzian, A. (2015). Simultaneous gas-chromatographic urinary measurement of sugar probes to assess intestinal permeability: use of time course analysis to optimize its use to assess regional gut permeability. *Clinica Chimica Acta; International Journal of Clinical Chemistry*, *442*, 24. https://doi.org/10.1016/J.CCA.2014.12.040

Sharkey, K. A., & Mawe, G. M. (2022). The enteric nervous system. *Physiological Reviews*, *103*(2), 1487. https://doi.org/10.1152/PHYSREV.00018.2022

Sharma, J. C., & Vassallo, M. (2014). Prognostic Significance of Weight Changes in Parkinson's Disease: the Park–weight Phenotype. *Neurodegenerative Disease Management*, *4*(4), 309–316. https://doi.org/10.2217/NMT.14.25

Shen, Z., Zhu, C., Quan, Y., Yang, J., Yuan, W., Yang, Z., Wu, S., Luo, W., Tan, B., & Wang, X. (2018). Insights into Roseburia intestinalis which alleviates experimental colitis pathology by inducing anti-inflammatory responses. *Journal of Gastroenterology and Hepatology*, *33*(10), 1751–1760. https://doi.org/10.1111/JGH.14144

Shults, C. W. (2006). Lewy bodies. *Proceedings of the National Academy of Sciences of the United States of America*, *103*(6), 1661–1668. https://doi.org/10.1073/PNAS.0509567103/SUPPL_FILE/09567FIG1.PDF

Siervo, M., Johnston, F., Calton, E., James, A., Stephan, B. C. M., Hornsby, A. K. E., Davies, J. S., & Burn, D. (2024). Metabolic biomarkers of appetite control in Parkinson's disease patients with and without cognitive impairment. *Clinical Nutrition ESPEN*, *64*, 425–434. https://doi.org/10.1016/J.CLNESP.2024.10.167

Singaram, C., Gaumnitz, E. A., Torbey, C., Ashraf, W., Quigley, E. M. M., Sengupta, A., & Pfeiffer, R. (1995). Dopaminergic defect of enteric nervous system in Parkinson's disease patients with chronic constipation. *Lancet (London, England)*, *346*(8979), 861–864. https://doi.org/10.1016/S0140-6736(95)92707-7

Singh, R. P., Halaka, D. A., Hayouka, Z., & Tirosh, O. (2020). High-Fat Diet Induced Alteration of Mice Microbiota and the Functional Ability to Utilize Fructooligosaccharide for Ethanol Production. *Frontiers in Cellular and Infection Microbiology*, *10*, 550086. https://doi.org/10.3389/FCIMB.2020.00376/BIBTEX

Skurk, T., Alberti-Huber, C., Herder, C., & Hauner, H. (2007). Relationship between Adipocyte Size and Adipokine Expression and Secretion. *The Journal of Clinical Endocrinology & Metabolism*, *92*(3), 1023–1033. https://doi.org/10.1210/JC.2006-1055

Smeyne, R. J., Noyce, A. J., Byrne, M., Savica, R., & Marras, C. (2021). Infection and risk of Parkinson's disease. *Journal of Parkinson's Disease*, *11*(1), 31–43. https://doi.org/10.3233/JPD-202279

Smith, P., Willemsen, D., Popkes, M., Metge, F., Gandiwa, E., Reichard, M., & Valenzano, D. R. (2017). Regulation of life span by the gut microbiota in the short-lived African turquoise killifish. *ELife*, *6*, e27014. https://doi.org/10.7554/ELIFE.27014

Smyth, G. K. (2004). Linear models and empirical bayes methods for assessing differential expression in microarray experiments. *Statistical Applications in Genetics and Molecular Biology*, *3*(1). https://doi.org/10.2202/1544-6115.1027/MACHINEREADABLECITATION/RIS

Soares, A., Beraldi, E. J., Ferreira, P. E. B., Bazotte, R. B., & Buttow, N. C. (2015). Intestinal and neuronal myenteric adaptations in the small intestine induced by a high-fat diet in mice. *BMC Gastroenterology*, *15*(1), 1–9. https://doi.org/10.1186/S12876-015-0228-Z/TABLES/4

Socha, E., Koba, M., & Kośliński, P. (2019). Amino acid profiling as a method of discovering biomarkers for diagnosis of neurodegenerative diseases. *Amino Acids*, *51*(3), 367–371. https://doi.org/10.1007/S00726-019-02705-6/TABLES/3

Sokol, H., Pigneur, B., Watterlot, L., Lakhdari, O., Bermúdez-Humarán, L. G., Gratadoux, J. J., Blugeon, S., Bridonneau, C., Furet, J. P., Corthier, G., Grangette, C., Vasquez, N., Pochart, P., Trugnan, G., Thomas, G., Blottière, H. M., Doré, J., Marteau, P., Seksik, P., & Langella, P. (2008). Faecalibacterium prausnitzii is an anti-inflammatory commensal bacterium identified by gut microbiota analysis of Crohn disease patients. *Proceedings of the National Academy of Sciences of the United States of America*, *105*(43), 16731–16736. https://doi.org/10.1073/pnas.0804812105

Soret, R., Chevalier, J., De Coppet, P., Poupeau, G., Derkinderen, P., Segain, J. P., & Neunlist, M. (2010). Short-Chain Fatty Acids Regulate the Enteric Neurons and Control Gastrointestinal Motility in Rats. *Gastroenterology*, *138*(5), 1772–1782. https://doi.org/10.1053/j.gastro.2010.01.053

Souza, A. P. da S., Barros, W. M. A., Silva, J. M. L., Silva, M. R. M., Silva, A. B. J., Fernandes, M. S. de S., Santos, M. E. R. A. dos, Silva, M. L. da, Carmo, T. S. do, Silva, R. K. P., Silva, K. G. da, Souza, S. L. de, & Souza, V. de O. N. (2021a). Effect of Metabolic Syndrome on Parkinson's Disease: A Systematic Review. *Clinics*, *76*, e3379. https://doi.org/10.6061/CLINICS/2021/E3379

Souza, A. P. da S., Barros, W. M. A., Silva, J. M. L., Silva, M. R. M., Silva, A. B. J., Fernandes, M. S. de S., Santos, M. E. R. A. dos, Silva, M. L. da, Carmo, T. S. do, Silva, R. K. P., Silva, K. G. da, Souza, S. L. de, & Souza, V. de O. N. (2021b). Effect of Metabolic Syndrome on Parkinson's Disease: A Systematic Review. *Clinics*, *76*, e3379. https://doi.org/10.6061/CLINICS/2021/E3379

Spencer, N. J., & Hu, H. (2020). Enteric nervous system: sensory transduction, neural circuits and gastrointestinal motility. *Nature Reviews Gastroenterology & Hepatology 2020 17:6*, *17*(6), 338–351. https://doi.org/10.1038/s41575-020-0271-2

Spencer, S. J., D'Angelo, H., Soch, A., Watkins, L. R., Maier, S. F., & Barrientos, R. M. (2017). High-fat diet and aging interact to produce neuroinflammation and impair hippocampal- and amygdalar-dependent memory. *Neurobiology of Aging*, *58*, 88–101. https://doi.org/10.1016/J.NEUROBIOLAGING.2017.06.014

Spillantini, M. G., Schmidt, M. L., Lee, V. M.-Y., Trojanowski, J. Q., Jakes, R., & Goedert, M. (1997). α-Synuclein in Lewy bodies. *Nature*, *388*(6645), 839–840. https://doi.org/10.1038/42166

Spohn, S. N., & Mawe, G. M. (2017). Non-conventional features of peripheral serotonin signalling — the gut and beyond. *Nature Reviews Gastroenterology & Hepatology 2017 14:7*, *14*(7), 412–420. https://doi.org/10.1038/nrgastro.2017.51

Statovci, D., Aguilera, M., MacSharry, J., & Melgar, S. (2017). The impact of western diet and nutrients on the microbiota and immune response at mucosal interfaces. In *Frontiers in Immunology* (Vol. 8, Issue JUL). Frontiers Media S.A. https://doi.org/10.3389/fimmu.2017.00838

Stenkamp-Strahm, C. M., Kappmeyer, A. J., Schmalz, J. T., Gericke, M., & Balemba, O. (2013). High-fat diet ingestion correlates with neuropathy in the duodenum myenteric plexus of obese mice with symptoms of type 2 diabetes. *Cell and Tissue Research*, *354*(2), 381. https://doi.org/10.1007/S00441-013-1681-Z

Steru, L., Chermat, R., Thierry, B., & Simon, P. (1985). The tail suspension test: A new method for screening antidepressants in mice. *Psychopharmacology*, *85*(3), 367–370. https://doi.org/10.1007/BF00428203/METRICS

Stitham, J., Midgett, C., Martin, K. A., & Hwa, J. (2011). Prostacyclin: An Inflammatory Paradox. *Frontiers in Pharmacology*, *2*, 24. https://doi.org/10.3389/FPHAR.2011.00024

Stocchi, F., Bravi, D., Emmi, A., & Antonini, A. (2024). Parkinson disease therapy: current strategies and future research priorities. *Nature Reviews Neurology 2024 20:12*, *20*(12), 695–707. https://doi.org/10.1038/s41582-024-01034-x

Stojanov, S., Berlec, A., & Štrukelj, B. (2020). The Influence of Probiotics on the Firmicutes/Bacteroidetes Ratio in the Treatment of Obesity and Inflammatory Bowel disease. *Microorganisms 2020, Vol. 8, Page 1715*, *8*(11), 1715. https://doi.org/10.3390/MICROORGANISMS8111715

Subramanian, A., Tamayo, P., Mootha, V. K., Mukherjee, S., Ebert, B. L., Gillette, M. A., Paulovich, A., Pomeroy, S. L., Golub, T. R., Lander, E. S., & Mesirov, J. P. (2005). Gene set enrichment analysis: A knowledge-based approach for interpreting genome-wide expression profiles. *Proceedings of the National Academy of Sciences of the United States of America*, *102*(43), 15545–15550. https://doi.org/10.1073/PNAS.0506580102/SUPPL_FILE/06580FIG7.JPG

Suez, J., Zmora, N., Segal, E., & Elinav, E. (2019). The pros, cons, and many unknowns of probiotics. In *Nature Medicine* (Vol. 25, Issue 5, pp. 716–729). Nature Research. https://doi.org/10.1038/s41591-019-0439-x

Sulzer, D., Alcalay, R. N., Garretti, F., Cote, L., Kanter, E., Agin-Liebes, J., Liong, C., McMurtrey, C., Hildebrand, W. H., Mao, X., Dawson, V. L., Dawson, T. M., Oseroff, C., Pham, J., Sidney, J., Dillon, M. B., Carpenter, C., Weiskopf, D., Phillips, E., … Sette, A. (2017). T cells from patients with Parkinson's

disease recognize α-synuclein peptides. *Nature 2017 546:7660*, *546*(7660), 656–661. https://doi.org/10.1038/nature22815

Sulzer, D., Bogulavsky, J., Larsen, K. E., Behr, G., Karatekin, E., Kleinman, M. H., Turro, N., Krantz, D., Edwards, R. H., Greene, L. A., & Zecca, L. (2000). Neuromelanin biosynthesis is driven by excess cytosolic catecholamines not accumulated by synaptic vesicles. *Proceedings of the National Academy of Sciences of the United States of America*, *97*(22), 11869–11874. https://doi.org/10.1073/PNAS.97.22.11869/ASSET/E816323D-1E85-4F12-8011-7ABC0F1CA80B/ASSETS/GRAPHIC/PQ2204087007.JPEG

Sulzer, D., Cassidy, C., Horga, G., Kang, U. J., Fahn, S., Casella, L., Pezzoli, G., Langley, J., Hu, X. P., Zucca, F. A., Isaias, I. U., & Zecca, L. (2018). Neuromelanin detection by magnetic resonance imaging (MRI) and its promise as a biomarker for Parkinson's disease. *Npj Parkinson's Disease 2018 4:1*, *4*(1), 1–13. https://doi.org/10.1038/s41531-018-0047-3

Sulzer, D., Mosharov, E., Talloczy, Z., Zucca, F. A., Simon, J. D., & Zecca, L. (2008). Neuronal pigmented autophagic vacuoles: lipofuscin, neuromelanin, and ceroid as macroautophagic responses during aging and disease. *Journal of Neurochemistry*, *106*(1), 24–36. https://doi.org/10.1111/J.1471-4159.2008.05385.X

Sulzer, D., & Surmeier, D. J. (2013). Neuronal vulnerability, pathogenesis, and Parkinson's disease. In *Movement Disorders* (Vol. 28, Issue 1, pp. 41–50). Mov Disord. https://doi.org/10.1002/mds.25095

Surmeier, D. J., Obeso, J. A., & Halliday, G. M. (2017). Selective neuronal vulnerability in Parkinson disease. *Nature Reviews Neuroscience 2017 18:2*, *18*(2), 101–113. https://doi.org/10.1038/nrn.2016.178

Suzuki, K., Simpson, K. A., Minnion, J. S., Shillito, J. C., & Bloom, S. R. (2010). The role of gut hormones and the hypothalamus in appetite regulation. *Endocrine Journal*, *57*(5), 359–372. https://doi.org/10.1507/ENDOCRJ.K10E-077

Suzuki, T. (2013). Regulation of intestinal epithelial permeability by tight junctions. *Cellular and Molecular Life Sciences : CMLS*, *70*(4), 631–659. https://doi.org/10.1007/S00018-012-1070-X

Svensson, E., Horváth-Puhó, E., Thomsen, R. W., Djurhuus, J. C., Pedersen, L., Borghammer, P., & Sørensen, H. T. (2015). Vagotomy and subsequent risk of Parkinson's disease. *Annals of Neurology*, *78*(4), 522–529. https://doi.org/10.1002/ana.24448

Swarup, S., Ahmed, I., Grigorova, Y., & Zeltser, R. (2024). Metabolic Syndrome. *StatPearls*. https://www.ncbi.nlm.nih.gov/books/NBK459248/

Tan, A. H., Chong, C. W., Lim, S. Y., Yap, I. K. S., Teh, C. S. J., Loke, M. F., Song, S. L., Tan, J. Y., Ang, B. H., Tan, Y. Q., Kho, M. T., Bowman, J., Mahadeva, S., Yong, H. Sen, & Lang, A. E. (2021). Gut Microbial Ecosystem in Parkinson Disease: New Clinicobiological Insights from Multi-Omics. *Annals of Neurology*, *89*(3), 546–559. https://doi.org/10.1002/ANA.25982

Tan, A. H., Hew, Y. C., Lim, S. Y., Ramli, N. M., Kamaruzzaman, S. B., Tan, M. P., Grossmann, M., Ang, B. H., Tan, J. Y., Manap, M. A. A. A., Tay, T. K., Tan, S. L., New, R. P., Fadzli, F., Yee, E. J., Moy, F. M., Mahadeva, S., & Lang, A. E. (2018). Altered body composition, sarcopenia, frailty, and their clinico-

biological correlates, in Parkinson's disease. *Parkinsonism & Related Disorders*, *56*, 58–64. https://doi.org/10.1016/J.PARKRELDIS.2018.06.020

Tan, A. H., Lim, S. Y., Chong, K. K., Manap, M. A. A. A., Hor, J. W., Lim, J. L., Low, S. C., Chong, C. W., Mahadeva, S., & Lang, A. E. (2021). Probiotics for Constipation in Parkinson Disease: A Randomized Placebo-Controlled Study. *Neurology*, *96*(5), E772–E782. https://doi.org/10.1212/WNL.0000000000010998

Tan, A. H., Lim, S. Y., & Lang, A. E. (2022). The microbiome–gut–brain axis in Parkinson disease — from basic research to the clinic. *Nature Reviews Neurology 2022 18:8*, *18*(8), 476–495. https://doi.org/10.1038/s41582-022-00681-2

Tanei, Z. ichi, Saito, Y., Ito, S., Matsubara, T., Motoda, A., Yamazaki, M., Sakashita, Y., Kawakami, I., Ikemura, M., Tanaka, S., Sengoku, R., Arai, T., & Murayama, S. (2020). Lewy pathology of the esophagus correlates with the progression of Lewy body disease: a Japanese cohort study of autopsy cases. *Acta Neuropathologica*, *141*(1), 25. https://doi.org/10.1007/S00401-020-02233-8

Tanner, C. M., Kame, F., Ross, G. W., Hoppin, J. A., Goldman, S. M., Korell, M., Marras, C., Bhudhikanok, G. S., Kasten, M., Chade, A. R., Comyns, K., Richards, M. B., Meng, C., Priestley, B., Fernandez, H. H., Cambi, F., Umbach, D. M., Blair, A., Sandler, D. P., & Langston, J. W. (2011). Rotenone, paraquat, and Parkinson's disease. *Environmental Health Perspectives*, *119*(6), 866–872. https://doi.org/10.1289/EHP.1002839/SUPPL_FILE/1002839ART_SUPPL.PDF

Tansey, M. G., Wallings, R. L., Houser, M. C., Herrick, M. K., Keating, C. E., & Joers, V. (2022). Inflammation and immune dysfunction in Parkinson disease. *Nature Reviews Immunology 2022 22:11*, *22*(11), 657–673. https://doi.org/10.1038/s41577-022-00684-6

Tasselli, M., Chaumette, T., Paillusson, S., Monnet, Y., Lafoux, A., Huchet-Cadiou, C., Aubert, P., Hunot, S., Derkinderen, P., & Neunlist, M. (2013). Effects of oral administration of rotenone on gastrointestinal functions in mice. *Neurogastroenterology & Motility*, *25*(3), e183–e193. https://doi.org/10.1111/NMO.12070

Thaler, J. P., Yi, C. X., Schur, E. A., Guyenet, S. J., Hwang, B. H., Dietrich, M. O., Zhao, X., Sarruf, D. A., Izgur, V., Maravilla, K. R., Nguyen, H. T., Fischer, J. D., Matsen, M. E., Wisse, B. E., Morton, G. J., Horvath, T. L., Baskin, D. G., Tschöp, M. H., & Schwartz, M. W. (2011). Obesity is associated with hypothalamic injury in rodents and humans. *The Journal of Clinical Investigation*, *122*(1), 153. https://doi.org/10.1172/JCI59660

Thi Lai, T., Kim, Y. E., Nguyen, L. T. N., Thi Nguyen, T., Kwak, I. H., Richter, F., Kim, Y. J., & Ma, H. il. (2024). Microglial inhibition alleviates alpha-synuclein propagation and neurodegeneration in Parkinson's disease mouse model. *Npj Parkinson's Disease 2024 10:1*, *10*(1), 1–10. https://doi.org/10.1038/s41531-024-00640-2

Tief, K., Schmidt, A., & Beermann, F. (1998). New evidence for presence of tyrosinase in substantia nigra, forebrain and midbrain. *Molecular Brain Research*, *53*(1–2), 307–310. https://doi.org/10.1016/S0169-328X(97)00301-X

Toh, T. S., Chong, C. W., Lim, S. Y., Bowman, J., Cirstea, M., Lin, C. H., Chen, C. C., Appel-Cresswell, S., Finlay, B. B., & Tan, A. H. (2022). Gut microbiome in Parkinson's disease: New insights from meta-analysis. *Parkinsonism and Related Disorders*, *94*, 1–9. https://doi.org/10.1016/j.parkreldis.2021.11.017

Tonneijck, L., Muskiet, M. H. A., Smits, M. M., Van Bommel, E. J., Heerspink, H. J. L., Van Raalte, D. H., & Joles, J. A. (2017). Glomerular hyperfiltration in diabetes: Mechanisms, clinical significance, and treatment. *Journal of the American Society of Nephrology*, *28*(4), 1023–1039. https://doi.org/10.1681/ASN.2016060666/-/DCSUPPLEMENTAL

Torrecillos, F., Tan, H., Brown, P., Capone, F., Ricciuti, R., Di Lazzaro, V., & Marano, M. (2022). Non-invasive vagus nerve stimulation modulates subthalamic beta activity in Parkinson's disease. *Brain Stimulation*, *15*(6), 1513–1516. https://doi.org/10.1016/j.brs.2022.11.006

Traserra, S., Alcalá-González, L. G., Barber, C., Landolfi, S., Malagelada, C., Lange, R., Forestier, S., Corsetti, M., & Jimenez, M. (2024). New insights into the characterization of the mechanism of action of hyoscine butylbromide in the human colon ex vivo. *European Journal of Pharmacology*, *972*, 176550. https://doi.org/10.1016/J.EJPHAR.2024.176550

Tremaroli, V., & Bäckhed, F. (2012). Functional interactions between the gut microbiota and host metabolism. *Nature 2012 489:7415*, *489*(7415), 242–249. https://doi.org/10.1038/nature11552

Tretiakoff C. (1919). *Contributions à l'étude de l'anatomie pathologique du locus niger de Soemmering avec quelques déductions relatives à la pathogénie des troubles de tonus musculaire et de la maladie de Parkinson.* .

Tribl, F., Arzberger, T., Riederer, P., & Gerlach, M. (2007). Tyrosinase is not detected in human catecholaminergic neurons by immunohistochemistry and Western blot analysis. *Journal of Neural Transmission. Supplementum*, *72*, 51–55. https://doi.org/10.1007/978-3-211-73574-9_8

Tsuboi, N., Okabayashi, Y., Shimizu, A., & Yokoo, T. (2017). The Renal Pathology of Obesity. *Kidney International Reports*, *2*(2), 251–260. https://doi.org/10.1016/J.EKIR.2017.01.007

Turnbaugh, P. J., Bäckhed, F., Fulton, L., & Gordon, J. I. (2008). Diet-Induced Obesity Is Linked to Marked but Reversible Alterations in the Mouse Distal Gut Microbiome. *Cell Host and Microbe*, *3*(4), 213–223. https://doi.org/10.1016/J.CHOM.2008.02.015

Turnbaugh, P. J., Ley, R. E., Mahowald, M. A., Magrini, V., Mardis, E. R., & Gordon, J. I. (2006). An obesity-associated gut microbiome with increased capacity for energy harvest. *Nature 2006 444:7122*, *444*(7122), 1027–1031. https://doi.org/10.1038/nature05414

Turner, J. R. (2009). Intestinal mucosal barrier function in health and disease. *Nature Reviews Immunology 2009 9:11*, *9*(11), 799–809. https://doi.org/10.1038/nri2653

Uemura, N., Yagi, H., Uemura, M. T., Hatanaka, Y., Yamakado, H., & Takahashi, R. (2018). Inoculation of α-synuclein preformed fibrils into the mouse gastrointestinal tract induces Lewy body-like aggregates in the brainstem via the vagus nerve. *Molecular Neurodegeneration*, *13*(1), 1–11. https://doi.org/10.1186/S13024-018-0257-5/FIGURES/6

Ulusoy, A., Phillips, R. J., Helwig, M., Klinkenberg, M., Powley, T. L., & Di Monte, D. A. (2017). Brain-to-stomach transfer of α-synuclein via vagal preganglionic projections. *Acta Neuropathologica*, *133*(3), 381–393. https://doi.org/10.1007/s00401-016-1661-y

Unger, M. M., Spiegel, J., Dillmann, K. U., Grundmann, D., Philippeit, H., Bürmann, J., Faßbender, K., Schwiertz, A., & Schäfer, K. H. (2016). Short chain fatty acids and gut microbiota differ between patients with Parkinson's disease and age-matched controls. *Parkinsonism and Related Disorders*, *32*, 66–72. https://doi.org/10.1016/j.parkreldis.2016.08.019

Ungerstedt, U. (1968). 6-Hydroxy-dopamine induced degeneration of central monoamine neurons. *European Journal of Pharmacology*, *5*(1), 107–110. https://doi.org/10.1016/0014-2999(68)90164-7

Uwada, J., Nakazawa, H., Muramatsu, I., Masuoka, T., & Yazawa, T. (2023). Role of Muscarinic Acetylcholine Receptors in Intestinal Epithelial Homeostasis: Insights for the Treatment of Inflammatory Bowel Disease. *International Journal of Molecular Sciences 2023, Vol. 24, Page 6508*, *24*(7), 6508. https://doi.org/10.3390/IJMS24076508

Valdearcos, M., Robblee, M. M., Benjamin, D. I., Nomura, D. K., Xu, A. W., & Koliwad, S. K. (2014). Microglia Dictate the Impact of Saturated Fat Consumption on Hypothalamic Inflammation and Neuronal Function. *Cell Reports*, *9*(6), 2124. https://doi.org/10.1016/J.CELREP.2014.11.018

Valdearcos, M., Xu, A. W., & Koliwad, S. K. (2015). Hypothalamic inflammation in the control of metabolic function. *Annual Review of Physiology*, *77*(Volume 77, 2015), 131–160. https://doi.org/10.1146/ANNUREV-PHYSIOL-021014-071656/CITE/REFWORKS

Van Den Berge, N., Ferreira, N., Gram, H., Mikkelsen, T. W., Alstrup, A. K. O., Casadei, N., Tsung-Pin, P., Riess, O., Nyengaard, J. R., Tamgüney, G., Jensen, P. H., & Borghammer, P. (2019). Evidence for bidirectional and trans-synaptic parasympathetic and sympathetic propagation of alpha-synuclein in rats. *Acta Neuropathologica*, *138*(4), 535–550. https://doi.org/10.1007/s00401-019-02040-w

Van Den Berge, N., & Ulusoy, A. (2022). Animal models of brain-first and body-first Parkinson's disease. *Neurobiology of Disease*, *163*, 105599. https://doi.org/10.1016/J.NBD.2021.105599

Van Der Heijden, R. A., Bijzet, J., Meijers, W. C., Yakala, G. K., Kleemann, R., Nguyen, T. Q., De Boer, R. A., Schalkwijk, C. G., Hazenberg, B. P. C., Tietge, U. J. F., & Heeringa, P. (2015). Obesity-induced chronic inflammation in high fat diet challenged C57BL/6J mice is associated with acceleration of age-dependent renal amyloidosis. *Scientific Reports 2015 5:1*, *5*(1), 1–15. https://doi.org/10.1038/srep16474

Van Ijzendoorn, S. C. D., & Derkinderen, P. (2019). The Intestinal Barrier in Parkinson's Disease: Current State of Knowledge. *Journal of Parkinson's Disease*, *9*(s2), S323–S329. https://doi.org/10.3233/JPD-191707/ASSET/IMAGES/10.3233_JPD-191707-FIG2.JPG

van Kessel, S. P., & El Aidy, S. (2019). Contributions of gut bacteria and diet to drug pharmacokinetics in the treatment of Parkinson's disease. *Frontiers in Neurology*, *10*(OCT), 466427. https://doi.org/10.3389/FNEUR.2019.01087/BIBTEX

van Kessel, S. P., Frye, A. K., El-Gendy, A. O., Castejon, M., Keshavarzian, A., van Dijk, G., & El Aidy, S. (2019). Gut bacterial tyrosine decarboxylases restrict levels of levodopa in the treatment of

Parkinson's disease. *Nature Communications*, *10*(1), 1–11. https://doi.org/10.1038/s41467-019-08294-y

Van Rooden, S. M., Colas, F., Martínez-Martín, P., Visser, M., Verbaan, D., Marinus, J., Chaudhuri, R. K., Kok, J. N., & Van Hilten, J. J. (2011). Clinical subtypes of Parkinson's disease. *Movement Disorders*, *26*(1), 51–58. https://doi.org/10.1002/MDS.23346

Vascellari, S., Palmas, V., Melis, M., Pisanu, S., Cusano, R., Uva, P., Perra, D., Madau, V., Sarchioto, M., Oppo, V., Simola, N., Morelli, M., Santoru, M. L., Atzori, L., Melis, M., Cossu, G., & Manzin, A. (2020). Gut Microbiota and Metabolome Alterations Associated with Parkinson's Disease. *MSystems*, *5*(5). https://doi.org/10.1128/msystems.00561-20

Vázquez-Vélez, G. E., & Zoghbi, H. Y. (2021). Parkinson's Disease Genetics and Pathophysiology. *Annual Review of Neuroscience*, *44*(Volume 44, 2021), 87–108. https://doi.org/10.1146/ANNUREV-NEURO-100720-034518/CITE/REFWORKS

Velloso, L. A., Folli, F., & Saad, M. J. (2015). TLR4 at the Crossroads of Nutrients, Gut Microbiota, and Metabolic Inflammation. *Endocrine Reviews*, *36*(3), 245–271. https://doi.org/10.1210/ER.2014-1100

Venables, W. N. & B. D. R. (2002). *Modern Applied Statistics with S, Fourth ed. New York Springer.* https://www.stats.ox.ac.uk/pub/MASS4/

Vendrik, K. E. W., Ooijevaar, R. E., de Jong, P. R. C., Laman, J. D., van Oosten, B. W., van Hilten, J. J., Ducarmon, Q. R., Keller, J. J., Kuijper, E. J., & Contarino, M. F. (2020). Fecal Microbiota Transplantation in Neurological Disorders. *Frontiers in Cellular and Infection Microbiology*, *10*, 522660. https://doi.org/10.3389/FCIMB.2020.00098/BIBTEX

Venegas, D. P., De La Fuente, M. K., Landskron, G., González, M. J., Quera, R., Dijkstra, G., Harmsen, H. J. M., Faber, K. N., & Hermoso, M. A. (2019). Short chain fatty acids (SCFAs)mediated gut epithelial and immune regulation and its relevance for inflammatory bowel diseases. In *Frontiers in Immunology* (Vol. 10, Issue MAR, p. 277). Frontiers Media S.A. https://doi.org/10.3389/fimmu.2019.00277

Vikdahl, M., Carlsson, M., Linder, J., Forsgren, L., & Håglin, L. (2014). Weight gain and increased central obesity in the early phase of Parkinson's disease. *Clinical Nutrition*, *33*(6), 1132–1139. https://doi.org/10.1016/J.CLNU.2013.12.012

Vila, M. (2019). Neuromelanin, aging, and neuronal vulnerability in Parkinson's disease. *Movement Disorders*, *34*(10), 1440. https://doi.org/10.1002/MDS.27776

Vila, M., Vukosavic, S., Jackson-Lewis, V., Neystat, M., Jakowec, M., & Przedborski, S. (2000). α-Synuclein Up-Regulation in Substantia Nigra Dopaminergic Neurons Following Administration of the Parkinsonian Toxin MPTP. *Journal of Neurochemistry*, *74*(2), 721–729. https://doi.org/10.1046/J.1471-4159.2000.740721.X

Villa, A., Vegeto, E., Poletti, A., & Maggi, A. (2016). Estrogens, Neuroinflammation, and Neurodegeneration. *Endocrine Reviews*, *37*(4), 372. https://doi.org/10.1210/ER.2016-1007

Villumsen, M., Aznar, S., Pakkenberg, B., Jess, T., & Brudek, T. (2019). Inflammatory bowel disease increases the risk of Parkinson's disease: a Danish nationwide cohort study 1977-2014. *Gut*, *68*(1), 18–24. https://doi.org/10.1136/GUTJNL-2017-315666

Vinaixa, M., Ángel Rodríguez, M., Rull, A., Beltrán, R., Bladé, C., Brezmes, J., Cañellas, N., Joven, J., & Correig, X. (2010). Metabolomic assessment of the effect of dietary cholesterol in the progressive development of fatty liver disease. *Journal of Proteome Research*, *9*(5), 2527–2538. https://doi.org/10.1021/PR901203W

Visanji, N. P., Brooks, P. L., Hazrati, L. N., & Lang, A. E. (2014). The prion hypothesis in Parkinson's disease: Braak to the future. *Acta Neuropathologica Communications*, *2*(1), 1–12. https://doi.org/10.1186/2051-5960-1-2/FIGURES/2

Volkow, N. D., Wang, G. J., & Baler, R. D. (2011). Reward, dopamine and the control of food intake: implications for obesity. *Trends in Cognitive Sciences*, *15*(1), 37–46. https://doi.org/10.1016/J.TICS.2010.11.001

Volpicelli-Daley, L. A., Luk, K. C., Patel, T. P., Tanik, S. A., Riddle, D. M., Stieber, A., Meaney, D. F., Trojanowski, J. Q., & Lee, V. M. Y. (2011). Exogenous α-Synuclein Fibrils Induce Lewy Body Pathology Leading to Synaptic Dysfunction and Neuron Death. *Neuron*, *72*(1), 57–71. https://doi.org/10.1016/J.NEURON.2011.08.033

Voss, U., Sand, E., Olde, B., & Ekblad, E. (2013). Enteric neuropathy can be induced by high fat diet in vivo and palmitic acid exposure in vitro. *PloS One*, *8*(12). https://doi.org/10.1371/JOURNAL.PONE.0081413

Wachsmuth, H. R., Weninger, S. N., & Duca, F. A. (2022). Role of the gut–brain axis in energy and glucose metabolism. *Experimental and Molecular Medicine*, *54*(4), 377–392. https://doi.org/10.1038/S12276-021-00677-W

Wakabayashi, K., Takahashi, H., Ohama, E., & Ikuta, F. (1990). Parkinson's disease: an immunohistochemical study of Lewy body-containing neurons in the enteric nervous system. *Acta Neuropathologica*, *79*(6), 581–583. https://doi.org/10.1007/BF00294234/METRICS

Wakabayashi, K., Takahashi, H., Takeda, S., Ohama, E., & Ikuta, F. (1988). Parkinson's disease: the presence of Lewy bodies in Auerbach's and Meissner's plexuses. *Acta Neuropathologica*, *76*(3), 217–221. https://doi.org/10.1007/BF00687767/METRICS

Wakamatsu, K., Fujikawa, K., Zucca, F. A., Zecca, L., & Ito, S. (2003). The structure of neuromelanin as studied by chemical degradative methods. *Journal of Neurochemistry*, *86*(4), 1015–1023. https://doi.org/10.1046/J.1471-4159.2003.01917.X

Wallen, Z. D., Appah, M., Dean, M. N., Sesler, C. L., Factor, S. A., Molho, E., Zabetian, C. P., Standaert, D. G., & Payami, H. (2020). Characterizing dysbiosis of gut microbiome in PD: evidence for overabundance of opportunistic pathogens. *Npj Parkinson's Disease*, *6*(1), 1–12. https://doi.org/10.1038/s41531-020-0112-6

Wallen, Z. D., Demirkan, A., Twa, G., Cohen, G., Dean, M. N., Standaert, D. G., Sampson, T. R., & Payami, H. (2022). Metagenomics of Parkinson's disease implicates the gut microbiome in multiple disease

mechanisms. *Nature Communications 2022 13:1*, *13*(1), 1–20. https://doi.org/10.1038/s41467-022-34667-x

Wang, I. K., Lin, C. L., Wu, Y. Y., Chou, C. Y., Lin, S. Y., Liu, J. H., Yen, T. H., Huang, C. C., & Sung, F. C. (2014). Increased risk of parkinson's disease in patients with end-stage renal disease: A retrospective cohort study. *Neuroepidemiology*, *42*(4), 204–210. https://doi.org/10.1159/000358921

Wang, J., Li, L., Chen, P., He, C., Niu, X., & Mei, Q. (2024). Homocysteine aggravates intestinal inflammation through promotion of 5-LOX and COX-2 in IBD. *European Journal of Medical Research*, *29*(1), 537. https://doi.org/10.1186/S40001-024-02125-7/FIGURES/8

Wang, K., Lai, W., Min, T., Wei, J., Bai, Y., Cao, H., Guo, J., & Su, Z. (2024). The Effect of Enteric-Derived Lipopolysaccharides on Obesity. *International Journal of Molecular Sciences 2024, Vol. 25, Page 4305*, *25*(8), 4305. https://doi.org/10.3390/IJMS25084305

Wang, K., Zhang, C., Zhang, B., Li, G., Shi, G., Cai, Q., & Huang, M. (2022). Gut dysfunction may be the source of pathological aggregation of alpha-synuclein in the central nervous system through Paraquat exposure in mice. *Ecotoxicology and Environmental Safety*, *246*, 114152. https://doi.org/10.1016/J.ECOENV.2022.114152

Wang, L., Magen, I., Yuan, P. Q., Subramaniam, S. R., Richter, F., Chesselet, M. F., & Taché, Y. (2012). Mice overexpressing wild-type human alpha-synuclein display alterations in colonic myenteric ganglia and defecation. *Neurogastroenterology and Motility*, *24*(9), e425. https://doi.org/10.1111/j.1365-2982.2012.01974.x

Wang, Q., Garrity, G. M., Tiedje, J. M., & Cole, J. R. (2007). Naïve Bayesian classifier for rapid assignment of rRNA sequences into the new bacterial taxonomy. *Applied and Environmental Microbiology*, *73*(16), 5261–5267. https://doi.org/10.1128/AEM.00062-07/SUPPL_FILE/SUMMARY_BYHIERARCHY.ZIP

Wang, W., Chen, L., Zhou, R., Wang, X., Song, L., Huang, S., Wang, G., & Xia, B. (2014). Increased proportions of Bifidobacterium and the Lactobacillus group and loss of butyrate-producing bacteria in inflammatory bowel disease. *Journal of Clinical Microbiology*, *52*(2), 398–406. https://doi.org/10.1128/JCM.01500-13/SUPPL_FILE/ZJM999093116SO2.XLSX

Wang, X., Li, L., Liu, D., Jin, Y., Zhao, X., Li, S., Hou, R., Guan, Z., Ma, W., Zheng, J., Lv, M., & Shi, M. (2025). LILRB4 as a novel immunotherapeutic target for multiple diseases. *Biochemical Pharmacology*, *233*, 116762. https://doi.org/10.1016/J.BCP.2025.116762

Weimers, P., Halfvarson, J., Sachs, M. C., Saunders-Pullman, R., Ludvigsson, J. F., Peter, I., Burisch, J., & Olén, O. (2019). Inflammatory Bowel Disease and Parkinson's Disease: A Nationwide Swedish Cohort Study. *Inflammatory Bowel Diseases*, *25*(1), 111–123. https://doi.org/10.1093/IBD/IZY190

Weis, S., Schwiertz, A., Unger, M. M., Becker, A., Faßbender, K., Ratering, S., Kohl, M., Schnell, S., Schäfer, K.-H., & Egert, M. (2019). Effect of Parkinson's disease and related medications on the composition of the fecal bacterial microbiota. *Npj Parkinson's Disease*, *5*(1), 28. https://doi.org/10.1038/s41531-019-0100-x

Wexler, A. G., & Goodman, A. L. (2017). An insider's perspective: Bacteroides as a window into the microbiome. *Nature Microbiology 2017 2:5*, *2*(5), 1–11. https://doi.org/10.1038/nmicrobiol.2017.26

Wexler, H. M. (2007). Bacteroides: the Good, the Bad, and the Nitty-Gritty. *Clinical Microbiology Reviews*, *20*(4), 593. https://doi.org/10.1128/CMR.00008-07

William Langston, J., Ballard, P., Tetrud, J. W., & Irwin, I. (1983). Chronic parkinsonism in humans due to a product of meperidine-analog synthesis. *Science*, *219*(4587), 979–980. https://doi.org/10.1126/SCIENCE.6823561

Willing, B. P., Russell, S. L., & Finlay, B. B. (2011). Shifting the balance: antibiotic effects on host–microbiota mutualism. *Nature Reviews Microbiology 2011 9:4*, *9*(4), 233–243. https://doi.org/10.1038/nrmicro2536

Wilms, H., Rosenstiel, P., Sievers, J., Deuschl, G., Zecca, L., & Lucius, R. (2003). Activation of microglia by human neuromelanin is NF-kappaB dependent and involves p38 mitogen-activated protein kinase: implications for Parkinson's disease. *The FASEB Journal : Official Publication of the Federation of American Societies for Experimental Biology*, *17*(3), 500–502. https://doi.org/10.1096/FJ.02-0314FJE

Wu, G., Jiang, Z., Pu, Y., Chen, S., Wang, T., Wang, Y., Xu, X., Wang, S., Jin, M., Yao, Y., Liu, Y., Ke, S., & Liu, S. (2022). Serum short-chain fatty acids and its correlation with motor and non-motor symptoms in Parkinson's disease patients. *BMC Neurology*, *22*(1), 13. https://doi.org/10.1186/S12883-021-02544-7

Wulf, M., Barkovits, K., Schork, K., Eisenacher, M., Riederer, P., Gerlach, M., Eggers, B., & Marcus, K. (2022). Neuromelanin granules of the substantia nigra: proteomic profile provides links to tyrosine hydroxylase, stress granules and lysosomes. *Journal of Neural Transmission*, *129*(10), 1257–1270. https://doi.org/10.1007/S00702-022-02530-4/FIGURES/5

Wuolikainen, A., Jonsson, P., Ahnlund, M., Antti, H., Marklund, S. L., Moritz, T., Forsgren, L., Andersen, P. M., & Trupp, M. (2016). Multi-platform mass spectrometry analysis of the CSF and plasma metabolomes of rigorously matched amyotrophic lateral sclerosis, Parkinson's disease and control subjects. *Molecular BioSystems*, *12*(4), 1287–1298. https://doi.org/10.1039/C5MB00711A

Xiang, J., Tang, J., Kang, F., Ye, J., Cui, Y., Zhang, Z., Wang, J., Wu, S., & Ye, K. (2024). Gut-induced alpha-Synuclein and Tau propagation initiate Parkinson's and Alzheimer's disease co-pathology and behavior impairments. *Neuron*, *112*(21), 3585-3601.e5. https://doi.org/10.1016/j.neuron.2024.08.003

Xicoy, H., Klemann, C. J., De Witte, W., Martens, M. B., Martens, G. J., & Poelmans, G. (2021). Shared genetic etiology between Parkinson's disease and blood levels of specific lipids. *Npj Parkinson's Disease 2021 7:1*, *7*(1), 1–8. https://doi.org/10.1038/s41531-021-00168-9

Xicoy, H., Wieringa, B., & Martens, G. J. M. (2019). The Role of Lipids in Parkinson's Disease. *Cells 2019, Vol. 8, Page 27*, *8*(1), 27. https://doi.org/10.3390/CELLS8010027

Xie, L., Chen, D., Zhu, X., & Cheng, C. (2023). Efficacy and safety of probiotics in Parkinson's constipation: A systematic review and meta-analysis. *Frontiers in Pharmacology*, *13*, 1007654. https://doi.org/10.3389/FPHAR.2022.1007654/FULL

Xu, J., Wang, L., Chen, X., & Le, W. (2022). New Understanding on the Pathophysiology and Treatment of Constipation in Parkinson's Disease. *Frontiers in Aging Neuroscience*, *14*, 917499. https://doi.org/10.3389/FNAGI.2022.917499

Xu, W., Yu, J., Yang, Y., Li, Z., Zhang, Y., Zhang, F., Wang, Q., Xie, Y., Zhao, B., & Wu, C. (2023). Strain-level screening of human gut microbes identifies Blautia producta as a new anti-hyperlipidemic probiotic. *Gut Microbes*, *15*(1), 2228045. https://doi.org/10.1080/19490976.2023.2228045

Xu, Y., Stokes, A. H., Freeman, W. M., Kumer, S. C., Vogt, B. A., & Vrana, K. E. (1997). Tyrosinase mRNA is expressed in human substantia nigra. *Molecular Brain Research*, *45*(1), 159–162. https://doi.org/10.1016/S0169-328X(96)00308-7

Xue, L. J., Yang, X. Z., Tong, Q., Shen, P., Ma, S. J., Wu, S. N., Zheng, J. L., & Wang, H. G. (2020). Fecal microbiota transplantation therapy for Parkinson's disease: A preliminary study. *Medicine*, *99*(35), e22035. https://doi.org/10.1097/MD.0000000000022035

Yamamoto, H., Kishi, T., Lee, C. E., Choi, B. J., Fang, H., Hollenberg, A. N., Drucker, D. J., & Elmquist, J. K. (2003). Glucagon-Like Peptide-1-Responsive Catecholamine Neurons in the Area Postrema Link Peripheral Glucagon-Like Peptide-1 with Central Autonomic Control Sites. *Journal of Neuroscience*, *23*(7), 2939–2946. https://doi.org/10.1523/JNEUROSCI.23-07-02939.2003

Yan, Z., Yang, F., Cao, J., Ding, W., Yan, S., Shi, W., Wen, S., & Yao, L. (2021). Alterations of gut microbiota and metabolome with Parkinson's disease. *Microbial Pathogenesis*, *160*, 105187. https://doi.org/10.1016/J.MICPATH.2021.105187

Yatsunenko, T., Rey, F. E., Manary, M. J., Trehan, I., Dominguez-Bello, M. G., Contreras, M., Magris, M., Hidalgo, G., Baldassano, R. N., Anokhin, A. P., Heath, A. C., Warner, B., Reeder, J., Kuczynski, J., Caporaso, J. G., Lozupone, C. A., Lauber, C., Clemente, J. C., Knights, D., … Gordon, J. I. (2012). Human gut microbiome viewed across age and geography. In *Nature* (Vol. 486, Issue 7402, pp. 222–227). NIH Public Access. https://doi.org/10.1038/nature11053

Ye, L., Hou, Y., Hu, W., Wang, H., Yang, R., Zhang, Q., Feng, Q., Zheng, X., Yao, G., & Hao, H. (2023). Repressed Blautia-acetate immunological axis underlies breast cancer progression promoted by chronic stress. *Nature Communications 2023 14:1*, *14*(1), 1–18. https://doi.org/10.1038/s41467-023-41817-2

Yeo, C. J., Couse, N. F., Antiohos, C., & Zinner, M. J. (1988). The effect of norepinephrine on intestinal transport and perfusion pressure in the isolated perfused rabbit ileum. *The Journal of Surgical Research*, *44*(5), 617–624. https://doi.org/10.1016/0022-4804(88)90170-9

Yoo, B. B., & Mazmanian, S. K. (2017). The Enteric Network: Interactions between the Immune and Nervous Systems of the Gut. *Immunity*, *46*(6), 910–926. https://doi.org/10.1016/J.IMMUNI.2017.05.011/ASSET/16399202-596E-4E27-8254-39DBD3D68324/MAIN.ASSETS/GR3.JPG

Yoo, D., Lim, Y., Son, Y., Rho, H., Shin, C., & Ahn, T. B. (2021). Dietary intake and plasma levels of polyunsaturated fatty acids in early-stage Parkinson's disease. *Scientific Reports 2021 11:1*, *11*(1), 1–9. https://doi.org/10.1038/s41598-021-92029-x

Zapała, B., Stefura, T., Milewicz, T., Wator, J., Piwowar, M., Wójcik-Pędziwiatr, M., Doręgowska, M., Dudek, A., Jania, Z., & Rudzińska-Bar, M. (2022). The Role of the Western Diet and Oral Microbiota in Parkinson's Disease. *Nutrients*, *14*(2), 355. https://doi.org/10.3390/NU14020355

Zatterale, F., Longo, M., Naderi, J., Raciti, G. A., Desiderio, A., Miele, C., & Beguinot, F. (2020). Chronic Adipose Tissue Inflammation Linking Obesity to Insulin Resistance and Type 2 Diabetes. *Frontiers in Physiology*, *10*, 505887. https://doi.org/10.3389/FPHYS.2019.01607/XML/NLM

Zecca, L., Bellei, C., Costi, P., Albertini, A., Monzani, E., Casella, L., Gallorini, M., Bergamaschi, L., Moscatelli, A., Turro, N. J., Eisner, M., Crippa, P. R., Ito, S., Wakamatsu, K., Bush, W. D., Ward, W. C., Simon, J. D., & Zucca, F. A. (2008). New melanic pigments in the human brain that accumulate in aging and block environmental toxic metals. *Proceedings of the National Academy of Sciences of the United States of America*, *105*(45), 17567–17572. https://doi.org/10.1073/PNAS.0808768105/SUPPL_FILE/0808768105SI.PDF

Zecca, L., Costi, P., Mecacci, C., Ito, S., Terreni, M., & Sonnino, S. (2000). Interaction of human substantia nigra neuromelanin with lipids and peptides. *Journal of Neurochemistry*, *74*(4), 1758–1765. https://doi.org/10.1046/J.1471-4159.2000.0741758.X

Zecca, L., Zucca, F. A., Wilms, H., & Sulzer, D. (2003). Neuromelanin of the substantia nigra: a neuronal black hole with protective and toxic characteristics. *Trends in Neurosciences*, *26*(11), 578–580. https://doi.org/10.1016/J.TINS.2003.08.009

Zhang, C., Jiang, J., Tian, F., Zhao, J., Zhang, H., Zhai, Q., & Chen, W. (2020). Meta-analysis of randomized controlled trials of the effects of probiotics on functional constipation in adults. *Clinical Nutrition (Edinburgh, Scotland)*, *39*(10), 2960–2969. https://doi.org/10.1016/J.CLNU.2020.01.005

Zhang, F., Yue, L., Fang, X., Wang, G., Li, C., Sun, X., Jia, X., Yang, J., Song, J., Zhang, Y., Guo, C., Ma, G., Sang, M., Chen, F., & Wang, P. (2020). Altered gut microbiota in Parkinson's disease patients/healthy spouses and its association with clinical features. *Parkinsonism and Related Disorders*, *81*, 84–88. https://doi.org/10.1016/j.parkreldis.2020.10.034

Zhang, H., Cao, X. yue, Wang, L. na, Tong, Q., Sun, H. min, Gan, C. ting, Shan, A. di, Yuan, Y. sheng, & Zhang, K. zhong. (2023). Transcutaneous auricular vagus nerve stimulation improves gait and cortical activity in Parkinson's disease: A pilot randomized study. *CNS Neuroscience & Therapeutics*, *29*(12), 3889. https://doi.org/10.1111/CNS.14309

Zhang, K., Xu, L., & Guo, J. (2024). Tarm1 may affect colitis by regulating macrophage M1 polarization in a mouse colitis model. *Pediatric Research 2024*, 1–8. https://doi.org/10.1038/s41390-024-03640-3

Zhang, W., Phillips, K., Wielgus, A. R., Liu, J., Albertini, A., Zucca, F. A., Faust, R., Qian, S. Y., Miller, D. S., Chignell, C. F., Wilson, B., Jackson-Lewis, V., Przedborski, S., Joset, D., Loike, J., Hong, J. S., Sulzer, D., & Zecca, L. (2009). Neuromelanin activates microglia and induces degeneration of dopaminergic

neurons: implications for progression of Parkinson's disease. *Neurotoxicity Research*, *19*(1), 63. https://doi.org/10.1007/S12640-009-9140-Z

Zhang, W., Zecca, L., Wilson, B., Ren, H. W., Wang, Y. J., Wang, X. M., & Hong, J. S. (2013). Human neuromelanin: an endogenous microglial activator for dopaminergic neuron death. *Frontiers in Bioscience (Elite Edition)*, *5*(1), 1. https://doi.org/10.2741/E591

Zhang, X., & Yi, N. (2020). NBZIMM: negative binomial and zero-inflated mixed models, with application to microbiome/metagenomics data analysis. *BMC Bioinformatics*, *21*(1), 1–19. https://doi.org/10.1186/S12859-020-03803-Z/FIGURES/7

Zhang, Y., He, X., Qian, Y., Xu, S., Mo, C., Yan, Z., Yang, X., & Xiao, Q. (2022). Plasma branched-chain and aromatic amino acids correlate with the gut microbiota and severity of Parkinson's disease. *Npj Parkinson's Disease 2022 8:1*, *8*(1), 1–10. https://doi.org/10.1038/s41531-022-00312-z

Zhao, Y., Lai, Y., Konijnenberg, H., Huerta, J. M., Vinagre-Aragon, A., Sabin, J. A., Hansen, J., Petrova, D., Sacerdote, C., Zamora-Ros, R., Pala, V., Heath, A. K., Panico, S., Guevara, M., Masala, G., Lill, C. M., Miller, G. W., Peters, S., & Vermeulen, R. (2024). Association of Coffee Consumption and Prediagnostic Caffeine Metabolites With Incident Parkinson Disease in a Population-Based Cohort. *Neurology*, *102*(8). https://doi.org/10.1212/WNL.0000000000209201/SUPPL_FILE/SUPPLEMENTARY_DATA1.PDF

Zhao, Z., Ning, J., Bao, X. qi, Shang, M., Ma, J., Li, G., & Zhang, D. (2021). Fecal microbiota transplantation protects rotenone-induced Parkinson's disease mice via suppressing inflammation mediated by the lipopolysaccharide-TLR4 signaling pathway through the microbiota-gut-brain axis. *Microbiome*, *9*(1), 1–27. https://doi.org/10.1186/S40168-021-01107-9/METRICS

Zhi, S. L., Schmauss, C., Cuenca, A., Ratcliffe, E., & Gershon, M. D. (2006). Physiological Modulation of Intestinal Motility by Enteric Dopaminergic Neurons and the D2 Receptor: Analysis of Dopamine Receptor Expression, Location, Development, and Function in Wild-Type and Knock-Out Mice. *Journal of Neuroscience*, *26*(10), 2798–2807. https://doi.org/10.1523/JNEUROSCI.4720-05.2006

Zhou, C., You, J., Guan, X., Guo, T., Wu, J., Wu, H., Wu, C., Chen, J., Wen, J., Tan, S., Duanmu, X., Qin, J., Huang, P., Zhang, B., Cheng, W., Feng, J., Xu, X., Wang, L., & Zhang, M. (2024). Microstructural alterations of the hypothalamus in Parkinson's disease and probable REM sleep behavior disorder. *Neurobiology of Disease*, *194*, 106472. https://doi.org/10.1016/J.NBD.2024.106472

Zhou, Q., Leeman, S. E., & Amar, S. (2009). Signaling mechanisms involved in altered function of macrophages from diet-induced obese mice affect immune responses. *Proceedings of the National Academy of Sciences of the United States of America*, *106*(26), 10740–10745. https://doi.org/10.1073/PNAS.0904412106/SUPPL_FILE/0904412106SI.PDF

Zhu, F., Li, C., Gong, J., Zhu, W., Gu, L., & Li, N. (2019a). The risk of Parkinson's disease in inflammatory bowel disease: A systematic review and meta-analysis. *Digestive and Liver Disease*, *51*(1), 38–42. https://doi.org/10.1016/j.dld.2018.09.017

Zhu, F., Li, C., Gong, J., Zhu, W., Gu, L., & Li, N. (2019b). The risk of Parkinson's disease in inflammatory bowel disease: A systematic review and meta-analysis. *Digestive and Liver Disease : Official Journal*

of the Italian Society of Gastroenterology and the Italian Association for the Study of the Liver, *51*(1), 38–42. https://doi.org/10.1016/J.DLD.2018.09.017

Zhu, Y., Yuan, M., Liu, Y., Yang, F., Chen, W. Z., Xu, Z. Z., Xiang, Z. B., & Xu, R. S. (2022). Association between inflammatory bowel diseases and Parkinson's disease: systematic review and meta-analysis. *Neural Regeneration Research*, *17*(2), 344–353. https://doi.org/10.4103/1673-5374.317981

Zizzo, M. G., Mulè, F., Mastropaolo, M., & Serio, R. (2010). D1 receptors play a major role in the dopamine modulation of mouse ileum contractility. *Pharmacological Research*, *61*(5), 371–378. https://doi.org/10.1016/J.PHRS.2010.01.015

Zucca, F. A., Basso, E., Cupaioli, F. A., Ferrari, E., Sulzer, D., Casella, L., & Zecca, L. (2014a). Neuromelanin of the human substantia Nigra: An update. *Neurotoxicity Research*, *25*(1), 13–23. https://doi.org/10.1007/S12640-013-9435-Y/FIGURES/2

Zucca, F. A., Basso, E., Cupaioli, F. A., Ferrari, E., Sulzer, D., Casella, L., & Zecca, L. (2014b). Neuromelanin of the human substantia nigra: an update. *Neurotoxicity Research*, *25*(1), 13–23. https://doi.org/10.1007/S12640-013-9435-Y

ANNEX

Annex Data Table 1. DEGs in tgNM females compared to wt littermates in the duodenum. Raw p. value ≤0.01, FC ≥|1.5|) in tgNM females compared to wt counterparts from duodenal samples.

Gene Symbol	Entrez	logFC	AveExpr	t	P.Value	adj.P.Val
Ccdc190	78465	-0,77933071	1,59959502	-5,29112628	2,755E-05	0,55314196
Ppp1r26	241289	0,98553885	3,93565243	4,79349783	9,0759E-05	0,691166
Parvb	170736	0,87017876	3,40323383	4,73995675	0,00010327	0,691166
Klk9	101533	-1,03696555	2,97721282	-4,49407407	0,00018717	0,78837558
Bhmt	12116	-1,00909704	3,1887043	-4,47056992	0,00019813	0,78837558
Crmp1	12933	-1,02691638	3,47844688	-4,3767536	0,00024871	0,78837558
Ptgis	19223	0,84643482	5,28850156	4,25326168	0,00033552	0,78837558
Rgr	57811	-0,64983305	2,26184996	-4,17327625	0,00040731	0,78837558
Gpihbp1	68453	0,76970073	3,93820411	4,16216393	0,00041843	0,78837558
Sohlh1	227631	-0,78841069	3,37155332	-4,01681848	0,00059501	0,91896458
Glyat	107146	0,75515442	1,9755891	3,93036941	0,00073339	0,99976613
1700125H20Rik	73634	0,75688234	2,32253882	3,88219301	0,00082391	0,99976613
Cpne6	12891	-0,86327001	3,55712173	-3,84359648	0,00090436	0,99976613
Ccl1	20290	0,62130668	2,3895462	3,77361247	0,00107055	0,99976613
Enthd1	383075	-0,67608065	3,96234053	-3,7626145	0,00109928	0,99976613
Cenpu	71876	-0,73435945	5,14930404	-3,68408422	0,00132777	0,99976613
Itih1	16424	-0,63042179	2,93347842	-3,6400559	0,00147575	0,99976613
Mdfic2	330390	0,85413723	2,32708259	3,63475475	0,00149462	0,99976613
Fbxl16	214931	0,65121113	4,1930323	3,62170277	0,00154212	0,99976613
Pou3f1	18991	-0,76719298	3,57746027	-3,57976159	0,00170504	0,99976613
Olfr849	258520	0,70977956	1,68940291	3,55514415	0,00180842	0,99976613
Atp6v1e2	74915	-0,74068902	4,60893868	-3,47544003	0,00218719	0,99976613
S100a7a	381493	0,65296039	2,67924425	3,46114545	0,0022629	0,99976613
2210408I21Rik	72371	-0,90434004	5,18307382	-3,41164143	0,00254544	0,99976613
Mog	17441	0,75995594	2,41845807	3,40164895	0,00260653	0,99976613
Foxb1	64290	-0,68916063	3,45281681	-3,39341122	0,00265796	0,99976613
Akr1c18	105349	-0,83638558	1,7754085	-3,38417076	0,00271683	0,99976613
Syt1	20979	0,7264483	5,96445979	3,36331612	0,00285441	0,99976613
Btbd35f28	627264	0,60916402	1,66953802	3,3491415	0,00295178	0,99976613
Cstdc6	100038854	-0,67238814	3,18205831	-3,34585747	0,0029748	0,99976613
R3hdml	100043899	0,60385484	3,79201011	3,32848079	0,00309954	0,99976613
Brinp3	215378	-0,68635842	1,87369382	-3,32173055	0,00314935	0,99976613
Tmem101	76547	0,69724658	4,20056348	3,28632846	0,00342367	0,99976613
Lrrc63	70859	0,74964673	2,10340844	3,26857041	0,0035699	0,99976613
Pxt1	69307	-0,67455967	3,11617999	-3,24094497	0,00380952	0,99976613
Igfbp3	16009	0,74746609	7,13760564	3,2025405	0,00416875	0,99976613
Lilrb4a	14728	0,70343939	4,78231923	3,19585483	0,00423456	0,99976613
Dcpp3	620253	0,6204512	2,41389904	3,16054963	0,00459913	0,99976613
Hpcal4	170638	0,88480552	3,37543347	3,1572983	0,00463419	0,99976613
Adam22	11496	0,68941911	4,41002016	3,14806435	0,00473518	0,99976613
Kndc1	76484	-0,67097536	3,17188535	-3,14003701	0,00482471	0,99976613

Taar3	493809	0,63556491	1,86805363	3,1386194	0,00484069	0,99976613
Gad2	14417	0,74193124	3,38551505	3,13809952	0,00484656	0,99976613
Rp1	19888	-0,61033499	2,41851904	-3,13593086	0,00487114	0,99976613
Olfr658	259051	0,64484319	1,94790954	3,13494343	0,00488237	0,99976613
Nsl1	381318	-0,63362626	5,59442322	-3,13294449	0,00490517	0,99976613
Padi3	18601	-0,60297106	2,69237402	-3,12569073	0,00498881	0,99976613
Upp2	76654	-0,95389541	3,87035445	-3,12024622	0,00505248	0,99976613
Gm15104	333588	-0,64358177	2,42464305	-3,07784794	0,00557595	0,99976613
Tarm1	245126	0,64400674	3,42249559	3,0663842	0,00572624	0,99976613
Pdgfrl	68797	-0,6531751	3,54397288	-3,04810546	0,00597399	0,99976613
Calhm4	270711	0,64764375	2,00951417	3,04592889	0,00600417	0,99976613
Cfap97d2	403185	0,85506231	2,26911678	3,03864384	0,00610626	0,99976613
Krtap31-1	70831	-0,88665633	2,87452662	-3,03833226	0,00611066	0,99976613
Trim42	78911	-0,64073929	2,26010261	-3,02900117	0,00624396	0,99976613
Fabp3	14077	0,68740997	3,43636634	3,01364252	0,00646947	0,99976613
Obsl1	98733	0,64464542	3,10244952	2,98976056	0,00683576	0,99976613
4930546C10Rik	78931	0,60775154	2,42450195	2,9794767	0,00699956	0,99976613
Olfr641	259075	0,66998177	2,63070825	2,96419001	0,00725003	0,99976613
Olfr1474	258123	-0,65453864	1,71079748	-2,95926537	0,00733253	0,99976613
Pla2g2c	18781	0,95558054	3,32676218	2,94887667	0,00750954	0,99976613
Wdr38	76646	-0,68697132	4,11395676	-2,94730169	0,00753673	0,99976613
Bpifb6	228796	0,69301615	2,69174192	2,92158895	0,0079942	0,99976613
Slfn1	20555	-0,67014149	2,38338965	-2,91807243	0,0080588	0,99976613
Vmn1r80	171238	-0,695973	1,87067163	-2,89191344	0,00855524	0,99976613
Trim46	360213	0,68552032	3,817273	2,88969795	0,0085986	0,99976613
Msh5	17687	-0,60559224	3,47516725	-2,88733419	0,0086451	0,99976613
Slc22a13	102570	-0,64206423	4,95225246	-2,88149051	0,00876108	0,99976613
Cacna1d	12289	0,76331323	4,62201521	2,87065068	0,00898017	0,99976613
H2al1m	76383	-0,92476099	3,46797487	-2,8603395	0,00919342	0,99976613
Kdm5d	20592	0,60262447	4,12213344	2,85805613	0,0092413	0,99976613
Taar4	209513	-0,73248527	2,30325053	-2,85480934	0,00930978	0,99976613
Nkx2-9	18094	-0,73009963	3,48162745	-2,83713752	0,00969109	0,99976613
Tlr7	170743	0,67062868	5,20817591	2,83654659	0,00970409	0,99976613
Xlr4a	434794	-0,90755867	3,77159838	-2,83629744	0,00970958	0,99976613

Annex Data Table 2. DEGs in tgNM males compared to wt littermates in the duodenum. Raw p. value ≤0.01, FC ≥|1.5|) in tgNM females compared to wt counterparts from duodenal samples.

Gene Symbol	Entrez	logFC	AveExpr	t	P.Value	adj.P.Val
Ccdc87	399599	1,07214595	2,64470779	4,87450185	7,4668E-05	0,99990874
Amh	11705	0,86746924	3,11096492	4,64927894	0,00012856	0,99990874
4933421I07Rik	71162	0,84273363	2,00322137	4,41160793	0,00022856	0,99990874
Zfp846	244721	0,62323693	5,91386531	4,03864561	0,00056438	0,99990874
Olfr1087	258843	1,00935445	2,56679016	3,89320704	0,00080228	0,99990874
Olfr347	258945	0,62062022	1,92224542	3,80979196	0,00098117	0,99990874

Pak3	18481	-0,884459	3,48359462	-3,75866159	0,00110979	0,99990874
Klre1	243655	0,73200339	3,27573651	3,73044804	0,00118775	0,99990874
Lrp1b	94217	-0,65579716	2,52116535	-3,5832717	0,00169078	0,99990874
A530053G22Rik	208079	-0,6408075	1,59413136	-3,55919693	0,00179099	0,99990874
Hrk	12123	0,69653541	4,24987571	3,53502333	0,00189748	0,99990874
Aanat	11298	0,78065882	2,46742407	3,50070726	0,00205938	0,99990874
Slc12a5	57138	0,6943155	2,69695363	3,47340017	0,00219784	0,99990874
Rrh	20132	0,63880276	3,2917138	3,45137858	0,00231609	0,99990874
Zfp763	73451	0,70710148	3,15008504	3,41670926	0,002515	0,99990874
Zfp267	241944	-0,74810588	4,35745885	-3,40272787	0,00259986	0,99990874
Pcdhb6	93877	1,03153776	2,66746468	3,36693901	0,00283003	0,99990874
Camk2a	12322	-0,68907151	4,29106596	-3,28875372	0,00340416	0,99990874
Tacstd2	56753	0,71650569	1,91236069	3,25544464	0,00368186	0,99990874
Gad2	14417	0,84516376	3,38551505	3,23052641	0,00390389	0,99990874
Kctd19	279499	0,84529754	2,24210475	3,22725774	0,00393396	0,99990874
Eya4	14051	-0,74399727	2,41004612	-3,22302041	0,00397328	0,99990874
Oit3	18302	0,60247287	4,02441698	3,21434719	0,00405495	0,99990874
Parvg	64099	0,69145322	4,25416749	3,19728896	0,00422036	0,99990874
D130040H23Rik	211135	-1,01984517	4,69158349	-3,18090775	0,00438535	0,99990874
Heatr9	629303	0,74364875	3,10690464	3,09676601	0,00533621	0,99990874
Dock4	238130	-0,78665221	6,35296028	-3,08531515	0,00548011	0,99990874
Htra4	330723	0,84927812	3,38326324	3,08371882	0,00550046	0,99990874
Slc38a8	234788	0,73039114	3,88704886	3,08089269	0,00553667	0,99990874
Kap	16483	-0,63923793	1,83661521	-3,07124709	0,00566202	0,99990874
Slc22a16	70840	0,99868559	2,60953751	3,02430677	0,00631207	0,99990874
Glycam1	14663	0,63247285	2,08915803	3,00958528	0,00653034	0,99990874
Phlda1	21664	-1,33468188	6,20049552	-2,96292605	0,00727112	0,99990874
Olfr954	258328	-0,64413518	1,45209218	-2,9479276	0,00752591	0,99990874
Cmya5	76469	0,69015836	3,06072496	2,92234411	0,0079804	0,99990874
Kcnh7	170738	0,75787414	2,75592669	2,92221844	0,00798269	0,99990874
Folh1	53320	-0,86489198	2,29450593	-2,90866805	0,00823401	0,99990874
Dnai3	242253	0,7010518	2,49894423	2,89227061	0,00854827	0,99990874
Gm6034	547347	0,86305815	3,39724881	2,88628166	0,00866588	0,99990874
Svopl	320590	-0,80238768	2,65373738	-2,86654092	0,00906459	0,99990874
Foxc1	17300	-0,65602098	3,57157401	-2,86424517	0,00911208	0,99990874
Olfr1086	258585	0,6720176	2,95870866	2,85772509	0,00924826	0,99990874
Upk2	22269	-0,62521824	2,07944141	-2,84700206	0,00947644	0,99990874
Ccdc7a	74703	0,70144301	4,21292823	2,83532913	0,00973094	0,99990874
Tmem52	69671	0,72866943	2,71459592	2,83344607	0,0097726	0,99990874
Zfp296	63872	-0,71487779	3,17917388	-2,83004548	0,00984827	0,99990874